

**REPORT NO. DOT-TSC-FAA-71-29**

# **MICROWAVE SCANNING BEAM APPROACH AND LANDING SYSTEM PHASED ARRAY ANTENNA**

**R.M. KALAFUS, P. HARRIS, F.J. LARUSSA,  
G.J. BISHOP, P.J. PANTANO, B. RUBINGER,  
G.G. HAROULES, R.S. YATSKO  
TRANSPORTATION SYSTEMS CENTER  
55 BROADWAY  
CAMBRIDGE, MA. 02142**



**SEPTEMBER 1971  
ANNUAL REPORT**

**Availability is Unlimited. Document may be Released  
To the National Technical Information Service,  
Springfield, Virginia 22151, for Sale to the Public.**

**Prepared for  
DEPARTMENT OF TRANSPORTATION  
FEDERAL AVIATION ADMINISTRATION  
WASHINGTON, D. C. 20590**



1. Report No. DOI-TSC-FAA-71-29	2. Government Accession No.	3. Recipient's Catalog No.	
4. Title and Subtitle Microwave Scanning Beam Approach and Landing System Phased Array Antenna		5. Report Date September 1971	6. Performing Organization Code TER
		8. Performing Organization Report No.	
7. Author(s) R.M. Kalafus, G.J. Bishop, G.G. Haroules,		10. Work Unit No. PPA FA209	
9. Performing Organization Name and Address Transportation Systems Center 55 Broadway Cambridge, MA 02142		11. Contract or Grant No. R1030	
		13. Type of Report and Period Covered Annual Report July 1970 - July 1971	
12. Sponsoring Agency Name and Address Federal Aviation Administration Systems Research and Development Service Washington, DC 20590		14. Sponsoring Agency Code	
		15. Supplementary Notes P. Harris, F.J. LaRussa, P.J. Pantano, B. Rubinger, R.S. Yatsko (Authors Cont)	
16. Abstract  The feasibility of the use of phased arrays for the proposed microwave landing guidance system (MLGS) is discussed. The effects of the use of planar and conical beam guidance on the choice of system configurations is investigated. The design of an experimental antenna to demonstrate feasibility is given.			
17. Key Words aircraft guidance; cylindrical arrays; linear arrays; planar arrays; air traffic control; C-band; components; stripline; microstrip; propagation, microwave sources		18. Distribution Statement Availability is Unlimited. Document may be Released To the National Technical Information Service, Springfield, Virginia 22151, for Sale to the Public.	
19. Security Classif. (of this report) Unclassified	20. Security Classif. (of this page) Unclassified	21. No. of Pages 312	22. Price



## PREFACE

The authors wish to acknowledge the contributions of the late David Friedman to this effort. His experience and enthusiasm were inspirational to his colleagues.



# TABLE OF CONTENTS

	Page
I. INTRODUCTION AND WORK STATEMENT.....	1
1.1 RTCA Recommendations.....	2
1.2 Coordinate System.....	3
1.3 RF Power Budget.....	7
1.4 Summary: Conclusions, Milestones, and Areas of Further Study.....	9
1.4.1 Results of the Effort, Arranged By Task.....	11
1.4.2 Results of the Effort, Arranged By Milestone.....	15
1.4.3 Experimental Program.....	16
1.4.4 Conclusions Regarding the Choice of Linear or Cylindrical Arrays.....	17
1.4.5 Areas of Further Study.....	19
II. THE IMPACT OF PLANAR VS. CONICAL GUIDANCE ON ANTENNA CONFIGURATION AND LOCATION.....	21
2.1 Planar and Conical Fan Beams-Descriptions.....	22
2.1.1 Azimuth Function.....	22
2.1.2 Elevation Function.....	24
2.2 Effect of Antenna Locations on Position-in- Space Determination--Initial Approach Region..	30
2.2.1 Exact (x, y, z) Calculation.....	35
2.2.2 Derivation of Range-To-Elevation #1....	38
2.2.3 Coverage Considerations.....	39
2.3 Effect of Site Locations on Position-in- Space Calculations in Final Approach Region...	41
2.3.1 Loss of Coverage Near Guidance Minimum.....	41
2.3.2 Glide Slope Error Due to Coning- Without DME Correction.....	46
2.3.3 Glide Slope Error Due to Coning- With DME Correction.....	47
2.3.4 Lateral Errors For Collocated Setup Without DME Correction.....	51
2.3.5 Lateral Errors For Collocated Setup With DME Correction.....	54
2.3.6 Lateral Errors For Split-Site Setup....	56
2.4 Effect of Antenna Locations on Position-in- Space Calculation in Landing and Rollout Region.....	58
2.4.1 DME At the Azimuth Site.....	61
2.4.2 DME At Elevation #2 Location.....	66
III. ANTENNA DESIGN STUDIES.....	68
3.1 Azimuth Antenna.....	68
3.1.1 Column Design-Multipath Considerations.....	69
3.1.2 Planar Array Design.....	83

# TABLE OF CONTENTS (CONT.)

	Page
3.1.3 Cylindrical Array Design.....	90
3.2 Elevation Antenna.....	108
3.2.1 Elevation Element Design.....	109
3.2.2 Linear Array Design.....	110
3.2.3 Cylindrical Array Design.....	112
IV. FEED NETWORK DESIGNS.....	119
4.1 Linear Arrays.....	119
4.2 Cylindrical Arrays.....	125
4.2.1 Transfer Matrix Feed.....	126
4.2.2 Lens Feed (R-2R).....	133
4.2.3 Electronic Attenuator (Vector Switch) Feed.....	137
4.2.4 Butler Matrix Feed.....	139
4.2.5 Advantages and Disadvantages of Candidate Feed Systems.....	141
4.2.5.1 One-Degree Beamwidth Antenna..	146
4.2.5.2 Two Degree Beamwidth Antenna..	151
4.2.5.3 Four-Degree Beamwidth Antenna..	157
4.2.5.4 Discussion of Various Feed Systems.....	162
V. EXPERIMENTAL LOGIC AND BEAM STEERING COMPUTER DESIGN.....	164
5.1 Control Logic Implementation.....	164
5.2 Control Unit Description.....	166
VI. RF POWER SOURCE DESIGN.....	172
6.1 Introduction.....	172
6.2 Source Requirements.....	173
6.2.1 RF Power Output Requirement.....	174
6.2.2 Summary of Source Requirements.....	176
6.3 Devices (C-Band, Solid State).....	176
6.3.1 Transistor Devices.....	180
6.3.2 Varactor Diodes.....	180
6.3.3 Step Recovery Diode.....	184
6.3.4 Bulk Effect and Avalanche Devices.....	186
6.3.4.1 Bulk Effect Devices.....	186
6.3.4.2 Avalanche Devices.....	187
6.3.5 Summary.....	188
6.4 RF Source Configuration.....	188
6.5 Initial Choice.....	191
6.5.1 Initial Source Specification.....	192
6.5.1.1 Electrical Requirements.....	192
6.5.1.2 Mechanical Requirements.....	193
6.5.1.3 Operational Effectiveness.....	194
6.5.1.4 Environmental Requirements.....	194
6.5.1.5 Design and Construction.....	194
6.5.1.6 Quality Assurance Provisions..	194



## TABLE OF CONTENTS (CONT.)

	Page
6.5.1.7 Drawing Applicability.....	195
6.5.1.8 Applicable Documents.....	195
6.6 Summary.....	195
VII. EXPERIMENTAL MODEL DESCRIPTION-GOALS OF EXPERIMENTAL PROGRAM.....	197
7.1 Lens Antenna System.....	198
7.1.1 Lens Antenna System-Discussion.....	198
7.1.2 Test Plan For the Microwave Lens.....	202
7.2 Test Plan for Components and Antenna Range Patterns.....	202
7.2.1 Component Tests - Evaluation of Candidate System Potential.....	202
7.2.2 Range Tests - Static Array Patterns....	203
7.2.3 Range Tests-Dynamic Array Patterns....	218
7.3 Antenna Elements-Development Plan.....	218
7.3.1 Column Element of Azimuth Antenna- Development Tasks.....	219
7.3.1.1 Elemental Dipole.....	219
7.3.1.2 Power Divider and Phasing.....	219
7.3.2 Elevation Antenna Element - Development Tasks.....	220
7.3.2.1 Element Design (Spec. H-Plane Pattern 120° @ 3dB).....	220
7.3.2.2 Power Divider and Phasing.....	220
7.4 Cost Estimates, Based on Component Production Costs.....	221
7.4.1 Azimuth Antenna Cost Estimates.....	223
7.4.2 Elevation Antenna Cost Estimate.....	224
Appendices	
A. Classes of Aircraft.....	A-1
B. Array Theory.....	B-1
C. Stripline Component Fabrication Considerations.....	C-1
D. Propagation Factors Which May Limit the Performance of Future Microwave Guidance Systems.....	D-1
E. Component Specifications.....	E-1
Glossary of Terms.....	G-1



# LIST OF ILLUSTRATIONS

		Page
1.1	SC-117 Landing System Configuration Data.....	4
1.2	LGS Signal Coverage.....	5
1.3	General Siting Plan Configuration "I" and "K".....	6
1.4	Runway Coordinate System.....	7
2.1	Guidance Contours Showing Coning in Linear Arrays...23	23
2.2	Azimuth Errors Due to Coning.....	25
2.3	Error Contours in Azimuth Due to Coning.....	26
2.4	Azimuth Errors Due to Coning-With Focusing at 5° Elevation.....	27
2.5	Guidance Path Using Conical Elevation Beams- Intersection of Plane and Cone.....	28
2.6	Coordinate Arrangement Relating Measured and Calculated Parameters.....	29
2.7	Typical Guidance Paths Using Conical Elevation Beams.....	31
2.8	"Droop" of Planar Beams Measured in True Elevation Coordinate.....	32
2.9	Schematic of High-Density Terminal Area Airspace....	33
2.10	Arrival Operation.....	34
2.11	Coordinate System for Split-Site (x,y,z) Calculation.....	35
2.12	Effect of Time Delay on Apparent Location of Zero Range.....	36
2.13	Planar Beam Contours in $\theta, \phi$ Coordinates.....	40
2.14	Elevation Coverage - Plan View.....	43
2.15	Elevation Coverage - Side View.....	44
2.16	Glideslope Limitations Due to Coverage Requirements.....	45
2.17	Coordinate System for Collocated Siting Beside Runway.....	52
2.18	Ground Range at Which Azimuth Error Exceeds 0.25°-Collocated Siting.....	53
2.19	Height at Which Error Exceeds 0.25°-Collocated Siting.....	53
2.20	Lateral Guidance Paths Using One-Term DME- Derived Correction.....	55
2.21	Guidance Contours Showing Coning in Linear Arrays.....	56
2.22	Relation of Glide Slope Elevation Angle and Elevation Angle as seen From the Azimuth Antenna- Split Site.....	57
2.23	Error Contours in Azimuth Due to Coning - Split Site Setup.....	59
2.24	DME Coverage Requirements When Located at Elevation #2.....	60

## LIST OF ILLUSTRATIONS (Cont)

	Page
2.25 Coordinate System for DME at Azimuth Antenna.....	61
2.26 (a) Height Error on Centerline Using Conical Guidance - No DME Correction.....	63
2.26 (b) Height Error on Centerline Using Conical Guidance - No DME Correction.....	64
2.27 Height Error on Centerline Using Conical (a&b) Guidance - With DME Correction.....	65
2.28 Coordinate System for DME at Elevation #2 Location.....	66
3.1 Geometry for Multipath Analysis (Azimuth Antenna).....	71
3.2 Variation of Azimuth Signal Level for Aircraft on 3° Glide Slope Angle.....	72
3.3 Synthesized Patterns in Elevation (Azimuth Antenna).....	76
3.4 Location of First Null and First Sidelobe as a Function of Aperture Height (Azimuth Antenna).....	77
3.5 Variation of Sidelobe Levels as a Function of the Parameter $\chi$ .....	77
3.6 Synthesized Antenna Patterns $\text{csc}^2\theta$ Patterns (Four Foot Aperture).....	78
3.7 Constant Field Intensity Contours Using Synthesized Antenna Patterns (Four Foot Aperture).....	80
3.8 Synthesized Antenna Pattern (Two Foot Aperture).....	82
3.9 Constant Field Intensity Contours Using Synthesized Antenna Patterns (Two Foot Aperture).....	84
3.10 Typical Printed Circuit Dipole Construction.....	85
3.11 Azimuth Errors Due to Coning.....	87
3.12 Error Contours in Azimuth Due to Coning (Focused for 0° Elevation).....	88
3.13 Error Contours in Azimuth Due to Coning (Focused for 8.94° Elevation).....	89
3.14 Element Pattern Contributions to Radiation from a Cylindrical Array.....	93
3.15 Scatter Plot of Sidelobe Level at 0° Elevation Vs. $\Phi_{err}$ .....	96
3.16 Variation of Sidelobe Level and Beamwidth with Focus Angle, 1° Design	
3.17 Variation of Sidelobe Level and Beamwidth with Focus Angle 2° Design	

# LIST OF ILLUSTRATIONS (Cont)

	Page
3.18 Variation of Sidelobe Level and Beamwidth with Focus Angle, 4° Design.....	101
3.19 Calculated Antenna Patterns of 1° Beamwidth Cylindrical Antenna.....	104
3.20 Calculated Antenna Patterns of 2° Beamwidth Cylindrical Antenna.....	105
3.21 Calculated Antenna Patterns of 4° Beamwidth Cylindrical Antenna.....	106
3.22 Dipole-Ground Plane Element.....	109
3.23 Principle-Plane Patterns for a Dipole-in-Front-of-a Ground-Plane.....	111
3.24 Configuration for Cylindrical Phased Arrays Sharing Elevation Coverage (Elevation Antenna)....	115
3.25 Configuration for Cylindrical Phased Arrays Sharing Azimuth Coverage (Elevation Antenna).....	116
4.1 Series - Series Feed Configuration.....	120
4.2 Corporate - Parallel Feed Configuration.....	121
4.3 Hybrid - Parallel Feed Arrangement.....	122
4.4 Series - Parallel Feed Arrangement.....	122
4.5 Phase Relations for a Linear Array.....	123
4.6 Boresight Shift in a Cylindrical Array Caused by Coarse Switching.....	125
4.7 Typical Layout Using Transfer Matrix.....	126
4.8 Schematic of 24 x 32 Switch.....	128
4.9a Circuit Diagram for 24 x 32 Transfer Matrix - Output in Rows.....	129
4.9b Board Arrangement for A 24 x 32 Transfer Matrix - Output in Rows.....	129
4.10 Possible Construction of 24 x 32 Transfer Matrix - 2 Layers.....	130
4.11 Possible Construction of Single Transfer Switch...131	131
4.12 Possible Construction of 24 x 32 Transfer Matrix - 3 Layers.....	132
4.13 R-2R Lens Geometry.....	133
4.14 Lens Geometry for Determining Scanning Limits for a Given Active Sector.....	135
4.15 R-2R Antenna System Configuration.....	136
4.16 Lens Illumination with One Probe Excited.....	137
4.17 Electronic Attenuator (Vector Switch) Antenna System.....	138
4.18 Butler Matrix Feed System - Standard Method.....	140
4.19 Butler Matrix Feed System - Switched Method.....	141
4.20 Diagram of Transfer Matrix Technique Feed System (1°BW).....	146

## LIST OF ILLUSTRATIONS (Cont)

	Page
4.21	Diagram of Butler Matrix Feed System ( $1^{\circ}$ BW).....147
4.22	Diagram of Electronic Attenuator Feed System ( $1^{\circ}$ BW).....148
4.23	Diagram of Butler Matrix Feed System ( $1^{\circ}$ BW).....149
4.24	Diagram of Butler Matrix Technique - Switched Feed System ( $1^{\circ}$ BW).....150
4.25	Diagram of Transfer Matrix Feed System ( $2^{\circ}$ BW).....152
4.26	Diagram of R-2R Lens Technique Feed System ( $2^{\circ}$ BW).153
4.27	Diagram of Electronic Attenuator Feed System ( $2^{\circ}$ BW).....154
4.28	Diagram of Butler Matrix Technique-Conventional Feed System ( $2^{\circ}$ BW).....155
4.29	Diagram of Butler Matrix Technique-Switched Feed System ( $2^{\circ}$ BW)
4.30	Diagram of Transfer Matrix Feed System ( $4^{\circ}$ BW).....157
4.31	Diagram of R-2R Lens Technique Feed System ( $4^{\circ}$ BW).158
4.32	Diagram of Electronic Attenuator Technique Feed System ( $4^{\circ}$ BW).....159
4.33	Diagram of Butler Matrix Technique-Conventional Feed System ( $4^{\circ}$ BW).....160
4.34	Diagram of Butler Matrix Technique-Switched Feed System ( $4^{\circ}$ BW).....161
5.1	Microwave Landing Guidance System Control Unit....168
5.2	Basic Timing Budget ( $\mu$ sec).....169
6.1	MLS RF Link.....175
6.2	Varactor Doubler Schematic.....181
6.3	Varactor/SRD Multiplier Chain Configurations.....183
6.4	Distributed "High-Efficiency" Varactor/SRD Multiplier Chain.....185
6.5	Bulk Effect and Avalanche Device Source Configurations.....189
7.1	Experimental Antenna Assembly Drawing.....199
7.2	Lens Geometry.....201
7.3	Block Diagram-Insertion Loss Measurement - Amplitude & Phase Swept Frequency Technique & Phase.....210
7.4	Block Diagram - VSWR and Isolation - Swept Frequency Technique.....211
7.5	Block Diagram - Insertion Loss Magnitude - Rapid Single Frequency Technique.....212
7.6	Block Diagram - Insertion Loss Magnitude and Isolation - Precision Single Frequency Technique.....213
7.7	Block Diagram - VSWR Measurement - Precision Single Frequency Technique.....214

# LIST OF ILLUSTRATIONS (Cont)

	Page
7.8	Block Diagram - Switching Characteristic Measurements.....215
7.9	Block Diagram - Bias Line RF Isolation and Dribble Measurements.....216
7.10	Block Diagram - Amplitude and Phase Balance Measurement.....217
B.1	General Array Geometry.....B-3
B.2	Azimuth Planar Array Geometry.....B-5
B.3	Geometry of Cylinder.....B-12
B.4	Relation of Width of Cylindrical Array to Active Sector and Coverage.....B-14
B.5a	Cylindrical Array Geometry - Elevation Antenna.....B-17
B.5b	Geometric Description of Phase Error for Elevation Antenna - Zero Error Along $\phi = 0$ .....B-17
B.6	Relation of Height of Cylindrical Array to Active Sector and Coverage.....B-19
C.1	Stripline Laminate with Etched Center Conductor.....C-7
C.2	One Sided Copper Clad Laminate.....C-7
C.3	Completed Structure.....C-8
C.4	Flow Chart for Photoengraving (Stripline).....C-9
D.1	Total Vertical Path Attenuation By Water Vapor Normalized To a Water Vapor Content of 1 GM/M <sup>3</sup> .....D-4
D.2	Total Vertical Path Microwave Attenuation By Atmospheric Oxygen.....D-5
D.3	Total Vertical Path Attenuation By Atmospheric Gases (Water Vapor Concentration: 7.5 GM/M <sup>3</sup> .....D-6
D.4	Attenuation Due to Clouds or Fog (Rogers).....D-8
D.5	Theoretical Values of Attenuation By Rain and Fog (Ryde and Ryde).....D-10
D.6	Rainfall Attenuation Versus Frequency For Various Precipitation Rates.....D-11
D.7	Sky Temperatures ( $T_{S\phi}$ ) and Average Sky Temperature ( $T_S$ ) As a Function of Wavelength and $\phi$ .....D-12
D.8	Sky Temperatures ( $T_{S\phi}$ ) and Average Sky Temperature ( $T_S$ ) As a Function of Wavelength and $\phi$ .....D-13
D.9	Sky Temperatures ( $T_{S\phi}$ ) and Average Sky Temperature ( $T_S$ ) As a Function of Wavelength and $\phi$ .....D-14
D.10	Probability Density Function of Attenuation at 15 GHz at Multiple Observing Angles.....D-16
D.11	Probability Distribution Functions of Attenuation at 15 GHz at Multiple Observing Angles.....D-18
D.12	Refraction Correction for a Standard Atmosphere as a Function of Elevation Angle.....D-20

# LIST OF TABLES

	Page
1.1	Summary of Element Power Requirements for Different Phased Array Configurations and Applications.....10
2.1	Coning Error at Coverage Limits.....46
2.2	Coning Error at Coverage Limits for Two Offset Distances-No DME Correction.....48
2.3	Coning Error at Coverage Limits - DME Correction.....50
2.4	Coning Error at Coverage Limits with Modified DME Correction.....51
3.1	Power Divider Coupling Values For Azimuth Antenna Vertical Column.....81
3.2	Relation Between Element Pattern Beamwidth and Element Spacing.....94
3.3	Calculated Physical Antenna Parameters.....97
3.4	Calculated 10dB Beamwidth Ratio: BW @ 20°/BW @ 0°.....102
3.5	Final Physical and Design Parameters For Azimuth Cylindrical Array Design.....103
3.6	Calculated Performance of Cylindrical Antenna Designs.....107
3.7	Linear Array Parameters for Elevation Function.....112
3.8	Elevation Antenna Coverage Limits Using a Cylindrical Array with an Active Sector of 60°.....113
3.9	Effect of Beamwidth on Physical Antenna Parameters Configuration K(±60° Azimuth Coverage).....113
3.10	Effect of Beamwidth on Physical Antennas Configuration I(±40° Azimuth Coverage).....114
3.11	Array Height for Shared Elevation Coverage.....115
3.12	Azimuth Coverage Sharing Scheme.....117
4.1	Component Symbols and Estimated Insertion Losses For Comparison of Various Feed Techniques.....143
6.1	General Source Requirements.....177
6.2	Device Performance Summary.....190
7.1	Tabulation of Test Planning for SP2T Switch.....204
7.2	Tabulation of Test Planning for SP4T Switch.....205
7.3	Tabulation of Test Planning for Phase-Balanced Transfer Switch.....206
7.4	Tabulation of Test Planning for Electrically Variable Attenuator.....207
7.5	Tabulation of Test Planning for 4-Bit Digital Phase Shifter.....208
7.6	Tabulation of Test Planning For 4-Way and 8-Way Power Divider.....209
7.7	Estimated Production Costs of Components Used in Electronic Attenuator Technique.....222



## LIST OF TABLES (CONT)

	Page
D.1 Anticipated Sky Noise Temperature Fluctuation, A, At 5 and 15 GHz for a 20% Change in Water Vapor Density In the First km Along the Path of Observation.....	D-7
D.2 List of Mean And Standard Deviations For Figures D.10 and D.11.....	D-17

## LIST OF SYMBOLS

*Abstract-The symbols used in this report are given and a discussion of the meaning included.*

a <sub>1</sub>	Distance from azimuth location to elevation #1 site.
a <sub>2</sub>	Distance from azimuth location to elevation #2 site.
b	Distance between locations of elevation #1 and Elevation #2 = a <sub>1</sub> -a <sub>2</sub> .
c	Velocity of light, 983. X 10 <sup>6</sup> feet per second.
d <sub>i</sub>	Spacing of antenna elements along the i-axis (i = x, y or z).
D	Maximum linear aperture.
e	Offset distance of elevation locations from runway centerline.
k	Wave number of radiation, equal to 2π/λ.
L	Length of chord of arc.
R	Distance of aircraft from DME location or center of coordinate system, or cylindrical array radius.
R <sub>a</sub>	Distance of aircraft from azimuth or DME location.
R <sub>a</sub> *	Distance of aircraft from zero range DME location.
R <sub>1</sub>	Distance of aircraft from elevation #1 location.
R <sub>2</sub>	Distance of aircraft from elevation #2 location.
R <sub>0</sub>	Distance of aircraft from spot on runway opposite elevation #2.
x	Coordinate parallel to runway centerline, parallel to ground.
x <sub>1</sub>	X-distance of aircraft to elevation #1 location.
x <sub>2</sub>	X-distance of aircraft to elevation #2 location.
y	Coordinate perpendicular to runway centerline, parallel to ground.
z	Coordinate perpendicular to ground
Δz	Deviation in height.
z <sub>err</sub>	Height error.
z <sub>0</sub>	Height coverage limit or decision height.
z <sub>1</sub>	Height above elevation #1 datum.
z <sub>2</sub>	Height above elevation #2 datum.
γ	Beam broadening factor, measured in degrees.
θ	True elevation angle (measured).
θ <sub>a</sub>	Elevation angle of aircraft as seen from azimuth location.
θ <sub>b</sub>	Elevation boresight or scan angle.
θ <sub>err</sub>	Error in elevation angle.
θ <sub>f</sub>	Focus angle in elevation.
θ <sub>1</sub>	Elevation angle of aircraft as seen from el. #1 location.
θ <sub>2</sub>	Elevation angle of aircraft as seen from el. #2 location.
ψ	Planar elevation angle (measured).
ψ <sub>1</sub>	Planar elevation angle as seen from el. #1 location.
ψ <sub>2</sub>	Planar elevation angle as seen from el. #2 location.

$\phi$  Azimuth angle (measured).  
 $\phi_a$  Azimuth angle as seen from azimuth location.  
 $\phi_b$  Boresight azimuth angle or scan angle.  
 $\phi_f$  Focus angle in azimuth.  
 $\phi_o$  Azimuth angle coverage limit.  
 $\phi_1$  Azimuth angle as seen from el. #1 location.  
 $\phi_2$  Azimuth angle as seen from el. #2 location.  
 $\phi_{err}$  Error in azimuth angle.  
 $\lambda$  Wavelength of radiation.



## CHAPTER I INTRODUCTION AND WORK STATEMENT

The purpose of the work contained in this report is to assess the feasibility of using phased arrays in the proposed microwave landing guidance system (MLGS). The work statement summary is the following:

RTCA SC-117 has adopted the scanning beam technique as the preferred concept for future landing system. Of the various methods which may be used for electronic scanning, the phased array antenna is adaptable to micro-electronic techniques offering potentials of small size, light weight and good beam shape control which are deemed worthy of further evaluation. Of prime consideration is the possibility of developing such an array at an effective cost to make it competitive with other designs. The object of this project is to conduct a design feasibility study of a phased array antenna for use with a proposed microwave scanning beam approach and landing system. The phased array to the operational requirements of the future system for both azimuth and vertical guidance.

The present ILS (Instrument Landing System) uses a localizer at about 110 MHz located at the stop end of the runway for the azimuth function. One path, along the runway centerline, is provided. For the elevation function, a glideslope transmitter provides a 330 MHz signal to the aircraft, again a single path at about 2.5-3.0 degrees elevation. The low frequencies involved result in a high degree of susceptibility to reflections, which cause bends in the course. The new microwave system uses frequencies of 5 GHz and 15 GHz, and will provide guidance with less susceptibility to reflections, and more flexibility in the choice of guidance paths. It is anticipated that the ability to determine location within a coverage volume will enable improved noise abatement routing,<sup>1</sup> and closer spacings between landing aircraft<sup>2</sup> to be achieved.

If phased arrays prove feasible and economical, they should be able to provide more reliable performance over a long period of time than can be achieved with mechanically scanned antennas.

1. ATCAC, Vol. 1, P. 60

2. Ibid., Vol. 2, pp. 2,64

In this report, frequent mention is made of two reports. One is the December 1970 document of the Radio Technical Commission for Aeronautics Special Committee 117, "A New Guidance System for Approach and Landing" (RTCA SC-117); this is hereafter referred to as the "RTCA Report". The other report is the "Report of Department of Transportation Air Traffic Control Advisory Committee" December 1969; this is hereafter referred to as the "ATCAC Report".

## 1.1 RTCA Recommendations

*Abstract-Some of the recommendations of the Radio Technical Commission for Aeronautics (RTCA) Special Committee No. 117 (SC-117) and their influence on the study are discussed.*

The Radio Technical Commission for Aeronautics Special Committee 117 (RTCA SC-117) issued their final report on December 18, 1970. Two options were cited: conventional scanning beams and doppler. This project is concerned primarily with the conventional scanning beam approach.

The recommendations of the committee were largely geared toward mechanically scanned antennas: (1) time-coding schemes were ruled out because mechanically scanned antennas cannot be controlled to the necessary accuracy; (2) planar fan beams were recommended which mechanical scanners naturally produce, and linear arrays do not; (3) continuous scan was recommended which mechanical scanners naturally produce, while phased arrays require added complexity to approach it; (4) a relatively low scan rate of scans-per-second was recommended (10 for fine elevation) -- higher scan rates would be difficult to achieve mechanically.

In Chapter VI of the RTCA report several recommendations are put forward which relate to the aims of this project. One is the problem of conical vs. planar beams<sup>1</sup>: "(a) Can planar beams be formed by electronic scanners? (b) If it is not feasible to produce planar beams with electronic scanners, what are the economic and implementational aspects?" A second is the technological investigation of C- and Ku-band phased array capabilities.

These represent the direct aims of the project. Additionally, the functional flexibility of phased arrays will facilitate the use of a feasibility model to be used as an investigative instrument in order to address other problems cited by the RTCA,

---

1. RTCA Report, p. 59

namely step vs. continuous scan, and sum vs. null beams.

This report draws heavily on the RTCA SC-117 report and assumes a familiarity with the basic format recommendations. Three figures which summarize the coverage, accuracy, and siting are given for reference purposes.<sup>1</sup> Most of the report is addressed to the requirements of configuration K, the most complex arrangement. It is recognized that there are permissible variations from the provisional format that were not exercised here. The modulation scheme, the accuracies, bandwidth, scan rate, and coverage were not questioned, even though these are far from being firm system design parameters. The beamwidths, the need for planar information, location of antennas, and power budget are questioned to some extent. The bulk of the report is addressed to the problem of the potential ability for phased arrays to accomplish the scanning of fan beams in azimuth and elevation.

## 1.2 Coordinate System

Abstract-A coordinate system is defined which differs from the conventional spherical system. Reasons for this choice are given.

The coordinate system to be used in this study is defined with respect to the runway orientation and is chosen to correspond to the pilot's conventional coordinate system of bearing, elevation, and range. The center of the coordinate system is at the glide path intercept point (GPIP) on the runway centerline; at close ranges, corrections will have to be made for the displacement of the actual elevation and azimuth antennas from this point. The elevation angle is  $\theta$ , and is related to the standard spherical coordinate  $\theta_{\text{sph}}$  by  $\theta = 90^\circ - \theta_{\text{sph}}$ . The azimuth angle  $\phi$  is essentially the negative of the spherical coordinate  $\phi_{\text{sph}}$ . It is chosen in this fashion so that increasing  $\phi$  corresponds to increasing bearing angle. The ranges of  $\theta$  and  $\phi$  are given by:

$$-90^\circ < \theta < +90^\circ$$

$$-180^\circ < \phi < 180^\circ$$

The coordinate system is shown in Figure 1.4 on page 7.

<sup>1</sup>. RTCA Report, pp. 17-19.

CONFIGURATION	B	D	E	F	G	I	K
	Straight Az Basic DME	Straight Az Straight EL Basic DME	Straight Az Select EL Basic DME	Straight Az Straight EL Basic DME	Straight Az Select EL Precise DME	Curved Az Curved EL Precise DME Missed Appr.	Curved Az Curved EL Precise DME Missed Appr.
FACILITY PERFORMANCE	CAT. I	CAT. I	CAT. I	CAT. II	CAT. II	CAT. III	CAT. III
MINIMUM GUIDANCE ALT	150 FT	150 FT	150 FT	50 FT	50 FT	TD	TD
COVERAGE							
ELEVATION	NA	8°	20°	8°	20°	20°	20°
AZIMUTH	+20°	+20°	+20°	+20°	+20°	+40°	+60°
MISSED APPROACH	---	---	---	---	---	+40°	+40°
ACCURACY* (noise)							
ELEVATION (2σ)	NA	7 FT	7 FT	1.4 FT	1.4 FT	1.4 FT	1.4 FT
AZIMUTH (2σ)	26 FT	26 FT	26 FT	11 FT	11 FT	9 FT	9 FT
RANGE (σ)	300 FT	300 FT	100 FT	100 FT	20 FT	20 FT	20 FT
DATA RATE (Max)	2.5 Hz	5 Hz	5 Hz	5 Hz	5 Hz	10 Hz	10 Hz
RUNWAY LENGTH	7000 FT			12,000 FT		14,000 FT	

\*Accuracy refers to the decision height for CAT. I and II Configurations and to the runway threshold for Configurations I and K.

Figure 1.1 SC-117 Landing System Configuration Data



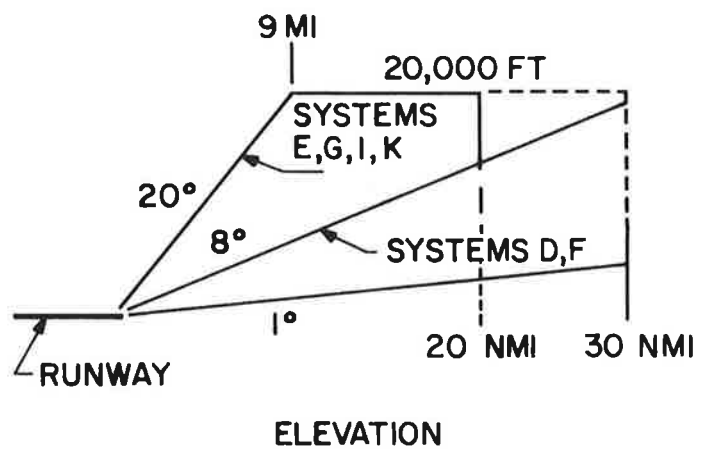
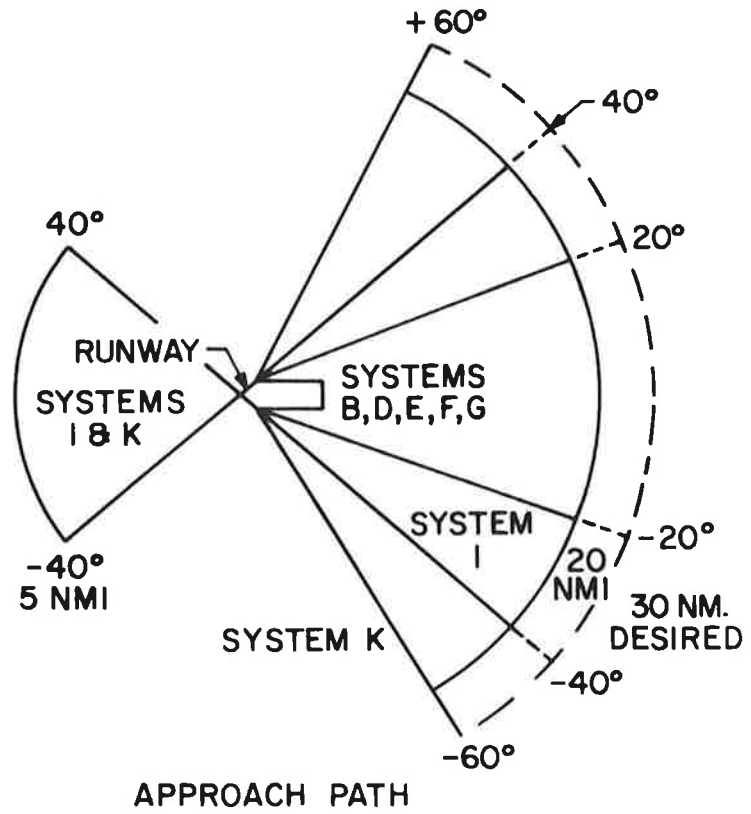


Figure 1.2 LGS Signal Coverage

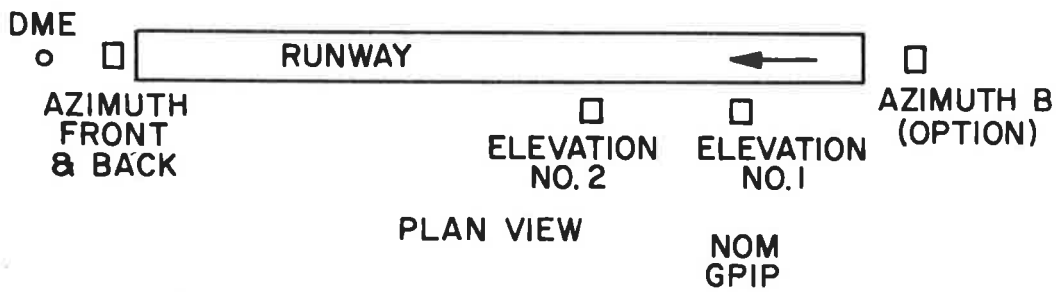
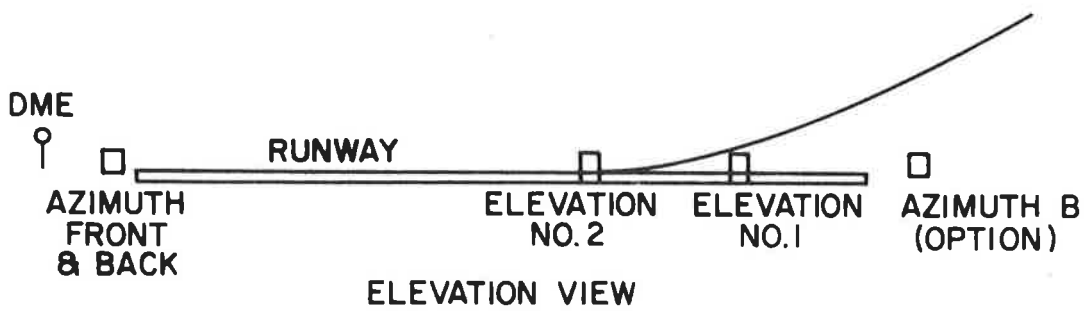


Figure 1.3 General Siting Plan Configuration "I" and "K"

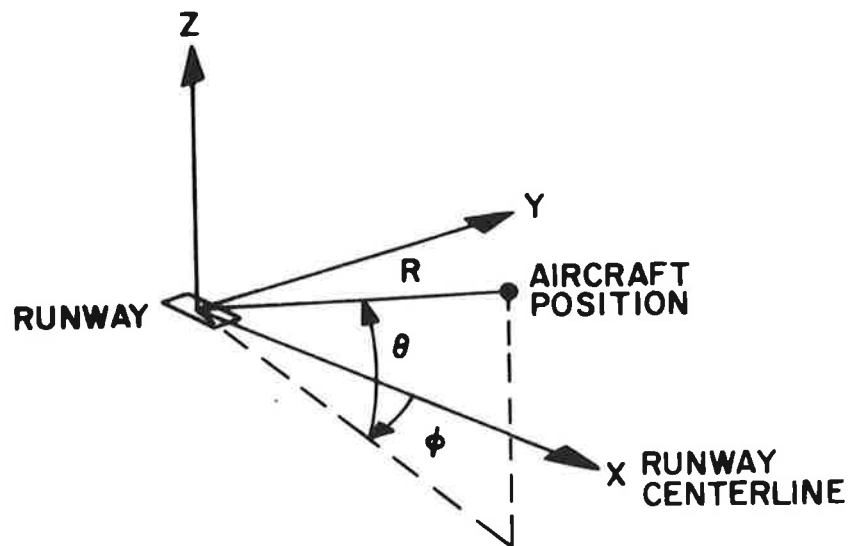


Figure 1.4 Runway Coordinate System

If the coordinates are all referenced to the GPIIP, the following relations apply:

$$x = R \cos \theta \cos \phi$$

$$y = -R \cos \theta \sin \phi$$

$$z = R \sin \theta$$

When coordinates are measured from origins other than the GPIIP, these relationships will be altered. In each of these cases the  $\gamma$  will be developed separately in the text.

### 1.3 RF Power Budget

Abstract-A discussion is presented of the RF power budget and the implications of different coverages and beamwidths are discussed.

A major factor influencing array complexity and cost is the RF power necessary for effective system performance. This paragraph presents the RF power required per element for three different azimuth and five different elevation array configurations.

The total effective radiated power from the antenna is a constant determined by (1) the maximum range between the ground and airborne systems and (2) the required signal level at the aircraft. The power per element is a function of the number of active antenna elements, antenna beamwidths, and illumination taper.<sup>1</sup>

The power required at the aircraft is a function of the airborne antenna gain, transmission line losses, receiver sensitivity, signal processing circuitry effectiveness and required azimuth and elevation position accuracies. SC-117's analysis of these elements resulted in a preliminary power requirement of -111dBW at the airborne antenna for azimuth guidance.<sup>1</sup> Since less accuracy is required for elevation guidance, a -120 dBW signal was determined adequate for this function. These estimates are used in the initial RF power budget estimate for the phased array. A range of 30 nautical miles is used for this derivation.

The effective radiated power for the azimuth and elevation antenna is 31 dBW and 22 dBW respectively as shown below.

	Azimuth Antenna	Elevation Antenna
Space Loss (30nmi)	142 dB	142 dB
Antenna Input Power	<u>-111</u> dBW	<u>-120</u> dBW
ERP	31 dBW or 1259 watts	22 dBW or 158 watts

The power per element is derived by dividing the effective radiated power by the antenna gain and the number of active array elements used to achieve this gain. A three dB factor is added to account for illumination taper. As an example, the power required per element for a 1° X 20°, 96 element array is derived below for the azimuth antenna application. A summary of power required for various antenna configurations is presented in Table 1-1.

Required ERP:	1259 watts
Antenna Gain*: (32.2dB or a ratio of 1650)	<u>1650</u>

<sup>1</sup> RTCA Report, p. E-2

\*Antenna Gain =  $10 \log_{10} \left( \frac{33000}{(BW_{az}^0 \times BW_{el}^0)} \right)$

Total Power to antenna	763 milliwatts
Number of elements:	<u>96</u>
Average power per element	7.95 milliwatts
Taper factor (3db)	<u>x 2</u>
Maximum element input power:	15.90 milliwatts

A wide variation in the required element power is evident from the table. It is desirable to keep the required power low in order to facilitate RF power source implementation. However, it can be seen from the table that low RF power requires a higher gain antenna; this increases system complexity in that a larger array utilizing more elements is required. These factors tend to negate the advantage of a low power RF source.

A trade off study is required to determine the best compromise of these factors and, of course, is one of the program objectives.

The values of Table 1-1 do not reflect system losses due to element components (e.g. phase shifters, attenuators and switches). Consequently depending on the array design, the powers supplied at the input of an element chain will be significantly larger than those presented. This topic is elaborated on in Chapter IV. Methods of generating the necessary RF power are discussed in Chapter VI.

It should be noted that the RF power estimates are preliminary and will be refined as system analytical work progresses. It is anticipated that the RF power requirement will decrease somewhat when the angle guidance format is defined (thereby permitting airborne receiver optimization). Future microwave device development will permit low noise preamplification for the airborne receiver, which will also reduce the RF power requirement for the ground system.

#### 1.4 Summary: Conclusions, Milestones, and Areas of Further Study

Abstract-This section summarizes the work of the project for the first year. Using the tasks of the work statement the results of the effort are described. The milestones as originally conceived are addressed and discussed. Finally, the work that remains to be done is indicated.

Table 1.1 Summary of Element Power Requirements for Different Phased Array Configurations and Applications

Application	Beam Width ( $A_z^\circ$ )	Beam Width ( $E_l^\circ$ )	Gain (dB)	Gain (Ratio)	Number of Active Elements	Maximum Power Per Element (mw)	Radiated Power (W)
Az Guidance	1	20	32.2	1650	96	15.9	.76
"	2	20	29.2	825	48	64	1.53
"	4	20	26.2	412	24	254	3.05
El Guidance	120	1	24.4	275	96	12	.58
"	120	2	21.4	138	48	48	1.15
"	120	4	18.4	69	24	192	2.31
"	180	2	19.6	96	48	69	1.66
"	180	4	16.6	48	24	276	3.31

$A_z ERP = 31dBW = 1259 \text{ watts}$   
 $E_l ERP = 22dBW = 158 \text{ watts}$   
 Power per element =  $\left[ \frac{ERP}{\text{Antenna Gain} + \text{number of active elements}} \right]$   
 X illumination taper factor.

$$\text{Gain (dB)} = 10 \log_{10} \frac{33000}{(BW_{az}^\circ \times BW_{El}^\circ)}$$

#### 1.4.1 RESULTS OF THE EFFORT, ARRANGED BY TASK

The project work statement requires that several tasks be performed in order to achieve the goals set forth by the FAA. These are the following:

- Task 1 array configuration
- Task 2 array design tradeoffs
- Task 3 antenna circuitries and element design
- Task 4 array cost and complexity
- Task 5 decorrelation effects due to atmospheric effects
- Task 6 monitoring

These are discussed separately below.

Task 1. Array Configuration. This task was originally addressed to the question of how planar beams can be generated by phased arrays, since the report of RTCA-SC-117 called for this use. The uncertainty of this requirement among the aerospace community along with the recommendations of the committee itself led to the expansion of this task to encompass the question of whether planar beams are necessary, or even desirable. This question has not yet been decided, and is expected to remain controversial for some time. Some of the considerations which bear on this question are discussed in Chapter II of the report as well as in section 1.4.4. Meanwhile, some conclusions can be stated:

- a. for configurations I and K, which require azimuthal coverages of  $\pm 40^\circ$  and  $\pm 60^\circ$  respectively, planar beams in azimuth are required;
- b. other configurations can use conical beams in azimuth if reduced elevation coverage ( $0^\circ$  to  $8^\circ$ ) is allowed;
- c. for the elevation antenna for flareout and touchdown, the choice of planar vs. conical beams depends on the location of the DME. Whether the elevation antenna for approach should have planar or conical beams is uncertain, since each has its advantages and limitations.

The question of how planar beams can be generated by phased arrays has been examined. Conclusions are the following:

- a. cylindrical arrays generate planar beams and can be designed to meet the azimuth function requirements for configurations I and K

- b. cylindrical arrays can theoretically be designed to meet the elevation requirements for any configuration, but the problems of implementation preclude its use for azimuth coverages beyond  $\pm 20^\circ$
- c. the use of spherical arrays, planar arrays employing beam shaping or multiple cylindrical arrays are not practical solutions.

Task 2. Array Design Tradeoffs. A computer program was written to assist in the tradeoff study. It is a very general program which calculates the far-field pattern of an arbitrary array of elements. The program accommodates linear, cylindrical or arbitrarily placed elements. Elevation and azimuth orientations are admissible, as well as vertical or horizontal (or both) polarizations. Several aperture distributions are provided, such as cosine-squared-on-a-pedestal, along with arbitrary element by element specification possible.

Several element patterns are available, including a dipole in front of a ground plane. Omni-directional as well as plane wave excitation can be employed. Phase shifts can be quantized or continuous. Beamwidths are accurately calculated using a four-term polynomial approximation; 3dB beamwidths are usually given, but provision is made for 10 dB beamwidths or any other specified ones. A plotting scheme is available for accurate drawing of patterns, which reduces the effort required to interpret the data. The program is designed to readily add modifications such as new distributions, element patterns, etc.

Some of the choices resulting from the tradeoff study are given for the azimuth antenna, a cylindrical array with a one-degree beamwidth:

- a. number of elements - 96 active, 288 total
- b. diameter - 706 cm (23.2 feet)
- c. spacing - 3.9 cm
- d. active sector ( $\phi_a$ ) -  $60^\circ$ , total sector -  $180^\circ$
- e. amplitude distribution - cosine-squared on a .5 pedestal  $|I_n| = .5 + \cos^2(2\phi_n/\phi_a)$
- f. sidelobe level due to this amplitude distribution - 26dB
- g. phase shifters - four bits

One of the interesting results of the tradeoff study is that the total number of elements is not strongly dependent on the size of the active sector angle  $\phi_a$ , making a wide range of design choices available.



Task 3. Antenna Circuitry and Element Design. Various methods of feeding cylindrical and linear arrays were investigated. In the case of linear arrays, corporate and series feeds were examined, and a preliminary judgment was made that a series feed, using parallel phase shifters whose commands incorporate the effects of frequency and line dispersion, is an attractive candidate network. In the case of cylindrical arrays, several feed networks were examined; the transfer matrix, the R-2R lens, the electronic attenuator feed, and the Butler matrix. Of these, the optimum choice depends on the component performance and the configuration, but the electronic attenuator approach offers higher flexibility, control, and economy than other means considered. The relative performance of the various systems can only be conclusively determined by experimental evaluation, since the components are state-of-the-art for these frequencies.

The element column design for the azimuth antenna has been chosen as a stripline array of dipoles. The number of sub-elements (or the size) depends on the amount of multipath rejection that is necessary to obtain good performance. From a cost standpoint the size should be kept as small as possible since the cost of the columns is a major part of the total antenna cost. However, the larger the size, the better the performance. A good compromise choice appears to be a column two feet high, having about 15 sub-elements. This choice depends on the terrain so that for some locations it may be desirable to use a larger vertical aperture. For these sites only the columns need to be redesigned-the rest of the antenna system is unaffected.

For the elevation antenna, simple dipoles backed by ground planes are adequate for most configurations. At  $60^\circ$  in azimuth for a quarter wavelength spacing between element and ground plane the signal is down by 3 dB which means the range is reduced by 30%. This is considered acceptable. If further coverage is required, it will be necessary to redesign the element.

For long life it is desirable to have an all-solid-state system, including the RF source. A survey was made of presently available C-band sources, described in Chapter VI of this report. It appears that techniques and power levels are available today which can meet the MLGS requirements, if somewhat inefficiently. Other methods are steadily improving at C-band frequencies, but there is no reliability data as yet. It is anticipated that reliable, high performance solid state sources will be available in the near future.

Task 4. Array Cost and Complexity. Beam steering computer requirements are included in this task. The actual beam steering design depends on the configuration chosen, but one design was completed for the most complicated (from a logic point of view) cylindrical array feed network. In this design read-only-memories (ROM's) are used extensively. Coarse beam steering is accomplished by straight readout from the ROM's.

Fine steering of the phase shifter is accomplished by a ROM readout followed by a shift register. Care was taken to select the most economical off-the-shelf logic components for the design. The initial design is more flexible than is necessary for the final configuration, since manual control is required for testing. The details are discussed in Chapter V of the report. The important feature is that it is a special-purpose computer made up of readily available logic modules. Other antenna configurations can also be controlled with this type of computer.

The relative material cost of the various approaches are not significantly different. The element columns for the azimuth antenna comprise about half the cost, and this is true for all antenna designs. An azimuth antenna having a one degree beamwidth and  $\pm 60^\circ$  coverage is estimated to have a component-and-structures cost in production of about \$150K, while the elevation antenna is costed at about \$40K. These figures are based on estimates from component manufacturers and do not include installation, assembly, or maintenance costs. Any comparison of these figures with those of other approaches should take into account costs of maintenance over a period of 10-15 years as well as comparative reliability. Phased arrays degrade gracefully and should provide virtually non-stop performance with routine scheduled maintenance.

Task 5. Decorrelation Effects Due to Atmospherics. At the request of the FAA technical monitor this task was not pursued to its experimental phase. However, the report has an appendix (Appendix D) which deals with rainfall attenuation. The results reported there were performed on a separate program but are applicable to the problem. The rain models used by the RTCA committee did not fully account for inhomogeneities in the rainfall rate for realistic conditions. Attenuation and radiometric temperature measurements are given in this report which are believed to be more relevant.

Task 6. Monitoring. This task was not pursued due to a lack of manpower. Present thinking in the antenna field is that monitoring drive currents to all switching diodes is sufficient to detect diode faults, and that by monitoring the power level at a couple of points in the circuit (per circuit path) the antenna performance is guaranteed. It is realized that this

may not be acceptable to pilots and controllers and that external monitoring will probably be needed as well. This will be pursued in the second year of the program.

#### 1.4.2 RESULTS OF THE EFFORT, ARRANGED BY MILESTONE

The original milestone chart represented an estimate of the issues to be resolved and the time involved to address them. Some of the issues turned out to be readily resolved, while others were much greater in depth than originally anticipated. The original manpower allocated was 7.5 man-years, which was reduced to 3.0 when it was apparent that adequate staffing would not be available. As a result, two large tasks were not carried through as scheduled, and a third was deleted. However, enough work has been performed on the antenna configuration and tradeoff studies to justify the procurement of components for a small feasibility experimental antenna. The milestones are discussed in the sections which follow.

a. Initial evaluation of subarray tradeoffs-(three months). The issue involved here was whether two or more linear sub-arrays could generate beams practically and are planar to the accuracy required. The answer is simply, no. The reason is that the coning requires a large number of subarrays, and the point is quickly reached where a cylindrical array is more practical.

b. Initial evaluation of curved array structures-(four months). Cylindrical arrays are the only practical curved array solution to the generation of planar beams and their capabilities and limitations are discussed in Chapter III. Spherical arrays offer no advantages for the azimuth function. For the elevation function a spherical array would exhibit appreciable beam spreading near the edges of the fan beam; it would present a complex problem in terms of layout and fabrication which would increase the cost significantly. At this time it is considered an undesirable design.

c. Decorrelation experiment-(four months). Due to lack of manpower this task was dropped. It is considered to be a lower priority item than the other tasks by the FAA contract monitor. Experimental data at 15 GHz is included in Appendix D of the annual report. This was obtained on a separate project, but made available here.

d. Beam monitoring techniques-(four months). This task was not addressed due to lack of manpower. It will be investigated in the next year's effort.

e. Evaluation of two dimensional phased array-(five months). It was ascertained that by expanding the aperture of a cylindrical array along the axis and separately controlling the amplitude and phase of the two-dimensional grid of elements that planar beams could be generated over  $\pm 40^\circ$  or  $\pm 60^\circ$ . It was

further determined that such a distribution could be generated by superimposing several distributions on the elements, rather than use separate amplitude-and-phase control. However, the complexity of the numerous feed systems was considered impractical, and the study was dropped.

f. Array configuration and array design tradeoffs-(six months). The first four monthly progress reports included the preliminary results in this area. Cylindrical arrays are recommended for the azimuth antenna for coverage beyond  $\pm 20^\circ$ ; below that, linear arrays will be adequate.

g. Beam steering computer requirements-(six months). The initial recommendation was not completed until the eleventh month. The preliminary beam steering model design originally scheduled for the eighth month, was re-scheduled for the sixth month of the next year. This area is now staffed, and the design and construction of the logic are expected to be completed well ahead of the schedule.

h. Array element and component costs-(ten months). The component costs under production conditions have been estimated by component manufacturers. Element costs for stripline dipole columns have been estimated as well. The cost study shows the importance of the element cost in the total system cost elevation.

i. Technical report-(twelve months).

#### 1.4.3 EXPERIMENTAL PROGRAM

It was apparent about halfway through the year that some of the most pressing questions were technological rather than conceptual. It was decided to build an experimental antenna to demonstrate the performance of components in an antenna system as a prelude to a full-size test antenna.

The initial unit is an azimuth antenna, but the feed network has been designed to be compatible with an elevation antenna, which can be conveniently added in the future. The initial unit uses simple monopoles as elements, but column elements utilizing shaped elevation distributions can be added after they have been independently designed and tested.

The chief purpose of the experimental model is to evaluate the beam steering methods used and the antenna performance achieved before extrapolating the design to a full-scale model.

The experimental model will be used to establish:

- a. insertion losses
- b. isolation between ports
- c. VSWR characteristics
- d. phase variations
- e. aperture illuminations

- f. fine phasing commands
- g. noise generated by beam switching
- h. effects of random and digital round-off errors on antenna patterns
- i. cost

The projected characteristics are the following:

- Number of active elements: 24
- Number of total elements: 32
- Active Sector:  $\pm 30^\circ$
- Radius of the array: 33.7 inches
- Element spacing: 1.53 inches ( $2.61^\circ$ )
- Beamwidth:  $4^\circ$  (sum beam)
- Sidelobe level: -26dB
- Frequency: 5.0-5.25 GHz
- Scan range:  $\pm 10^\circ$

By altering the aperture distribution and reducing the number of active elements (easily achieved) the beamwidth can be broadened to  $5.2^\circ$ ; this will allow step-scanned operation with two beams per 3dB beamwidth. Initially, beams will be steered manually, but the circuitry will be compatible with logic hardware, which will be added later.

Contracts for the fabrication of phased array components were awarded. There are two techniques (an R-2R lens and electronic attenuator) which will be completely implemented, while a limited number of components were purchased for a third technique (or class of techniques) to allow its evaluation (transfer matrix). The relative merit of the different choices must be determined by experimental measurements. The most promising technique will be fully implemented with logic, and tested with a receiver.

#### 1.4.4 CONCLUSIONS REGARDING THE CHOICE OF LINEAR OR CYLINDRICAL ARRAYS

Based on the results of this section, there are several conclusions which can be reached. These are not all-encompassing, since there are several areas of uncertainty which remain. Probably there is no unique answer to the question of the "best" system arrangement--there are shortcomings in any choice. It is hoped that the discussion above will help in pinpointing the performance tradeoffs involved in making choices for particular airports providing particular air traffic control requirements.

a. Determination of exact position-in-space in the initial approach region is very difficult when split siting is used. This is due to the mathematical complexity of the

expressions for position throughout the required coverage to the required accuracy. This holds for planar as well as conical guidance. By the same token, range to elevation #1 is readily calculated only when the aircraft is along the runway centerline at low elevation angles. Either complex calculating machinery is needed on board, or else relative (as opposed to exact) position-in-space information must be used. In the latter case, there is no advantage to planar over conical guidance; in the former case, the advantage is slight.

b. The use of planar beams in elevation results in a loss of elevation coverage at azimuth coverage extremes. This is due to the off-center "droop" of planar beams. This is no significant for azimuth coverage of  $\pm 20^\circ$ , but is a problem for the I and K configurations. Typical proposed curved path trajectories approach predict aircraft MLGS intercepts at high elevation angles at wide azimuth angles; this means that the reduced elevation coverage occurs where the wide angle coverage is most needed.

c. In the final approach region the elevation antenna coverage in azimuth must be wider than the system coverage in order to accommodate steep glide slope angles down to guidance minimums without loss of signal. The severity of this problem is dependent on the offset distance of elevation #1 location from the runway centerline. This problem can be reduced either by increasing the azimuth coverage of the elevation antenna or by locating the antenna close to the runway centerline.

d. If the offset distance is 200 feet or less, conical beams give acceptable straight-line guidance in the final approach region for CAT-I conditions for glideslope angles of  $5^\circ$  or less. With an added one-term DME-derived correction, this can be extended to offset distances of 300 feet and  $9^\circ$  glideslope angles. This applies to installations where the elevation antenna is located beside the runway. These conditions satisfy most present and near-future situations. For V/STOL applications separate runways are likely to be used. There, collocated equipment is a more natural choice and conical guidance is actually preferable.

e. When the azimuth antenna is located at the stop end of the runway, the azimuth errors are negligible in the final approach region using conical guidance. This is because the aircraft is near the runway centerline.

f. When the azimuth antenna is located beside the runway, azimuth guidance down to CAT-I minimums within the required accuracy is not possible without a DME-derived correction. A one-term DME-derived correction results in satisfactory guidance.

g. In the landing and rollout region the location of the DME determines whether planar or conical elevation beams are the more satisfactory choice. If the DME is located at the stop end of the runway, the use of planar elevation beams

allows the calculation of height by the simple product of range and elevation angle. Similarly, if the DME is located at the elevation #2 site, the use of conical elevation beams allows the calculation of height by a simple product. However, if the opposite combinations are used, an additional on-board computation is necessary to correctly derive height information. This correction is fairly simple for small offset distances.

One overall conclusion that can be reached is that if the offset of elevation antennas is small, say 200 feet or less, conical beams in elevation result in adequate guidance information without DME corrections for all present and near-future applications for civil use. If highly maneuverable craft using gates very close in are to be accommodated in a mixed environment (not anticipated in near-future civil air traffic schemes), or if V/STOL craft use steep glideslopes on major runways in IFR situations, more flexibility might be deemed desirable..

#### 1.4.5 AREAS OF FURTHER STUDY

Some of the issues which will be addressed in the coming year are the following:

- a. Near-field guidance. In the final approach region and for flareout and touchdown, the aircraft can be in the near field of the elevation antennas. This must be investigated.
- b. Effect of reflections on accuracy. This must be carried out further to generate terrain siting criteria for both elevation and azimuth antennas.
- c. Further work in feed network design for cylindrical arrays. Improvements must be sought to reduce insertion loss and complexity of the feed networks.
- d. Further effort in low-cost element design. The use of shaped reflectors and lower-cost dipole array design should be investigated further.
- e. Monitoring. Techniques for internal monitoring of components will be reviewed, and promising methods incorporated into final designs. The external monitoring problem will be studied, and recommendations completed.
- f. Antenna system arrangement. Arrangements of the various antennas other than those in the RTCA report will be investigated, drawing on the results of Chapter II.
- g. Component development. Methods of improving reliability and reducing production costs by combining several functions on one board or substrate will be investigated. Layout techniques for building matrices from modules will be studied.
- h. Source Development. While a full-scale development program in the area of sources is beyond the resources of this project, every effort to incorporate promising devices

into the system will be made.

The areas listed above are over and above the requirement of testing, fabrication, and evaluation of antenna components, test receiver, and subsystems; these are the primary concerns of the task.



## CHAPTER II THE IMPACT OF PLANAR VS. CONICAL GUIDANCE ON ANTENNA CONFIGURATION AND LOCATION

The RTCA report calls for planar guidance in both azimuth and elevation, and lists reasons for this choice.<sup>1</sup> In the recommendations for further study, the question of planar and conical beams is raised to some extent<sup>2</sup>, although it is given relatively little attention. The choice of planar beams rules out the use of linear or planar arrays over wide coverage angles. It is shown in this report that cylindrical arrays can provide planar beams over limited coverage angles in the non-scan plane, but are more expensive than linear arrays by a factor of two or three, and cannot achieve the wide azimuth coverages of configurations I ( $\pm 40^\circ$ ) and K ( $\pm 60^\circ$ ) without further complexity. Furthermore the reasons given in the RTCA report are not considered to be exhaustive. Accordingly, a review was made of the implications of planar and conical beams and their effects on antenna locations and system complexity, and presented in this chapter.

The first section introduces the concept of planar and conical beams, and states some of their general features. The second section deals with the effect of antenna locations on the determination of aircraft position-in-space in the initial approach region. The initial approach region describes the region from initial acquisition of the landing guidance signal to the point where the aircraft is on the straightline final approach.

The third section deals with the final approach region in which the aircraft is on a straight line path down to the guidance minimum for CAT-I or CAT-II operation. If guidance is maintained below the guidance minimum, the fine guidance elevation antenna is assumed to have taken over at some prior point in the final approach region.

The fourth section deals with guidance for landing and rollout.

1. RTCA Report, pp. IV-24 through 26.
2. Ibid, p. V-3.

## 2.1 Planar and Conical Fan Beams-Descriptions

*Abstract-Expressions are given for the differences between planar and conical fan beams for azimuth and elevation guidance. The differences are small for narrow coverages. Conical beams cause bias errors in azimuth; in elevation this is not necessarily true.*

The words "planar" and "conical" when used to describe microwave scanning beams imply that fan beams are in use, that is, that the beamwidth in azimuth is narrow and the beamwidth in elevation is wide, or vice versa. The surface swept out in space by a line hinged at the antenna center and passing through the maximum of the fan beam can be planar or conical in shape. A line source (a pill box horn or linear array) which is phased for broadside radiation generates a planar beam; if it is phased for other than broadside, it generates a conical beam.

A series of planar beams can be generated by mechanically rotating a line source phased for broadside. A series of conical beams can be generated by electronically phasing a line source with a varying linear phase taper, or by rotating the feed of a fixed reflector.

Using scan angles near broadside, the differences between planar and conical beams are slight.

### 2.1.1 AZIMUTH FUNCTION

In a "rho-theta" guidance system, the assumption that the azimuth angle is independent of the elevation angle is implicit. Another way of defining the angular guidance surfaces is by the condition  $\phi = \text{constant}$  where  $\phi$  is the azimuth angle.

Applied to the scanning beam system, the guidance surfaces correspond to the fans of the beams. In order to generate fan beams which are narrow in azimuth, the antenna dimensions must be narrow in the vertical dimension and wide horizontally. Since aperture length and antenna beamwidth are inversely related (beamwidth in degrees  $\approx 61^\circ \cdot \lambda/L$ ). The antenna configuration needed for the azimuth plane should have its long dimension parallel to the ground.

In Appendix B it is shown that a linear array parallel to the y-axis, and scanned to an angle  $\phi_0$  off broadside, produces a fan beam whose locus in  $\theta$ - $\phi$  coordinates is given by

$$\phi = \sin^{-1}(\sin \phi_b / \cos \theta) \quad (2.1.1)$$

where  $\theta$  is the elevation angle (equation B.11). If the beam were planar, the equation would be given by

$$\phi = \phi_b \quad (2.1.2)$$

Figure 2.1a shows the ideal guidance surfaces, which are planar. Figure 2.1b shows the guidance surfaces obtained by a linear array; the bowing which results is called "coning".

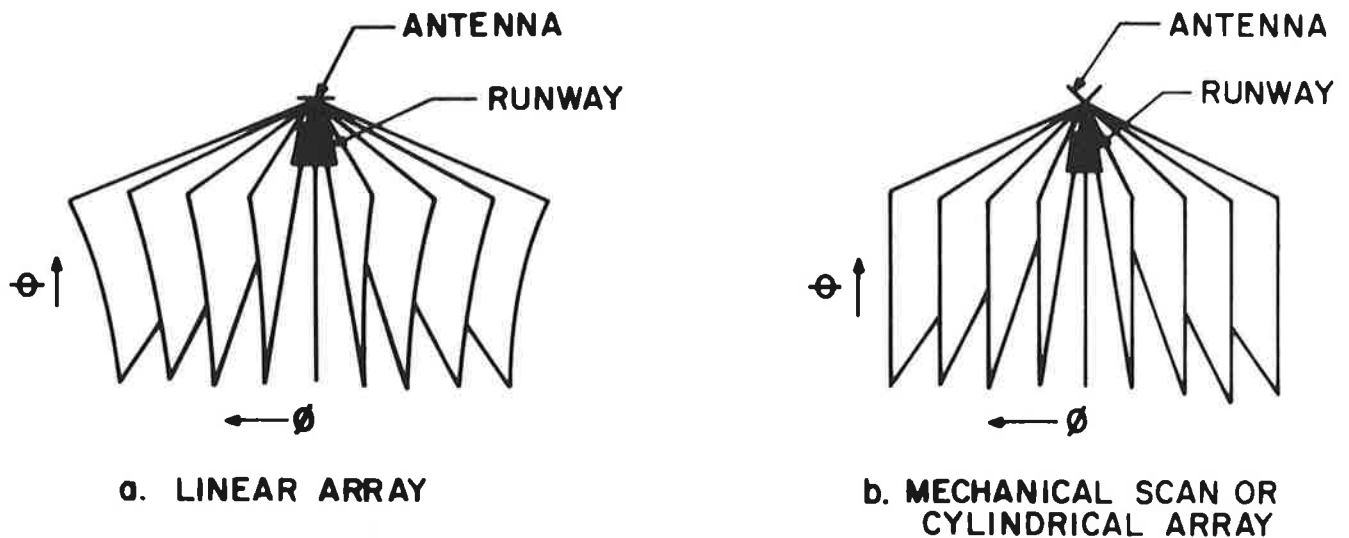


Figure 2.1 Guidance Contours Showing Coning in Linear Arrays

An aircraft receiving the signal (anticipating planar information) would interpret its angular azimuth position as  $\phi_b$ . Its actual position would be at  $\phi$ , given by equation 2.1.1. Since  $\phi$  is greater than  $\phi_b$  (which can be seen from 2.1.1) the aircraft would interpret its position as being closer to the runway centerline (given by  $\phi=0$ ) than it actually would be. The error in a measurement is equal to the measured value minus the actual value. Here the measured value is  $\phi_b$ ; the actual value is given by equation 2.1.1.

Thus the error due to coning (for positive angles) would be negative, and given by

$$\phi_{err} = \phi_b - \sin^{-1} \left( \frac{\sin \phi_b}{\cos \theta} \right) \quad (2.1.3)$$

This is plotted in Figure 2.2, where the error is understood to be negative. Constant-error curves are plotted in Figure 2.3, obtained by rewriting equation 2.1.3:

$$\cos \theta = \sin \phi_b / \sin (\phi_b - \phi_{err}) \quad (2.1.4)$$

The fact that coverage below the horizon is not needed allows an increased coverage to be attained within the same error envelope. This is accomplished by focusing the fan beam at an elevation angle  $\theta_f$  other than zero. This deteriorates the performance at the horizon but improves it at higher angles. From the focus, in  $\theta$ - $\phi$  coordinates is now given by

$$\phi = \sin^{-1} (\sin \phi_b \cos \theta_f / \cos \theta) \quad (2.1.5)$$

This reduces equation 2.1.1 when  $\theta_f=0$ .

The coning error (still negative) is given by

$$\phi_{err} = \phi_b - \sin^{-1} (\sin \phi_b \cos \theta_f / \cos \theta) \quad (2.1.6)$$

which is plotted in Figure 2.4 for a focused elevation angle of  $5^\circ$ .

## 2.1.2 ELEVATION FUNCTION

The elevation function differs from the azimuth function in that planar beams are no more "natural" than conical beams. Indeed, the common spherical coordinate system incorporates the true elevation angle ( $\theta$ ) which suggests ( $\theta=\text{constant}$ ) conical beams. However, the RTCA SC-117 has chosen planar beams in elevation (as well as azimuth) for the following reason: for most configurations of the RTCA SC-117 the azimuth and elevation sites are separated, the azimuth site being located on the runway centerline at the stop end of the runway, while the elevation site is near the touchdown point off the runway centerline. The runway centerline is thus located along the guidance surface given by  $\phi=0$ . By providing planar guidance in elevation, two things are accomplished: (1) the guidance path given by  $\phi=0$ ,  $\psi=\text{constant}$  (where  $\psi$  is the planar elevation angle) is a straight line path to the GPIP, since the intersection of two planes is a straight line; (2) the path in space is not sensitive to the distance of the elevation site from the runway centerline. On the other hand, if conical guidance in elevation is provided,

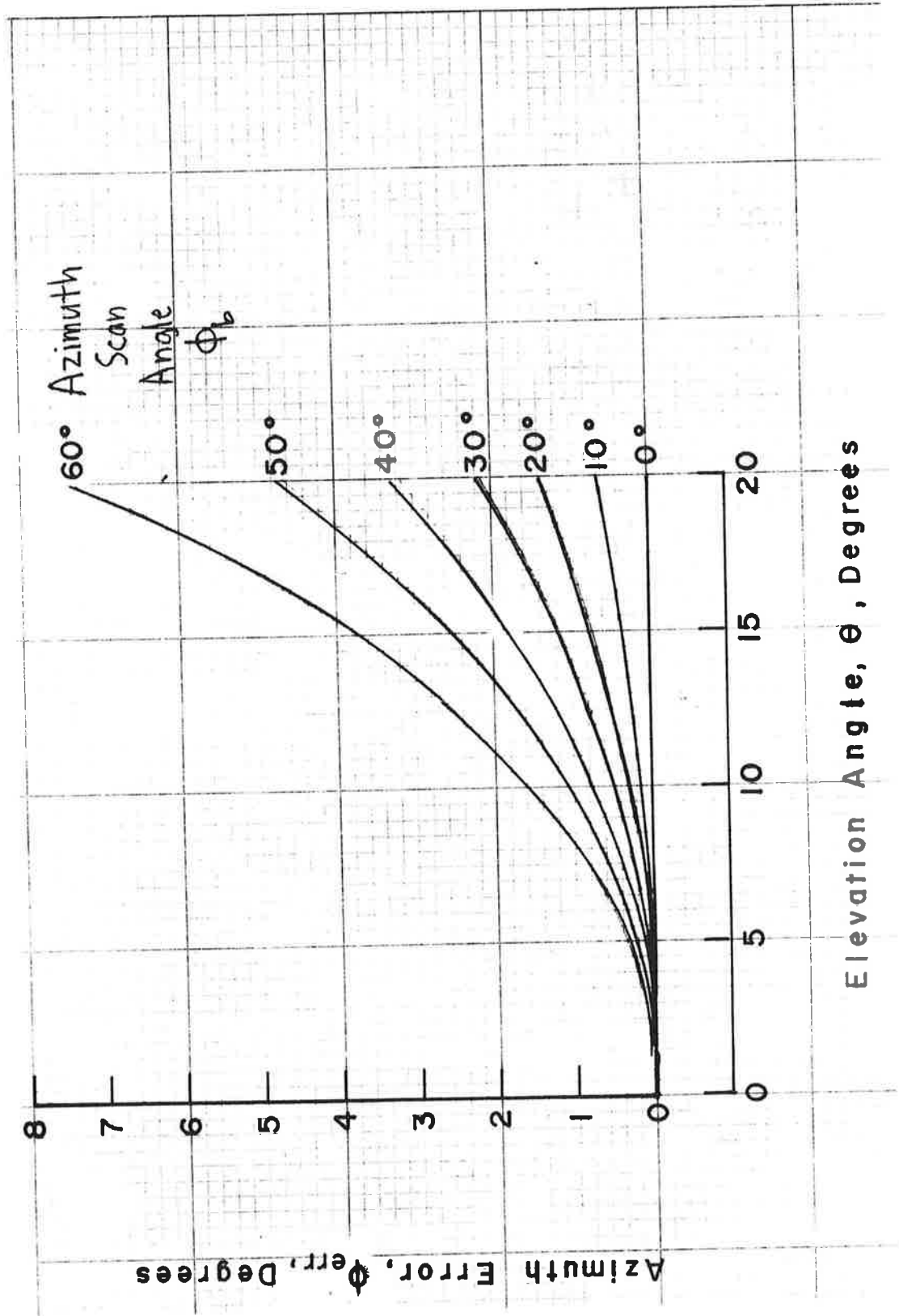


Figure 2.2 Azimuth Errors Due to Coning

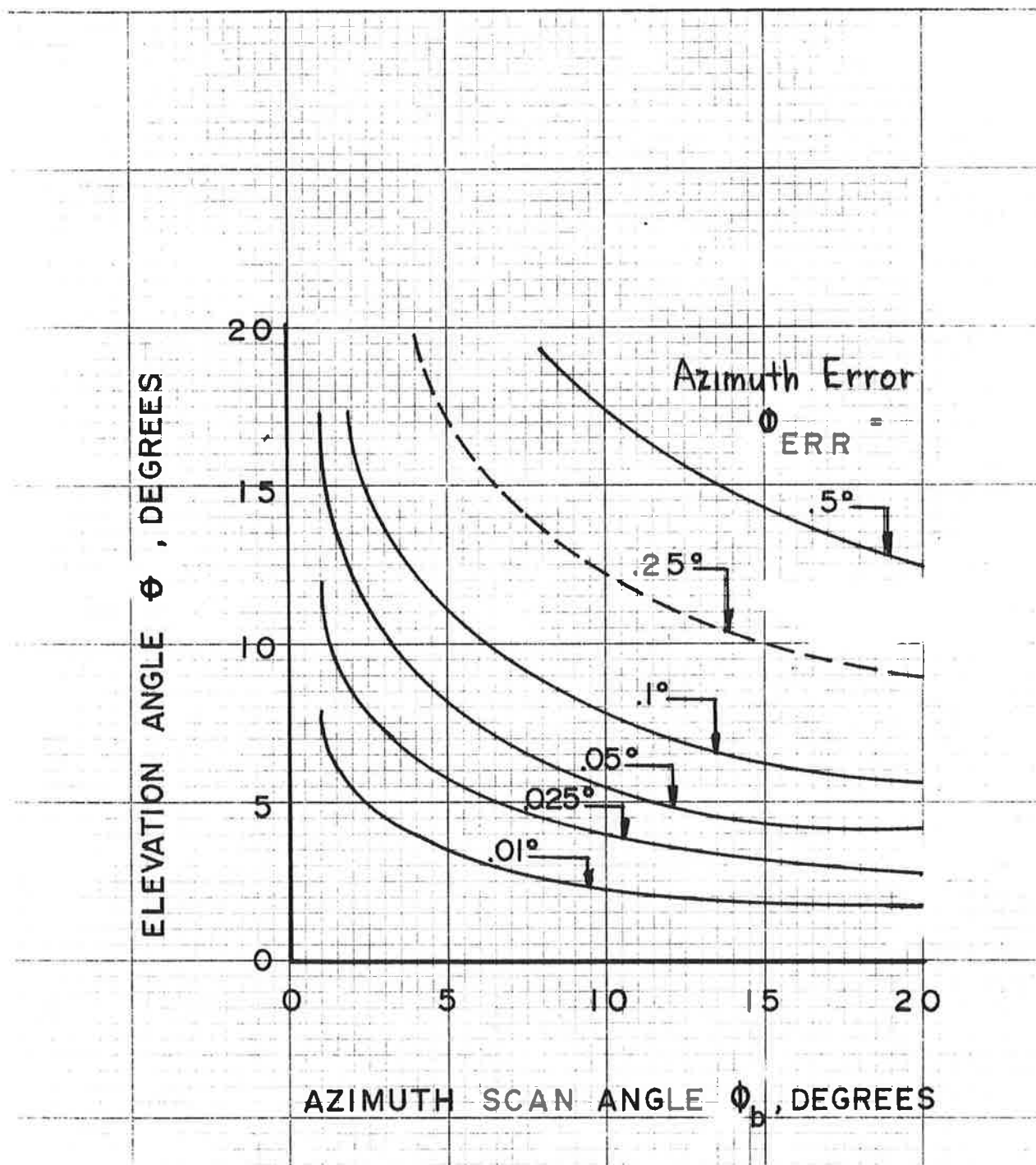


Figure 2.3 Error Contours in Azimuth Due to Coning

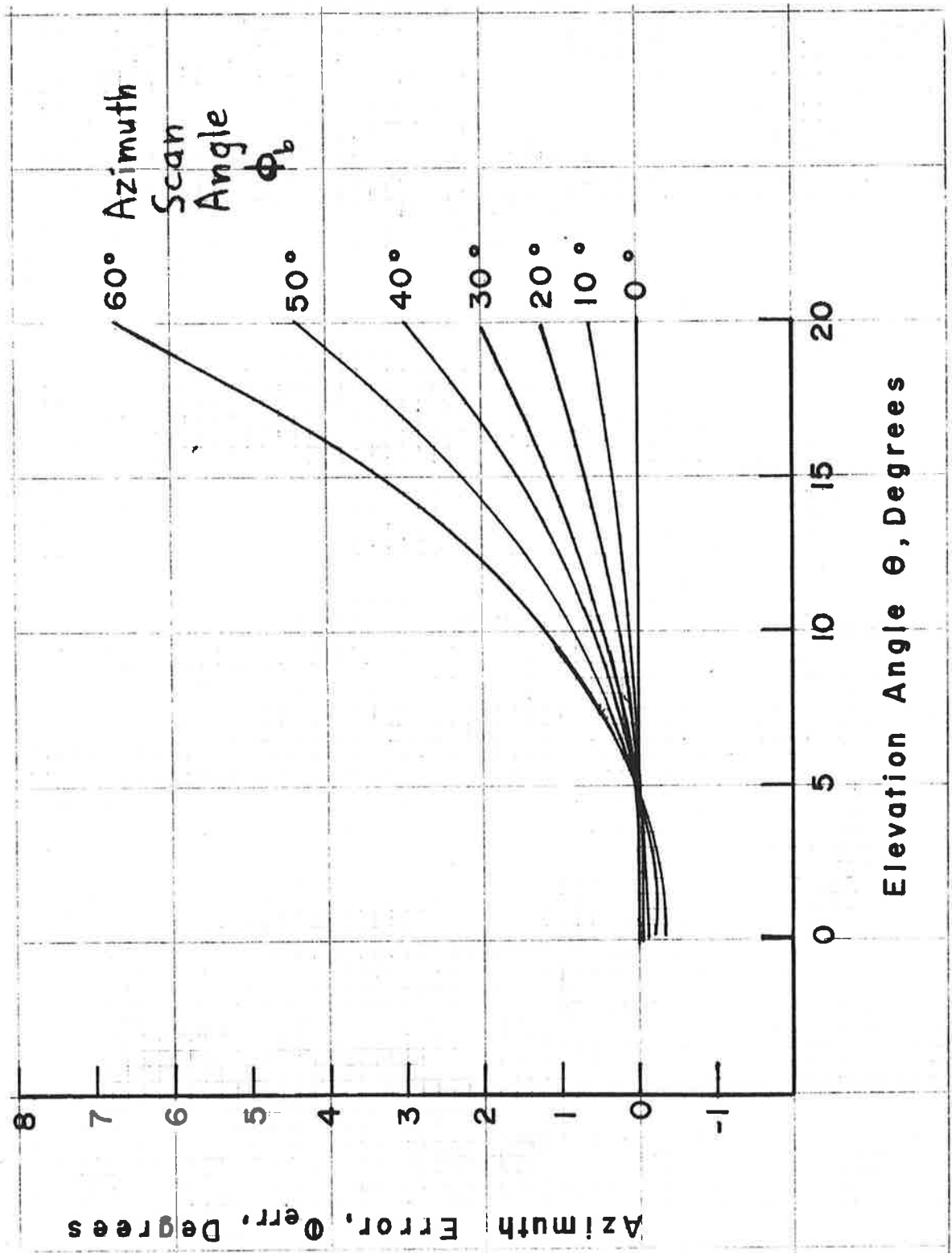


Figure 2.4 Azimuth Errors Due to Coning-With Focusing at 5° Elevation

the path in space is hyperbolic, rather than straight, since the intersection of the azimuth plane  $\phi=0$  and the cone  $\theta=\text{constant}$  is a hyperbola.

Thus the planar guidance offers straight line paths to the GPIIP; an aircraft following the conical guidance path given by  $\phi=0$ ,  $\theta=\text{constant}$ , on the other hand, would fly somewhat above the (straight line) glideslope path; this is shown in Figure 2.5. The deviation from a straight line increases with elevation angle, and with the distance of the elevation site from the runway centerline.

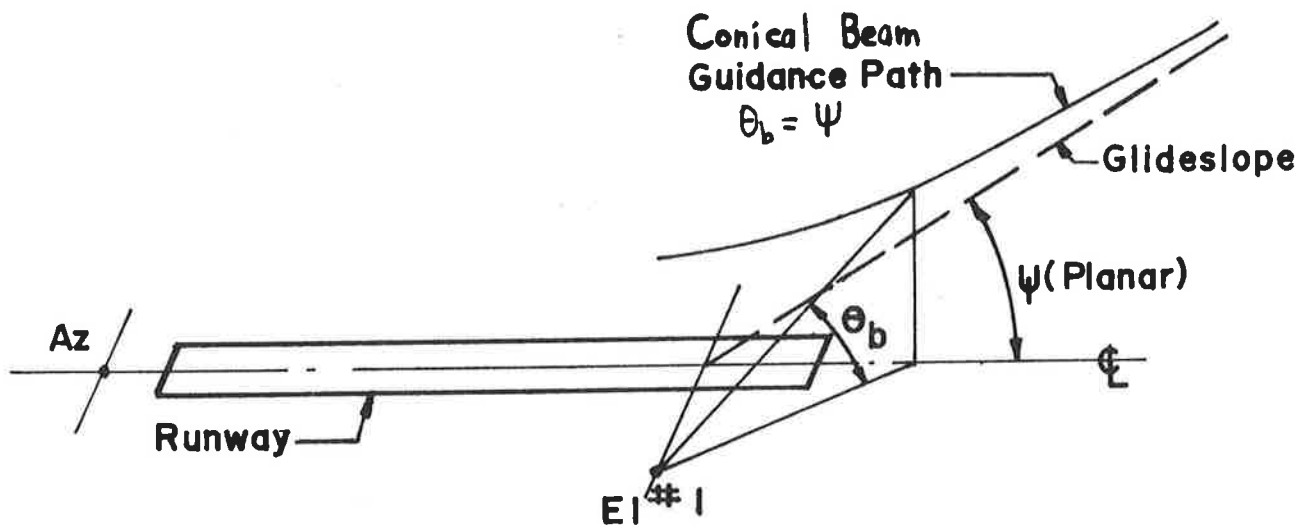


Figure 2.5 Guidance Path Using Conical Elevation Beams- Intersection of Plane and Cone

Quantitatively, the deviation from a straight line can be determined as follows: with reference to Figure 2.6, the offset distance is "e", the x-axis is along the runway centerline, and the z-axis is vertical. The azimuthal guidance plane along the runway centerline is given by  $y=0$ ; the vertical guidance cone is given by  $\theta=\theta_b$ . The relations between the Cartesian coordinates and the (offset) spherical coordinates are given by

$$x = R \cos \theta \cos \phi$$

$$y = -R \cos \theta \sin \phi - e$$



$$z = R \sin \theta \quad (2.1.8)$$

By setting  $y=0$ ,  $\theta=\theta_b$ , and solving for  $z$  in terms of  $x$ :

$$\begin{aligned} z &= x \tan \theta_b / \cos \phi \\ \text{or} \quad z &= \sqrt{x^2 + e^2} \tan \theta_b \end{aligned} \quad (2.1.9)$$

where  $\cos \phi = x / \sqrt{x^2 + e^2}$

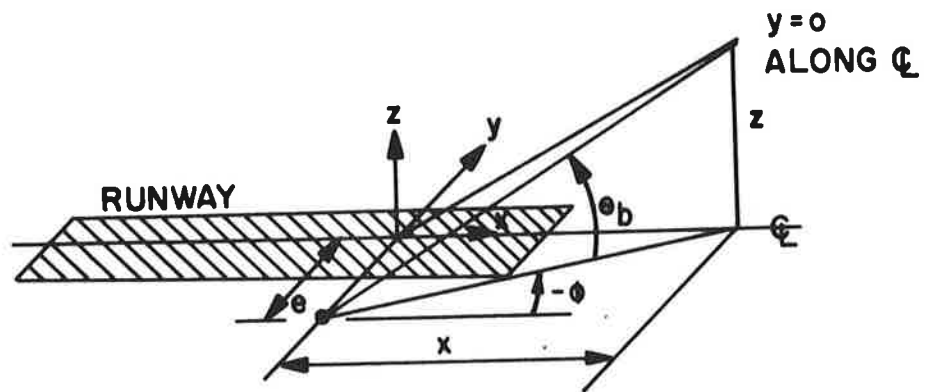


Figure 2.6 Coordinate Arrangement Relating Measured and Calculated Parameters

The straightline path which corresponds to the curved path above is given by

$$z = x \tan \theta_b \quad (2.1.10)$$

Thus, the deviation of the curved path from the straight line is given by the difference between 2.1.9 and 2.1.10:

$$\Delta z = (\sqrt{x^2 + e^2} - x) \tan \theta_b \quad (2.1.11)$$

It can be seen that the deviation is always positive, and increases with elevation angle. Several representative paths

are given in Figure 2.7.

It should be noted that the deviation does not necessarily constitute an error in the case of elevation. It would only if the aircraft interpreted the conical guidance as planar guidance. This is discussed further in section 2.3.1.

The coverage in elevation offered by planar beams is severely reduced at wide azimuth angles, since planar beams "droop". This is shown schematically in Figure 2.8. The result is to increase reflections (since reflecting objects are generally near the ground) and reduce coverage in the region where high elevation coverage is most needed. This is discussed in section 2.2.3.

## 2.2 Effect of Antenna Locations on Position-in-Space Determination--Initial Approach Region

*Abstract-Determination of exact position-in-space in the initial approach region is very difficult using the siting configuration recommended by RTCA SC-117 regardless of whether planar or conical beams are used. Planar beams in elevation cause a loss of coverage in the region it is most needed.*

Curved path approaches have been proposed as providing solutions to some air traffic control problems by increasing flexibility in the choice of feeder paths preparatory to the final approach and by allowing positive control on curved-path noise abatement routing. The RTCA SC-117 proposed that additional coverage in azimuth be provided for these approaches in the I and K configurations.<sup>1</sup> The ATCAC Report also recommends curved path approaches;<sup>2</sup> two concepts from that report are shown in Figures 2.9 and 2.10 where at least part of the "in-trail" region lies within the specified range of the landing system. (It should be noted that this is a significant extension of the approach concept over the present ILS, and that it overlaps the terminal area navigation function). For paths like A & B in Figure 2.9 the aircraft will be coming in at high altitudes, necessitating coverage at elevations above 9° in the region near coverage extremes. This requirement is discussed below in section 2.2.3

1. RTCA pages 19-69/SC 117-46 Jan. 27, 1969, p. 25
2. ATCAC Appendices, pp. 74 and 79.

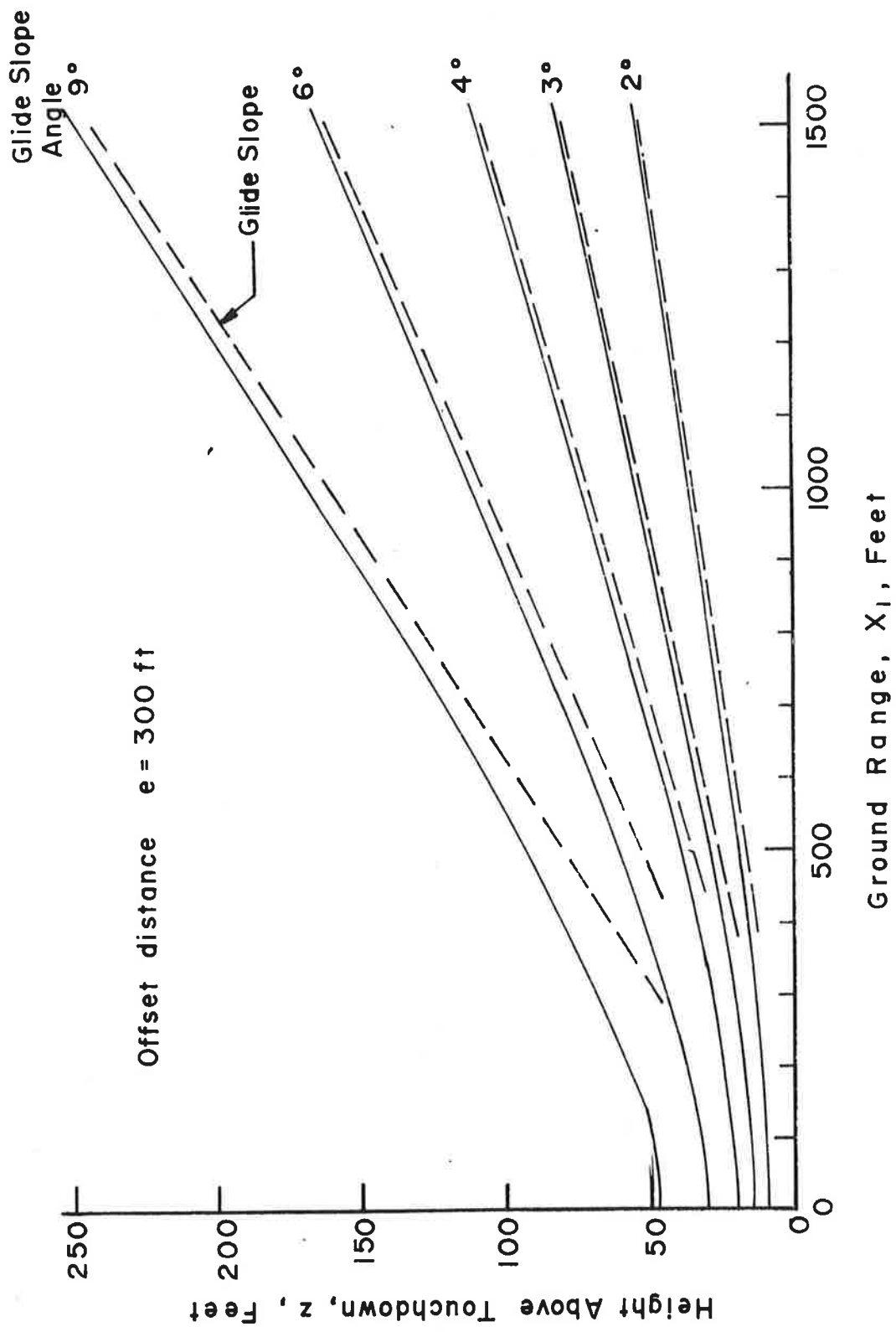


Figure 2.7 Typical Guidance Paths Using Conical Elevation Beams

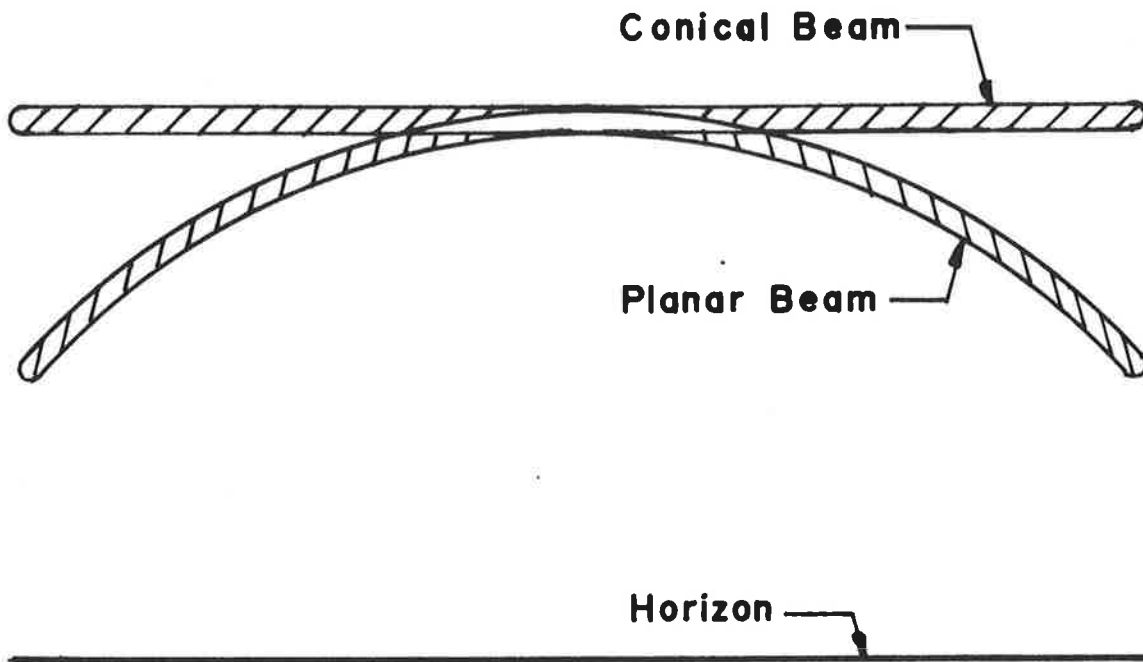


Figure 2.8 "Droop" of Planar Beams Measured in True Elevation Coordinate

The accuracy requirements given by RTCA-SC-117 on the angular and range information may be interpreted in two ways: (1) absolute, in that the position of an aircraft is known in relation to a fixed position on the ground, or (2) relative, in that the deviation between absolute and measured location is the same for all aircraft in the area. The second allows skew and calculation errors which are biased beyond the accuracy requirements; this would maintain aircraft separation and assure smooth feeding into the final approach (NOTE: in the final approach region, measurement accuracy must be absolute, not relative). If absolute measurements are required, the use of planar beams (as well as conical) in the RTCA-SC-117 configuration results in a calculation complexity which is excessive. If relative measurements are adequate, then planar beams offer no simplicity in calculation. This is discussed in sections 2.2.1 and 2.2.2 below. The output data suggested by the

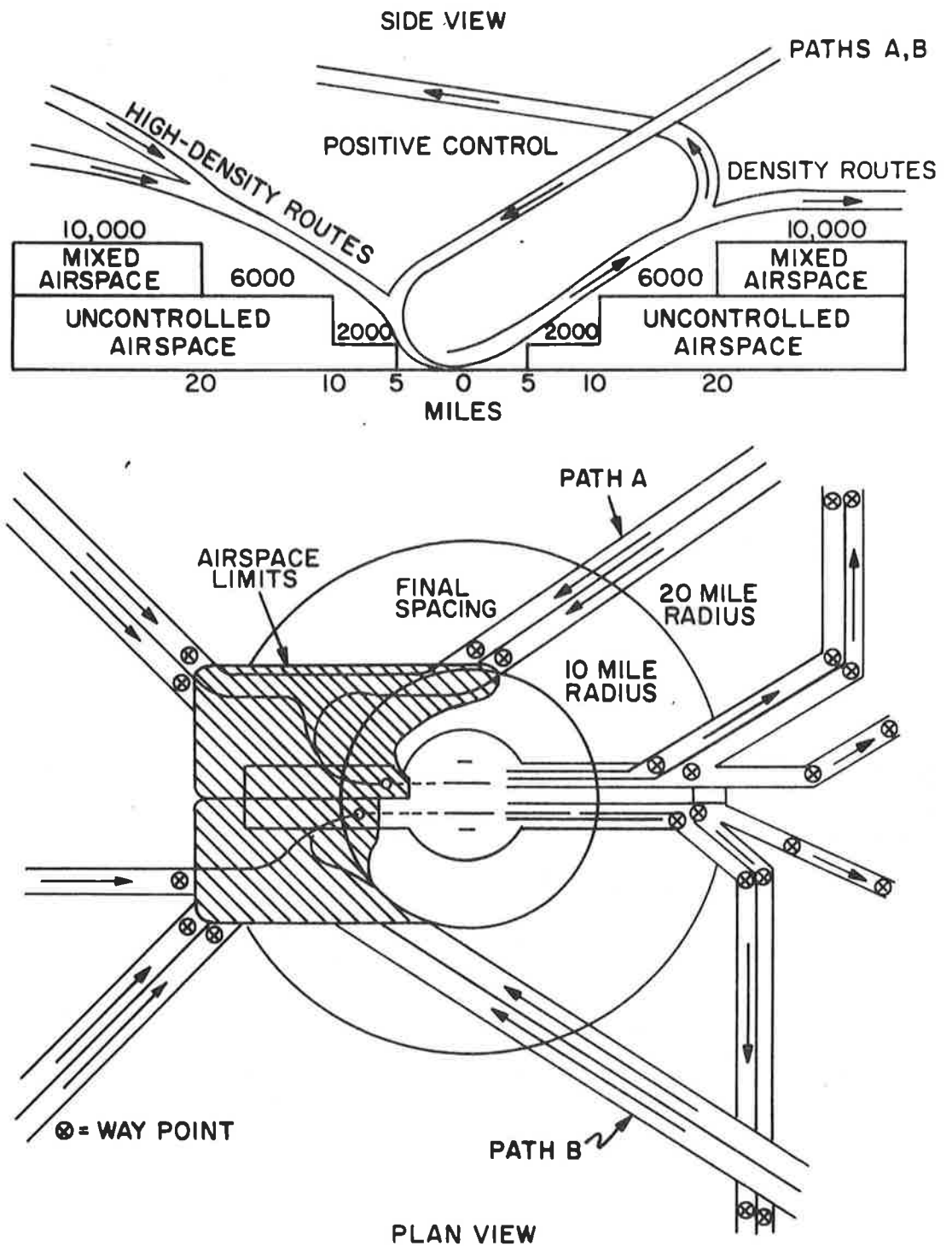


Figure 2.9 Schematic of High-Density Terminal Area Airspace

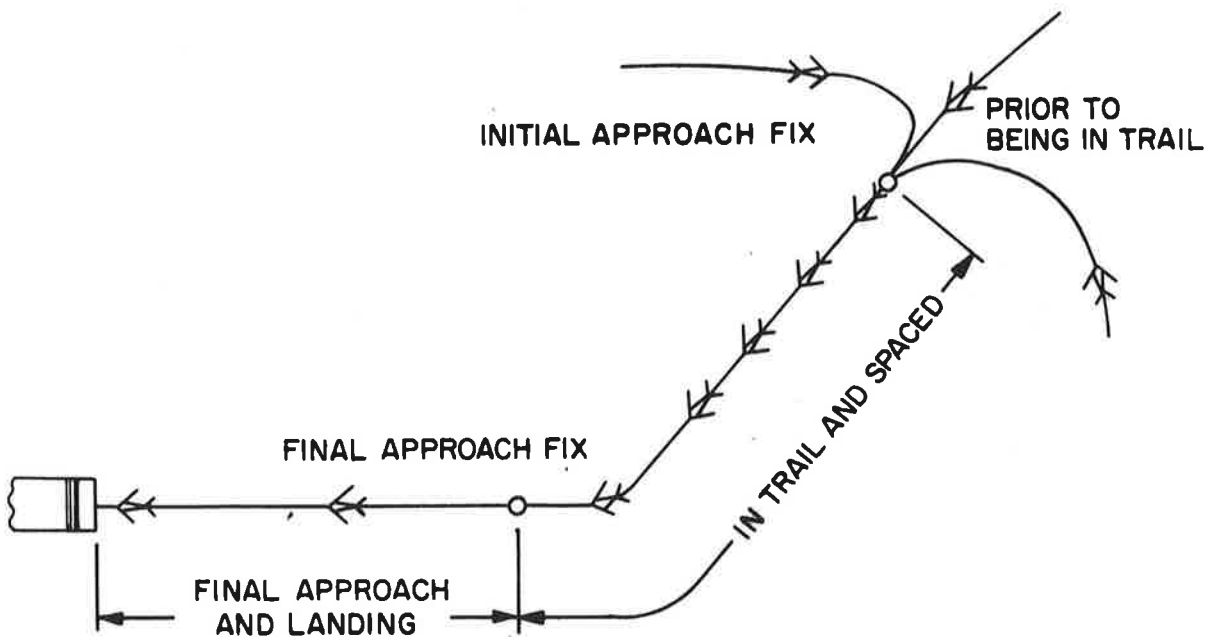


Figure 2.10 Arrival Operation

RTCA SC-117<sup>1</sup> for the initial approach region is given below. It can be seen that the question of absolute or relative position information is not resolved.

- a. Elevation Path Deviation. - Compatible with ILS glideslope outputs. Will be course-softened at short range and referenced to offset GPIIP.
- b. Azimuth Path Deviation. - Compatible with ILS localizer outputs. Will be course-softened during roll-out and missed approach. Can be optionally referenced to curved approach courses in some configurations.
- c. Elevation #1 Angle.- Used for computation of curved elevation paths. Used for air-selectable glide-paths.
- d. Azimuth Angle. - Used for computation of curved approach courses.

1. RTCA Report, p. IIIA-17

e. Range to Elevation #1. - Used for numerous functions of navigation, approach, landing and possibly roll-out service. This output will become negative when the aircraft flies past the elevation #1 site.

### 2.2.1 EXACT (X, Y, Z) CALCULATION

The exact determination of position-in-space is complicated by three factors: (1) the split siting, whereby

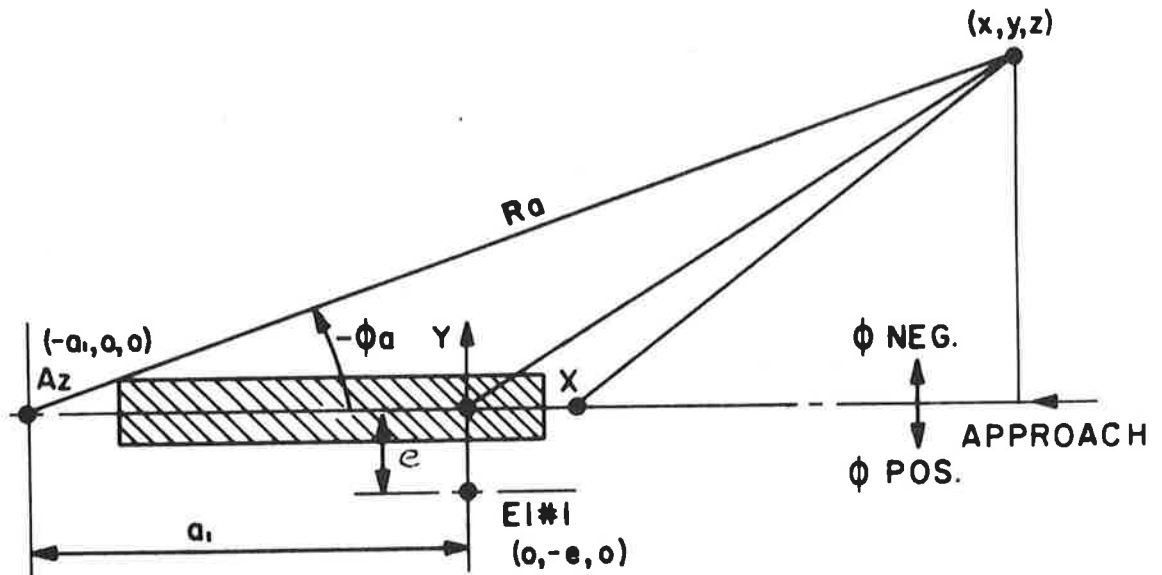


Figure 2.11 Coordinate System for Split-Site (x,y,z) Calculation

azimuth and range information are acquired from one location, and elevation from another location several thousand feet away; (2) the fact that slant range, not its projection along the ground, is measured; and (3) the DME bias<sup>1</sup>, whereby a 60 microsecond delay corresponds to the range at elevation number 1.

<sup>1</sup> RTCA Report, p.34

The DME bias problem is brought about by the technique proposed by the RTCA-SC-117, i.e., to calibrate the DME at all airports so that the time delay is always 60 microseconds at the GPIIP at the elevation #1 location. This is accomplished by a time delay in the ground DME transponder which is set on-site for each airport runway. The effect of this is that zero range does not correspond to a point, but a circle centered at the DME site and passing through the GPIIP.

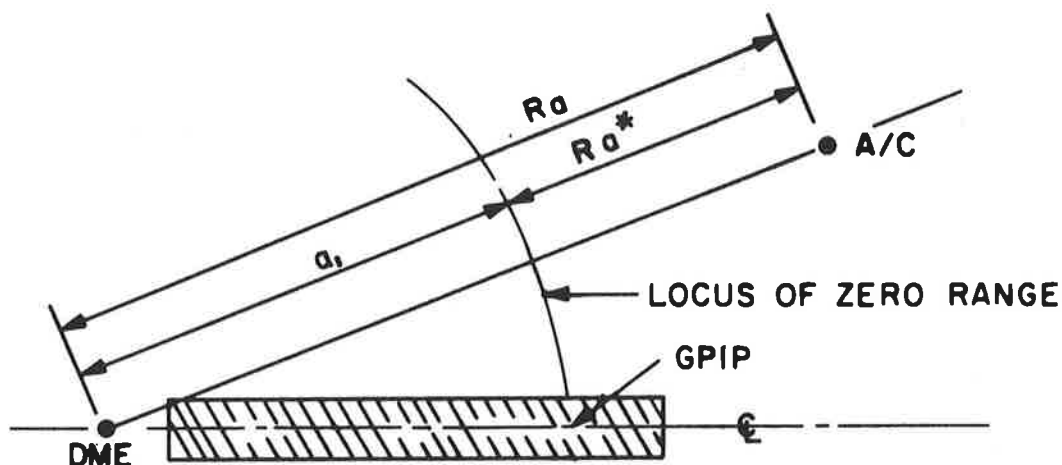


Figure 2.12 Effect of Time Delay on Apparent Location of Zero Range

The apparent (measured) range  $R_a^*$  is related to the actual range  $R_a$  by

$$R_a^* = R_a - a_1 \quad (2.2.1)$$

Using planar beams, the following relations hold:  
(see Figure 2.11)

$$y = -(x+a) \tan \phi_a \quad (\text{azimuth plane}) \quad (2.2.2)$$

$$z = x \tan \psi_1 \quad (\text{elevation plane}) \quad (2.2.3)$$

$$R_a^2 = (R_a^* + a_1)^2 \quad (2.2.4)$$

$$= (x+a_1)^2 + y^2 + z^2 \quad (\text{range with DME bias}) \quad (2.2.5)$$



The measured quantities are  $R_a^*$ ,  $\phi_a$  and  $\psi_1$ , the quantity " $a_1$ " is a siting constant of the runway, and  $x$ ,  $y$  and  $z$  are to be determined. Eliminating  $y$  and  $z$ , the following quadratic form can be obtained for  $x+a_1$ ;

$$(x+a_1)^2 [1+\tan^2\phi_a + \tan^2\psi_1] + (x+a_1) \cdot 2a_1 \tan^2\psi_1 + a_1^2 \tan^2\psi_1 - (R_a^* + a_1)^2 = 0 \quad (2.2.6)$$

Over coverages of  $\pm 60^\circ$  in azimuth and  $20^\circ$  in elevation, none of the terms can be ignored in general. Thus the solution will be of the form

$$x+a_1 = \frac{-B}{2A} \pm \frac{1}{2A} \sqrt{B^2 - 4AC} \quad (2.2.7)$$

where

$$A = 1 + \tan^2\phi_a + \tan^2\psi_1$$

$$B = -2a_1 \tan^2\psi_1$$

$$C = a_1^2 \tan^2\psi_1 - (R_a^* + a_1)^2$$

and  $y$  and  $z$  are found from (2.2.3) and (2.2.4). This is a very complex set of equations to be calculated without an expensive special-purpose computer; the time used up with a general purpose computer is considerable.

Using planar azimuth beams and conical elevation beams, the expressions are somewhat more complex:

$$y = -(x+a_1) \tan\phi_a \quad (2.2.8)$$

$$z = \sqrt{x^2+(y+e)^2} \tan\theta_1 \quad (2.2.9)$$

$$(R_a^* + a_1)^2 = (x+a_1)^2 + y^2 + z^2 \quad (2.2.10)$$

Eliminating  $y$  and  $z$ , the following quadratic form results:

$$(x+a_1)^2 (1+\tan^2\phi_a) (1+\tan^2\theta_1) - 2(x+a_1) (a_1+e \tan\phi_a) \tan^2\theta_1 + (a_1^2 + e^2 \tan^2\phi_a) \tan^2\theta_1 - (R_a^* + a_1)^2 = 0 \quad (2.2.11)$$

This can be written in the form of equation (2.2.7), where

$$A = (1+\tan^2\phi_a) (1+\tan^2\theta_1)$$

$$B = 2(a_1+e \tan\phi_a) \tan^2\theta_1$$

$$C = (a_1^2 + e^2 \tan^2\phi_a) \tan^2\theta_1 - (R_a^* + a_1)^2 \quad (2.2.12)$$

This requires knowledge of the elevation offset distance "e" as well as "a". The fact that the quantity "e" is between 150 feet and 600 feet means that some simplification could occur, but not a great deal.

The conclusion is that exact position-in-space requires an excessive amount of computation, necessitating a relatively complex on-board computer. This holds for planar as well as conical beams. While the computation could be made periodically every few scans, while using small-angle correction computations in between, the scheme is still highly complex.

### 2.2.2 DERIVATION OF RANGE-TO-ELEVATION #1

One of the outputs that is specified by the RTCA SC-117 is the range to elevation #1 site. Since this is not independently generated, it must be calculated. Along the runway centerline for low elevation approaches, the range is approximately given by the measured range  $R_a^*$ . However, this approximation does not hold throughout the coverage volume: the exact form is given by

$$R_1 = \sqrt{x^2 + (y + e)^2 + z^2} \quad (2.2.13)$$

where x, y, and z are found from section 2.2.1. From equation 2.2.1,

$$R_a = R_a^* + a_1 \quad (2.2.14)$$

where  $R_a^*$  is measured, and  $a_1$  is the siting parameter.

Thus,  $R_1$  can be expressed in terms of  $R_a$ :

$$\begin{aligned} R_1 &= \sqrt{(x+a_1)^2 + y^2 + z^2 - 2a_1x - a_1^2 + 2ey + e^2} \\ &= R_a \sqrt{1 - \frac{2a_1x + a_1^2 - 2ey - e^2}{R_a^2}} \end{aligned} \quad (2.2.15)$$

where x and y still have to be computed as shown in section 2.2.1.

This in general can not be simplified if high accuracy is required, except that the term  $e^2/R_a^2$  might be ignored. Since  $a_1$  could be two miles, the terms involving  $a_1$  are not small enough for using two-term expansions, regardless of whether planar or conical elevation guidance is used.

Thus the computation of range-to-elevation #1 can not be easily computed from the data available in the RTCA format in the initial approach region.

### 2.2.3 COVERAGE CONSIDERATIONS

It was noted in section 2.1.2 that the elevation coverage offered by planar guidance is less than that obtained with conical guidance. This can be seen by plotting constant planar elevation contours in true elevation-azimuth coordinates shown in Figure 2.13. These curves are derived as follows: let the origins of the coordinate systems described in Figure 2.6 coincide by setting  $e=0$ . Then a planar guidance surface is given by

$$z/x = \tan \psi_b \quad (2.2.16)$$

where  $\psi_b$  is the planar elevation angle. In general,  $z$  and  $x$  are related by (see equation 2.1.8)

$$z/x = \tan \theta / \cos \phi \quad (2.2.17)$$

Thus equating (2.1.12) and (2.1.13) gives

$$\tan \psi_b = \tan \theta / \cos \phi \quad (2.2.18)$$

Rewritten to give contours of  $\theta$  as a function of  $\phi$ :

$$\theta = \tan^{-1} (\tan \psi_b \cos \phi) \quad (2.2.19)$$

The curves of Figure 2.13 show that there is a loss in coverage at wide azimuth angles using planar guidance (conical guidance curves are horizontal straight lines on this plot). Figure 2.9 shows the significance of this: a typical approach profile is path A or B: here the aircraft is in the initial approach region preparatory to final approach at relatively high elevation angles near the coverage extremes. On the other hand, an aircraft approaching from the left of the diagram would be at a low elevation angle at the entry point into the initial approach region. Thus the high-angle coverage offered by planar beams is lost in the coverage sector it is most needed.

Also, at low glideslope angles, planar beams are more subject to reflections from objects near the coverage extremes, due to the "droop" in the beam. Thus a beam at  $4^\circ$  elevation along the runway centerline will be at  $2^\circ$  elevation for azimuth angles of  $\pm 60^\circ$ , and will be more likely to suffer from reflections than a conical beam which holds at  $4^\circ$  regardless of azimuth angle. This is indicated schematically in Figure 2.8. How severe this problem is depends on the site.

Elevation Angle of Planar Beam

$$\tan \theta = \tan \psi \cos \phi$$

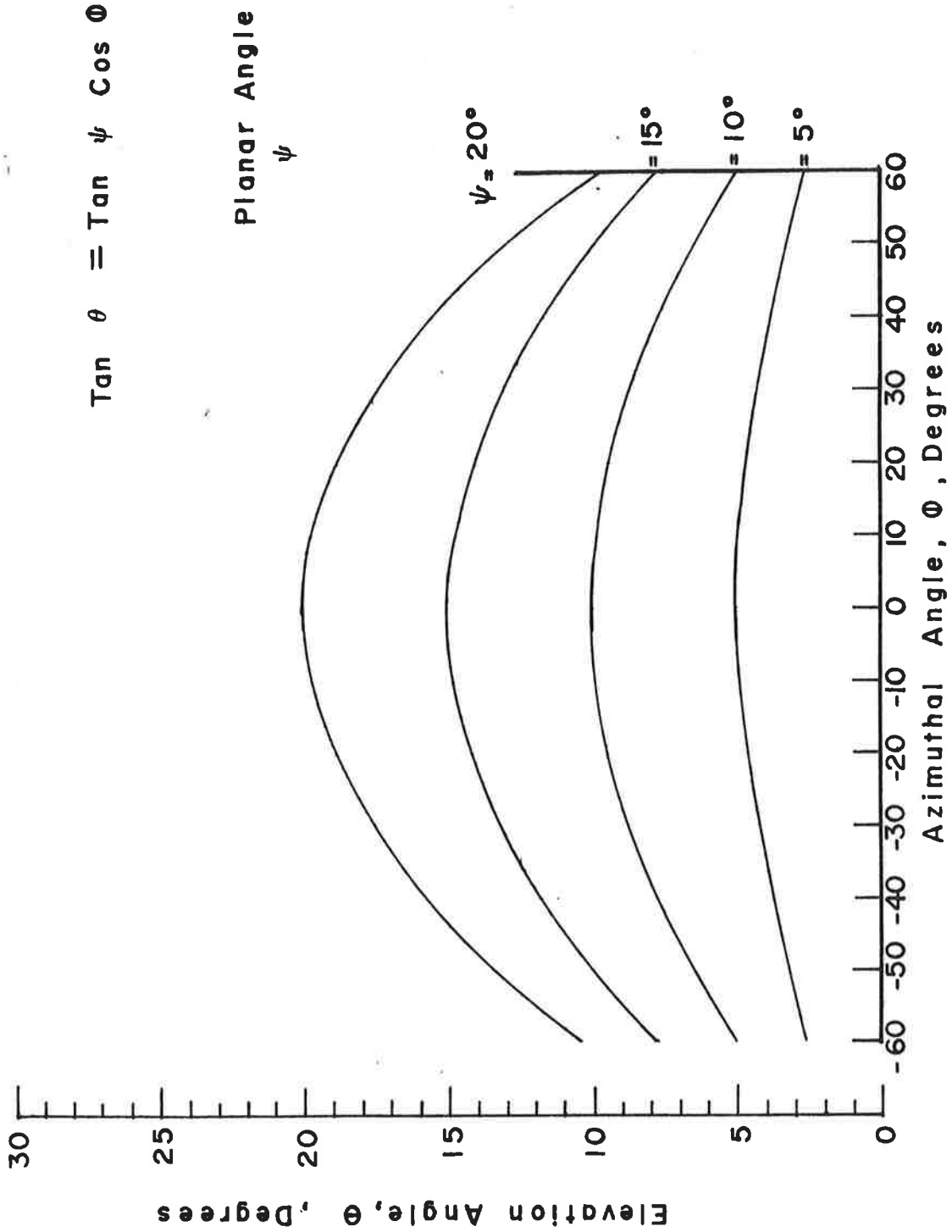


Figure 2.13 Planar Beam Contours in  $\theta, \phi$  Coordinates

## 2.3 Effect of Site Locations on Position-in-Space Calculations in Final Approach Region

*Abstract-It is shown that the elevation coverage must be wider than the system coverage in azimuth in order to accommodate steep glide slope angles down to guidance minimums without loss of signal. Without DME corrections conical guidance in elevation results in errors which, while not serious for present approach angles ( $3^{\circ}$  or less), do exceed the accuracy requirements posed by RTCA-SC-117. A correction term derived from the DME results in satisfactory accuracies for elevation #1 offset distances of 300 feet or less. Azimuth errors are negligible in the final approach region using linear arrays.*

In the final approach region the function of the elevation antenna (#1) is to provide glide path information to the aircraft. For aircraft without DME, one aiming point is presented; for those with DME it is possible to calculate paths using other aiming points. When planar guidance in elevation is presented to the aircraft, the guidance path is a straight line. Conical elevation guidance uncorrected by DME information results in a hyperbolic path somewhat above the straight line path. The deviation is more severe for larger elevation #1 offset distances and steep glide paths. The result is an upward pitch command which occurs in the region of the decision height for categories I and II; at this time the pilot is in the process of overriding the autopilot in order to land (or execute a missed approach).

The sections which follow deal with the effect of offset distance and coverage on coning errors, and the effectiveness of DME corrections in reducing them.

It is assumed that for configurations I and K, in case of a failure of the flareout antenna, the glide path antenna (#1) will provide CAT-II guidance. The considerations of the final approach region which refer to configurations I and K are discussed in this light.

### 2.3.1 LOSS OF COVERAGE NEAR GUIDANCE MINIMUM

It is important to note the relationship between the offset distance "e" of the elevation antenna #1 from the runway centerline, and the maximum allowable glide slope angle. This comes about as a result of the coverage and applies to both conical and planar beams. It can be seen

from Figure 2.14 that an aircraft landing along the runway will lose guidance at an azimuth angle  $\phi_0$ , which is the coverage limit. From Figure 2.15, it is evident that in order to maintain guidance down to some minimum height above the runway, there is a maximum glide slope allowable; i.e., aircraft approaching along steeper glideslopes will lose the guidance signal before reaching the required minimum height. The determination of this glide slope is now discussed.

For CAT-I conditions, the decision height is 200 feet, and guidance to 150 feet above the runway is the projected requirement for configuration B, D, and E. For CAT-II conditions the decision height is 100 feet and the projected requirement for configurations F and G as well as for elevation #1 or I and K is for guidance down to 50 feet. The relation of maximum glide path slope to offset distance can be found as follows; from Figure 2.14, it is evident that

$$x_1 = e \cot \phi_0 \quad (2.3.1)$$

and from Figure 2.15 that

$$\psi_{\max} = \tan^{-1} (z/x_1) \quad (2.3.2)$$

where  $z$  is the desired minimum height. Eliminating  $x_1$  from the equation gives

$$\psi_{\max} = \tan^{-1} \left( \frac{z}{e} \tan \phi_0 \right) \quad (2.3.3)$$

This is plotted in Figure 2.16. For a given offset distance, allowable glide slope paths are limited to angles below the curves. Conversely, if it is desired to accommodate glide slope angles up to some maximum angle, the antenna must be sited some distance to the left of the curves. Since configurations I and K have increased coverage, they can accommodate steeper glide slopes or larger offset distances. (The more sophisticated systems will probably be used on wider runways, requiring larger offsets.) It should be noted that this severely limits the choice in offset distance  $e$  for all RTCA configurations. For an offset distance of 500 feet, the requirement of accommodation of glide slopes up to  $20^\circ$  could not be reached for any configuration, for example.

Another conclusion to be drawn from this is that even in the lower configurations, the elevation antenna must in general have coverage wider in azimuth than that which is required by the configuration coverage in order to accommodate steeper

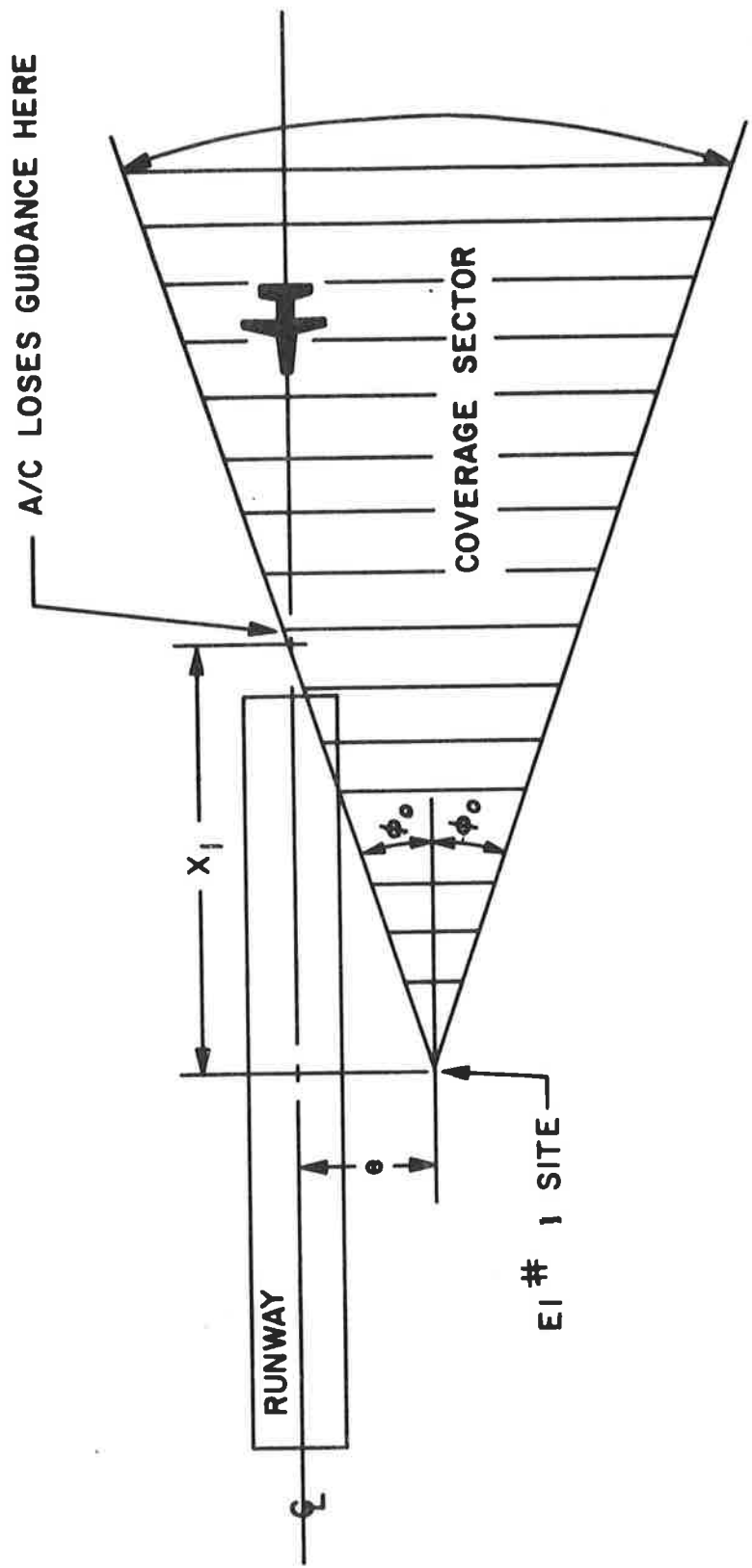


Figure 2.14 Elevation Coverage- Plan View

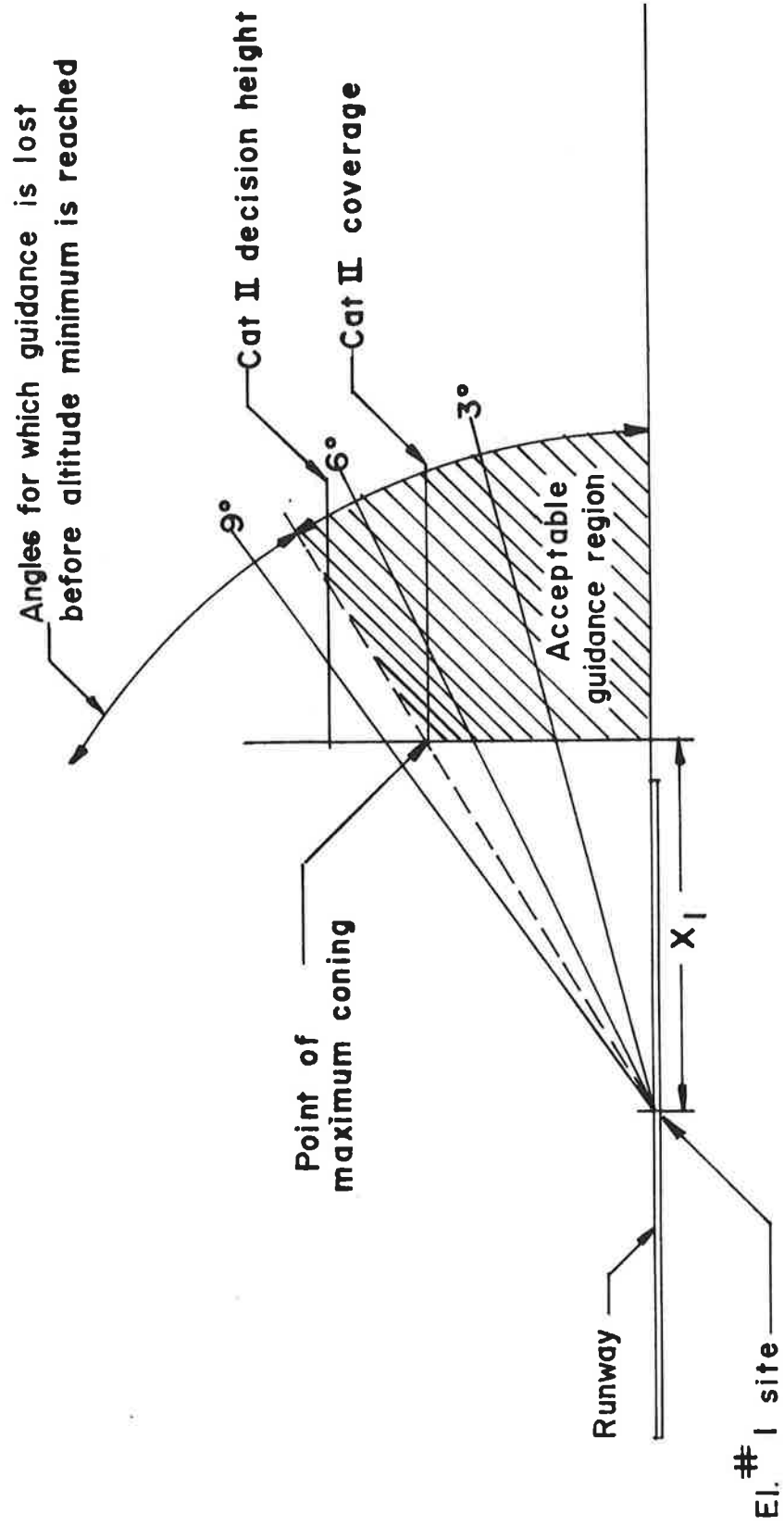


Figure 2.15 Elevation Coverage - Side View



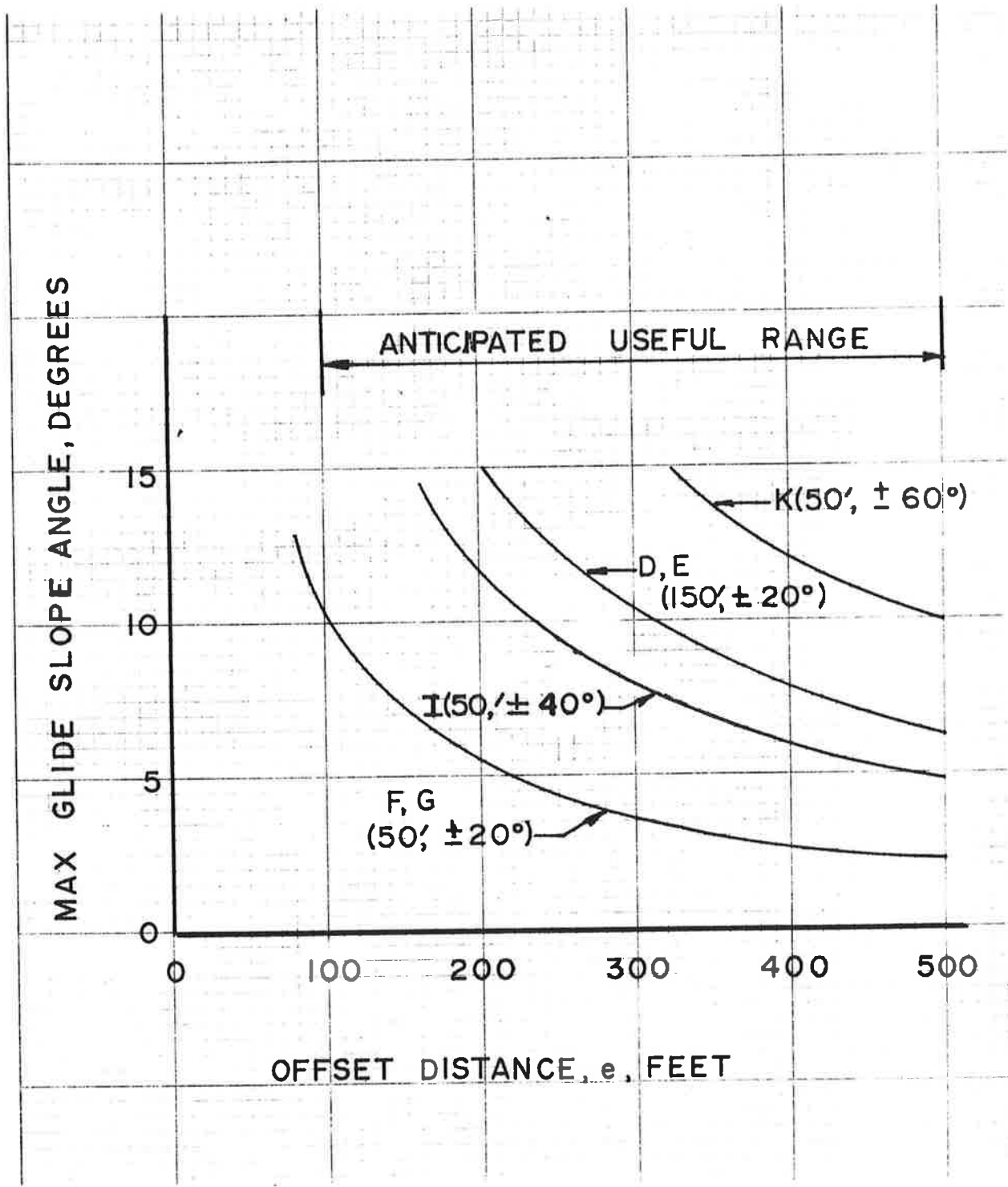


Figure 2.16 Glideslope Limitations Due to Coverage Requirements

glide paths.

### 2.3.2 GLIDE SLOPE ERROR DUE TO CONING-WITHOUT DME CORRECTION

If the on-board processor interpreted conical beam data as if it were planar, an error would result, called the coning error. The coning error causes the glide slope guidance path to bend slightly above a straight line path to the GPIIP, assuming no corrections are made. This error increases with increasing glideslope angle, and as a result is maximum at the steepest glide slope allowable (given by equation 2.3.3 above). The deviation  $\Delta z$  expressed earlier in equation 2.1.11 is an error  $z_{err}$  in this case:

$$z_{err} = (\sqrt{x^2 + e^2} - x) \tan \theta_b \quad (2.3.4)$$

where  $\theta_b$  is the glide slope angle equal to the planar angle  $\psi$ . If  $\phi_1$  is the azimuth angle of the aircraft along the runway centerline as seen from elevation #1 site, this error can be written as

$$z_{err} = z(\sec \phi_1 - 1) \quad (2.3.5)$$

At the coverage extreme,  $\phi_1 = \phi_0$ ,  $z = z_0$  (where  $z_0$  is the required minimum guidance height), or

$$z_{err} = z_0(\sec \phi_0 - 1) \quad (2.3.6)$$

The errors which result are listed in Table 2.1 for the coverage extremes. It should be noted that these errors are maximum, i.e., the errors in height are at most those indicated in Table 2.1.

Table 2.1 Coning Error at Coverage Limits

Configurations	$z_0$	$\phi_0$	$z_{err}$	RTCA allowable error
D, E	150 ft.	$\pm 20^\circ$	9.6 ft.	7.0 ft.
F, G	50 ft.	$\pm 20^\circ$	3.2 ft.	1.4 ft.
I	50 ft.	$\pm 40^\circ$	15.3 ft.	1.4 ft.
K	50 ft.	$\pm 60^\circ$	50 ft.	1.4 ft.

For the configurations D through G, the maximum errors are slightly higher than the recommended ones. This implies that if no DME correction were made, glide slopes would be limited somewhat. This is shown in Table 2.2. The coning error is given by equation 2.3.4, and the ground range  $x$  by equation 2.3.1:

$$x = e \cot \phi_0 \quad (2.3.6)$$

The coning errors are high for configurations I and K, but correspond to very steep glide slope angles. In order for the uncorrected coning error to be kept below 1.4 feet down to 50 feet, the elevation offset distance would have to be less than 225 feet, and the allowable glide slope angle less than three degrees. This does not appear to be a serious constraint when it is considered that no DME corrections are made, and that the use of steep glide slopes in CAT-II conditions is unlikely.

The glide slopes of Table 2.2 were chosen to represent the maximum glide path angles used by various classes of aircraft. This is discussed in Appendix A. Only the more maneuverable aircraft with slower approach speeds would use glide slopes above  $3^\circ$ , so that deviations above the slide slope are less serious. For the fast, less maneuverable aircraft the coning errors are quite small. Furthermore, the larger aircraft will be equipped with DME in general. This makes possible simple corrections discussed in the next section.

### 2.3.3 GLIDE SLOPE ERROR DUE TO CONING-WITH DME CORRECTION

If the (conical) elevation guidance angle signal is modified by a DME-derived corrective term, the effect can be determined by repeating the argument of section 2.1.2 with the modified elevation angle. Replacing  $\theta_b$  by

$$\theta_b \left[ 1 - \frac{1}{2} \left( \frac{e}{R_a} \right)^2 \right]$$

the height corresponding to equation (2.1.9), i.e., the height of an aircraft following this modified guidance path, is

$$z = \sqrt{x^2 + e^2} \tan \left\{ \theta_b \left[ 1 - \frac{1}{2} \left( \frac{e}{R_a} \right)^2 \right] \right\} \quad (2.3.7)$$

Table 2.2 Coning Error at Coverage Limits for Two  
Offset Distances-No DME Correction

Offset Distance of Elevation #1 Site: 500 ft.			
Glide Slope Angle	3°	6°	9°
Configuration	Coning Error, Ft./Ground Range, Ft.		
D, E Decision Ht.-200 ft. Coverage Limit-150 ft.	1.7/3816 2.3/2862	6.8/1902 8.9/1427	No Coverage N.C.
F, G D.H. - 100 ft. C.L. - 50 ft.	N.C. N.C.	N.C. N.C.	N.C. N.C.
I (#1) C.L. - 50 ft.	6.4/954	N.C.	N.C.
K (#1) C.L. - 50 ft.	6.4/954	22.5/476	43.6/316

Offset Distance: 300 ft.			
Glide Slope Angle	3°	6°	9°
Configuration	Coning Error, Ft./Ground Range, Ft.		
D, E D.H. - 200 ft. C.L. - 150 ft.	.6/3816 .8/2862	2.5/1902 3.3/1427	5.6/1262 7.3/947
F, G D.H. - 100 ft. C.L. - 50 ft.	1.2/1908 2.4/954	N.C. N.C.	N.C. N.C.
I (#1) C.L. - 50 ft.	2.4/954	9.1/476	N.C.
K (#1) C.L. - 50 ft.	2.4/954	9.1/476	19.0/316

The straight-line (desired) guidance path is still

$$z = x \tan \theta_b \quad (2.3.8)$$

so that the error is given by the difference between these two heights. Since the DME for the RTCA recommended configuration is located several thousand feet away at the stop end of the runway, the slant range and ground range are almost indistinguishable, so that

$$x \approx R_a^* \quad (2.3.9)$$

to a very good approximation. The error can thus be written:

$$z_{\text{err}} = \sqrt{x^2 + e^2} \tan \left\{ \theta_b \left( 1 - \frac{1}{2} \frac{e^2}{x^2} \right) \right\} - x \tan \theta_b \quad (2.3.10)$$

At the guidance minimum height  $z_0$ ,  $x = z_0 \cot \theta_b$ . Using this relation and equation (2.3.10) the error in height can be calculated for various minimum heights, offset distances, and glide slope angles. Some results are given in Table 2.3. These show marked improvement for the D and E configurations and shallow glide slope angles, but are still outside the allowed bias errors for steep glide slopes.

Further improvement can be obtained by using fractions other than  $\frac{1}{2}$  in equation (2.3.10). In fact, by using  $1/3$  for an offset distance of 300 feet, the error can be reduced to well within the required bias error for approach angles up to about  $8^\circ$ . This is shown in Table 2.4. The best fraction for an offset distance of 500 feet is between  $1/3$  and  $1/4$ , indicating a dependence of the multiplying fraction on the offset distance. This could be objectionable, in that another piece of information would have to be transmitted up to the aircraft. However, since this is the only situation where the information is needed, the offset distance information  $e$  can be modified from its actual value to incorporate this factor. For example, suppose the offset distance is 300 feet, and suppose the processor is using

$$\theta_b \left[ 1 - \frac{1}{2} \left( \frac{e}{R_a^*} \right)^2 \right]$$

instead of  $\theta_b$  as the angle. Rather than transmit the actual offset distance of 300 feet, the offset distance sent up is modified to be

Table 2.3 Coning Error at Coverage Limits - DME Correction

Deviation Above Glide Slope, Ft./ Ground Range, Ft.

Offset Distance of Elevation #1 Site: 500 Ft.			
Glide Slope Angle	3°	6°	9°
Configuration	Coning Error, Ft./Ground Range, Ft.		
D, E Decision Ht. -200 ft. Coverage Limit-150 ft.	0/3816 -.1/2862	-.4/1902 -.9/1427	No Coverage N.C.
F, G D.H. - 100 ft. C.L. - 50 ft.	N.C. N.C.	N.C. N.C.	N.C. N.C.
I (#2) C.L. - 50 ft.	-.3/954	N.C.	N.C.
K (#1) C.L. - 50 ft.	-1.3/954	-17.6/476	-73.5/316

Offset Distance: 300 Ft.			
Glide Slope Angle	3°	6°	9°
Configuration	Coning Error, Ft./Ground Range Ft.		
D, E D.H. - 200 ft. C.L. - 150 ft.	0/3816 0/2862	-.1/1902 -.1/1427	-.3/1262 -.7/947
F, G D.H. - 100 ft. C.L. - 50 ft.	0/1908 -.2/954	N.C. N.C.	N.C. N.C.
I (#1) C.L. - 50 ft.	-.2/954	-2.7/476	N.C.
K (#1) C.L. - 50 ft.	-.2/954	-2.7/476	-12.3/316

Table 2.4 Coning Error at Coverage Limits with Modified DME Correction

Offset Distance: 300 ft.			
Glide Slope Angle	3°	6°	9°
Configuration	Coning Error, Ft./Ground, Range Ft.		
D, E D.H. - 200 ft. C.L. - 150 ft.	.2/3816 .3/2862	.8/1902 1.0/1427	1.6/1262 2.0/947
F, G D.H. - 100 ft. C.L. - 50 ft.	.4/1908 .7/954	N.C. N.C.	N.C. N.C.
I (#1) C.L. - 50 ft.	.7/954	1.2/476	N.C.
K (#1) C.L. - 50 ft.	.7/954	1.2/476	1.9/316

$$e = 300 \cdot \sqrt{\frac{1}{3}} / \sqrt{\frac{1}{2}} = 244 \text{ ft.} \quad (2.3.11)$$

This will result in the errors shown in Table 2.4

Thus for an offset distance of 300 feet or less, the errors in the DME - corrected glide slope path using conical beams in elevation are acceptable. How far beyond 300 feet this holds has not yet been determined.

#### 2.3.4 LATERAL ERRORS FOR COLLOCATED SETUP WITHOUT DME CORRECTION

Configuration E of the RTCA SC-117 report, a collocated setup, was cited for use with STOL or small airports and thus admits the possibility of an azimuth location which is not along the runway centerline. The limitation on this configuration is the topic of this section.

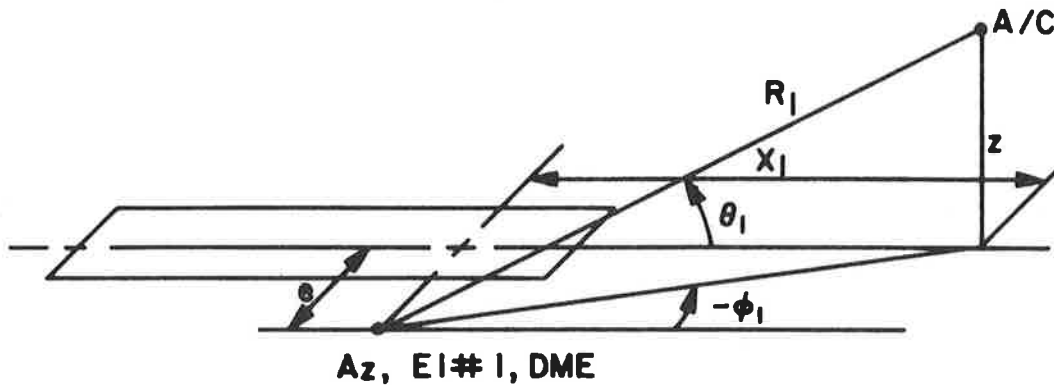


Figure 2.17 Coordinate System for Collocated Siting Beside Runway

An aircraft following the guidance path given by  $\phi_1 = 0$  will aim directly at the azimuth antenna, and will then always be a distance  $e$  from the runway centerline. The RTCA SC-117 accuracy requirements for configuration E call for a bias error of 50 feet or  $0.25^\circ$ . Since the offset distance will always be greater than 50 feet the angular error is the dominant factor in determining the point in the coverage where the limits are exceeded.

With reference to Figure 2.17, the angle  $\phi_1$  will exceed  $0.25^\circ$  when

$$x_1 < e \cot (.25^\circ) = 229 e \quad (2.3.12)$$

This is shown in Figure 2.18. The height at which this occurs is given by

$$z = x_1 \tan \theta_1 = e \cot (.25^\circ) \tan \theta_1 \quad (2.3.13)$$

This is plotted in Figure 2.19. It can be seen that in general, CAT-I guidance for this is not possible without a DME correction.



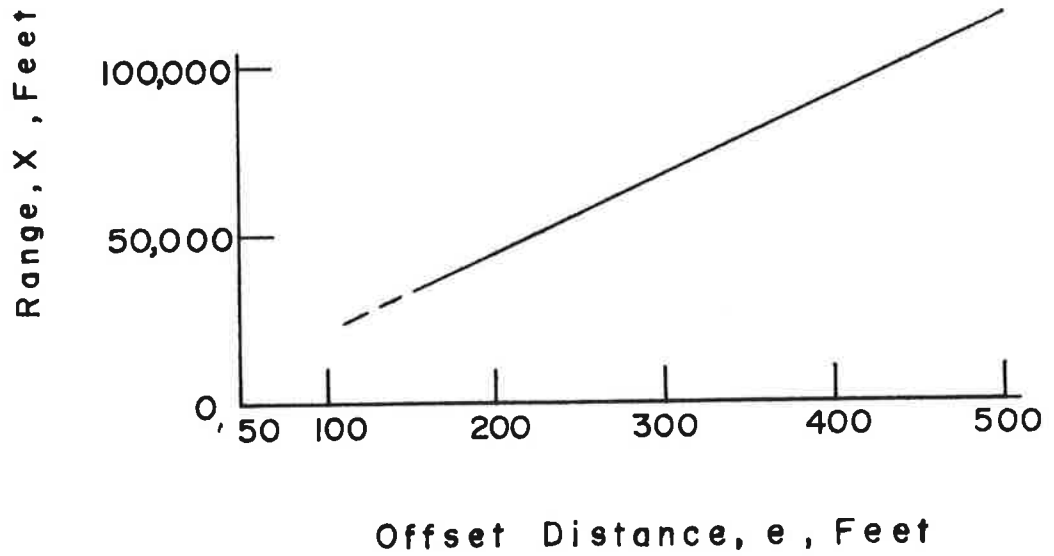


Figure 2.18 Ground Range at Which Azimuth Error Exceeds  $0.25^\circ$  Collocated Siting

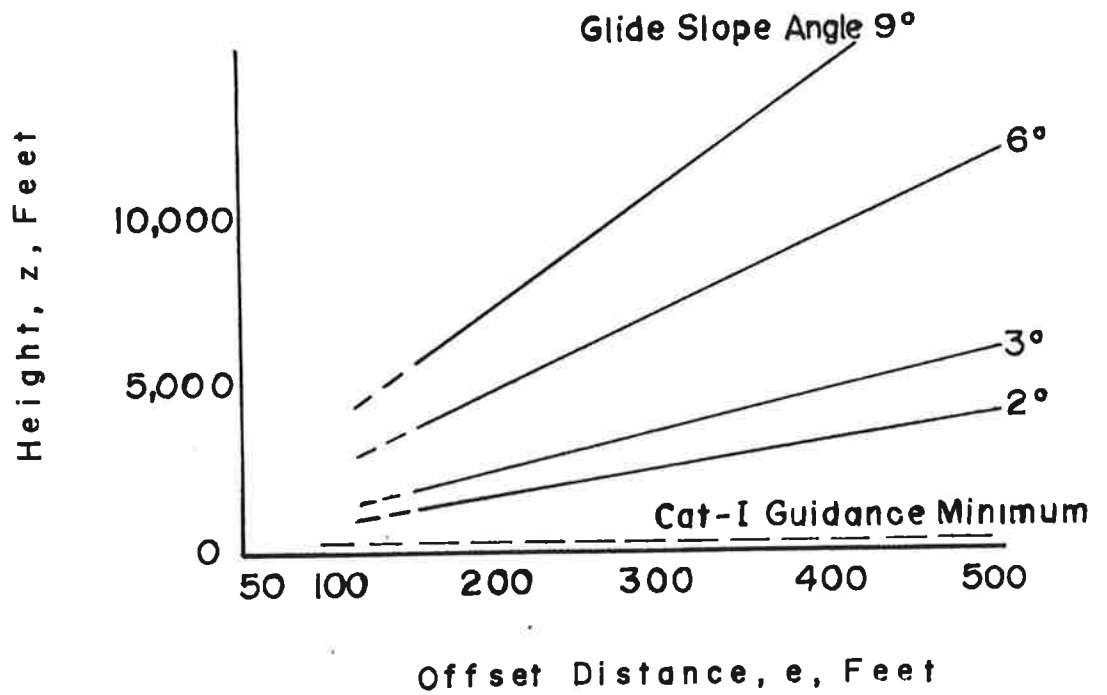


Figure 2.19 Height at Which Error Exceeds  $0.25^\circ$  - Collocated Siting

For STOL runways, it has been suggested by Fombonne<sup>1</sup> that a collocated setup with conical guidance in elevation along with a DME is a natural choice, since it allows approaches from a variety of directions, all aimed (in azimuth) directly at the antenna site. Here the DME would be used to calculate aiming points other than at the antenna site and allow CAT-III landings.

### 2.3.5 LATERAL ERRORS FOR COLLOCATED SETUP WITH DME CORRECTION

In order to maintain a path along the centerline of the runway ( $y=0$ ), it is necessary that

$$\phi_1 = -\sin^{-1} \left( \frac{e}{R_1 \cos \theta} \right) \quad (2.3.14)$$

The logical approximation is

$$\phi_1 + e/R_1 = 0 \quad (2.3.15)$$

as a control equation. The deviation from the runway centerline using this equation is given by  $y_1$ , where

$$\begin{aligned} y_1 &= R_1 \cos \theta \sin \phi_1 - e \\ &= R_1 \cos \theta \sin(e/R_1) - e \end{aligned} \quad (2.3.16)$$

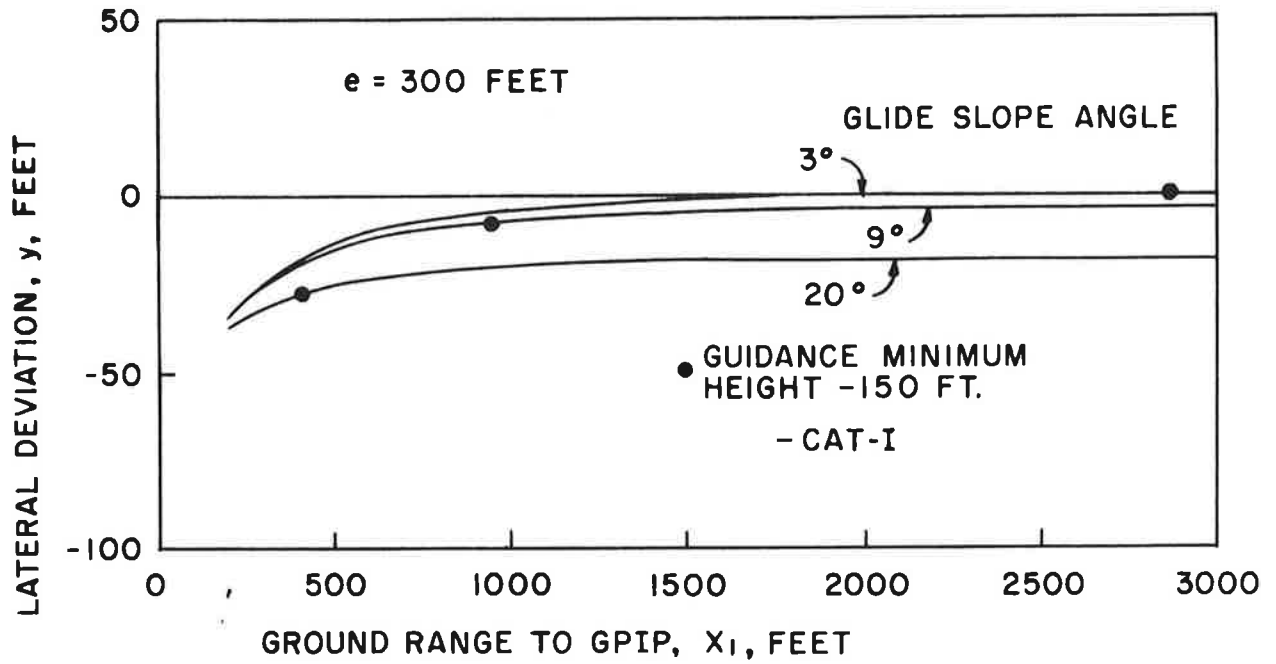
Some tracks projected on to the x-y plane are shown in Figure 2.20, where  $x_1$  is given by

$$x_1 = R_1 \cos \theta \cos(e/R_1) \quad (2.3.17)$$

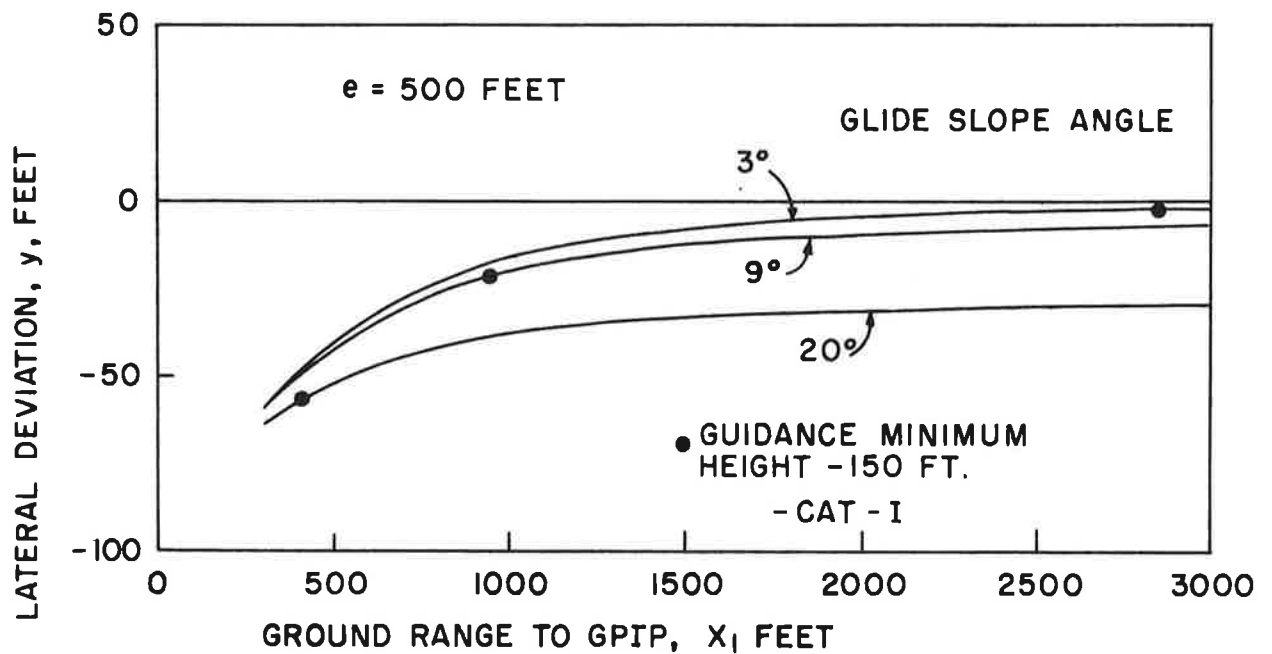
The tracks bend toward the antenna site as the aircraft approaches. It can be seen that for offset distances of 300 feet or less that the deviation is negligible for glideslopes of  $9^\circ$  or less down to 100 feet from touchdown. For larger offset distances, the error is more severe, and could result in a lateral command prior to the pilot's override of the autopilot (if it is used). It is thus recommended that for the collocated setups that the offset distance not exceed about 300 feet, and that glideslopes be limited to about  $6^\circ$ .

Another point to be noticed is that since the guidance equation 2.3.15 does not involve the glideslope angle  $\theta$ , the tracks are offset somewhat from the runway centerline for the steep glide slope angles. This is given by

<sup>1</sup> I. P. Fombonne, "Coordinate Systems" RTCA SC-117 Supplementary Report AT. DTRN 2-159, March, 1970, p. 4.



(A) OFFSET DISTANCE ( $e$ ): 300 FEET



(B) OFFSET DISTANCE ( $e$ ): 500 FEET

Figure 2.20 Lateral Guidance Paths Using One-Term DME-Derived Correction

$$y_1 \approx e(1-\cos\theta) \quad (2.3.18)$$

Thus for an offset of 300 feet and a glideslope angle of  $20^\circ$ , the track taken by the aircraft is about 30 feet off the runway centerline; for glideslope angles of  $9^\circ$  or less, this error is less than 7 feet and will cause no problems.

### 2.3.6 LATERAL ERRORS FOR SPLIT-SITE SETUP

If purely planar beams are used in azimuth there is no lateral error from the guidance surface geometry. If a linear array is used, the guidance surfaces are not quite planar but are conical (see section 2.1). The guidance surface generated would be given by  $\gamma = \text{constant}$ , where  $\gamma$  is the angle measured from the antenna axis, which in the coordinate used here, is the y-axis. The locus of this surface expressed in  $\theta$ - $\phi$  coordinates is

$$\phi = \sin^{-1} \left( \frac{\sin\phi_b}{\cos\theta} \right) \quad (2.3.19)$$

where  $\phi_b$  is the angle to which the fan beam is steered; this is equal to the planar beam when measured along the horizon (Figure 2.21). The locus of the planar beam corresponding to equation 2.3.19 above is given by  $\phi = \phi_b$

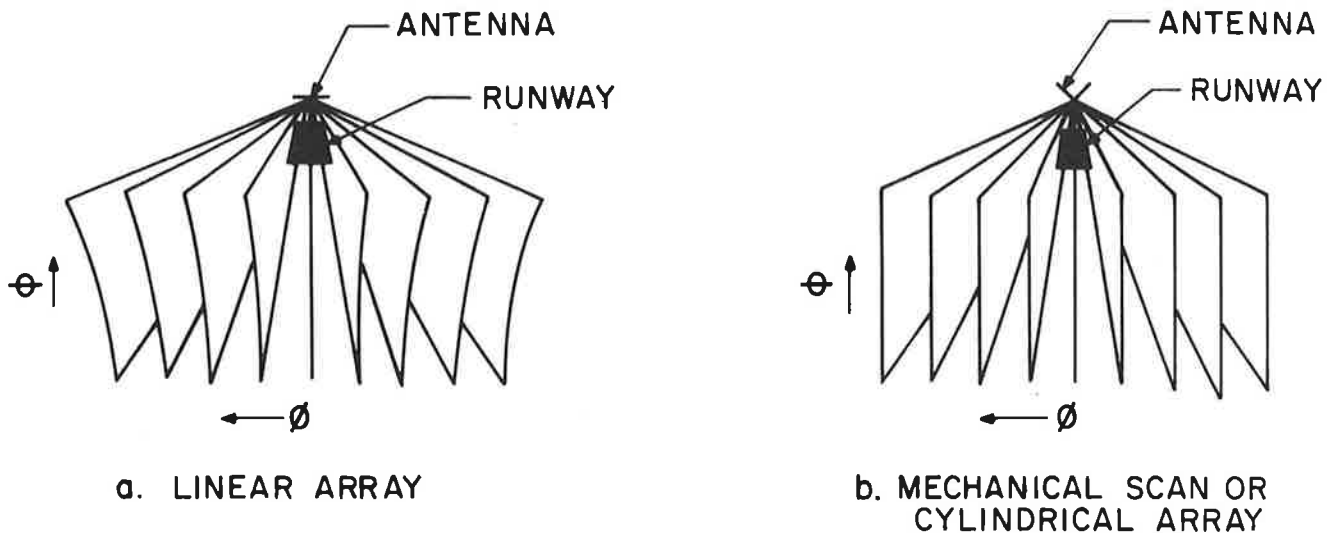


Figure 2.21 Guidance Contours Showing Coning in Linear Arrays

An aircraft receiving the guidance angle information  $\phi_b$  would interpret its position as in the plane  $\phi = \phi_b$ , whereas its actual position would be given by equation (2.3.19). Thus the error is given by the difference between its measured position and its actual position, or

$$\phi_{err} = \phi_b - \sin^{-1} \left( \frac{\sin \phi_b}{\cos \theta} \right) \quad (2.3.20)$$

It is evident that the coning error is zero at the horizon, where  $\theta = 0$ .

Stated another way, the contours in the  $\theta$ - $\phi$  plane for a given azimuth error  $\phi_{err}$  is given by

$$\cos \theta = \sin \phi_b / \sin (\phi_b + \phi_{err}) \quad (2.3.21)$$

In the split-site arrangement, the azimuth antenna is located on the runway centerline at some distance (typically 1000 feet) off the end of the runway. Thus the elevation angle of an aircraft seen from the azimuth antenna is significantly smaller than the measured elevation angle, which is determined by the elevation antenna. The latter is located at the glide path intercept (GPIP), typically 1500 feet from the threshold.

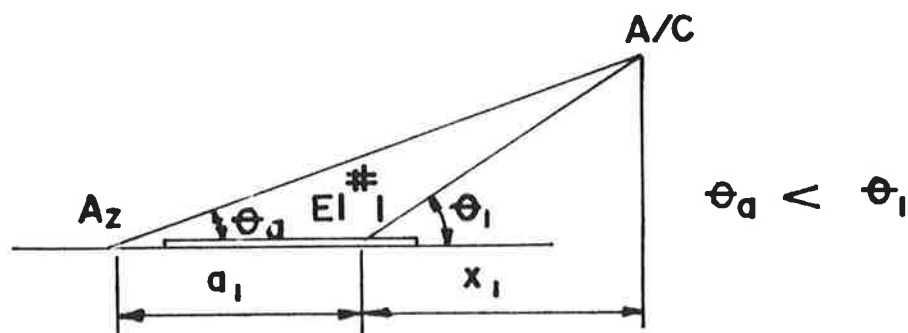


Figure 2.22 Relation of Glide Slope Elevation Angle and Elevation Angle as seen From the Azimuth Antenna-Split Site

This can be seen from Figure 2.22 which illustrates the relation between the two elevation angles for aircraft along the runway centerline. The relation is given

mathematically by

$$\tan \theta_1 = \left( \frac{x_1 + a_1}{x_1} \right) \tan \theta_a \quad (2.3.22)$$

A more exact formula, accounting for azimuth angles other than zero (the runway centerline), is

$$\tan \theta_1 = \left( \frac{x_1 + a_1}{x_1} \right) \tan \theta_a \sqrt{1 + \frac{2a_1}{x_1} + \frac{a_1^2}{x_1^2} \sin^2 \phi_a} \quad (2.3.23)$$

where  $\phi_a$  and  $\theta_a$  are measured with respect to the azimuth datum, and  $\theta_1$  with respect to the elevation datum #1. The error contours due to the coning of a linear array are shown in Figure 2.23 for the parameters of configuration K ( $a_1 = 14,000$  feet,  $\phi_{err} = .072$ ,  $x_1 = 4,000$  feet). It is obvious that the coning is insignificant, since in this region the azimuth angle will be at most a few degrees.

Thus, in the final approach region the coning error due to the use of a linear array in azimuth is negligible, when the azimuth antenna is at the stop end of the runway.

#### 2.4 Effect of Antenna Locations on Position-in-Space Calculation in Landing and Rollout Region

*Abstract-A general discussion of DME siting is presented. Location of the DME at the azimuth results in planar beams as a less restricting choice. Conical beams are more natural when the DME is located at Elevation #2.*

Much of the discussion of planar vs. conical beams for the flare guidance in the landing region centers around the location of the DME. The RTCA committee recommends placing the DME at the azimuth location. This turns out to be essential if planar beams are used, a topic discussed below. In any case the function of the elevation flare antenna (#2) is to provide height and/or sink rate information to the aircraft. It should be noted that height here strictly means "height above touchdown point".

The discussion in this section applies to the elevation function. It is assumed that the azimuth antenna for a landing system will be along the runway centerline at the stop end of the runway. The issue of planar vs. conical beams in azimuth does not come up, since there is negligible difference between the two in the landing and rollout region.

There are considerations affecting the location of the DME which do not involve the question of planar vs. conical

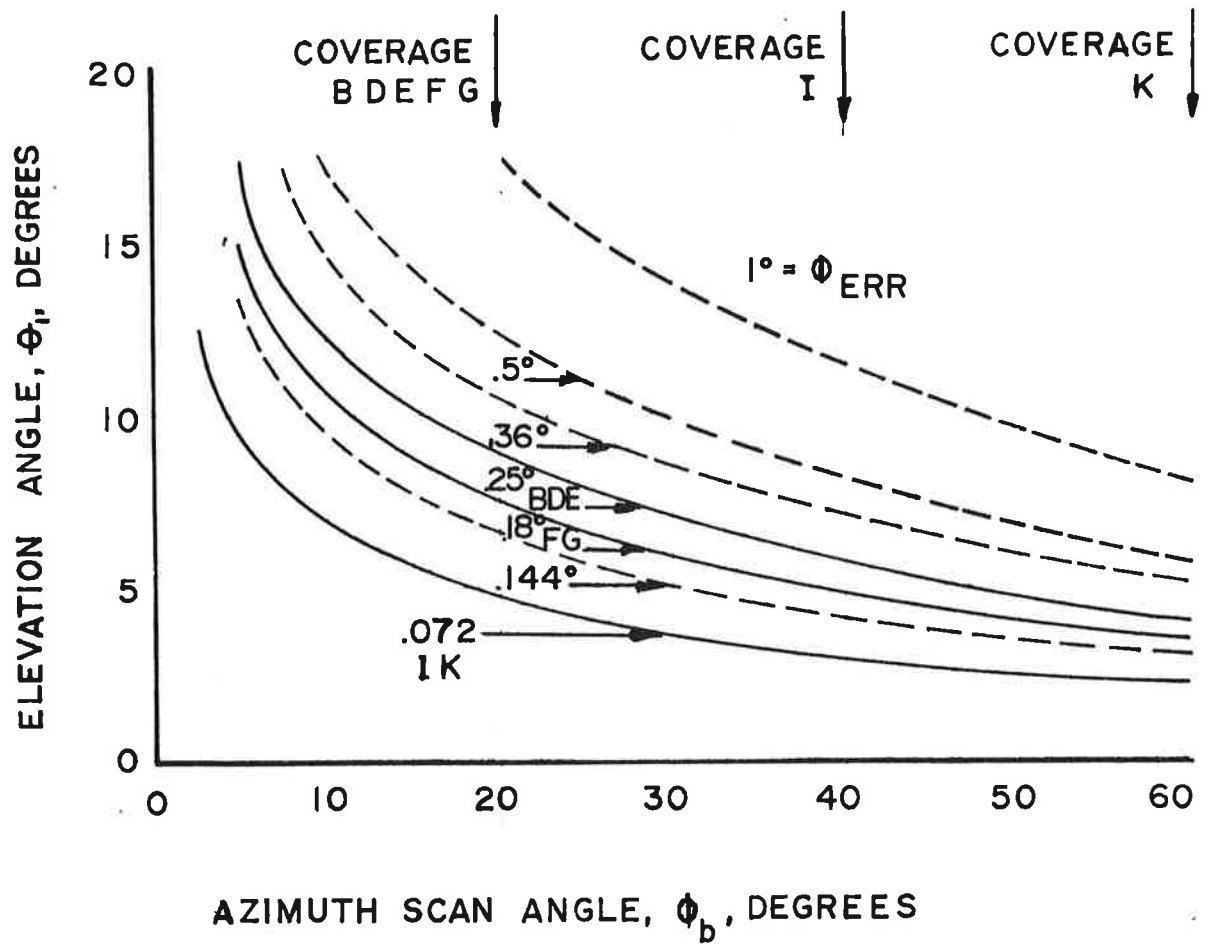


Figure 2.23 Error Contours in Azimuth Due to Coning - Split Site Setup

beams. One important consideration is that the placement of the DME along the runway centerline at the stop end of the runway makes possible continuous coverage throughout landing and rollout, using only the forward antenna of the aircraft. Placing the DME at the elevation location, on the other hand, puts the requirement on the DME that it "look backwards", i.e., cover the rear region, and perhaps the side region as well, in order to maintain coverage throughout rollout. This is illustrated in Figure 2.24. The aircraft must pick up the signal on its rear antenna in order to be covered through rollout.

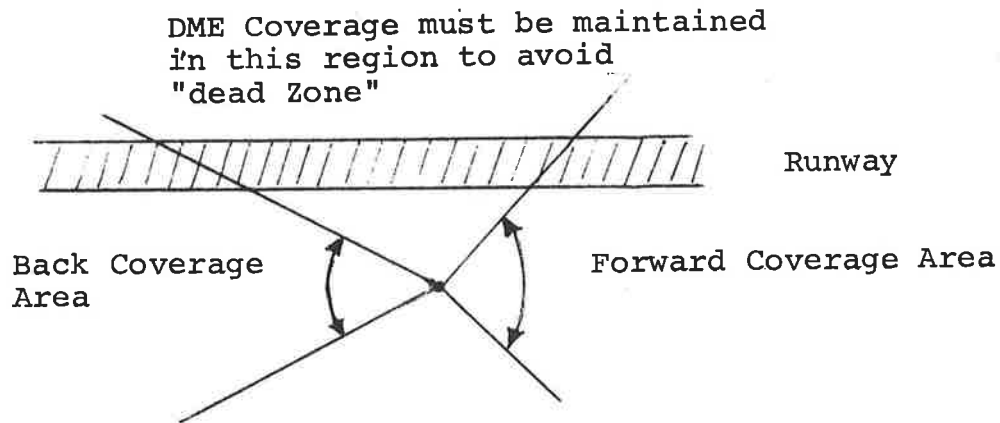


Figure 2.24 DME Coverage Requirements When Located at Elevation #2

Another point to be considered is that the level of the DME signal varies fairly rapidly in the vicinity of the transmitter (power varies as  $1/R^2$ ). This might present a problem in the case of placement of the DME at Elevation #2. How serious this is has not yet been assessed.

In spite of the discussion above, it may yet prove unfeasible to site the DME at the stop end of the runway. The reason for this is that the DME range error is made up of a range-proportional error and a range independent error. With the DME so far away, the range-proportional error may prove to be too large to obtain the accuracy



necessary for guidance to touchdown; or, the circuitry necessary to perform this function properly may prove too costly; or, the collective effect of these errors and calibration errors involved in the delay may exceed allowable tolerances. This important issue has not yet been resolved.

It has been suggested that siting of the DME at the stop end of the runway removes the necessity for transmitting the site parameter  $a_2$  (or  $a_1$ ) to the aircraft. (The purpose is to inform the pilot during rollout of the distance to the end of the runway). This is incorrect. The use of a variable delay which calibrates a 60 microsecond delay corresponding to the GPIIP removes the knowledge of the actual distance to the DME site (Figure 2.10 and discussion). Thus, this parameter must be transmitted as auxiliary data regardless of the DME location. The issue of DME location is not closed, and for that reason, both possible locations are discussed in the following sections.

#### 2.4.1 DME AT THE AZIMUTH SITE

This is the configuration recommended by RTCA SC-117. The azimuth antenna is located at the stop end of the runway along the runway centerline; the elevation antenna is a distance  $a_2$  away beside the runway (Figure 2.25).

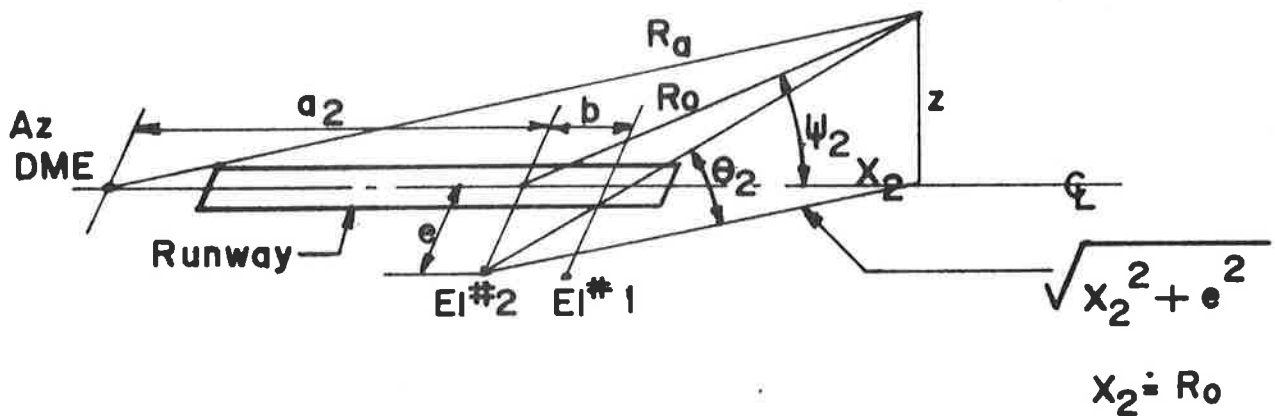


Figure 2.25 Coordinate System for DME at Azimuth Antenna

The range information sent to the aircraft in the RTCA format is  $R_a^*$ ; from equation 2.2.2, the fact that  $a_2 = a_1 - b$ , and from Figure 2.25,

$$R_O \doteq R_a - a_2 = R_a^* + b \quad (2.4.1)$$

The distance between the elevation locations, given by  $b$ , is a number which must be transmitted to the aircraft.

It is reasonable to assume that elevation angles are small in the flareout region, and thus that elevation angles, their sines, and their tangents are all the same. From Figure 2.25 it can be seen that height is given by

$$z = R_O \sin \psi_2 \doteq R_O \psi_2 \quad (2.4.2)$$

for planar elevation beams. Conical beams, on the other hand, require a correction

$$\begin{aligned} z &= \sqrt{x_2^2 + e^2} \tan \theta_2 \doteq \sqrt{R_O^2 + e^2} \theta_2 \\ &\doteq \left( R_O + \frac{e^2}{2R_O} \right) \theta_2 \end{aligned} \quad (2.4.3)$$

This approximation only holds for  $e \ll R_O$ , which requires that the minimum value of  $R_O$  (the distance from the point on the runway centerline opposite Elevation #2 to the furthest required touchdown point) be considerably larger than the offset distance  $e$ . This in turn would require locating the Elevation #2 antenna further down the runway.

Figures 2.26a and b show the height error due to coning when no correction term (i.e., using only the first term in equation 2.4.3) is used. It can be seen that in order to provide coverage up to 60 feet without exceeding the RTCA bias error requirement, the antenna must be located about 1300 feet down the runway from the furthest anticipated touchdown point.

With the correction, the errors are those shown in Figures 2.27a and b. Thus, if conical elevation beams are used in this configuration, there is a tradeoff involving the offset distance, the siting parameter  $b$ , the allowable error, and the altitude coverage, as against the added on-board complexity necessary to calculate the corrected height of Equation 2.4.3.

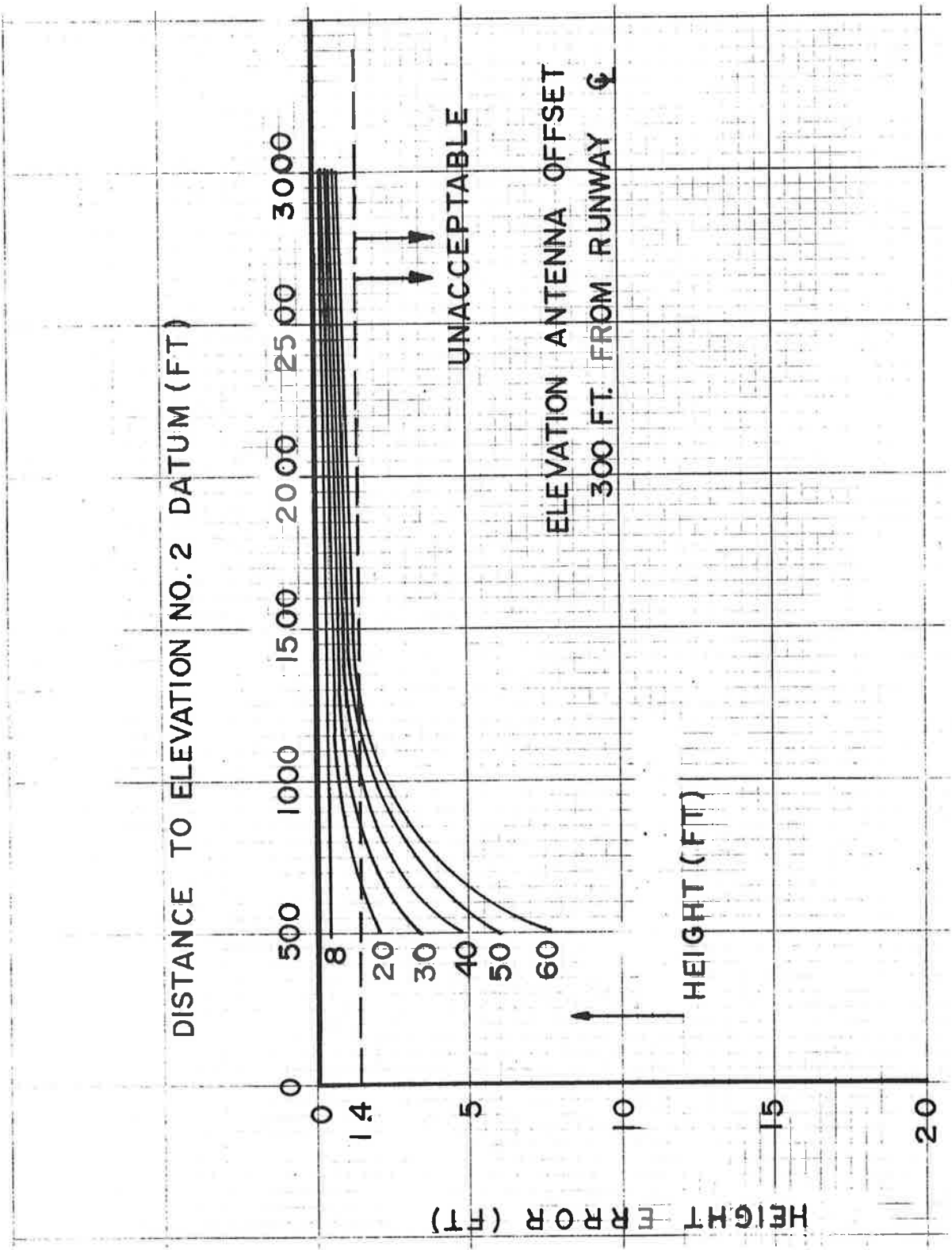


Figure 2.26(a) Height Error on Centerline Using Conical Guidance - No DME Correction

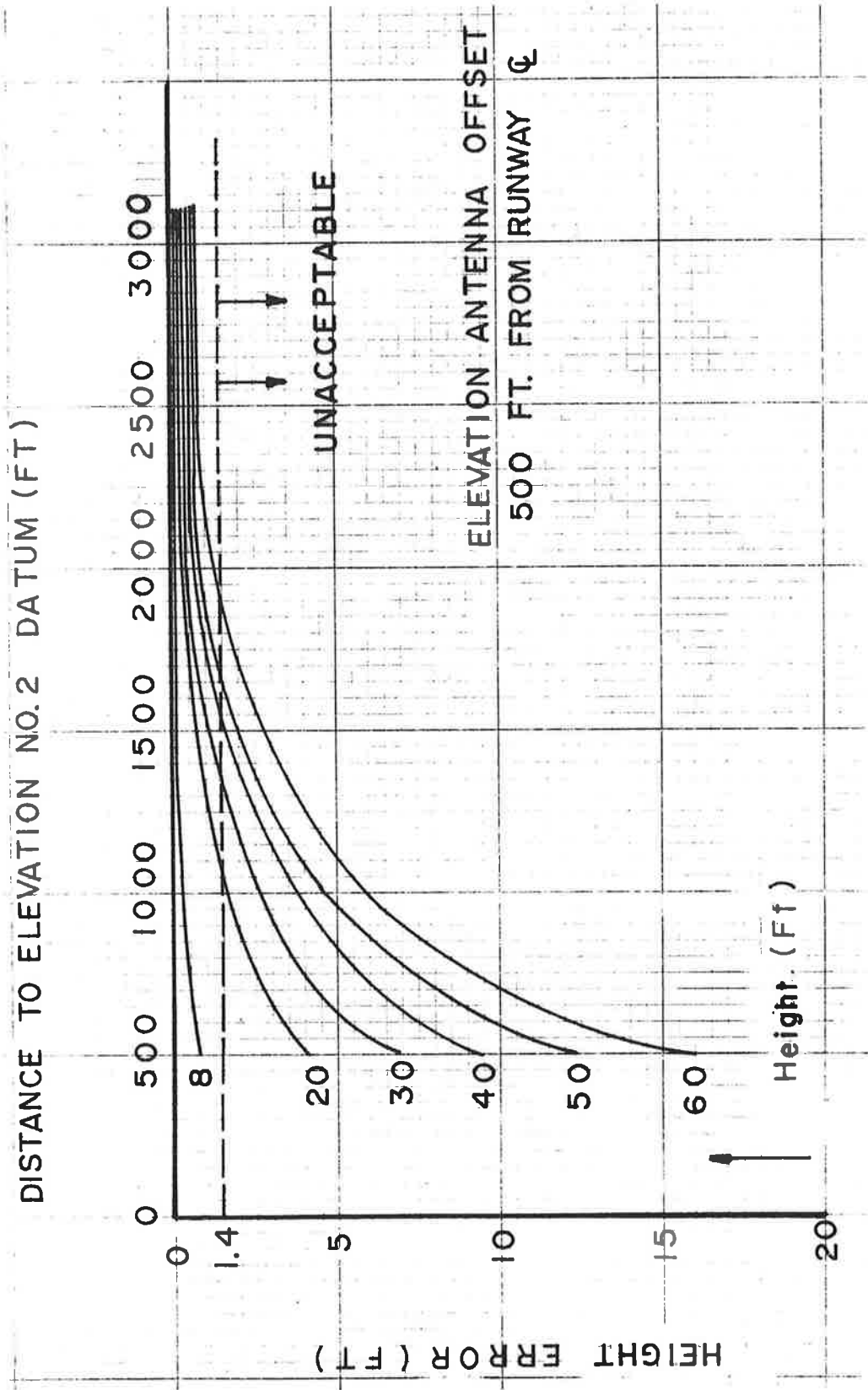


Figure 2.26 (b) Height Error on Centerline Using Conical Guidance - No DME Correction

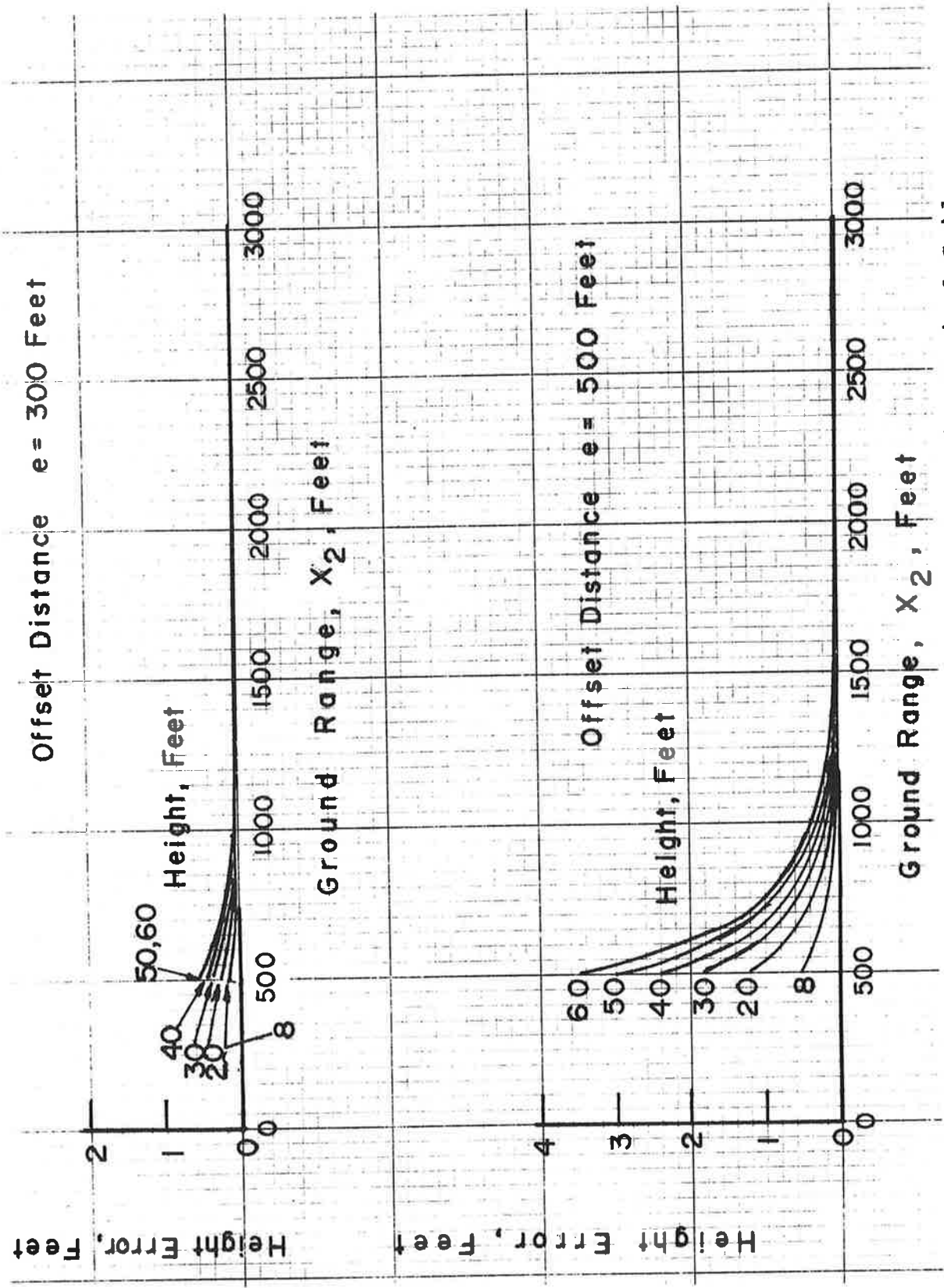


Figure 2.27 (a & b) Height Error on Centerline Using Conical Guidance - With DME Correction

Siting of the DME at the azimuth antenna results in lower complexity using planar elevation beams. Conical beams can be used under conditions described in this section.

#### 2.4.2 DME AT ELEVATION #2 LOCATION

When the DME is at the elevation antenna, height information is best obtained with conical beams.

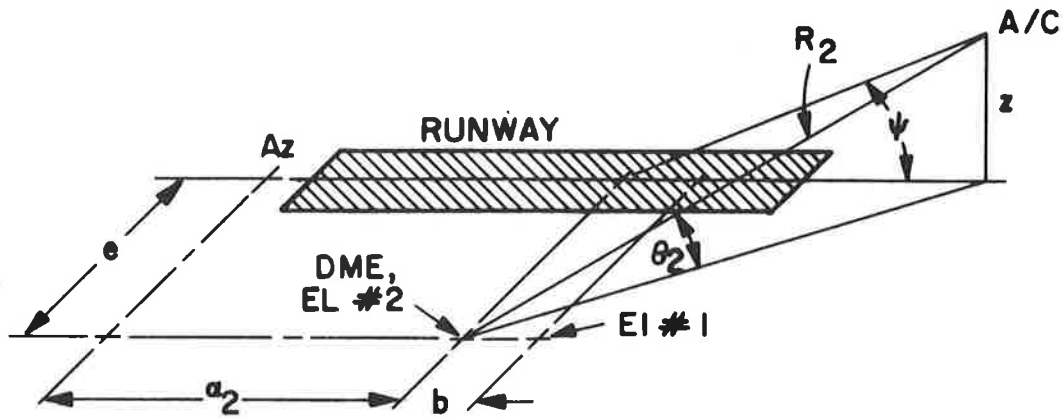


Figure 2.28 Coordinate System for DME at Elevation #2 Location

$$z = R_2 \sin \theta_2 \doteq R_2 \theta_2 \quad (2.4.4)$$

using the conical beam angle  $\theta$ . Using planar beams with angle  $\theta$ , on the other hand,

$$\begin{aligned} z &= x_2 \tan \psi_2 \doteq \sqrt{R_2^2 - e^2} \psi_2 \quad (2.4.5) \\ &= \left( R_2 - \frac{e^2}{2R_2} \right) \psi_2 \end{aligned}$$

Comparison with 2.4.3 shows that this requires the same correction, except for sign, used in section 2.4.1. The errors encountered using planar beams are essentially the negative of the errors using conical beams before.

In conclusion, conical beams are a natural choice when the DME is at the elevation antenna. The conditions under which planar beams can be used are those described in the last paragraphs of section 2.2.1.

## CHAPTER III ANTENNA DESIGN STUDIES

This chapter gives some of the results of the tradeoff study performed during the year. In order to facilitate the study, a computer program was written which allows a wide variety of geometries, orientations, polarizations, aperture distributions and element patterns to be used. The basic calculation is that given by equation B.4 for the far-field. The output of the program involves a printout of the pattern data for selected azimuth and elevation cuts, a calculation of the beamwidth (3dB, 10dB or arbitrary) using a 4 point polynomial interpolation, and an optional plot capability. The program is written to allow the ready addition of new geometries, aperture distributions, and element patterns. Digitized phase shifters may be specified, as well as quantized or digitized amplitude levels. Plane wave (cophasal) excitation and omnidirectional patterns may be specified. At this time, the limitations of the program are that gain is not directly calculated, only separable two-dimensional geometries (e.g., planar and cylindrical) can be accommodated, and only one excitation at a time can be used. It may prove necessary to add these capabilities at a later time.

The azimuth and elevation antennas are considered separately. Element or element column designs, linear and cylindrical geometries are discussed. Other geometries were not considered feasible, or were too complex. The emphasis was on stripline and microstrip techniques, as opposed to waveguide techniques, in order to keep costs down, and to make the design compatible with high production manufacturing techniques.

### 3.1 Azimuth Antenna

*Abstract - Since the antenna will be elevated, and since the coverage should extend to  $-1^\circ$ , some multipath is unavoidable. It is seen, using the  $(\sin x)/x$  pattern synthesis method for the column design, that the sidelobe level, (and thus multipath), depends largely on the pattern level at the horizon. It is shown that the  $3^\circ \csc \theta$  power pattern requirement of RTCA SC-117 is not consistent with the coverage requirements at 20,000 feet. Using a 15 element aperture a pattern is generated that will meet the requirements, at the expense of 3.5 dB increase in transmitter power.*

*It is shown that the coning errors of a linear array are acceptable for  $\pm 20^\circ$  coverage in azimuth, thus linear arrays can be used for all configurations except I and K. Linear array*



designs for  $1^\circ$ ,  $2^\circ$ , and  $4^\circ$  beamwidths are presented.

*It is noted that a cylindrical array design can meet the azimuth coverage requirements of the I and K configurations. The design procedure is explained and it is shown that once the active sector is chosen all other variables except the focus angle are determined. The active sector is chosen from considerations of defocusing, structural problems, and component complexity. The optimum focus angle is determined from the results of computer studies. Cylindrical array designs for  $1^\circ$ ,  $2^\circ$  and  $4^\circ$  beamwidths are presented and their calculated performance is tabulated.*

The RTCA Committee recommended locating the azimuth antenna along the runway centerline at the stop end of the runway, near the present localizer. Since the localizer will not be removed, at least for some time, the azimuth antenna design must account for this. It is assumed here that the azimuth antenna will be behind the localizer so as not to disrupt the localizer guidance. It will be elevated in order to "look over" the localizer antenna, probably on the order of 20 feet.

The RTCA committee also recommended a beamwidth of one-degree in azimuth. Several considerations surrounding this are tentative: (1) a coarse-fine system of two azimuth antennas is not ruled out; (2) the final code format may require longer dwell times or higher scan rates necessitating larger beamwidths. This being the case, beamwidths of  $2^\circ$  and  $4^\circ$  and the associated designs are also considered and discussed.

One of the conclusions drawn is that for configurations B through G a planar array can be used for azimuth guidance; the skew error caused by coning is not serious over the azimuthal coverage of  $\pm 20^\circ$ . For configurations I ( $\pm 40^\circ$  coverage) and K ( $\pm 60^\circ$  coverage), the coning is more serious, and causes unacceptable skew errors. Cylindrical array designs are given for  $\pm 60^\circ$  of coverage. The designs can be extended to cover the back course or even a complete  $360^\circ$  coverage.

### 3.1.1 COLUMN DESIGN-MULTIPATH CONSIDERATIONS

The element design for the azimuth antenna depends on the elevation coverage required and the reduction of multipath effects. Multipath effects depend on the siting, environment, runway surface material and wetness condition, as well as the antenna pattern. The azimuth antenna located at the stop end of the runway must be elevated so as to "look over" the present ILS localizer. This means that it will be on the order of 20 feet high.

The narrow beam in azimuth of the azimuth antenna is effective in providing protection against reflections from buildings and other objects outside a narrow swath; these reflections cause signal variation and course bending. The beam is wide in elevation, so that reflections from the runway can involve ray paths within the fan beam itself. The precise shaping of the beam near the horizon is crucial to good multipath characteristics, and warrants appreciable study and care.

In Appendix B it is shown that the vertical column design can for the most part proceed independently of the horizontal characteristics. It is anticipated that the element will be a vertical array of vertical dipoles. The problem is to synthesize an appropriate pattern in the elevation plane which will provide the coverage intended and exhibit low multipath characteristics. Concurrently, it is necessary to define in quantitative terms what the appropriate pattern is, and what constitutes acceptably low multipath. It is desirable from a cost aspect to keep the number of dipoles (and the aperture dimension) as small as possible, while from a performance point of view larger apertures are preferable. It is thus desirable to reduce radiation below the horizon and shape the beam above the horizon to give the desired range over the desired coverage. Actually it is not desirable to have a null at elevation angle zero, because this would cause the lateral guidance to unlock near touchdown. This is due to the fact that the antenna is elevated. Since the azimuth antenna is typically 1000 ft. beyond the end of the runway, a null should not be in the antenna pattern above  $-1^{\circ}$ , typically. Signal coverage is required during rollout to the end of the runway.

Figure 3.1 shows the geometry of the situation. The main beam must extend somewhat below the horizon. This means that a certain amount of multipath from the runway is inevitable. The effect of this is a fluctuation in signal level. Figure 3.2 shows the variation in signal level for an aircraft on a  $3^{\circ}$  glide slope in a worst case situation (total reflection, perfectly flat surface, diffuse scattering ignored).

The antenna patterns used in this figure are for a four-foot aperture, described below. The antenna is assumed to be 20 feet high, 14,000 feet from the GPIIP. In each case the signal level at the threshold, 1000 ft. out from the GPIIP, was chosen as the reference level and fixed at 0 dB. It can be seen that the swing of signal level can be appreciable. To estimate the sample-to-sample signal level variation, consider a ground speed of 200 knots. For an update rate of 5 per second, this corresponds to a sample every 70 feet, or three for every small division on the chart. The angle processor

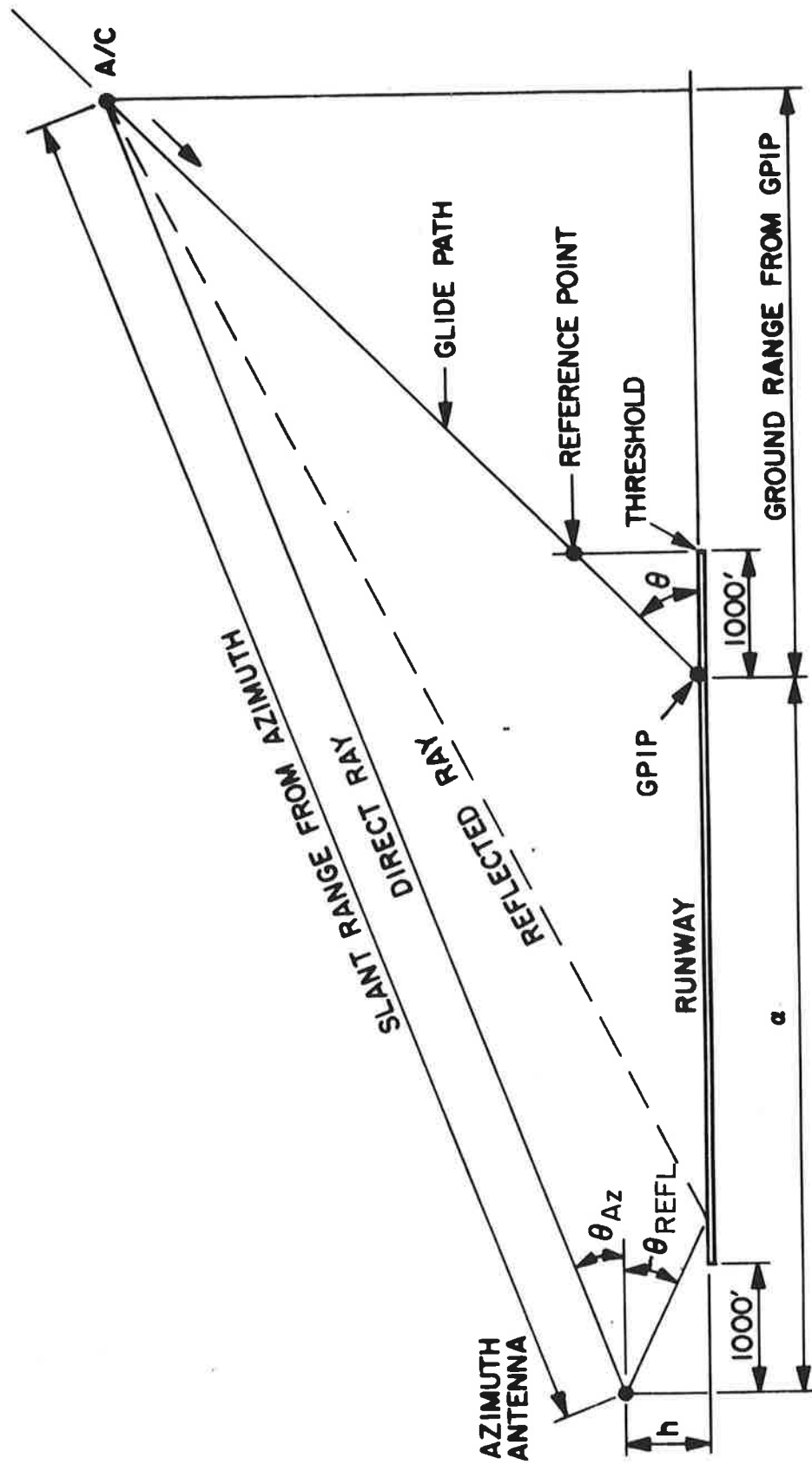


Figure 3.1 Geometry for Multipath Analysis (Azimuth Antenna)

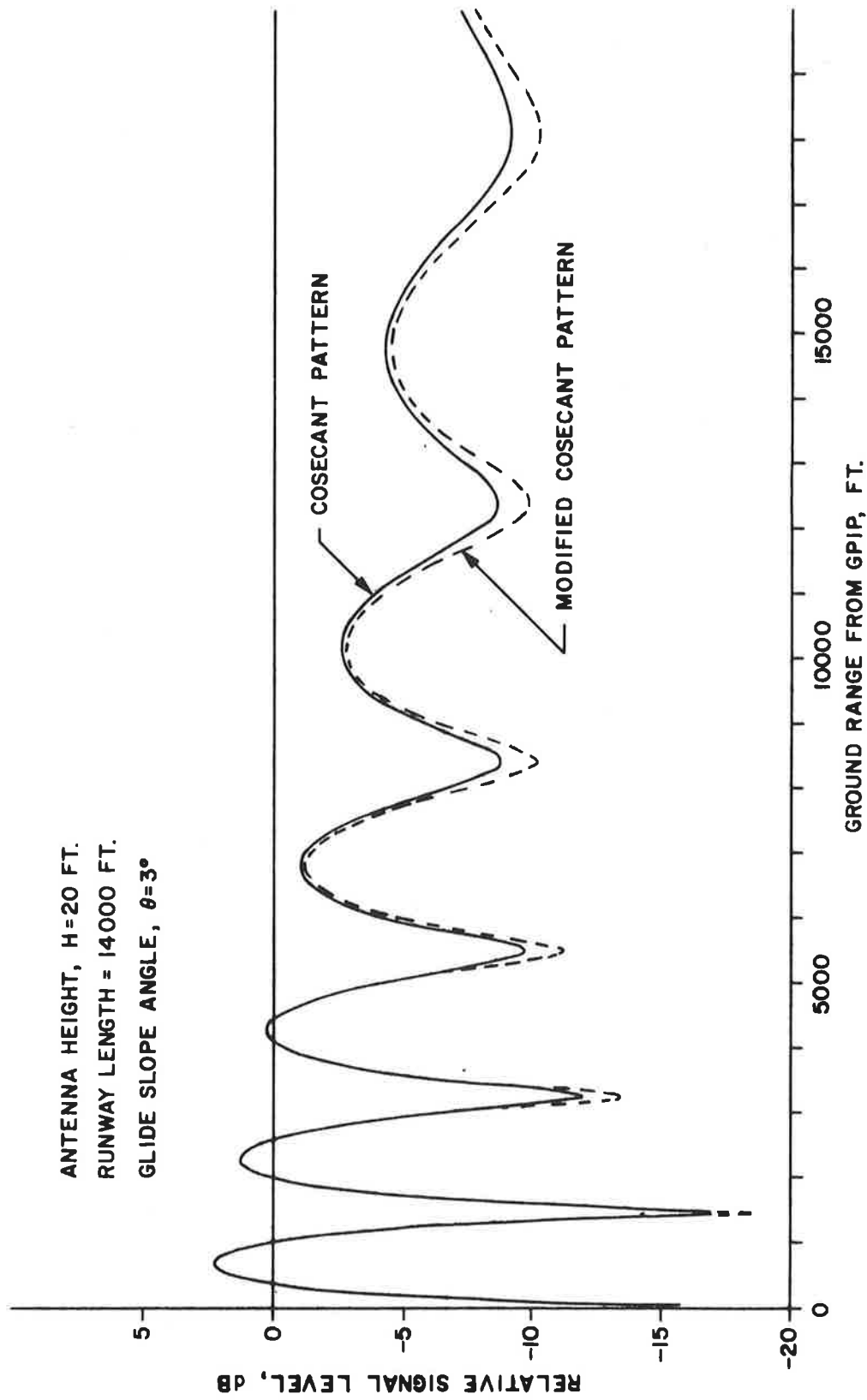


Figure 3.2 Variation of Azimuth Signal Level for Aircraft on  $3^\circ$  Glide Slope Angle

on-board the aircraft should be designed to accommodate variations and variation rates of this nature. In practice the nulls will probably not be as deep as the figure indicates, since the reflection will not be exactly total; however, the reflection coefficient will be close to unity for the shallow grazing angles encountered in this configuration.

One of the most popular pattern synthesis methods is the  $(\sin x)/x$  method, which has the advantages of computational simplicity and realizable illuminations. It is not the only method, nor is it necessarily optimum for this application, but it can be used as a starting point, and refinements added later if desired.

The method is essentially one of point matching to the desired pattern at equally spaced intervals in  $\sin \theta$ . It is based on the assumption of a continuous aperture, rather than an array, so that a complete study involves exciting the array elements with the illumination sampled at their respective locations and calculating the resulting pattern.

Consider an aperture of height  $L$  representing the vertical array radiating face; let  $\mu = (L/\lambda) \sin \theta$ , where  $\lambda$  is the wavelength, and let  $F_d(\mu)$  be the desired field pattern. The pattern is sampled at  $N$  points given by  $\mu_n = n$ . The resulting pattern  $F_r(\mu)$  is then simply given by

$$F_r(\mu) = \sum_{n=-N}^N F_d(n) \frac{\sin \pi(\mu-n)}{\pi(\mu-n)} \quad (3.1.1)$$

Realizable illuminations are obtained if  $N < L/\lambda$ ; the reason for this lies in the fundamental limitations of antennas, because excitations using higher terms result in excessive tolerance and bandwidth problems. The illumination across the aperture which generates this pattern is given by

$$g(p) = \sum_{n=-N}^N F_d(n) e^{-jnp} \quad (3.1.2)$$

where  $p = 2\pi z/L$ , and  $-\frac{L}{2} < z < \frac{L}{2}$

If the aperture is an array of  $M$  elements, the aperture is sampled at intervals  $L/(M-1)$  wide. That is,  $p$  in equation 3.1.2

takes on values given by  $p_m = (m-1)/(M-1)$ , where  $m=1, \dots, M$ , and

$$b_m = \sum_{n=-N}^N F_d(n) e^{-jn(m-1)/(M-1)} \quad (3.1.3)$$

where  $b_m$  is the excitation coefficient of the  $m$ -th radiator. The resulting pattern is found from B.27 to be:

$$\begin{aligned} f(\theta, \phi) &= g(\theta, \phi) \sum_{m=1}^M b_m e^{jkz_m \sin \theta} \\ &= g(\theta, \phi) \sum_{n=-N}^N F_d(n) \sum_{m=1}^M e^{-j \frac{(m-1)}{(M-1)} (n - \frac{L}{\lambda} \sin \theta)} \end{aligned} \quad (3.1.4)$$

where  $g(\theta, \phi)$  is the element pattern. Over a  $\pm 20^\circ$  range in elevation, the element pattern can be considered unity as a good approximation.

Further design flexibility can be obtained by a trans-  
lation of the zeros, which entails redefining the variable  $\mu$  to be  $\mu = (L/\lambda)(\sin \theta - \sin \theta_0)$ ; the angle  $\theta_0$  can now be shifted as well.

The next step is to choose the desired distribution  $F_d(\mu)$ . The RTCA report suggests a  $3^\circ$  cosecant-square beamshape.<sup>1</sup> This means that the field pattern should have a peak at  $3^\circ$  and fall off as the cosecant of the elevation angle for higher angles, up to the coverage limit. Expressed in terms of the parameter  $\mu$ ,

$$F_d(\mu) = \left\{ \begin{array}{l} 0, \quad \mu < 0 \\ \chi, \quad \mu = 0 \\ \frac{1}{\mu}, \quad \mu > 0 \end{array} \right\} \quad (3.1.5)$$

<sup>1</sup>. RTCA Report, p: III A-11 and p. K-4

and the aperture dimensions and the translation angle  $\theta_0$  are chosen to yield a maximum at  $3^\circ$ , and proper fall-off below the horizon. Then equation 3.1.1 becomes

$$F_r(\mu) = \left[ \frac{\chi}{\mu} + \sum_{n=1}^N \frac{(-1)^n}{n(\mu-n)} \right] \frac{\sin \pi \mu}{\pi} \quad (3.1.6)$$

It can be seen that the pattern has nulls at  $\mu=-n$ . In addition the bracketed term can become zero for one negative value of  $\mu$  (assuming  $0 < \chi < 1$ ), giving an additional null. The pattern resulting is shown in Figure 3.3 for  $\chi=.4$ ,  $N=19$ ,  $\theta_0=0$ , and  $L/\lambda=19.11$ . The lobes below the horizon are 35dB down in this idealized case, and above the horizon the pattern is within  $\pm 1.5$ dB of the desired  $\csc \theta$  pattern.

A study of the patterns reveals that for apertures wider than five wavelengths, the sidelobe (or downlobe) level is relatively independent of the aperture height. However, the position of the nulls and lobes directly depends on aperture height. This is indicated in Figure 3.4. The sidelobe level depends largely on the parameter indicated in Figure 3.5. It can be seen that a null at zero ( $\chi=0$ ) gives a fairly high lobe level but it improves for larger values up to a point.

Similarly equation 3.1.3 becomes

$$b_m = g(p_m) = \chi + \sum_{n=1}^N \frac{\exp[-jn(m-1)/(M-1)]}{n} \quad (3.1.7)$$

If  $N=37$ , the elements are approximately a half-wavelength apart, and give a pattern indicated in Figure 3.3. The lobes shift in position but change little in amplitude from the continuous aperture, and the patterns are almost indistinguishable above the horizon. Coverage plots showing constant field intensity contours reveal that this excitation results in a rapid fall-off in range for elevation angles below  $2.5^\circ$ . The low angle range can be improved by using  $\chi=.7$ . The resulting pattern is shown by the solid line antenna pattern in Figure 3.6.

Furthermore the  $3^\circ \csc^2 \theta$  power pattern requirement mentioned in the antenna requirements of the RTCA SC-117 is not consistent with the coverage requirements of

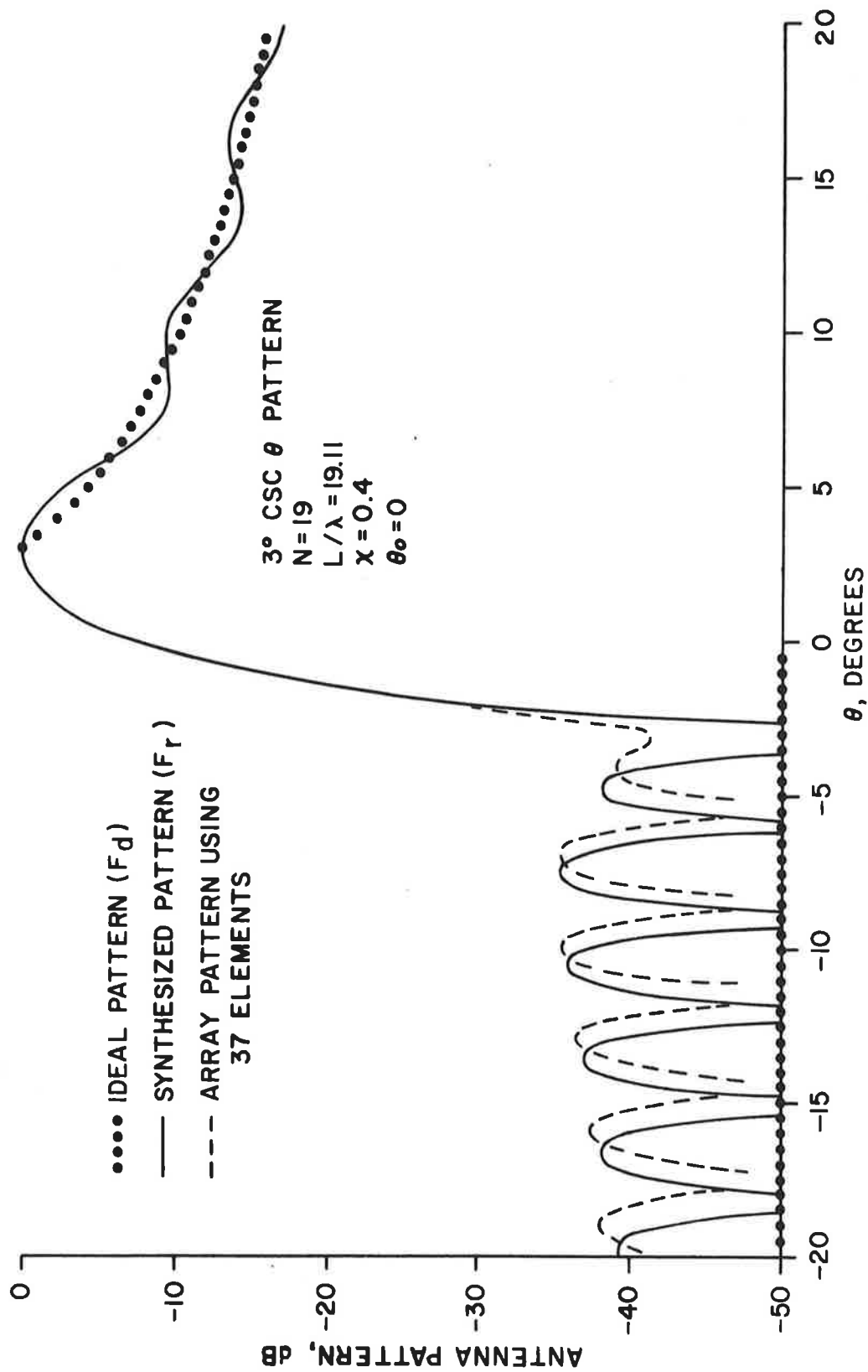


Figure 3.3 Synthesized Patterns in Elevation (Azimuth Antenna)



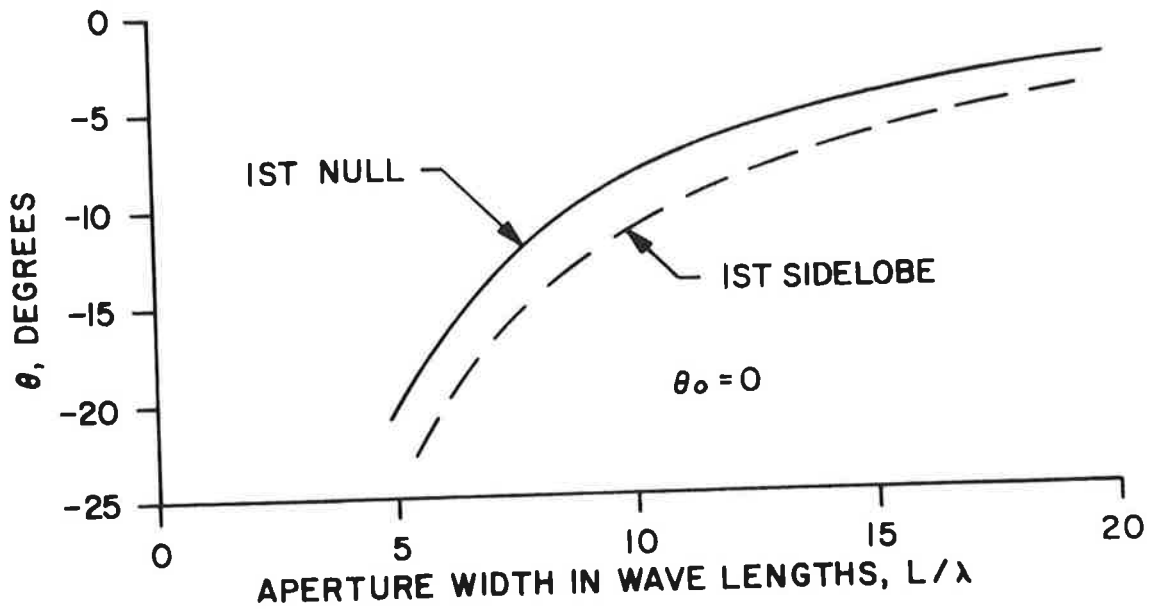


Figure 3.4 Location of First Null and First Sidelobe as a Function of Aperture Height (Azimuth Antenna)

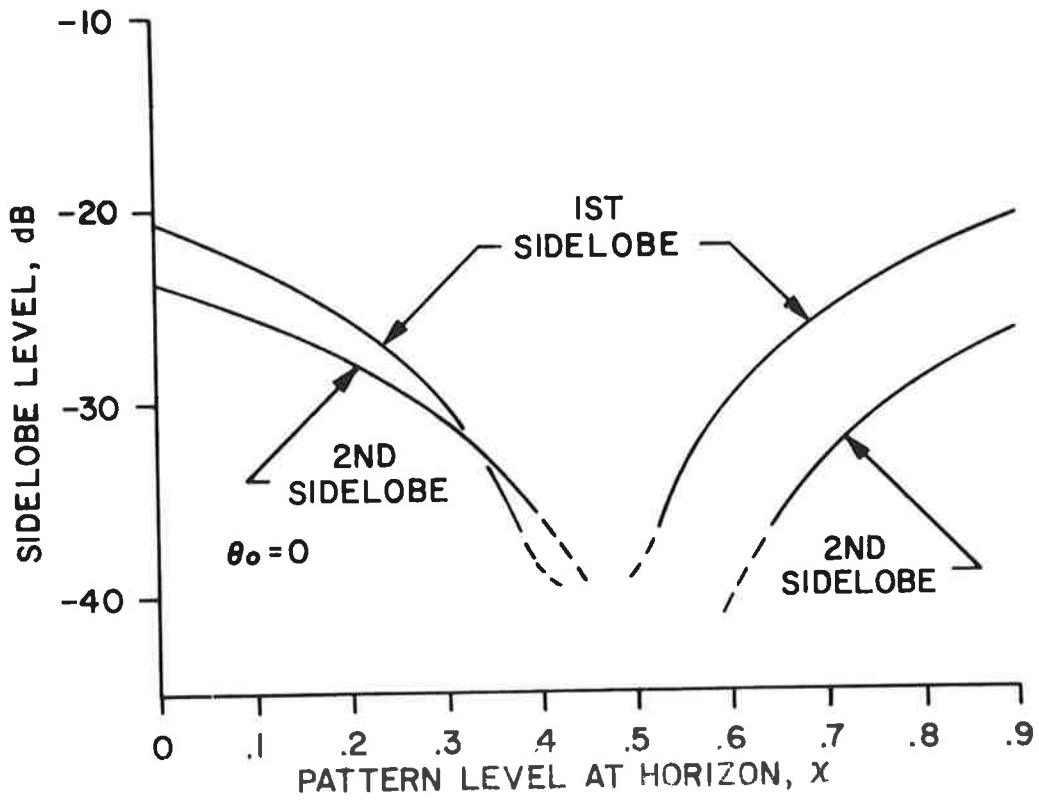


Figure 3.5 Variation of Sidelobe Levels as a Function of the Parameter  $x$

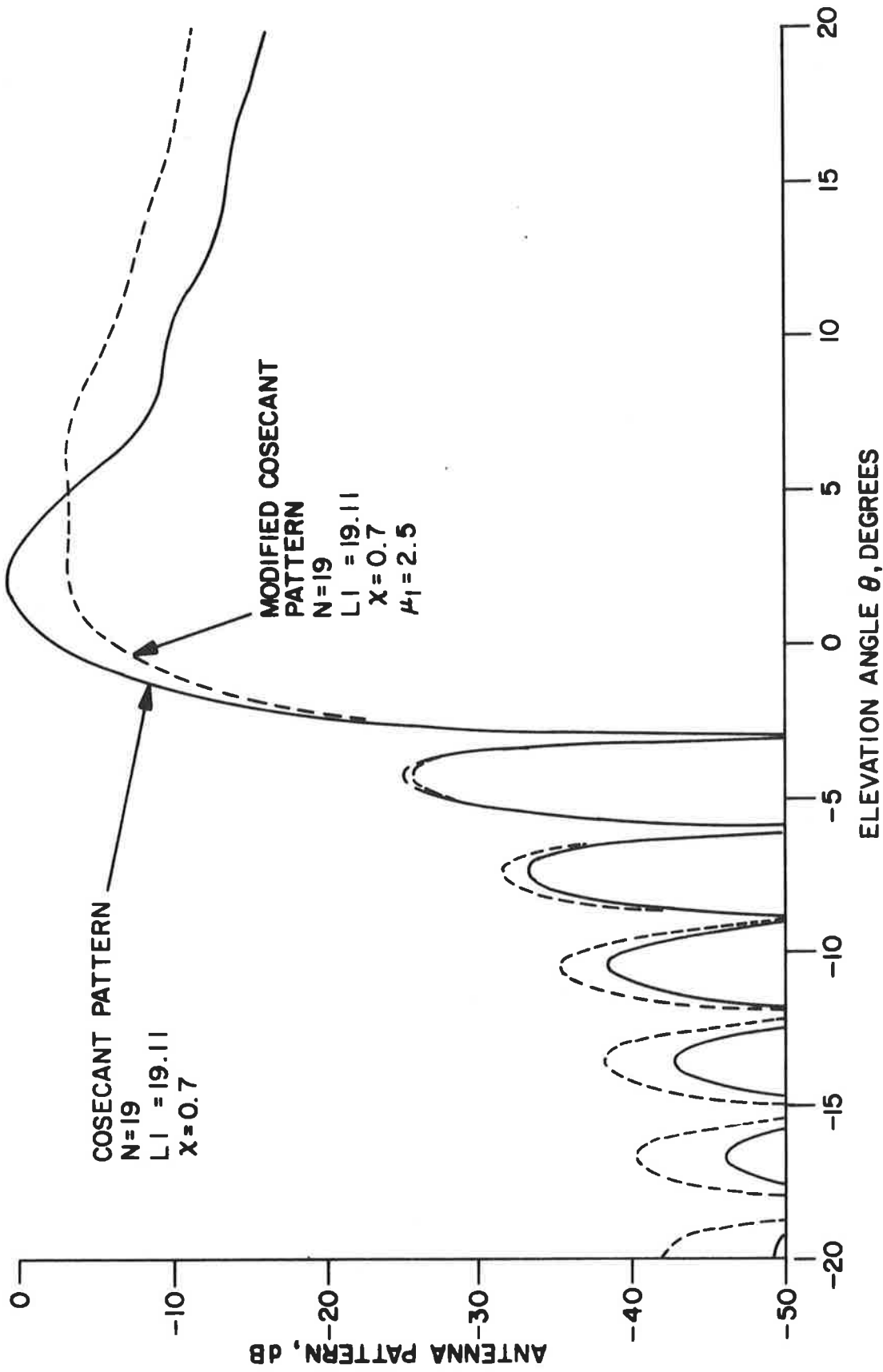


Figure 3.6 Synthesized Antenna. Patterns,  $\text{csc}^2\theta$  and Modified  $\text{csc}^2\theta$  Patterns (Four Foot Aperture)

20,000 feet<sup>1</sup>. The coverage plot in Figure 3.7 gives the constant field intensity contour for a transmitter power level yielding a 25 NM range at 3° elevation. This range assumes no signal attenuation by the medium. It can be seen that the coverage does not extend beyond 10,000 feet. (Changing  $\chi$  to .7 shifts the beam peak down to about 2.3°; a strict 3° csc<sup>2</sup>  $\theta$  pattern gives similar results.) Since the coverage requirements extend to 20,000 feet, a 3° csc<sup>2</sup>  $\theta$  type of beam is not appropriate if coverage above 10,000 feet is operationally necessary.

A pattern can be generated by the same aperture which will meet the requirements, but at the expense of transmitter power. A pattern can be tailored according to the coverage requirements, given mathematically by

$$F_d(\mu) = \begin{cases} 0, & \mu < 0 \\ \chi, & \mu = 0 \\ 1, & 0 < \mu < \mu_1 \\ \mu_1/\mu, & \mu > \mu_1 \end{cases} \quad (3.1.8)$$

where  $\mu = (L/\lambda)(\sin \theta - \sin \theta_0)$ . By choosing  $\chi = .7$ ,  $\theta_0 = 0^\circ$  and  $\mu_1 = (L/\lambda)\sin 7.5^\circ = 2.5$ , where  $N = 19$ ,  $L/\lambda = 19.11$  as before, then the pattern is tailored to the coverage requirements at 25 NM. The resulting pattern is given by

$$F_r(\mu) = \left[ \frac{\chi}{\mu} + \sum_{n=1}^{[\mu_1]} \frac{(-1)^n}{(\mu-n)} + \sum_{[\mu_1+1]}^N \frac{\mu_1(-1)^n}{n(\mu-n)} \right] \frac{\sin \pi \mu}{\pi} \quad (3.1.9)$$

( [ ] indicate that the number is the largest integer  $\leq$  the term within.)

which is shown as a function of elevation angle in Figure 3.6 as the dashed curve. The level has been adjusted to the same transmitter power as the unmodified beam. The resulting coverage is shown as the dashed curve of Figure 3.7. By increasing the transmitter power by 3.5dB the dot-dash coverage is obtained. In view of this, the coverage requirement should be reviewed, since it requires more than a doubling of transmitter power to get the required range.

An examination of the coefficients of excitation required to generate this modified cosecant pattern reveals that the ratios of power required to be delivered to the various elemental dipoles vary over an impractical range. It is

---

1.

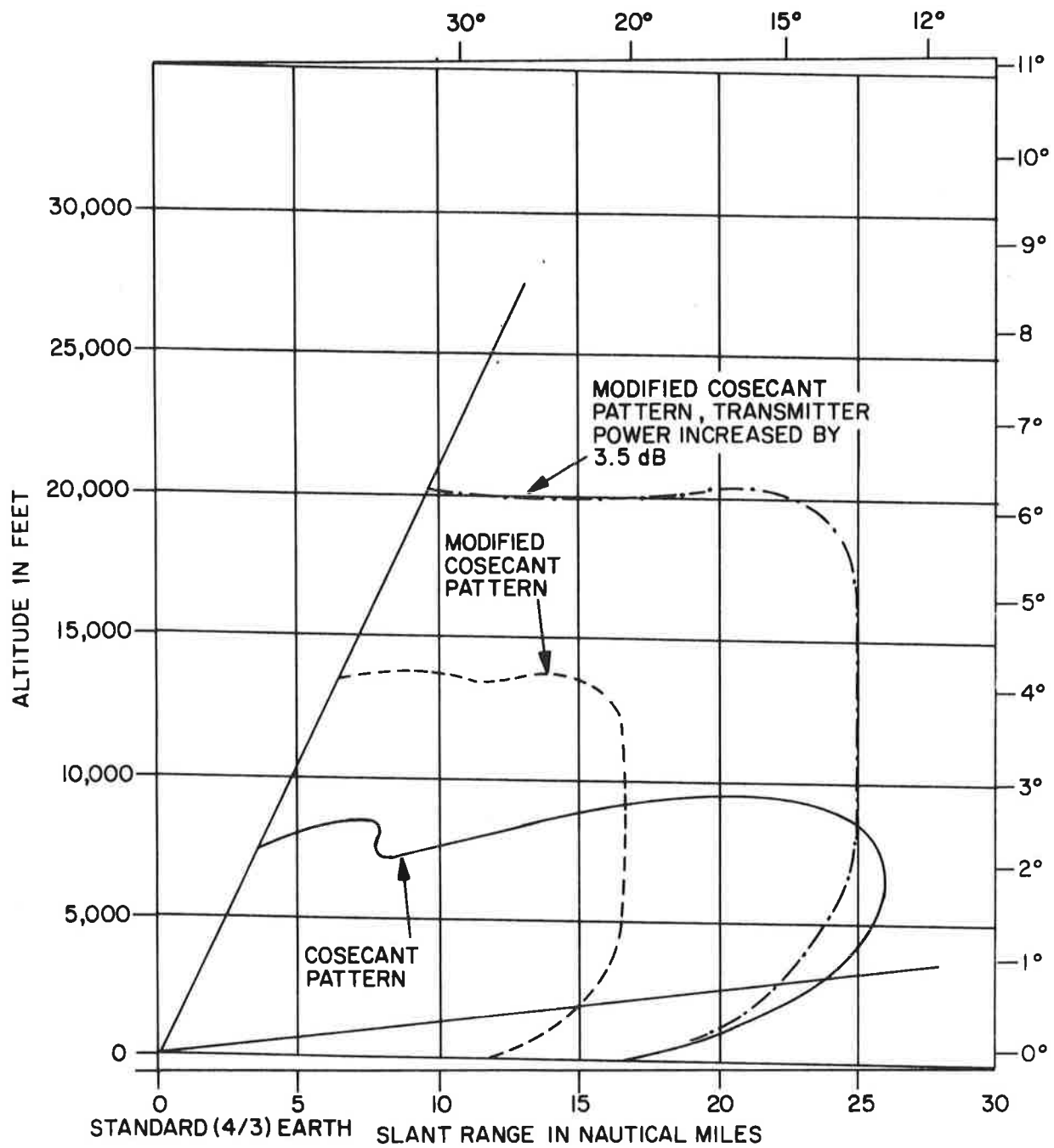


Figure 3.7 Constant Field Intensity Contours Using Synthesized Antenna Patterns (Four Foot Aperture)

important to introduce this constraint into the problem. Since the beam is actually wider for the modified pattern, it seems reasonable that less aperture may be used, even though the fall-off of "down" lobes will be less steep. The resulting current distribution turns out to be more practical.

The criterion used in constraining the range of currents set up in the column is that the coupling values vary by less than 30 dB. The design which follows uses a two foot aperture, has 15 elements, and has a pattern null at  $-6^\circ$ . The coupling values are given in Table 3.1. If the values of power are added up, the result is unity. That is, the coupling values represent the power division distribution.

Table 3.1 Power Divider Coupling Values For Azimuth Antenna Vertical Column

Element Number	Power, dB	Phase, Degrees
1	-30.4	-34.7
2	-24.1	-77.0
3	-22.9	-71.7
4	-17.2	-67.5
5	-15.5	-71.0
6	-11.8	-50.9
7	- 7.9	-51.9
8	- 3.7	0.0
9	- 7.9	51.9
10	-11.8	50.9
11	-15.5	71.0
12	-17.2	67.5
13	-22.9	71.7
14	-24.1	77.0
15	-30.4	34.7

This is not considered to be a difficult distribution to achieve in practice. It is possible that by altering the phase of the  $(\sin x)/x$  beams, that further improvement in cut-off performance below the horizon can be achieved. This will be studied further in the next year.

The resulting pattern is shown in Figure 3.8. It has its peak around  $4.5^\circ$ , and is down by less than 2 dB at  $1^\circ$  elevation, has a null at  $-6^\circ$ , and "down-lobes" 23 dB below the peak. The constant field intensity contours are shown

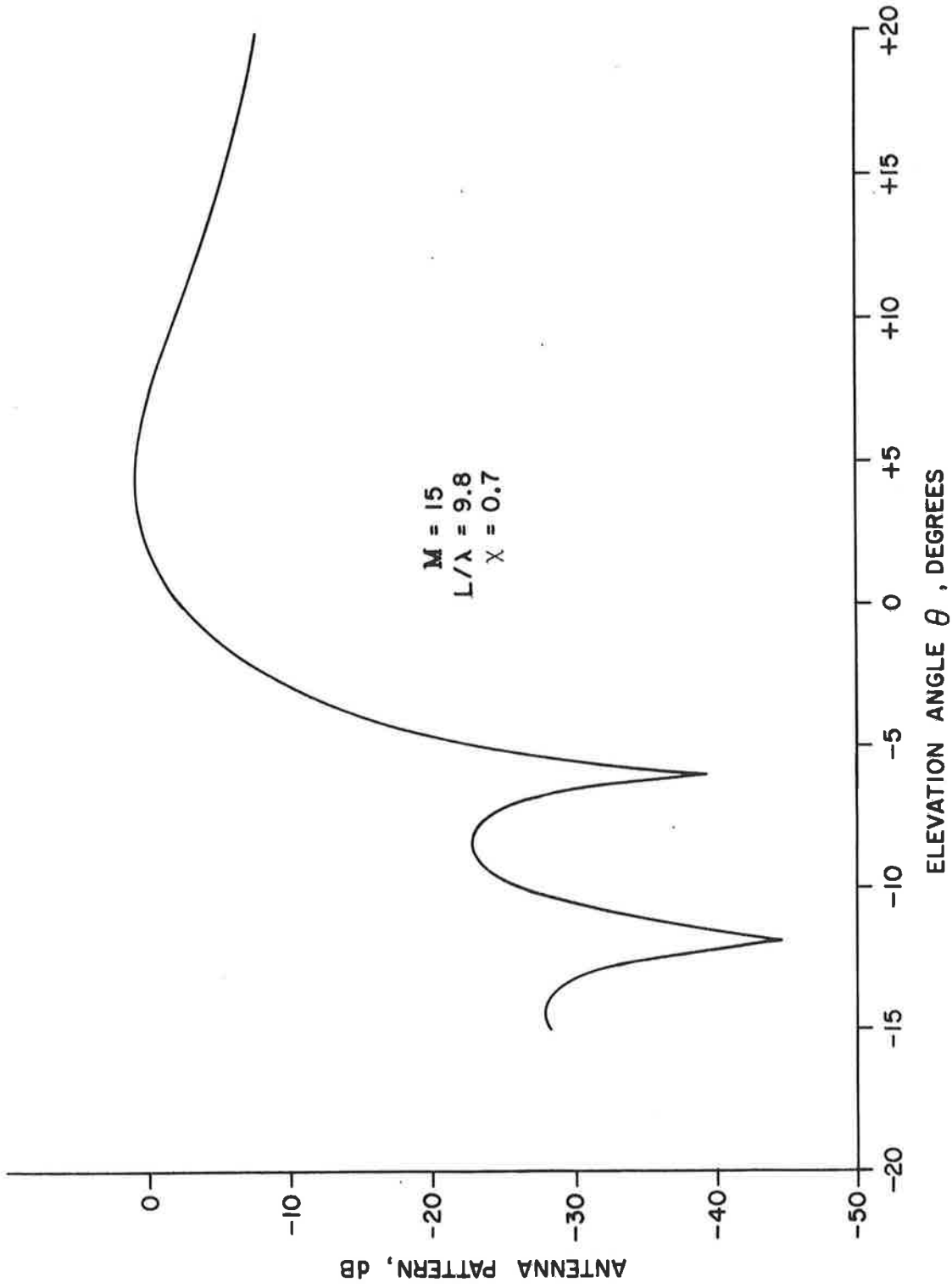


Figure 3.8 Synthesized Antenna Pattern (Two Foot Aperture)

in Figure 3.9. It can be seen that the full coverage recommended by the RTCA committee is achieved.

The elements themselves are assumed to be in stripline. A typical layout is shown in Figure 3.10. Other designs are also under consideration. It is important to reduce the amount of work involved in its fabrication in order to keep costs down, since the element costs are a large part of the total array costs.

### 3.1.2 PLANAR ARRAY DESIGN

It is shown in Appendix B.1 that a planar array pattern is given by the product of two perpendicular linear arrays. That is, for the azimuth antenna, the columns can be designed as in section 3.1.1; the azimuthal behavior is entirely contained in the results of a linear array along the y-axis. From equation (b.9), the far-field of this linear array can be written

$$f(\theta, \phi) = g(\theta, \phi) S_M(\theta) \sum_{n=1}^N C_n e^{-jknd_y(\cos \theta \sin \phi - \cos \theta_f \sin \phi_b)} \quad (3.1.10)$$

The  $C_n$ 's must be chosen to give a low sidelobe level in azimuth. Here a -25dB design was chosen, which can be generated by a cosine-squared on a pedestal distribution, where the pedestal height is 0.5. Specifically,

$$C_n = \cos^2 \left[ \left( \frac{n-1}{N-1} - \frac{1}{2} \right) 180^\circ \right] + .5 \quad (3.1.11)$$

When  $n=1$  or  $N$ , then  $C_n=.5$  (edge elements), and when  $n=\frac{N-1}{2}$ ,  $C_n=1.5$  (center element). (If  $N$  is even, there is no element actually located exactly in the center; the two central elements will have coefficients  $C_n$  approximately equal to 1.5).

The total width of the array is given by

$$L = (N-1) d_y \quad (3.1.12)$$

The width must be adjusted for a given distribution to give the desired beamwidth. The length is related inversely to the beamwidth, so that this is an easy task:

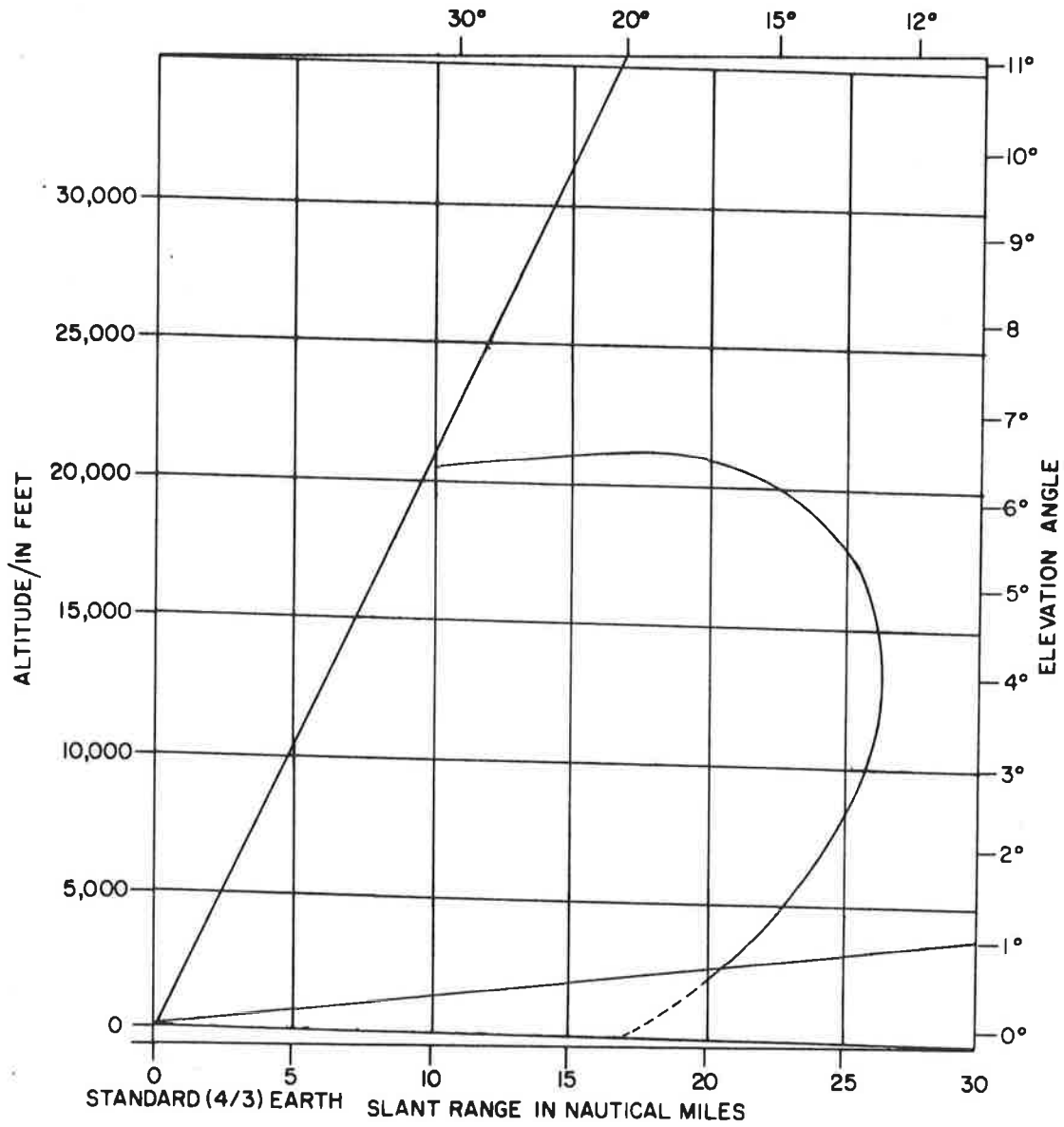


Figure 3.9 Constant Field Intensity Contours Using Synthesized Antenna Patterns (Two Foot Aperture)



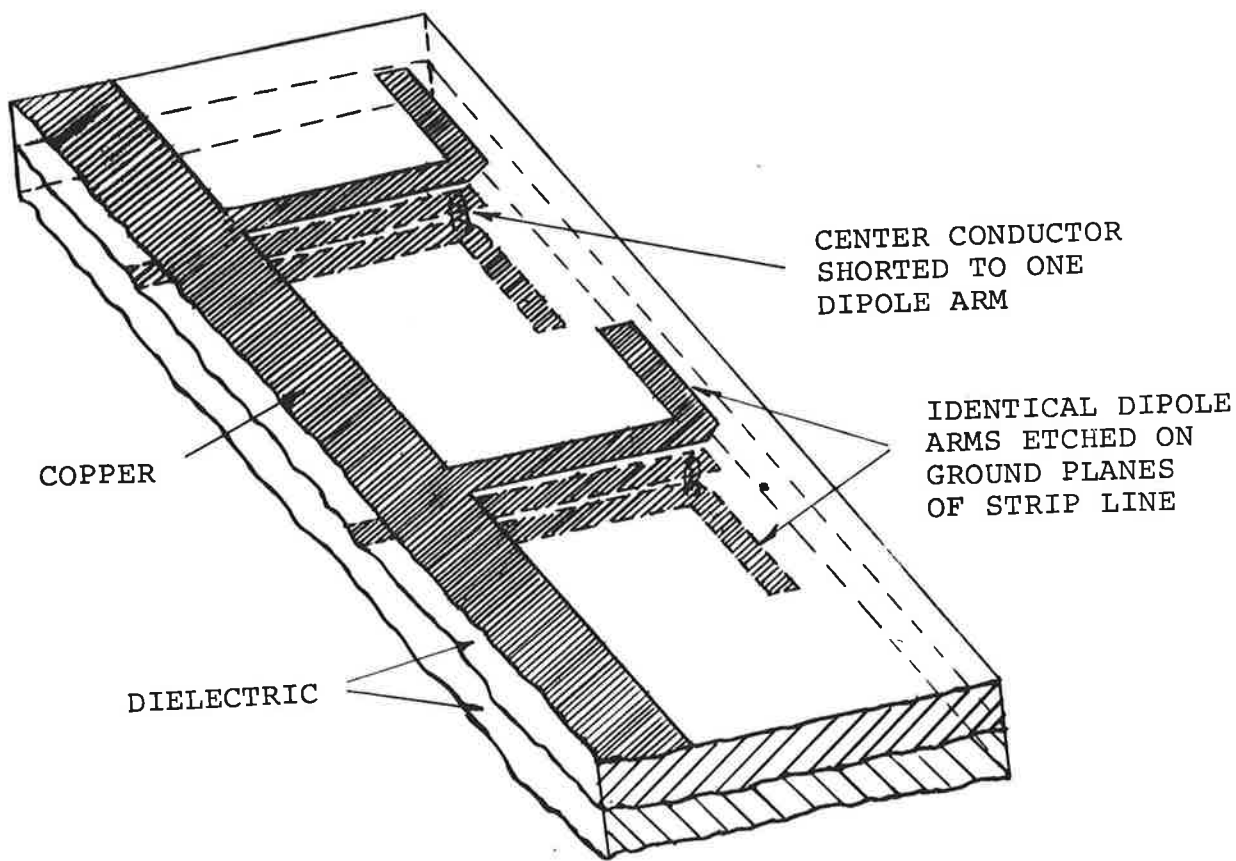


Figure 3.10 Typical Printed Circuit Dipole Construction

$$BW = \frac{\gamma L}{L} = \frac{\gamma \lambda}{(N-1) d_y} \quad (3.1.13)$$

The beam broadening factor,  $\gamma$ , for this distribution is  $61^\circ$ , which can be established from one pattern.

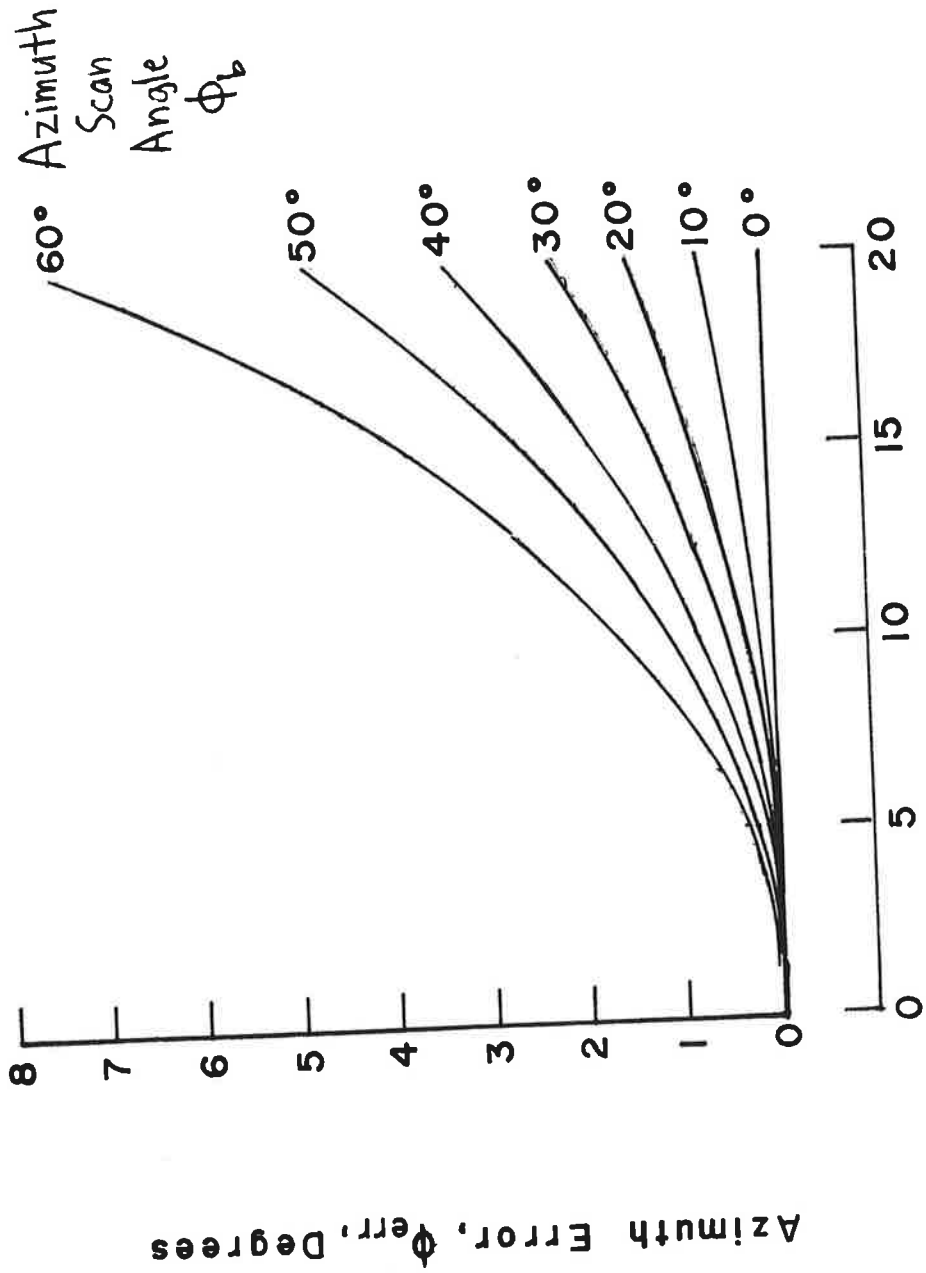
The choice of element spacing  $d_y$  is premised on the basis of cost and the avoidance of grating lobes. To keep costs down the spacing should be as wide as possible. As the spacing is increased, however, unwanted grating lobes form at the scan coverage limits. This results in unacceptable reflections and sidelobes. The criterion for spacing is:

$$\frac{d}{\lambda} < \frac{1}{1 + |\sin \phi_0|} \quad (3.1.14)$$

where  $\phi_0$  is the maximum scan angle.

The major limitation in the use of linear arrays for the azimuth function is the problem of coning, which is described in section 2.1.1. The error due to coning (called skew) is given in Figures 3.11 and 3.12 which are the same as Figures 2.2 and 2.3. It is evident that the skew error is unacceptably large for configurations I ( $\pm 40^\circ$  coverage) and K ( $\pm 60^\circ$  coverage). Other configurations require  $\pm 20^\circ$  coverage in azimuth, and the situation is not so bad. From Figure 3.12 it can be seen that the skew error is less than half a degree over the coverage except for a region at the upper right hand corner of the diagram; this is not a serious reduction in coverage. The worst error is  $1.4^\circ$ , and occurs in a region where accuracy is not critical-for the final approach, aircraft would be comfortably in the lower control region where the accuracy is high.

The curves given in Figures 3.11 and 3.12 use a focus angle  $\theta_f$  of zero, which means that at the horizon there is no skew error. If some other focus angle is used the skew error will be zero at that elevation but not at the horizon. By choosing a focus angle of  $8.94^\circ$ , the skew error at the low end of the elevation coverage (namely  $1^\circ$ ) and at the azimuth coverage extreme ( $\pm 20^\circ$ ) will be  $-.25^\circ$ . However, the error at higher elevations than the focus angle will be reduced. This is shown in Figure 3.13. The worst error is  $1.07^\circ$  in the coverage volume.



Elevation Angle,  $\theta$ , Degrees

Figure 3.11 Azimuth Errors Due to Coning

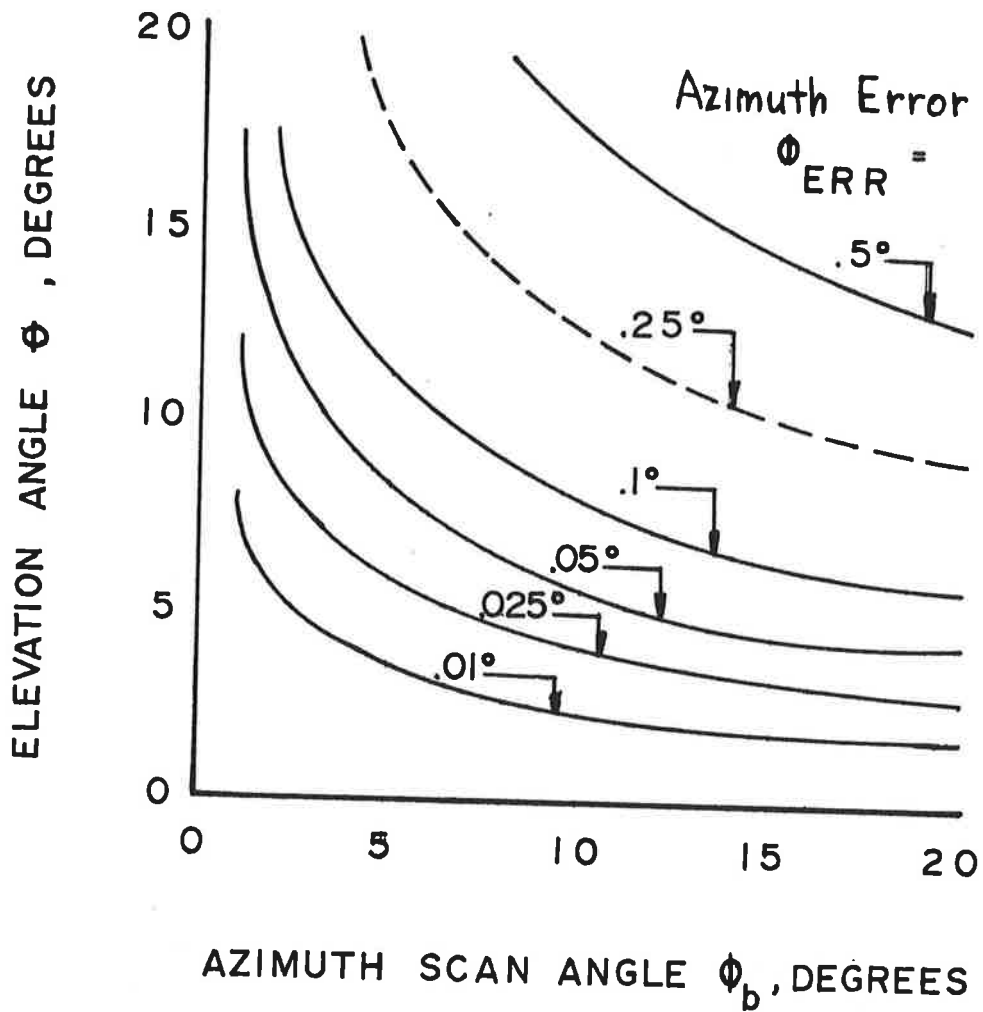


Figure 3.12 Error Contours in Azimuth Due to Coning  
 (Focused for 0° Elevation)

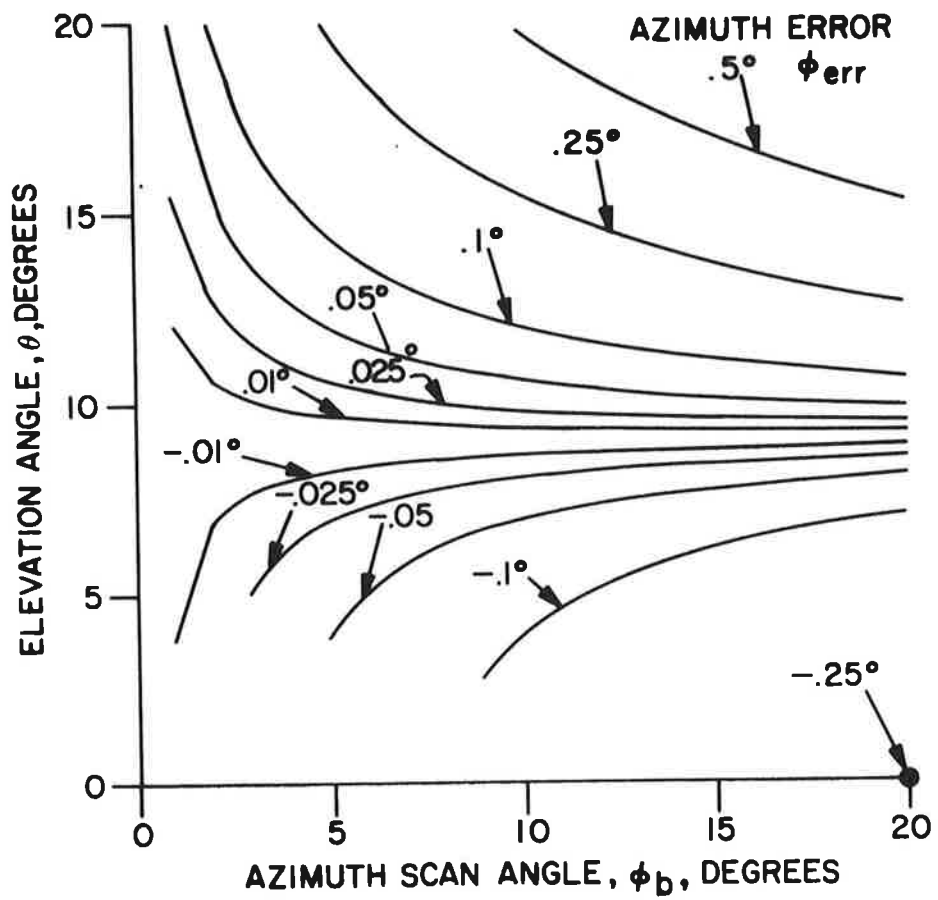


Figure 3.13 Error Contours in Azimuth Due to Coning (Focused for  $8.94^\circ$  Elevation)

Since linear arrays are only being considered for configurations having  $\pm 20^\circ$  azimuth coverage, the grating lobe criterion on the spacing yields, from (3.1.14);

$$\frac{d}{\lambda} < \frac{1}{1 + |\sin 20^\circ|} = .74 \quad (3.1.15)$$

Actually, it is best to use spacings substantially less than that required by this criterion, since sidelobes begin to rise before the full-blown grating lobe appears. Also, a convenient element number,  $N$ , should be chosen. Thus, for a  $1^\circ$  beamwidth, 96 elements spaced at about  $0.65\lambda$  apart is the choice made here. For  $2^\circ$ , 48 elements are chosen with the same spacing; for  $4^\circ$ , 24 elements. (The elements referred to here are actually vertical columns of elements, designed separately in section 3.1.1).

There is another problem which should be mentioned in relation to linear arrays, namely squint error. Squint errors result from asymmetries in the main beam. When linear arrays are scanned off broadside, the beam becomes slightly asymmetric, so that a processor which interprets the bore-sight as being located halfway between the 1/10 power points on the beam will locate the beam center at an angle other than the angle where the beam peaks. For  $\pm 20^\circ$  of scan this problem is negligible.

The parameters chosen here along with the feed network described in Section 4.1, and the element columns of section 3.1.1, constitute the azimuth linear array design.

### 3.1.3 CYLINDRICAL ARRAY DESIGN

The column design, discussed in section 3.1.1, can proceed independently of the horizontal design to a great degree. The elevation pattern obtained, however, must be multiplied by a slowly varying function in elevation, namely  $R_N(\theta, \phi)$  of equation B.27. The variations in elevation are related to the defocusing exhibited by cylindrical arrays. The effects of defocusing on the azimuth pattern are beam broadening and sidelobe degradations at elevation angles other than one chosen elevation angle  $\theta_f$ , the focus angle. The criterion for the allowable degradation at the elevation coverage limits is not certain. The RTCA recommendations are for 2:1 decrease in accuracy requirement at the coverage extremes, which suggests that a 2:1 increase in beamwidth would be tolerable, as long as other factors don't degrade accuracy at the same time. The RTCA report also calls for sidelobes of less than -20dB to keep interchannel interference down. For the azimuth antenna a design goal of -25dB was chosen to allow room for random errors and other imperfections. While one-degree beam-

widths have been specified, it is possible that time bandwidth limitations or scan rate changes may necessitate larger beamwidths, so that  $2^\circ$  and  $4^\circ$  designs are considered as well.

Several variables are utilized in determining which antenna specifications are required in order to have the antenna performance meet the far field antenna pattern criteria mentioned above. These variables and some of their effects on antenna performance are listed below.

Beam broadening factor,  $\gamma$  -- equal to the product of the aperture in wavelengths and the antenna beamwidth. It depends primarily on the distribution of energy or excitation across the aperture. This factor varies from  $52^\circ$  for a uniform aperture distribution to  $70^\circ$  for a typical reflector. Here  $\gamma$  is about  $61^\circ$ . Increasing  $\gamma$  allows higher sidelobe suppression.

Aperture width,  $L$  -- the width of the projection of the illuminated portion of the antenna on a line perpendicular to the boresight direction. Increasing the aperture narrows the beamwidth.

Active sector,  $\phi_a$  -- that angular portion of the antenna which is actually transmitting energy, as the active sector is decreased while maintaining the aperture width  $L$  the sidelobe level goes down and the beamwidth decreases but the radius of the antenna must be increased. Thus the size of the antenna and probably the cost increases also.

Antenna radius,  $R$  -- as the radius of the antenna is increased while aperture is held constant, the active sector decreases.

Element spacing,  $d$  -- the distance between the elements. As  $d/\lambda$  is increased beyond a certain point grating lobes begin to appear and the sidelobes well away from the main beam increase. As  $d/\lambda$  is decreased antenna performance does not deteriorate but the cost increases since more elements are required to excite the same aperture.

Angular element spacing,  $\phi$  -- determined by  $R$  and  $d$ .

Azimuth coverage angle,  $\phi_c$  -- the minimum angular distance through which the antenna must be capable of steering the beam.

Number of elements in the active sector,  $N_a$ .

Total number of elements in the antenna,  $N_T$ . Since the complexity and cost of the antenna is closely related to  $N_T$ ,

(see section 7.5), it is desirable to keep  $N_T$  as low as good performance allows.

Elevation focus angle,  $\theta_f$ . Optimum patterns are only obtained at an elevation angle called the focus angle. At angles above and below the focus angle defocusing causes gradual broadening of the beamwidth and deterioration of the sidelobes. Since it is more important to have good performance at the horizon than at high elevations, the focus angle is chosen with this in mind.

Azimuth beamwidth, BW.

Design azimuth beamwidth,  $BW_d$ .

Azimuth beamwidth at zero degrees elevation,  $BW_0$ .

Azimuth beamwidth at the focus angle,  $\theta_f$ ,  $BW_f$ .

Azimuth beamwidth at twenty degrees elevation,  $BW_{20}$ .

Sidelobe level, SLL, dB.

Sidelobe level at zero degrees elevation,  $SLL_0$ .

Sidelobe level at twenty degrees elevation,  $SLL_{20}$ .

Defocusing phase error,  $\bar{\Phi}_{err}$  (see equations B-30, B-31).  $\bar{\Phi}_{err}$  represents the phase difference between the contributions from the elements at the center and the edge of the active sector at a given elevation angle, ( $\bar{\Phi}_{err} = 0$  at  $\theta_f$ ).

Two antenna designs for the same beamwidth that have different  $\phi_a$ 's and/or  $\theta_f$ 's but that have the same  $\bar{\Phi}_{err}$  at a given elevation angle will have a very similar antenna pattern at that elevation angle. This fact makes  $\bar{\Phi}_{err}$  a useful parameter for assessing the effects of changes in physical antenna parameters.

The physical antenna parameters are the radius, element spacing, aperture, and the number of elements (active and total). The design parameters (active sector, focus angle, beam broadening factor, and defocusing phase error) along with the physical parameters determine the performance parameters (beamwidths and sidelobe levels). The performance parameters are the requirements which must be met, and the other parameters must be derived from them.

The sidelobe level was chosen as -25dB; it is expected that the actual performance obtained will be at least -20dB. The difference is due to phase shift quantization errors, random phase and amplitude errors, and defocusing. Several aperture distributions were considered, but the cosine-squared on a pedestal of .5 distribution was chosen, which results in a -25dB sidelobe level in the ideal case (focused, no phase or amplitude errors). This distribution is very similar to the Taylor distribution designed for -25dB sidelobes. This corresponds to a beam broadening factor  $\gamma$  of  $61^0$ .



The remainder of the parameters are chosen so as to minimize beam broadening and sidelobe level deterioration by keeping defocusing down, but avoiding costly solutions. The treatment which follows differs from conventional approaches in that variations of element pattern with spacing are tacitly considered. This leads to the conclusion that for a given aperture width the total number of elements is not strongly dependent on the radius, a fact which allows wide latitude in the choice of parameters. The number of elements is a good measure of the cost of the array.

The fact that the active sector is switched (or otherwise translated) around the arc of the array means that little phase scanning takes place, thus coning errors are insignificant. (This technique allows the coverage to be extended to  $\pm 40^\circ$  or  $\pm 60^\circ$  to meet the requirements of the I and K configurations.) The center element of the active sector always is phased for essentially broadside scan. Similarly, edge elements contribute to beams formed at an angle equal to half the active sector. This is shown in Figure 3.14. The elements at the edge do not contribute to the main beam at their pattern maximums.

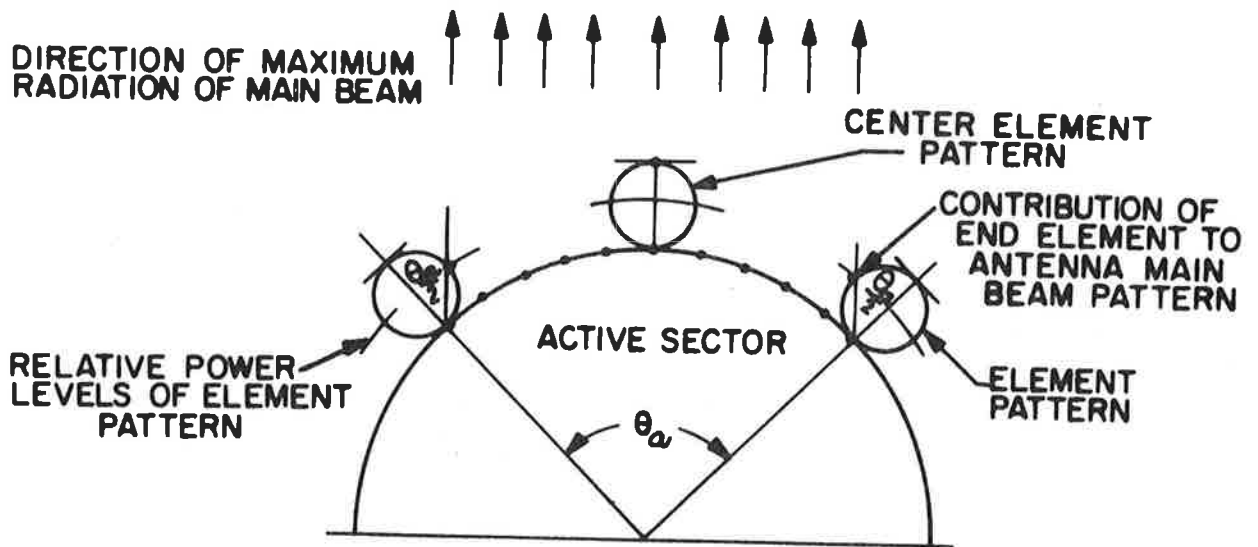


Figure 3.14 Element Pattern Contributions to Radiation from a Cylindrical Array

(It should be noted that the phase should be the same over the element pattern. This subject is not thoroughly treated in the literature.)

The elements in the vicinity of the center of the active sector are essentially "scanned" to broadside, while the elements near the edge are "scanned" to an angle given by  $\phi_a/2$ . Arguing by analogy with linear arrays, the center elements "see" a broadside scan environment, while edge elements "see" a  $\phi_a/2$  scan environment. It is assumed that the active element pattern is essentially that of a linear array in the respective scan state. The active element pattern, which takes into account mutual coupling between elements, depends strongly on the spacing.<sup>1</sup> The case here corresponds to H-plane element patterns for dipoles in front of a ground plane. For a dipole-to-reflector spacing of  $.25\lambda$  (used throughout this report), the 3dB element pattern beamwidth has a dependence on spacing given in Table 3.2.

Table 3.2 Relation Between Element Pattern Beamwidth and Element Spacing

Element Spacing, Wavelengths	Element Pattern Beamwidth
.5	111°
.6	80°
.7	57°
.8	38°

It can be seen from this table that the wider spacings cause narrower element patterns. If the edge element look angle ( $\phi_a/2$ ) is greater than the element pattern half-beamwidth, the contribution will be smaller than predicted by an assumed pattern based on an isolated dipole in front of a ground plane. For look angles less than the element pattern half-beamwidth, the main beam pattern and first few sidelobes are not sensitive to the choice of element patterns used for computation.

Once the active sector is assumed, the spacing is chosen by interpolation from Table 3.2. When the active sector and

<sup>1</sup> J. L. Allen, et.al., "Phased Array Radar Studies," Technical Report #381, March 1965, pp. 292, 294.

element spacing are fixed the number of active elements,  $N_a$ , required for each angular active sector can be determined. Where this value is non-integer it is rounded up so as not to increase the element spacing beyond the maximum. After rounding, the spacing is re-calculated to make  $N_a$  exactly fit the active sector.

The total number of elements required for each design is determined from:

$$N_T = N_A \left( \frac{\phi_c + \phi_a}{\phi_a} \right) \quad (3.1.16)$$

where:  $N_a$  is not rounded up prior to being used in the equation and  $N_T$  is rounded up.

All these calculated values are tabulated in Table 3.3 for maximum element spacings determined by Table 3.1.

A useful observation can be made from this table for maximum element spacings; although the number of elements required for the active sector increases as the size of the active sector increases, the total number of elements is not strongly dependent on the size of the active sector, for a given aperture width. (On the other hand, for a fixed spacing the total number of elements varies significantly with the active sector.)

The reason for this behavior can be seen by rewriting equation 3.1.16:

$$N_T = \left( 1 + \frac{\phi_c}{\phi_a} \right) N_A \quad (3.1.17)$$

wider active sectors decrease the bracketed term; at the same time wider active sectors require broader element patterns, which from Table 3.2 require narrower spacing, thus increasing  $N_A$ . The two factors tend to neutralize each other.

From the discussion in Appendix B it can be seen that better performance is obtained from narrower active sectors. This can be seen from equation B.37:

$$\bar{\phi}_{err} = \frac{180^\circ \gamma}{\phi_{BW}} \tan \left( \frac{\phi_a}{4} \right) (\cos \theta_f - \cos \theta) \quad (3.1.18)$$

where the elevation angle  $\theta$  is taken at the horizon or at  $20^\circ$ , the coverage limit. The defocusing error  $\bar{\phi}_{err}$  is a good measure of the performance, in that higher defocusing errors imply higher sidelobes and beam broadening. This can be seen from Figure 3.15, which shows a typical set of

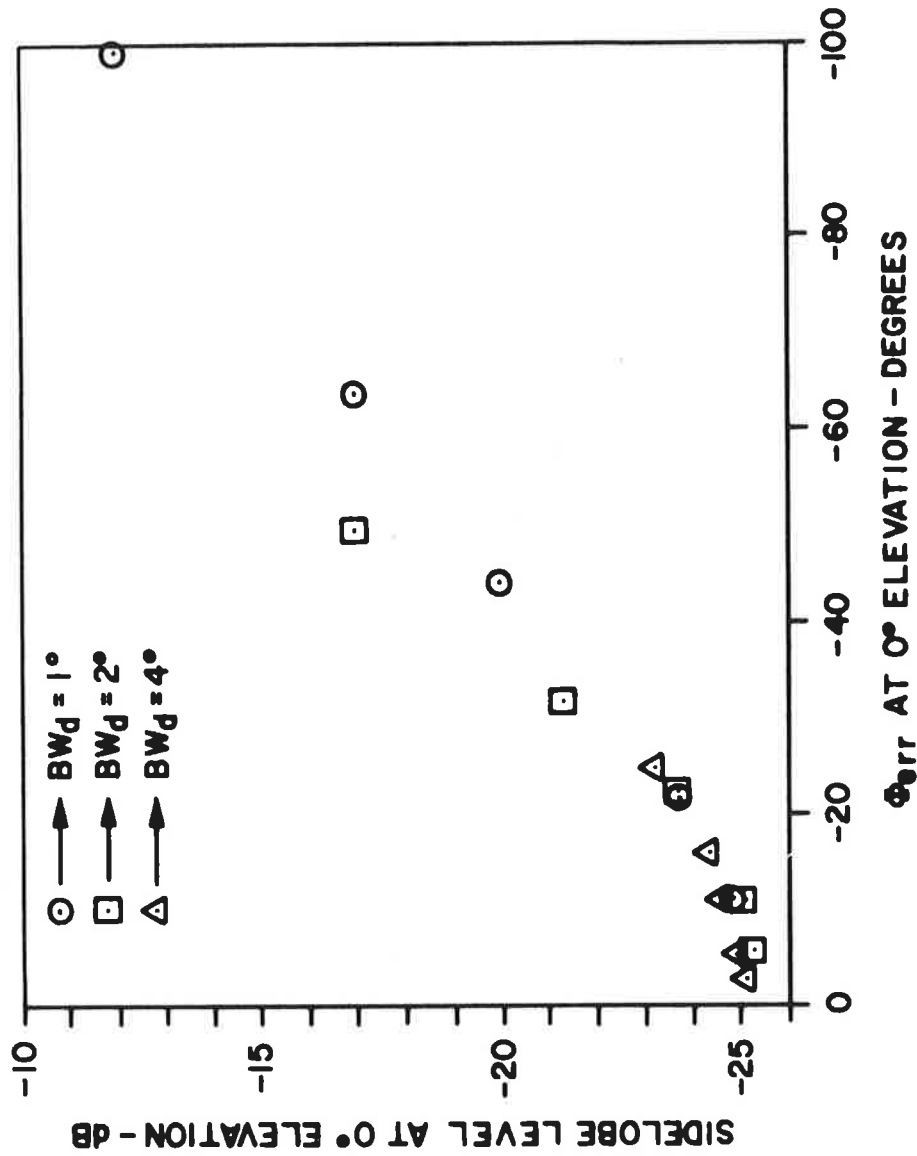


Figure 3.15 Scatter Plot of Sidelobe Level at 0° Elevation Vs.  $\Phi_{err}$

Table 3.3 Calculated Physical Antenna Parameters

	$\phi_a^\circ$	R (cm)	Na	Nominal Spacing (MAX)		Spacing for Na To Exactly Fit $\phi_a$		$\phi_c=80^\circ$	$\phi_c=120^\circ$
				$d/\lambda$	$d/\lambda$	$N_T$	$N_T$		
BW=1° L=353.304 CM	40	516.496	78	0.79	0.786	233	310		
	45	461.614	82	0.76	0.752	228	297		
	50	417.994	84	0.74	0.739	218	285		
	55	382.572	88	0.71	0.710	215	279		
	60	353.304	93	0.68	0.677	216	273		
	65	328.778	97	0.66	0.654	215	274		
	70	307.983	101	0.64	0.634	215	272		
	75	290.183	105	0.62	0.615	216	271		
80	274.822	109	0.60	0.599	217	272			
BW=2° L=176.652 CM	40	258.248	39	0.79	0.786	116	155		
	45	230.807	41	0.76	0.752	113	149		
	50	308.997	42	0.74	0.739	109	142		
	55	191.286	44	0.71	0.710	107	139		
	60	176.652	47	0.68	0.670	108	139		
	65	164.389	49	0.66	0.647	108	137		
	70	153.992	51	0.64	0.628	108	136		
	75	145.091	53	0.62	0.610	108	136		
80	137.411	55	0.60	0.593	109	136			
BW=4° L= 88.326 CM	40	129.124	20	0.79	0.767	58	78		
	45	115.404	21	0.76	0.734	57	75		
	50	104.499	21	0.74	0.739	54	71		
	55	95.643	22	0.71	0.710	53	69		
	60	88.326	24	0.68	0.656	54	70		
	65	82.194	25	0.66	0.634	54	69		
	70	76.996	26	0.64	0.615	54	68		
	75	72.546	27	0.62	0.598	54	68		
80	68.705	28	0.60	0.583	55	68			

points. From equation B.37 above it can be seen that for active sectors of  $90^\circ$  or less, the defocusing error is almost proportional to active sector.

This would suggest using the narrowest active sector possible. However, there are two reasons for avoiding this: (1) the radius increases significantly--the structural problem in maintaining tolerances becomes more severe; cable lengths become greater, resulting in higher losses and more serious tolerance problems; and the structure becomes more bulky; (2) components become more complicated--lenses are larger, switching designs require higher order switches. An example of the latter is that for a coverage of  $\pm 60^\circ$ , an active sector of  $60^\circ$  calls for SP3T switches; to use a smaller active sector, SP4T switches would be required. Another point is that if full  $360^\circ$  coverage is eventually required, an active sector should be divisible into  $360^\circ$ . This would admit active sectors of  $90^\circ$ ,  $72^\circ$ ,  $60^\circ$  and  $45^\circ$ . The studies performed indicate that an active sector of  $60^\circ$  results in patterns that are adequate in terms of the criteria set down in this report. In the event that these criteria are changed, the choice of  $60^\circ$  will have to be reviewed.

It remains to determine the focus angle,  $\theta_f$ .

Using  $\phi_a=60^\circ$  and the corresponding dimensions from the above table, computer calculations (using continuous phase shifters) were executed to determine the 3dB beamwidth (BW) at  $0^\circ$ , at the focus angle, and at  $20^\circ$ , and to determine the sidelobe level (SLL) at  $0^\circ$  and  $20^\circ$ . These calculations were executed for focus angles of  $5^\circ$ ,  $7^\circ$ ,  $10^\circ$ ,  $12^\circ$  and  $15^\circ$  for the design beamwidths of  $1^\circ$ ,  $2^\circ$ , and  $4^\circ$ . The results of these computer calculations are plotted in Figures 3.16, 3.17 and 3.18

The determination of an optimum focus angle,  $\theta_f$ , for an active sector of  $60^\circ$  involves a trade-off between poor performance at  $20^\circ$  elevation and good performance at the horizon for the lower focus angles. The  $2^\circ$  and  $4^\circ$  beamwidth cases appear to have a range of focus angles over which the calculated beamwidths are sufficiently close to nominal and the calculated SLL at  $0^\circ$ ,  $SLL_0$ , is close to  $-25\text{dB}$ .

Determination of focus angle only presents a problem in the  $1^\circ$  beamwidth case. From the plot of the computer results it was determined that  $\theta_f$  should probably lie between  $7^\circ$  and

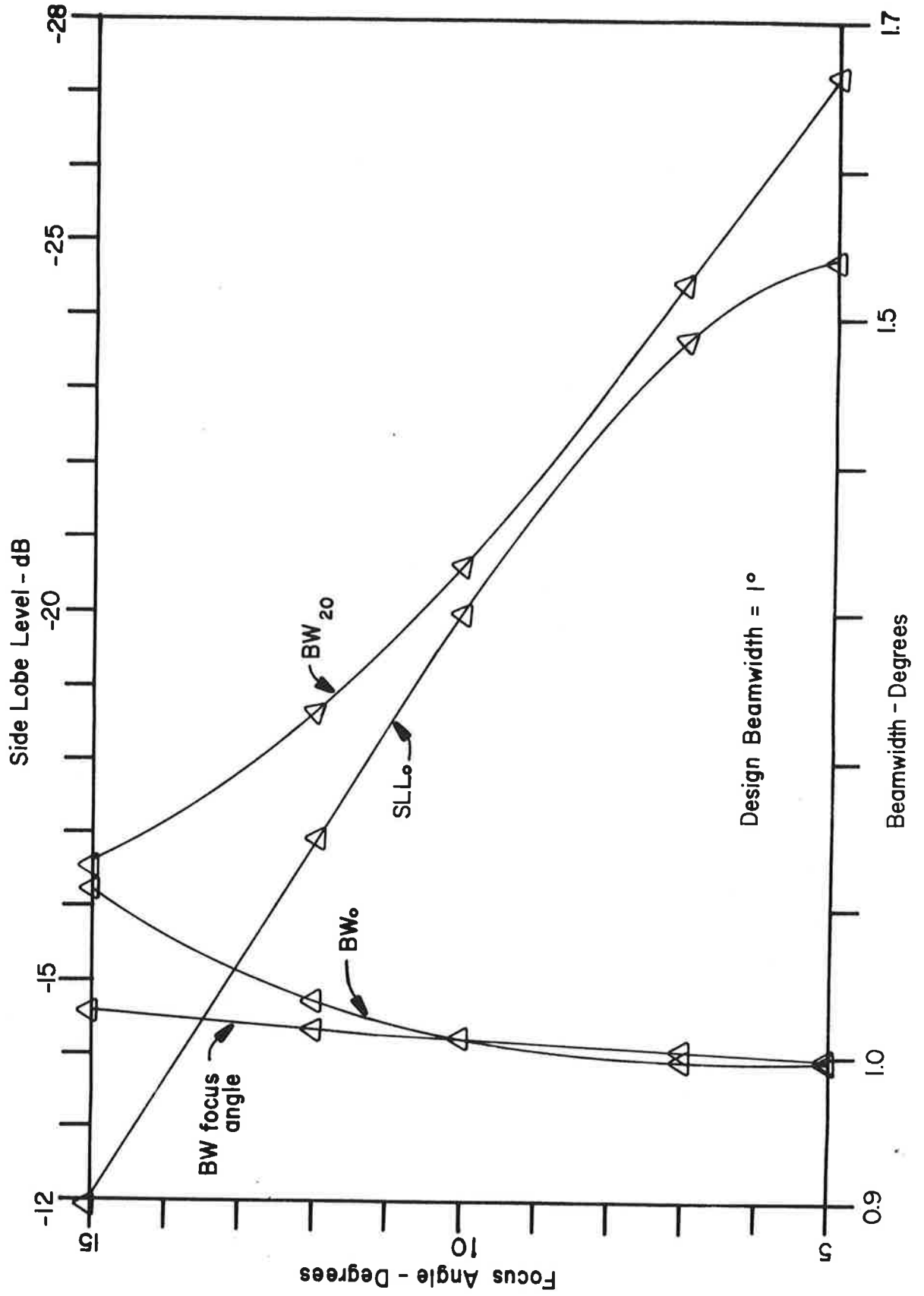


Figure 3.16 Variation of Sidelobe Level and Beamwidth with Focus Angle, 1° Design

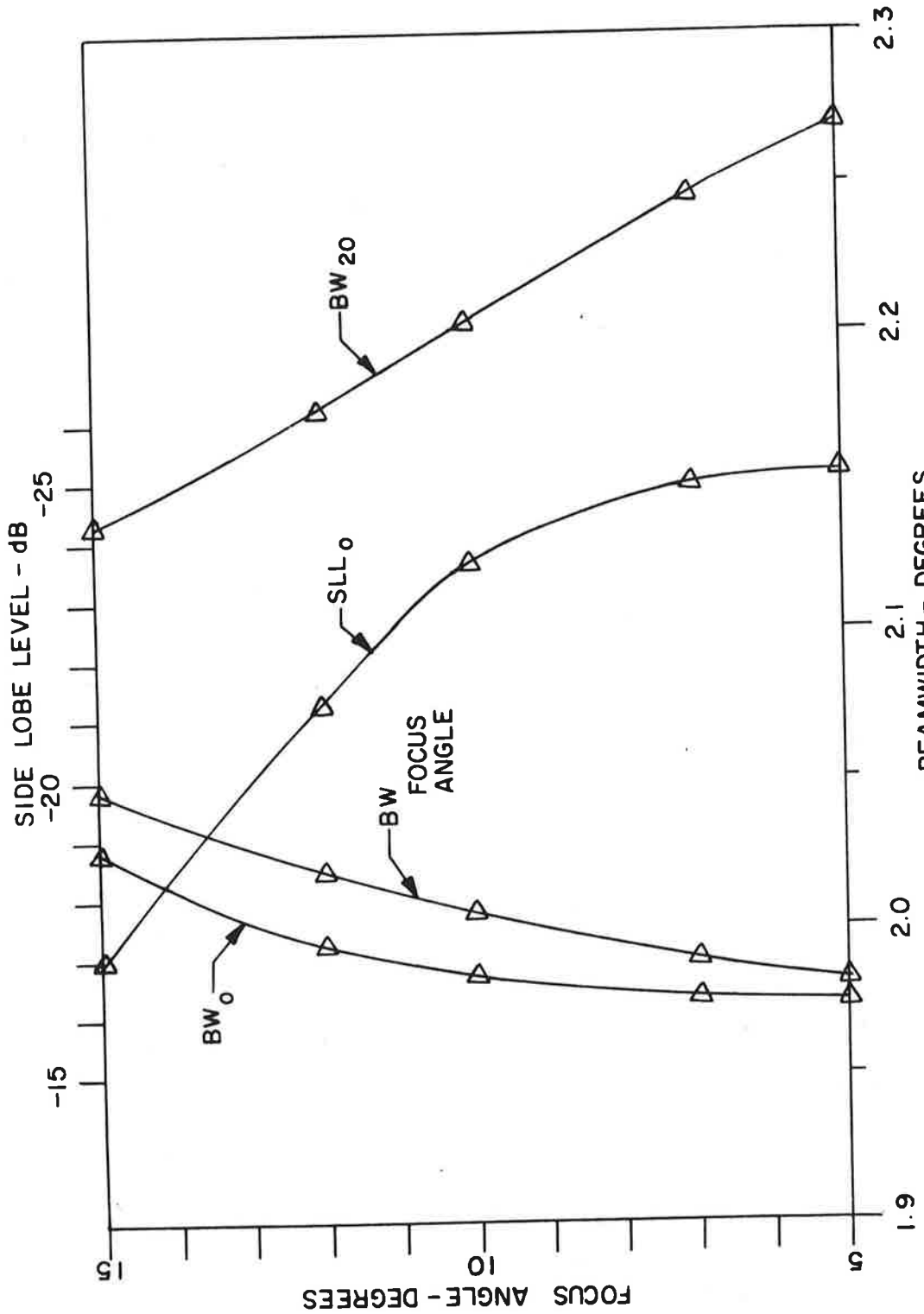


Figure 3.17 Variation of Sidelobe Level and Beamwidth with Focus Angle 2° Design



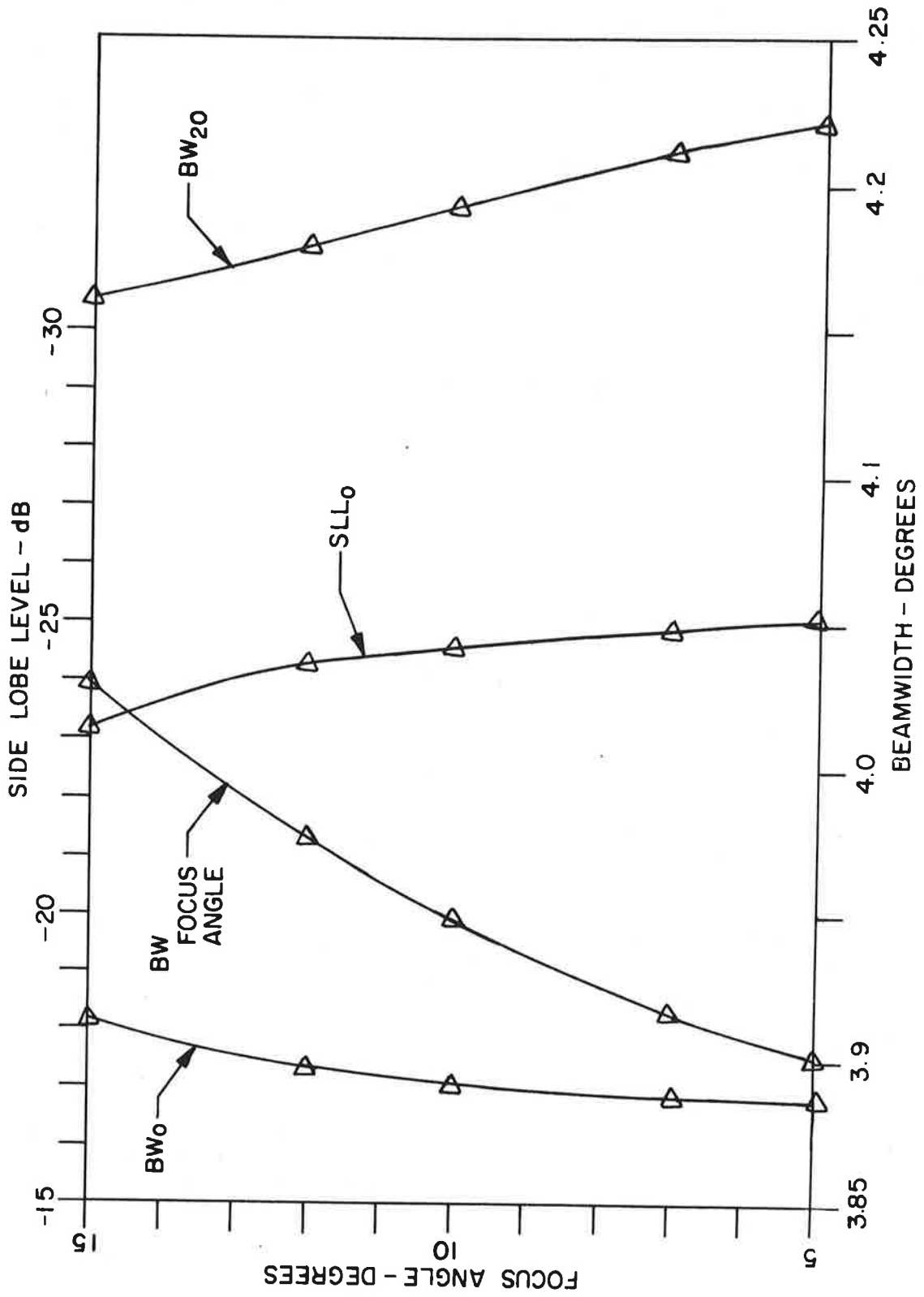


Figure 3.18 Variation of Sidelobe Level and Beamwidth with Focus Angle, 4° Design

10°. If  $\theta_f$  is greater than 10° SLL<sub>0</sub> is too high, and if  $\theta_f$  is less than 7° then BW<sub>20</sub> is too large.

To facilitate making the choice of  $\theta_f$  the ratio of the 10dB beamwidth at 20° to the 10dB beamwidth at 0° was calculated and tabulated for different  $\theta_f$ 's. This was also done for the 2° and 4° beamwidth cases (Table 3.4). The RTCA format gave no guidelines as to the variation of beamwidth that would be allowed by the on-board processor. For lack of a firm criterion, a variation of 2:1 at 20° elevation was considered allowable, which is consistent with the RTCA requirement that accuracy not degrade by more than 2:1 at the coverage extremes.<sup>1</sup>

Table 3.4 Calculated 10dB Beamwidth Ratio:  
BW @ 20°/BW @ 0°

BW <sub>d</sub>	$\theta_f$	$\frac{BW_{20}}{BW_0}$
1°	5°	1.96
	7°	1.87
	10°	1.69
2°	5°	1.18
	7°	1.187
	10°	1.181
4°	5°	1.16
	7°	1.11
	10°	1.09

The best ratio occurs at  $\theta_f=10^\circ$ . Focus angles greater than 10° tend to provide a better beam at 20° elevation than at 0°, but it is desirable to have the highest accuracy near the horizon, where almost all aircraft will require the most accurate information.

Using these considerations and the trade-off between SLL<sub>0</sub> and BW<sub>20</sub> in Figure 3.16 mentioned above,  $\theta_f$  was chosen to be 10° for the 1° design beamwidth case. Since the 2° and 4° beamwidth cases are more flexible in what will constitute an acceptable design, and since the above considerations apply to the larger beamwidths also,  $\theta_f$  was chosen

<sup>1</sup>. RTCA Report, p. A-1

to be  $10^\circ$  in these cases.

The other specifications for the design are taken from the tables presented above. The entire design is tabulated in Table 3.5.

Table 3.5 Final Physical and Design Parameters  
For Azimuth Cylindrical Array Design

BW <sub>d</sub>	DESIGN
$1^\circ$	R = 353.304 cm = Aperture $\phi_a = 60^\circ$ $N_a = 96$ elements $\theta_f = 10^\circ$ $d = 0.656\lambda$
$2^\circ$	R = 176.652 cm = Aperture $\phi_a = 60^\circ$ $N_a = 48$ elements $\theta_f = 10^\circ$ $d = 0.656\lambda$
$4^\circ$	R = 88.326 cm = Aperture $\phi_a = 60^\circ$ $N_a = 24$ elements $\theta_f = 10^\circ$ $d = 0.656\lambda$

It will be noted that the spacing chosen is actually slightly less than required by Table 3.3, and uses more elements (active and total). This was done to add a certain safety margin and to achieve  $N_a$ 's which allow power dividers to be made up of combinations of small numbers. For example, 96 elements can be fed by a power divider made up of four-way and six-way power dividers.

Using these specifications, the antenna patterns can be calculated from equation B.27. The computer program written for the tradeoff study provides for the use of digital phase shifters, rounded to the nearest level (as opposed to truncated). The patterns in Figures 3.19, 3.20, and 3.21 were calculated for a cosine-squared-on-a 0.5 pedestal using four-bit phase shifters. The patterns shown are for the coverage extremes (horizon and  $20^\circ$  elevation) and represent

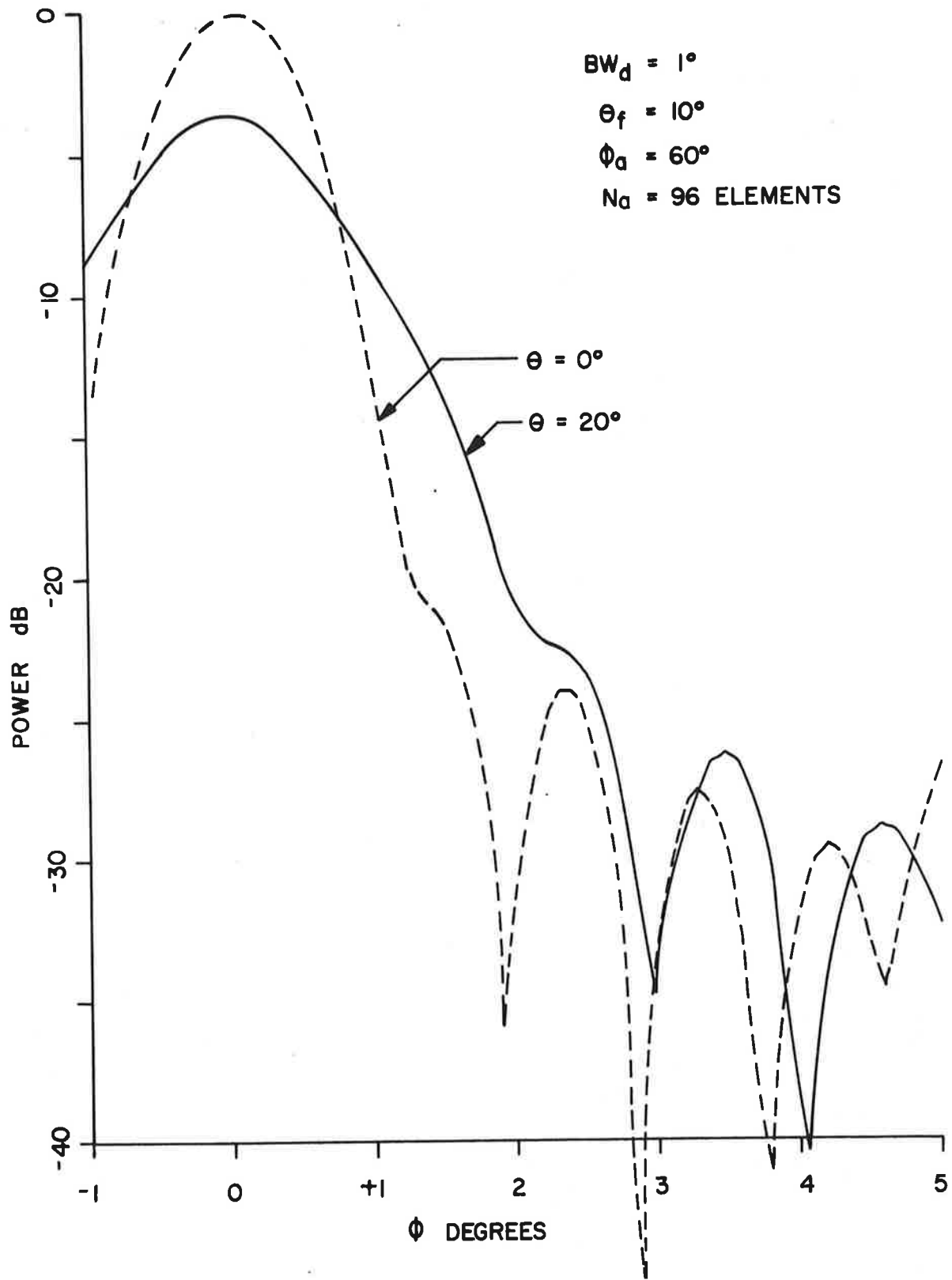


Figure 3.19 Calculated Antenna Patterns of  $1^\circ$  Beamwidth Cylindrical Antenna

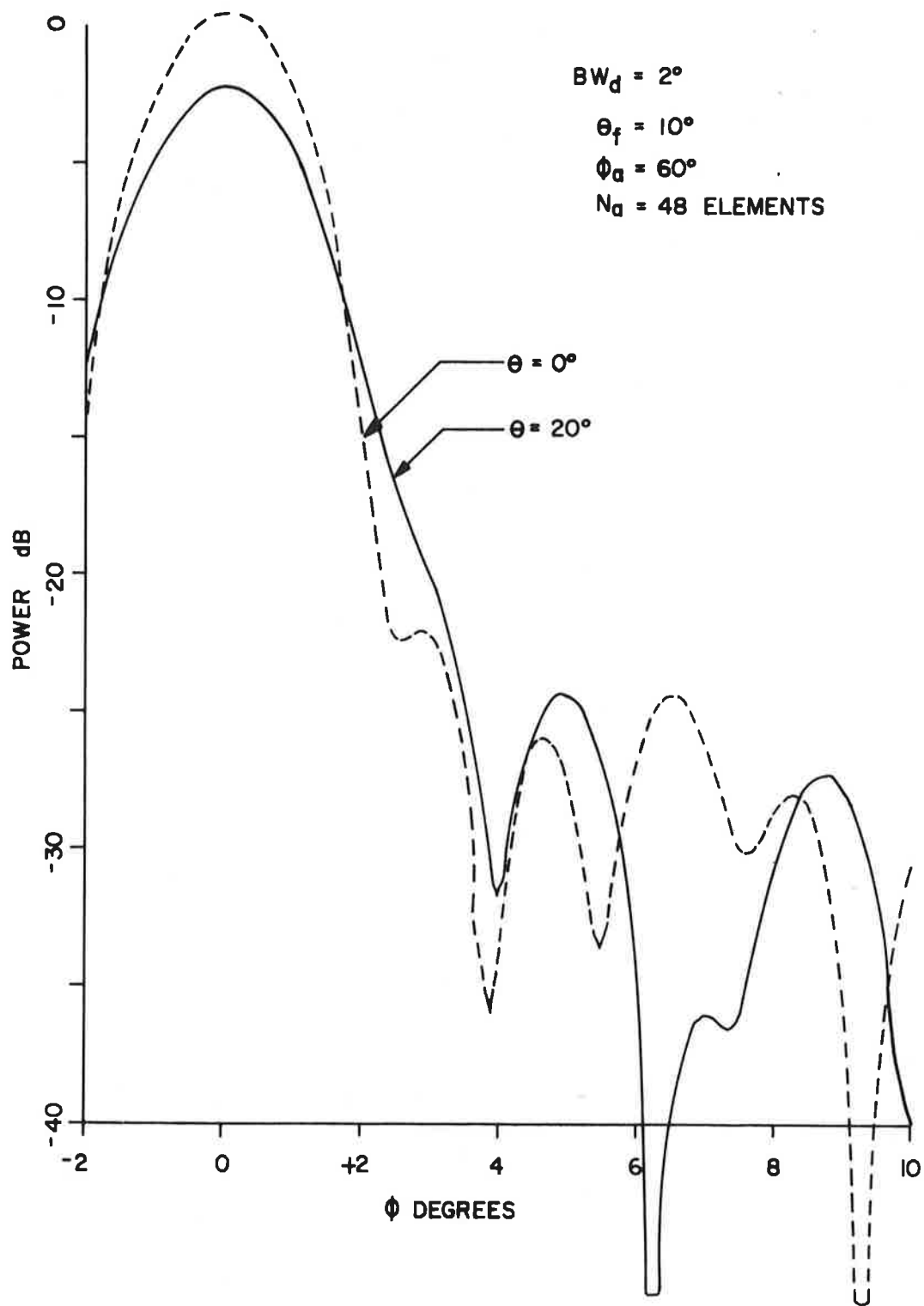


Figure 3.20 Calculated Antenna Patterns of  $2^\circ$  Beamwidth Cylindrical Antenna

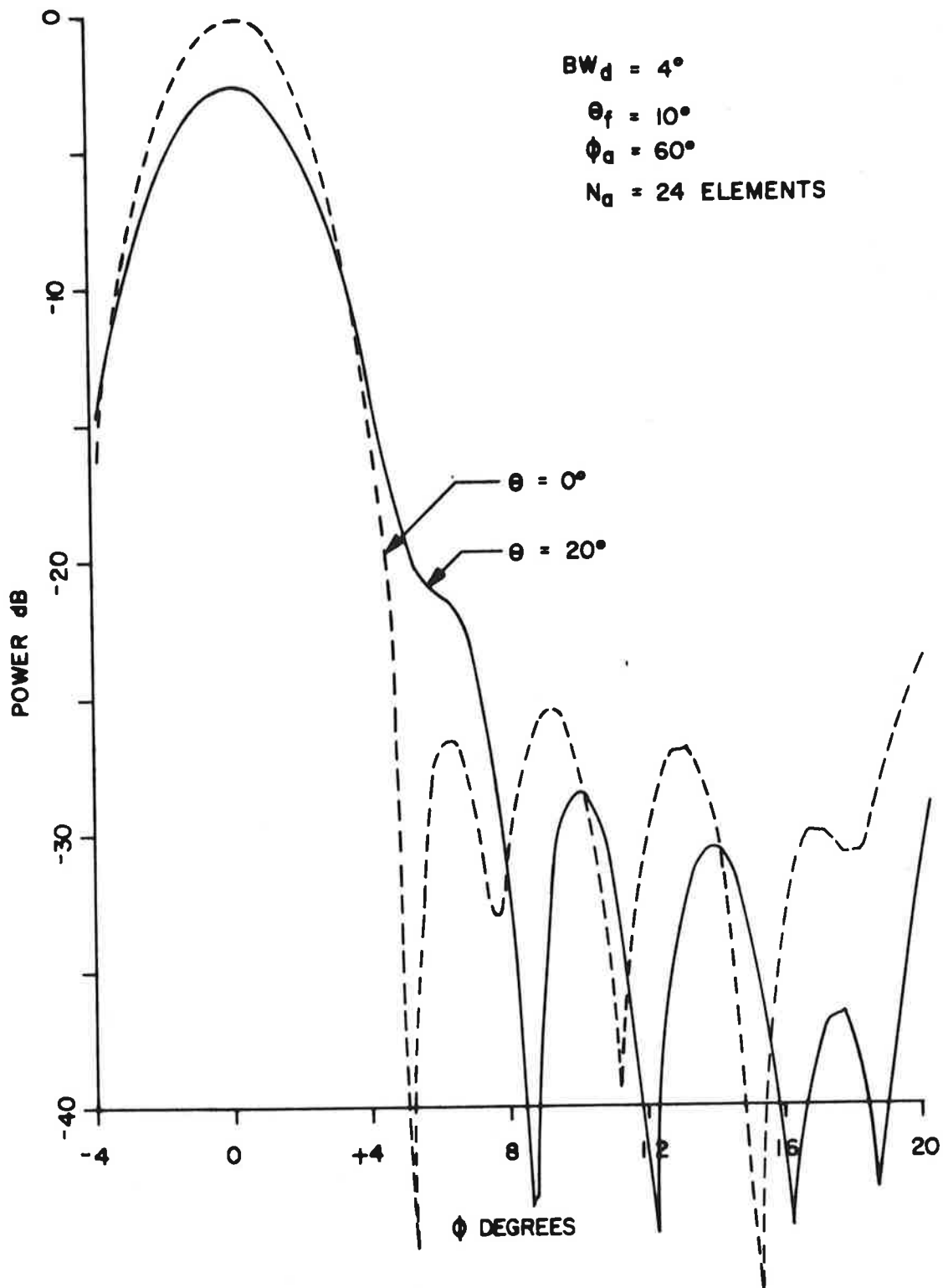


Figure 3.21 Calculated Antenna Patterns of  $4^\circ$  Beamwidth Cylindrical Antenna

the worst patterns encountered. The curves of Figure 3.21 in particular are the patterns the experimental antenna, described in Chapter VII, are expected to produce.

The performance is summarized in Table 3.6. The 3dB and 10dB beamwidths are included along with the sidelobe level. The sidelobe figures need some explanation: as patterns are taken further from the focal elevation angle, the first sidelobe begins to merge with the main beam; i.e., the first null fills in, then the lobe looks like a shoulder, and finally is merged until there is only a slight distortion of a widened main beam. The same thing occurs at higher angles for the second lobe as well (only observed here in the 1° beamwidth design). As mentioned before, the most serious defocusing problem occurs in the 1° beamwidth antenna; Table 3.6 shows that the 10dB beamwidth varies by less than 2:1, which meets the requirements set down earlier in this section. Larger beamwidths have smaller ratios.

The design parameters of Table 3.5 along with the column design of section 3.1.1 constitute the electrical design parameters of the array itself. The feed network required to set up the required distribution is discussed in section 4.1.

Table 3.6 Calculated Performance of Cylindrical Antenna Designs

BW <sub>d</sub>	$\theta$	3 dB BW	10 dB BW	SLL <sub><math>\theta</math></sub>
1°	0°	1.01°	1.76°	-24.0 dB
	5°	1.01°	1.74°	-24.4
	10°	1.01°	1.73°	-25.2
	15°	1.07°	1.94°	-18.2
	20°	1.37°	3.10°	-10.5*
2°	0°	1.98°	3.43°	-22.3 dB
	5°	1.99°	3.43°	-23.3
	10°	2.01°	3.44°	-24.8
	15°	2.06°	3.57°	-23.5
	20°	2.21°	4.01°	-18.1**

\*The first sidelobe has merged into the main beam. The second sidelobe has the behavior below.\*\*

\*\*Appears as a shoulder, but is located where lobes exist at elevation focus angle. Lobing is down by more than 20 dB below main below.

Table 3.6 Calculated Performance of Cylindrical Antenna Designs  
(Continued)

BW <sub>d</sub>	θ	3 dB BW	10 dB BW	SSL <sub>θ</sub>
4°	0°	3.89°	6.68°	-25.1 dB***
	5°	3.90°	6.73°	-25.2***
	10°	3.94°	6.79°	-24.8***
	15°	4.03°	6.99°	-22.2***
	20°	4.16°	7.39°	-18.6**

\*\*\* Quantization lobes about 22 dB down appear for this case at about 21° off boresight. These are reduced when the beam is scanned away from broadside.

### 3.2 Elevation Antenna

*Abstract - The elevation element can be simple and inexpensive since it needs no sharp cutoff at the limits of azimuth coverage. The design of a linear array for the elevation antenna is very similar to the design for the azimuth antenna, however, the problem of ground reflections from 'down-lobes' may necessitate a higher antenna. To achieve the coverage requirements with one cylindrical array large radii and small active sectors are required, making the height prohibitive in the case of 1° and 0.5° beamwidths. This problem could be overcome using several arrays and dividing the elevation or azimuth coverage between them. However, this method has high complexity and other difficulties.*

The RTCA Committee recommended a coarse-fine elevation guidance format, with a forward coarse C-band antenna having a 1° beamwidth, and a 0.5° beamwidth fine Ku-band system located beyond the touchdown point. The C-band antenna is supposed to provide accurate guidance down to 1° elevation.<sup>1</sup> This requirement along with the accuracy required suggest a 1° beamwidth, although this is not absolutely essential. The Ku-band antenna is supposed to provide coverage down to 8 feet above the touchdown point,<sup>1</sup> a requirement which is difficult at C-band, since a 0.5° beamwidth implies an aperture of about 12 feet.

The recommendation of planar beams in elevation would not allow the use of linear arrays. This recommendation is discussed in sections 2.3 and 2.4. The use of linear arrays is considered

<sup>1</sup>. RTCA Report, p. A-7



possible, however, and is discussed in section 3.2.2. Cylindrical arrays and multiple-array configurations which meet the planar beam criterion are discussed in section 3.2.3. The conclusions there are that cylindrical arrays can generate  $1^\circ$  beamwidth planar beams with azimuthal coverage of  $\pm 20^\circ$ . Beyond that, multiple arrays or multiple feeds would be necessary, which are complex and costly. The element design is substantially simpler than for the azimuth antenna. It is discussed in section 3.2.1 below.

### 3.2.1 ELEVATION ELEMENT DESIGN

The element design for the elevation antenna is less stringent than for the azimuth antenna. This is due to the fact that the reflections from the ground are naturally suppressed by the narrow-beamed antenna pattern. While it is desirable for the radiation to be suppressed outside the azimuth coverage  $\pm 60^\circ$  (for configuration K) the element pattern need not have sharp cutoff at the coverage limit. This allows the use of a simple element. One candidate is the dipole-ground plane combination, shown in Figure 3.22. If the width is infinite, the pattern is given by

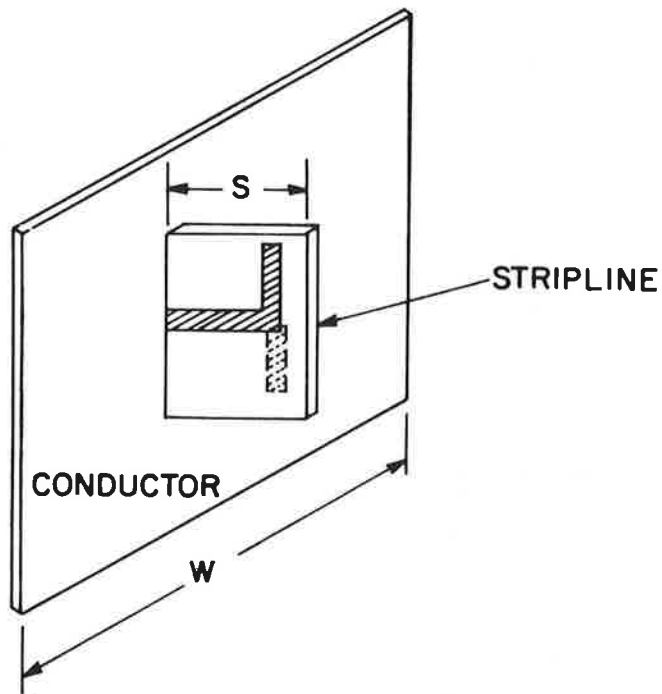


Figure 3.22 Dipole-Ground Plane Element

$$g(\theta, \phi) = \frac{\sin(ks \cos\theta \cos\phi) [\cos(kl \sin\theta) - \cos(kl)]}{\sin(ks) \cos\theta [1 - \cos(kl)]} \quad (3.2.1)$$

Principle-plane patterns are shown in Figure 3.22 for a dipole-ground plane spacing of a quarter wavelength and a dipole length (2) of a half-wavelength. For a dipole-to-ground plane spacing(s) of a quarter wavelength, the 3dB beamwidth in azimuth is 120°. Thus at ±60° the pattern is at the half power points. Thus the range at the coverage extremes would be reduced by a factor of 0.7 from the range along the runway centerline. This is not considered serious for the elevation function.

The effect of the finite width of conductor is to cause lobing at far angles from broadside. The width will be experimentally determined, but it is anticipated that a two-foot width will be adequate.

This element will be quite inexpensive and is not expected to be a major cost factor.

### 3.2.2 LINEAR ARRAY DESIGN

If a linear array is used for the elevation function conical elevation guidance is generated. In this case, a feed arrangement involving a power divider and a number of phase shifters feeding elements of the band described in section 3.2.1 is anticipated. This feed network is described in section 4.1.

The linear array design for the elevation antenna is very similar to that for the azimuth antenna. Since the array is vertical, and polarization is vertical, the array scans in the "E-plane" (the azimuth linear array scans in the "H-plane"). The mutual coupling effects are somewhat different in the two cases, but the fact that scan is only required over 20° means that the variation in impedance looking into the antenna elements is not severe. The difference in element patterns for the elevation and azimuth antennas is not significant, either, for the coverage involved.

One difference that should be given consideration is the different multipath requirements. For the azimuth antenna reflections off the ground are primarily within the main beam, and do not cause serious pointing errors. In the elevation antenna, reflections through sidelobes (more precisely, "downlobes") can result in serious pointing errors. This may require better sidelobe characteristics than the cosine-

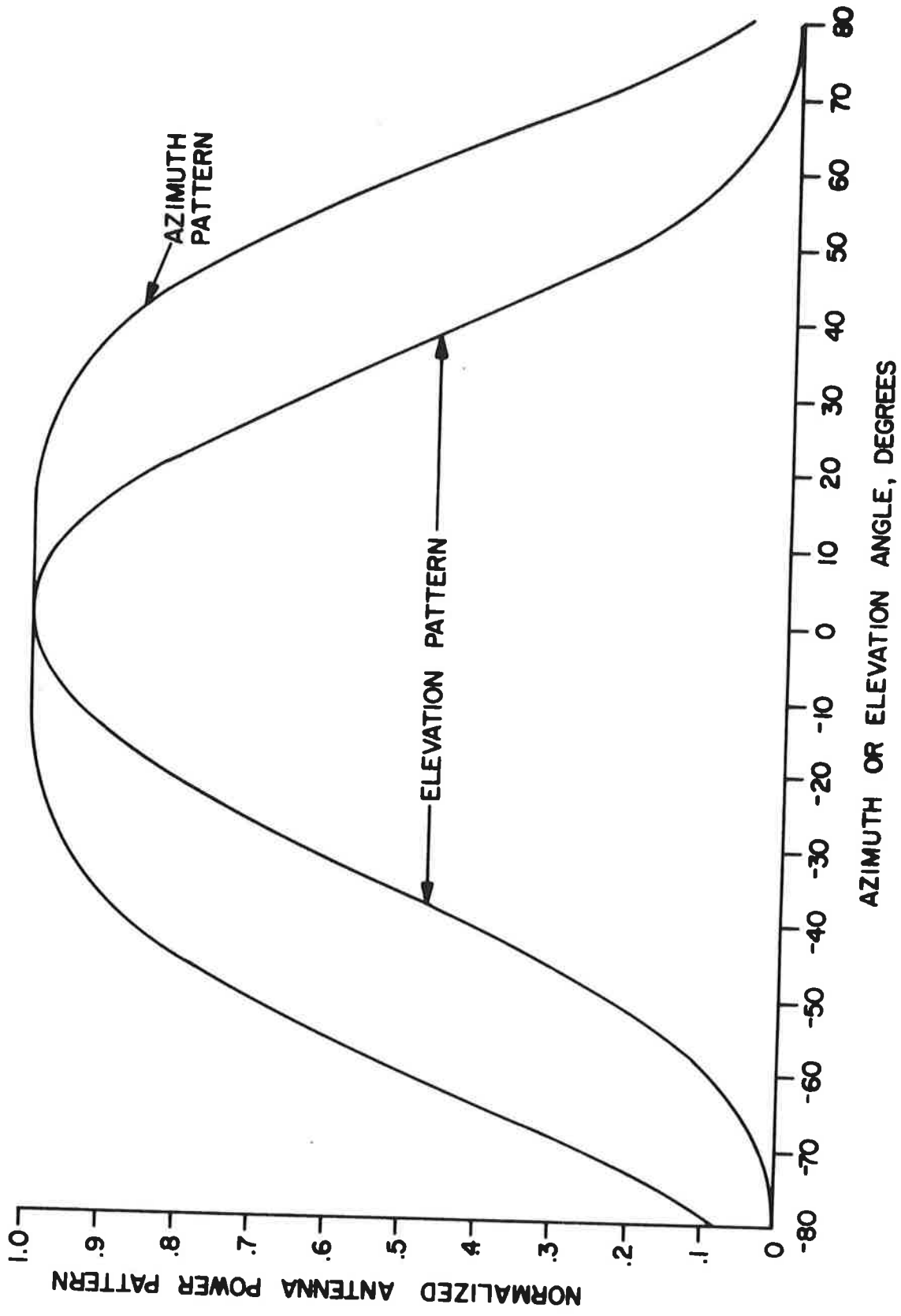


Figure 3.23 Principle-Plane Patterns for a Dipole-in-Front-of-a Ground-Plane

squared-on-a .5 pedestal allows, and a sharper aperture taper may be required, which will increase the height requirements by 10-15%. Using the above distribution the linear array requirements are tabulated in Table 3.7 below:

Table 3.7 Linear Array Parameters for Elevation Function

Beamwidth	Number of Elements	Height, ft.
.5	192	23.6
1	96	11.8
2	48	5.9
4	24	3.0

### 3.2.3 CYLINDRICAL ARRAY DESIGN

The application of cylindrical arrays to the elevation function in order to generate planar beams is discussed in section B.2 of Appendix B. The defocusing problem is much more severe than for the azimuth function, which requires only 20° of coverage; here ±60° of coverage is needed, and the degradation occurs more rapidly at wider angles. This can be seen by equation B.48 for the defocusing error:

$$\Phi_{err} = \frac{180^\circ \gamma}{\theta_{BW}} \tan(\theta_a/4) (\cos\phi_f - \cos\phi) \quad (3.2.2)$$

The coverage limits for a given beamwidth can be calculated from equations B.49 and B.50 by setting an allowable defocusing error, and determining the focus angle and coverage limits. Table 3.8 shows the focus angles and coverage limits for several beamwidths using an active sector of 60° and a beam broadening factor of 61°.

Table 3.8 Elevation Antenna Coverage Limits Using a Cylindrical Array with an Active Sector of 60°

Beamwidth BW, degrees	Focus Angle $\phi_f$ , degrees	Coverage Limit $\phi_o$ , degrees
0.5	± 10.0	± 14.2
1	± 14.2	± 20.1
2	± 20.1	± 28.6
4	± 28.6	± 40.9

If ±60° or ±40° of azimuth coverage were to be attained with one cylindrical array, large radii and small active sectors would be necessary. The height can be found from equation (B.52). The height, radius, and active sector using the 90° defocusing criterion above for the various beamwidths are given in Tables 3.9 and 3.10. The active sector is found by eliminating  $\phi_f$  from (B.49) and (B.50) and solving for the active sector. This gives

$$\theta_a = 4 \tan^{-1} \left[ \frac{\theta_{BW} |\bar{\phi}_{err}|}{90^\circ \gamma (1 - \cos \phi)} \right] \quad (3.2.3)$$

Here  $\bar{\phi}_{err} = 90^\circ$ ,  $\gamma = 61^\circ$ , and the frequency chosen is at the lower end of the band, namely 5.0 GHz.

Table 3.9 Effect of Beamwidth on Physical Antenna Parameters Configuration K(±60° Azimuth Coverage)

Beamwidth BW, degrees	Active Sector $\theta_a$ , degrees	Radius R, feet	Height h, feet
0.5	3.8	366	148
1	7.5	91.7	42.9
2	15.0	23.0	13.6
4	29.9	5.82	4.8

Table 3.10 Effect of Beamwidth on Physical Antennas  
Configuration I ( $\pm 40^\circ$  Azimuth Coverage)

Beamwidth BW, degrees	Active Sector $\theta_a$ , degrees	Radius R, feet	Height h, feet
0.5	8.0	172	81.9
1	16.0	43.1	26.2
2	31.9	10.9	9.4
4	62.6	2.9	3.8

It is apparent that for beamwidths of  $\frac{1}{2}^\circ$  and  $1^\circ$  the height is prohibitively high, while for  $2^\circ$  and  $4^\circ$  beamwidths this approach is possible. Since the RTCA committee recommends a beamwidth of  $1^\circ$  for the coarse guidance and  $0.5^\circ$  for the fine guidance (at 15 GHz, however), the question arises of whether a combination of cylindrical arrays of a reasonable height can yield planar beams over the entire coverage. The discussion below is aimed at providing planar beams for a  $1^\circ$  beamwidth antenna over  $\pm 60^\circ$  of coverage in azimuth, and  $20^\circ$  in elevation.

Attempts have been made during the year to design array geometries which meet these requirements. The results are not encouraging, but for completeness sake, some configurations are discussed below.

#### A. Switched Cylindrical Arrays, Each with Full Azimuth Coverage

In order to achieve  $\pm\phi_0$  azimuth coverage, the active sector of a cylindrical array must satisfy the relation

$$\tan(\theta_a/4) \leq \frac{\Phi_{err}}{180^\circ \gamma (1 - \cos\phi_0)} \quad (3.2.4)$$

for some selected defocusing error  $\Phi_{err}$ . For  $\gamma = 61$ ,  $\phi_0 = 60^\circ$ , and  $\Phi_{err} = 180^\circ$ , this dictates that  $\theta_a = 3.8^\circ$ . If one antenna were used, it would have to be 43 feet high; less than 16% of the aperture would be used at one time. By requiring that the elevation coverage be shared by  $n$  arrays, such as in Figure 3.24 the height of each would be given by

$$h = \frac{\gamma\lambda}{2} \left[ 1 + \frac{\sin(\theta a/2 + 20^\circ/h)}{\sin(\theta a/2)} \right] \quad (3.2.5)$$

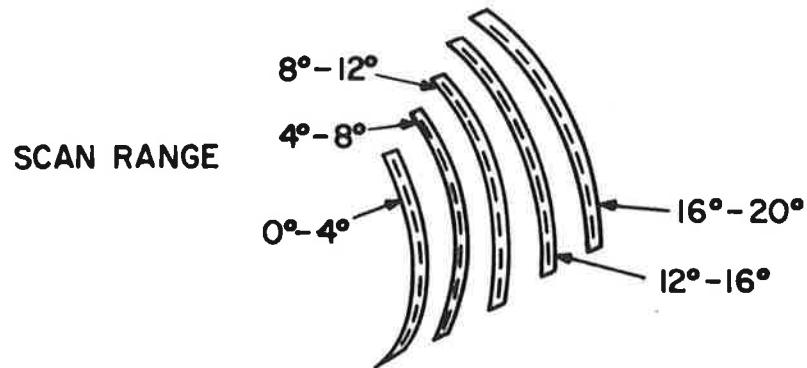


Figure 3.24 Configuration for Cylindrical Phased Arrays Sharing Elevation Coverage (Elevation Antenna)

This is indicated in Table 3.11:

Table 3.11 Array Height for Shared Elevation Coverage

Number of Arrays	Height, ft.
1	42.9
2	27.8
3	22.6
4	20.0
5	18.4
6	17.3
7	16.6

The difficulties with this method are the following:

1. Antenna height is somewhat excessive.
2. Antenna complexity is high.
3. Elevation datum shifts by several feet with the array used.

## B. Arrays Which Share Azimuth Coverage

Since aspect ratios of 40:1 are feasible with cylindrical arrays of an acceptable height the question arises of whether the azimuth coverage could be shared by several arrays. This has the attractive feature that the various configurations could be modularized, i.e., additional coverage added at a later time by adding more sections if it were deemed desirable.

This approach is best illustrated by an example. Using the  $90^\circ$  defocusing error criterion, the focus angle can be found from equation B.49 for the center element. The limit of coverage is determined by (B.50). Using this limit as the lower limit of the next array, the focus angle can be found from (B.49) by replacing the "I" by  $\cos \phi_0$  where  $\phi_0$  is this limit. This process is repeated until the coverage is attained. With a height of 19 ft., a frequency of 5 GHz, and an active sector angle of  $31.0^\circ$ , the center element in the array of Figure 3.25 will give a coverage of  $\pm 20^\circ$  in azimuth within the  $90^\circ$  criterion for  $\gamma = 61$ . The coverage will be shared by the nine arrays in a manner indicated by Table 3.12.

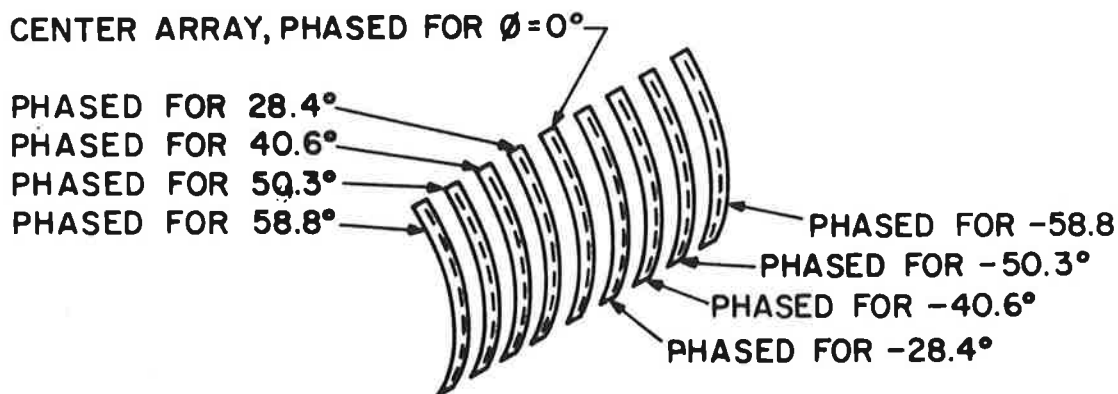


Figure 3.25 Configuration for Cylindrical Phased Arrays Sharing Azimuth Coverage (Elevation Antenna)



Table 3.12 Azimuth Coverage Sharing Scheme

Array	-90° Error	Zero Error	90° Error	Configuration
Center	-20°	0°	20°	B,D,E,F,G,I,K
1st Left 1st Right	-35.0° 20.0°	-28.4° 28.4°	-20.0° 35.0°	I,K
2nd Left 2nd Right	-45.7° 35.0°	-40.6° 40.6°	-35.0° 45.7°	
3rd Left 3rd Right	-54.7° 45.7°	-50.3° 50.3°	-45.7° 54.7°	K
4th Left 4th Right	-62.8° 54.7°	-58.8° 58.8°	-54.7° 62.8°	

The phase advance required at each element to achieve a perfectly aligned beam at some azimuth angle  $\phi_f$  for an elevation scan angle of zero is given by

$$\bar{\phi}_n = kR \cos\phi_f (1 - \cos\theta_n) \quad (3.2.6)$$

Since this depends on the coverage center angle  $\phi_f$ , the phasing differs from element to element, so that each array has to have different commands.

The difficulties with this configuration are the following:

1. Antenna height is high, but not as high as for case "a".
2. Complexity is high for configurations I and K.
3. Different and more complex software is needed for configurations I and K.
4. The result of the shared coverage is that the antenna pattern will deteriorate at the crossover points, and exhibit scalloping and possibly deep nulls.

Rather than use separate arrays, the same effect can be obtained by combining the signals properly on the elements. This meets objection 4 above, but the other difficulties still apply. A separate feed system would be necessary for each azimuthal coverage, or nine in the example used.

The elevation antenna design is not carried as far as the

azimuth design because of uncertainties in the eventual requirements. The design procedure is very similar to that of cylindrical arrays for the azimuth function. Certain differences exist, however, which need further treatment. For one thing, the sidelobe requirement for the elevation antenna is probably more severe than for the azimuth antenna; this is due to the requirement for good performance at low elevation angles, i.e., down to  $1^\circ$ . Sidelobes ("downlobes" might be more descriptive) can be reflected upward and affect the guidance signal. The requirement for good multipath rejection may require sidelobes more like -30dB. This would result in a larger beam-broadening factor, and a requirement for less defocusing error; these in turn imply larger antenna heights. Additionally, phase variations would have to be held to tighter tolerances. This will be studied further.

The conclusions from this study are as follows:

- (1) cylindrical arrays with  $2^\circ$  and  $4^\circ$  beamwidths can generate planar beams having the necessary coverage with minimum complexity;
- (2) cylindrical arrays with this amount of complexity but having beamwidths of  $0.5^\circ$  or  $1^\circ$  will not generate planar beams wide enough to meet the coverage requirements of configurations I and K, assuming heights above 20 feet are undesirable. Applications to other configurations are not considered-- $\pm 20^\circ$  coverage in azimuth is achievable for a  $1^\circ$  beamwidth, but wider elevation coverage is desirable in order to maintain an adequate guidance volume (see section 2.3.1).

## CHAPTER IV FEED NETWORK DESIGNS

### 4.1 Linear Arrays

*Abstract-Variou s methods of signal distribution for linear arrays are discussed. The most promising method appears to be a series feed with parallel phase shifters. The associated logic is straight forward.*

In linear arrays all elements are fed simultaneously with amplitudes which do not normally change. Steering of the beam is done entirely with phase shifters which usually are adjusted to give a linear phase front. The spacing between adjacent elements is sometimes varied in order to eliminate grating lobes and allow wider average spacings, thus reducing the number of elements, and therefore the cost. This increases the complexity of the control circuitry. Since scan angles for linear arrays are not anticipated to vary more than  $\pm 20^\circ$ , this technique is of limited value, and only uniformly spaced arrays will be discussed further.

As linear arrays are scanned from broadside, several phenomena occur:

1. The main beam broadens. This is caused by the fact that the projected radiating aperture decreases by the cosine of the scan angle.
2. The gain decreases. This is caused by the first factor mentioned, plus the fact that the element pattern has its maximum at broadside, and is reduced in magnitude elsewhere.
3. The boresight shifts. The definition of boresight depends on the processing used, but generally is either the angle midway between the 10 dB points (or other reference level) or the center of gravity of the beam (usually that part of the main beam higher in amplitude than the 10 dB point). In either case, the beam is asymmetrical and the beam peak does not usually coincide with the boresight. (The beam peak is always at the angle at which the linear phase front is aimed.) This effect, called squint, is not appreciable for small angles, but becomes more critical when wider beamwidths and/or wide scan angles are employed. The effect is to cause an error in the angle measurement.

4. The sidelobes are asymmetrical and maximum side-lobe level increases. This is caused by the fact that the element pattern does not change with scan angle, while the array pattern does. This is not a significant problem for this application.

Linear arrays can be fed by a series, corporate, or mixed feed circuit. Additionally, the phase shifters may be in series or parallel. One possibility is the series - series feed, illustrated in Figure 4.1.

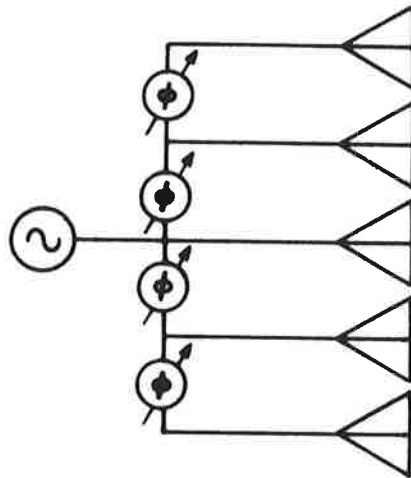


Figure 4.1 Series - Series Feed Configuration

This has the simplest control, since each phase shifter receives the same command. Its disadvantages are first that it is narrow-band, (its bandwidth is inversely proportional to the number of elements used); second, analog phase shifters must be used which do not mate well with a digital control circuit; third, errors accumulate toward the edge elements.

The other extreme is the completely corporate - parallel feed, shown in Figure 4.2.

This approach has a large bandwidth since line lengths are the same to all elements. The phase shifters can be digital, but must be separately controlled. This approach uses longer lengths of line, in general, which increases the insertion loss.

A hybrid - parallel arrangement can be used to keep line lengths down while providing more bandwidth than a series feed. Here a corporate feed is used for one or two

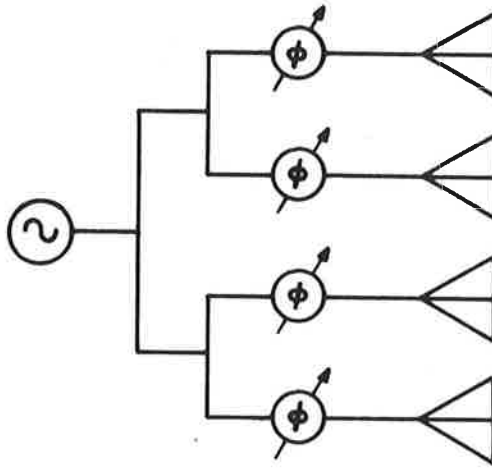


Figure 4.2 Corporate - Parallel Feed Configuration

stages of power division, followed by series feeds.

The choice of feed network depends on the bandwidth required. Bandwidth, as used here, can mean one of two things: (1) the bandwidth of the channel used by the particular antenna or (2) the bandwidth including all channels allocated to the function. Clearly, the second is desirable because if the channel bandwidths only were used, the power divider design would vary from channel to channel, making inconvenient (if not impossible) a change in channel assignments. Accordingly, the design must accommodate the entire band allocated to the function.

The RTCA SC-117 allocates the frequency band 5130 to 5250 MHz for the angle function, while reserving 5000 to 5130 to the DME. However, there is enough uncertainty in the RTCA choices to admit the possibility that the additional band may need to be covered by the same antenna. Thus it is best to require that the feed network accommodate the entire 5000 - 5250 MHz band.

The possibilities for the landing system reduce to two basic types:

- (1) one in which the phase shift settings depend only on the frequency and boresight angle - this requires the corporate - parallel arrangement shown in Figure 4.2;

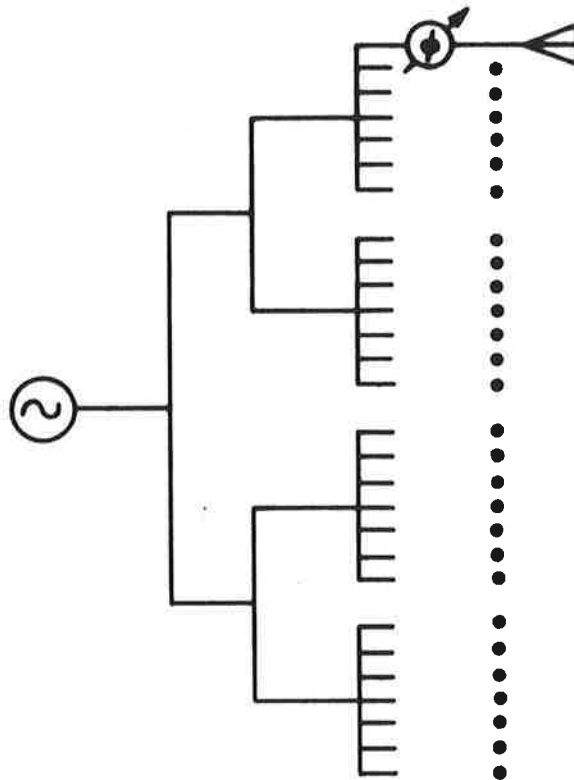


Figure 4.3 Hybrid - Parallel Feed Arrangement

- (2) one in which the phase shift calculations compensate for dispersion in the power dividing network - this allows the use of the series - parallel arrangement shown in Figure 4.4.

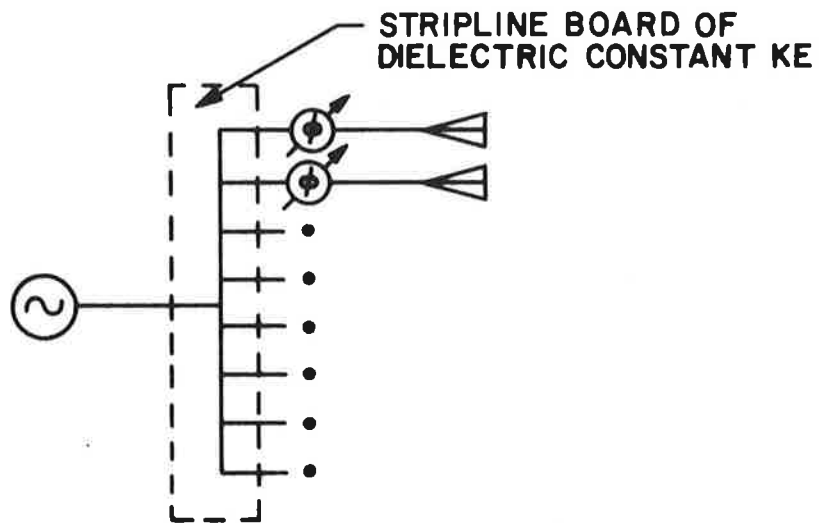


Figure 4.4 Series - Parallel Feed Arrangement

With the corporate feed, the phase shift settings depend only on the spacing and the direction of the beam. Suppose the elevation antenna feed is under consideration, and the direction of boresight is  $\theta_b$ . Assuming an even number of elements the command to the  $n$ -th phase shifter is given by (see equation B.6)

$$\phi_n = 360^\circ \cdot \frac{fd}{c} (n-\frac{1}{2}) \sin \theta_b \quad (4.1.1)$$

where

$$\frac{-N}{2} + 1 \leq N \leq \frac{N}{2}$$

and  $N$  is the total number of elements. This relation can be seen from Figure 4.5.

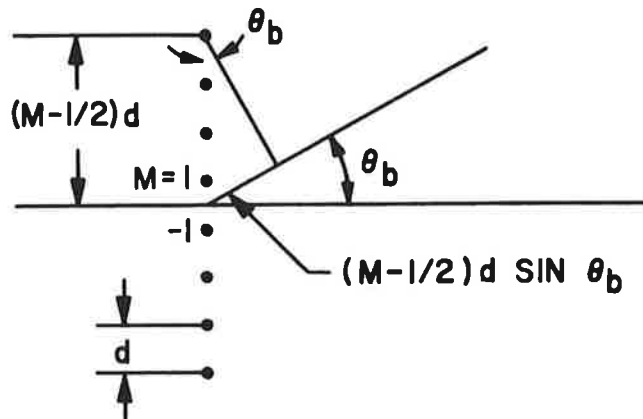


Figure 4.5 Phase Relations for a Linear Array

If the series - parallel feed arrangement is used, the phase shift setting must compensate for the dispersive effect of the power divider. If the power divider is a stripline transmission line with a dielectric constant  $K_e$ , the correction term is

$$360^\circ \cdot \frac{fd}{c} \sqrt{K_e} (n-\frac{1}{2}) \text{ resulting in a phase setting:}$$

$$\phi = 360^\circ \cdot \frac{fd}{c} (n - \frac{1}{2}) (\sin\theta_b - \sqrt{K_e}) \quad (4.1.2)$$

In either case the frequency must be known, since it can be shown that the error involved in trying to cover the entire 250 MHz band with a single frequency command is much too large. Thus in either case a change in channel assignments will require a change in software.

One way of achieving the calculation is to store a separate constant for each beam position, given by

$$b(\theta_b) = 360^\circ \frac{fd \sin\theta_b}{c} \quad (4.1.3)$$

At each element a constant given by  $n - \frac{1}{2}$  is stored and multiplied by the constant in (4.1.3) and sent to the driver circuits. (How this multiplication is implemented will have to be determined.) There would be approximately 640 words to be stored for a one-degree beamwidth antenna covering  $20^\circ$  in elevation (20 beamwidths) using 32 beam positions per beamwidth. This Read-Only-Memory (ROM) would be replaced if a channel reassignment were made. This scheme would accommodate the series - parallel arrangement as well by storing the constants

$$b(\theta_b) = \frac{360^\circ fd}{c} (\sin\theta_b - \sqrt{K_e}) \quad (4.1.4)$$

instead of the constant in (4.1.3).

An attractive feature of the Read-Only-Memory is that the boresight shift (squint) discussed above can be compensated for by storing the appropriate angles. For example, if the desired boresight were  $\theta_b$ , and if  $\theta_b$  were used in equation 4.1.3 or 4.1.4 to calculate phase shifter commands, the beam peak would be at  $\theta_b$ , the midpoint between 10 dB points or the main beam would be at some other angle  $\theta_b'$  and the difference  $\theta_b' - \theta_b$  would be the squint error. By using an angle  $\theta_b''$  as the command, where  $\theta_b'' = \theta_b - (\theta_b' - \theta_b)$  the 10 dB midpoint will occur at  $\theta_b$  as desired. This is all accomplished by storing the corrected commands when setting the ROM's initially.

Based on the above consideration, it appears that a series-parallel feed arrangement is the best choice, since it offers lower insertion loss without any added control



complexity. This will be subject to further review.

## 4.2 Cylindrical Arrays

*Abstract-Various methods for feeding cylindrical arrays are discussed and compared from the point of view of complexity, susceptibility to failure, flexibility, expandability, and performance. It is concluded that the best choice will depend on component performance, which is not clearcut. It will depend on the results of tests soon to be performed on state-of-the-art components.*

Cylindrical arrays require more complicated feed circuits than linear arrays, and allow for a wide variety of approaches, each with its own advantages and limitations. In each case in order to steer the beam, advantage is taken of the circular symmetry and the aperture distribution is translated in angle around the array. This is illustrated in Figure 4.6. When the aperture distribution is translated by one element, the beam moves in angle an amount given by the

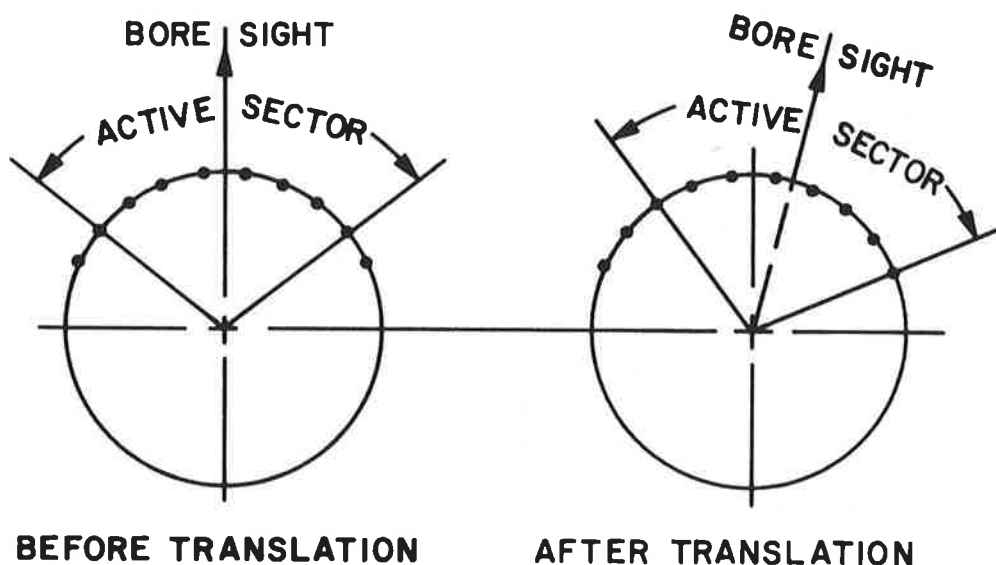


Figure 4.6 Boresight Shift in a Cylindrical Array Caused by Coarse Switching

angular spacing of the elements. Except for angle, all other antenna parameters are unchanged (skew, sidelobe level, beamwidth, etc.).

In addition to steering the distribution around, the feed network must provide a plane wave, and thus compensate for the cylindrical geometry. This process is called collimation.

Collimation is accomplished automatically in some methods, and must be provided by the phase shifters in others. The discussion which follows describes how these two functions, steering and collimation, are performed in the various methods, and treats the advantages and disadvantages of each.

Since there are three beamwidths being considered ( $1^\circ$ ,  $2^\circ$ , and  $4^\circ$ ), the  $4^\circ$  beamwidth designs are presented, along with indications of how the methods can be expanded to meet the  $1^\circ$  and  $2^\circ$  requirements.

#### 4.2.1 TRANSFER MATRIX FEED

The transfer matrix method performs steering by switching a set of RF inputs to a set of outputs while maintaining the order, but performing a translation, very much like a shift register in a logic circuit.

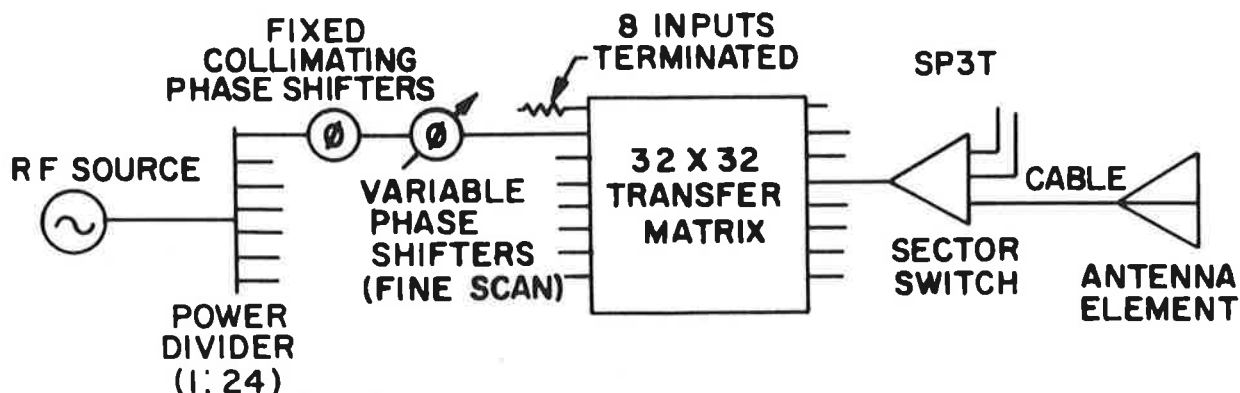


Figure 4.7 Typical Layout Using Transfer Matrix

A typical layout is shown in Figure 4.7. This has been reported by Giannini.<sup>1</sup> In the form shown there are 24 active inputs, and 32 outputs in the matrix. Collimating can be performed by using fixed phase shifters (actually line lengths), with variable phase shifters used to fine-steer the beam.

In order to explain the operation, suppose that inputs 1 through 24 are connected to outputs 1 through 24 in the initial transfer matrix switch position. In the next switch position, these inputs are connected (maintaining the same sequential order) to outputs 2 through 25 (and routed to antenna elements 2 through 25 as well). This can be repeated until outputs 9 through 32 are active. The next step will connect input 1 with output 10, 2 with 11, etc., but input 24 will be connected with output 1. Up to this point the sector switches have remained in their initial position. Now the sector switch at output 1 of the transfer matrix is thrown, so that instead of activating antenna element number 1, the signal is routed to antenna element 33, so that antenna elements 10 through 33 are properly excited, as desired for coarse steering.

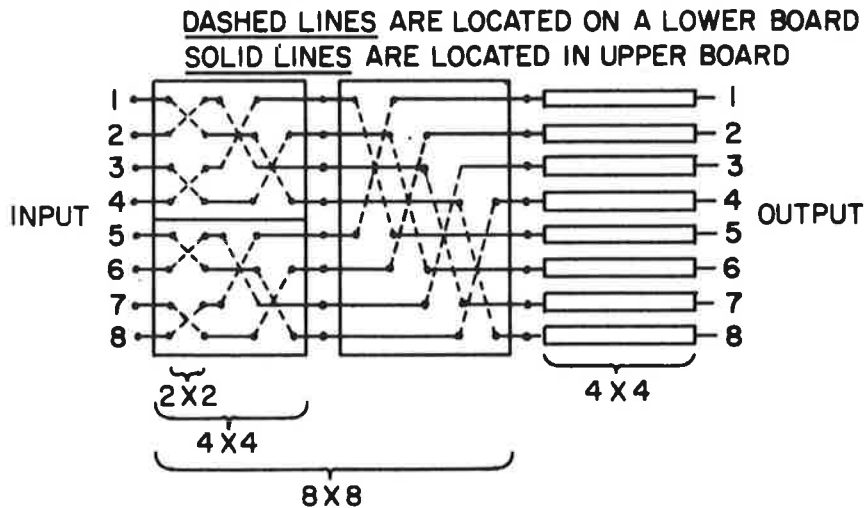
The fabrication of the transfer matrix is a design challenge. Figure 4.8 shows the schematic of such a matrix, where the dots represent a double-pole double-throw switch (transfer switch). Attempting to fabricate this from a single stripline board is poor design, because the lines cross at many points. These crossovers are a major problem in the layout of RF matrices, since they give rise to reflections and phase perturbations, and make line lengths unnecessarily long (and thus causing additional losses).

One way to reduce the number of crossovers is to modularize the matrix and orient the boards in perpendicular fashion. This is shown in Figure 4.9. The heavy lines in Figure 4.9a indicate how the fourth and fifth column of switches can be connected to give a 4 x 4 module, and Figure 4.9b shows its physical orientation. Using this technique, three rows of eight inputs feed 4 x 4's which connect (without connectors) to the third column of switches, and finally through another set of 4 x 4's (orientated perpendicularly) to give four rows of eight outputs.

1. R. J. Giannini, "An Electronically-Scanned Cylindrical Array for IFF Based as a Switching - and - Phasing Technique", IEEE G-AP Symposium, pp. 199-207, December 1969

However, there still are some crossovers: a 4 x 4 has two crossovers, and the center bank has twelve. One technique that could be used is to use two stripline boards, one with switches, and the other with the transmission lines. Connections between the boards are accomplished by right-angle feed-through connectors. The resulting board is shown in Figures 4.10 and 4.11. The 8 x 8 can be on one board set. This eliminates cross-overs entirely. It can be seen that this technique maintains equal line lengths.

2 - LAYER CONSTRUCTION



1	2	3	4	5	6	7	8
9	10	11	12	13	14	15	16
17	18	19	20	21	22	23	24

1	2	3	4	5	6	7	8
9	10	11	12	13	14	15	16
17	18	19	20	21	22	23	24
25	26	27	28	29	30	31	32

Figure 4.10 Possible Construction of 24 x 32 Transfer Matrix - 2 Layers

Alternatively, a three-board assembly can be used, with the center board carrying the transmission lines. This has the advantage of reducing the transmission line lengths, and thus insertion losses. This is shown in Figure 4.12.

The question of feed-throughs and crossovers is a significant technological problem. Crossovers in microstrip have been built which exhibit 40 dB isolation and low VSWR, but no phase information is available. Crossovers are not available for stripline boards using one center conductor. Striplines with two center conductors can accommodate some

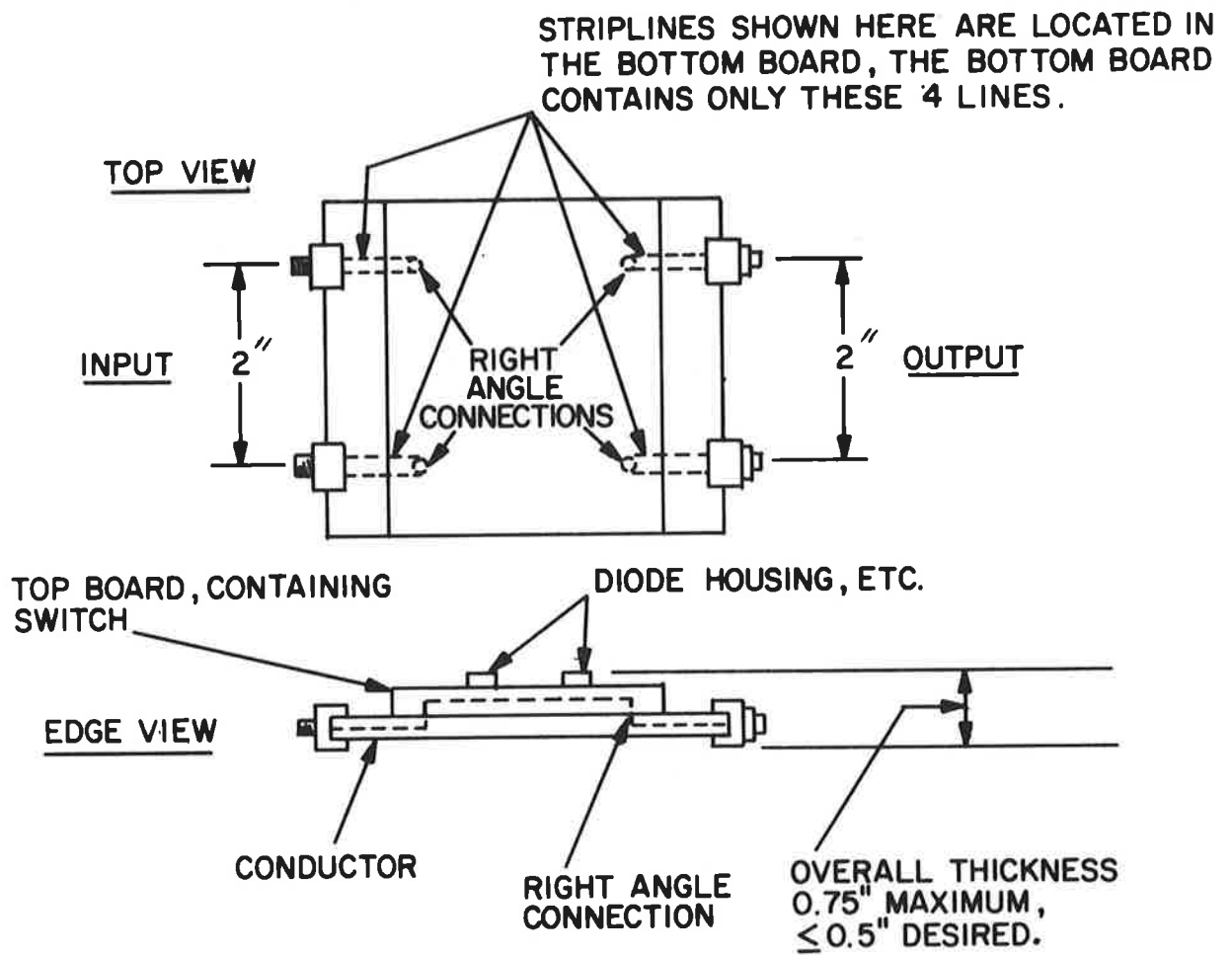


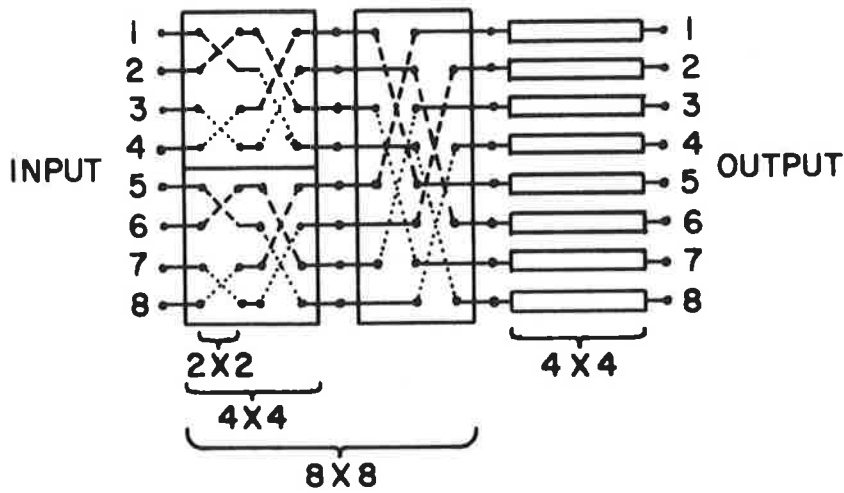
Figure 4.11 Possible Construction of Single Transfer Switch

**3-LAYER CONSTRUCTION**

**DASHED LINES ARE LOCATED ON BOTTOM BOARD**

**SOLID LINES ARE LOCATED ON MIDDLE BOARD**

**DOTTED LINES ARE LOCATED ON TOP BOARD**



ON EACH PATH { 10 INTERLAYER CONNECTIONS  
4 INTERBOARD CONNECTIONS

Figure 4.12 Possible Construction of 24 x 32 Transfer Matrix-  
3 Layers

crossovers, but with unknown phase perturbations. This technique has not been explored at C-band. The feasibility of feed-throughs at this frequency has not been established for this application. In general, standard right-angle connectors do not perform well at this frequency band. Also, it is not easy to suppress higher order stripline modes which are excited by the connector.

These problems need to be explored and solutions demonstrated.

#### 4.2.2 LENS FEED (R-2R)

A beam-steering lens is usually a parallel plate cavity with probes located at the periphery, sometimes filled with dielectric material, usually flat. A small number of probes (1-4) are used as inputs, and the lens distributes the power to the larger number of output probes. The size and shape of the lens are usually chosen to achieve collimation.

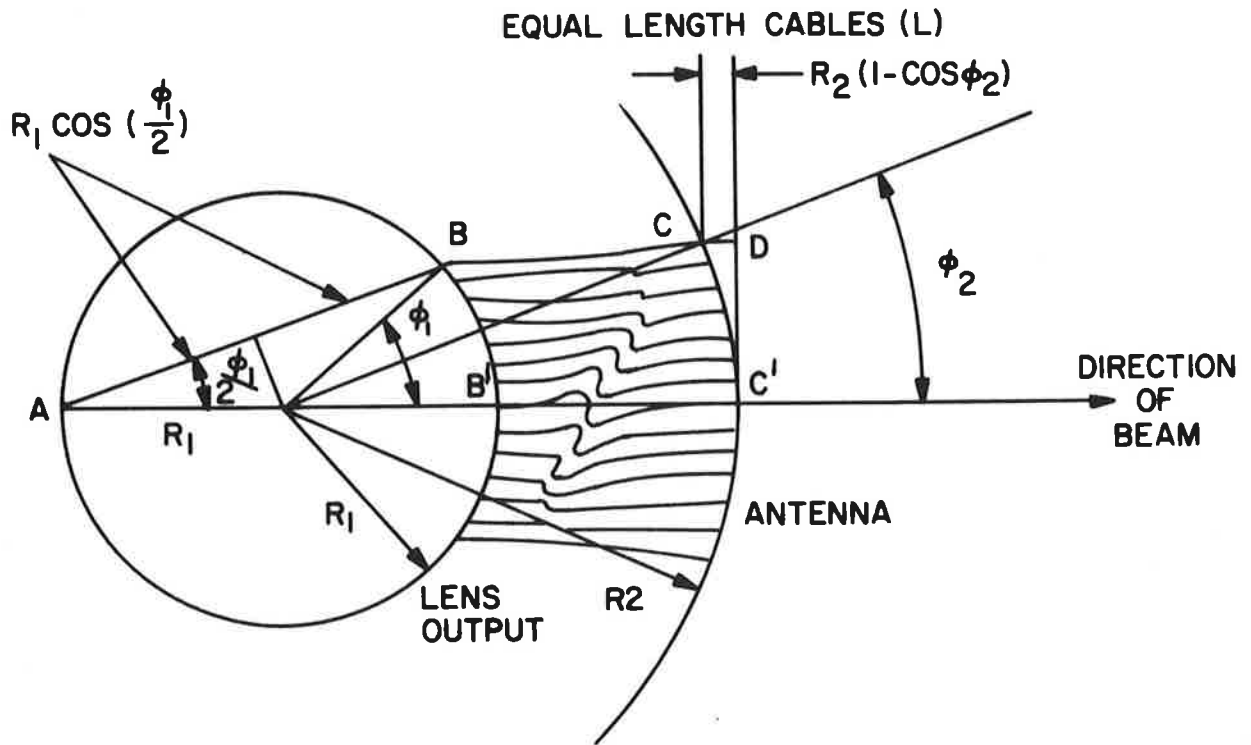


Figure 4.13 R-2R Lens Geometry

A popular lens which is appropriate to the MLGS is the R-2R lens, described by Boyns, et. al.<sup>1</sup>

To explain the operation, suppose that one probe is excited at A in Figure 4.13. One signal path is through the lens to B, through a cable, of length L, to C, and through air to point D on the phase front. Another path is straight through (A'B'C'). For collimation, these paths should be equal. The length AB is  $2R_1 \cos(\phi_1/2)$ ; CD is  $R_2(1-\cos \phi_2)$ ; AB' is  $2R_1$ , so that equating the two path lengths gives

$$2R_1 \cos\left(\frac{\phi_1}{2}\right) + L + R_2(1-\cos\phi_2) = 2R_1 + L$$

or

$$R_2(1-\cos\phi_2) = 2R_1\left(1-\cos\left(\frac{\phi_1}{2}\right)\right) \quad (4.2.1)$$

If  $R_2 = 2R_1$ , and if the lens probe spacing is chosen to give  $\phi_1 = 2\phi_2$ , this becomes an identity. The antenna has thus twice the radius of the lens (hence the name R-2R lens), and the lens probe spacing is twice the spacing (in angle) of the antenna elements. The probe spacing in units of electrical length are approximately the same for lens and antenna. The size of the lens can be reduced with the addition of dielectric material if this is necessary from the point of view of size.

If the input probe at an angle  $\Delta\phi$  clockwise from the initial probe is excited instead, the beam will move an angle  $\Delta\phi/2$  clockwise in space. If this process is continued, eventually the input probe will be an output probe for one of the prior beam positions. If coverage this wide were necessary, a signal routing problem would occur, since the lens probe would be connected to both an antenna element and the source network, necessitating either a switch or circulator. This is to be avoided if possible in order to keep insertion loss and complexity down. Quantitatively, the coverage limits imposed by this criterion can be calculated from the active sector angle  $\phi_a$ . If the antenna active sector is  $\phi_a$ , the lens active sector must be  $2\phi_a$ .

1. J.E. Boyns, A.D. Munger, J.H. Provencher, J. Reindel, and B.I. Small, "A Lens Feed for a Ring Array," IEEE Trans. Ant. & Prop., Vol AP-16, No. 2, pp. 264-267, March, 1968



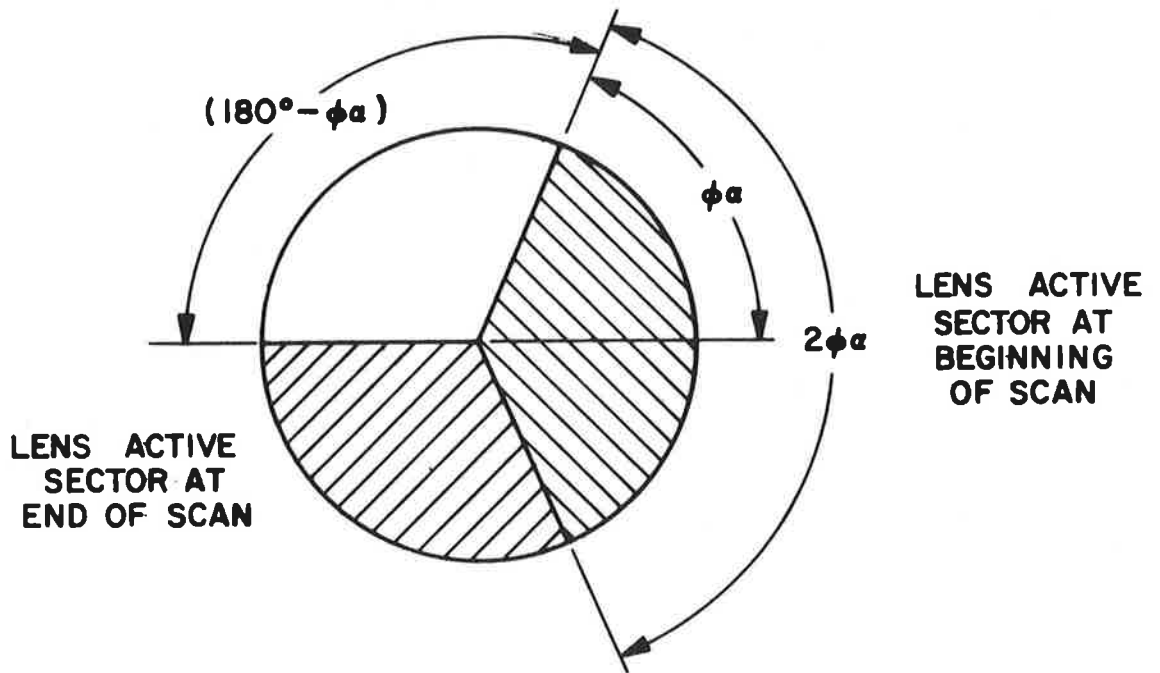


Figure 4.14 Lens Geometry for Determining Scanning Limits for a Given Active Sector

Moving the input probe clockwise, it can go no further than  $180^\circ - \phi_a$ .

Thus, the scan coverage in space must be  $\frac{1}{2}(180^\circ - \phi_a)$ , or

$$\phi_c \leq 90^\circ - \frac{\phi_a}{2}$$

Thus, for an active sector of  $60^\circ$ , the scan limits are  $\pm 30^\circ$ . In order to achieve a coverage of  $\pm 60^\circ$ , the active sector would have to be  $30^\circ$  or less, which would constitute an inefficient use of aperture, and require a large radius antenna. This does not rule it out as a possibility, but it is a significant cost disadvantage.

Another feature of the independent input and output probes is that the spacings can be different: the output probe spacing is dictated by the antenna spacing, but the input probe spacing can be chosen to optimize the aperture taper and sidelobe level.

If the same antenna is to be used for front and back course azimuth guidance, input and output probes must overlap and the discussion above does not apply.

Used in the landing system context, there are two methods of achieving fine steering. One is by "center-of-gravity" steering, wherein some form of variable power division network is used between source and lens so that the signal appears to emanate from a position between the actual probe positions. The second method is by fine steering with phase shifters placed after the lens (i.e., between lens and radiating elements). In a full circular R-2R lens, this would require a large number of phase shifters, since there must be one per radiating antenna element. For limited scan, this is not so serious. The disadvantage of the variable power division method is that more highly critical components are placed between source and lens increasing the probability of catastrophic failure. For these reasons the second method has been chosen for this application. It is shown in Figure 4.15 for symmetrical sum-beam patterns.

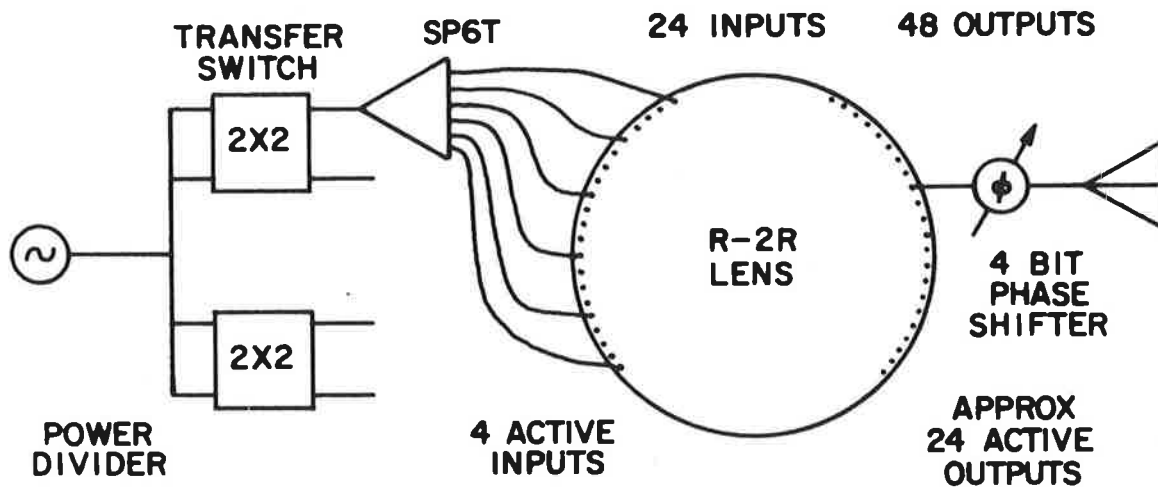


Figure 4.15 R-2R Antenna System Configuration

The system shown in the figure has four inputs, while the discussion considered only one. The reason for this is that exciting one input probe results in an aperture distribution which does not have sufficient taper to it, and as a result,

has unacceptably high side lobes. This can be seen with reference to Figure 4.16. Also, probes at the side of the

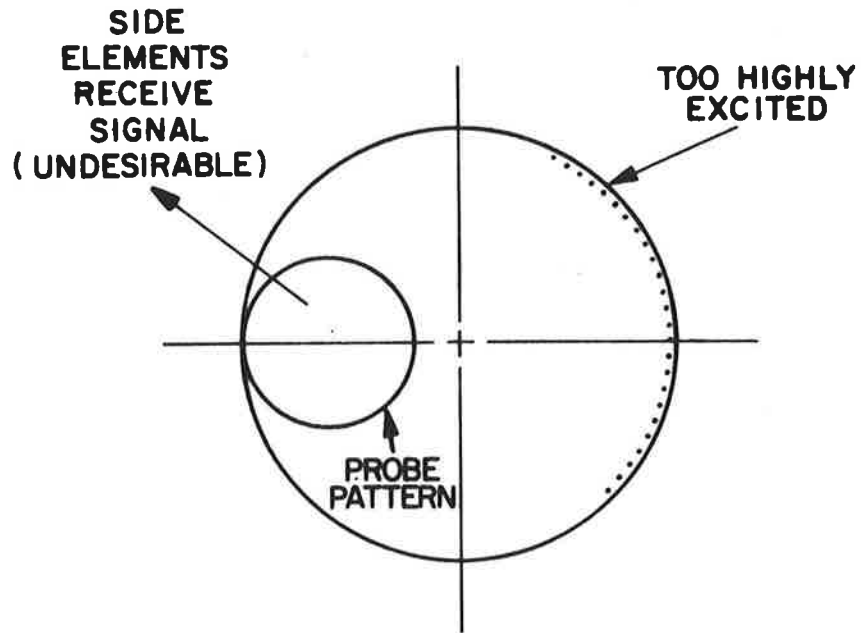


Figure 4.16 Lens Illumination with One Probe Excited

lens receive too much signal, and aggravate the defocusing problem. By simultaneously exciting several adjacent probes, the input pattern can control the aperture distribution. The distribution can be tapered to some extent to increase the signal to the center output probes, decrease that to the side probes, increase the aperture taper, and reduce sidelobes. The actual excitations have not yet been determined; this will be a matter of study in the early part of the next year.

#### 4.2.3 ELECTRONIC ATTENUATOR (VECTOR SWITCH) FEED

A design which at first glance seems undesirable, but which has many attractive features is the electronic attenuator approach.<sup>1</sup> This is illustrated in Figure 4.17.

1. J.E. Boyns, C.W. Gorham, A.D. Manger, J.H. Provencher, J. Reindel, and B.I. Small, "Step-Scanned Circular Array Antenna," IEEE Trans. Ant. & Prop., AP-13, No. 5 pp. 590-595, September 1970

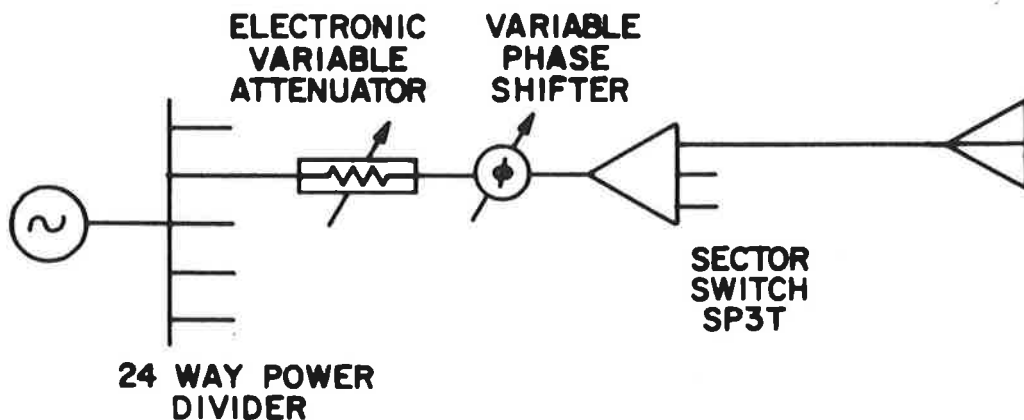


Figure 4.17 Electronic Attenuator (Vector Switch) Antenna System

Here the aperture distribution is set by electronically controlled attenuators. Coarse steering is accomplished by shifting the commands to the attenuators, shift register style, and resetting one sector switch. Fine steering is accomplished by the phase shifters. To illustrate, suppose initially that attenuators 1 through 24 are connected to antenna elements 1 through 24 respectively. Number 1 attenuator has a setting appropriate to the edge element. At the next coarse position it is desirable that number 2 antenna element have the edge distribution signal, and that number 25 element have the other edge signal. This is accomplished by resetting the sector switch which feeds antenna elements 1 and 25 (and 49) from number 1 position to number 25 position. At the same time, the electronic attenuators are all reset so that attenuator number 2 has the edge setting (formerly at 1), and number 1 has the other edge setting (formerly at 24), while others at number  $n$  have the setting formerly at  $n-1$ .

The obvious disadvantage of this approach is that power is absorbed by the attenuators in setting up the aperture distribution, which greatly increases insertion loss. For example, an aperture distribution given by cosine-squared-on-a-pedestal with 3:1 edge taper voltage represents a 3 dB insertion loss. This loss is offset by the reduction in the number of components in the signal path, which is less than any other approach. The advantages of this approach are discussed more fully in section 4.2.5.

The electronic attenuator itself requires a 3-bit control. It has been determined that eight levels of amplitude, equally spaced, are sufficient to suppress grating lobes, and cause no appreciable deterioration in sidelobe level from a continuous amplitude distribution.

The most straightforward attenuator technique is the PIN diode transmission-type attenuator. The attenuator levels are controlled by the drive current, and are approximately linear (in decibels) with current out to 10 dB of attenuation, which is sufficient for this application. This requires a three bit digital-to-analog converter in the drive circuitry, which does not appear to be difficult to achieve for the accuracies needed.

This approach has the advantage of reduced size. The attenuator, phase shifter, and sector switch could all be part of the same module. The power divider, or part of it, could also be included in the module.

Even if the loss proves to be higher than with alternative approaches, the extreme flexibility of this approach, which can easily accommodate optimized difference patterns, alterable beam shapes, larger antennas with narrower beamwidths, and step scan, may well justify this method.

#### 4.2.4 BUTLER MATRIX FEED

A Butler matrix is a passive network having  $N$  inputs and  $N$  outputs whose output distribution is a sampled Fourier transform of the input distribution. To understand the significance of this statement, several examples are cited for illustration: (1) if one input port is excited, all outputs are excited equally in amplitude, but with a phase that varies linearly with position, i.e., the difference in phase between adjacent ports is constant. The constant phase difference between ports depends on which input port is excited. (2) If the  $N$  input ports are excited equally in amplitude, but with a linear phase taper corresponding to one of those in (1), all the signal will come out of one port. (3) If the  $N$  input ports are excited equally in amplitude, but with a linear phase taper other than those in (1), the output distribution will be a sampled distribution of  $\sin x/x$ . (4) If a given phase and amplitude input distribution gives a desired output distribution, changing the input by a linear phase taper shifts the output distribution along the ports. If the phase taper corresponds to (1) the shift is perfect, i.e., the original output distribution is exactly reproduced, but translated.

If not there results an output distribution which is a translated approximation to the original.

The fourth property listed above means that both coarse and fine phasing can be accomplished with a bank of phase shifters as shown in Figure 4.18. The power divides

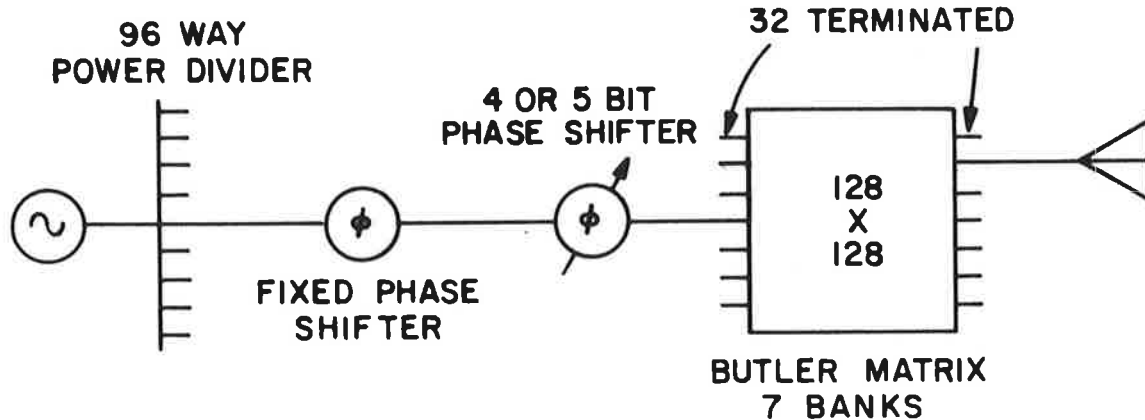


Figure 4.18 Butler Matrix Feed System - Standard Method

and fixed phase shifters set up the initial distribution, and the second bank of phase shifters serve to steer the beam. The desirable features are that it uses only one kind of active element, and exhibits graceful degradation and broad bandwidth (this is due to the fact that the fixed phase shifters can be collimating line lengths). The undesirable features are the higher tolerances on the Butler matrix hybrid components and lines, the difficulty of laying out a stripline design which has short enough line lengths to keep losses down at this frequency (in stripline), and the fact that quantization errors cause sidelobes, necessitating 5 bit phase shifters or special techniques.

A second technique is to use a suitable Butler matrix technique, as shown in Figure 4.19. This approach is probably no less lossy than the first one, since it has a SP3T switch where the other has two banks of hybrids. However, the diode count is very low, and 5-bank Butler matrix layouts have been built, although the authors are unaware of any at this frequency.

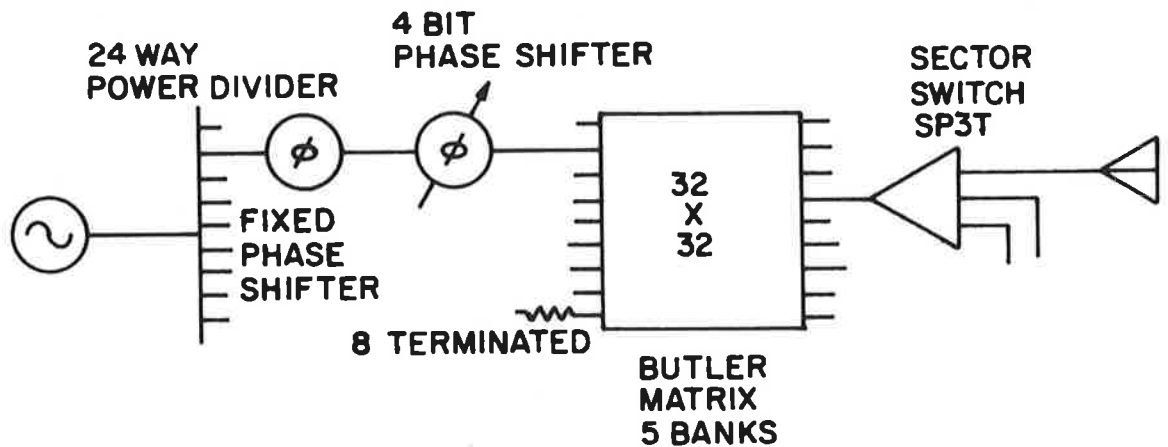


Figure 4.19 Butler Matrix Feed System - Switched Method

The chief difficulty with this design is the fact that narrower beamwidths require higher order Butler matrices, so it is not considered a serious contender for the  $1^\circ$  or  $2^\circ$  beamwidth cases.

#### 4.2.5 ADVANTAGES AND DISADVANTAGES OF CANDIDATE FEED SYSTEMS

The discussion which follows treats several designs which exist in the literature. It is important to note that these have only undergone minor modifications in the arrangements shown. Further modifications are anticipated in the future which will reduce the number of components and improve performance. The reason for this is that the full flexibility has not yet been sufficiently explored; for example, grouping elements in amplitude and/or phase may allow simpler designs.

It turns out that some designs which are better for large antennas are not the best choice for smaller ones. The discussion below tabulates some of the parameters for beamwidths of  $1^\circ$ ,  $2^\circ$ , and  $4^\circ$ .

There are many considerations which bear on the problem. Those which at this point are considered most important are now discussed.

1. Number of components. This impacts on the cost and the relative reliability.
2. Number of diodes. This is generally considered the most important measure of reliability in the sense of maintenance. The rationale for this is that active elements are expected to have a higher failure rate than passive ones. In an environment where limited mechanical and thermal stresses are encountered, this appears to be reasonable. This is the case for the landing system. The MTBF is a measure of the frequency of routine maintenance necessary.
3. Number of critical diodes. Diodes are considered critical if their failure results in a significant pointing error. Non-critical diode failures result in negligible pointing errors - this is called "graceful degradation", a desirable feature. It means that the system can continue to operate, and replacement or repair can be made at routine intervals.
4. Number of high power components. In some schemes there are components which pass a large fraction of the signal. This means that special techniques will have to be employed which sacrifice other properties, especially insertion loss.
5. Number of isolation, or leakage, points in directional signal path. By this is meant the number of junctions where energy is leaked out of the desired path, or where unwanted energy is fed into a signal path. An example is a transfer switch, where the isolation between paths is not perfect. This is particularly critical where several banks of these components are used. Other components are switches and hybrids.
6. Insertion loss. This is an extremely important criterion, because added insertion loss reduces the range of the system for a given source power, or increases the power requirements in order to achieve a given range. For example, a source which is 10% efficient feeding a system with 10 dB insertion loss radiates only 1% of the power supply input as RF energy.

In all of the parameters listed above, it is desirable to keep the numbers as low as possible, from both a cost and performance viewpoint



Table 4.1  
Component Symbols and Estimated Insertion Losses  
For Comparison of Various Feed Techniques

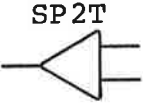
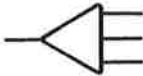
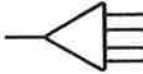
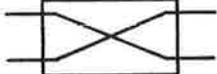
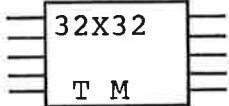
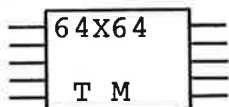
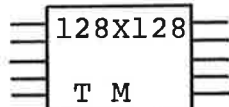
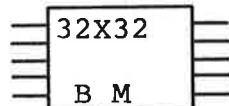
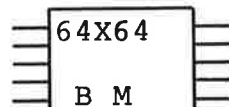
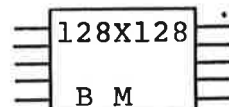
COMPONENT	SYMBOL	EST. IL, db
SP2T Switch	SP2T 	1.2
SP3T Switch	SP3T 	1.5
SP4T Switch	SP4T 	1.8
Transfer Switch (2X2)		1.1
Transfer Matrix (32X32)		5.1
Transfer Matrix (64X64)		6.1
Transfer Matrix (128X128)		7.1
Butler Matrix (32X32)		2.5
Butler Matrix (64X64)		3.0
Butler Matrix (128X128)		3.5

Table 4.1 (Continued)

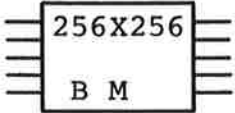
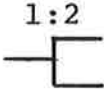
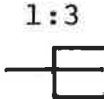
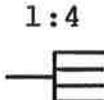
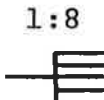
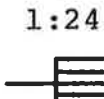
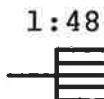
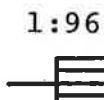
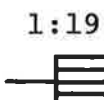
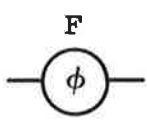
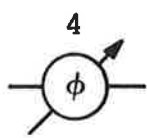
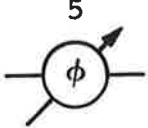


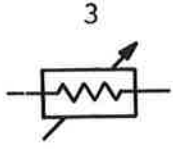
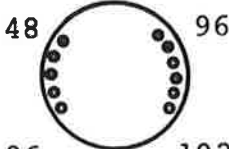
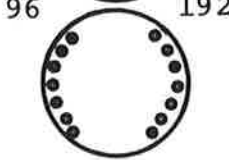
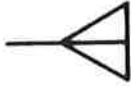

COMPONENT	SYMBOL	EST. IL, db
Butler Matrix (256X256)		4.0
1:2 Power Divider		0.4
1:3 Power Divider		0.6
1:4 Power Divider		0.8
1:8 Power Divider		1.2
1:24 Power Divider (1:2, 3, 4)		1.8
1:48 Power Divider (1:3, 4, 4)		2.2
1:96 Power Divider (1:2, 3,4,4)		2.6
1:192 Power Divider (1:3,4,4,4)		3.0
Phase Shifter, Fixed		0.1
Phase Shifter, 4 bit		1.7

Table 4.1 (Continued)

COMPONENT	SYMBOL	EST. IL, db
Phase Shifter, 5 bit		1.9
Hybrid (180°)		0.5
Hybrid (Quadrature)		0.4
Electrically Variable Attenuator (including 3 dB of Amplitude Tapering)		4.0
Lens (48 inputs, 96 outputs)		1.0
Lens (96 inputs, 192 outputs)		1.0
Antenna Module		1.0
Antenna Cable		1.0

#### 4.2.5.1 One-Degree Beamwidth Antenna

##### General characteristics:

Scan range:  $\pm 60^\circ$   
 Current distribution:  $\cos^2 x + .5$   
 Active sector:  $60^\circ$   
 Number of elements, total: 288  
 Number of active elements: 96  
 Element spacing:  $.65\lambda$   
 Radius: 11.59 feet  
 Sidelobe level: -26 dB

##### A. Transfer Matrix Technique

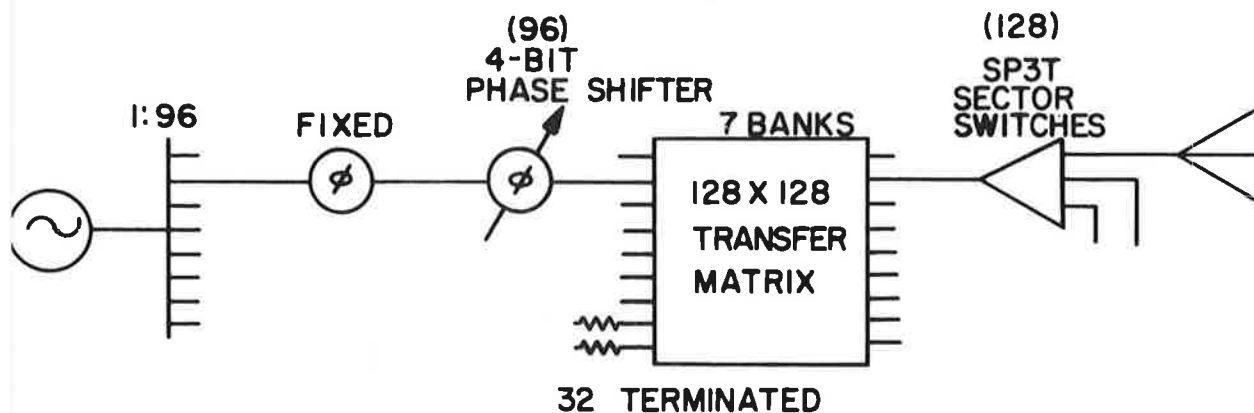


Figure 4.20 Diagram of Transfer Matrix Technique Feed System ( $1^\circ$  BW)

Number of SP3T Switches - 128

Diode Count -  $128 \times 3 = 384$

Leakage points - 1

Number of Transfer Switches:

Before removal of unused switches:  $7 \text{ banks} \times 64 = 448$

Unused switches  $5 \text{ banks} \times 16 = 80$

After removal of unused switches:  $448 - 80 = 368$

Diode Count:  $368 \times 4 = 1472$

Leakage points in directional path - 7

Number of Phase Shifters - 96

Diode Count (Est.) -  $96 \times 8 = 768$

Total Diode Count:  $384 + 1472 + 768 = 2624$

Critical Diode Count 0

High Power Diode Count 0

Number of Leakage Points 8

Insertion loss:  $2.6 + 0.1 + 1.7 + 7.1 + 1.5 + 1.0$   
 $+ 1.0 = 15.0$  dB

Remarks: (a) The scheme as it is allows  $\pm 90^\circ$  scan. If SP2T sector switches are used,  $\pm 50^\circ$  is achieved.

(b) Fixed phase shifters are passive collimating lengths of transmission line.

#### B. R-2R Lens Technique

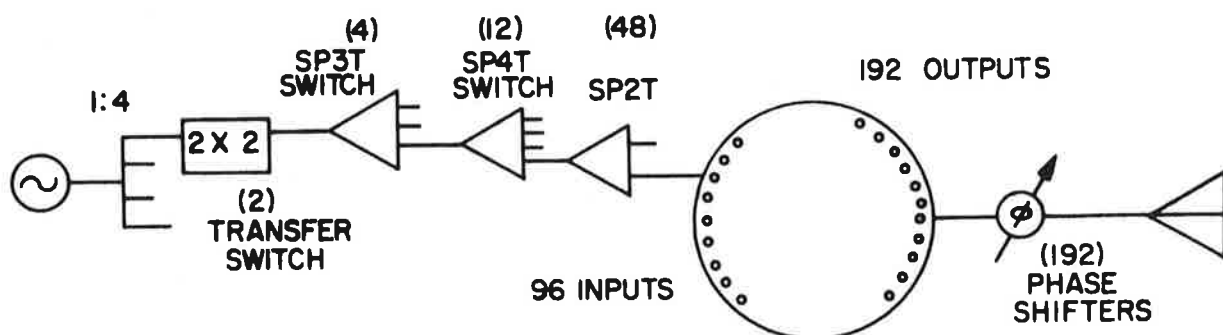


Figure 4.21 Diagram of Butler Matrix Feed System ( $1^0$ BW)

Number of Transfer Switches - 2

Diode Count -  $2 \times 4 = 8$

Leakage Points - 1

Number of SP3T Switches - 4

Diode Count -  $4 \times 3 = 12$

Leakage Points - 1

Number of SP4T Switches - 12

Diode Count -  $12 \times 4 = 48$

Leakage Points - 1

Number of SP2T Switches - 48

Diode Count -  $48 \times 2 = 96$

Leakage Points - 1

Number of Phase Shifters - 192

Diode Count -  $192 \times 8 = 1536$

Total Diode Count -  $8 + 12 + 48 + 96 + 1536 = 1700$

Critical Diode Count - 164

High Power Diode Count - 164

Number of Leakage Points - 4

Insertion loss:  $0.8 + 1.1 + 1.5 + 1.8 + 1.2 + 1.0$   
 $+ 1.7 + 1.0 + 1.0 = 11.1$  dB

- Remarks: (a) This scheme is limited to a scan range of  $\pm 30^\circ$ . The reason for this is that wider scans would require that some lens probes be used for input and output, necessitating added circuitry.
- (b) The fact that only one bank of transfer switches is used is premised on the assumption that the distribution is symmetric. If a different pattern were used, another bank would be necessary.
- (c) It is possible to build switches with larger numbers of throws, e.g., a SP6T switch. This could reduce insertion loss somewhat.

### C. Electronic Attenuator Technique

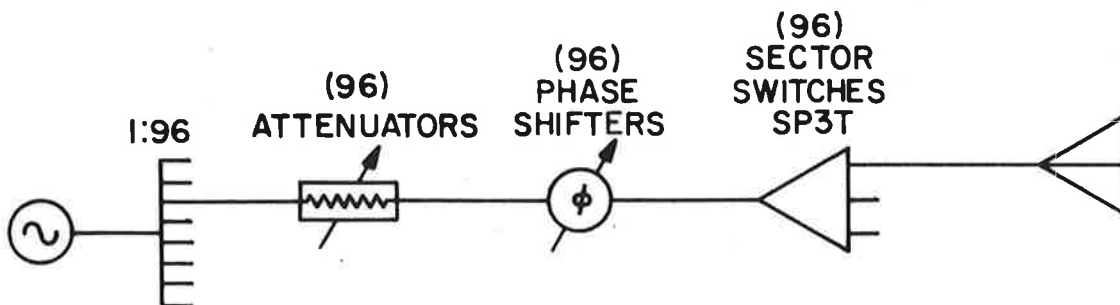


Figure 4.22 Diagram of Electronic Attenuator Feed System ( $1^\circ$ BW)

Number of Attenuators - 96

Diode Count -  $96 \times 2 = 192$

Number of Phase Shifters - 96

Diode Count -  $96 \times 8 = 768$

Number of SP3T Switches - 96

Diode Count -  $96 \times 3 = 288$

Leakage Points - 1

Total Diode Count -  $192 + 768 + 288 = 1248$

Critical Diode Count 0

High Power Diode Count 0

Number of Leakage Points 1

Insertion loss:  $2.6 + 4.0 + 1.7 + 1.5 + 1.0 + 1.0$   
 $= 11.8 \text{ dB}$

D. Butler Matrix Technique-Conventional

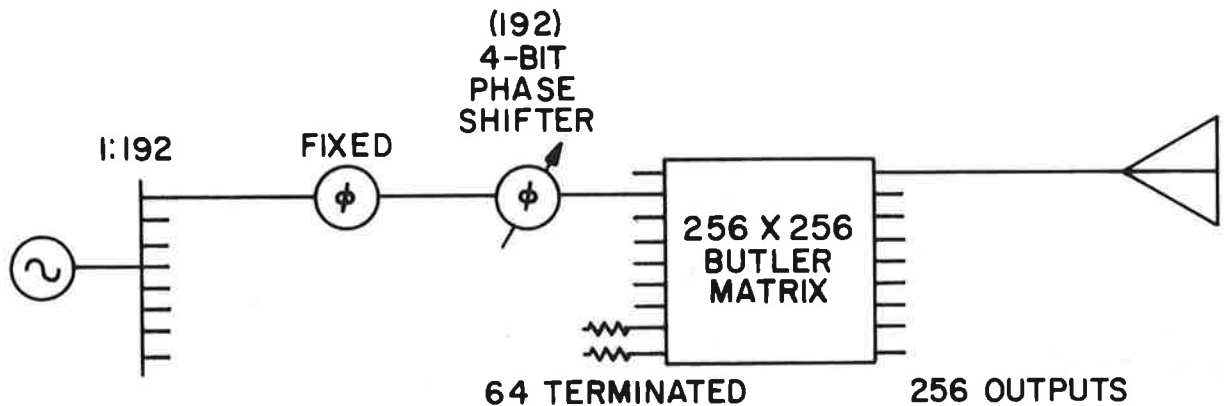


Figure 4.23 Diagram of Butler Matrix Feed System ( $1^\circ\text{BW}$ )

Number of Phase Shifters - 192

Diode Count -  $192 \times 8 = 1536$

Number of Hybrid Banks - 8

Number of Hybrids -  $128 \times 8 - 32 \times 6 = 832$

Number of Leakage Points - 8

Total Diode Count - 1536

Critical & High Power Diode Count 0

Number of Leakage Points - 8

Insertion loss:  $3.0 + 0.1 + 1.7 + 4.0 + 1.0 + 1.0$   
 $= 10.8 \text{ dB}$

- Remarks:
- (a) Fixed phase shifters are passive collimating lengths of line.
  - (b) This scheme gives coverage of  $\pm 50^\circ$  only; more could require a larger Butler matrix.
  - (c) The large number of phase shifters is necessary for suppressing currents on non-active elements. This might be reduced somewhat.

E. Butler Matrix Technique-Switched

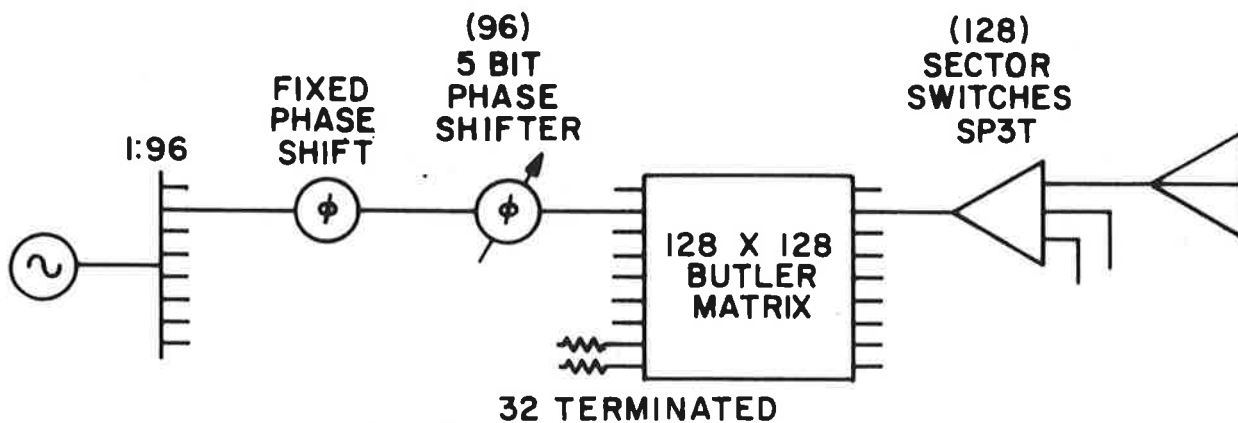


Figure 4.24 Diagram of Butler Matrix Technique - Switched Feed System ( $1^\circ$ BW)



Number of Phase Shifters - 96

Diode Count -  $96 \times 10 = 960$

Number of Banks of Hybrids - 7

Number of Hybrids -  $64 \times 7 - 16 \times 4 = 362$

Number of Leakage Points - 7

Number of SP3T Switches - 128

Diode Count -  $128 \times 3 = 384$

Leakage Points - 1

Total Diode Count -  $960 + 384 = 1344$

Critical Diode Count - 0

High Power Diode Count - 0

Number of Leakage Points - 8

Insertion loss:  $2.6 + 0.1 + 1.9 + 3.5 + 1.5 + 1.0$   
 $+ 1.0 = 11.6$  dB

- Remarks: (a) The scheme as it is allows  $\pm 90^\circ$  scan. If SP2T sector switches are used,  $\pm 50^\circ$  is achieved.
- (b) Fixed phase shifters are passive collimating lengths of transmission line.
- (c) Five bit phase shifters are necessary in order to keep the quantization sidelobes down.

#### 4.2.5.2 Two Degree Beamwidth Antenna

##### General Characteristics:

Scan range:  $\pm 60^\circ$

Current distribution:  $\cos^2 x + .5$

Active sector:  $60^\circ$

Number of elements, total: 144

Number of active elements: 48

Element spacing:  $.65\lambda$

Radius: 5.80 feet

Sidelobe level: -26 dB

##### A. Transfer Matrix Technique

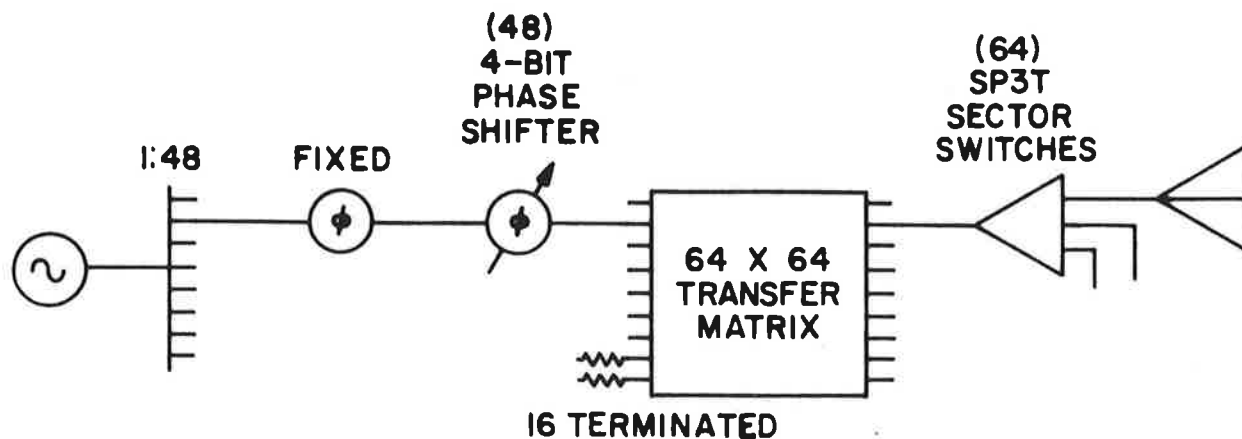


Figure 4.25 Diagram of Transfer Matrix Feed System ( $2^\circ$ BW)

Number of SP3T Switches - 64

Diode Count -  $64 \times 3 = 192$

Leakage Points - 1

Number of Transfer Switches -  $32 \times 6 - 8 \times 4 = 160$

Diode Count -  $160 \times 4 = 640$

Leakage Points - 6

Number of Phase Shifters - 48

Diode Count -  $48 \times 8 = 384$

Total Diode Count -  $192 + 640 + 384 = 1216$

Critical and High Power Diode Circuit - 0

Number of Leakage Points - 7

Insertion loss:  $2.2 + 0.1 + 1.7 + 6.1 + 1.5 + 1.0 + 1.0 = 13.6$  dB

Remarks: (a) The scheme as it is allows  $\pm 90^\circ$  scan. If SP2T sector switches are used,  $\pm 50^\circ$  is achieved.

(b) Fixed phase shifters are passive collimating lengths of transmission line.

B. R-2R Lens Technique

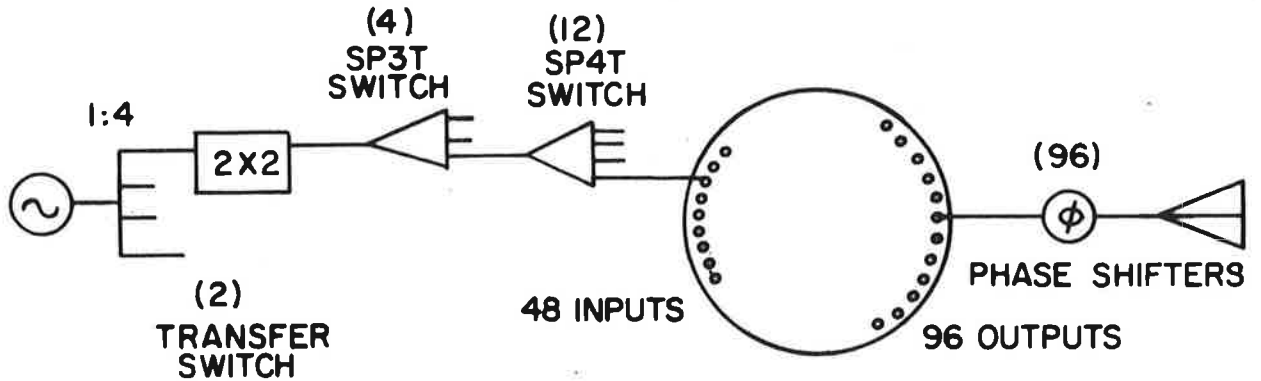


Figure 4.26 Diagram of R-2R Lens Technique Feed System (2°BW)

Number of Transfer Switches - 2

Diode Count -  $2 \times 4 = 8$   
Leakage Points - 1

Number of SP3T Switches - 4

Diode Count -  $4 \times 3 = 12$   
Leakage Points - 1

Number of SP4T Switches - 12

Diode Count -  $12 \times 4 = 48$   
Leakage Points - 1

Number of Phase Shifters - 96

Diode Count -  $96 \times 8 = 768$

Total Diode Count -  $8 + 12 + 48 + 768 = 836$

Critical and High Power Diode Count - 68

Number of Leakage Points - 3

Insertion loss:  $0.8 + 1.1 + 1.5 + 1.8 + 1.0 + 1.7$   
 $+ 1.0 + 1.0 = 9.9$  dB

- Remarks:
- (a) This scheme is limited to a scan range of  $\pm 30^\circ$ . The reason for this is that wider scans would require that some lens probes be used for input and output, necessitating added circuitry.
  - (b) The fact that only one bank of transfer switches is used is premised on the assumption that the distribution is symmetric. If a different pattern were used, another bank would be necessary.
  - (c) It is possible to build switches with larger numbers of throws, e.g., a SP6T switch. This could reduce insertion loss somewhat.

C. Electronic Attenuator Technique

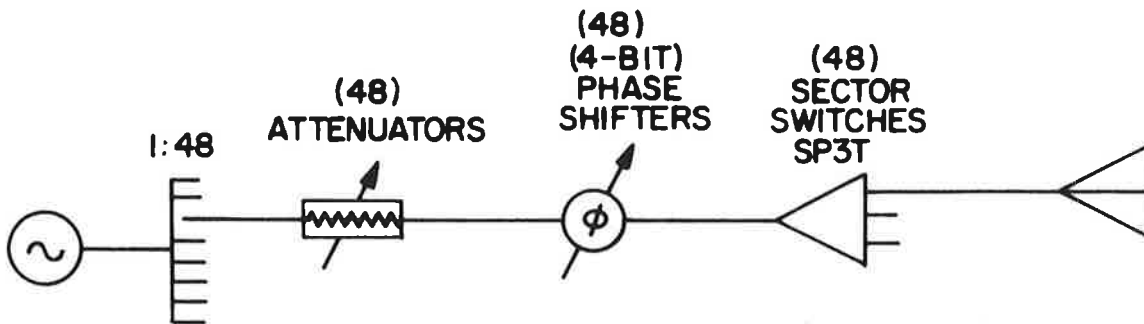


Figure 4.27 Diagram of Electronic Attenuator Feed System ( $2^\circ$  BW)

Number of Attenuators - 48

Diode Count -  $48 \times 2 = 96$

Number of Phase Shifters - 48

Diode Count -  $48 \times 8 = 384$

Number of SP3T Switches - 48

Diode Count -  $48 \times 3 = 144$

Leakage Points - 1

Total Diode Count -  $96 + 384 + 144 = 624$   
 Critical and High Power Diode Count - 0  
 Number of Leakage Points - 1  
 Insertion loss:  $2.2 + 4.0 + 1.7 + 1.5 + 1.0 + 1.0$   
 $= 11.4 \text{ dB}$

D. Butler Matrix Technique-Conventional

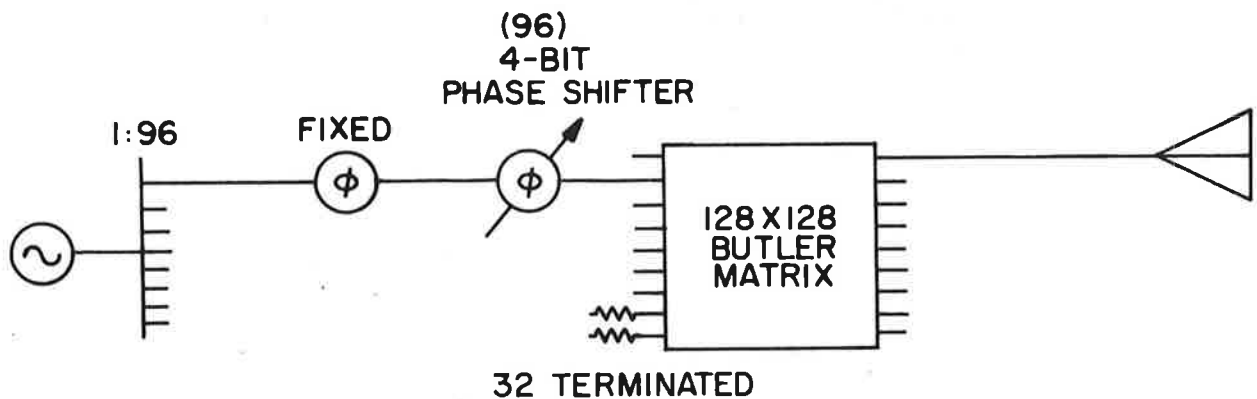


Figure 4.28 Diagram of Butler Matrix Technique-Conventional Feed System (  $2^{\circ}$ BW)

Number of Phase Shifters - 96

Diode Count -  $96 \times 8 = 768$

Number of Hybrid Banks - 7

Number of Hybrids -  $64 \times 7 - 16 \times 5 = 368$

Number of Leakage Points - 7

Total Diode Count - 768

Critical and High Power Diode Count - 0

Number of Leakage Points - 8

Insertion loss:  $2.6 + 0.1 + 1.7 + 3.5 + 1.0 + 1.0$   
 $= 9.9 \text{ dB}$

Remarks: (a) Fixed phase shifters are passive collimating lengths of line.

(b) This scheme gives coverage of  $\pm 50^{\circ}$  only--

- more could require a larger Butler matrix.
- (c) The large number of phase shifters is necessary for suppressing currents on non-active elements. This might be reduced somewhat.

E. Butler Matrix Technique-Switched

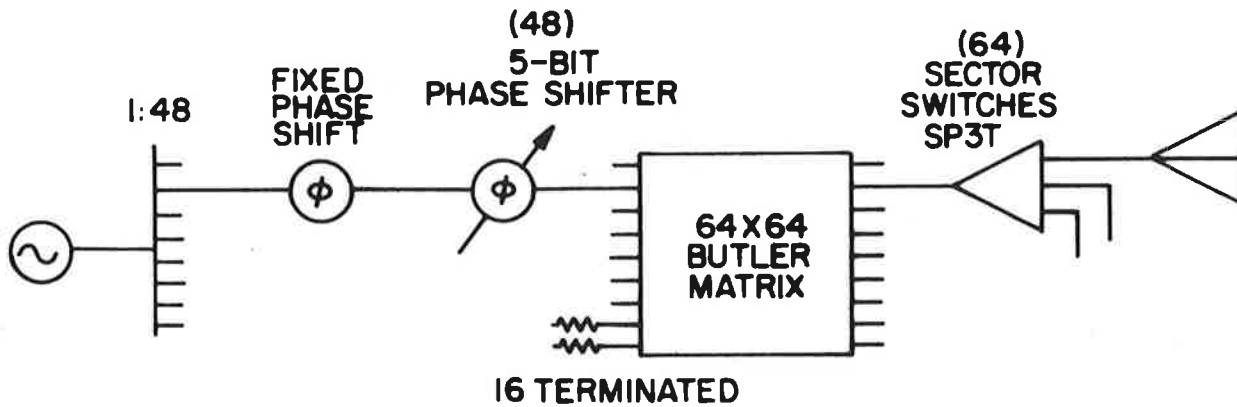


Figure 4.29 Diagram of Butler Matrix Technique-Switched Feed System ( $2^{\circ}$ BW)

Number of Phase Shifters - 48

Diode Count  $48 \times 10 = 480$

Number of Banks of Hybrids - 6

Number of Hybrids -  $32 \times 6 - 8 \times 4 = 160$

Number of Leakage Points - 6

Number of SP3T Switches - 64

Diode Count -  $64 \times 3 = 192$

Leakage Points - 1

Total Diode Count -  $480 + 192 = 572$

Critical Diode Count - 0

High Power Diode Count - 0

Number of Leakage Points - 7

Insertion loss:  $2.2 + 0.1 + 1.9 + 3.0 + 1.5 + 1.0$   
 $+ 1.0 = 10.7$  dB

- Remarks: (a) The scheme as it is allows  $\pm 90^\circ$  scan. If SP2T sector switches are used,  $\pm 50^\circ$  is achieved.
- (b) Fixed phase shifters are passive collimating lengths of transmission line.
- (c) Five bit phase shifters are necessary in order to keep the quantization sidelobes down.

#### 4.2.5.3 Four-Degree Beamwidth Antenna

##### General characteristics:

Scan range:  $\pm 60^\circ$   
 Current distribution:  $\cos^2 x + 0.5$   
 Active sector:  $60^\circ$   
 Number of elements, total: 72  
 Number of active elements: 24  
 Element spacing:  $.65\lambda$   
 Radius: 2.90 feet  
 Sidelobe level: -26 dB

##### A. Transfer Matrix Technique

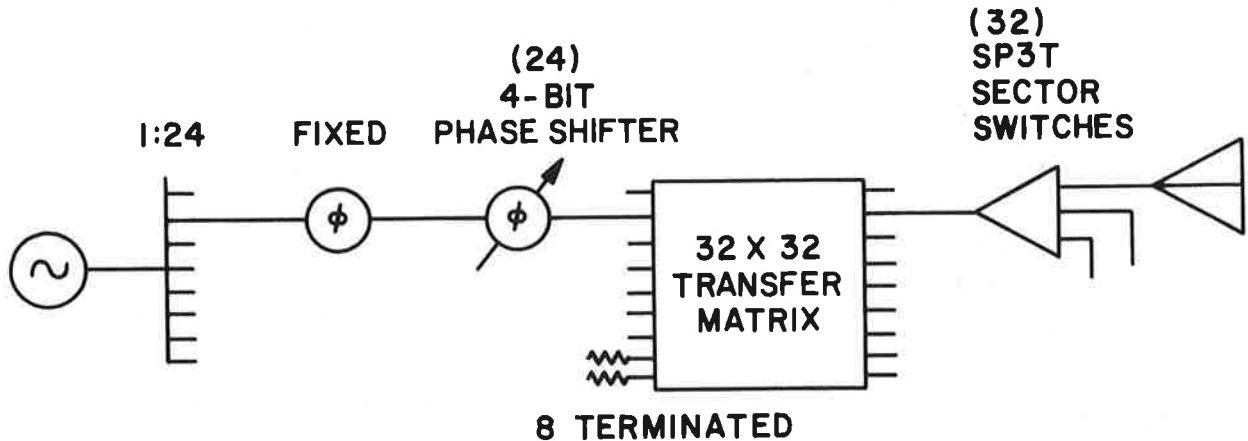


Figure 4.30 Diagram of Transfer Matrix Feed System ( $4^\circ$ BW)

Number of SP3T Switches - 32

Diode Count -  $32 \times 3 = 96$

Leakage Points - 1

Number of Transfer Switches -  $16 \times 5 - 4 \times 3 = 68$

Diode Count -  $68 \times 4 = 272$

Leakage Points - 5

Number of Phase Shifters - 24

Diode Count -  $24 \times 8 = 192$

Total Diode Count -  $96 + 272 + 192 = 560$

Critical Diode Count - 0

High Power Diode Count - 0

Number of Leakage Points - 6

Insertion loss:  $1.8 + 0.1 + 1.7 + 5.1 + 1.5 + 1.0$   
 $+ 1.0 = 12.2$  dB

- Remarks: (a) The scheme as it is allows  $\pm 90^\circ$  scan. If SP2T sector switches are used,  $\pm 50^\circ$  is achieved.  
(b) Fixed phase shifters are passive collimating lengths of transmission line.

#### B. R-2R Lens Technique

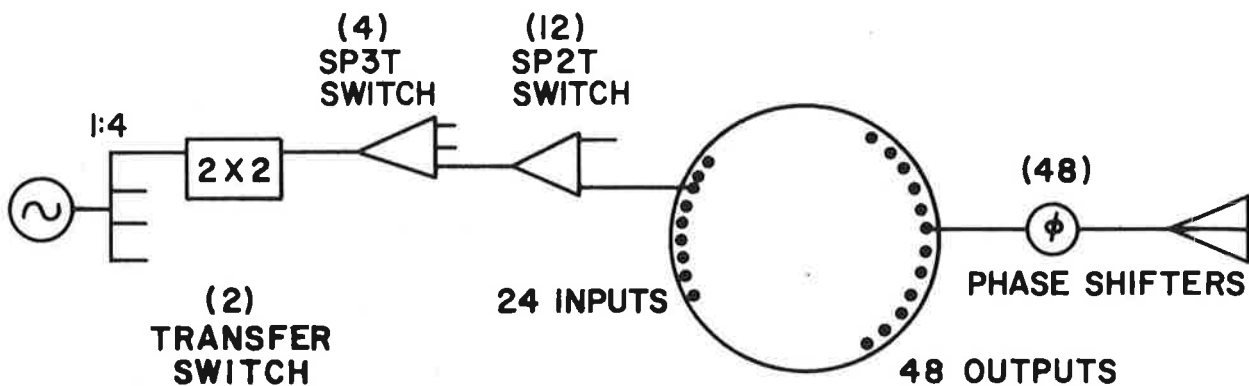


Figure 4.31 Diagram of R-2R Lens Technique Feed System ( $4^\circ$ BW)

Number of Transfer Switches - 2

Diode Count -  $2 \times 4 = 8$

Leakage Points - 1

Number of SP3T Switches - 4

Diode Count -  $4 \times 3 = 12$

Leakage Points - 1



Number of SP2T Switches - 12

Diode Count -  $12 \times 2 = 24$   
Leakage Points - 1

Number of Phase Shifters - 48

Diode Count -  $48 \times 8 = 384$

Total Diode Count -  $8 + 12 + 24 + 384 = 428$

High Power and Critical Diode Count - 44

Number of Leakage Points - 3

Insertion loss:  $0.8 + 1.1 + 1.5 + 1.2 + 1.0 + 1.7$   
 $+ 1.0 + 1.0 = 9.3$  dB

- Remarks:
- (a) This scheme is limited to a scan range of  $\pm 30^\circ$ . The reason for this is that wider scans would require that some lens probes be used for input and output, necessitating added circuitry.
  - (b) The fact that only one bank of transfer switches is used is premised on the assumption that the distribution is symmetric. If a different pattern were used, another bank would be necessary.
  - (c) It is possible to build switches with larger numbers of throws, e.g., a SP6T switch. This could reduce insertion loss somewhat.

### C. Electronic Attenuator Technique

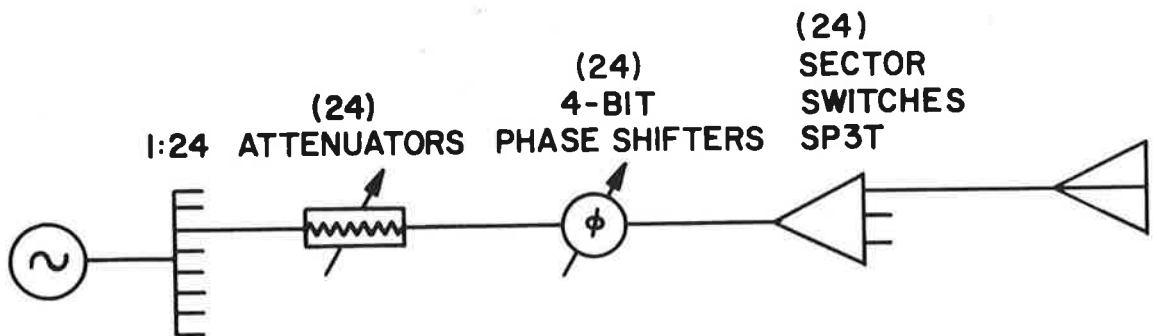


Figure 4.32 Diagram of Electronic Attenuator Technique Feed System (4°BW)

Number of Attenuators - 24

Diode Count -  $24 \times 2 = 48$

Number of Phase Shifters - 24

Diode Count -  $24 \times 8 = 192$

Number of SP3T Switches - 24

Diode Count -  $24 \times 3 = 72$

Total Diode Count -  $48 + 192 + 72 = 312$

Critical Diode Count - 0

High Power Diode Count - 0

Number of Leakage Points - 1

Insertion loss:  $1.8 + 4.0 + 1.7 + 1.5 + 1.0$   
 $+ 1.0 = 11.0$  dB

D. Butler Matrix Technique-Conventional

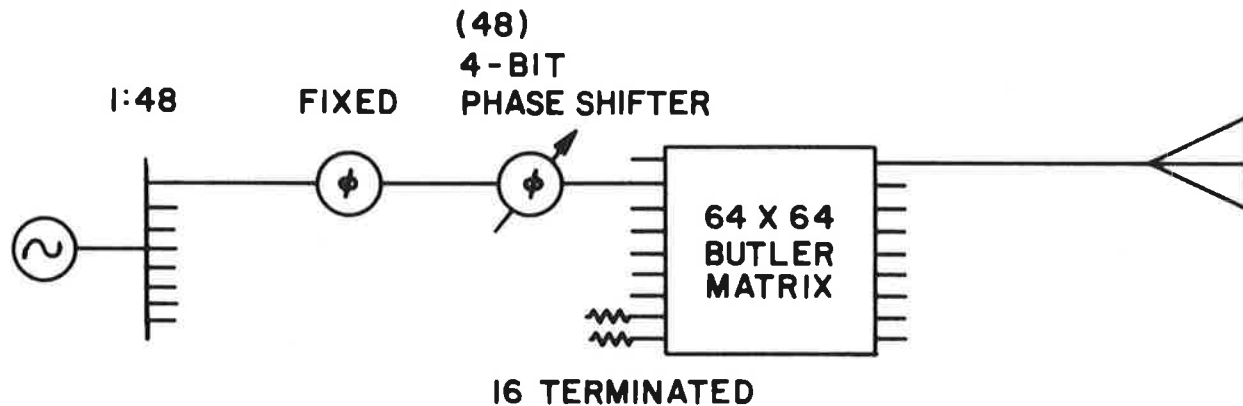


Figure 4.33 Diagram of Butler Matrix Technique-Conventional Feed System ( $4^0$ BW)

Number of Phase Shifters - 48

Diode Count -  $48 \times 8 = 384$

Number of Hybrid Banks - 6

Number of Hybrids -  $32 \times 6 - 8 \times 4 = 160$

Number of Leakage Points - 7

Total Diode Count - 384

Critical Diode Count - 0

High Power Diode Count - 0

Number of Leakage Points - 7

Insertion loss:  $2.2 + 0.1 + 1.7 + 3.0 + 1.0$   
 $+ 1.0 = 9.0 \text{ dB}$

- Remarks: (a) Fixed phase shifters are passive collimating lengths of line.  
(b) This scheme gives coverage of  $\pm 50^\circ$  only -- more would require a larger Butler matrix.  
(c) The large number of phase shifters is necessary for suppressing currents on non-active elements. This might be reduced somewhat.

E. Butler Matrix Technique-Switched

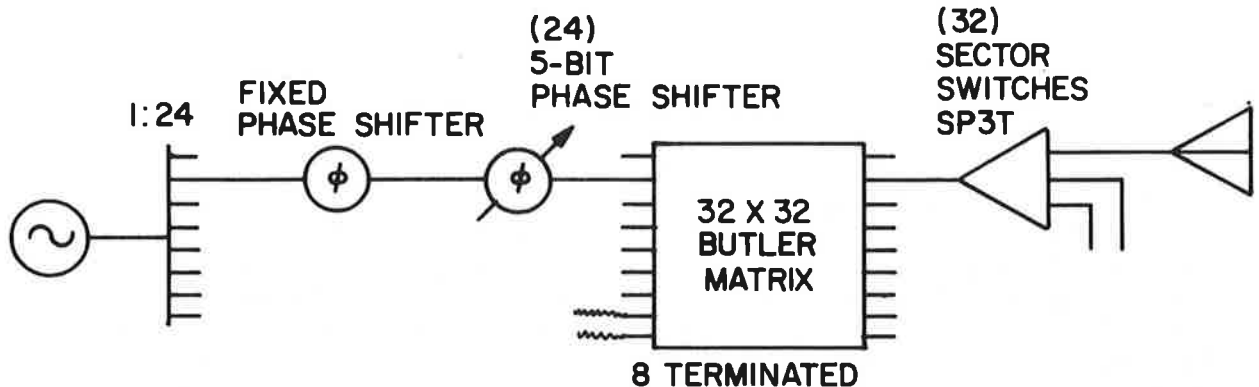


Figure 4.34 Diagram of Butler Matrix Technique-Switched Feed System ( $4^\circ \text{BW}$ )

Number of Phase Shifters - 24

Diode Count -  $24 \times 10 = 240$

Number of Banks of Hybrids - 5

Number of Hybrids -  $16 \times 5 - 4 \times 3 = 68$

Number of Leakage Points - 5

Number of SP3T Switches - 32

Diode Count -  $32 \times 3 = 96$

Leakage Points - 1

Total Diode Count -  $240 + 96 = 336$

Critical Diode Count - 0

High Power Diode Count - 0

Number of Leakage Points - 6

Insertion loss:  $1.8 + 0.1 + 1.9 + 2.5 + 1.5 + 1.0$   
 $+ 1.0 = 9.8$  dB

- Remarks: (a) The scheme as it is allows  $\pm 90^\circ$  scan. If SP2T sector switches are used,  $\pm 50^\circ$  is achieved.
- (b) Fixed phase shifters are passive collimating lengths of transmission line.
- (c) Five bit phase shifters are necessary in order to keep the quantization sidelobes down.

#### 4.2.5.4 Discussion of Various Feed Systems

It is apparent from the information tabulated above that for a one-degree beamwidth, the electronic attenuator method is the best candidate system. It has the lowest diode count, no critical diodes or high power diodes and the lowest number of leakage points. Only the conventional Butler matrix approach offers a significantly better insertion loss (namely, 1 dB), a fact offset by the other considerations. It has the advantage that the attenuator, phase shifter, and sector switch can be constructed on one module, eliminating the need for two sets of connector pairs, thus improving the reliability. The other approaches offer very difficult fabrication problems.

For the four degree beamwidth antenna, the lens and Butler matrix methods offer about 2 dB improvement, and the fabrication problems are not so severe. The electronic attenuator still uses the smallest number of diodes, but the difference is not great. The lens uses twice the number

of phase shifters, about two-thirds the number of switches (high power, however) and no attenuators. The lens itself is small, (about three feet in diameter using an air dielectric) and is relatively cheap. If  $\pm 30^\circ$  of scan is sufficient, it is a possible candidate. The Butler matrix methods use larger matrices than have been fabricated on one stripline board. Using this approach fabrication and layout methods would have to be explored further before confidence could be had in the technique.

The two-degree antenna is even more uncertain, since the tradeoff between insertion losses and other parameters is not clear. It remains to be established how severe the RF power requirements are, and how critical the range of the system is. The actual performance obtained from the various approaches must be determined experimentally from measurements on components specially designed for the MLGS.

It should again be emphasized that the above approaches do not represent the only possible approaches, and that new concepts may emerge in the future which are superior in performance and/or cost than those cited here.

Another consideration that should not be overlooked deals with the possibility that back course guidance may be required from the same antenna; or, a full  $360^\circ$  capability may be desirable every few scans. Both the lens and the conventional Butler matrix become so complex and lossy as to render them out of competition. The switching approaches all require merely changing the sector switches to SP6T switches, and  $360^\circ$  coverage is attained. The electronic attenuator looks more attractive than ever under this condition.

## CHAPTER V EXPERIMENTAL LOGIC AND BEAM STEERING COMPUTER DESIGN

Since the final choice as to the feed network awaits experimental results, it is premature to fix the computer design at this time. However, it is well to think through the problems associated with its design. Accordingly, a beam steering design has been completed which meets satisfactorily the requirements of the most complex candidate feed network for a cylindrical array, namely, the electronic attenuator, or vector switch, approach. For this experimental model there are 24 phase shifters, and 24 single pole double throw switches. The 24 phase shifters perform the fine scanning and may be required to generate as many as 32 beam positions per coarse position, or about 50 beam positions per beamwidth. In order to accommodate the RTCA format, about 1 millisecond per beamwidth is the scan speed used. This implies about 20 microseconds per beam position, or a clock rate of 50 kHz. A variable clock rate of 10 kHz to 100 kHz allows for a range of variation around 50 kHz of faster scans by 2:1 and slower scans (or increased dwell time) of 5:1.

If switching time between states is 500 nanoseconds, the ratio of off-time to on-time is  $.5/20 = 2.5\%$  which appears to be an acceptable figure. This will be subject to revision.

In the experimental phase, it will be necessary to use more flexible (and thus more costly) components. For example, the number of fine scan beam positions will be variable; the memories will be alterable; a manual override will allow placement of the beam by an operator. These conditions will not be necessary once the design decisions are made.

The design presented here is based on the laboratory model requirements, and would require some added complexity and appreciable added size in order to accommodate a narrow beamwidth. (The memory size is approximately inversely proportioned to beamwidth.)

### 5.1 Control Logic Implementation

*Abstract-The memory requirements associated with various control logic implementation are compared.*

Several techniques for implementing the control logic were considered. Among the basic approaches studied were: (1) stored memory only (2) stored memory plus shift registers, and (3) stored memory plus a switch matrix.

The first solution, stores all control commands on alterable ROM's. The memory required for this purpose is:

- (1) Attenuator settings  
24 paths X 24 coarse positions X 3 bits = 1728 bits
- (2) Sector switches  
24 paths X 24 coarse positions X 1 bit = 576 bits
- (3) Phase shifters  
24 paths X 24 coarse X 32 fine positions  
X 4 bits = 73,728 bits

TOTAL MEMORY = 76,032 bits

The above technique requires a considerable amount of memory, the bulk of which is needed for phase information. It would be desirable to use any symmetry the system possesses to reduce this number which is the motivation behind the second approach.

A comparison of the phase settings for two different coarse positions (assuming the same fine scan position) reveals that the phase commands are shifted in accordance with the coarse position displacement. If this symmetry were utilized the phase data memory could be reduced by a factor of twenty-four. Under this scheme, the phase settings required for all fine positions are stored, and then rotated with shift registers to achieve the final ordering.

The third solution is a further refinement of the above approach and employs a switch matrix to rotate the phase settings. Such a matrix consists of five banks of switches, each of which commutes the input by  $2^n$  positions, where  $n=0, 1, 2, 3, 4$ .

The memory required for the second and third approaches is:

Attenuator settings	1728 bits
Sector switches	576 bits
Phase shifters	<u>3072 bits</u>

TOTAL MEMORY 5376 bits

The beam steering control unit described in the following sections is based on the second solution.

## 5.2 Control Unit Description

*Abstract-The digital logic required for steering the MLGS beam is derived. The solution is based upon the use of field alterable memory and shift registers. Operation of the control logic is discussed, and the associated timing and logic flow diagrams presented.*

The logic required for steering the beam of the microwave guidance landing system antenna is provided by the control unit. For each beam pointing position, it supplies 192 bits of data. This information is used to set the 4-bit phase shifters, the 3-bit attenuators, and the sector switches.

The MLGS control unit incorporates the following features.

- (1) Fine increment granularity control: Allows the number of fine steering increments associated with each coarse position to be varied among 4, 8, 16 and 32 steps. This flexibility is necessary in the study phase in establishing the number of fine steps per beam width in the final model.
- (2) Manual input: Placing the AUTO/MANUAL switch in the MANUAL position enables the operator to select any of the available 1024 beam positions. This is accomplished in conjunction with a set of 10 toggle switches located on the control panel. Manual operation allows the beam to be held in any pointing position, providing the flexibility necessary for testing the system, position by position.
- (3) Variable internal clock: The system incorporates a central clock which is continuously variable over the range 10KC to 100KC. This allows the scan rate to vary over a 10:1 range.
- (4) Control Unit Monitoring: The commands generated by the control unit may be monitored by observing the output on a bank of minilamps. This is accomplished by switching the input mode switch to MANUAL and comparing the settings on the lamps to the desired values for select azimuth positions.

The landing guidance system control unit is made up of four major functional blocks: these are: (1) azimuth position selection; (2) system timing; (3) control command generation and (4) switch drivers. These sub-blocks perform the following operations.



### Azimuth position selection:

Establishes the appropriate azimuth pointing position and enters this information into a central storage register. This data is then used to generate the required steering commands.

The azimuth selection unit allows the operator to choose between a manual input and free running mode. When the automatic mode is employed, the user selects the central clock frequency, and fine steering granularity.

### System Timing:

Supplies the timing pulses and enable signals required by the storage registers, shift registers and memory unit.

### Control Command Generator:

The control generator translates the azimuth pointing position into appropriate commands for setting the phase shifters, attenuators and sector switches. It is implemented with alterable read only memory (ROM) logic on which digital data for beam positioning control is stored.

### Switch Drivers

The settings on the phase shifters, attenuators, and sector switches are established by proper biasing of the associated PIN diodes. Therefore, in order to point the beam, each PIN diode is assigned a conduction state, either forward biased or backward biased; this task is accomplished by the switch drivers.

### System Operation

A flow chart describing the operation of the landing Guidance System control unit is presented in Fig. 5.1 and the associated timing diagrams illustrated in Fig. 5.2. The system presented is for the second method where ROM's and a shift register are employed. Detailed diagrams covering the other designs will not be presented since their implementation is basically the same.

Operation of the system proceeds in the following manner:

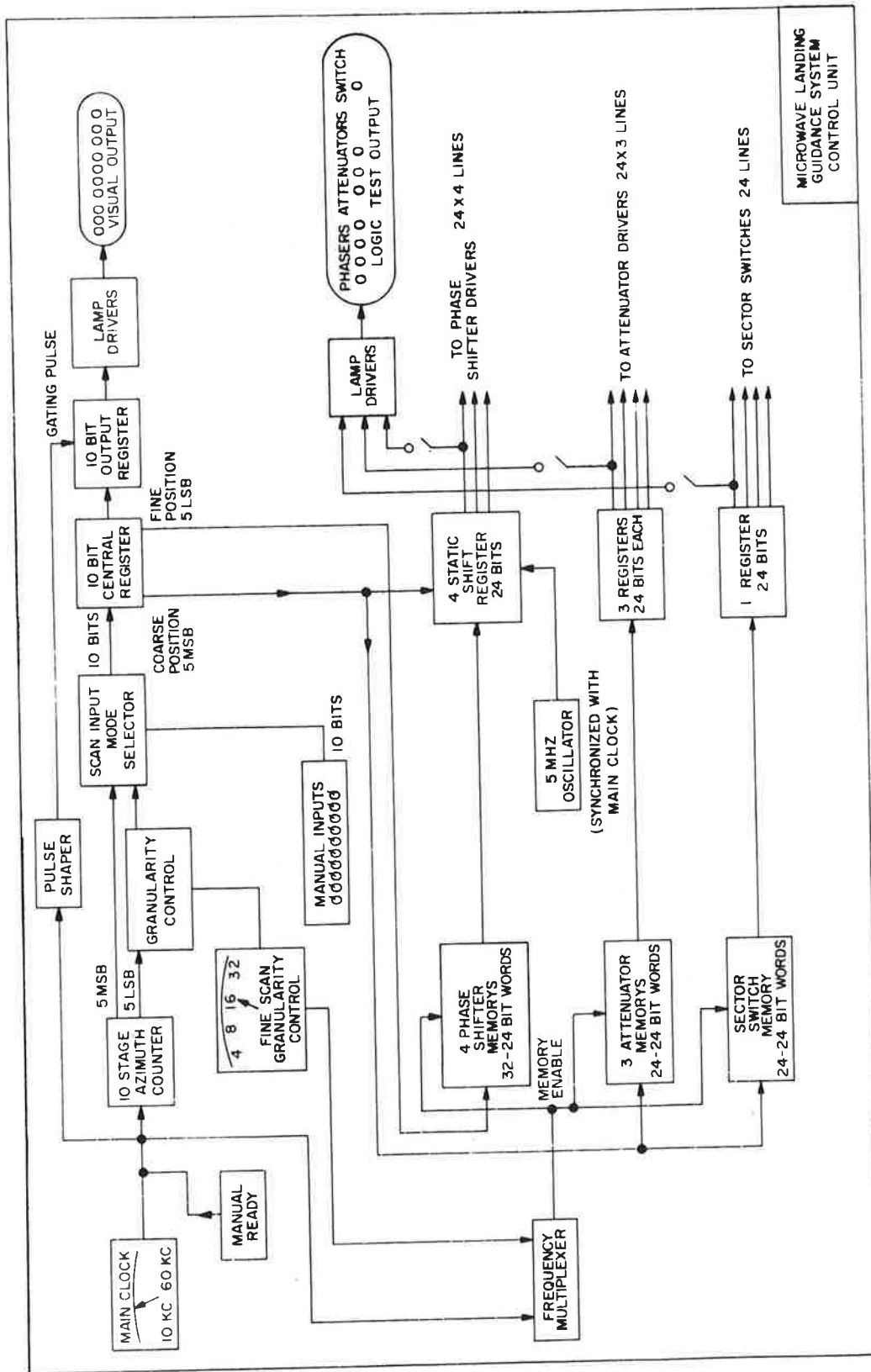


Figure 5.1 Microwave Landing Guidance System Control Unit

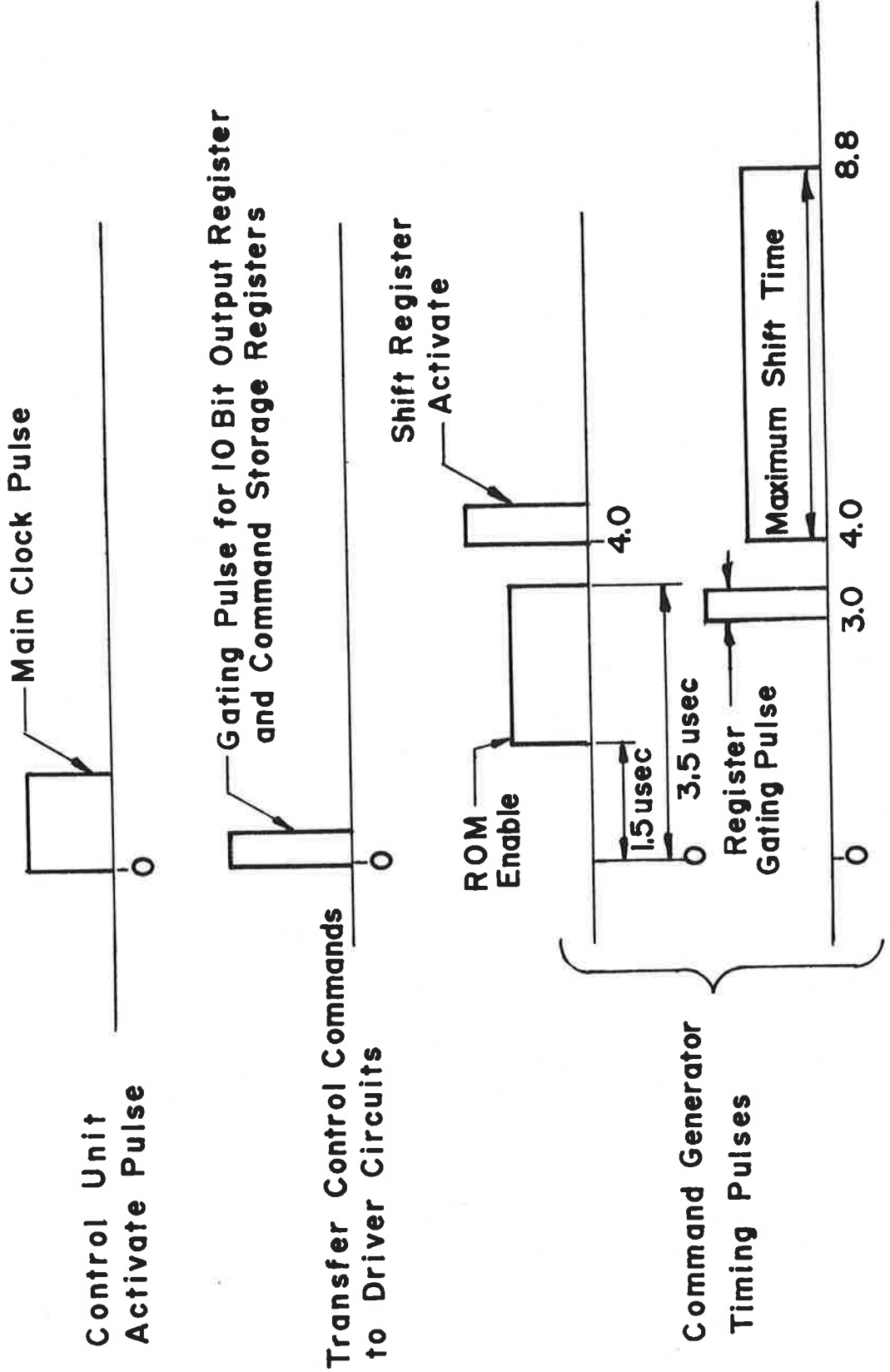


Figure 5.2 Basic Timing Budget ( $\mu$  sec)

A pulse from the main clock causes the antenna to shift to the next position; this is accomplished by outputting the phase, attenuator and sector switch settings which were precomputed and held in storage registers. This data is sent to the driver circuits and the new antenna beam is formed. Simultaneously, the control logic performs the operations required to establish the next antenna pointing position.

The control unit executes the following sequence of operations in deriving the beam steering commands:

The cycle is initiated by a pulse from the main clock which increments the azimuth position counter. This information (10 bits) is then transferred to the "input mode select" switch which chooses automatic or manual entry of azimuth pointing position. Next, this data is entered into a central storage register; the 5 MSB (most significant bits) indicating the desired coarse steering position and the 5LSB (least significant bits) defining the fine steering position.

The coarse steering position, together with a read enable is then supplied as the input to the attenuator and sector switch ROM's. Steering data from these units then appear on the output lines and is entered into the storage registers by a gating pulse. Simultaneously, the fine scan position is employed as the input to the phase setting memory and its output clocked into a static shift register. At this point an "excite" pulse turns on a high frequency clock which produces shift pulses at a 5 MHz rate. The shift register circuit also incorporates a down counter and a "zero compare". It will continue to operate until it achieves the number of shifts specified by the coarse position. When this limit is reached, an input gate is closed and the circuit frozen. The phase information is then in the proper order and will be stored in the shift register until the next main clock pulse comes along. At that time, all the commands will be transferred from the registers to the driver circuits and the new beam established. This completes the cycle.

The system also includes provisions for varying the fine scan granularity. Nominally, there are 32 fine positions between each coarse steering position. In order to reduce this number by a factor of N, the procedure for updating the central register is altered. In addition, it is required that the command logic respond to only a fraction (i.e.,  $1/N$ ) of the main clock pulses. To accomplish this the control

logic incorporates a pulse suppression unit (the frequency multiplexer) which passes only 1 out of N input pulses.

When the scan input mode selector is on MANUAL, the operator chooses any of the 1024 azimuth pointing positions with 10 toggle switches. After the switches are set, the user presses a ready button which generates timing pulses, in essence simulating the main clock. Two pulses are generated; the first initiates the control logic and establishes the beam steering commands, whereas the second causes this data to be transferred to the driver circuits and the new beam is formed.

## CHAPTER VI RF POWER SOURCE DESIGN

### 6.1 Introduction

This section discusses the requirements and selection of an RF power source for the phased array. Program efforts for this subject consist of the following:

1. Determine the RF power source requirements for various system configurations;
2. Review the present state of the art of microwave energy sources;
3. Determine feasible source designs for present and future source technology;
4. Procure a source suitable for the present program needs.

In the design of single feed microwave antennas, the RF source is not an integral part of the antenna design, for there is little, if any, antenna performance improvement to be gained through the selection and application of the RF source.

However, in the design of electronically scanned microwave antennas, and in particular the phased array, optimum performance can be obtained only when careful attention is given to the method of supplying RF to its elements.

The importance of the RF source and feed method for this application results from the losses associated with the phased array RF distribution networks, beam forming networks and beam steering networks. These losses can be minimized by tailoring the RF source, and feed system to a selected antenna design. For example, amplification after the element phase shifter negates the loss of this device and reduces the required power from the source.

In our work, a universal RF source approach is required in order to investigate several phased array configurations. Consequently, the source approach chosen will not be the optimum performance or cost solution for a final design; however, it will be program cost effective, representative of present technology and thus permit the evaluation of the source approach, antenna components and the landing system performance.

Preliminary review of antenna configurations (section 1.4) led to the selection of a X48 amplifier multiplier which will provide one watt output in C-band. This device is readily available (90 day delivery) at moderate cost (≈\$2500) and is discussed in detail in section 6.5.

A single RF source will be used to feed the various array configurations. This design permits the substitution of laboratory signal generators and TWT amplifiers (presently available in house) for performance comparison and provides back-up in the event of failure or late delivery of the desired sources.

The remainder of this section will present the RF source requirements, representative microwave source devices, source configurations and describe the sources to be used in this program.

## 6.2 Source Requirements

*Abstract-General source requirements are discussed and summarized in Table 6.1.*

The source design is influenced by the following system parameters:

### Ground System:

- Transmission losses
- Effective antenna gain
- Antenna Design and Feed Network
- Maintenance

### Airborne System:

- Antenna gain
- Transmission losses
- Receiver sensitivity
- Signal processing circuitry effectiveness

### Overall:

- Range
- Dwell time
- Environmental factors, particularly those affecting the propagation path.

A detailed analysis of all of these parameters has not been completed at this time. Therefore preliminary estimates and experience provided the basis for the source

selection.

### 6.2.1 RF POWER OUTPUT REQUIREMENT

The desired source power output was derived from the RTCA recommended -111 dBw signal level at the aircraft antenna at a range of 30 nautical miles.<sup>1</sup> This figure will provide a predetection signal-to-noise ratio of approximately 23 dB in a one MHz bandwidth as shown. It is expected that the effective predetection bandwidth will be less than 100 kHz thereby improving the above figure to 33 dB.

#### Airborne Receiver-Predetection Signal-to-Noise Ratio

##### Effective Input Noise

kTB:	-144 dBW/MHz
Noise Figure:	10 dB
	<hr/>
	-134 dBW/MHz

##### Input Signal:

Antenna Signal	-111 dBW
Antenna Gain and Transmission Loss	0
	<hr/>
	-111 dB

Predetection Signal-to-Noise Ratio: 23 dB/MHz

A simplified block diagram depicting the RF link is shown in Figure 6-1. The required power at point B is determined below.

Path loss (30nm @ 5 GHz)	142 dB
Power at point C:	-111 dBW
Power at point B:	<hr/>
	31 dBW

31 dBW represents the effective radiated power of the ground guidance antenna.

The power required from the source (point A) is determined by the transmission losses and antenna gain as can be seen from Figure 6.1. A large variation in these parameters can be expected. They are a function of the array configuration and antenna application (e.g. coarse or precision guidance) as discussed in section VII. From that section it can be seen that the losses may vary from 1 to 13 dB and that the gain may vary from 24 to 32 dB.

1. RTCA Report, p. 24



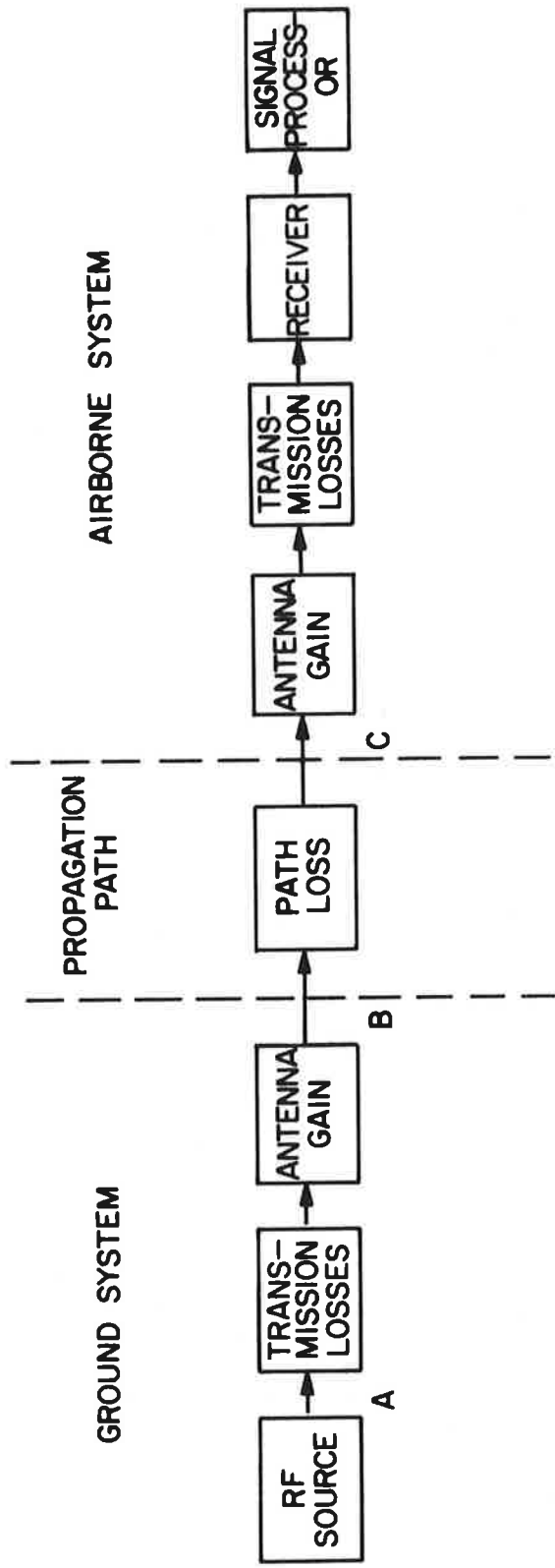


Figure 6.1 MLS RF Link

From these considerations the minimum power (maximum antenna gain and minimum transmission loss) needed for a single source is 0 dBW and the maximum power (minimum antenna gain and maximum transmission losses) is 20 dBW.

	Minimum Power	Maximum Power
ERP =	+31 dBW	31 dBW
Loss=	<u>1 dB</u>	<u>13 dB</u>
	32 dBW	44 dBW
-Ant. Gain	<u>32 dB</u>	<u>24 dB</u>
Source Power	0 dBW	20 dBW

In general relatively low cost, reliable, solid state sources are available in the 10 mw to 2w power level range for our requirement. Thus it can be seen that the antenna gain should be as high as practical and that the losses be kept to an absolute minimum in order to achieve the recommended -111 dBW signal level at the aircraft with currently available sources.

### 6.2.2 SUMMARY OF SOURCE REQUIREMENTS

General source requirements are tabulated on the next three pages with a rational explanation for their need. These requirements were used as guidelines in arriving at the initial selection of a suitable RF source for the phased array.

### 6.3 Devices (C-Band, Solid State)

*Abstract-Performance characteristics of transistor, varactor diode, step recovery diode, bulk effect, and avalanche devices are presented. It is shown how these devices may be utilized in the development of RF power for the MLS.*

The configuration of the microwave source is in large dependent on the availability of suitable devices for the generation of C-band power. The C-band frequency range is an awkward one in which to generate substantial power from solid state sources. Transistors which are presently supplying up to 10 watts (single devices) of power at S-band generate only milliwatts of power at C-band. Similarly, TRAPATT diodes generate watts of power at L and S band frequencies but at this time are inefficient and not practical to use in our application at C-band. At the other end of the spectrum, Impatt and bulk-effect devices are pushing the state of the art in solid state power generation from X-band through the millimeter wavelength frequency range. However, efficient, high power devices

Table 6.1 General Source Requirements

No.	Description	Limits	Rationale/Explanation
1	Frequency	5.0 to 5.25 GHz	Consistent with program goals, currently available for aeronautical radio-navigation (per Spectrum usage chart prepared by Frequency Management Division of the FAA)
2	Bandwidth	250 MHz desired	Full band coverage desired to permit complete frequency flexibility, particularly since no fixed channelization has been assigned as yet.
3	Output Power	1 to 100 watts	Consistent with achieving -111 dBw at 30nm (an RTCA SC-117 recommendation), dependent on design of landing system, particularly antenna gain and transmission losses.
4	RFI, Spurious Signals, & Noise	Consistent with the state of the art	No formal regulations have been set up for this service as yet. Not critical for technique evaluation at this time.
5	Amplitude Stability	$\pm 1$ dB/da in operating environment	Depends on the approach used, amplitude variation should not degrade fidelity of the signal in space, i.e., amplitude perturbations should be small, particularly in terms of the dwell time. Requirement can be significantly tighter with multiple sources as explained in section 7.

Table 6.1 (continued)

No.	Description	Limits	Rationale/Explanation
6	Phase Stability	$\pm 10^\circ$	Depends on antenna design approach and effects caused by modulation. Should be consistent with errors discussed in paragraph 3.3.
7	Frequency Stability	Capable of $\pm 1$ part in $10^6$ /year	From RTCA requirements, this requirement permits efficient spectrum usage and low cost hardware implementation technique for ground and airborne equipment.
8	Modulation Capability	FM, Pulse	Dependent on approach used. Source should be capable of being modulated with these functions or capable of transmitting this modulation when driven by a low level source containing this modulation for the TSC program.
9	Reliability	As great as economically possible	10,000 hours looks practical. Solid state source definitely desired.
10	Environmental Conditions	Outdoor, world-wide, ground based	It is desirable that the landing system components not require an environmentally controlled housing order to simplify installation and logistic support in general.

Table 6.1 (continued)

No.	Description	Limits	Rationale/Explanation
11	Producibility/ Availability	Off the shelf, with estab- lished perfor- mance history	These limits are desired from a reliability point of view. In fact, it may not be possible to achieve this goal without substantial development for the final system.
12	Cost	Lower life cycle costs than of tube approaches	Cost should not be prohibitive and at least should be competitive with that of mechanical scan antenna systems.

have yet to be demonstrated at C-band. This situation is a result of device development history and the lack of a large and immediately demanding market to spur device development.

Despite the lack of highly efficient low cost devices for C-band, there are a number of good prospects that may be practically utilized in the RF source at this time. They include: transistors, varactor/step recovery diodes, bulk effect devices and avalanche devices.

A brief discussion describing these devices and their application follows.

#### 6.3.1 TRANSISTOR DEVICES

The transistor cannot be considered a practical output device at this time. Although technology has progressed to the point of producing small signal (milliwatts and lower) amplifiers and oscillators in the C-band and low X-band frequency regions, these units are laboratory devices and are not suitable for this application. The transistor does play an important part in generating C-band power because it can be followed by a varactor or step recovery diode multiplier chain. The advent of high power (10w) S-band transistor devices makes possible improved multiplier chain efficiency and simplifies multiplier design by reducing the number of directly cascaded multiplier stages.

#### 6.3.2 VARACTOR DIODES

The varactor approximates an ideal non-linear variable capacitor. The varactor diode was the first major source of solid state microwave energy in the low (milliwatts) to medium power (watts) power level region. At this time it is the only established source of power in the one to five watt power level for the C-band frequency range. The varactor's characteristics first made it very popular in the parametric amplifier, down converter and up converter applications. Its use as an harmonic multiplier soon followed. The varactor rapidly developed into a relatively efficient source of phase coherent microwave energy over the frequency range spanning L-band through  $K_u$  band. A simple representative schematic of a lumped element doubler is shown in Figure 6.2. Many variations in circuits are possible and users adopted their favorites, primarily dependent on ease of alignment, circuit stability and in-house analytical and empirical capabilities.

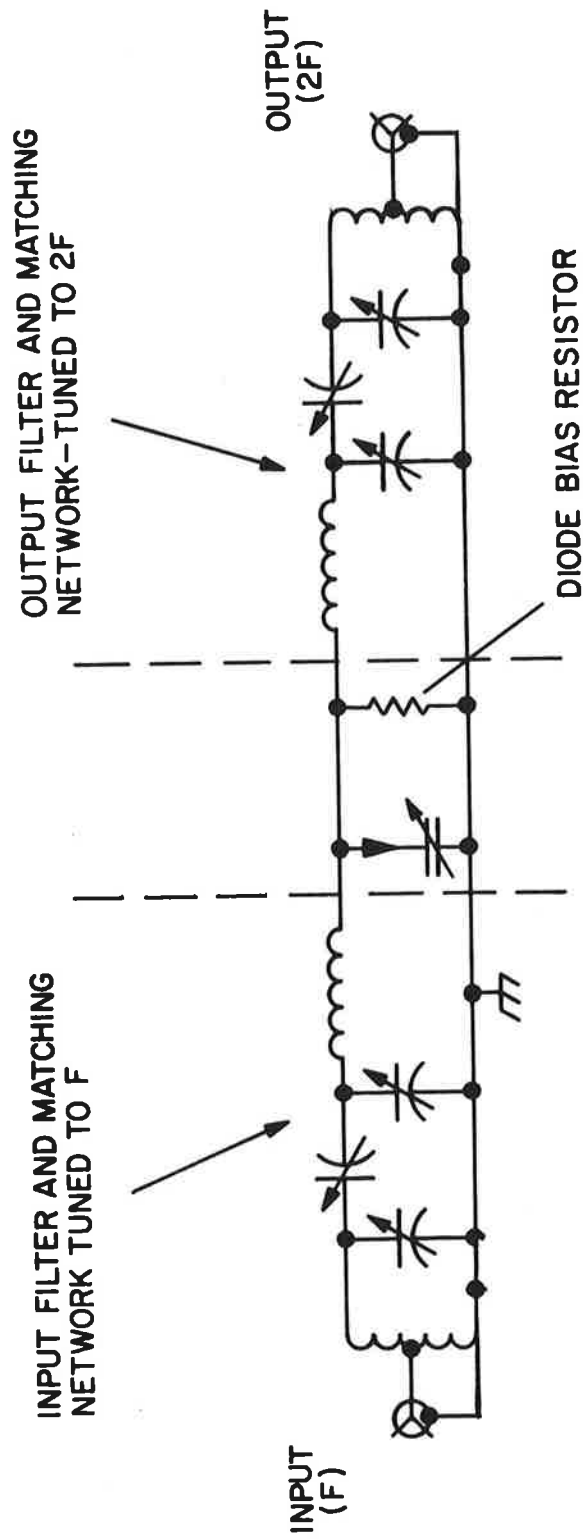


Figure 6.2 Varactor Doubler Schematic

Higher order multiplication (> 2 times) is implemented by the addition of an "idler" circuit across the diode. This series resonant circuit enables harmonic currents to be more efficiently circulated through the diode and makes possible the sum of these currents and the fundamental input frequency. In tripler operation the idler is tuned to the second harmonic, thereby enabling the second harmonic energy to combine with the fundamental energy to produce third harmonic output.

Likewise in quadrupler (X4) operation the idler is tuned to third harmonic permitting this current and the fundamental to combine and produce the fourth harmonic energy.

Higher order single varactor multiplication is possible by the addition of more idler circuits. Generally this technique is avoided because of the extreme tuning complexity involved with such assemblies and the associated poor efficiencies. For higher order multiplication the use of cascaded low order multipliers is preferred.

The exact operation of these devices is complex and really is not as cleanly defined as explained above. In actual practice alignment of the device is complicated by the fact that the varactor impedance changes as a function of frequency and drive level. Being a two terminal device, load variations may drastically effect the multiplier input impedance, thus complicating the cascading of multiplier stages. Being a relatively low loss non-linear reactance, parametric effects are quite common and can cause circuit instabilities.

Despite these difficulties, manufacturers have learned to control these problem areas such that efficient stable sources of microwave energy can be supplied up into the 90 to 100 GHz region through the use of cascaded multiplier stages driven by a power source in the low to high UHF frequency band.

As mentioned before, the advent of higher frequency (S-band), high power transistors improves chain efficiency by permitting low level multiplication schemes followed by amplification at the higher frequencies which is subsequently followed by additional high frequency multipliers. An example illustrating this improvement in a C-band application is shown in Figure 6.3.

The lower part of the figure illustrates a multiplier chain configuration more representative of 1971 technology. The lower RF and DC power levels reduces the stress on the individual transistor amplifiers and diode multipliers. This factor along with the improvement in DC to RF efficiency improves multiplier reliability.



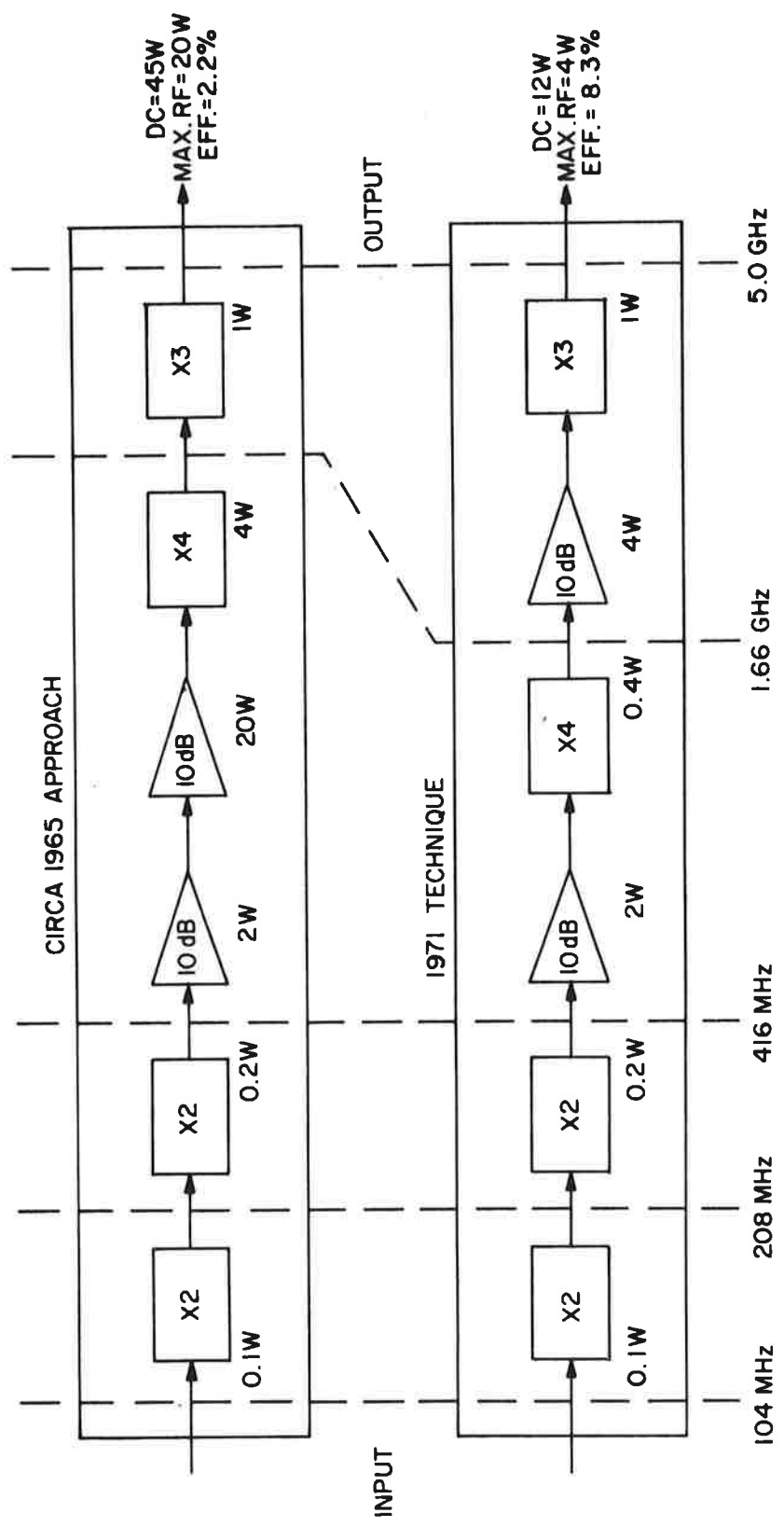


Figure 6.3 Varactor/SRD Multiplier Chain Configurations

The coherent phase characteristics make the varactor multiplier chain ideal for phased array applications. Several modern designs utilize separate low level varactor multipliers for each element. These element chains are fed from a common low frequency driver similar to that shown in the Figure 6.4. This approach has been successfully demonstrated and was considered seriously for the MLS application, as discussed in paragraph 6.5.

The prime advantages of the above described distributed approach are the built in source redundancy and the possibility of placing amplification after lossy element networks (e.g., the phase shifters).

The prime disadvantage of this distributed approach is that of insuring identical phase characteristics of the individual amplifier and multipliers.

### 6.3.3 STEP RECOVERY DIODE

The step recovery diode (SRD) has in general replaced the varactor in high order multiplication applications. This device approximates a two state capacitor, possessing high capacitances in one state and very low capacitance in the other state.

When driven by rf energy, this diode generates very fast impulses at the drive frequency rate. These devices can be used in high order multipliers without the use of idler circuits and can obtain efficiencies of  $1/n$  to  $2/n$  where  $n$  is the multiplication ratio. These devices are now generally preferred in the design of multiplier chains, because of their simplicity.

Both the varactor and SRD offer the possibility of simultaneously supplying microwave energy and phase shift capability. The phase shift is achieved by varying the bias voltage across the diode. This approach has been successfully implemented and patented by Ryan-Teledyne. This permits the elimination of the discrete phase shifter normally associated with each element. Other advantages include low drive power (for the phase shifter), simple driving networks and smaller size. The disadvantages of this approach include: narrow bandwidth operation, low output power capabilities and phase tracking errors.

Operating bandwidths for varactor/SRD multipliers vary from approximately 2% to 20%, depending on output power, spurious suppression requirements, flatness and multiplication ratio. Power outputs of 10 watts with bandwidths of 5% have been demonstrated by industry at C-band. Broad bandwidths and high power generally involve amplification, balanced broadband

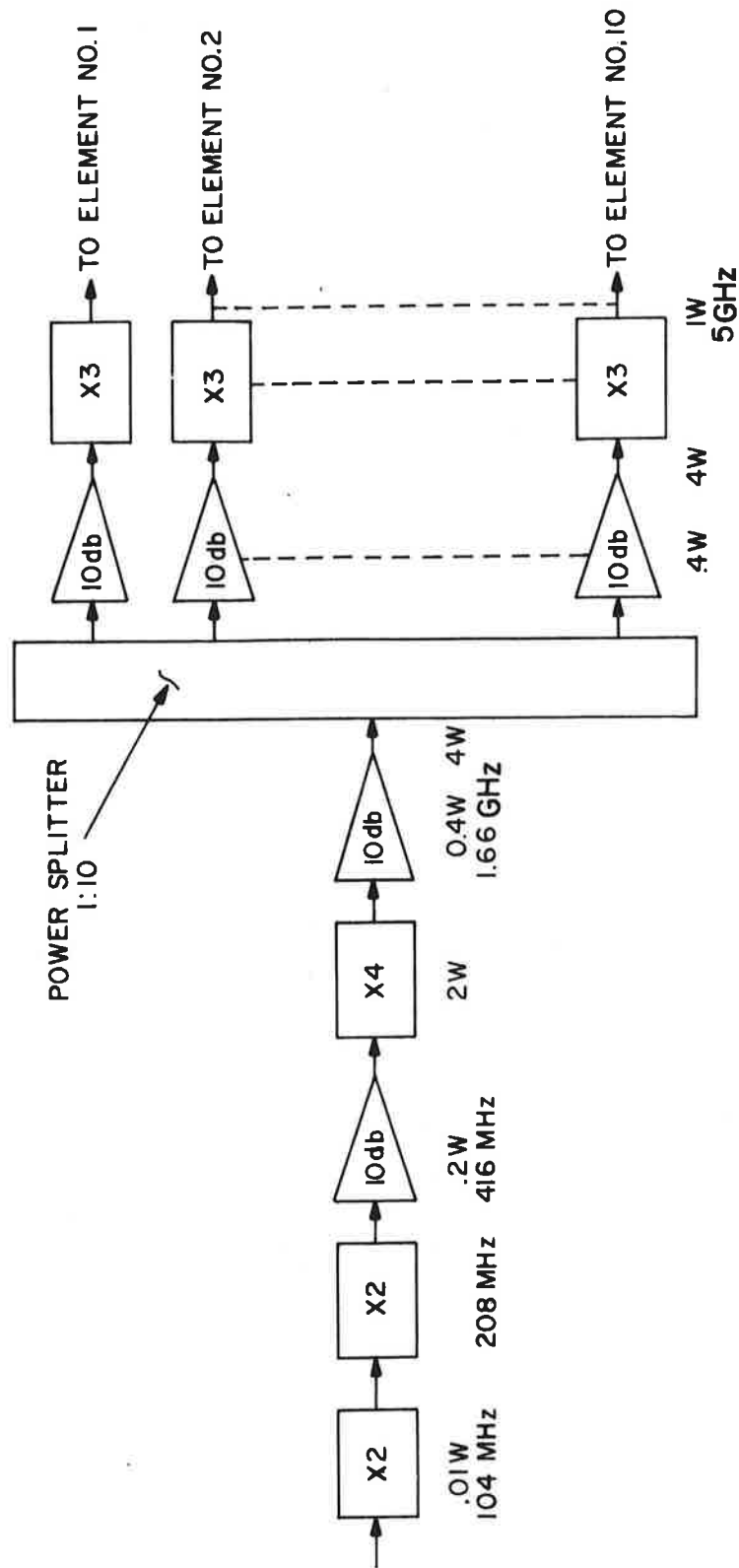


Figure 6.4 Distributed "High-Efficiency" Varactor/SRD Multiplier Chain

multipliers with hybrid combining or some variation of these schemes.

#### 6.3.4 BULK EFFECT AND AVALANCHE DEVICES

These devices are the newest entrants into the microwave RF source field. They are exciting devices because of their inherent simplicity and ease of operation. The devices are two terminal elements, packaged in typical microwave diode configurations and provide RF power when they are placed in a "resonant" cavity and DC voltage is applied across them. Although simple in appearance and application, the physics of their operation is quite complex. The inventors and users of these devices have been debating and refining the principles of operation since the discovery of the Gunn diode\*.

##### 6.3.4.1 Bulk Effect Devices

Both the Gunn diode and LSA diode are in a class of devices known as bulk effect devices. This class of devices has several "modes" of operation as discussed in the literature\*. The devices are capable of pulsed, CW and amplifier operation.

##### Gunn Diode

The Gunn diode (generic name: Transferred Electron Oscillator or Transferred Electron Amplifier depending on its use) was predicted by Dr. Cyril Hilsum of Britain and physically discovered by Dr. J. B. Gunn of IBM in 1963. It is the oldest of the "modern generation" of solid state microwave energy sources.

The diode itself is a very simple device and does not contain a PN junction per se but rather consists of a continuous semiconductor material with ohmic contacts on either end. When the proper voltage is placed on the device rf, output may be obtained and sustained when the diode is placed in a cavity tuned to its self resonant frequency. The frequency of oscillation is a function of the applied voltage, the semiconductor material and its doping.

The power output of this device varies inversely as the square of the frequency.

\*"Microwaves" Hayden Publishing Company, Inc., New York, February 1971, pp. 30, 36, 43.

In CW operation, Gunn diodes are readily available that will provide 250 mw output from C through X bands.

The gun oscillator is suitable for phase lock loop or injection locking type frequency stabilizing systems.

#### LSA (Limited Space Charge Accumulation) Diode

This device, physically similar to the Gunn diode, was discovered in 1966 by Dr. John A. Copeland of BTL when in the process of analytically analyzing and verifying the operation of the Gunn oscillator. He found a new mode of operation when the voltage applied to the semiconductor was about two times greater than that normally applied to the Gunn diode. In this new mode, the power output from the device was found to vary inversely as a function of frequency and consequently this device looked more suitable for higher power and higher frequency operation. Such was the case for in 1967, the Microwave Journal\* reported that BTL had obtained 20 mw of CW power at 88 GHz with 2% efficiency and 50 mw of pulsed power at 88 GHz with 4% efficiency. The LSA diode is more efficiently operated in the pulse mode and currently is the highest power solid state pulse source available, providing more than 2KW of peak power at C-band.\*\*

LSA devices could not be located for immediate program application. However, when DME is incorporated into the landing system, this device will certainly be the leading candidate for the pulse transmitter.

#### 6.3.4.2 Avalanche Devices

##### Impatt (Impact Avalanche and Transit Time) Diode

This device and its performance was predicted by Dr. W. T. Read of BTL in 1957. Performance was demonstrated in 1965. Currently the diodes consist of PN junctions of either silicon, germanium, or gallium arsenide materials.

\* The Microwave Journal, Horizon House, Dedham, Massachusetts, March 1967, p. 28.

\*\* Eastman, L.F., William O. Comp, Jr., Joseph S. Browman, "LSA- New Peaks in Microwave Power," Microwaves, Hayden Publishing Co., Inc., New York, February 1971, p. 43.

Power output is inversely proportional to the frequency squared. Source configuration is similar to that of the bulk effect devices. The most common method of frequency stabilization is by injection locking.

#### Trapatt Diode

This mode of operation of an avalanche diode was discovered by RCA accidentally in 1967 while experimenting with the Impatt mode of operation. BTL gave the device the name Trapatt an abbreviation for "Trapped Plasma Avalanche Triggered Transit", which describes its mode of operation. The mode is also described as anomalous or "high efficiency" mode. This device is operated in a resonant circuit much below its normal self-resonant frequency, typically 1/3 of its self resonant frequency with approximately three times the efficiency than when used in the Impatt mode of operation.

These devices are currently producing 10 watts of power at L-band and up to 2 watts of power at S-band. High power C-band devices are not currently available.

Of the available bulk effect and avalanche devices, the Gunn and Impatt diodes are currently the most suitable for our application. Figure 6.5 presents block diagrams of possible RF source configurations utilizing these devices.

#### 6.3.5 SUMMARY

From the discussion above it can be seen that power in the 1 to 10 watt power level region can be generated by several devices with several approaches.

Table 6.2 summarizes the devices considered and their more important characteristics for this application.

#### 6.4 RF Source Configuration

*Abstract-Single high power and distributed low power source techniques are considered for supplying RF power to the phased array antenna. The single source approach was chosen for reasons of program expediency and ease of implementation.*

A number of techniques may be utilized to construct the desired source using the devices described above. The

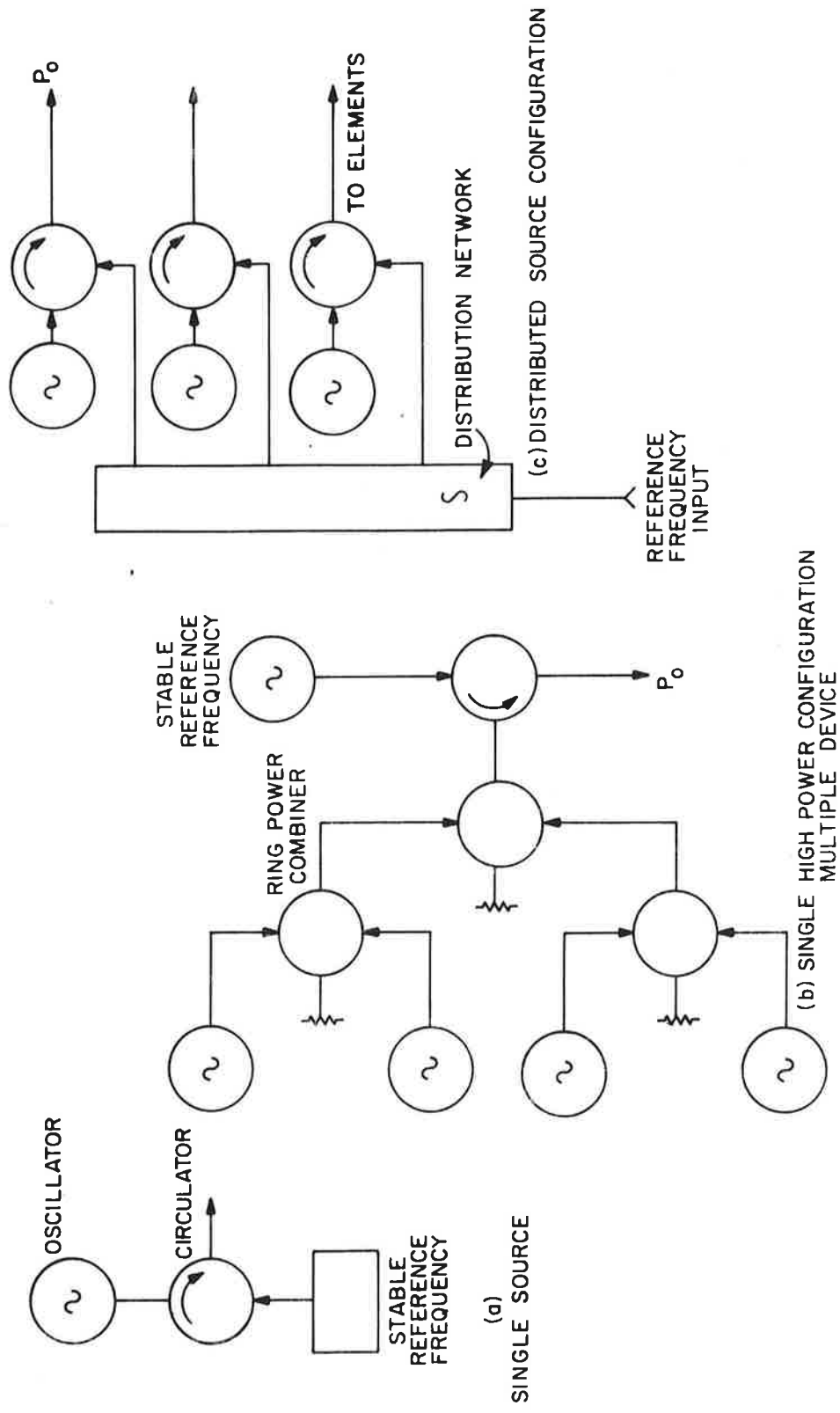


Figure 6.5 Bulk Effect and Avalanche Device Source Configurations

Table 6.2 Device Performance Summary

<u>Device</u>	<u>Mode of Operation</u>	<u>Frequency</u>	<u>Power</u>	<u>Efficiency</u>	<u>Instantaneous Bandwidth</u>	<u>Nomenclature</u>	<u>Manufacturer</u>	<u>Gain</u>
Transistor	Oscillator	6 GHz	20mw	20%	10%	MS0146	TI	
Transistor	Amplifier	5 GHz	0.4w	20%	10%	MS0146	TI	5dB
Transistor	Amplifier	3 GHz	2.5w	30%	10%	MSC 3003	MSC	6dB
Transistor	Amplifier	2.3 GHz	3.7w	40%	10%	MSC 3003	MSC	7.5dB
Transistor	Amplifier	2.0 GHz	10w	40%	10%	MSC 2010	MSC	5dB
Transistor	Amplifier	1 GHz	20w	60%	10%	MSC 2010	MSC	10dB
Varactor/ SRD	Multiplier X3	5-8.0 GHz	10w	50%	5%	VAB-814A-3	Varian	-3dB
Gunn Diode	Oscillator	5 GHz	1w	4-5%	Narrow		*	na
LSA	Pulse Oscillator	5GHz	2KW	5%	Narrow		*	na
Impatt	Oscillator	5GHz	4w	8%	Narrow	MS838A	Microstate	na Eastman
Trapatt	Pulsed Oscillator	5GHz	2KW	15%	Narrow		*	na

\*Microwaves, Hayden Publishing Co., Inc. New York, February 1971, p. 30, 36, 43.



technique chosen is primarily a function of the device itself, total power required, the method of feeding the array, as well as the other general requirements presented in paragraph 6.2.

Two general approaches have been considered in the source design, namely

1. single high power source, and
2. distributed lower power sources

Single source feeds are used in phased arrays, in which distribution losses are low and the radiated power is low in terms of available device power capabilities.

The distributive feed approach is used in arrays that generally require more power than available from a single source. The distributed approach permits more efficient generation of power by eliminating losses that are incurred in the generation and distribution of RF that is normally associated with the single source approach.

In large arrays the distributed source approach provides the further advantage of increased reliability, since the failure of a number of power sources will not significantly impair the performance of the antenna.

The prime disadvantage of the distributed source approach is the requirement for phase coherence and phase stability that are now placed on the individual source elements.

In view of the added system complexity of the distributed approach and the time allotted for this program, the single source feed approach has been selected for implementation. The choice is elaborated upon in paragraph 6.5.

## 6.5 Initial Choice

*Abstract-A times 48 amplifier multiplier chain has been selected to supply RF power to the antenna. The rationale for this choice and the specification for the hardware are presented.*

A preliminary survey of the source market showed that the only readily available devices for single-source application were impatt diodes and varactor/SRD multiplier chains. Both of these approaches can provide watts or power at C-band. Low power (50 to 200 mw) devices in the form of Gunn oscillators and transistor VCO's followed by a single SRD multiplier were also readily available and were considered for a distributed source approach.

From a cost point of view the distributed approach was ruled out. Low cost Gunn oscillators are not available for this frequency range. Furthermore, the cost of this approach is increased by the additional circuitry needed to stabilize and modulate the Gunn oscillator. These same considerations also apply to the transistor VCO/SRD combination. Cost estimates for these sources ran from \$1500 to \$3500 each depending on the stability, modulation capability and power output required. The distributed varactor multiplier approach (similar to that shown in Figure 6.4) also proved expensive with prices ranging from \$70,000 to \$100,000 for a complete RF source system.

It is emphasized that these prices result from non-recurring charges due to the lack of source development in this area, and that production prices would be significantly lower.

From a technical point, the added hardware complexities of system implementation with Gunn and Impatt sources is not warranted. The distributed varactor multiplier approach is quite attractive in that phased array antennas have been successfully implemented with them in the past. Even though the varactor approach is a much more complicated method of generating RF power than that of the simple Gunn and Impatt devices, it has the advantages of being presently available, practical to integrate into the system, an established performance history and moderate cost.

Based on the considerations presented in this section it was decided to procure a 1 watt, X48 amplifier-multiplier as specified below.

#### 6.5.1 INITIAL SOURCE SPECIFICATION

X48 Amplifier-Multiplier Assembly, to generate C-band energy from amplitude (on/off) frequency or frequency hopping modulated source in the 100 MHz frequency region, in accordance with the following specifications:

##### 6.5.1.1 Electrical Requirements:

- (a) Operating Modes: CW, CW with narrow/wideband FM: up to 200 kHz, sequential frequency hopping, and pulse.
- (b) Output Frequency:  $5190 \pm 20$  MHz min. (instantaneous bandwidth)
- (c) RF Power Output: 1 watt min.
- (d) Input Frequency: Output frequency/48
- (e) RF Input Power: +10dBm  $\pm$  3dB

- (f) Undesired signal levels:  
Output harmonics and signals related to the input frequency: >40dB below the fundamental - C-band Output
- (g) Broadband Noise: Not to exceed - 40dBm/MHz over the 5190 ± 90 MHz frequency band. The noise shall roll off at least 6dB/octave thereafter
- (h) Spurious Signals: signals not related to the above shall be equal to or greater than 80dB below the C-band output signal level.
- (i) Input Impedance: 50 ohms, VSWR<1.5
- (j) Output Impedance (load): 50 ohms, VSWR<2.0. The unit will not be damaged under "no load" operating conditions.
- (k) Power Source Requirement:
  1. Voltage: 28 ± 0.5 VDC
  2. Current: <1.3 amp., 500 ma desired
  3. The unit will not be damaged by operation during a power source voltage variation of 0 to 30 VDC. The unit will not exhibit any deterioration other than changes in output power and undesired signal levels when the power source voltage varied from 26 to 30 VDC. Undesired signal "break-up", parasitic signals etc., will not be caused by such operation.
- (l) RFI: The generation of radio-frequency interference by the multiplier and the vulnerability of the multiplier to radio-frequency interference shall meet the limits of specification MIL-I-6181D.

#### 6.5.1.2 Mechanical Requirements:

- (a) Connectors: RF, input/output: SMA Female  
DC, Solder Terminal
- (b) Weight: <5 pounds
- (c) Size: <150 cubic inches, excluding connectors.
- (d) Mounting: The assembly shall hard mount to a flat surface with surface tolerance of ± 1/64".
- (e) Finish: Corrosion resistant, the assembly will be suitably finished to prevent deterioration of the assembly housing material over the operating and environmental conditions called out in this specification.
- (f) Cooling: The unit shall be designed to be cooled by conduction to the mounting surface.
- (g) Marking: All units shall have a label that contains at least the following information:

1. Manufacturer
2. Model No.
3. Serial No.
4. TSC Contract No.
5. Device Nomenclature

#### 6.5.1.3 Operational Effectiveness:

The Contractor warrants the unit for a period of at least one year after final acceptance. Multiplier failures occurring during this period (when operated in accordance with this specification) shall be repaired by the vendor at no cost to the Government.

#### 6.5.1.4 Environmental Requirements:

(a) Ambient Temperature:

1. Operational:  $-20^{\circ}\text{C}$  to  $+50^{\circ}\text{C}$ , Mounting Surface Temp:  $-10^{\circ}\text{C}$  to  $+60^{\circ}\text{C}$
2. Degraded Performance:  $-30^{\circ}\text{C}$  to  $-20^{\circ}\text{C}$  and  $+50^{\circ}\text{C}$  to  $+70^{\circ}\text{C}$

(b) Humidity: 0 to 100%

(c) Shock and Vibration: Must withstand normal handling procedures involved in shipment and laboratory work.

(d) General: Condensation is expected within the temperature range of  $+70^{\circ}\text{C}$  to  $-30^{\circ}\text{C}$ . A salt laden moisture is to be considered. Sand, dust and wind loading are not directly applicable.

#### 6.5.1.5 Design and Construction:

(a) This specification is not intended to define the internal structure of the network. Any reasonable configuration is acceptable as long as overall specification is maintained, but efforts should be oriented to a minimal size where possible. The design approach shall be amenable to large quantity production. The design should feature modular construction and be readily maintainable by technicians skilled with these devices.

(b) All components will be accessible, that is to say, potting will not be used, and components will not be epoxied in place, etc.

#### 6.5.1.6 Quality Assurance Provisions:

(a) The Contractor shall provide test data to show general specification compliance.

- (b) Final Test Notification: The contractor shall notify the Contracting Officer at least five (5) working days prior to the commencement of final tests.

#### 6.5.1.7 Drawing Applicability:

- (a) The Contractor shall supply informal, non-proprietary block diagrams, parts list and assembly drawings suitable for engineering use and analyses.
- (b) The Contractor shall supply an outline drawing of the amplifier multiplier within 30 days after receipt of order.

#### 6.5.1.8 Applicable Documents:

The following document forms a part of the technical requirements. In areas of conflict, the above specifications take precedence of the document listed below:

MIL-I-6181D Interference Control Requirements, Aircraft Equipment

Two types of sources have been ordered. One to the specification above and a wideband unit ordered to a similar specification which covers the complete 5.0 to 5.25 GHz band.

These devices do not represent the final choice for the phased array RF source. However, they do represent a good compromise between technical, price and program goals. Their performance requirements will enable the planned antenna program to be carried out permitting component evaluation, antenna testing and realistic flight testing (10 to 30 nm range).

#### 6.6 Summary

For the antenna configurations of section VII it has been determined that a net source power of 1 to 100 watts is required for full system performance. The exact amount of power and optimum source design will be determined upon the selection of a final antenna configuration and its specific function in the overall landing system plan.

A review of available microwave energy sources revealed several devices suitable for source design. Of the sources constructed from these devices, an amplifier-multiplier configuration utilizing transistors and SRD's appeared to be readily available and easily implemented into the system.

Four one watt sources, two narrow band ( $5190 \pm 20$  MHz) and two wide band ( $5125 \pm 125$  MHz) devices have been ordered. These will supply the RF energy for the initial phased array landing system.

Future landing systems will probably utilize high power transistor amplifiers or Trapatt diodes operating directly at C-band in either single or multiple source configurations as required. These devices presently show the most promise of providing significant power (50 to 100w) and efficiency (50%) within the next five years.

Future program work in this area consists of three major tasks:

1. Updating the information obtained for the tasks outlined in paragraph 6.1 so that more quantitative information may be provided for use in the selection of a source suitable for the final recommended phased array configuration.
2. Design/Development/Fabrication and/or procurement of a driver modulator for the X48 amplifier-multiplier; and
3. System test of the complete modulator-source system.

## CHAPTER VII EXPERIMENTAL MODEL DESCRIPTION-GOALS OF EXPERIMENTAL PROGRAM

In order to establish positive feasibility of phased arrays for the MLGS it is necessary to have a demonstration model fabricated and tested which reflects the technological characteristics of the final system. There are a number of questions relating to phased array technology at C-band which can only be resolved by a hardware demonstration. For example, non-linearities in components, switching noise, system insertion loss, and cost must be examined from measured performance. Analytical estimates do not suffice. It is not necessary to have all 200 proposed channels, or to have the scan coverage of the final design, as long as the extension to the full-blown capability requires no new major components.

It is desirable to have an instrument with which to address some of the problem areas of the RTCA recommendation, specifically step scan vs. continuous scan, sum beams vs. difference beams, the generation of planar beams, and variable scan rate. It is possible to incorporate this flexibility into a phased array without compromising the system performance.

It is apparent from the discussion on feed networks that there are several possible designs which can be used, each of which are comparable on paper, but which have individual problems which may prove costly to surmount in practice. Accordingly, two parallel techniques (R-2R lens and electronic attenuator) are being pursued which can be completely implemented with parts procured during the FY-72 fiscal year, and a third which can be evaluated on the basis of measured component performance (transfer matrix). Simultaneously, analytical work will proceed on the design of new techniques that may prove superior.

The basic parameters chosen for the experimental antenna are the following:

<u>Function</u>	<u>Azimuth</u>
Number of active elements	24
Number of total elements	32
Active Sector	60°
Radius of the array	33.7 inches
Element spacing	1.53 inches (2.61°)
Beamwidth	4° (sum beam)
Sidelobe level	-26 dB

<u>Function</u>	<u>Azimuth</u>
Frequency	5.0 - 5.25 GHz
Scan Range	$\pm 10^\circ$

More elements can be added if additional coverage is desired. If planar beam generation is desired for experiments in elevation, the same feed network can be used, but a new structure will be necessary, as well as new feed elements.

The antenna itself uses monopoles as elements protruding out of a conducting apron. A cylindrical reflector is mounted about a quarter wavelength behind the elements as shown in Figure 7.1. The apron edge is serrated in order to break up edge reflections. The apron acts to reduce the energy spilled below the horizon. This does not result in optimum multipath rejection but is adequate for testing the scanning technique. It is planned to proceed with the design of element columns of printed circuit dipoles which will be tailored to give a more desirable elevation pattern. These can be used with any of the feed networks later on.

For the elevation antenna, the polarization and coverage are different. This requires a redesign of the antenna element and backup structure if it is desired to test planar beams in elevation. It has not yet been determined whether this will be done.

In the sections which follow, the experimental designs, tests and costs are discussed. The experimental evaluation of the components will allow an assessment of their system potential. The lens design is given in some detail. The test plans are included for the components and antenna patterns. The procedure by which the element column design is expected to proceed is also included. Finally some costs are given, based purely on component cost estimates by component manufacturers, which will prove helpful in assessing the economics of phased arrays.

## 7.1 Lens Antenna System

*Abstract-The experimental lens design is discussed and the associated plan for its testing given.*

### 7.1.1 LENS ANTENNA SYSTEM - DISCUSSION

The lens antenna approach uses an R-2R parallel plate constrained lens with a cylindrical antenna array. The "constraining" elements are the equal length cables which



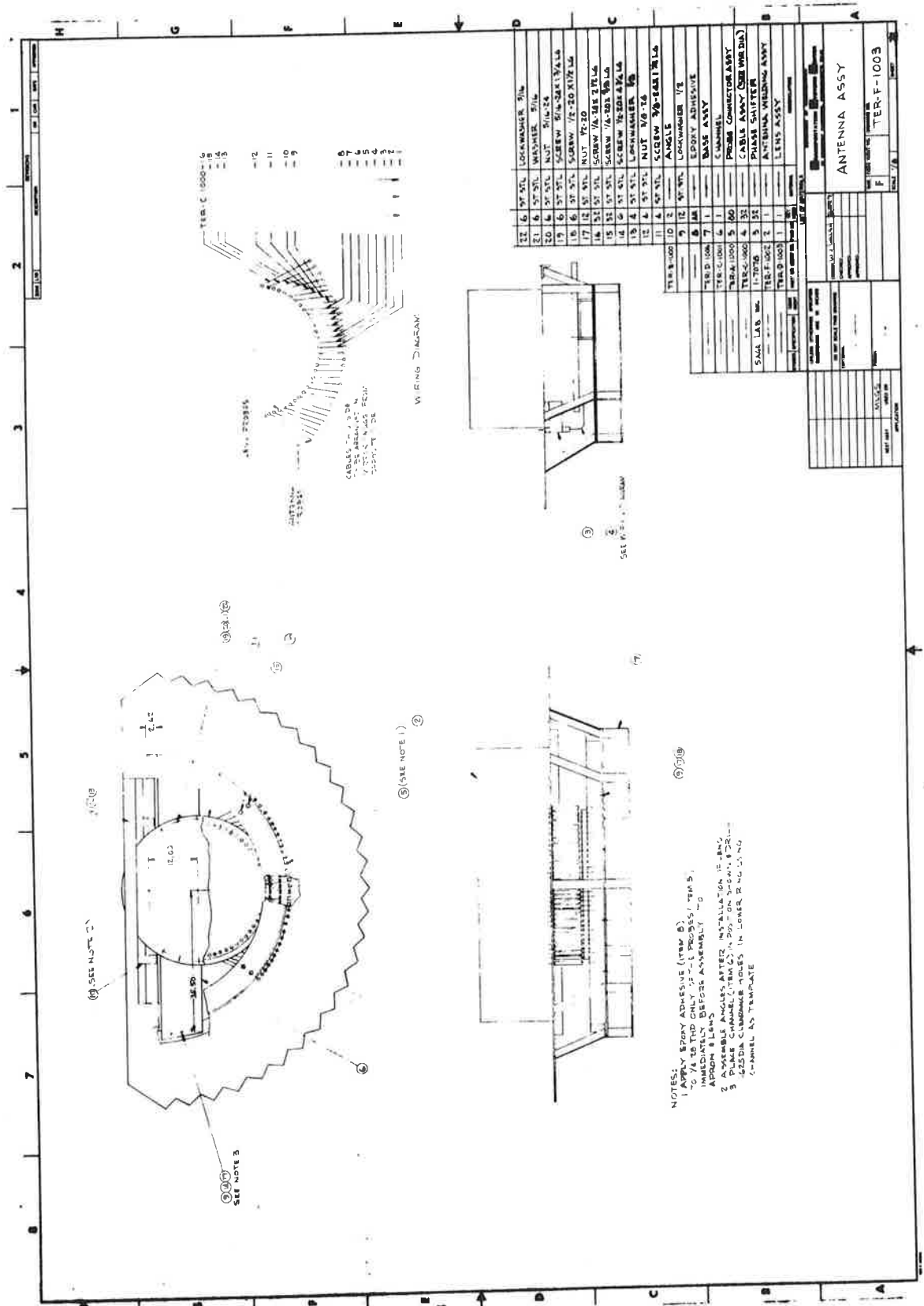


Figure 7.1 Experimental Antenna Assembly Drawing

connect the output probes of the lens to the antenna radiators of the cylindrical array. The lens consists of a circular parallel plate transmission line and the constraining elements. (See Figure 7.2) If the ratio at lens radius to array radius is  $R/2R$  then a collimated beam will be produced in space at an azimuth angle  $\phi/2$  when an RF source along the focal arc is located at an angle of  $\phi$  with respect to the centerline axis. A certain degree of far field radiation pattern control can be obtained by varying the radiating aperture on the focal arc of the lens.

Because of the  $R/2R$  relationship, the probe spacing on the lens is equal to the inter-element spacing of the array, and the angular sector scanned in space will be one half the angular sector travelled by the RF source along the focal arc. Moving the RF distribution one probe at a time along the focal arc "coarse scans" the beam in space. "Fine scanning" between coarse probe positions can be implemented by using variable phase shifters on each of the output cables and setting up the desired phase taper. This method requires phase shifters on each of the output cables and can be complex and costly because of the large number of phase shifters required.

Another method of fine scanning the beam is by adjusting the amplitude of the RF excitation to each of the focal arc probes in order to move the center of gravity of the distribution to intermediate points between two probe positions.

In the test model this will be accomplished by the use of variable attenuators. However, in the actual system, this technique would not be used because of the resultant system losses.

In order to test the lens technique, a small lens antenna scanning system design will be fabricated using  $\lambda/4$  vertical monopoles on a ground plane as the radiating elements. The parameters of the antenna are as follows:

Antenna radius: 33.661"  
Active Sector:  $60^\circ$  (33.661" aperture  $\approx 15\lambda$ )  
Probes in Active Sector: 24  
Total Number of Output Probes: 32  
Scan Limits:  $\pm 10^\circ$   
Coarse Scan Interval:  $2.61^\circ$   
Coarse Beam Positions:  $\pm 4$  either side of  $0^\circ$   
Half-Power Beamwidth:  $4.0^\circ$ - $5.0^\circ$  depending on radiating aperture distribution and frequency.

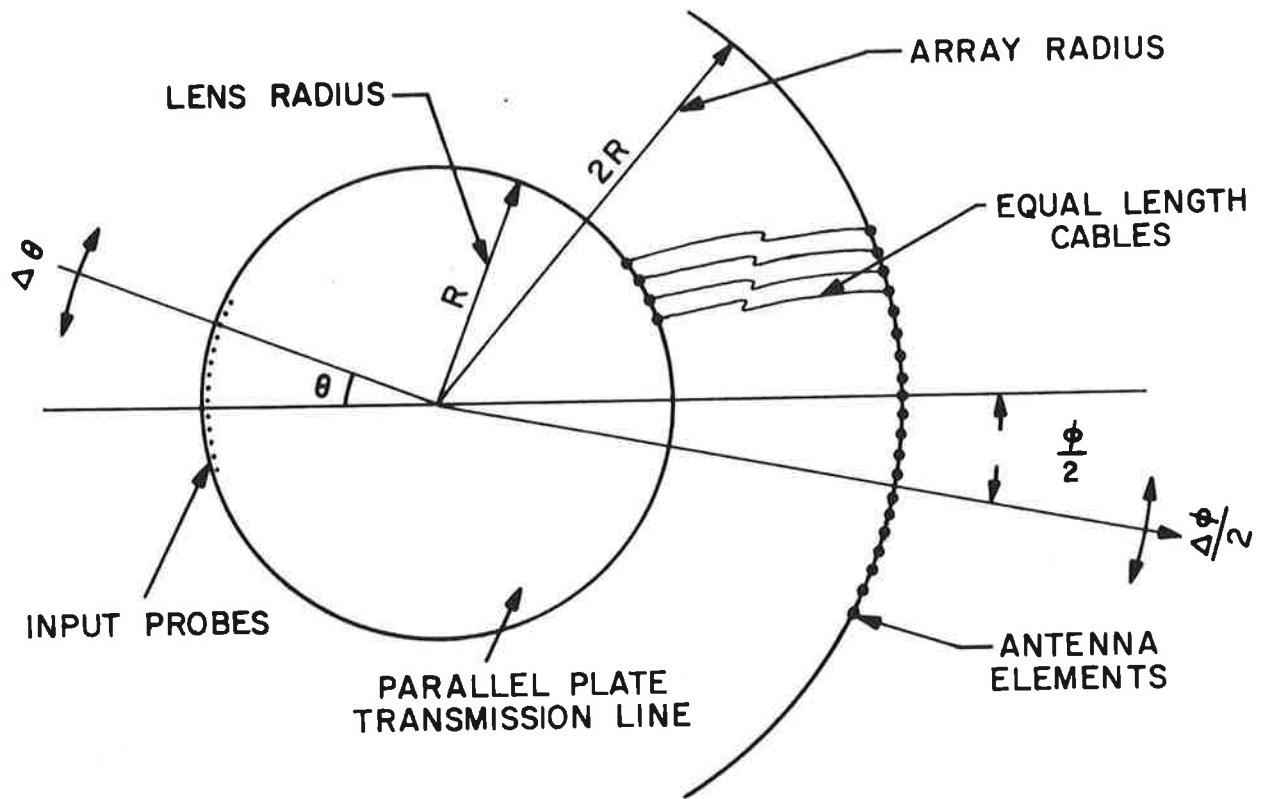


Figure 7.2 Lens Geometry

### 7.1.2 TEST PLAN FOR THE MICROWAVE LENS

- a. With all probes installed check impedance of a single probe with all others terminated.
  - b. Measure amplitude and phase of output probes as a function of excitation on focal arc. Check for-  
1 probe }  
2 probe } excitation  
3 probe }
- Phase should have  $r(1-\cos\theta)$  progression and amplitude taper should change with the focal arc excitation.
- c. Once proper focal arc distribution has been obtained (i.e., 1, 2, or 3 probes) for proper edge level (10db) move this illumination around to different positions along focal arc and check amplitude and phase at the output probes to determine how well the distribution is maintained as a function of coarse scan.
  - d. Once these tests on the lens have been completed connect the lens to the antenna probes and perform the radiation pattern measurements indicated in section 7.2.2.

### 7.2 Test Plan for Components and Antenna Range Patterns

*Abstract-The tests and block diagrams of test setups are given in tabular form. The test procedures for obtaining antenna pattern information are described.*

#### 7.2.1 COMPONENT TESTS - EVALUATION OF CANDIDATE SYSTEM POTENTIAL

Information is presented in tabular and diagrammatic formats to permit accurate evaluations of the components being purchased. The components under consideration are electronically controlled switches, phase shifters and attenuators, and passive power dividers.

This test plan includes eight test system block diagrams for evaluating the components relative to their specifications listed in Appendix E. Six tables are included to aid the evaluator in systematically and effectively verifying the level of performance of each component or group of components. This information will assist in the evaluation of candidate systems and will aid in determining the system sensitivity to parameter variations.

The tables are to serve as guidelines rather than as a mandatory list of duties. As examples, it may be unnecessary to check VSWR, insertion loss magnitude, or isolation on a single frequency basis. However, if the need arises, pertinent information is provided by the tables and diagrams.

Temperature and humidity measurements may be performed using the indicated test set-ups by mounting the Device Under Test, D.U.T., in an appropriate environmental chamber.

If RFI evaluations are required, additional procedures or diagrams can be supplied as required.

### 7.2.2 RANGE TESTS-STATIC ARRAY PATTERNS

This section provides general instructions for range testing the static array patterns. Part (a) relates to the azimuth antenna lens system. Part (b) relates to the switching matrix design with shaped elevation beam column elements. Parts (c) and (d) relate to the electronically controlled attenuator and a second switching matrix techniques, respectively, and use the same instructions as part (b).

#### (a) Lens System Using Monopole Array - Azimuth Antenna

- (1) Take azimuth radiation patterns to determine the distribution on the focal arc of the lens required to produce "satisfactory" radiation patterns over the frequency range 5.0 GHz-5.25 GHz.
- (2) Once "satisfactory" radiation patterns have been obtained, take patterns at one frequency for a number of different coarse scan positions including the scan limits of the lens and a group of consecutive coarse positions.
- (3) Repeat step 2 above for a representative number of frequencies over the 5.0 GHz to 5.25 GHz range.
- (4) Take consecutive fine scan radiation patterns between the coarse positions of step 2 and step 3.

#### (b) Switching Matrix Design with Shaped Elevation Beam Column Elements

- (1) Take azimuth radiation patterns at  $0^{\circ}$  azimuth and  $0^{\circ}$  elevation at a single frequency and check 2 complete cycles (one on either side of  $0^{\circ}$ ) of fine scan beams. Include coarse beam positions as well.
- (2) Spot check 3 other azimuth scan positions on either side of  $0^{\circ}$ .
- (3) Repeat 1 and 2 for 2 other frequencies in the band.
- (4) Repeat 1 through 3 for elevation angles of  $10^{\circ}$ ,  $20^{\circ}$ ,  $30^{\circ}$  and  $40^{\circ}$  at the same scan positions and at the same frequencies.
- (5) Take elevation patterns at those scan positions and those frequencies used in 1 through 3.

Table 7.1 Tabulation of Test Planning for SP2T Switch

Parameter Under Test	Test System Fig. No.	Port Connections Input - Output	Spec. Limit	Freq. Eval. Mode	Spec. Para. No.
VSWR	7.4	1, 2, 3	1.5	Swept	E.1 (7)
VSWR	7.4 or 7.7	1, 2, 3	1.5	Single	E.1 (7)
IL Mag, Absolute	7.3	1-2, 1-3	1.2db	Swept	E.1 (3)
IL Mag, Absolute	7.3, 7.5 or 7.6	1-2, 1-3	1.2db	Single	E.1 (3)
IL Mag, Variation	7.3	1-2, 1-3	0.3, 0.4db	Swept	E.1 (4)
IL Mag, Variation	7.3, 7.5 or 7.6	1-2, 1-3	0.3, 0.4db	Single	E.1 (4)
IL Phase, Diff	7.3	1-2, 1-3	10 deg.	SW. or SIN.	E.1 (5)
Isolation	7.4	On to Off Ports	30db	Swept	E.1 (6)
Isolation	7.4 or 7.6	On to Off Ports	30db	Single	E.1 (6)
Switching Char.	7.8	1-2, 1-3	See Specs.	SW. or SIN.	E.1 (8)
Switching Transients	7.9	1-2, 1-3	See Specs.	SW. or SIN.	E.1 (8)
RF Isolation	7.9	RF Port-Bias Port	30db	Swept	E.1 (8)
RFI	7.3 thru 7.9 as req.	To be performed as and when required			E.1 (9)
Temp. & Humidity		To be performed as and when required			
Mech. Insp.		To be performed as and when required			

NOTE: Test Power Levels for each test are +27, 0, and -20dbm.

Table 7.2 Tabulation of Test Planning for SP4T Switch

Parameter Under Test	Test System Fig. No.	Port Connections Input - Output	Spec. Limit	Freq. Eval. Mode	Spec. Para. No.
VSWR	7.4	1,2,3,4,5	1.5	Swept	E.2 (7)
VSWR	7.4 or 7.7	1,2,3,4,5	1.5	Single	E.2 (7)
IL Mag, Absolute	7.3	1-2,1-3,1-4,1-5	1.8	Swept	E.2 (3)
IL Mag, Absolute	7.3,7.5 or 7.6	1-2,1-3,1-4,1-5	1.8	Single	E.2 (3)
IL Mag, Variation	7.3	1-2,1-3,1-4,1-5	0.3,0.4db	Swept	E.2 (4)
IL Mag, Variation	7.3,7.5 or 7.6	1-2,1-3,1-4,1-5	0.3,0.4db	Single	E.2 (4)
IL Phase, Diff	7.3	1-2,1-3,1-4,1-5	10 deg	SW.or SIN.	E.2 (5)
Isolation	7.4	On to Off Ports	30db	Swept	E.2 (6)
Isolation	7.4 or 7.6	On to Off Ports	30db	Single	E.2 (6)
Switching Char.	7.8	1-2,1-3,1-4,1-5	See Specs.	SW.or SIN.	E.2 (8)
Switching	7.9	1-2,1-3,1-4,1-5	See Specs.	Single	E.2 (8)
Transients	7.9	RF Port-Bias Port	30db	Swept	E.2 (8)
RF Isolation		To be performed as and when required			E.2 (9)
RFI	7.3 thru 7.9	To be performed as and when required			
Temp. & Humidity	as req.	To be performed as and when required			
Mechanical Insp.		To be performed as and when required			

NOTE: Test Power Levels for each test are +34.8, 0, and -20dbm.

Table 7.3 Tabulation of Test Planning for Phase-Balanced Transfer Switch

Parameter Under Test	Test System Fig. No.	Port Connections Input - Output	Spec. Limit	Freq. Eval. Mode	Spec. Para. No.
VSWR	7.4	1, 2, 3, 4	1.5	Swept	E.3 (10)
VSWR	7.4 or 7.7	1, 2, 3, 4	1.5	Single	E.3 (10)
IL Mag, Absolute	7.3	1-3,1-4,2-3,2-4	1.1,0.9db	Swept	E.3 (4)
IL Mag, Absolute	7.3,7.5, or 7.6	1-3,1-4,2-3,2-4	1.1,0.9db	Single	E.3 (4)
IL Mag, Variation	7.3	1-3,1-4,2-3,2-4	0.3db	Swept	E.3 (5)
IL Mag, Variation	7.3,7.5, or 7.6	1-3,1-4,2-3,2-4	0.3db	Single	E.3 (5)
IL Phase, Variation	7.3	1-3,1-4,2-3,2-4	10 deg.	SW.or SIN.	E.3 (8)
Balance, Ampl & Phase	7.10	1&2-3&4	0.3db, 5 deg.	SW.or SIN.	E.3 (7)
Isolation	7.4	See Spec.	30db	Swept	E.3 (11)
Isolation	7.4 or 7.6	See Spec.	30db	Single	E.3 (11)
Switching Char.	7.8	1-3,1-4,2-3,2-4	See Specs.	SW.or SIN.	E.3 (12)
Switching Transients	7.9	1-3,1-4,2-3,2-4	See B3.3 (8)	Single	E.3 (8)
RF Isolation	7.9	RF Port-Bias Port	See B3.3 (8)	Swept	E.3 (8)
RFI					
Temp. & Humidity	7.3 thru 7.10 as req.				
Mechanical Insp.					

NOTE: Test Power Levels for Each Test are +30, 0, and -20dbm.



Table 7.4 Tabulation of Test Planning for Electrically Variable Attenuator

Parameter Under Test	Test System Fig. No.	Port Connections Input - Output	Spec. Limit	Freq. Eval. Mode	Spec. Para. No.
VSWR	7.4	1, 2	1.5	Swept	E.4 (4)
VSWR	7.4 or 7.7	1, 2	1.5	Single	E.4 (4)
IL Mag, Absolute	7.3	1-2	1db	Swept	E.4 (7)
IL Mag, Absolute	7.3, 7.5 or 7.6	1-2	1db	Single	E.4 (7)
IL Mag, Diff	7.3	1-2	0.3, 0.5db	Swept	E.4 (7)
IL Mag, Diff	7.3, 7.5 or 7.6	1-2	0.3, 0.5db	Single	E.4 (7)
Atten. Range	7.3	1-2	0-10db	Swept	E.4 (5)
Atten. Accuracy	7.3	1-2	See Specs.	Swept	E.4 (6)
Atten. Accuracy	7.3, 7.5 or 7.6	1-2	See Specs.	Single	E.4 (6)
Ins. Phase Var.	7.3	1-2	+5 deg	SW.or SIN.	E.4 (8)
Switching Char.	7.8	1-2	See Specs.	SW.or SIN.	E.4 (9)
Switching	7.9	1-2	See Specs.	Single	E.4 (9)
Transients	7.9	1-2	30db	Swept	E.4 (9)
RF Isolation					E.4 (10)
RFI					
Temp. & Humidity	7.3 thru 7.9 as req.	To be performed as and when required			
Mechanical Insp.		To be performed as and when required			

NOTE: Test Power Levels for each test are +30, 0, and -20dbm.

Table 7.5 Tabulation of Test Planning for 4-Bit Digital Phase Shifter

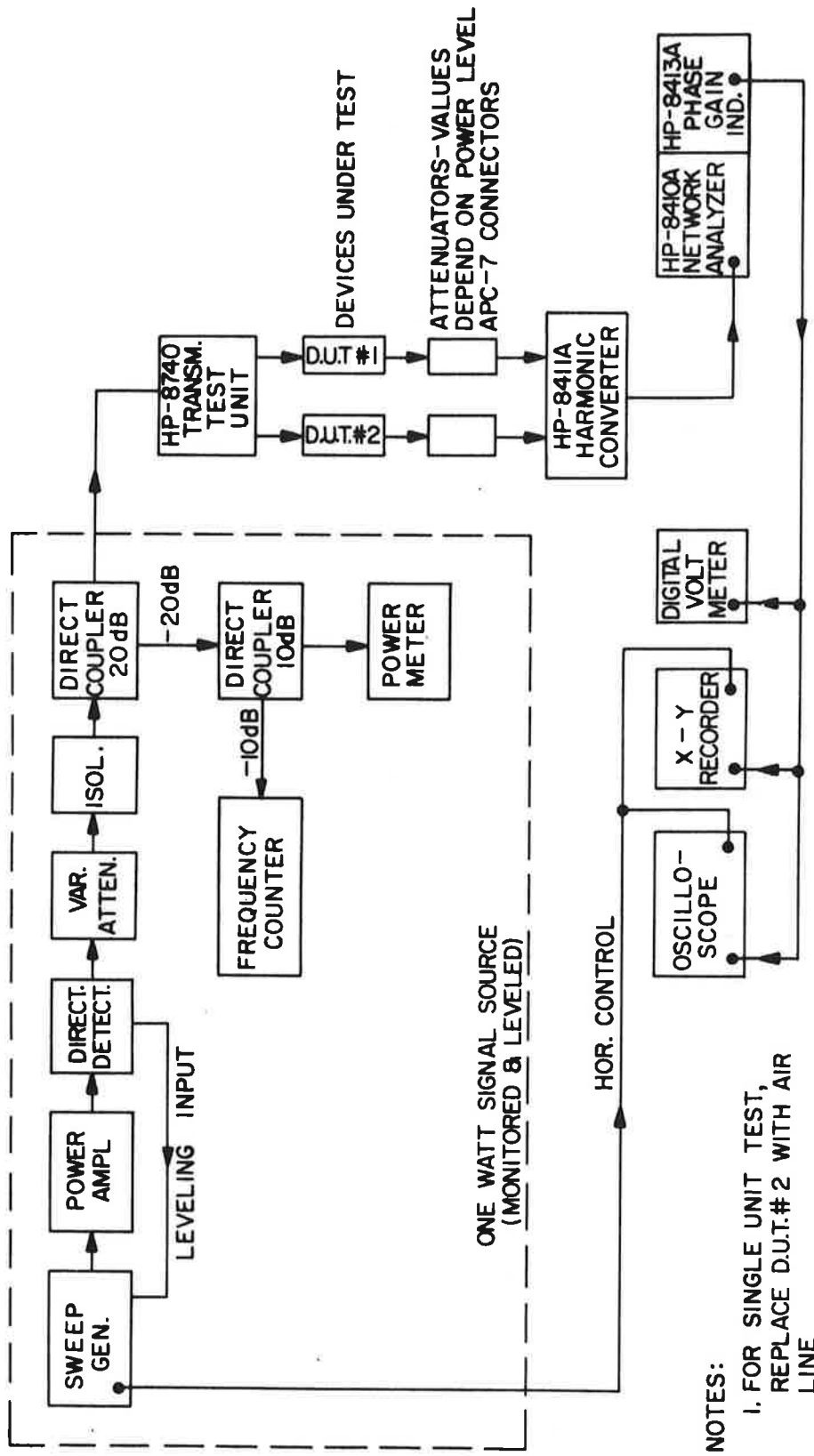
Parameter Under Test	Test System Fig. No.	Port Connections Input - Output	Spec. Limit	Freq. Eval. Mode	Spec. Para. No.
VSWR	7.4	1, 2	1.35	Swept	E.5 (2)
VSWR	7.4 or 7.7	1, 2	1.35	Single	E.5 (2)
IL Mag, Absolute	7.3	1-2	1.7, 1.5db	Swept	E.5 (3)
IL Mag, Absolute	7.3, 7.5 or 7.6	1-2	1.7, 1.5db	Single	E.5 (3)
IL Mag, Variation	7.3	1-2	0.25, 0.2db	Swept	E.5 (3)
IL Mag, Variation	7.3, 7.5 or 7.6	1-2	0.25, 0.2db	Single	E.5 (3)
Phase Shift	7.3	1-2	See Specs.	SW.or SIN.	E.5 (5)
Ins. Phase Var.	7.3	1-2	±5°	SW.or SIN.	E.5 (6)
Switching Char.	7.8	1-2	See Specs.	SW.or SIN.	E.5 (7)
Switching Transients	7.9	1-2	See Specs.	Single	E.5 (9)
RF Isolation	7.9	RF Port-Bias Port	30db	Swept	E.5 (10)
RFI		To be performed as	and when required		
Temp. & Humidity	7.3 thru 7.9 as req.	To be performed as	and when required		
Mechanical Insp.		To be performed as	and when required		

NOTE: Test Power Levels for each test are +28.5, 0, and -20dbm.

Table 7.6 Tabulation of Test Planning For 4-Way and 8-Way Power Divider

Parameter Under Test	Test System Fig. No.	Port Connections Input - Output	Spec. Limit	Freq. Eval. Mode	Spec. Para. NO.
Item 1: 8-way power divider					
RF Input Power (2)	7.5(1)	See Spec.	See Specs.	Single	E.6 (1)
VSWR (4)	7.4	All Ports	1.5	Swept	E.6 (6)
VSWR (4)	7.4 or 7.7	All Ports	1.5	Single	E.6 (6)
Coupling & IL Mag (4)	7.3	See Spec.	10.2, 1.2db	Swept	E.6 (2)
Coupling & IL Mag (4)	7.3, 7.5 or 7.6	See Spec.	10.2, 1.2db	Single	E.6 (2)
Isolation (4)	7.4	See Spec.	20db	SW.or SIN.	E.6 (3)
Amplitude Balance (4)	7.3	See Spec.	0.3db	Swept	E.6 (4)
Amplitude Balance (4)	7.3, 7.5 or 7.6	See Spec.	0.3db	Single	E.6 (4)
Phase Balance (4)	7.3	See Spec.	10 deg	Single	E.6 (5)
RFI (4)	7.3 thru 7.11 as req.	To be performed as and when required			E.6 (7)
Temp. & Humidity (4)					
Mechanical Insp.		To be performed as and when required			
Item 2: 4-way power divider; same as item 1 except the following					
RF Input Power (3)	7.5(1)	See Spec.	See Specs	Single	
Coupling & IL Mag (4)	7.3	See Spec.	6.8, 0.8db	Swept	
Coupling & IL Mag (4)	7.3, 7.5 or 7.6	See Spec.	6.8, 0.8db	Single	

NOTE: (1) Terminate ports per spec paragraph No. F3.3(1)  
 (2) Test power levels of +44.8, 0, and -20dbm  
 (3) Test power levels of +37, 0, and -20dbm  
 (4) Test power levels of +30, 0, and -20dbm



- NOTES:
1. FOR SINGLE UNIT TEST, REPLACE D.U.T.#2 WITH AIR LINE
  2. FOR COMPARISON TEST, INSTALL BOTH D.U.T.#1 AND D.U.T.#2

Figure 7.3 Block Diagram - Insertion Loss Measurement - Amplitude & Phase Swept Frequency Technique & Phase.

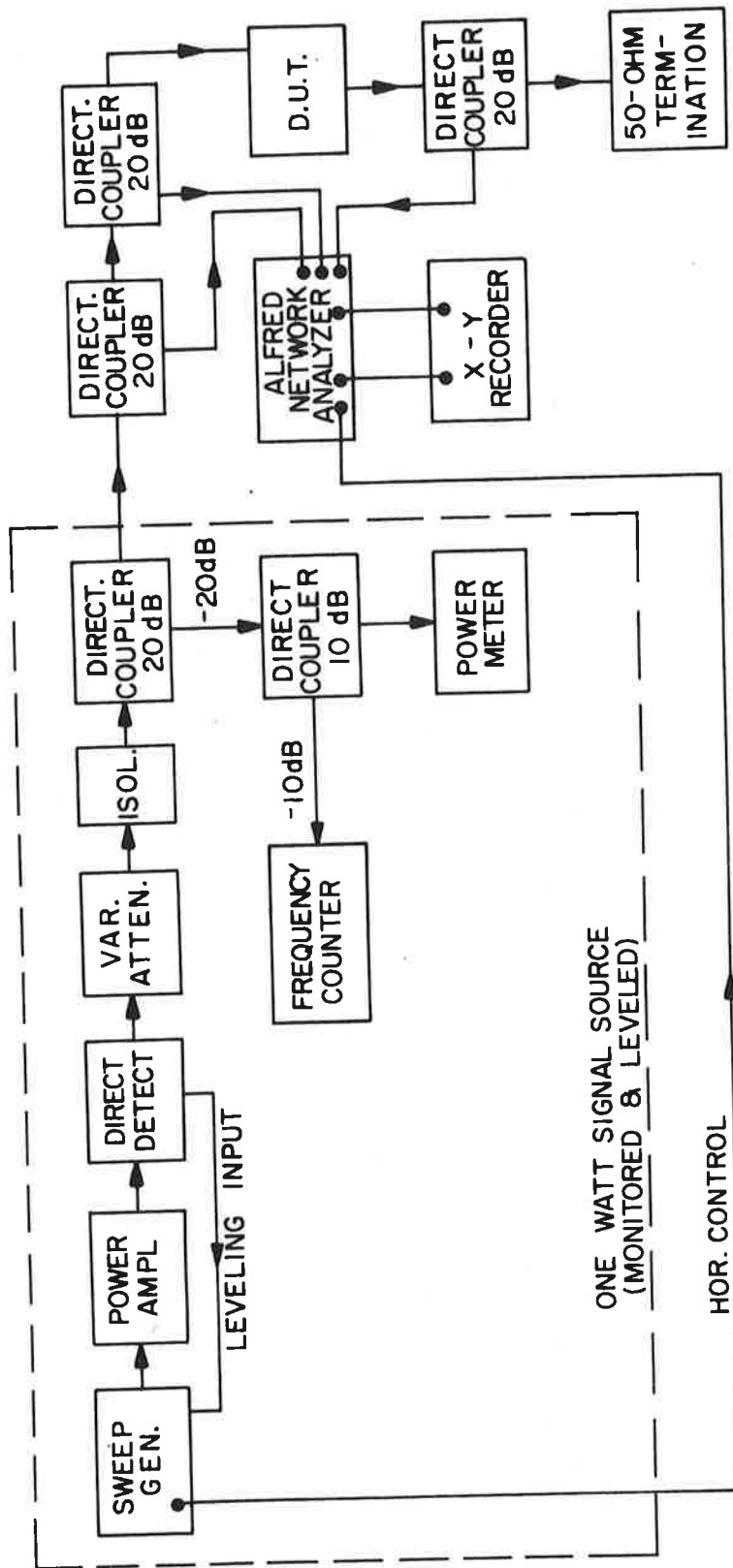


Figure 7.4 Block Diagram - VSWR and Isolation - Swept Frequency Technique

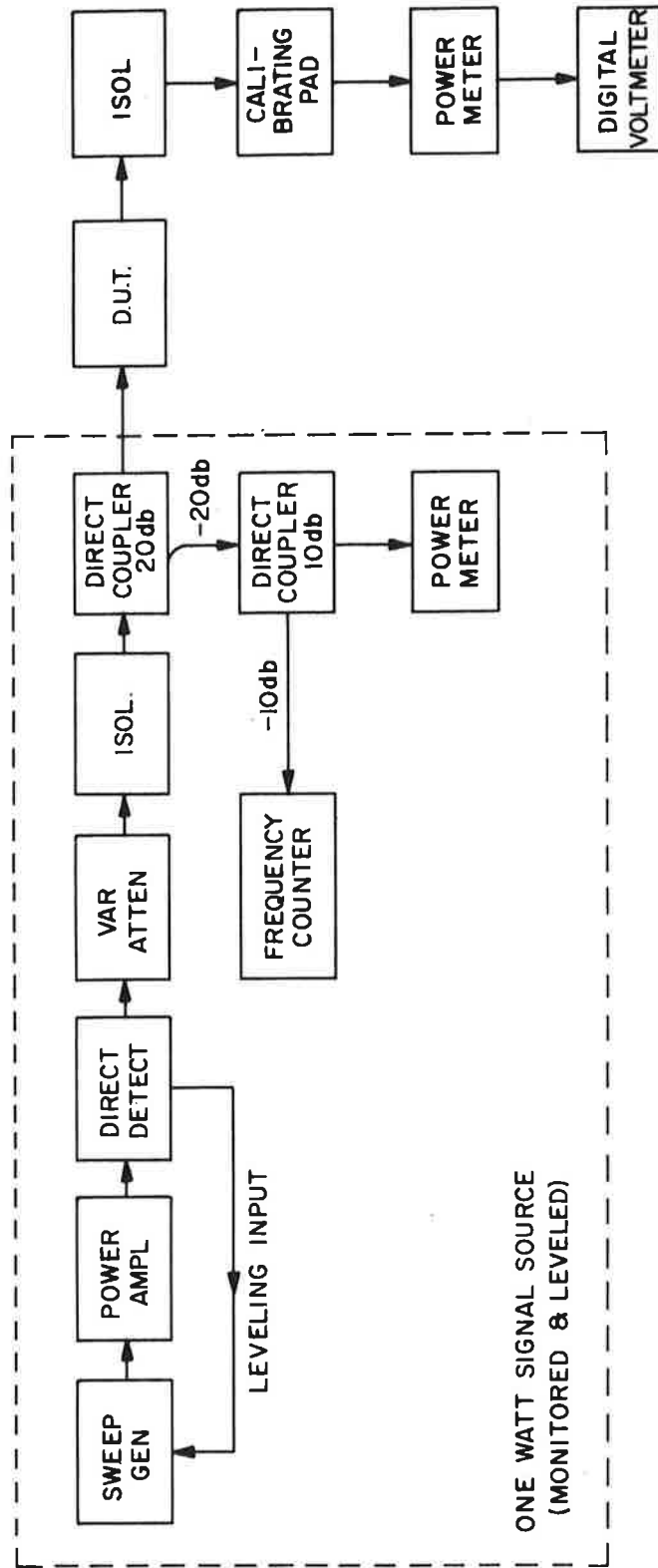


Figure 7.5 Block Diagram - Insertion Loss Magnitude - Rapid Single Frequency Technique

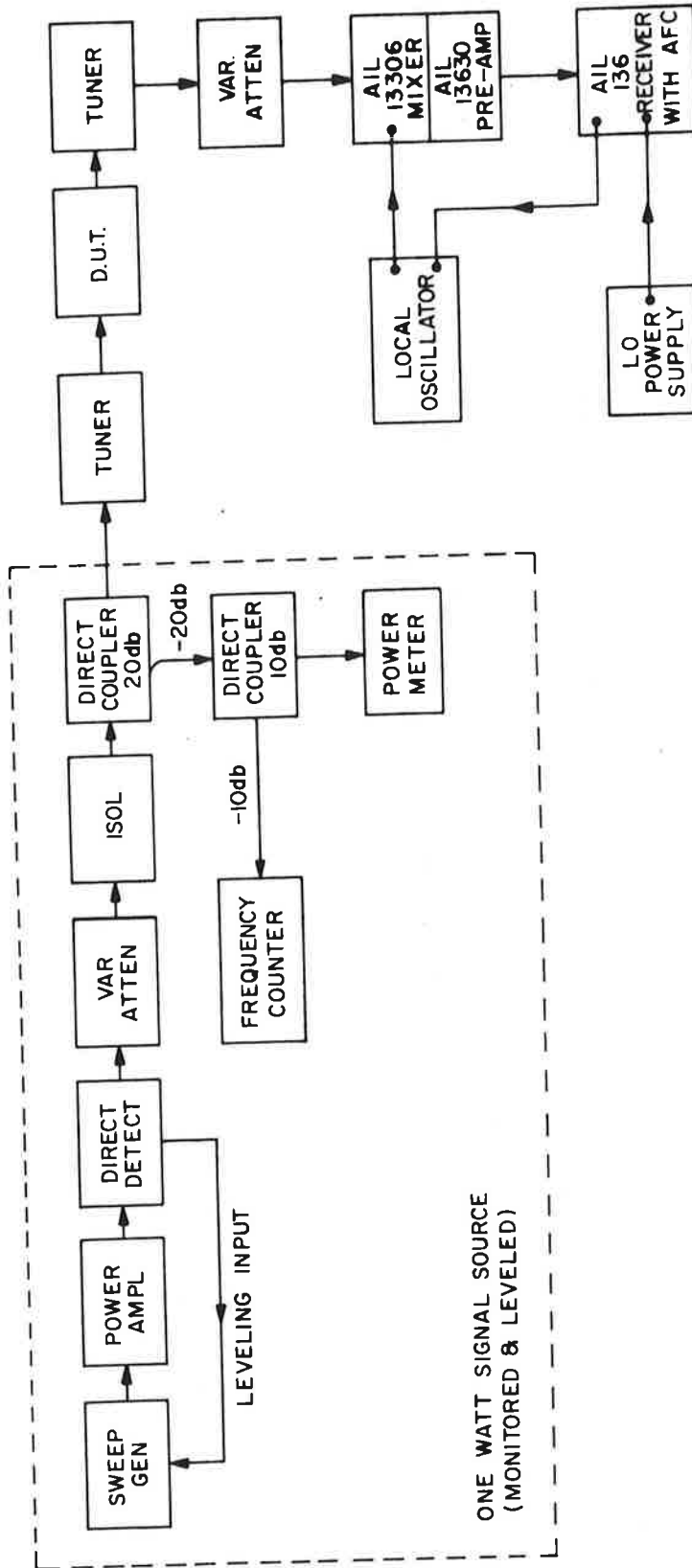


Figure 7.6 Block Diagram - Insertion Loss Magnitude and Isolation - Precision Single Frequency Technique

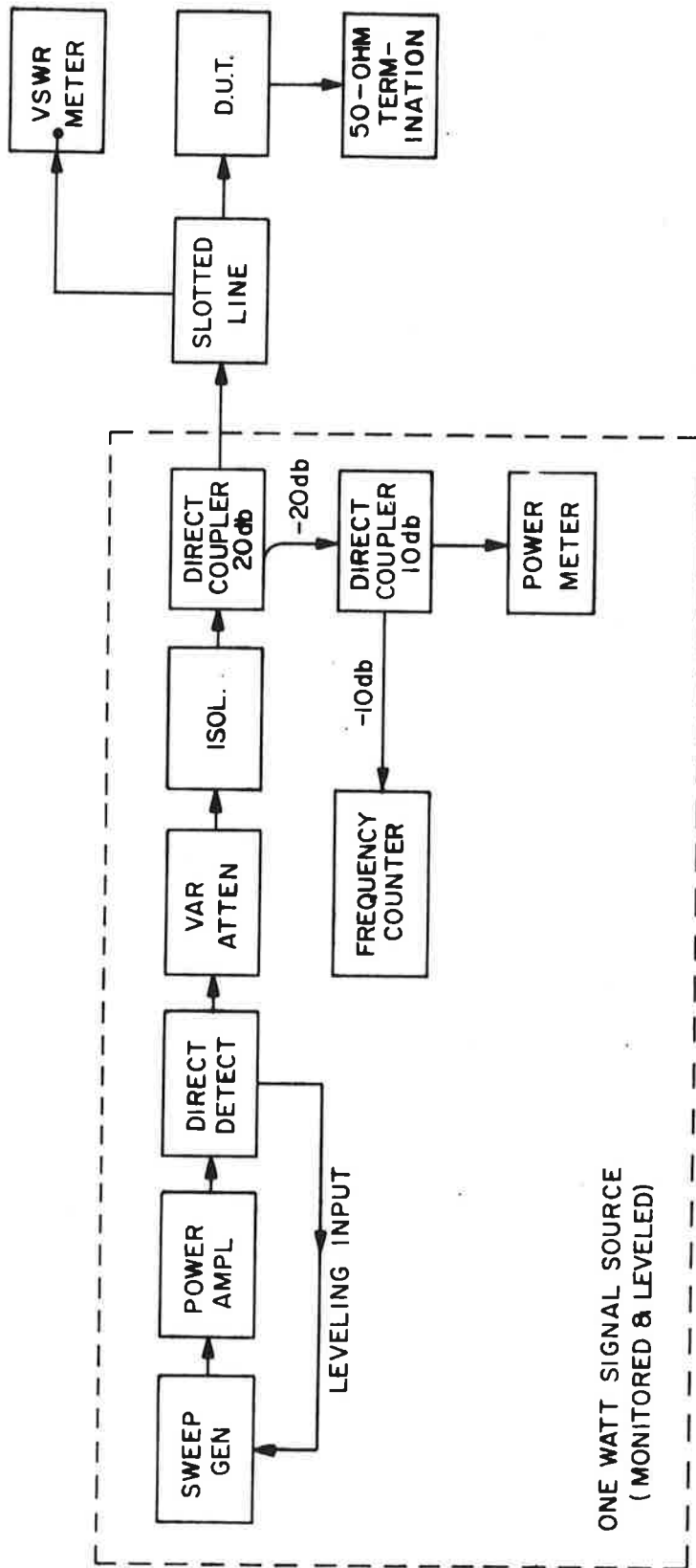


Figure 7.7 Block Diagram - VSWR Measurement - Precision Single Frequency Technique



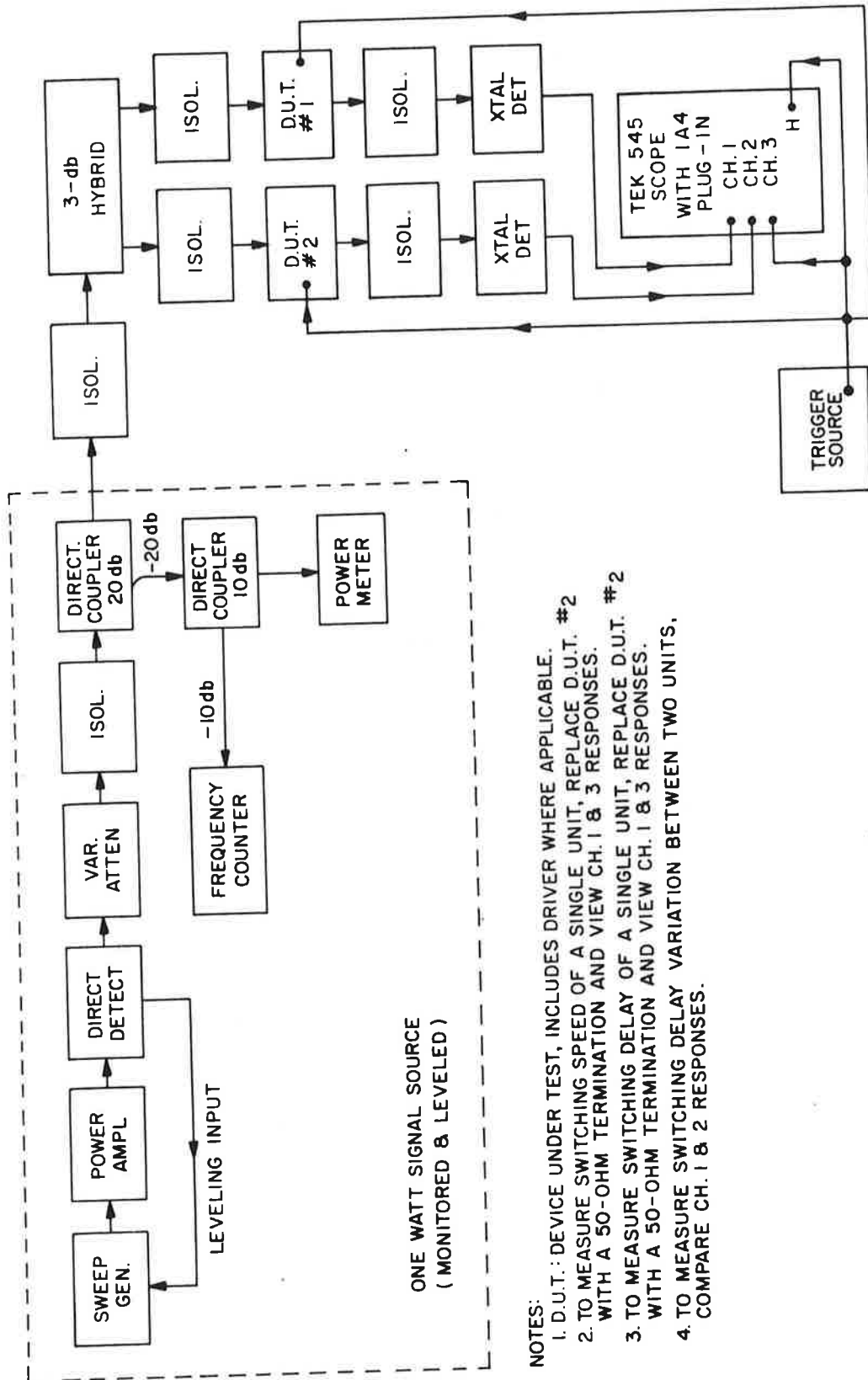
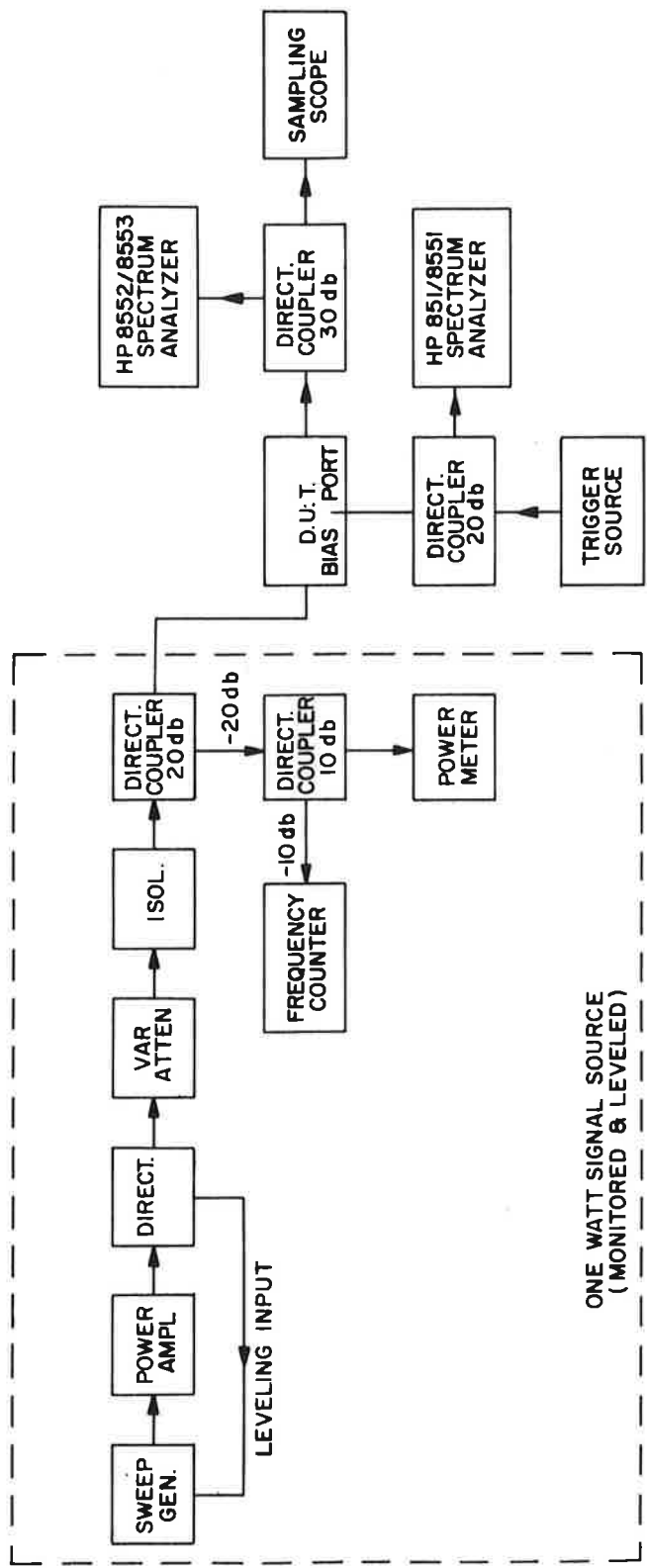


Figure 7.8 Block Diagram- Switching Characteristic Measurements



NOTE:  
D.U.T.: DEVICE UNDER TEST INCLUDES DRIVER WHERE APPLICABLE.

Figure 7.9 Block Diagram - Bias Line RF Isolation and Dribble Measurements

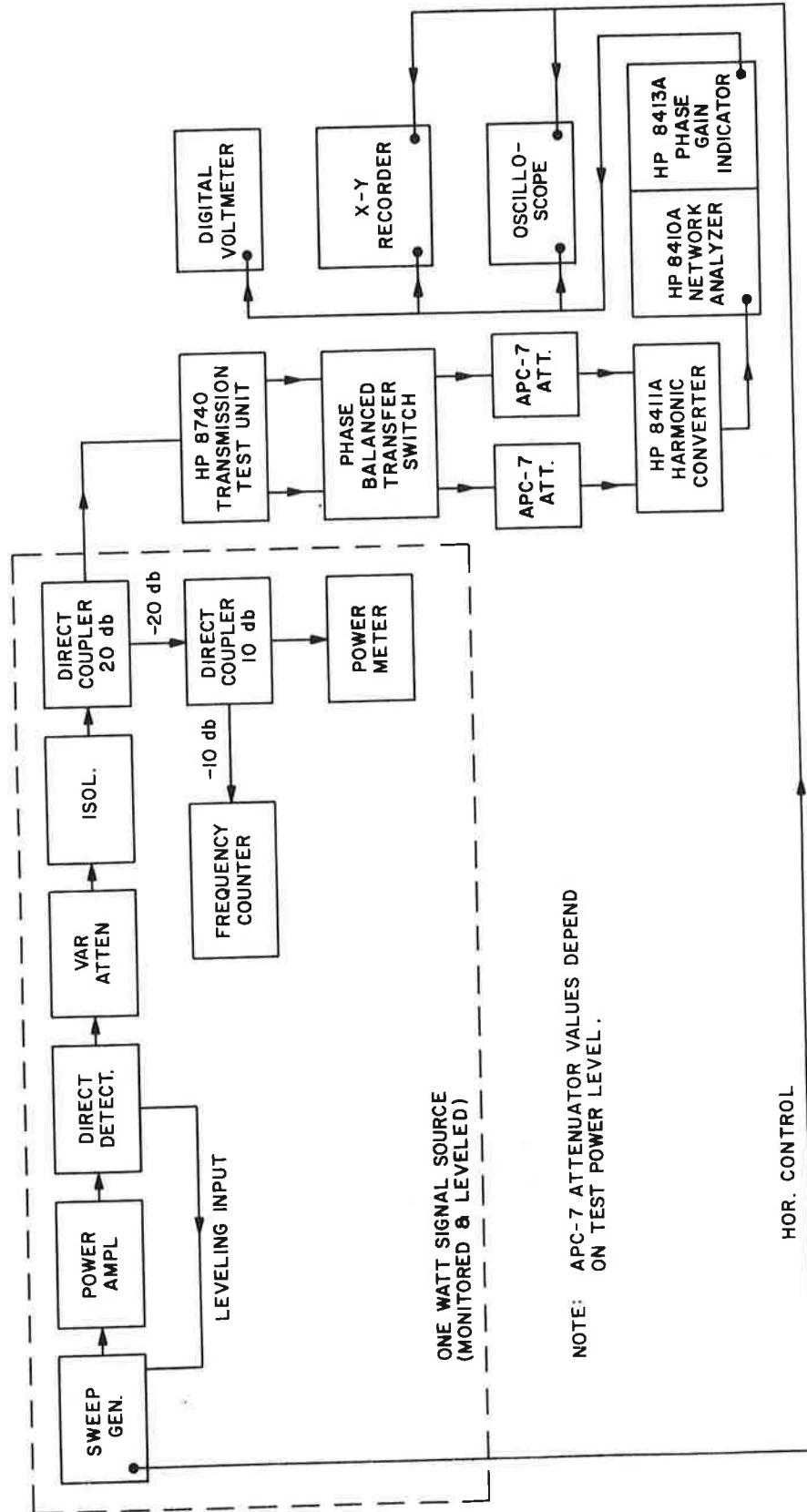


Figure 7.10 Block Diagram - Amplitude and Phase Balance Measurement

- (c) Electronically controlled attenuator approach with shaped elevation beam column elements. Steps (1) through (4); same as (b) above.
- (d) Second switching matrix design with shaped elevation beam column elements. Steps (1) through (4); same as (b) above.

### 7.2.3 RANGE TESTS-DYNAMIC ARRAY PATTERNS

This section provides generalized guidelines on dynamically range testing the array patterns.

- (a) Position antenna in azimuth and at  $0^{\circ}$  elevation and electronically scan the antenna in azimuth. The output of the receiving antenna will vary with the scan angle of the antenna under test. Test at 3 frequencies in the 5.0-5.25 GHz range.
- (b) Repeat (a) above for a number of azimuth scan angles at the same test frequencies as (a).
- (c) Reposition antenna in elevation and repeat steps (a) and (b) above using the same test frequencies and the same scan angles.

### 7.3 Antenna Elements-Development Plan

*Abstract-The element columns for the azimuth antenna must be designed to meet low multipath requirements. The proper currents must be setup using a properly designed power divider. The procedure is discussed herein.*

The following sections outline a step by step procedure anticipated for the development of the antenna elements. The fact that the vertical beam shaping is largely independent of the horizontal scanning design for the azimuth antenna allows the element column design to proceed in parallel with the feed network study. The azimuth column design requires a power division-phasing network feeding an array of stripline dipoles. For the elevation antenna, similar stripline dipoles appear to be adequate at present to give the required coverage in azimuth.

These procedures represent a conservative estimate of the effort required. The variation of impedance with scan affects cylindrical array design, since the elements near the edge of the distribution are essentially in a wide scan position. Also, any given element is sometimes in an edge position, sometimes in a center position in the distribution. One technique is to match the element in its isolated state, is, with no neighboring elements. This has proved to be a good

compromise match for some applications. If it works here, many of the steps can be eliminated.

### 7.3.1 COLUMN ELEMENT OF AZIMUTH ANTENNA-DEVELOPMENT TASKS

#### 7.3.1.1 Elemental Dipole

- a. Design dipole element over ground plane for use in column array.
- b. Match the dipole to a  $50\Omega$  transmission line in the frequency range 5.0 GHz to 5.25 GHz.
- c. Fabricate 12 dipoles to the "matched" design dimensions with connectors.
- d. Assemble a 4-element by 3-element array of dipoles.
- e. Measure the variation of impedance of a single dipole in the array over the frequency range 5.0 GHz to 5.25 GHz. Measure variations with respect to the phase and amplitude of the E and H plane coupling.
- f. If results of (e) above indicate large impedance variations, adjust dipole element design to minimize them.
- g. Once design is satisfactory, fabricate enough dipole elements with connectors to make 3 complete column arrays.

#### 7.3.1.2 Power Divider and Phasing

- a. Calculate amplitude and phase distribution required at each dipole of the column array (Computer-program).
- b. Design power divider to produce the distribution calculated in (a).
- c. Fabricate one power divider with connectors.
- d. Test fabricated power divider with matched loads. Tests over the frequency range 5.0 to 5.25 GHz will include:
  1. Input VSWR with output parts terminated in matched loads
  2. Insertion loss
  3. Amplitude and Phase of each output port with all other output ports terminated
  4. Isolation between ports. Measure amplitude and phase variation of each output port as each of the other terminated outputs is short-circuited and open-circuited
- e. Redesign power divider and repeat steps c. and d. if results of d. are poor.
- f. Measure input VSWR of power divider with dipoles connected in place of matched loads over the frequency range 5.0 GHz to 5.25 GHz.

- g. Take antenna radiation patterns over the frequency range 5.0 to 5.25 GHz of single column.
- h. If antenna radiation patterns not satisfactory (i.e. do not compare with the calculated) determine cause and correct.
- i. When radiation patterns are satisfactory, design power divider and dipoles combined.
- j. Verify the "combined" array by taking VSWR, and antenna radiation patterns over the frequency range 5.0 GHz to 5.25 GHz.
- k. Fabricate 32 column arrays for the experimental antenna.

### 7.3.2 ELEVATION ANTENNA ELEMENT - DEVELOPMENT TASKS

#### 7.3.2.1 Element Design (Spec. H-Plane Pattern $120^\circ$ @ 3dB)

- a. Survey literature for possible stripline element.
- b. Fabricate those element types that appear promising.
- c. Take antenna radiation patterns of candidate antennas and select the one that meets the spec. (If none meet the spec. select the most promising and attempt to widen the beam).
- d. Match the antenna selected, to minimize the variation of impedance over the frequency range 5.0 GHz to 5.25 GHz.
- e. Fabricate 5 "matched" antennas with connectors.
- f. Fabricate a 4-element linear array.
- g. Measure the impedance of a single element in the array with the adjacent elements driven. Measure the variation of impedance with respect to the phase and amplitude of the E-Plane coupling.
- h. If results of g. indicate large impedance variations, adjust element design so as to minimize them.
- i. Once the design is satisfactory, fabricate enough for a complete elevation antenna array. (Without connectors)

#### 7.3.2.2 Power Divider and Phasing

- a. Calculate the amplitude and phase distribution required at each element of the elevation antenna array. (Computer program)
- b. Design power divider to produce the distribution calculated in a.
- c. Fabricate one power divider with connectors.
- d. Test fabricated power divider with matched loads. Tests over the frequency range 5.0 GHz to 5.25 GHz will include:
  - 1. Input VSWR with output ports terminated in matched loads.
  - 2. Insertion Loss.

3. Amplitude and phase of each output port with all other output ports terminated.
4. Isolation between ports. Measure amplitude and phase variation of each output port as each of the other terminated outputs is short-circuited and open-circuited.
- e. Redesign power divider and repeat steps c. and d. if results of d. are poor.
- f. Test fabricated power divider (with connectors) with the matched antenna elements. Perform the following tests over the frequency range 5.0 GHz and 5.25 GHz.
  1. Input VSWR with antenna elements on the output ports.
- g. Take antenna radiation patterns over the frequency range 5.0 to 5.25 GHz of the array. Also check pattern at various scan angles.

#### 7.4 Cost Estimates, Based on Component Production Costs

*Abstract-The costs involved in component procurement are estimated for the electronic attenuator method. The effect of beamwidth on cost is discussed.*

The cost estimates for the feed network components are given in Table 7.7. In addition to these are the costs of logic, RF sources, antenna elements (including cables), and structural costs.

a. Component Costs. The estimates in Table 7.7 are based on conversations with several component houses and are not considered as final, since they are not standardized in any way. For example, the phase shifter cost is low from the point of view of the number of diodes relative to the cost of the SP4T switches. These estimates will be refined during the next year so that comparable techniques are used throughout. In this section, only the costs of the electronic attenuator design are used, since it appears at present to be the most immediately realizable scheme which yield full coverage in azimuth.

b. Logic Costs. This can only be roughly estimated at present, but it is not critical since it represents a small percentage of total cost. The following costs are assumed for both azimuth and elevation:

One-degree beamwidth	\$10,000
Two-degree beamwidth	\$ 5,000
Four-degree beamwidth	\$ 2,500

Table 7.7 Estimated Production Costs of Components Used  
in Electronic Attenuator Technique

ITEM	ESTIMATED COST
1:4 Power Divider	\$ 130
1:6 Power Divider	\$ 160
1:8 Power Divider	\$ 190
SP2T Switch, with Driver	\$ 150
SP3T Switch, with Driver	\$ 250
SP4T Switch, with Driver	\$ 340
4-Bit Diode Phase Shifter, with Driver	\$ 130
Electronic Attenuator, with Driver	\$ 190
Vertical Dipole Column (Azimuth Antenna)	\$ 150
Dipole Assembly ( Elevation Antenna )	\$ 30



c. Source Cost. The figure of \$1000 per watt is used as a baseline. This is based on the present cost of applicable commercial solid-state sources. It is reasonable to assume that this cost will decrease by 5:1 or more in the next five years. The power needed for the three beam widths is quite different (see Table 1.1) since the wider beamwidths propagate energy over widely different regions (the power requirement is proportional to beamwidth). The losses of the system are assumed to be those of the electronic attenuator scheme. The requirements are thus given as follows:

One-degree beamwidth: the radiated power of .76 watts through an insertion loss of 11.8 dB requires 11.5 watts at the source: cost: \$11,500.

Two-degree beamwidth: the radiated power of 1.53 watts through an insertion loss of 11.4 dB requires 21.2 watts at the source: cost \$21,200.

Four-degree beamwidth: the radiated power of 3.05 watts through an insertion loss of 11.0 dB requires 38.4 watts at the source: cost: \$38,400.

d. Antenna element costs. Based on the requirement for a power divider feeding an array of stripline dipoles fed by a phase-stable low loss cable, each azimuth antenna column is estimated to cost about \$200. For the narrow beam azimuth antenna, this turns out to be almost half the cost of the array. It may prove necessary to use an hour-glass type reflector in order to keep costs down. This requires further consideration. For the elevation antenna, this is not so critical.

e. Structural costs. Since the same tolerances must be held over a wider region for the narrower beam antenna, the cost will rise at a rate faster than the aperture rate of increase. Thus the costs are estimated at \$2000, \$4500, and \$12,000 for the 4°, 2°, and 1° beamwidth azimuth antennas, respectively.

#### 7.4.1 AZIMUTH ANTENNA COST ESTIMATES

##### a. One-degree beamwidth antenna.

Feed System	\$57,930
Logic	\$10,000
Source	\$11,500
Elements: 288 x \$200 =	\$57,600
Structural	\$12,000
	<u>\$149,030</u>

b. Two-degree beamwidth antenna:

Feed System	\$28,660
Logic	\$ 5,000
Source	\$21,200
Elements: 144 x \$200 =	\$28,800
Structural	\$ 4,500
	<u>\$88,160</u>

c. Four-degree beamwidth antenna:

Feed System	\$14,450
Logic	\$ 2,500
Source	\$38,400
Elements: 72 x \$200 =	\$14,400
Structural	\$ 2,000
	<u>\$71,750</u>

It should be pointed out that the above costs do not take into account assembly costs, monitors, or additional software or hardware above the basic scanning requirements. It should also be noted, however, that a thorough cost study should really consider the maintenance and down-time user cost since the inherent reliability and graceful-mode failure of phased array systems make them much more attractive when these are taken into account.

7.4.2 ELEVATION ANTENNA COST ESTIMATE

The elevation antenna costs are premised on the assumption of a linear array, with a similar aperture distribution to that of cylindrical arrays. Thus there are 96, 48, and 24 elements for beamwidths of  $1^\circ$ ,  $2^\circ$ , and  $4^\circ$ , respectively. Since there was no cost and insertion loss breakdown in Section IV, it will be carried out here. The logic is similar to that used in cylindrical arrays, and will be comparably priced. The elements will be cheaper, as will the structure.

a. One-Degree beamwidth. The 1:96-way (unequal) power divider is assumed to be made up of 1:4; four 1:4's and 16-1:6-way power dividers. There are 96 phase shifters, 96 cables, and 96 elements:

1:4 power divider	.8 dB
1:4 power divider	.8 dB
1:6 power divider	1.0 dB
4-bit phase shifter	1.7 dB
Cable	1.0 dB
Element	0.4 dB
	<u>5.7 dB</u> Insertion loss

The source requirements are for .58 watts radiated, corresponding to a source of 2.15 watts, or a cost of \$2150. The cost breakdown then becomes:

1 Source		=	\$2150
5 - 1:4 power dividers	5x\$130	=	\$ 650
16-1:6 power dividers	16x\$160	=	\$2560
96 - 4 bit phase shifters	96x\$130	=	\$12480
96 - element + cable complexes	96x\$50		\$4800
Logic			\$10000
Structure			\$ 6000
			<u>\$38,640</u>

b. Two-degree beamwidth. The 1:48-way (unequal) power divider is assumed to be made up of 1:6, and 6-1:8 way power dividers. There are 48 phase shifters, 48 cables, and 48 elements:

1:6 power divider	1.0 dB
1:8 power divider	1.2 dB
4-bit phase shifters	1.7 dB
Cable	1.0 dB
Element	0.4 dB
	<u>5.3 dB</u> Insertion loss

The source requirements are for 1.15 watts radiated, corresponding to a source of 3.89 watts, or a cost of \$3,890. The cost breakdown then becomes:

1 Source	\$3,890
1-1:6 power divider	\$ 160
6-1:8 power dividers - 6x\$190	\$1,140
48 - 4-bit phase shifters - 48x\$130	\$6,240
48 - element & cable complexes - 48x\$50	\$2,400
Logic	\$4,000
Structure	\$3,000
	<u>\$20,830</u>

c. Four-degree beamwidth. The 1:24 way (unequal) power divider is assumed to be made up of 1:4, and 4-1:6-way power dividers. There are 24 phase shifters, 24 cables, and 24 elements:

1:4 power divider	.8 dB
1:6 power divider	1.0 dB
4-bit phase shifter	1.7 dB
Cable	1.0 dB
Element	0.4 dB
	<u>4.9 dB</u> Insertion loss

The source requirements are for 2.31 watts radiated, corresponding to a source of 7.15 watts, or a cost of \$7150. The cost breakdown then becomes:

1 - source	\$7150
1 - 1:4 power divider	\$ 130
4 - 1:6 power dividers - 4 x \$160	\$ 640
24 - 4 bit phase shifters - 24 x \$130	\$3120
24 - element & cable complexes 24 x \$50	\$1200
Logic	\$2500
Structure	\$1500
	<u>\$16240</u>

# APPENDIX A

## CLASSES OF AIRCRAFT<sup>1</sup>

I. Tentative Operational Requirements, RTCA Paper 19-69/  
SC117-46, pp. 5-6

*Abstract-Definitions of aircraft classes are described as defined by RTCA-SC-117.*

#### A. General

The character of the guidance system should not impose limitations on the aircraft utilizing the system. Therefore, existing and future programmed aircraft have been grouped into five classes by consideration of approach and landing velocities, handling characteristics, lateral and vertical approach angles and runway requirements. Further, since propeller-driven aircraft, jet aircraft and aircraft with other propulsion systems will use the system, the performance of the guidance system must not be affected by propulsion system characteristics such as propeller or rotor speeds.

#### B. Classes of Aircraft

1. Class I - Final approach speeds from 60-100KIAS. Final approach descent flight path angles to be utilized will be those that are optimum for the user aircraft. Descent angles may range from 2 degrees to 9 degrees maximum. Included in this class are reciprocating engines, turbo-props and turbo-jet conventional aircraft.
2. Class II - Final approach speeds of 101-135 KIAS. Final approach descent flight path angles to be utilized will be those that are optimum for the user aircraft. Descent angles may range from 2 degrees to 9 degrees maximum. This class is composed of higher performance, less maneuverable aircraft than Class I.
3. Class III - Final approach speeds of 136-165 KIAS. Final approach descent flight path angles to be utilized will be those that are optimum for the user aircraft. Descent angles may range from 2 degrees to 6 degrees maximum. This class is composed of higher performance, less maneuverable aircraft than Class II.
4. Class IV - Final approach speeds of 166 KIAS or greater. Final approach descent flight path angles to be utilized will be those that are optimum for the user aircraft. These descent angles may range from 2 degrees to 2.5 degrees maximum.
5. Class V - Helicopter, vertical take-off and landing (VTOL) or short take-off and landing (STOL) aircraft. Experiments have indicated that these aircraft may require approach angles that vary from 3 degrees to 30 degrees depending on type aircraft, load, terrain,

wind conditions, etc.<sup>1/</sup> The STOLs will include a variety of aircraft configurations including rotor, propeller and jet-lift types. The VTOLs will include a variety of configurations including rotor, propeller and jet-lift types.

<sup>1/</sup> The 0-15 degree vertical coverage specified in Sections IV and V satisfies existing requirements. However, consideration should be given to accommodating higher approach angles that may be required in the future. This could be accomplished either by rotating the 15 degree coverage or increasing the total angular coverage.





# APPENDIX B

## ARRAY THEORY

*Abstract-General antenna array theory is discussed. Relationships are developed for planar, linear and cylindrical arrays. These relationships are then used in developing the basis for azimuth and elevation antenna configurations for the MLS. For the azimuth antenna, a cylinder around the z-axis is the appropriate geometry. A cylindrical antenna with its axis along the y-axis appears to hold promise for generating planar beams for the elevation antenna.*

The purpose of this appendix is to present a discussion of arrays appropriate to the landing system using the runway coordinates of Section I. Radiation is assumed to originate independently (mutual coupling is ignored) from a set of points corresponding to the phase centers of some elementary antennas. The field point, corresponding to the location of the aircraft, is considered to be in the far field: i.e., the range is large compared to the quantity  $2D^2/\lambda$ , where  $D$  is the maximum linear dimension of the ground antenna, and  $\lambda$  is wavelength of the radiation. This condition, it should be noted, is not always met at close range. Near field effects will be considered during the next phase of the project.

The element pattern of a radiator is assumed to be given by  $g_n(\theta, \phi)$ , where  $\theta$  and  $\phi$  refer to a fixed geometry, whose origin is at the element, and the index  $n$  is included to emphasize the fact that different elements may be differently oriented. This factor includes polarization characteristics of both the ground and aircraft antennas. If the phase center of the element is located at  $(X_n, Y_n, Z_n)$ , the pattern expressed in the coordinates of the fixed system is different, due to the translation (without rotation) of the phase center from the origin.

The field due to a radiator at the origin with element pattern  $g_n(\theta, \phi)$  is

$$f_n(\theta, \phi) \sim \frac{e^{-jkR}}{R} g_n(\theta, \phi) \quad (\text{B.1})$$

When the origin is translated, but the aircraft is still far enough away that  $r$  and  $R$  in Figure B.1 are essentially parallel,

$$f_n(\theta, \phi) \sim \frac{e^{-jkr_n}}{r_n} g_n(\theta, \phi)$$

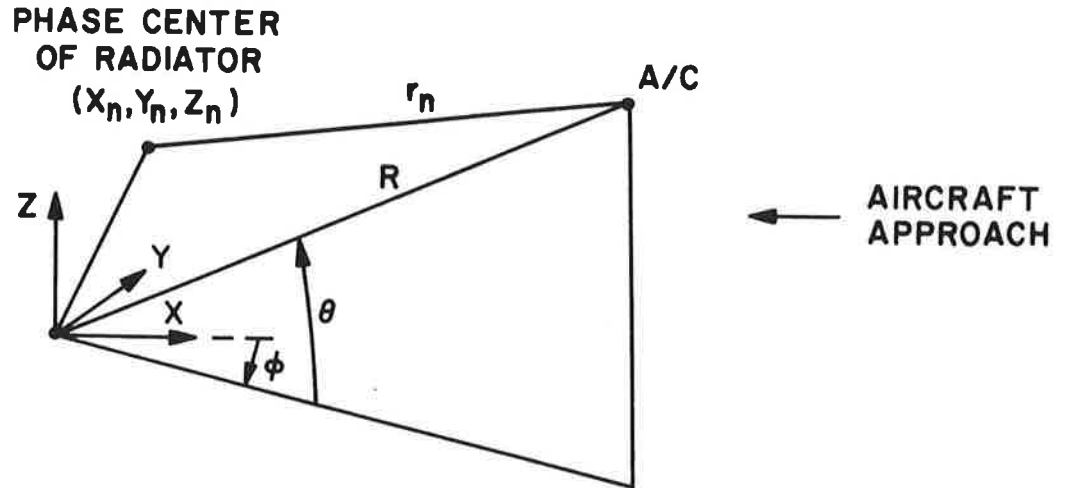


Figure B.1 General Array Geometry

$$= \frac{e^{-jkR}}{R} g_n(\theta, \phi).$$

$$e^{jkx_n \cos \theta \cos \phi} e^{-jky_n \cos \theta \sin \phi} e^{jkz_n \sin \theta}$$

(B.2)

since  $1/r_n = 1/R$ , and

$$r_n = \sqrt{(R \cos \theta \cos \phi - x_n)^2 + (R \cos \theta \sin \phi + y_n)^2 + (R \sin \theta - z_n)^2}$$

or

$$r_n = \sqrt{R^2 - 2x_n R \cos \theta \cos \phi + 2y_n R \cos \theta \sin \phi - 2z_n R \sin \theta}$$

$$= R - x_n \cos \theta \cos \phi + y_n \cos \theta \sin \phi - z_n \sin \theta$$

(B.3)

The field of an array of sources is given by a linear combination of terms like that of Equation B.2. Since the term

$$e^{-jkR/R}$$

is common to all elements, it may be dropped. The reason for this is that the field strength depends on the source power, and antenna properties, since they are independent of power, are all defined in terms of ratios of powers and as such do not depend on the absolute value of the field strengths. Thus the total field for an array of N radiators is given by

$$f(\theta, \phi) = \sum_{n=1}^N a_n g_n(\theta, \phi) e^{+jk(x_n \cos \theta \cos \phi - y_n \cos \theta \sin \phi + z_n \sin \theta)}$$

(B.4)

where the  $a_n$ 's are the (complex) excitation coefficients of the radiators.

If the array is supposed to generate a plane wave in the direction  $(\theta_b, \phi_b)$ , the phase of the coefficients  $a_n$  must be chosen properly. Usually they are chosen to be cophasal; i.e., they are chosen so that when  $\theta = \theta_b$ ,  $\phi = \phi_b$ , all terms in the sum (B.4) are real (or cophasal). From a vector point of view, all the vectors will be parallel, adding "head-to-tail" in this condition. Assuming  $g_n(\theta, \phi)$  is real and positive,

$$a_n = A_n e^{j\phi_n} \tag{B.5}$$

where  $A_n$  is the amplitude, and  $\phi_n$  the phase, of the coefficient  $a_n$ . Thus, for cophasal excitation,

$$\phi_n = -k(x_n \cos \theta_b \cos \phi_b - y_n \cos \theta_b \sin \phi_b + z_n \sin \theta_b) \tag{B.6}$$

All the properties which are discussed below are derived from (B.4) through (B.6).

### B.1 Planar and Linear Arrays

Planar arrays are more complicated than linear arrays but are discussed first because their performance can be derived from that of linear arrays. Planar arrays could be

used for the azimuth function; the scanning is in the horizontal plane, while the vertical beam shaping is accomplished by the vertical aperture. The antenna is thus in the y-z plane, so that at broadside the beam points down the runway centerline.



Figure B.2 Azimuth Planar Array Geometry

Then  $x_n = 0$ , and the summation must be a double summation, representing a grid of  $N$  vertical columns of  $M$  elements each. Uniformly spaced arrays are assumed, for reasons given in section 4.1. The elements are all parallel, so that the element pattern is the same for all radiators. The element pattern can now come outside the summation:

$$f(\theta, \phi) = g(\theta, \phi) \sum_{n=1}^N \sum_{m=1}^M a_{mn} e^{-jk(nd_y \cos\theta \sin\phi - md_z \sin\theta)}$$

(B.7)

where  $d_y$  is the spacing in the horizontal, and  $d_z$  in the vertical. For plane wave excitation (cophasal), this can be written

$$f(\theta, \phi) = g(\theta, \phi) \sum_{n=1}^N e^{-jknd_y (\cos\theta \sin\phi - \cos\theta_b \sin\phi_b)} \sum_{m=1}^M A_{mn} e^{jkm d_z (\sin\theta - \sin\theta_b)}$$

(B.8)

It is desirable to use identical columns if possible. This poses no problem. It requires that the ratios of the excitations of any two elements in a column be the same for any two columns. This means that

$$A_{mn} = B_m C_n$$

so that (B.8) can be written

$$f(\theta, \phi) = g(\theta, \phi) \left( \sum_{n=1}^N C_n e^{-jknd_y (\cos\theta \sin\phi - \cos\theta_b \sin\phi_b)} \right) \\ \cdot \left( \sum_{m=1}^M B_m e^{-jkmd_z (\sin\theta - \sin\theta_b)} \right) \\ = g(\theta, \phi) R_N(\theta, \phi) S_M(\theta) \quad (B.9)$$

Each of the bracketed terms in (B.9) represents the pattern of a linear array. Thus, the field of a planar array can be expressed as the product of two linear arrays.

The second conclusion is that, except for the element pattern, the azimuthal variation is entirely contained in the first bracketed term. This means that the horizontal beam shaping is independent of the vertical column design. The coefficients  $B_m$  can be chosen to shape the vertical pattern to give sharp cutoff below the horizon.

Thirdly, the coning problem can be seen from this equation. Usually  $\theta_b$  is chosen as zero, which means that there is no coning error at the horizon. It is evident that since the  $C_n$ 's are real (and positive), the vectors of  $R_N(\theta, \phi)$  will be head-to-tail collinear when

$$\cos\theta \sin\phi - \sin\phi_b = 0 \quad (B.10)$$

This condition defines the beam maximum in  $\theta$ - $\phi$  coordinates. When  $\theta$  is small;  $\cos\theta \doteq 1$ , and  $\phi \doteq \phi_b$ ; this means that for small elevation angles, the coning error is small. Otherwise  $\phi$  is different from  $\phi_b$  and given by

$$\phi = \sin^{-1} \left( \frac{\sin \phi_b}{\cos \theta} \right) \quad (\text{B.11})$$

It is evident that  $\phi$  is generally greater in magnitude than  $\phi_b$ .

Fourthly, beamwidth variations with scan can be demonstrated. Suppose the elements are equally excited; i.e.,  $C_n = 1$ . Letting  $u = kd_y(\cos \theta \sin \phi - \cos \theta_b \sin \phi_b)$ , we have

$$R_N(\theta, \phi) = \sum_{n=1}^N e^{jnu} \quad (\text{B.12})$$

This is a standard form which can be solved to give

$$R_N(\theta, \phi) = e^{j \left( \frac{N+1}{2} \right) u} \frac{\sin \left( \frac{Nu}{2} \right)}{\sin \left( \frac{u}{2} \right)} \quad (\text{B.13})$$

The phase term is of little significance. The numerator is a rapidly varying function compared with the denominator due to the presence of the factor  $N$ . Thus, the numerator will pass through zero several times ( $N$  times, in fact) while the denominator passes through twice. At  $u = 0$ ,  $R_N(\theta, \phi) = N$ ; the main beam is contained between

$$\frac{Nu}{2} = -\pi \text{ and } \frac{Nu}{2} = +\pi,$$

where the numerator vanishes. At these points (called  $u_0$ )

$$u_0 = \pm \frac{2\pi}{N} = kd_y (\sin \phi_0 - \sin \phi_b) \quad (\text{B.14})$$

assuming  $\theta = \theta_b = 0$ . This can be written

$$\sin \phi_0 = \sin \phi_b \pm \frac{2\pi}{kd_y N} \quad (\text{B.15})$$

The second term is very small, so that  $\phi_0$  is very close to  $\phi_b$ ; this allows the following approximation:

$$\sin\phi_o \doteq \sin\phi_b + (\phi_o - \phi_b)\cos\phi_b \quad (\text{B.16})$$

Using this, the nulls are at

$$\phi_o = \phi_b \pm \frac{2\pi}{kd_y N \cos\phi_b} \quad (\text{B.17})$$

and the null beamwidth is thus

$$\Delta\phi = \frac{4\pi}{kd_y N \cos\phi_b} \quad (\text{B.18})$$

It is apparent from this that for scan angles away from broadside (where  $\phi_b = 0$ ) that the beamwidth increases, namely by the factor  $\sec \phi_b$ . Thus at  $\phi_b = 60^\circ$ , the beam broadens by a factor of two.

For the elevation function, a vertical linear array may prove to be the most desirable configuration. In that case,  $x_n = y_n = 0$ ; the elements are parallel and uniformly spaced, so that  $f(\theta, \phi)$  from equation B.4 becomes

$$f(\theta, \phi) = g(\theta, \phi) \sum_{n=1}^N a_n e^{jkz_n \sin\theta} \quad (\text{B.19})$$

The array can be scanned to a desired elevation angle  $\theta_b$  if

$$a_n = A_n e^{-jkz_n \sin\theta_b} \quad (\text{B.20})$$

yielding

$$f(\theta, \phi) = g(\theta, \phi) \sum_{n=1}^N A_n e^{jkz_n (\sin\theta - \sin\theta_b)} \quad (\text{B.21})$$



The locus of the main beam can be found by setting the exponent equal to zero as before; this gives

$$\theta = \theta_b \tag{B.22}$$

independently of  $\phi$ . This represents a conically shaped beam around the z-axis. The azimuth coverage is only limited by the element pattern, which can be designed to give the desired coverage. The coefficients  $A_n$  are chosen to minimize sidelobes.

## B.2 Cylindrical Arrays

In the case of cylindrical arrays it is convenient to recast equation B.4. The method is the same, but the formulas are different for elevation and azimuth. The azimuth antenna will be discussed first, and the formulas for the elevation antenna will be derived by analogy.

### B.2.1 Azimuth Antenna

For the azimuth antenna, a cylinder around the z-axis is the appropriate geometry. The location of the elements can be identified by the z and  $\phi$  coordinates, where

$$\begin{aligned} X_n &= R \cos \phi_n \\ Y_n &= -R \sin \phi_n \end{aligned} \tag{B.23}$$

and R is the array radius. Also, the element patterns are not identical, since they are mounted around the cylinder. If the element at  $\phi = 0$  has a pattern  $g(\theta, \phi)$ , the element pattern at other locations is given by

$$g_n(\theta, \phi) = g(\theta, \phi - \phi_n) \tag{B.24}$$

Equation B.24 can now be written:

$$\begin{aligned} f(\theta, \phi) &= \sum_{n=1}^N \sum_{m=1}^M a_{mn} g(\theta, \phi - \phi_n) e^{jkR \cos \theta \cos(\phi - \phi_n)} \\ &\quad e^{jkz_m \sin \theta} \end{aligned} \tag{B.25}$$

For reasons identical to the discussion on linear arrays, the vertical element column design and horizontal feed network design can proceed independently, and

$$a_{mn} = b_m c_n \quad (\text{B.26})$$

so that (B.25) becomes

$$f(\theta, \phi) = \left( \sum_{n=1}^N c_n g(\theta, \phi - \phi_n) e^{jkR \cos \theta \cos(\phi - \phi_n)} \right) \cdot \left( \sum_{m=1}^M b_m e^{jkz_m \sin \theta} \right)$$

$$= R_N(\theta, \phi) S_M(\theta) \quad (\text{B.27})$$

The  $c_n$ 's can be chosen to give a plane wave in a desired direction  $(\theta_b, \phi_b)$  and to achieve low sidelobes, while the  $b_m$ 's can be chosen to shape the vertical pattern. The vertical pattern is also affected by the factor  $R_N(\theta, \phi)$  but it is slowly varying in  $\theta$  and can be accounted for once the  $c_n$ 's are chosen.

In order to obtain a cophasal distribution such that a plane wave is generated in the direction  $\phi_b$ , and focused at an elevation angle  $\theta_b$  and assuming momentarily that  $g_n(\theta_b, \phi_b - \phi_n)$  is real for the coverage considered, the coefficients  $c_n$  are

$$c_n = C_n e^{-jkR \cos \theta_b \cos(\phi_b - \phi_n)} \quad (\text{B.28})$$

The phase of  $R_N(\theta, \phi)$  can be written

$$\phi_n = kR \left[ \cos \theta \cos(\phi - \phi_n) - \cos \theta_b \cos(\phi_b - \phi_n) \right] \quad (\text{B.29})$$

To get a coherent plane wave, the  $\phi_n$ 's for  $\phi = \phi_b$  must be the same for all  $n$ ; this only occurs when  $\theta = \theta_b$ . The phase error at other elevation angles is the difference between the actual phase given by (B.29) and the exact phase obtained by substituting  $\theta = \theta_b$  into that equation:

$$\phi_{err} = -kR(\cos\theta_b - \cos\theta)\cos(\phi - \phi_n) \quad (B.30)$$

If a fixed phase shift is added to all phase shift commands in (B.28), i.e., independent of  $n$ , the antenna characteristics remain the same. Only relative phase errors are significant, so one can add a term to equation (B.30) and require that the center element have zero reference phase, and relate the errors to that one. The resulting error is thus meaningful in an absolute sense. The resulting error is obtained by setting  $\phi_n = \phi_b$  (center element); this gives

$$\phi_{err} = kR(\cos\theta_b - \cos\theta) [\cos(\phi - \phi_b) - \cos(\phi - \phi_n)] \quad (B.31)$$

This is when  $\phi_n = \phi_b$  or when  $\theta = \theta_b$

This error is worst at the edge of the distribution; if  $\phi_a$  is the active sector, then the following elements are excited:

$$\phi_b - \frac{\phi_a}{2} \leq \phi_n \leq \phi_b + \frac{\phi_a}{2} \quad (B.32)$$

No generality is lost if  $\phi_b$  is chosen as zero; then the worst error occurs when  $\phi_n = \phi_a/2$ . Furthermore, for narrow beam antennas, the main lobe and first few side lobes are contained in a region where  $\phi$  is close to  $\phi_b$  ( $= 0$ ). Near the main beam, then,  $\cos\phi \doteq 1$ , and the maximum phase error is given by

$$\phi_{err} = kR(\cos\theta_b - \cos\theta) \left( 1 - \cos\left(\frac{\phi_a}{2}\right) \right) \quad (B.33)$$

This quantity turns out to be an important design parameter.

Other useful relationships can be derived by analogy with linear arrays. The beamwidth obtained by exciting the cylindrical sector AB in Figure B.3 will be about the same as that from a linear array along the chord AB. The

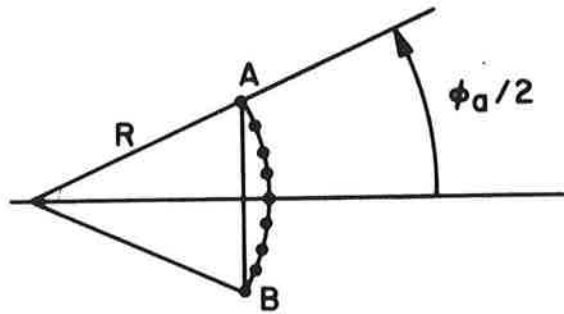


Figure B.3 Geometry of Cylinder

beamwidth is related to the arc length  $L_{AB}$  by

$$\phi_{BW} = \gamma\lambda/L_{AB} \quad (B.34)$$

where  $\lambda$  is the wavelength, and  $\gamma$  is a beam broadening factor, greater than  $52^\circ$ , but less than  $70^\circ$ . It depends primarily on the aperture distributions, and weakly on the active sector. It is considered constant in the discussion. For a cosine-squared-on-a pedestal, where the ratio between center element current and end element current is 3:1,  $\gamma$  is about  $61^\circ$ . From Figure B.3,

$$L_{AB} = 2R \sin\left(\frac{\phi_a}{2}\right) \quad (B.35)$$

which gives

$$R = \frac{\gamma\lambda}{2\phi_{BW}\sin\left(\frac{\phi_a}{2}\right)} \quad (B.36)$$

Using this relation in (B.33), the phase error can be related to the beamwidth and active sector (using  $k = 360^\circ/\lambda$ )

$$\phi_{\text{err}} = \frac{180^\circ \gamma \left(1 - \cos\left(\frac{\phi_a}{2}\right)\right)}{\phi_{\text{BW}} \sin\left(\frac{\phi_a}{2}\right)} (\cos\theta_b - \cos\theta)$$

or

$$\phi_{\text{err}} = \frac{180^\circ \gamma}{\phi_{\text{BW}}} \tan\left(\frac{\phi_a}{4}\right) (\cos\theta_b - \cos\theta)$$

(B.37)

Several conclusions regarding the phase error can be noted: (1) the problem is worse for narrow beamwidths; (2) for active sectors less than  $90^\circ$ , the error is almost linear with active sector; and (3) the error is proportional to the beam-broadening factor  $\gamma$ .

Equation (B.37) can be used to determine the limits of coverage in elevation. Suppose that some prescribed  $\phi_{\text{err}}$  e.g.,  $\pm 90^\circ$ , were considered as tolerable. Then the coverage limits are given by:

$$\theta \begin{matrix} \text{(upper)} \\ \text{(lower)} \end{matrix} = \cos^{-1} \left\{ \cos\theta_b \left( \pm \frac{\phi_{\text{BW}} |\phi_{\text{err}}|}{180^\circ \gamma \tan\left(\frac{\phi_a}{4}\right)} \right) \right\}$$

(B.38)

In Section III the significance of  $\phi_{\text{err}}$  is discussed further.

It is evident that if the active sector is  $\phi_a$  and the scan coverage is  $\phi_c$  that the total sector of the array must be  $\phi_a + \phi_c$ . In azimuth the array scans an angle of  $\pm \phi_c/2$  degrees. From Figure B.4 it can be seen that the width  $W$  is given by

$$W = 2R \sin\left(\frac{\phi_a + \phi_c}{2}\right)$$

(B.39a)

if  $\phi_a + \phi_c < 180^\circ$ , and by

$$W = 2R$$

(B.39b)

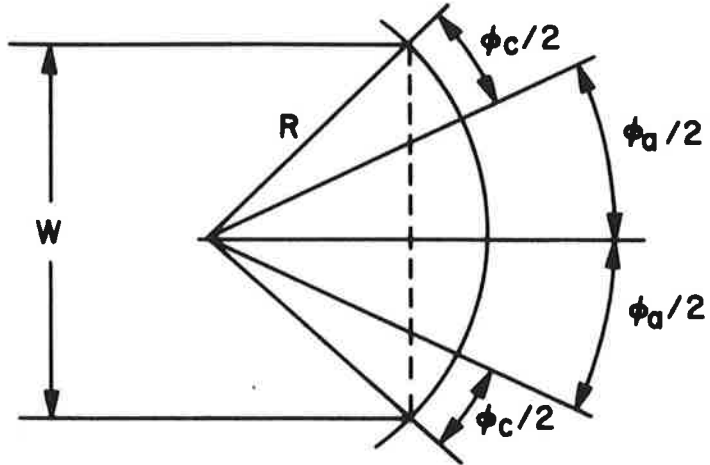


Figure B.4. Relation of Width of Cylindrical Array to Active Sector and Coverage

if  $\phi_a + \phi_c \geq 180^\circ$ . Using the relation for R in equation B.36, this can be written

$$W = \left\{ \begin{array}{l} \frac{\gamma\lambda}{\phi_{BW}} \cdot \frac{\sin\left(\frac{\phi_a + \phi_c}{2}\right)}{\sin\frac{\phi_a}{2}} \quad , \quad \phi_a + \phi_c < 180^\circ \\ \frac{\gamma\lambda}{\phi_{BW}} \quad , \quad \phi_a + \phi_c \geq 180^\circ \end{array} \right\}$$

(B.40)

The spacing between elements, is usually chosen, at least approximately, from grating lobe, mutual coupling, and cost considerations; that is, the number of elements in the active sector is chosen to give a reasonable spacing:

$$s = \frac{R\phi_a}{N_a} = \frac{\gamma\lambda\phi_a}{2\phi_{BW}N_a\sin\left(\frac{\phi_a}{2}\right)} \quad (\text{B.41})$$

The angular spacing  $\Delta\phi$  is simply

$$\Delta\phi = \frac{\phi_a}{N_a - 1} \quad (\text{B.42})$$

These are some of the relations between the various parameters of cylindrical arrays.

The amplitude coefficient,  $C_n$  in equation B.28 are chosen by analogy with linear arrays. If the active sector is not more than  $90^\circ$ , the chord and arc are quite close to each other, and one can reasonably expect similar behavior in the region of the main beam. This is discussed further in Chapter III.

### B.2.2 Elevation Antenna

A cylindrical array with its axis along the y-axis appears to hold promise as a means of generating planar beams since for a given sector being activated, the fan of the beam would be described by a plane through the y-axis and the center (active) array element. This is the case for beams with aspect ratios (ratio of maximum to minimum beamwidth of a fan beam) which are not too large. For this application where the desired aspect ratio is 120:1, the fan degenerates at azimuth angles greater than  $20^\circ$ , typically. This was discussed by a SFDT working paper by ITT Gilfillan<sup>1</sup>.

1. "Limitations in the Use of Cylindrical Arrays, " ITT Gilfillan, RTCA-SC-117 SFDT, Special Working Group Paper SWG-13, February 18, 1970.

The derivation of formulas for the elevation antenna if a cylindrical array is employed is largely a matter of exchanging the roles of  $\theta$  and  $\phi$ . Some differences occur which arise from the fact that the azimuth scans  $\pm\phi_c/2$  while the elevation scans from  $0^\circ$  (or  $1^\circ$ ) to some limit  $\theta_a$ , and from the fact that the coverages in the non-scan plane are different. For example, an elevation antenna focused for some angle  $\phi_f$  is also focused for  $-\phi_f$  as well.

Rather than rewriting the formulas entirely from analogy, a geometric description is given to give a more intuitive picture of the phase error. Consider a cylindrical array of radius  $R_\phi$  whose elements between  $-\theta_a/2$  and  $+\theta_a/2$  are activated, corresponding to a scan plane in the x-y plane. (See Figure B.5a.) The length of the projection of the arc on the z-axis must be

$$L_{\text{arc}} = \frac{\gamma\lambda}{\theta_{\text{BW}}} \quad (\text{B.43})$$

where  $\lambda$  is the wavelength,  $\theta_{\text{BW}}$  is the beamwidth in the elevation, and  $\gamma$  is a factor, usually between  $55^\circ$  and  $70^\circ$ , which depends on the aperture illumination. The ITT Gilfillan paper uses  $\gamma = 61$ . The radius is then given by

$$R = \gamma\lambda/2\theta_{\text{BW}}\sin(\theta_a/2) \quad (\text{B.44})$$

For ordinary illumination (cophasal) the phases of the elements are advanced with respect to the center element to produce a plane wave. The required phase advance for an element located at  $\theta_n$  is given by

$$\phi_{\text{adv}} = kR(1-\cos\theta_n) \quad (\text{B.45})$$

Once the phase shift is set, the contributions from the various elements add up perfectly along the x-axis. In Figure B.5b this is shown for the top end element ( $\theta_n = \theta_a/2$ ); at azimuth angles  $\phi$  other than zero, it can be seen that the contributions are not in phase, and in fact can differ significantly. The error  $\phi_{\text{err}}$  is given by

$$\phi_{\text{err}} = kR(1-\cos\theta_n)(1-\cos\phi) \quad (\text{B.46})$$

A comparison with (B.31) shows that (B.46) is a special case. Its generalization, i.e. for arbitrary focus angle  $\phi_f$  and boresight angle  $\theta_b$  is



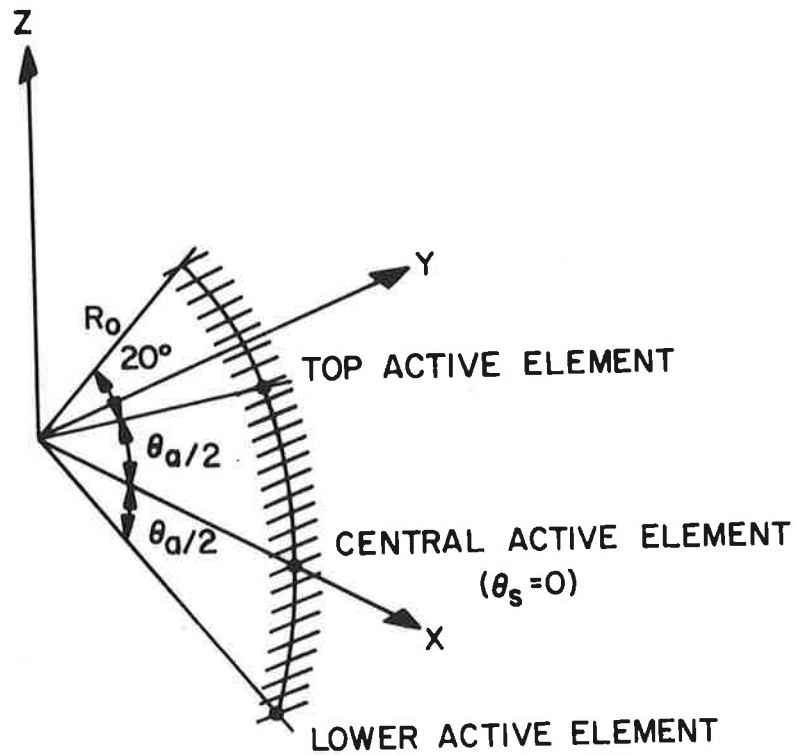


Figure B.5a Cylindrical Array Geometry - Elevation Antenna

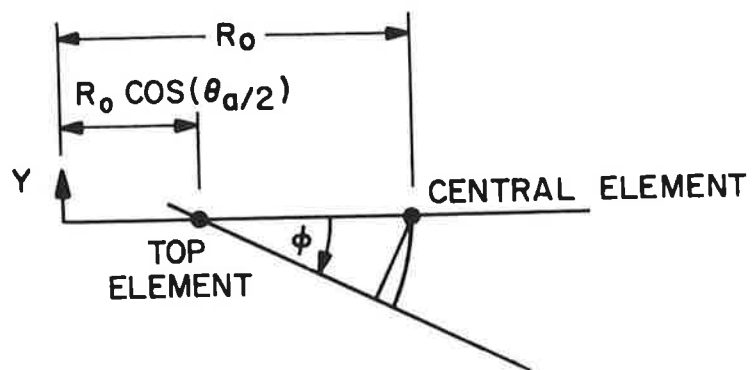


Figure B.5b Geometric Description of Phase Error for Elevation Antenna - Zero Error Along  $\phi = 0$

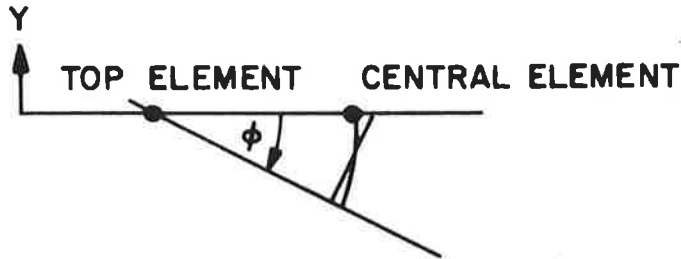


Figure B.5c Geometric Description of Phase Error for Elevation Antenna -  $90^\circ$  Error Along  $\phi = 0$

$$\Phi_{\text{err}} = kR(\cos\phi_f - \cos\theta) \left[ \cos(\theta - \theta_b) - \cos(\theta - \theta_n) \right] \quad (\text{B.47})$$

For an active sector of  $\theta_a$  the worst error becomes

$$\Phi_{\text{err}} = \frac{180^\circ \gamma}{\theta_{\text{BW}}} \tan(\theta_a/4) (\cos\phi_f - \cos\phi) \quad (\text{B.48})$$

By choosing a focus angle other than zero the beam is "spoiled" at broadside. By fixing this error at some figure like  $90^\circ$ , the proper focus angle can be calculated from (B.48):

$$\phi_f = \cos^{-1} \left\{ 1 - \frac{\theta_{\text{BW}} |\Phi_{\text{err}}|}{180^\circ \gamma \tan(\theta_a/4)} \right\} \quad (\text{B.49})$$

The coverage limit is found once the focus angle  $\phi_f$  is known:

$$\phi_{\text{limit}} = \cos^{-1} \left\{ \cos \phi_f - \frac{\theta_{\text{BW}} |\phi_{\text{err}}|}{180^\circ \gamma \tan(\theta_a/4)} \right\} \quad (\text{B.50})$$

As was mentioned above, if the array is focused at  $\phi_f$  it is also focused at  $-\phi_f$  so that the total coverage for which the phase error is less than some specified figure, is given by twice the amount from (B.50):

$$\phi_c = 2 \cos^{-1} \left\{ 1 - \frac{\theta_{\text{BW}} |\phi_{\text{err}}|}{90^\circ \gamma \tan(\theta_a/4)} \right\} \quad (\text{B.51})$$

The antenna height is given by a formula quite different from (B.40). From Figure B.6 it can be seen

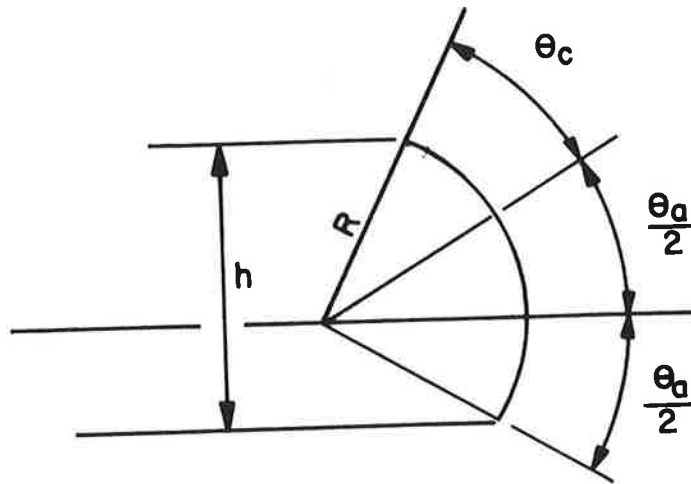


Figure B.6. Relation of Height of Cylindrical Array to Active Sector and Coverage

that

$$h = R \sin(\theta_a/2) + R \sin(\theta_a/2 + \theta_c)$$

or,

$$h = \frac{\gamma\lambda}{2\theta_{BW}} \left[ 1 + \frac{\sin(\theta_a/2 + \theta_c)}{\sin(\theta_a/2)} \right]$$

(B.52)

The discussion above assumes that the active sector moves smoothly along so that the center of the active sector always coincides in angle with the boresight. In fact, however, since an array of discrete elements is used, and not a continuum, the active sector moves in jumps. (This is not strictly true for lens feeding using center-of-gravity steering or for Butler matrix feeds; there the amplitude distribution changes smoothly.) The fine scanning positions between these coarse positions have the characteristic coning of linear arrays. If the amplitude distribution is switched every time the boresight shifts by an angle corresponding to the angular spacing between elements, the coning is negligible. This is discussed further in Section 3.3.

## **APPENDIX C**

STRIPLINE COMPONENT FABRICATION CONSIDERATIONS

*Abstract-Stripline and photoengraving process details are presented. These techniques will be used in the development of in-house prototype components. There appears to be no obvious obstacle to fabricating stripline components.*

### C.1 STRIPLINE PROCESSING

To fabricate prototype striplines of special designs requires a number of processing steps with associated equipment. The processing steps and equipment needed are listed below:

1. Design
2. Adequate drawing of design (sketch or drafting type)
3. Artwork-layout or Topology of Schematic (Rubylith)
4. Photographic Reproduction and Reduction
5. Mask Fabrication
6. Microwave Circuit Laminates (metal clad)-purchase
7. Cleaning of laminates
8. Photolithography (alignment, exposure, etc.)
9. Etching and Photoresist Removal
10. Assembly of etched printed circuit laminate

The ten steps listed above are essential to fabrication of stripline structures. Some equipment needed is available. However, additional equipment will be required. The equipment status will be presented in detail according to the process steps enumerated above.

1. Design-no significant equipment except pencil, paper, and knowledge required.
2. Drawing-drafting equipment available in the Center.
3. Artwork and Layout:
  - a. Coordinatograph-instrument available for our use elsewhere on limited basis.
  - b. Artwork layout materials such as Rubylith, Stabiline or Cut "N" strip required. These materials use a Mylar backing which exhibits better dimensional stability than do paper or similar materials.
4. Photographic Reproduction
  - a. Suitable reduction camera must be capable of reducing at least 10X and have a distortion free lens. This equipment is available in the photographic department in the Center and can handle a 16" x 20" master.
  - b. Additional equipment would be normal photographic development apparatus-available in the photographic department in the Center.

5. Mask Fabrication
  - a. Apparatus to hold mask rigid such as a vacuum frame.
  - b. Other equipment required same as (4b).
6. Microwave Circuit Laminates (Copper Clad)

Laminates of various types depending on the application can be purchased commercially with copper or other metal cladding on one or two sides or if preferred unclad. It is more economical to purchase the metal clad boards. To deposit or plate the metal in-house requires costly electrochemical plating equipment.
7. Cleaning of Laminates

This is straightforward and requires high purity water and some organic and inorganic chemicals. However, the quality of the final product is dependent on the removal of contamination from the laminates prior to other steps in the processing.
8. Photolithography

Dependent on the requirements, it is necessary to have a light source rich in ultra-violet preferably collimated. This equipment can be purchased. Also needed is an optical alignment system with low magnification and a positioner to hold and move the mask and substrate assembly. This is required for exposing the photoresist patterns. Ovens and/or hot plates are required to pre-bake and post-bake the photoresist. Spraying guns, beakers, etc. are additional accessory equipment required. All these items can be purchased or in some cases fabricated in house. Commercial equipment to perform this task is readily available. See attached appendix for more details on this process.
9. Etching and Photoresist Removal

Etching of metal on laminates requires etching solutions for the metals selected. All etching must be done in a well ventilated area, i.e., a fume hood. Most of the photolithographic operations must also be done in a well ventilated area. Etching can be done in beakers or commercial equipment specifically designed for this processing. Glass beakers can be used for photoresist removal with appropriate stripper solutions.
10. Assembly Fabrication

Depending on the process, fusion bonding or screw bonding assembly of the stripline requires either a press with heated platens or accurate mechanical machinery, in particular, drill presses.

A materials group in the Center has a press with platens on order expected to arrive shortly which can be used for the fusion process. Our machine shop can perform the mechanical fastening process. Launches or connectors

for test purposes can be soldered to the boards.

With this equipment in-house or elsewhere there are no obvious obstacles to fabricating stripline except a little practice. This would enable us to evaluate special designs of stripline in prototype quantities.

## C.2 PHOTOENGRAVING PROCESS DETAILS

### 1. Cleaning

Boards as received must be cleaned. A rinse at room temperature using high purity demineralized, distilled water is the least cleaning required. Copper readily forms  $\text{CuO}$  which may be removed with mild etchant or by mechanical abrasion.

### 2. Coating Resist

Spin techniques assure more uniform coating of resist material on substrate. For better resolution a thin coating is desired as long as it holds up against the etching solution. A thick coating spun on at low speeds (75 to 100 RPM) is generally used on copper clad sheets with 1 oz. metal. Such a coating may be non-uniform on the stripline laminate. However, it appears adequate for most stripline applications. Other techniques can be used. Resists may be KPR or KMER (Kodak Photoresists) used with full strength or thinned if desired. For fine line work other resists such as KTFR may be used. The Kodak resists are negative resists. Shipley makes several types of positive resists (a positive mask must be used). For stripline work Shipley AZ111 is adequate. For finer line work AZ1350 or 1350H is needed.

Other methods for applying a protective mask coating are:

- a. Spraying
- b. Dipping

These two methods suffer from non-uniformity as well as reproducibility of coating thickness on the substrate. Other photoresists are available if desired. Equipment needed: Hood, spinner, photoresist, applicator.

### 3. Drying

Drying of photoresist can be done by several different methods. Some of these are listed below:

- a. hot plate-air drying
- b. oven-forced air circulation
- c. infrared



For stripline work, the various laminates used cannot be heated to excessively high temperatures. Generally air drying at room temperature followed by a bake at 82° C is sufficient to cause good photoresist adherence to the substrate and "drive out" unwanted solvents and moisture. The final temperature selected depends on the thermal characteristics of the substrate. Equipment required: hot plate, small air circulation drying oven, infrared light source.

#### 4. Aligning and Printing

Alignment between mask and substrate must be accurate and requires precision equipment. The substrate is held in place in a frame and the mask with the desired pattern is placed in intimate contact with the substrate. This is accomplished in several ways. Precise alignment holes in both the mask and substrate can be used to accurately align the elements. Pins protruding through these holes hold the work in place. Cruder alignment methods may be employed depending on the accuracy required.

Once the mask and substrate are firmly held and aligned an appropriate ultraviolet source (Mercury Arc lamp) is used for exposure of the photoresist. This normally takes 5 to 10 seconds. The source should be collimated.

In this process the image is projected on the substrate exposing the photoresist. The photoresist is polymerized wherever the light encounters a light area on the mask. The exposed regions are resistant to solvents and acids required to delineate the pattern geometry. The unexposed regions are soluble in certain acids and solvents.

The images must be developed. The photoresists mentioned previously use developers specifically made for each type photoresist. After developing, the substrates with a photoresist covering are rinsed to remove the unexposed photoresist regions so that the etchants to be used later on in the process can dissolve the underlying metal. The process is completed by a post bake at a higher temperature than the previous bake.

The next step involves etching the metal in the regions which have been cleared of photoresist in the previous step. This normally takes 3 to 4 minutes depending on the metal thickness. Generally Ferric Chloride is used to etch copper in stripline work. After the photoresist has been removed one section of the stripline configuration has been completed. The assembly consists of a completely copper clad backed laminate (ground plane),

a dielectric, and an etched strip line pattern. To complete the assembly a single copper clad laminate must be fused or connected by bolts to the prepared stripline laminate.

Figure C.1 shows the assembly after etching and photoresist removal. Figure C.2 shows the single copper clad laminate. Figure C.3 shows the completed assembly.

Another technique for forming the completed stripline assembly is a fusion process. Heat and pressure are applied to the sub-assembly parts until a good bond is achieved. However, this technique is not applicable to all types of dielectric material. Some companies have developed this technique for PTFE glass non-woven microfibre reinforced. This material is difficult to fuse or bond, however, since it does not readily form a melted phase at the required temperatures. Another form of Teflon, FEP, is more adaptable to this process. However, to the writers knowledge no laminates of this type are presently commercially available. A check on the commercial availability of FEP laminates copper clad will be made. The advantage of this technique is improved reliability due to the sealed package. In addition stresses set up in the dielectric boards fastened by normal techniques are eliminated.

#### 5. Resist Removal

Finally, the photoresist is removed from the substrate. J-100 stripping solution heated can be used to remove the photoresist. The metal is unaffected by this process. With this step the photolithography process is completed. Equipment required: fume hood, beakers, spray gun, solvents, alignment fixtures, collimated ultra-violet light source, good H<sub>2</sub>O, alignment positioner, masks.

**STRIPLINE ASSEMBLY**

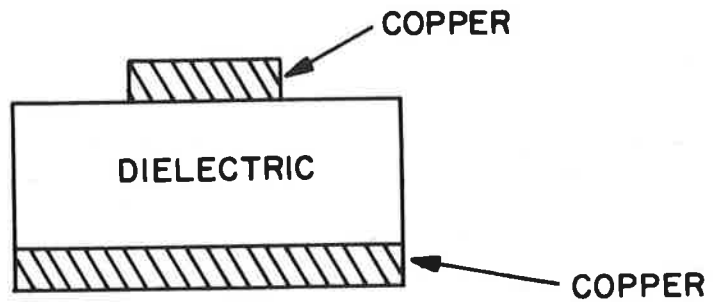


Figure C.1 Stripline Laminate with Etched Center Conductor

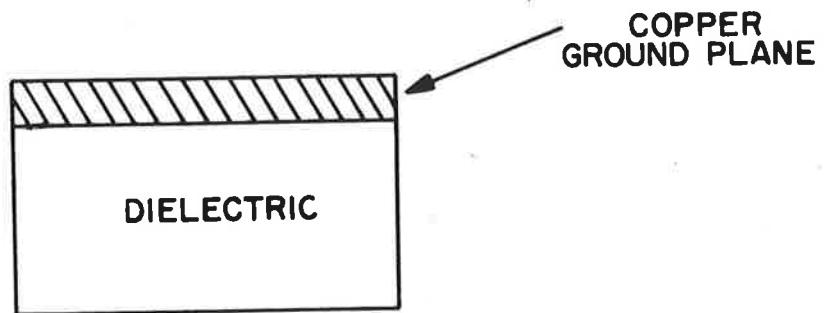


Figure C.2 One Sided Copper Clad Laminate

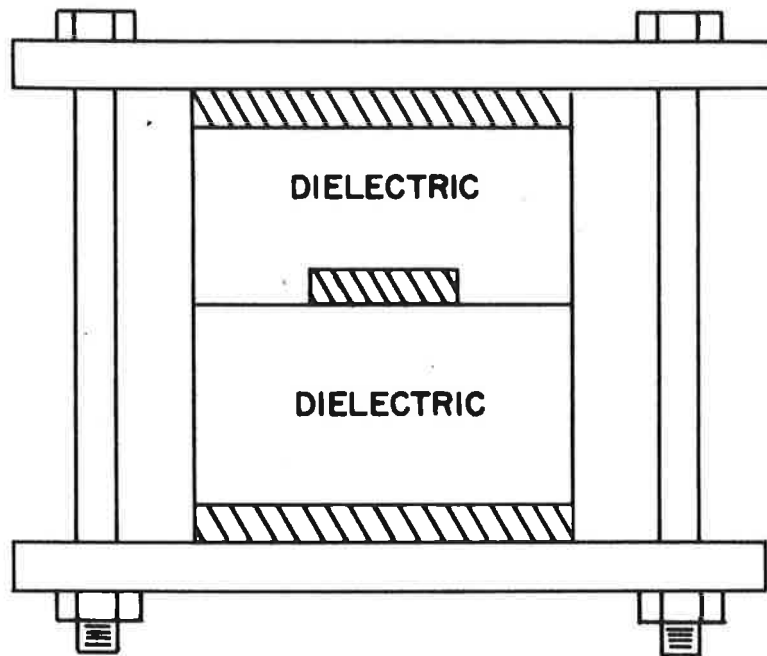


Figure C.3 Completed Structure

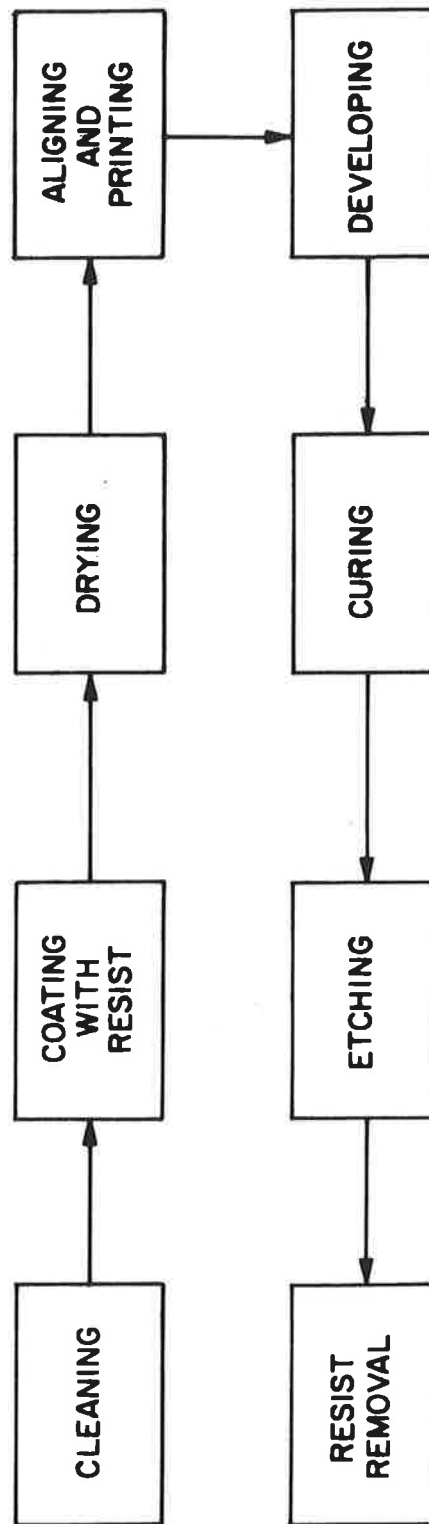


Figure C.4 Flow Chart for Photoengraving (Stripline)



## **APPENDIX D**

**PROPAGATION FACTORS WHICH MAY LIMIT THE PERFORMANCE  
OF FUTURE MICROWAVE GUIDANCE SYSTEMS**

*Abstract-The potential near future use of the microwave spectrum at frequencies of 5 GHz and 15 GHz have produced recent interest in these higher frequencies for satisfying the projected needs of the aviation community for a more precise vertical and horizontal guidance system. At these higher frequencies relatively high gain antennas are achieved with modest aperture diameter; broad channel capability allows high information capacity and the total available bandwidth exceeds the entire spectrum below 5 GHz. Those atmospheric effects which may seriously limit the performance of systems above 10 GHz are absorption, emission and refraction (Ref. 1).*

#### D.1 Review of Current State-of-the-Art Knowledge

A review of the literature used by RTCA SC-117 does not necessarily support the choice of frequencies at 5 GHz and 15 GHz in terms of the fact that the most severe parameter is attenuation. Sampson et al (Ref. 2) conclude that a 15 GHz system could be designed with sufficient high reliability even in areas of heavy rainfall. No data however is given which shows the effects of measured refraction on a half degree beamwidth at either  $K_u$  or C band during rainfall rates of 50 millimeters per hour when the antenna is pointed at angles of less than two degrees from the horizon. Simultaneously no consideration was given to the effects of decorrelation across the aperture of an antenna at either  $K_u$  or C band for beamwidths on the order of a half degree. These two effects alone could produce a pointing error in an RF generated beam as well as distort the radiated wave front. The dispersion of a ranging system utilizing a narrow pulse could also become marginal under atmospheric conditions of heavy rainfall or precipitation by snow and sleet.

The properties of backscatter and forward scatter during meteorological conditions of melting snow and hail are another set of meteorological phenomenon which could cause distortion of electromagnetic energy both at C band and  $K_u$  band. Inadequate experimental data exists at these frequencies concerning narrow beam microwave systems operating at low elevation angles.

The work of Hogg (Ref. 3) and Semplak and Turrin (Ref. 4) support the fact that attenuation at frequencies above 10 GHz are a severe limit to electromagnetic propagation. The RTCA-117 report however does not support the choice of these two frequencies in terms of the by-product effects caused by attenuation when applied to electromagnetic propagation



at these frequencies.

## D.2 Effects of Atmospheric Constituents

### D.2.1. Emission

It is well known that the atmospheric noise level at microwave frequencies is determined by the absorption and radiation of atmospheric gases and associated condensation and precipitation products. The main contribution is due to pure rotational transitions at 22 GHz and the pressure broadened skirts of the absorption lines.

Oxygen absorption is associated with a magnetic dipole resonance leading to a series of transitions between fine structure levels of various rotational states of the molecule. The resonance occurs in the region about 60 GHz. The oxygen absorption dominates over that of water except in the immediate region of the water vapor line, even though the mass absorption coefficient of the two gases are of the same order of magnitude. This occurs as a consequence of the large density ratio of oxygen to water vapor in the atmosphere.

The radiation temperature along a vertical path through the atmosphere may be expressed in the form

$$T_{\text{sky}} = \int_0^{\infty} \alpha T \exp\left(-\int_0^h \alpha dh\right) dh \quad (\text{D-1})$$

where  $\alpha$  and  $T$  are the absorption coefficient and temperature at the height  $h$ . Evaluation of Eq. (D-1) requires that the magnitudes of  $\alpha$  and  $T$  be known as a function of position in the atmosphere. The vertical atmospheric attenuation contributed by atmospheric oxygen, that contributed by water vapor, and a composite of oxygen and water vapor have been derived by Van Vleck (Refs. 5, 6). Graphical plots are shown in Figs. D.1 through D.3. Variations in the corresponding atmospheric temperature can be expected with variation in pressure, temperature, and water vapor density. Large variations will normally occur over long time intervals and will be associated with major changes in the air mass type at the observing site.

Of particular interest is the spatial distribution of water vapor content in a given air mass which would give rise to variations in the atmospheric water vapor absorption coefficient due to motion of the air mass relative to the antenna beam. If we assume that a change in the absorption

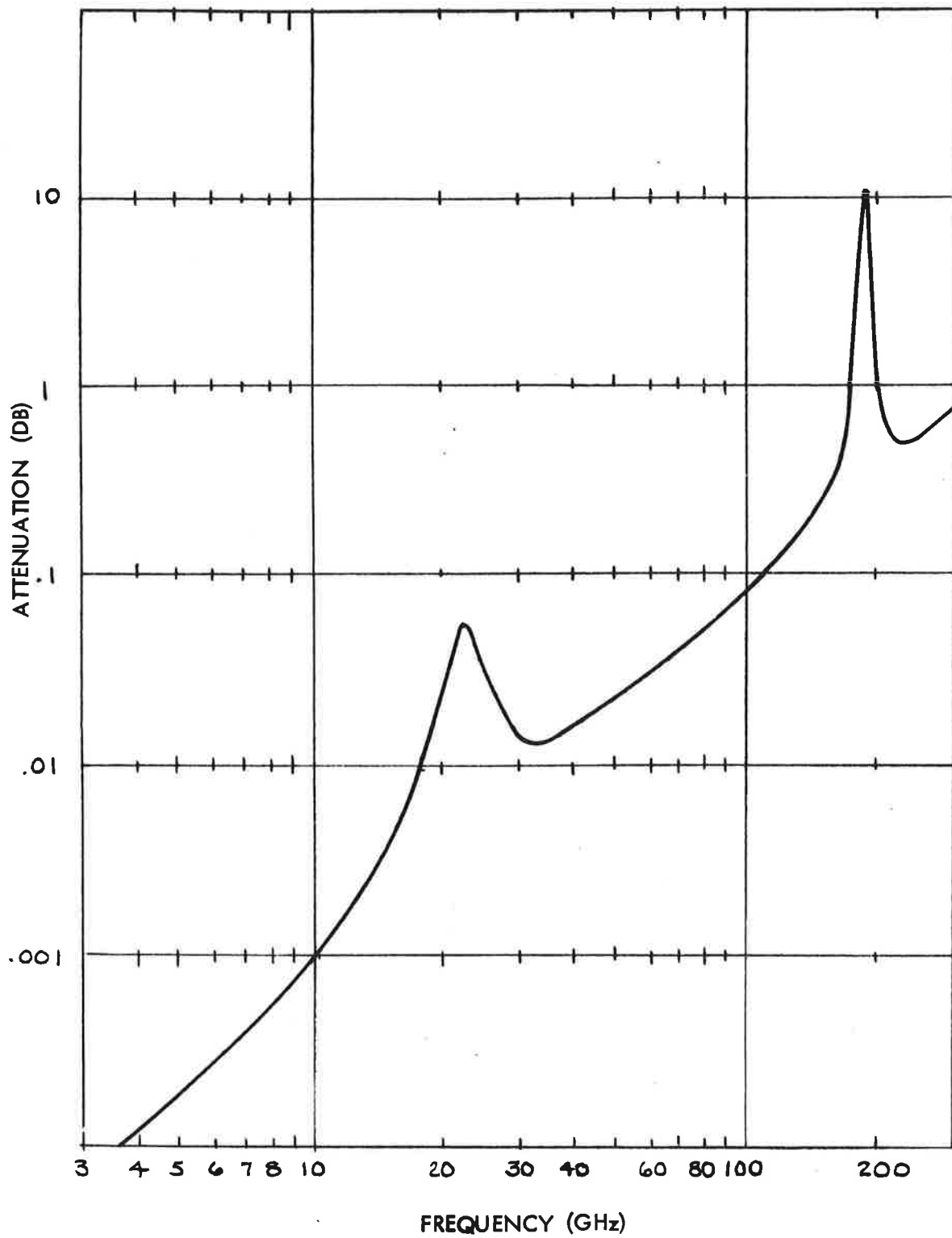


Figure D.1 Total Vertical Path Attenuation By Water Vapor Normalized To a Water Vapor Content of 1 GM/M<sup>3</sup>

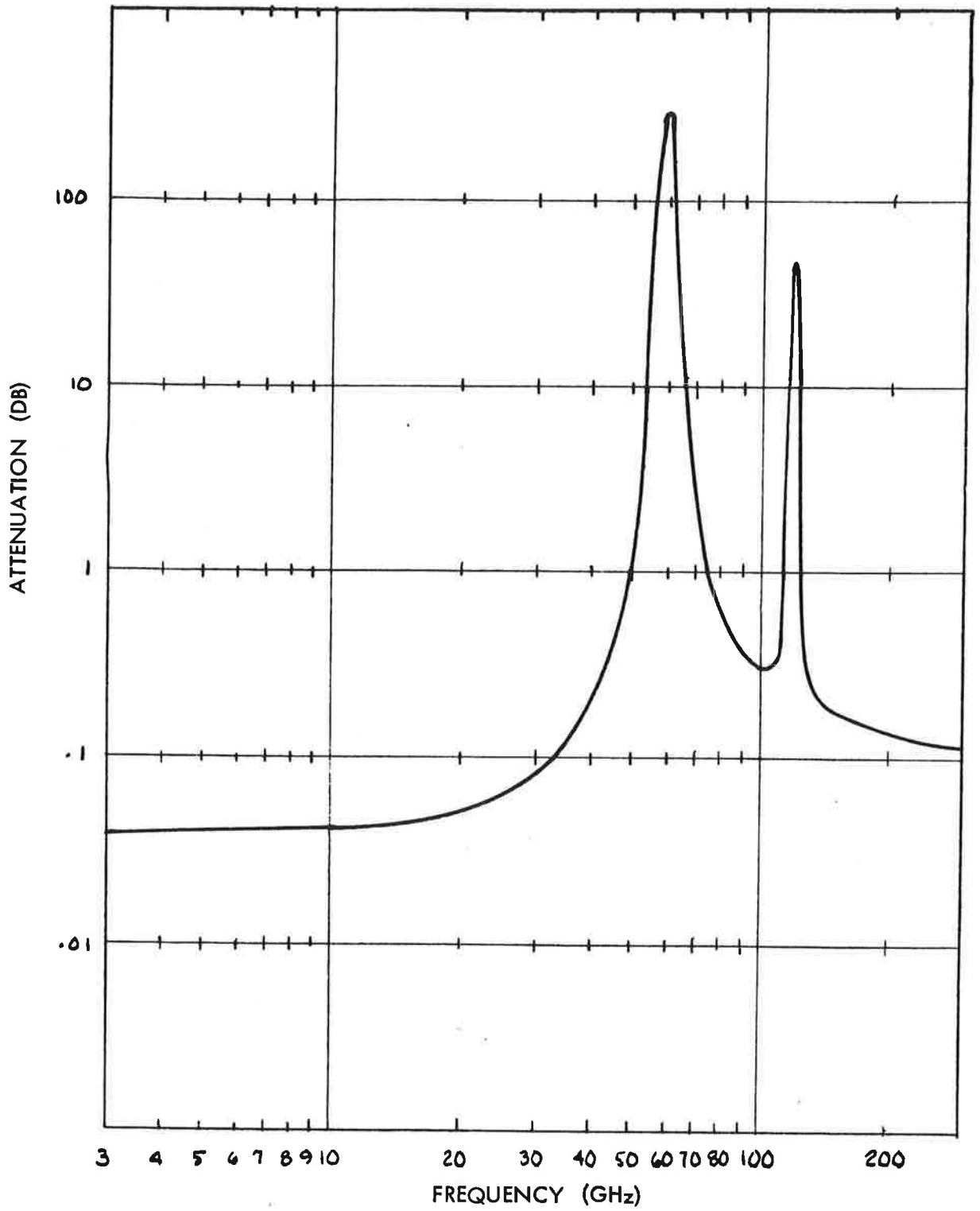


Figure D.2 Total Vertical Path Microwave Attenuation  
By Atmospheric Oxygen

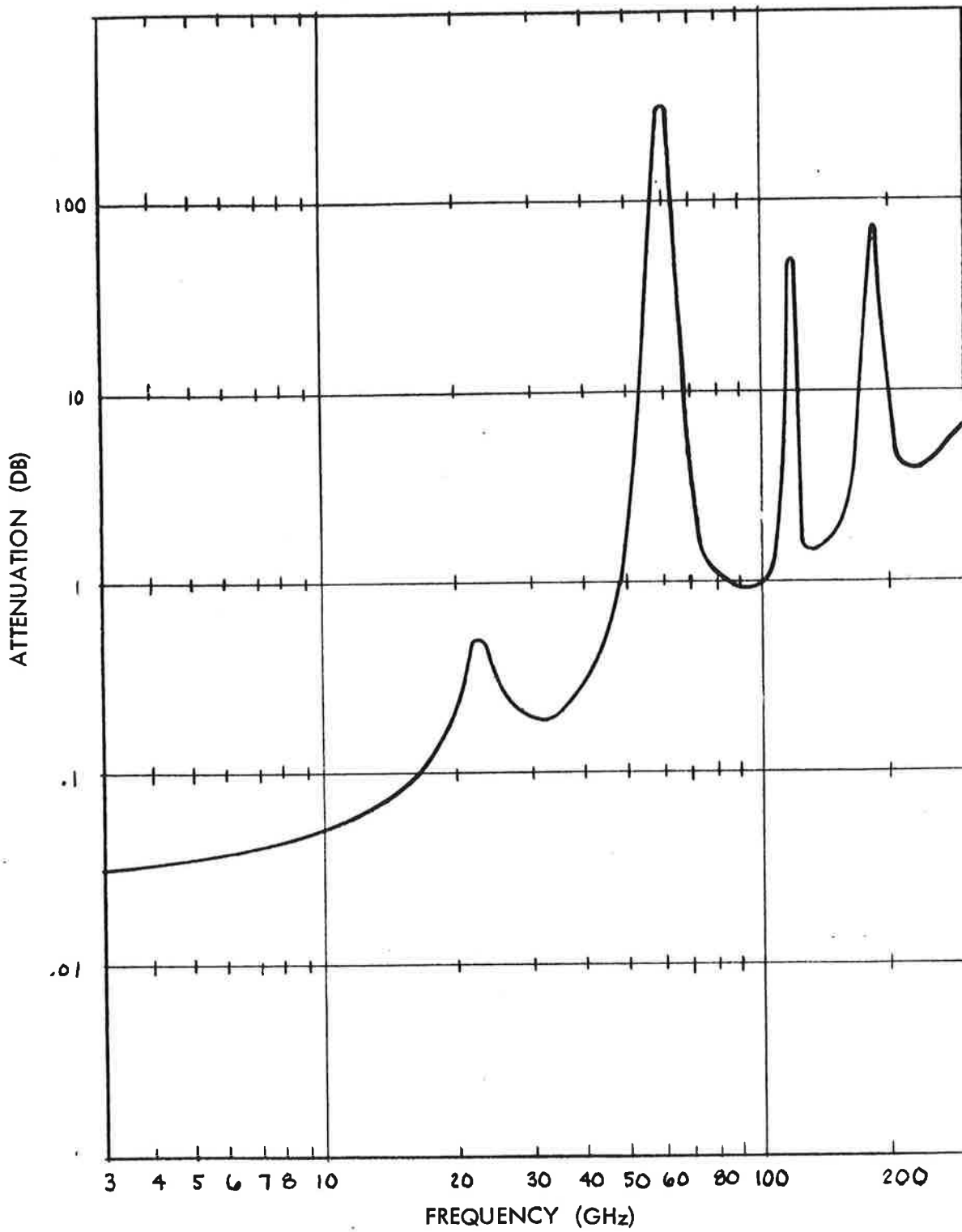


Figure D.3 Total Vertical Path Attenuation By Atmospheric Gases (Water Vapor Concentration: 7.5 GM/M<sup>3</sup>)

coefficient  $\alpha$  occurs in the first kilometer  $\Delta h$ , the corresponding variation in sky brightness temperature will be

$$\Delta T_{\text{sky}} = T \Delta \alpha \Delta h \exp(-\alpha \Delta h) \quad (\text{D-2})$$

where the absorption coefficient is  $\alpha + \Delta \alpha$  in the interval  $\Delta h$ . Since the water vapor absorption coefficient is believed to be directly proportional to water vapor density  $\rho$  (in grams per cubic meter), then

$$\Delta \alpha = \alpha \frac{\Delta \rho}{\rho} \quad (\text{D-3})$$

The anticipated sky noise temperature fluctuation level  $\Delta A$  at selected frequencies for a 20 percent change in water vapor density in the first kilometer along the path of observation is shown in Table D.1. An atmospheric temperature of 300° K was assumed along the path in which the water vapor density change occurs.

Table D.1 Anticipated Sky Noise Temperature Fluctuation,  $\Delta A$ , At 5 and 15 GHz for a 20% Change in Water Vapor Density In the First km Along the Path of Observation

Frequency (GHz)	$\alpha$ (dB/km)	$\alpha_n$ (Np/km)	$\Delta A$ (°K)
5	0.01	$2.3 \times 10^{-3}$	0.13
15	0.05	$11.5 \times 10^{-3}$	0.69

The effects of condensation and precipitation products (clouds, rain, and snow) are less susceptible to practical analysis and measurement than the gaseous constituents of the atmosphere as a consequence of uncertainties concerning spatial distribution and homogeneity. Suspended water drops in the atmosphere have the dual effect of absorbing and scattering microwave energy. For extremely small drops, such as those in fog or clouds, the liquid water acts as an imperfect dielectric and consequently absorbs energy from the incident electromagnetic field. The attenuation at a given frequency is proportional to the total liquid water content per unit volume and is normally expressed in terms of absorption values. Typical values as determined by Rogers (Ref. 7) are shown in Fig. D.4.

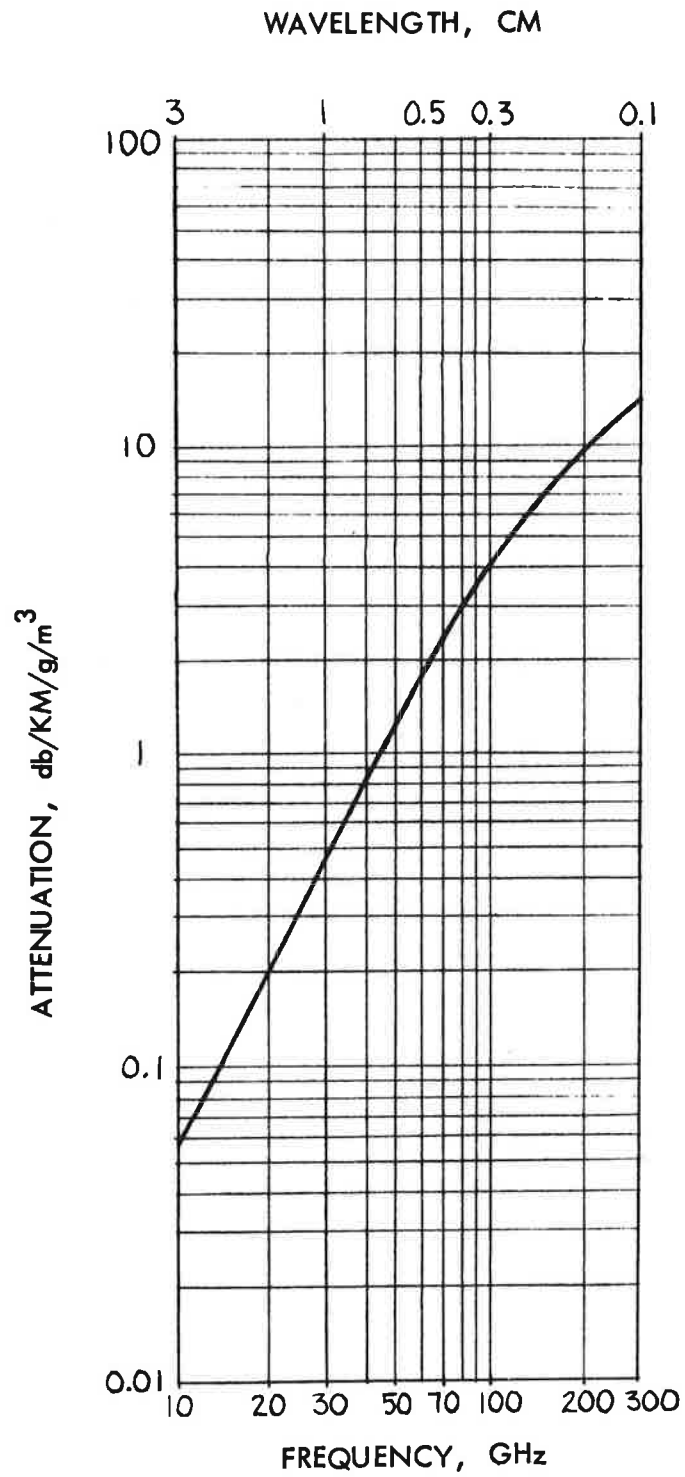


Figure D.4 Attenuation Due to Clouds or Fog (Rogers)

As water droplet size increases, the attenuation effects become more pronounced and depend on the size of the drops as well as the volumetric water content; the absorption process increases in complexity and wavelength dependent scattering effects become important. The attenuation resulting from these effects can be determined for drops of any diameter; however, the non-uniformity of drop size in typical rain fall and the inconvenience of describing rainfall in terms of drop diameter has led to the correlation of drop size with precipitation rate in millimeters per hour to arrive at a relationship between attenuation and precipitation rate. Measurements indicate that even for very short path lengths rainfall is both spatially non-uniform and varies rapidly with time. Thus the calculated attenuation values by Ryde and Ryde (Ref. 8) for various rainfall rates, as shown in Fig. D.5, are useful only for comparative purposes and provide little direct information on the anticipated total attenuation over an extended path for a given time of observation. The relationship of rainfall rate has been calculated as a function of frequency and attenuation to depict large variations between the theoretical value derived from the previous curves by Ryde and Ryde. The results are shown in Figure D.6, and account for higher rainfall rates than in Figure D.5.

#### D.2.2 Absorption

The composite effect of the absorption by atmospheric gases and associated condensation and precipitation products has been reported by Weger (Ref. 9) in terms of the corresponding sky temperature as a function of zenith angle and frequency of observation. These calculated values are shown in Figs. D.7, D.8 and D.9 for weather Cases I through III, as defined in the *Handbook of Geophysics* (Ref. 10).

A recent publication by Medhurst (Ref. 11) has refined the theoretical approach of Ryde and Ryde but indicates that theoretical values are usually lower than measured values. The measured data presented by Medhurst also indicates that in most cases rain parameters were inadequately measured due to difficulties in measuring instantaneous drop-size distribution over practical path lengths. In addition the ability to determine the average over the path length from measurements made at discrete points along the path contributes to the main source of error when correlating attenuation directly with rainfall rate. Finally most rainfall measurements assume that the precipitation is uniform which is not consistent with information published on the variability of rain under thunderstorm conditions.

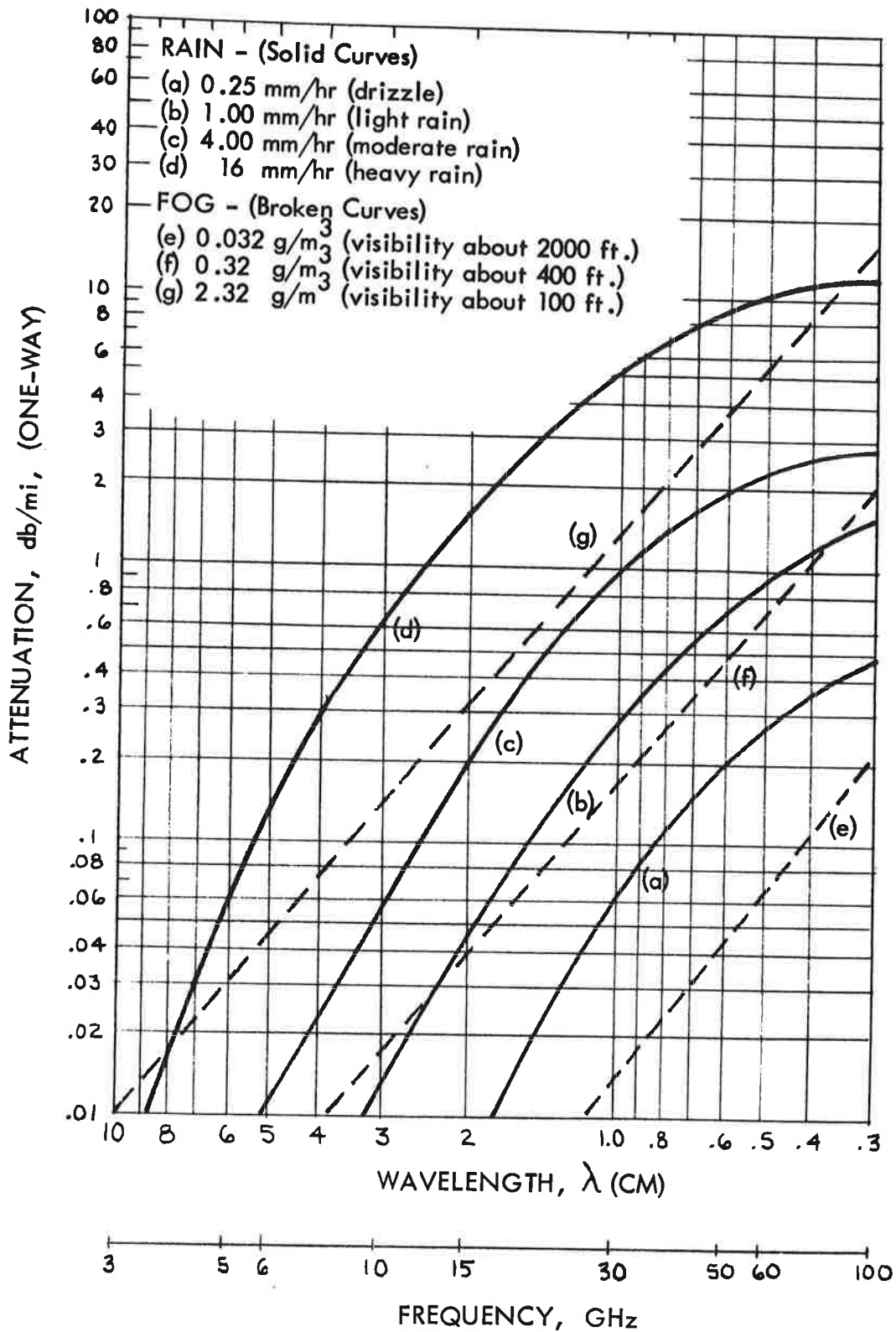


Figure D.5 Theoretical Values of Attenuation By Rain and Fog (Ryde and Ryde)



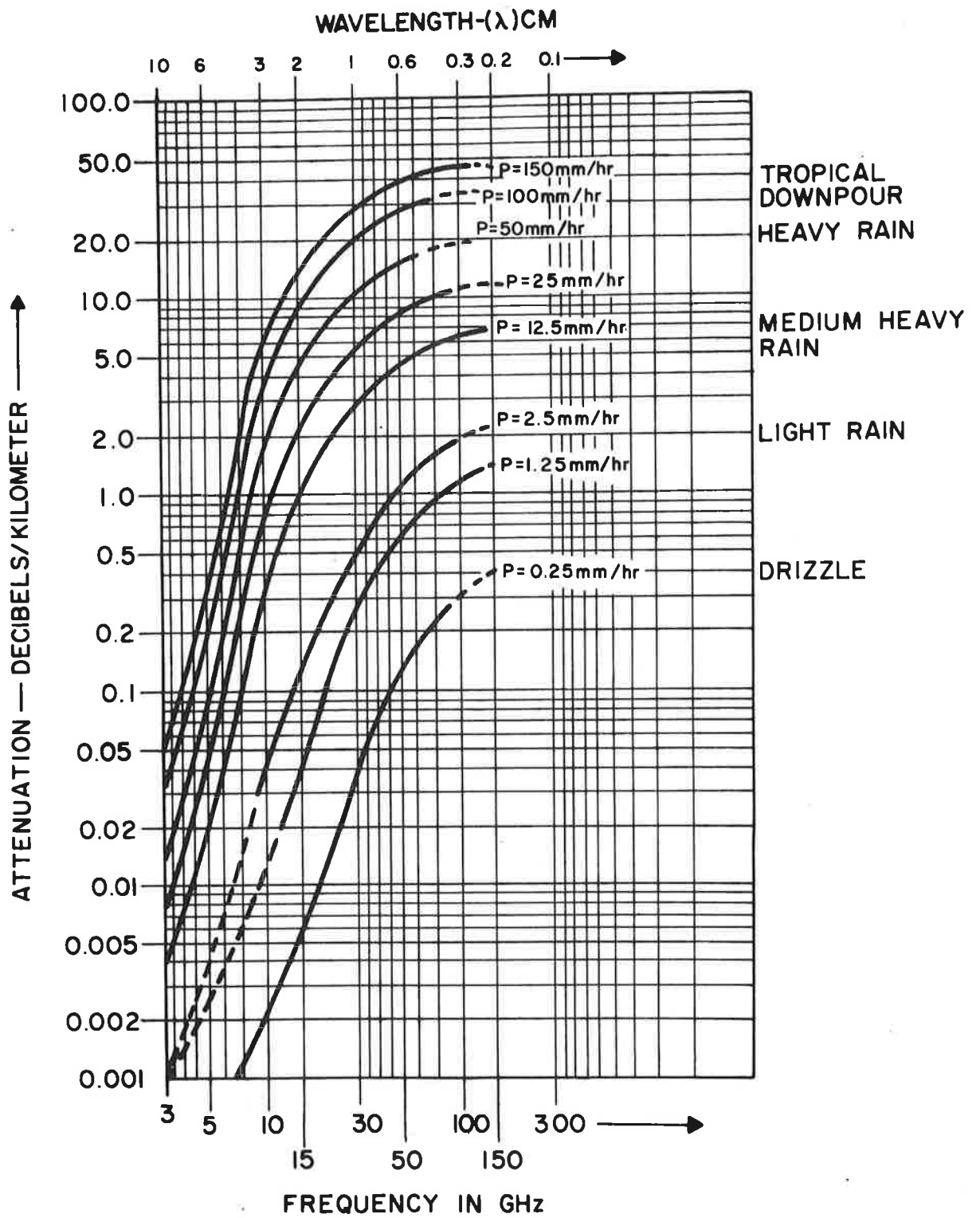


Figure D.6 Rainfall Attenuation Versus Frequency For Various Precipitation Rates

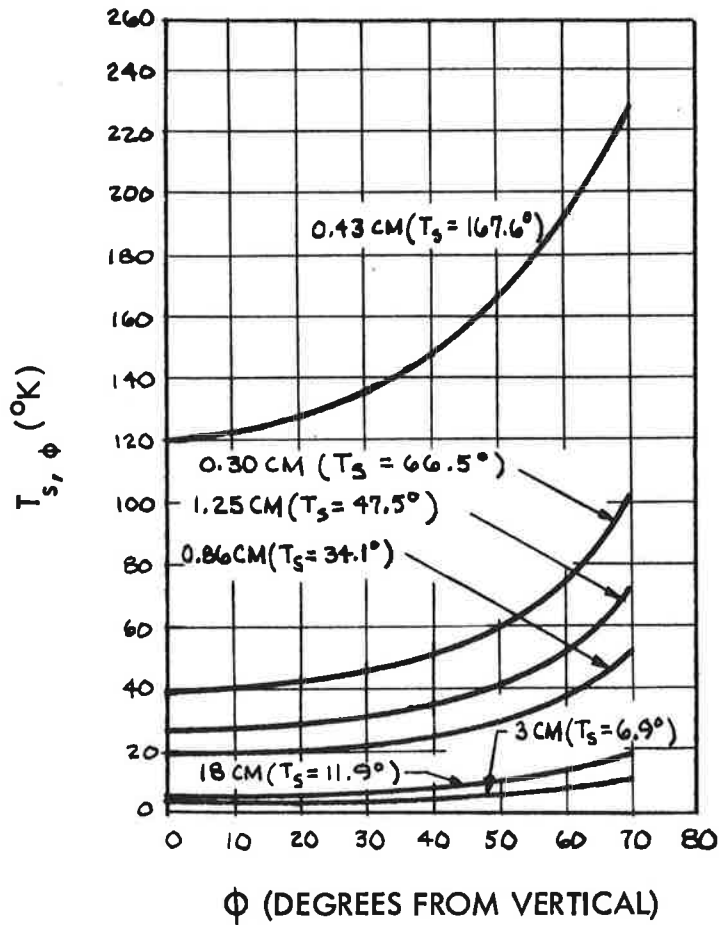


Figure D.7 Sky Temperatures ( $T_{s, \phi}$ ) and Average Sky Temperature ( $T_s$ ) As a Function of Wavelength and  $\phi$

Case I Conditions: Clear sky (water vapor content at sea level  $7.5 \text{ g/m}^3$ ; sea level temperature 290K (Weger)

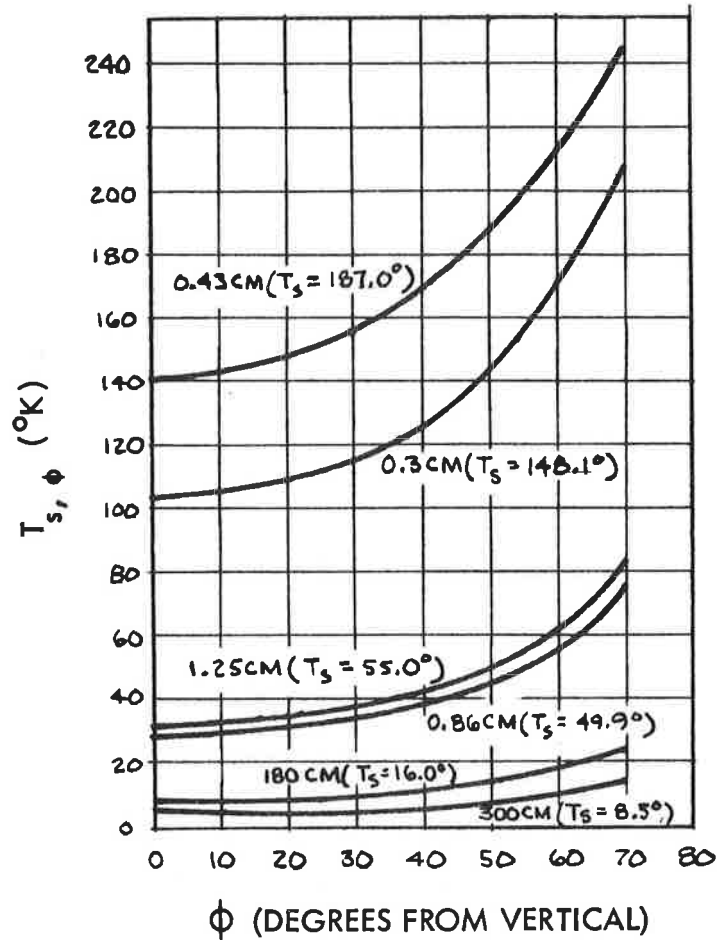


Figure D.8 Sky Temperatures ( $T_{S, \phi}$ ) and Average Sky Temperature ( $T_S$ ) As a Function of Wavelength and  $\phi$

Case II Conditions: Moderate cloud cover (0.3 g water/m<sup>3</sup>) between 900 and 1800 m; sea-level temperature 290K

(Weger)

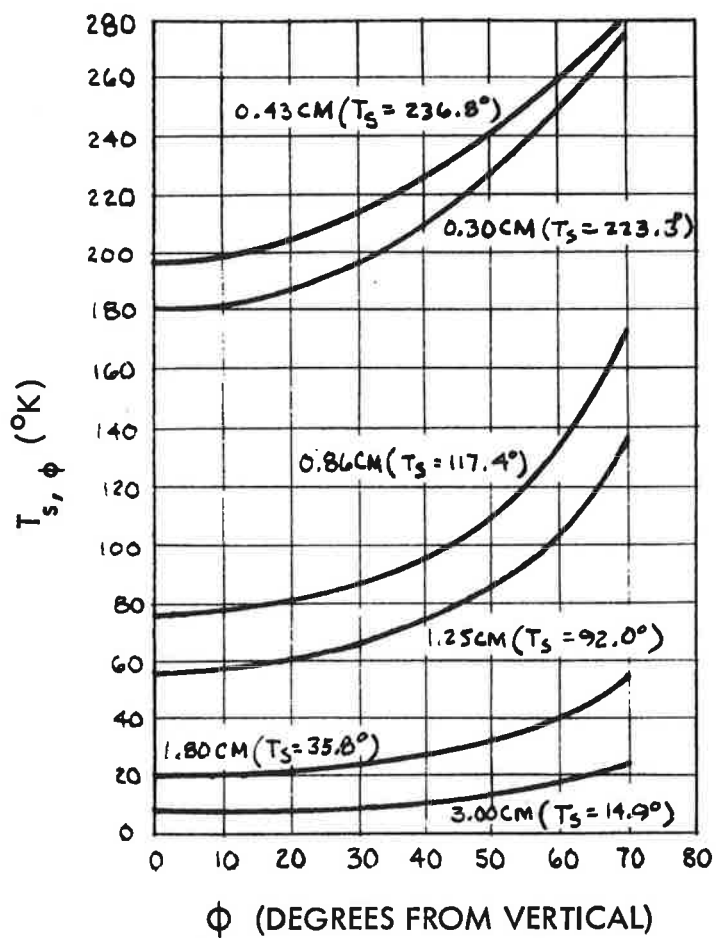


Figure D.9 Sky Temperatures ( $T_{S\phi}$ ) and Average Sky Temperature ( $T_S$ ) As a Function of Wavelength and  $\phi$

Case III Conditions: Moderate rain (4 mm/hr)  
 Between 0 and 900 m; moderate cloud cover (0.3 g water m<sup>3</sup>)  
 Between 900 and 1800 m; sea-level temperature 290K

(Weger)

Most important however is the lack of data concerning the magnitude of atmospheric attenuation and the relative time interval of its occurrence at microwave frequencies when considering the elevation angle of observation. Knowledge of the percentage of time during which relatively high values of attenuation are observed is irrelevant without consideration of the elevation angle of observation at the time of occurrence. Shown in Figure D.10 is a plot of the probability density function of attenuation data measured at 15 GHz by utilizing a radiometric sensor and the sun as an exoatmospheric source (Ref. 12).

The probability density function describes the probability that the data will assume a value within a defined range of percent attenuation at any instant of time. Shown in Table D.2 is the value of the mean and standard deviation for the plot. The data at each elevation angle is presented separately and all types of weather are included in the data. The mean or expected value given in the tables are the statistical average or the first moment of the data for each particular elevation angle or range of elevation angles. For example in referring to Figure D.10 at an elevation angle of 42° the value of attenuation that a systems designer may expect is about 21% or 1 dB with a standard deviation of 11% at 15 GHz (Table D.2). Figure D.11 is a plot of the probability distribution function of the percent attenuation as a function of a given elevation angle represents the sum of the probability density values for all the percent attenuation values at that angle. This type of data indicates the marginality of a system operating at 15 GHz at low elevation angles and is typical of a New England environment on a seasonal basis.

### D.2.3 Refraction

An electromagnetic wave upon passing from one medium to another undergoes a change in velocity and if it enters the second medium obliquely it experiences a bending called refraction. The index of refraction of the earth's atmosphere at microwave frequencies is given by the expression:

$$N = (n-1) \times 10^6 = 77.6 \frac{P}{T} + 3.73 \times 10^5 \frac{e}{T^2} \quad (D-4)$$

where

n = index of refraction  
 N = refractivity  
 P = air pressure, millibars

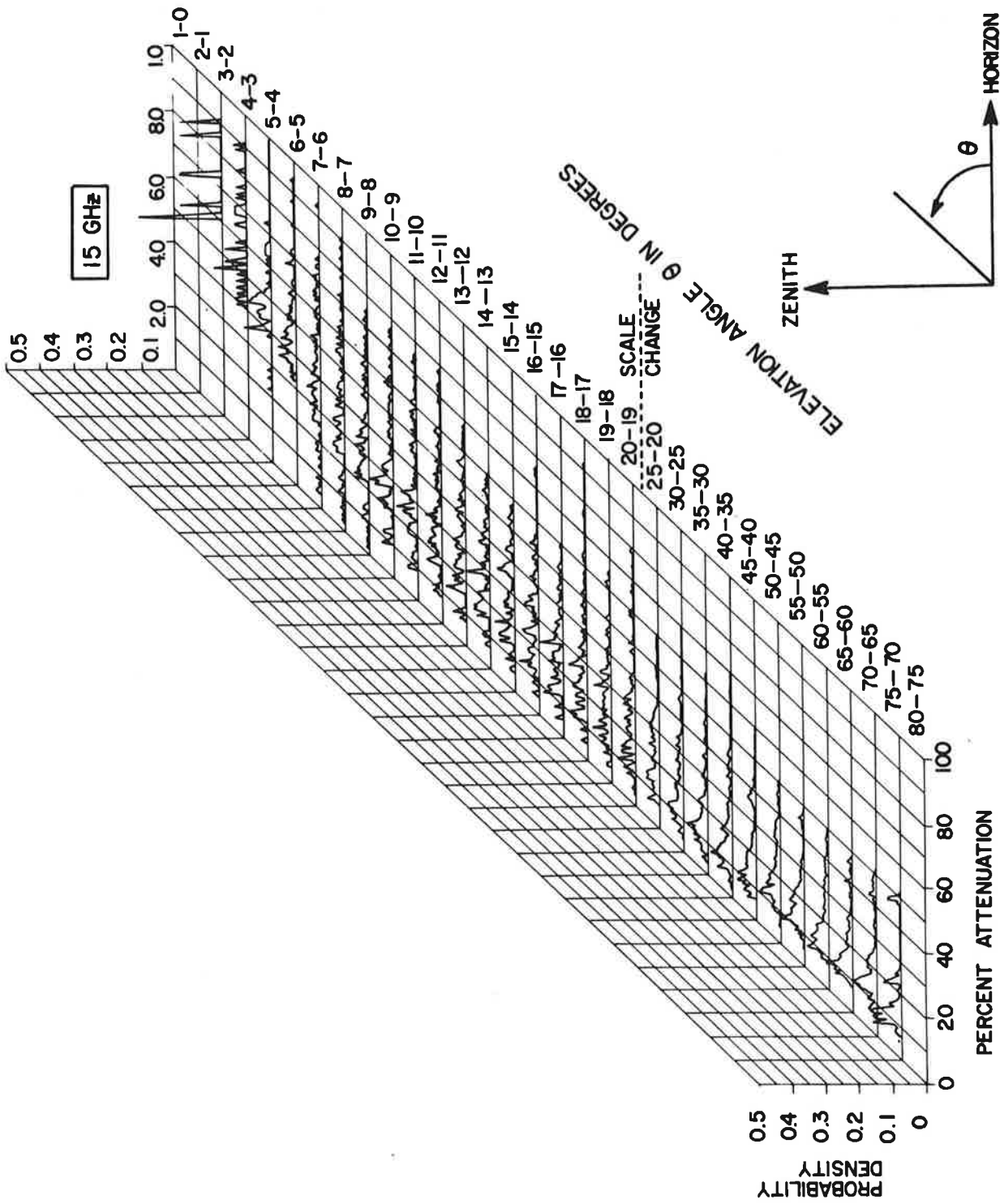


Figure D.10 Probability Density Function of Attenuation at 15 GHz at Multiple Observing Angles

Table D.2 List of Mean And Standard Deviations For  
Figures D.10 And D.11

15 GHz ELEVATION ANGLE (DEGREES)	PERCENT ATTENUATION		TOTAL OBSERVING TIME (SECONDS)
	MEAN	DEVIATION	
80-75	0.0	0.0	0
75-70	19.0	10.8	16770
70-65	22.3	11.5	123320
65-60	20.7	9.7	104091
60-55	21.1	9.0	133460
55-50	20.6	8.3	109290
50-45	23.0	9.4	105960
45-40	20.6	10.4	147436
40-35	21.4	13.4	140198
35-30	20.4	11.9	152157
30-25	23.4	13.3	144410
25-20	25.9	13.1	125347
20-19	27.2	14.5	19117
19-18	26.5	12.3	18693
18-17	27.1	12.9	18055
17-16	26.6	11.1	15083
16-15	28.2	12.7	13726
15-14	29.6	12.7	13804
14-13	29.7	12.7	13307
13-12	31.5	13.4	12727
12-11	32.6	14.9	12038
11-10	33.8	15.1	11444
10-9	34.7	14.8	10468
9-8	36.3	16.0	9490
8-7	39.8	18.5	7720
7-6	42.3	17.6	6550
6-5	48.2	14.6	5830
5-4	51.5	12.6	3588
4-3	62.2	13.6	1510
3-2	72.5	11.0	400
2-1	0.0	0.0	0
1-0	0.0	0.0	0

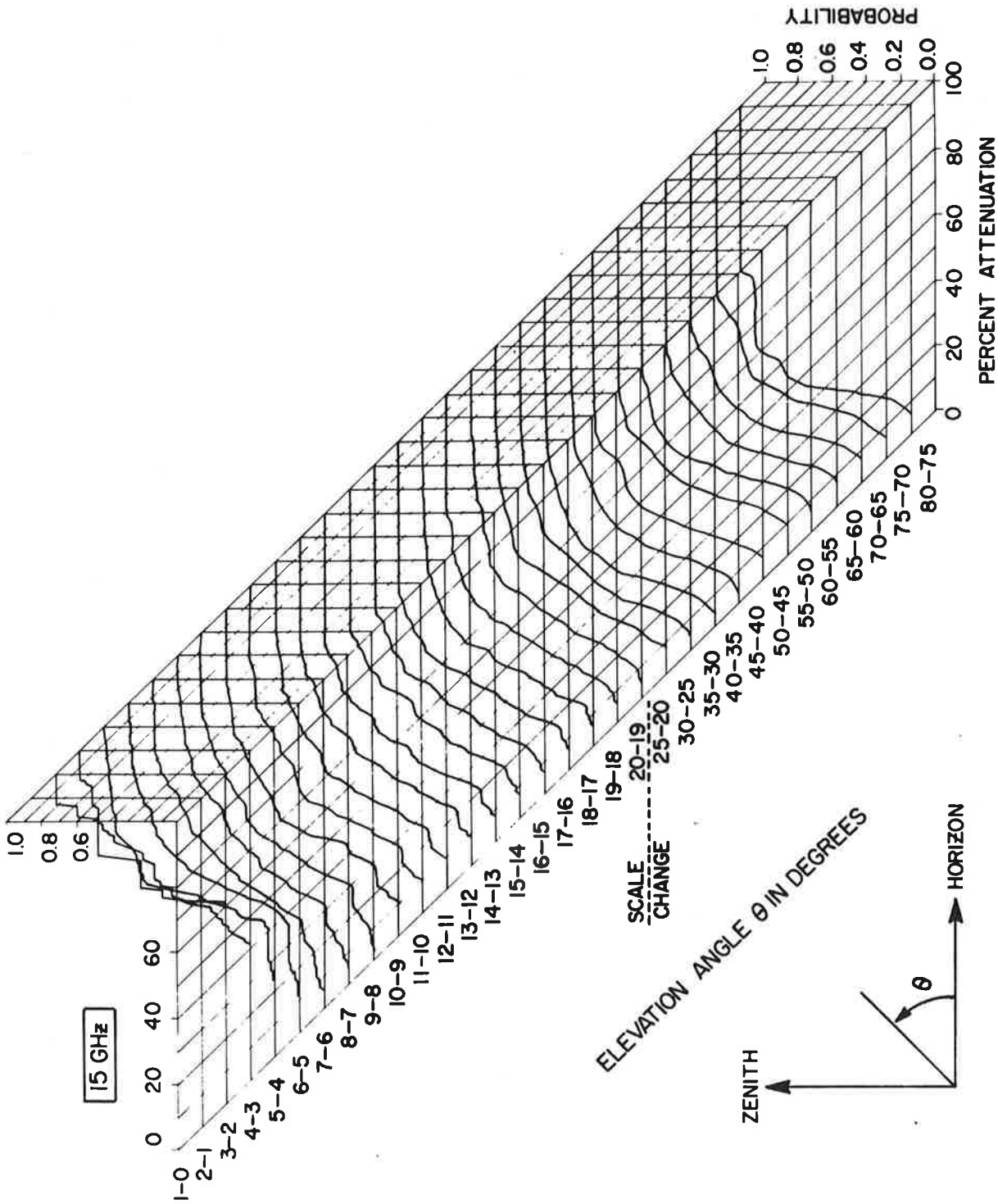


Figure D.11 Probability Distribution Functions of Attenuation at 15 GHz at Multiple Observing Angles



T = temperature, °K  
e = partial pressure of water vapor, millibars

For a standard atmosphere, assumed to consist of horizontally stratified layers, P and e decrease rapidly with height and T decreases slowly. Therefore, n decreases with height and a wave passing from a lower to upper layer is bent downward. Under these conditions, the apparent position of a source outside the lower atmosphere appears at an elevation angle slightly greater than that corresponding to the true position. The refraction correction for a standard atmosphere is shown in Fig. D.12 as a function of elevation angle for both microwave and optical wavelengths (Ref. 1, p. 173). For a dry atmosphere the index of refraction is almost constant for the entire electromagnetic spectrum. When water vapor is added it can be shown that the dipole moment of the molecule tends to follow electric-field changes at microwave frequencies but not at optical frequencies; as a result, the microwave index of refraction is greater.

Refractive effects vary widely with meteorological conditions, and for some abnormal cases the wave bends sharply downward (super-refraction), upward (sub-refraction), or becomes trapped (ducting). A loss in signal due to refraction should be distinguished from attenuation by absorption or multiple scattering. In the latter case the energy is for all practical purposes lost, whereas in the former case the wave is only bent, thereby resulting in a change in angle of arrival at the antenna. Bertram (Ref. 13) in a recent publication shows a method of compensating for this angle change when it is known.

Changes in the index of refraction of the medium will cause variations in the propagation velocity. This in turn will cause the energy ray paths to be delayed and bent resulting in differences between the apparent and true distances and direction of the target of interest. Another way of expressing this is that a shift in the radio bore-sight from the true boresight will occur.

The need for tropospheric refractive error compensation has encouraged extensive research into experimental measurement and correction for these effects.

In general data is corrected on the basis of meteorological measurements taken at the site or available from past records. Perfect compensation for refractive effects is not possible since there is usually a time lag or space difference between gathering of the meteorological data and the received radio signal. The error that remains following

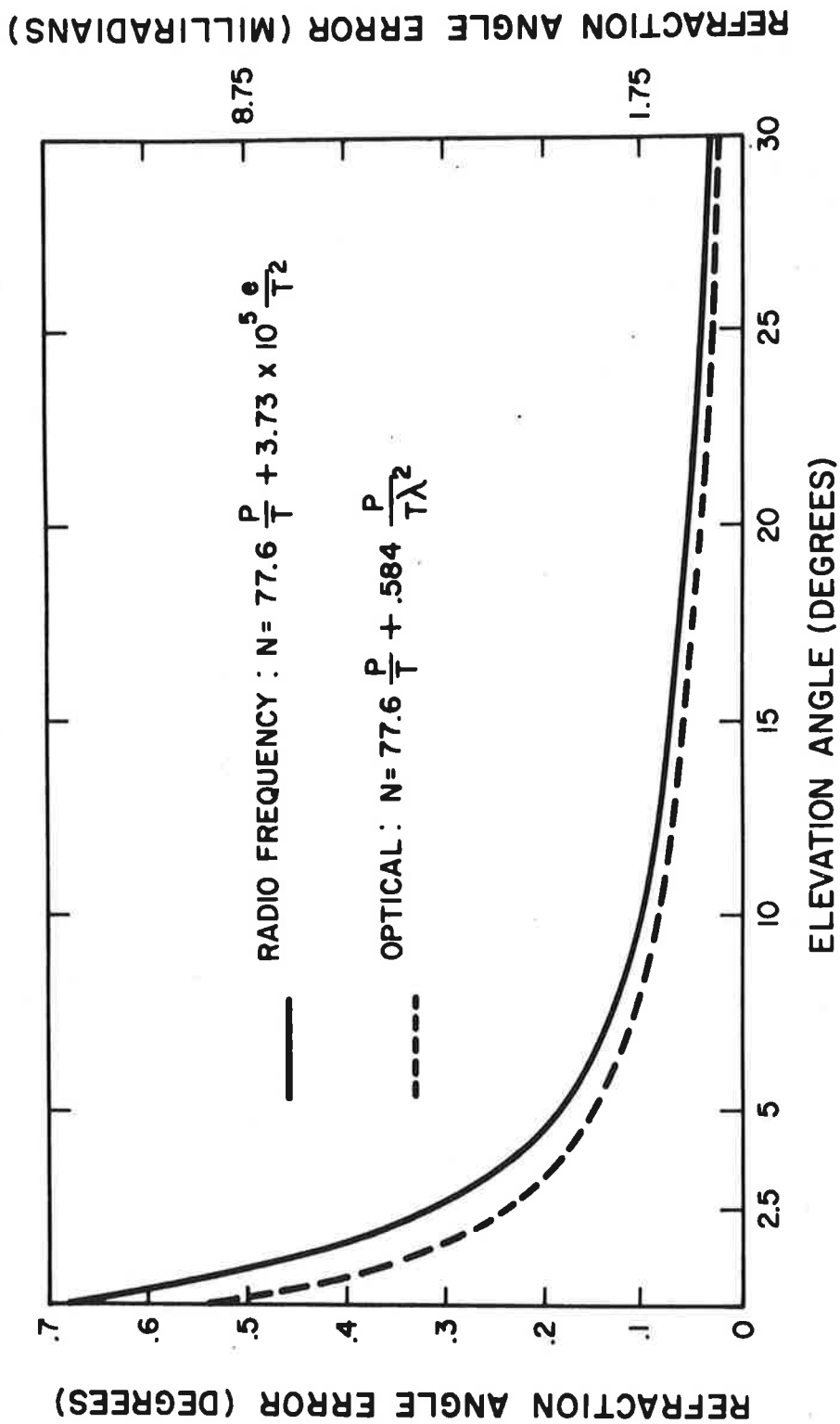


Figure D.12 Refraction Correction for a Standard Atmosphere as a Function of Elevation Angle

the correction process is termed residual error.

The errors caused by a varying refractive index of the lower troposphere can be evaluated by assuming that the atmosphere is horizontally stratified and is homogeneous. By a simple application of Snell's law, the total bending of a ray between the surface and any point can be calculated.

Radio systems utilized to measure range have an error introduced by refraction which is composed of two parts. The two contributors are (1) a geometric error resulting from the difference between a curved path length and a straight line, and (2) a velocity error due to the lower velocity of propagation in the medium.

Correction for refractive errors can be accomplished in varying degrees of sophistication depending on the accuracy requirement that is existent. Sufficient curves and tables exist in the literature which give the required correction for any altitude or range (Ref. 1). This technique gives a good first order approximation. A more useful procedure is the one employing the use of a standard model of the refractivity profile and the local surface refractivity at the time of measurement. Finally if a full refractivity profile can be measured at the same time as the radio transmission is made, then the standard deviation of the residual error may be taken from curves in the literature.

### D.3 Summary

In summary, although RTCA-117 suggested that attenuation from rain fall might be the meteorological parameter that would most seriously limit the performance of future microwave landing systems operating at 5 GHz and 15 GHz, no data was given to adequately substantiate this point. Furthermore, the effects of decorrelation across the aperture resulting from spatial and temporal variations along the transmission path induced by atmospheric homogeneities was not addressed. The combination of atmospheric emission, attenuation, and refraction could also cause range errors in the use of DME by dispersion of the pulse width resulting from atmospheric inhomogeneities. Thus the correlation bandwidth of the atmosphere at both 5 and 15 GHz could be determined so that a proper modulation and coding scheme be designed for the Microwave Landing System. Failure to acknowledge these effects could seriously impose a time bandwidth product limitation on the available spectrum required for future landing systems operating at these frequencies. If an experiment is to be run to determine the magnitude of these parameters and their effect on system

design. The data should be collected utilizing site characteristics and equipment performance parameters typical of the proposed system suggested by RTCA-SC-117.

#### D.4 References

Note: Certain citations have document accession numbers such as Axx-xxxxx or Nxx-xxxxx. These are defined in Table 5-1 of Ref. 1.

1. Thompson, W. I., III, (1971), Atmospheric Transmission Handbook: A Survey of Electromagnetic Wave Transmission in the Earth's Atmosphere over the Frequency (Wavelength) Range 3 kHz(100km) - 3,000 THz(0.1 micron), Report No. DOT-TSC-NASA-71-6, DOT Transportation Systems Center, Cambridge, MA, N71-20121#, p. 47.
2. Samson, C. A., B. A. Hart, and R. E. Skerjanec, (1970), Weather Effects on Approach and Landing Systems, Report No. FAA-RD-70-47, ESSA Research Labs., Institute for Telecommunication Sciences, Boulder, CO.
3. Hogg, D. C. (1969), Statistics on Attenuation of Microwaves by Intense Rain, Bell System Technical J., 48, 2949-2962, A70-16575.
4. Semplak, R. A. and R. H. Turrin, (1969), Some Measurements of Attenuation by Rainfall at 18.5 GHz, Bell System Technical J., 48, 1767-1787.
5. Van Vleck, J. H. (1947), The Absorption of Microwaves by Oxygen, Physical Review, 71, 413-424.
6. Van Vleck, J. H. (1947), The Absorption of Microwaves by Water Vapor, Physical Review, 71, 425-432.
7. Rogers, T. F. (1953), An Estimate of Influence of the Atmosphere on Airborne Reconnaissance Radar Performance, Propagation Lab. Report, Air Force Cambridge Research Center, Bedford, MA, Jan. 4.
8. Ryde, J. W. and D. Ryde, (1945), Attenuation of Centimetre and Millimetre Waves by Rain, Hail, Fog and Clouds, Report No. 8670, General Electric Co., Research Labs., Wembly, England.
9. Weger, E. (1960), Apparent Sky Temperatures in the Microwave Region, J. Meteorology, 17, 159-165.
10. Campen, C. F., A. E. Cole, T. P. Condron, W. S. Rysley, and N. Sissenwine, Editors, Handbook of Geophysics, Revised Edition, MacMillan, New York.

11. Medhurst, R. G. (1965), Rainfall Attenuation of Centimeter Waves: Comparison of Theory and Measurement, IEEE Trans. Antennas & Propagation, AP-13, 550-564.
12. Haroules, G. G., W. E. Brown, III, and G. J. Bishop, (1971), Measurements of transatmospheric attenuation statistics at the microwave frequencies: 15, 19, and 34 GHz, Report No. DOT-TSC-NASA-71-10, DOT Transportation Systems Center, Cambridge, MA.
13. Bertram, S. (1971), Compensating for Propagation Errors in Electromagnetic Measuring Systems, IEEE Spectrum, 8, #3, 58-63, A71-22356.

# **APPENDIX E**

## **COMPONENT SPECIFICATIONS**

*Abstract-General performance tradeoffs required in the development of the major array components are discussed. Specifications for the antenna switches, attenuators, phase shifters and power dividers are presented.*

Electronically controlled switches, phase shifters and attenuators, and passive power dividers are the major components to be incorporated into the proposed landing systems. The decisions on component specifications have been made based on discussions with component designers and manufacturers. State-of-the-art performance was requested in accordance with manufacturing feasibility.

Tradeoffs on various electrical parameters were made to obtain components which satisfied the overall requirements of the system. For example, although lower insertion loss levels are achievable as a separate entity, requesting same could result in poorer phase balance and bandwidth. Thus the final specifications represent the best balance of performance achievable in manufacturable quantities. The electrical specifications of the seven components being purchased are listed below.

#### E.1 Specification: Single Pole Double Throw Switch

Scope: This document defines the performance and data requirements for a single pole double throw (SPDT) switch to be used in controlling RF energy in a phased array antenna.

#### Applicable Documents:

Specifications: MIL-I-6181D Interference Control Requirements, Aircraft Equipment

#### Electrical Requirements:

- (1) Frequency: 5.0 to 5.25 GHz
- (2) RF Power Input: Thermal noise to 0.5 w max. C.W.
- (3) Insertion Loss: 1.2 dB max.
- (4) Insertion Loss Variation:

Port-to-Port: Maximum and minimum insertion losses shall not differ by more than 0.4 dB between switch positions.

Switch-to-Switch: Maximum and minimum insertion loss shall not differ by more than 0.3 dB between switches (with the same switch positions used).



(5) Differential Insertion Phase:

Port-to-Port: The insertion phase difference between switch ports will not exceed ten degrees.

Switch-to-Switch: The insertion phase difference between switches (same switch position) shall not exceed ten degrees.

(6) Isolation: 30 dB min. from any selected "on" port to "off" port.

(7) Impedance: 50 ohms, VSWR 1.5 max. at input port when other ports are terminated in a 50 ohm load having a VSWR of 1.1.

(8) Switching Characteristics:

Speed: <500 nanosec. max. (full on to full off and full off to full on).

Repetition rate: 0 to 40 kHz Max.

Delay: <200 nanoseconds.

Delay Variation: <100 nanoseconds.

Control: Electronic, vendor will specify control signal characteristics and will supply schematic of circuit used to test the switch. Control voltages will be specified in the response to any solicitation for this item.

Switching Transients ("Dribble"): Care will be taken to minimize the generation of energy on the RF input and output ports commonly caused by the switch control signals. Maximum advantage will be taken of the slow switching time requirement in achieving this requirement.

RF Isolation: C-band energy on the switch control leads shall be at least 30 dB below the RF input signal under any test condition.

(9) RFI: Interference Control) - the generation of radio-frequency interference by the network and the vulnerability of the network to radio-frequency interference shall be controlled within the limits

of Specification MIL-I-6181D.

E.2 Specification: Single Pole Four Throw Switch

Scope: This document defines the performance and data requirements for a single pole four throw (SP4T) switch to be used in controlling RF energy in a phased array antenna.

Applicable Documents:

Specifications

Military

MIL-I-6181D Interference Control Requirements,  
Aircraft Equipment

Electrical Requirements:

- (1) Frequency: 5.0 to 5.25 GHz.
- (2) RF Power Input: thermal noise to 3.0 watts max., CW.
- (3) Insertion loss: 1.8 dB Max.
- (4) Insertion loss variation:

Port-to-Port: Maximum and minimum insertion losses shall not differ by more than 0.4 dB between switch positions. (Port 1 - Port 2 path used as reference)

Switch-to-Switch: Maximum and minimum insertion loss shall not differ by more than 0.3 dB between switches (with the same switch positions used).

- (5) Differential Insertion Phase:

Port-to-Port: The insertion phase difference between switch ports will not exceed ten degrees. (Port 1 - Port 2 path used as reference)

Switch-to-Switch: The insertion phase difference between switches (same switch position) shall not exceed ten degrees.

- (6) Isolation: 30 dB min. from any selected "on" port to any "off" port.

- (7) Impedance: 50 ohms, VSWR 1.5 Max, at input port when other ports terminated in 50 ohms, VSWR = 1.1.

(8) Switching Characteristics:

Speed: <500 nanosec. Max. (Full on to full off and full off to full on)

Repetition rate: 0 to 40 kHz Max.

Delay: <200 nanoseconds.

Delay Variation: <100 nanoseconds

Control: Electronic, vendor will specify control signal characteristics and will supply schematic of circuit used to test the switch. Control voltages will be specified in the response to any solicitation for this item.

Switching Transients ("Dribble"): Care will be taken to minimize the generation of energy on the RF input and output ports commonly caused by the switch control signals. Maximum advantage will be taken of the slow switching time requirement in achieving this requirement.

RF Isolation: C-band energy on the switch control leads shall be at least 30 dB below the RF input signal under any test condition.

- (9) RFI: (Interference control): The generation of radio-frequency interference by the network and the vulnerability of the network to radio-frequency interference shall be controlled within the limits of Specification MIL-I-6181D.

E.3 Specification: Phase-Balanced Transfer Switch

Scope: This document defines the performance and data requirements for a phase balanced transfer switch (double pole double throw switch) to be used in controlling RF energy in a phased array antenna.

Applicable Documents:

Specifications:

Military: MIL-I-6181D Interference Control Requirements, Aircraft Equipment

### Electrical Requirements:

- (1) Frequency: 5.0 to 5.25 GHz
- (2) RF Power Input: 20 dB variation typical, 1.0 watt (cw) maximum at each input terminal.
- (3) Switch Routing: (refer to Figure 1)  
Position 1: Terminal 1 connected to Terminal 3.  
Terminal 2 connected to Terminal 4.  
  
Position 2: Terminal 1 connected to Terminal 4.  
Terminal 2 connected to Terminal 3.
- (4) Insertion Loss: 1.1 dB maximum, 0.9 dB average, (0.7 dB average desired)
- (5) Insertion Loss Variation:
  - (a) The maximum and minimum insertion losses for different units (input applied at the corresponding terminal and the switch being set to the same position in each case) shall not differ by more than 0.3 dB.
  - (b) The maximum and minimum insertion losses for any one unit shall not differ by more than 0.3 dB.
- (6) Amplitude Balance: With equal amplitude signals applied at terminals 1 & 2, the difference in amplitude between the output signals shall not exceed 0.3 dB in either switch position.
- (7) Phase Balance: With in-phase signals applied at terminals 1 and 2, the phase difference between the signals measured at ports 3 and 4 shall not exceed 5° in either switch position.
- (8) Insertion Phase Variation:
  - (a) The maximum and minimum electrical path length for different units (input applied at the corresponding terminal and the switch being set to the same position in each case) shall not differ by more than ten degrees.
  - (b) The maximum and minimum electrical path length for any one unit shall not differ by more than ten degrees.
- (9) Impedance: 50 ohms.
- (10) VSWR: All terminals not greater than 1.5 when other terminals are terminated with 50 Ohms (VSWR<1.05)

(11) Isolation: The power measured at either of the two terminals not designated as input or output shall be down by at least 30 dB from the power measured at the designated output terminal - for the input located at either input terminal and for either position of the switch.

(12) Switching Characteristics:

Speed: <500 nanoseconds maximum (Full On to Full Off and Full Off to Full On)

Repetition Rate: 0 to 40 kHz maximum.

Delay: <200 nanoseconds

Delay Variation: <100 nanoseconds

Control: Electronic. Vendor will specify control signal characteristics and recommend drivers suitable for interface with logic drive units. The vendor will also supply a schematic of the circuit used to test the switch.

(13) RFI: (Interference Control) - The generation of radio frequency interference by the network and the vulnerability of the network to radio frequency interference shall be controlled within the limits of Specification MIL-I-6181D.

E.4 Specification: Electronically Controlled Variable Attenuator

Scope: This document defines the performance and data requirements for a continuously variable electronically controlled attenuator to be used to control power level in a phased array antenna.

Applicable documents:

Specification - MIL-I-6181D - Interference control requirements, aircraft equipment.

Electrical Requirements:

- 1) Type: Absorptive Variable Attenuator
- 2) Frequency Range: 5.0 - 5.25 GHz
- 3) Input Power: 1 watt CW maximum
- 4) V.S.W.R.: 1.5 max referred to 50 ohm coaxial line at any attenuation setting and any input power level up to the maximum.

- 5) Attenuation Range: 0 to 10 dB continuously variable.
- 6) Attenuation Accuracy: Linear with drive current and resettable to within 5% of attenuation value for a given drive current over extended time periods and temperature cycles.
- 7) Insertion loss at zero setting: 1.0 dB maximum.
  - a) Insertion loss of any two units at zero setting shall not differ by more than .3 dB.
  - b) Attenuation values of any two units having the same drive current shall not differ by more than .5 dB.
- 8) Variation of Phase with attenuation:  $\pm 5^\circ$  max. at any input level from 0 dBm to +30 dBm. Phase at any attenuation setting shall not vary more than  $\pm 5^\circ$  with power over an input power range of 0 dBm to 30 dBm.
- 9) Switching Characteristics:
  - a) Speed: 500 nanoseconds max. between any two attenuation settings.
  - b) Rep. Rate: 0 - 40 kHz
  - c) Delay: 200 nanoseconds max.
  - d) Delay variation: 100 nanoseconds max.
  - e) Control: Vendor shall specify control signal characteristics and recommend drivers suitable for interface with 3 bit TTL logic drive units.
  - f) Switching Transients (Dribble): Care will be taken to minimize the generation of energy on the RF input and output ports commonly caused by the switch control signals. Maximum advantage should be taken of the slow switching time requirement in achieving this.
  - g) RF Isolation: C-band power on the switch control leads shall be at least 30 dB below the RF input signal under any test condition.
- 10) RFI: (Interference Control) - The generation of radio-frequency interference by the network and the vulnerability of the network to radio-frequency interference shall be controlled within the limits of Specification MIL-I-6181D.

#### E.5 Specifications: 4-bit Digital Phase Shifter

Scope: This document contains the performance and data requirements for a four-bit digital diode phase shifter to be used for fine phasing in a phased array antenna.

Applicable Documents: MIL-I-6181D, Interference Control Requirements, Aircraft Equipment

### Electrical Requirements:

- 1) Frequency Range: 5.0 - 5.25 GHz
- 2) VSWR: 1.35 Max to 50 ohm coaxial line.
- 3) Insertion Loss: Maximum for any setting shall not exceed 1.7 dB. Average over all settings, 1.5 dB or less. Amplitude variations between settings on one unit shall not exceed  $\pm 0.25$  dB. Amplitude variations between units at same setting shall not exceed  $\pm 0.2$  dB.
- 4) Power handling capability: Shall be 700 mW minimum, with one watt desired, with no deterioration of electrical performance.
- 5) Phase Shift:  $0^\circ$  to  $337.5^\circ$  in steps of  $22.5^\circ$ . RMS phase error at various settings:  $5^\circ$  or less. Unit-to-unit variations shall be within  $\pm 5^\circ$  at each setting.
- 6) Insertion Phase: Unit-to-unit variations at zero phase shift setting shall be within  $\pm 5^\circ$ .
- 7) Switching Time, full off to full on (and vice versa): 500 nanoseconds including driver. Repetition rate: up to 40 kHz. Delay less than 200 nanoseconds. Delay variations less than 100 nanoseconds.
- 8) Control: Drive circuitry shall be designed to interface with TTL logic, with 2.5 to 5 volts representing a "1", and 0 to 0.8 volts representing a "zero".
- 9) Switching Transients (dribble): Care will be taken to minimize the generation of energy on the RF input and output ports commonly caused by the switch control signals. Maximum advantage will be taken of the relatively slow switching time to achieve this end.
- 10) RF Isolation: C-band energy on the switch control leads shall be down by at least 30 dB below the RF input signal under any test condition.
- 11) RFI: The generation of RFI by the network and the vulnerability of the network to RFI shall be controlled within the limits of specification MIL-I-6181D.

### E.6 Specification: Power Dividers, 1 to 8 and 1 to 4

Scope: This document defines the performance and data requirements for two types of power dividers, a one input-eight output type, and a one input-four output type.

#### Applicable Documents:

#### Specifications:

MIL-I-6181D Interference Control Requirements, Aircraft Equipment

## Electrical Requirements

(Item 1: 8-way power divider)

- 1) RF Power Input: up to 30 watts CW. Outputs are anticipated to feed into components with VSWR's of 1.5 maximum, but power divider shall be able to dissipate the reflected signal from a VSWR of 2.0 at one output poer without destruction.
- 2) Coupling and insertion loss: the ratio of output power at any port to the power at the input shall be at least -10.2 dB (Insertion loss of 1.2 dB)
- 3) Isolation: 20 dB minimum. Specifically this means that if the input port and all but two output ports are terminated in matched loads, and a signal fed into one of the two remaining ports, the signal observed at the other port shall be down by 20 dB or more from the input signal.
- 4) Amplitude balance between output ports: the signal at the maximum port and the minimum port shall not differ by more than 0.3 dB for any unit. The coupling to any port of any unit shall not differ from the coupling to the same port of any other unit by more than 0.3 dB.
- 5) Phase balance between output ports: the signal phase at any output port shall not differ from the signal phase at any other output port by more than 10 degrees, for any unit. The phase to any port of any unit shall not differ from the phase of the same port of any other unit by more than 10 degrees.
- 6) VSWR: 1.5 max. to 50 ohms, with matched terminations at output.
- 7) RFI: shall meet the requirements of MIL-I-6181D.

(Item 2: 4-way power divider)

- 1) RF Power Input: Up to 5 watts CW. Outputs are anticipated to feed into components with VSWR's of 1.5 maximum, but power divider shall be able to dissipate the reflected signal from a VSWR of 2.0 at one output port without destruction.
- 2) Coupling and Insertion Loss: the ratio of output power at any port to the power at the input shall be at least -6.8 dB. (This corresponds to an insertion loss of .8 dB)
- 3) Isolation: 20 dB minimum. Specifically this means that if the input port and all but two output ports are terminated in matched loads, and a signal fed into one of the two remaining ports, the signal observed at the other port shall be down by 20 dB or more.
- 4) Amplitude balance between output ports: the signal at the maximum port and the minimum port shall not



differ by more than 0.3 dB for any unit. The coupling to any port of any unit shall not differ from the coupling to the same port of any other unit by more than 0.3 dB.

- 5) Phase balance between output ports: the signal phase at any output shall not differ from the signal phase at any other output port by more than 10 degrees, for any unit. The phase to any port of any unit shall not differ from the phase of the same port of any other unit by more than 10 degrees.
- 6) VSWR: 1.5 max to 50 ohms, with matched terminations.
- 7) RFI: shall meet the requirements of MIL-I-6181D.



taken at approximately 700 ft. altitude and represent roughly the average over the entire approach. All the variables except pitch angle deviation and airspeed deviation at flare altitude exceed their limits for one or more of the conditions shown.

There is a dramatic decrease in elevator activity (Fig. 7-37) and pitch rate activity (Fig. 7-38) at 1 scan per second, indicating the tendency of high frequency variables to settle between scans at low scan rates, but the pitch angle deviation, produced by the pitch rate activity prior to settling remains constant between scans, accounting for the subsequent increase in rms pitch angle (Fig. 7-36) at 1 scan per second.

Figure 7-43(a) is the composite plot for the PA-30 showing acceptable beam noise-scan rate values for the longitudinal channel. As with the CV-880, the region of acceptable values is severely limited by noise sensitive variables, in this case indicated glideslope deviation,  $Z_I$ , and pitch rate,  $q$ . Figure 7-43(b) shows the improvement with a 0.5 second coupler filter.

#### 7.4 SUMMARY

By way of summary, the reader is referred to the important figures of this section, the various beam noise-scan rate tradeoffs:

##### Azimuth:

CV-880 Safety Factors	Fig. 7-8(a) Fig. 7-8(b)
Pilot Acceptability Factors	Figs. 7-16(a) & (b) Figs. 7-24(a) & (b)

##### Elevation #1

CV-880 Safety Factors	Figs. 7-28(a) & (b)
Pilot Acceptability Factors	Figs. 7-35(a) & (b) Figs. 7-43(a) & (b)

#### 7.5 INTERPRETATIONS

##### 7.5.1 IMPLICATIONS OF A PERCENTAGE INCREASE IN $1\sigma$ VALUE TO THE PROBABILITY OF EXCEEDING A LIMIT - CRITICAL VARIABLES AT TOUCHDOWN

All of the results of Section 7 related to safety criteria

at touchdown are expressed in terms of percentage increase in  $1\sigma$  value as beam noise and scan rate are varied from the perfect continuous case with worst case wind.

Without knowledge of the absolute dispersion for the baseline case, this percentage increase has no direct implication for the probability of exceeding a specific limit.

It is illuminating, however, to postulate hypothetical relationships between the limit and the  $1\sigma$  value and, over a range of interest to at least bound probability variation as a function of percentage variation.

If the variables of interest are gaussian, then this is easily done with the aid of tables for the gaussian cumulative distribution function. Table 7-3 shows probability of exceeding a limit for various percentage increases and various baseline probabilities. As an example, let the limit,  $L$ , on a variable,  $X$ , be 10 and its  $1\sigma$  value under baseline conditions be 2.35; then the limit represents a  $4.26\sigma$  value of that variable and will be exceeded once in  $10^5$ . For an increase of 0.5% in the  $1\sigma$  value, the limit now represents a  $4.24\sigma$  value and will be exceeded 1.12 times in  $10^5$  events, an increase of 12%.

It is felt that a probability budget of 12% for LGS imperfections is certainly reasonable (but probably unachievable) and that it would be unrealistic to limit possible acceptable scan rates and beam noise by variables whose increase in  $1\sigma$  values are less than 0.5%.

What the preceding paragraphs suggest with respect to the results on safety factors is that there is room for deterioration in some of the critical variables when compared with conventional ILS performance while picking up significant improvements in others at moderate scan rates and beam noise. In particular, rather than constrain performance in  $\dot{Y}_A$  and  $\dot{Z}$  (Figs. 7-8(a) and 7-28(a) respectively), by conventional ILS performance, it would be more realistic to use a flat 1% or 0.5% constraint. (1% increase in corresponds to a 25-30% probability budget for LGS).

It should be noted further that, in an absolute sense, these increases in probability are significant only if  $\dot{Y}_A$  or  $\dot{Z}$  is truly a limiting factor in determining the probability of a successful landing. For instance, if the probability of landing off the runway is 1 in  $10^6$  and that of exceeding the cross track velocity limit ( $\dot{Y}_A$ ) is 1 in  $10^8$ , then an increase to 1.15 in  $10^8$  for exceeding cross track velocity limit is insignificant in comparison with the limiting factor, 1 in  $10^6$ .

TABLE 7-3  
 EFFECTS OF PERCENTAGE INCREASE IN  $1\sigma$  VALUE ON  
 PROBABILITY OF EXCEEDING A LIMIT FOR A GAUSSIAN RANDOM VARIABLE

Ratio of Limit to $1\sigma$ Value for 0% (Baseline)	Probability of Exceeding Limit for Percentage Increase in Value Shown				
	0.0%	0.1%	0.5%	1.0%	5.0
5.99	1 in $10^9$	1.03 in $10^9$	1.18 in $10^9$	1.37 in $10^9$	5.2 in $10^9$
5.61	1 in $10^8$	1.03 in $10^8$	1.15 in $10^8$	1.35 in $10^8$	4.8 in $10^8$
5.20	1 in $10^7$	1.03 in $10^7$	1.13 in $10^7$	1.35 in $10^7$	4.7 in $10^7$
4.75	1 in $10^6$	1.02 in $10^6$	1.12 in $10^6$	1.3 in $10^6$	3.3 in $10^6$
4.26	1 in $10^5$	1.02 in $10^5$	1.12 in $10^5$	1.25 in $10^5$	2.4 in $10^5$
3.72	1 in $10^4$	1.02 in $10^4$	1.1 in $10^4$	1.18 in $10^4$	1.9 in $10^4$
3.09	1 in $10^3$	1.02 in $10^3$	1.08 in $10^3$	1.14 in $10^3$	1.7 in $10^3$
2.33	1 in $10^2$	1.01 in $10^2$	1.05 in $10^2$	1.1 in $10^2$	1.35 in $10^2$

Therefore, in interpreting scan rate beam noise trade-offs for safety factors for the CV-880, it is felt that Figures 7-8(b) and 7-28(b) which use the hybrid constraint on critical variables (dispersion increases half that with conventional ILS or 0.5%, whichever is greater) are still conservative but more realistic than ones generated based solely on either a flat percentage or a specific improvement over conventional ILS.

#### 7.5.2 PILOT ACCEPTABILITY FACTORS - THE EFFECTS OF A COUPLER FILTER

As was seen in Section 7 [Figs. 7-16(b), 24(b), 35(b) and 43(b)] a coupler filter significantly reduces activity in higher frequency variables, thereby enlarging the region of acceptable noise and scan rate values for pilot acceptability factors. It is more critical in the longitudinal system, to an extent that, with effectively no filter, neither aircraft satisfies all pilot acceptability constraints for reasonable values of noise and scan rate.

It is certainly reasonable to assume that a significant amount of work will go into designing a coupler filter for each aircraft that intends to fly the LGS and that the filter design will be based on both the scanning rate and the aircraft dynamics. No attempt has been made during this study to accomplish such a design for the aircraft under consideration.

The results, however, do reflect the sensitivity of pilot acceptability factors to filtering and do point out the need for considering filter configurations in further performance studies concerning scanning rate and beam noise. It is felt that results based on a rational filter design would more closely approximate those with a 0.5 second filter than those with the 0.025 second filter.

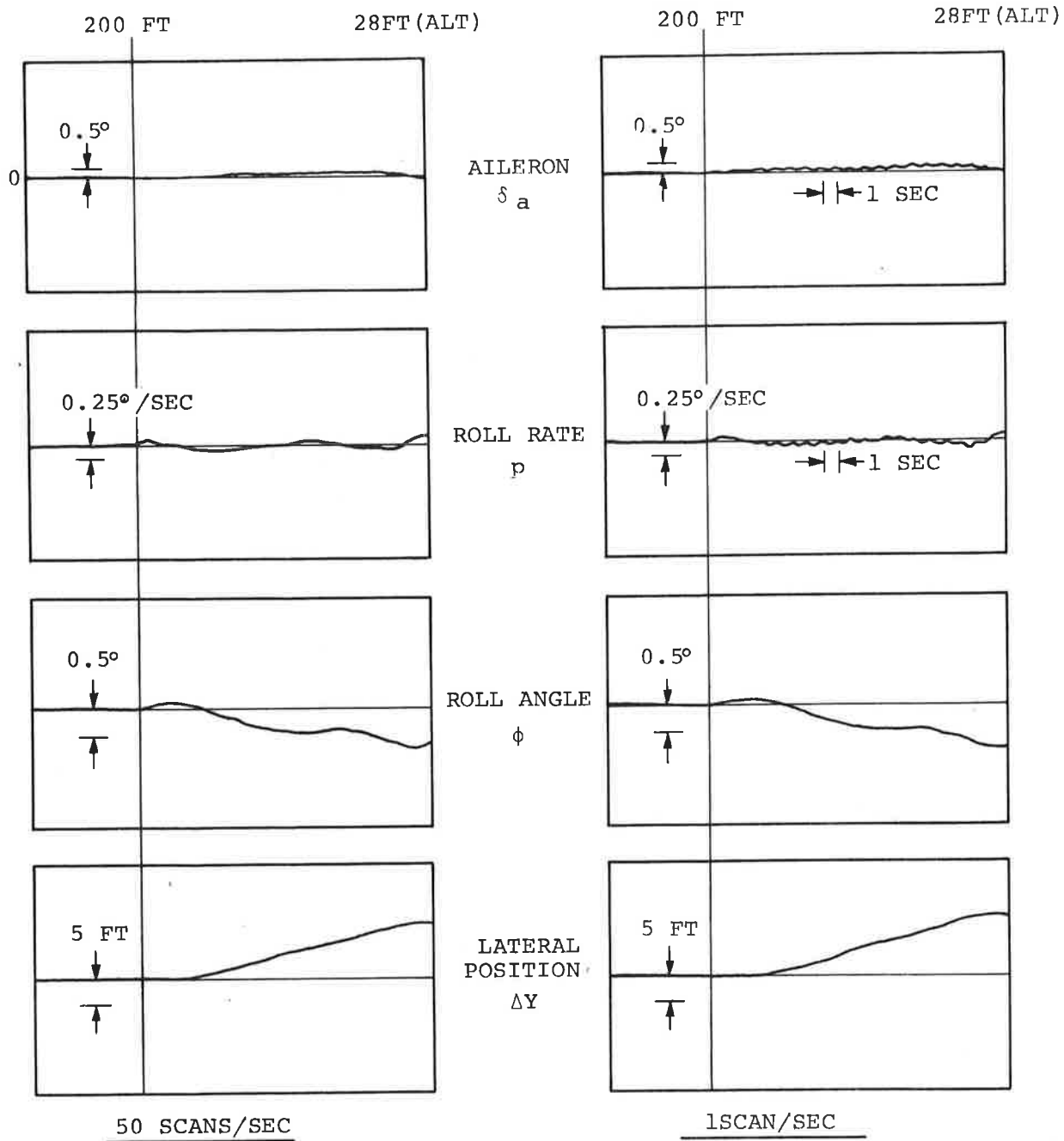


Figure 7-1. CV-880 Lateral System Response to Wind Shear At 50 and 1 Scans Per Second

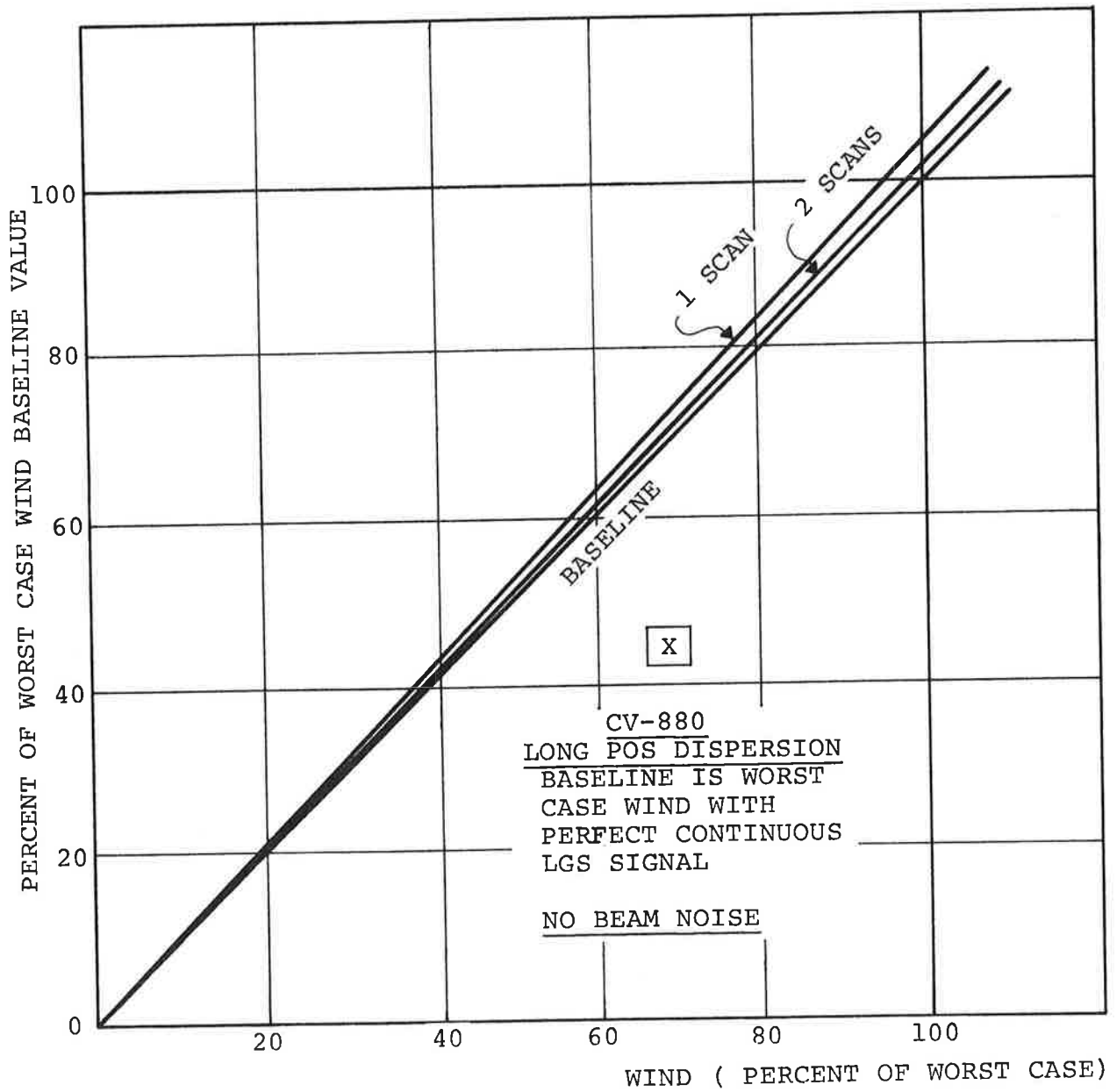


Figure 7-2. Relative Dispersion in Longitudinal Position Vs. Relative Gust Intensity (No Beam Noise)



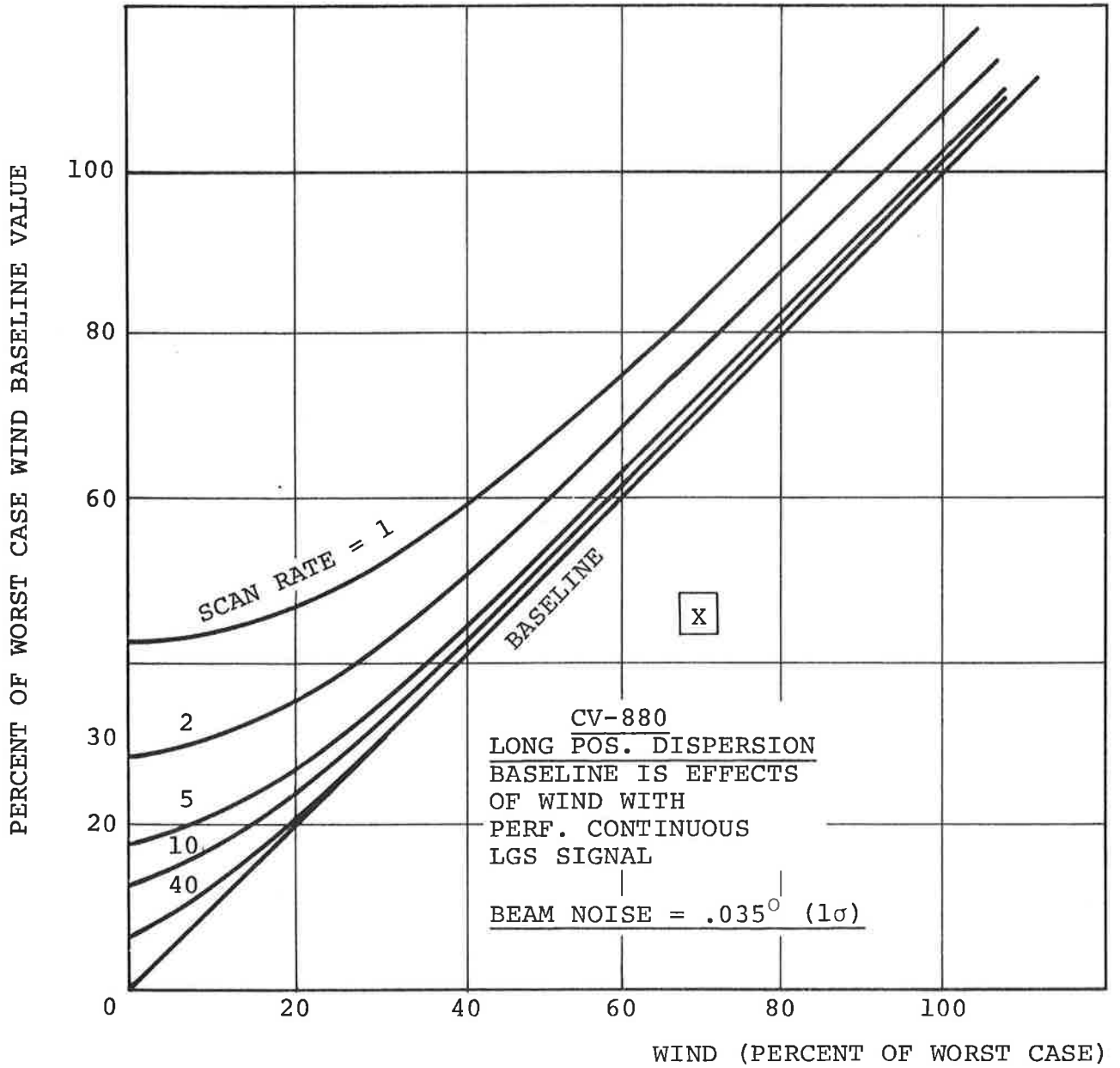


Figure 7-3. Relative Dispersion in Longitudinal Position Vs. Relative Gust Intensity With Beam Noise

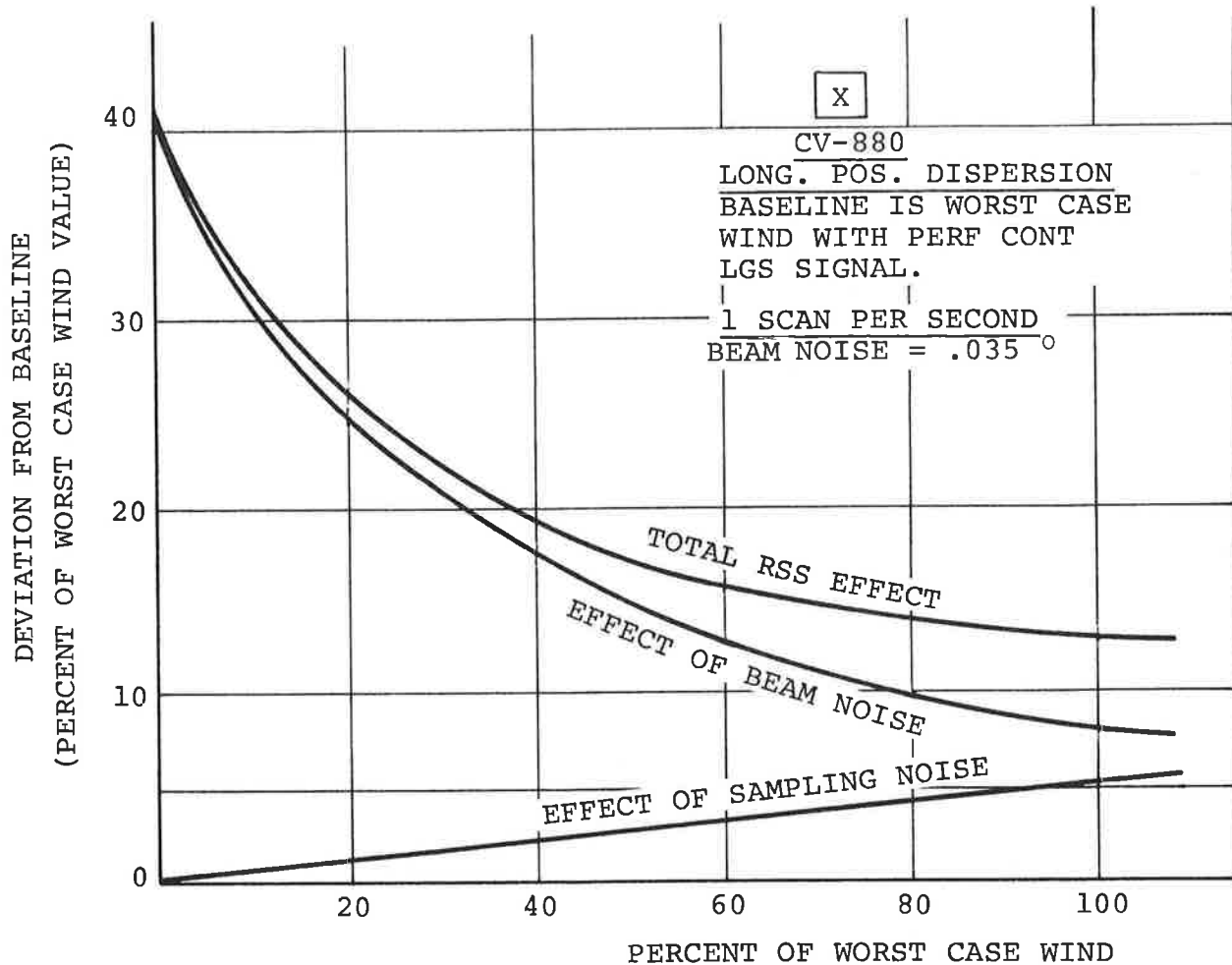


Figure 7-4. Relative Effects of Beam Noise and Sample Noise Vs. Wind

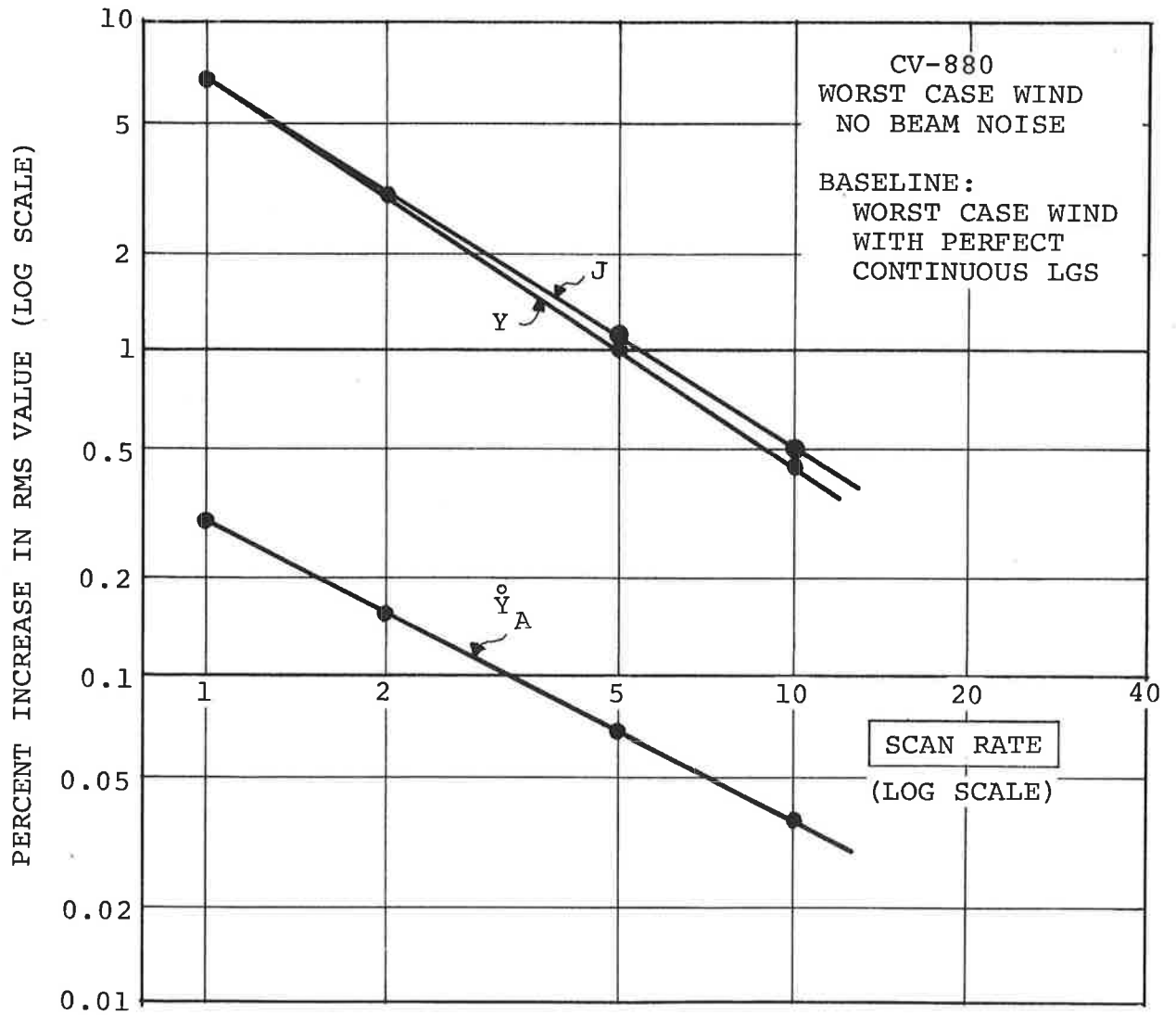


Figure 7-5. Relative Effect of Scan Rate on Lateral Touchdown Variables - Worst Case Wind - No Beam Noise

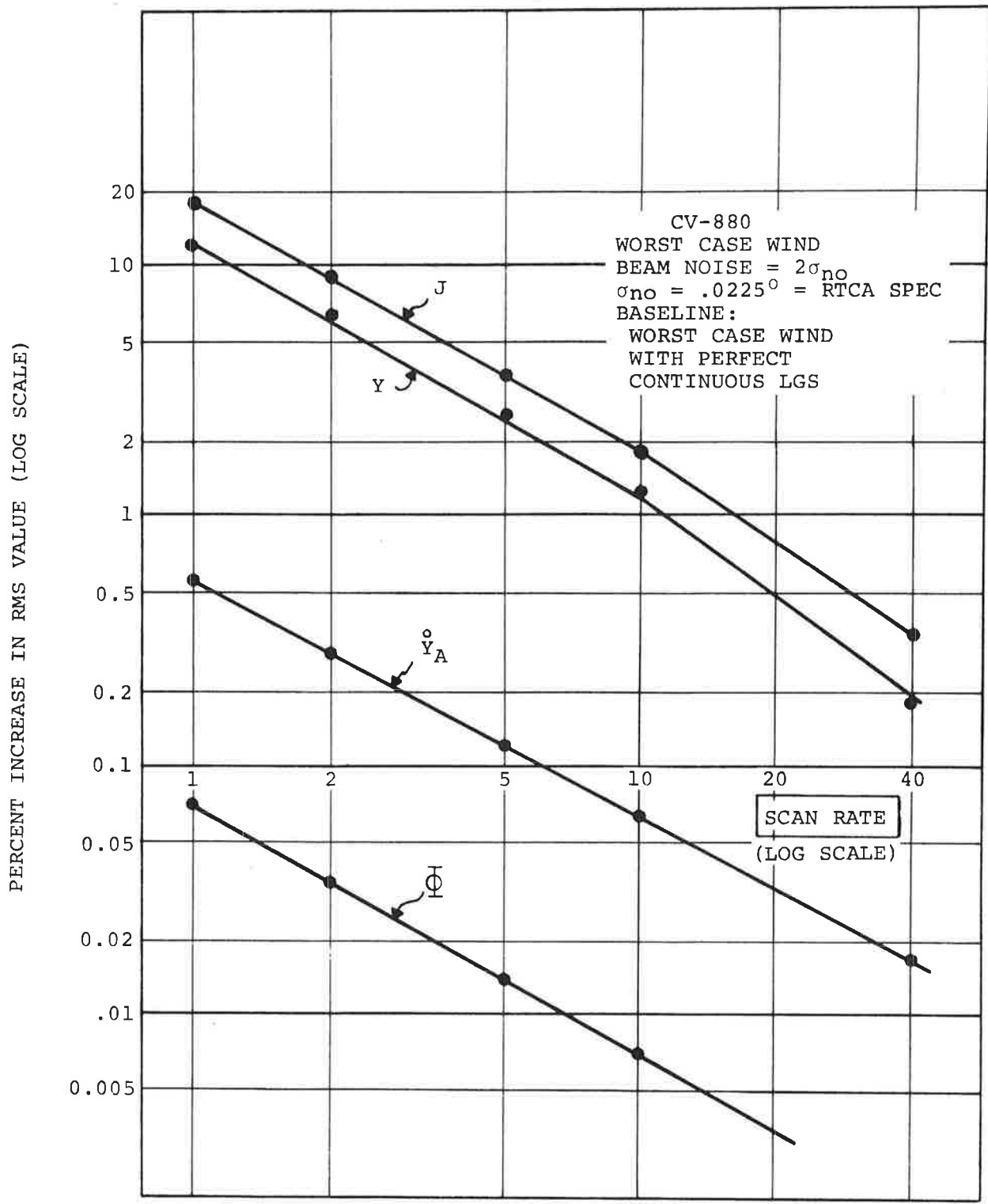


Figure 7-6. Relative Effect of Scan Rate on Lateral Touchdown Variables, Worst Case Wind + Beam Noise

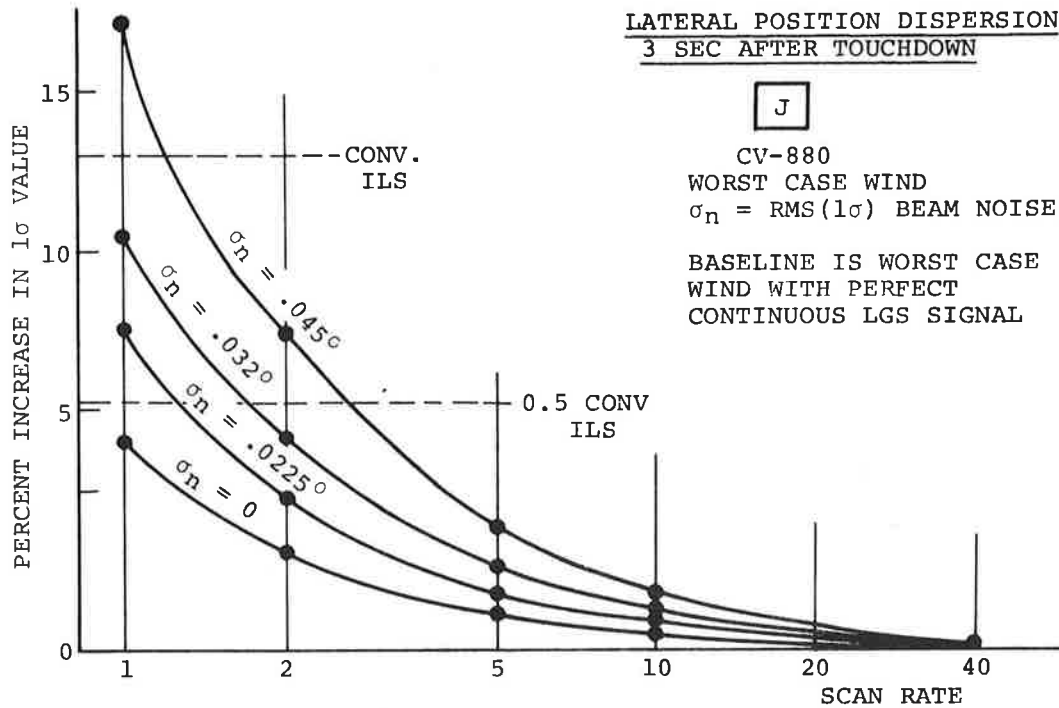


Figure 7-7(a).  $1\sigma$  Lat. Pos. (3 Sec. After TD) Vs. Scan Rate

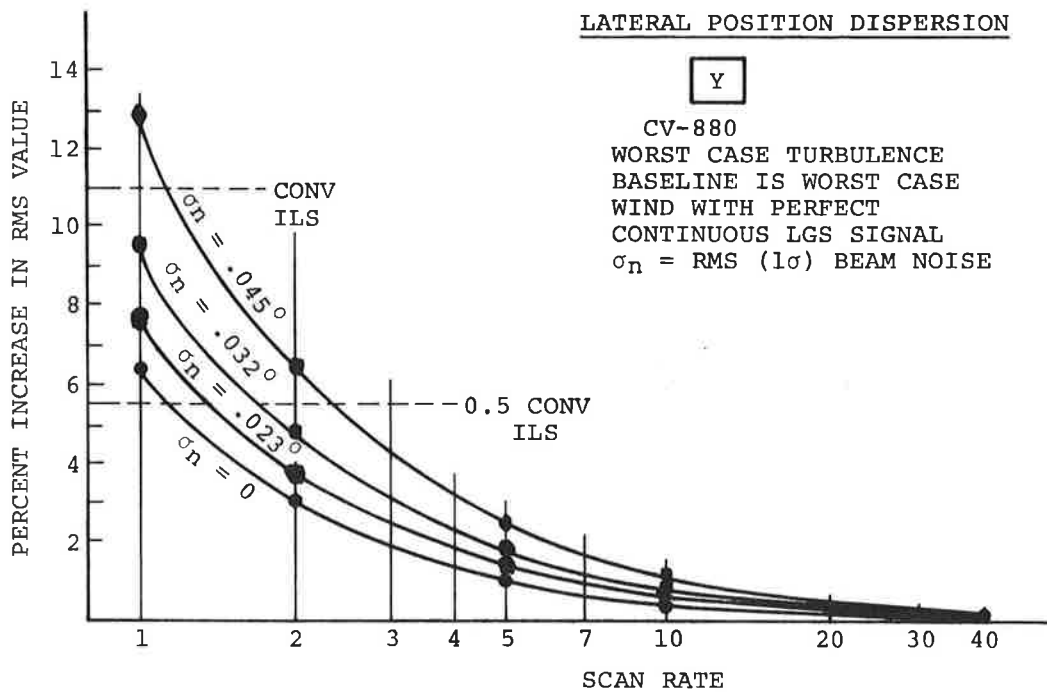


Figure 7-7(b). Lateral Position Dispersion Vs. Scan Rate

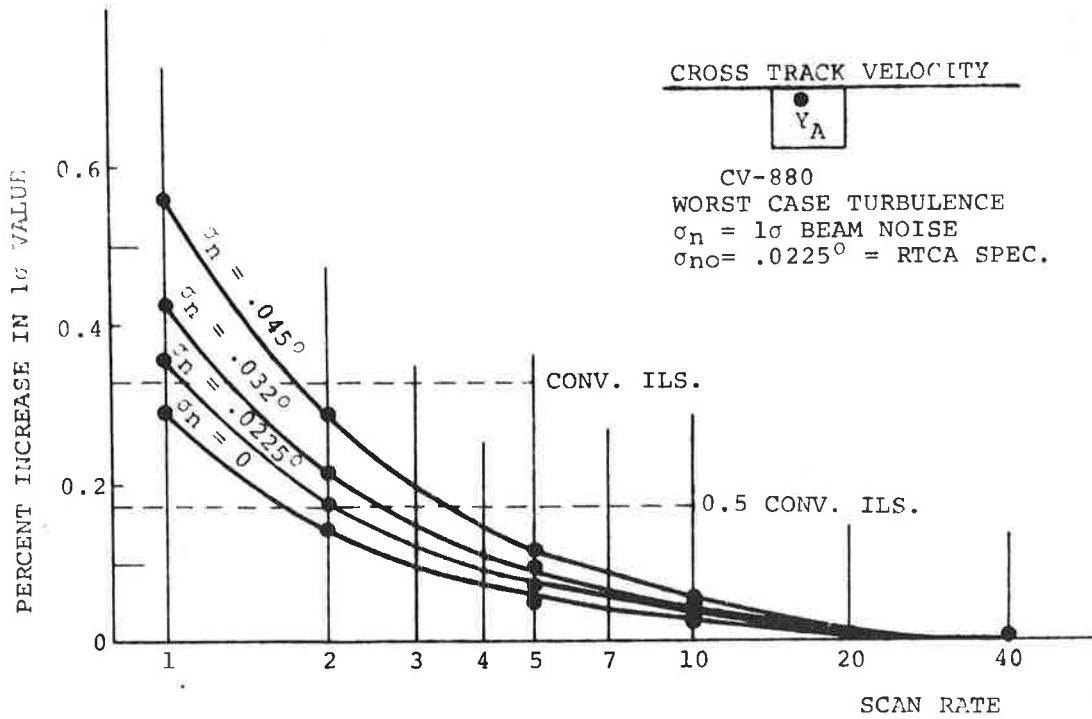


Figure 7-7(c). Cross Track Velocity Dispersion Vs. Scan Rate

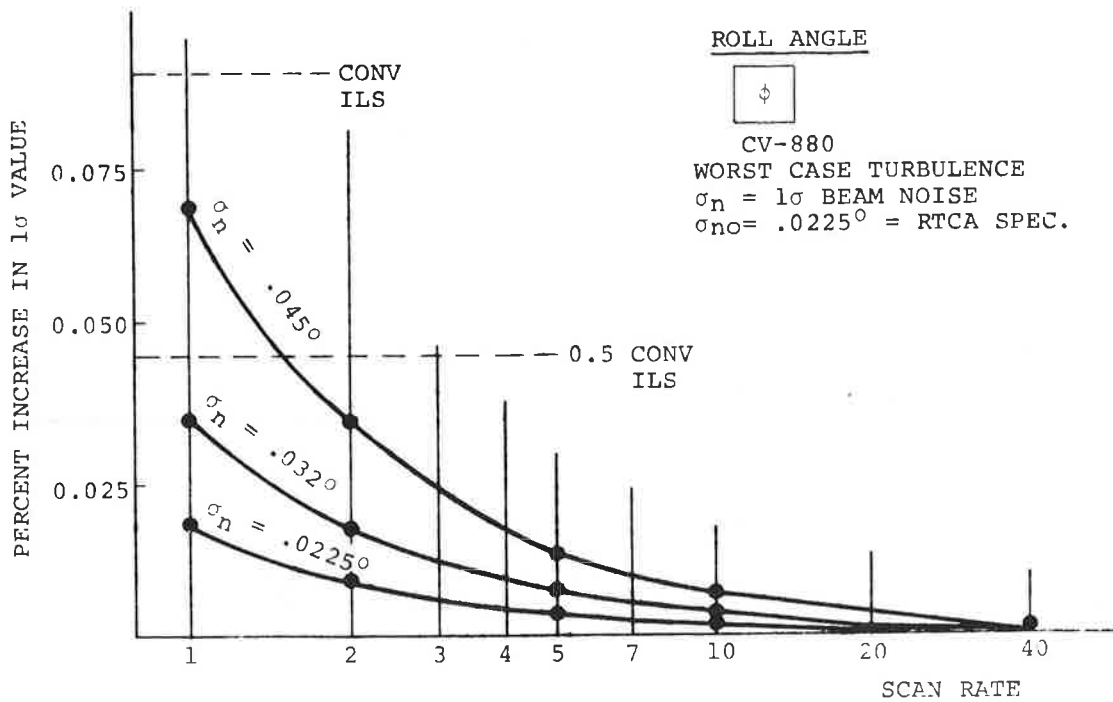


Figure 7-7(d). Roll Angle Dispersion Vs. Scan Rate

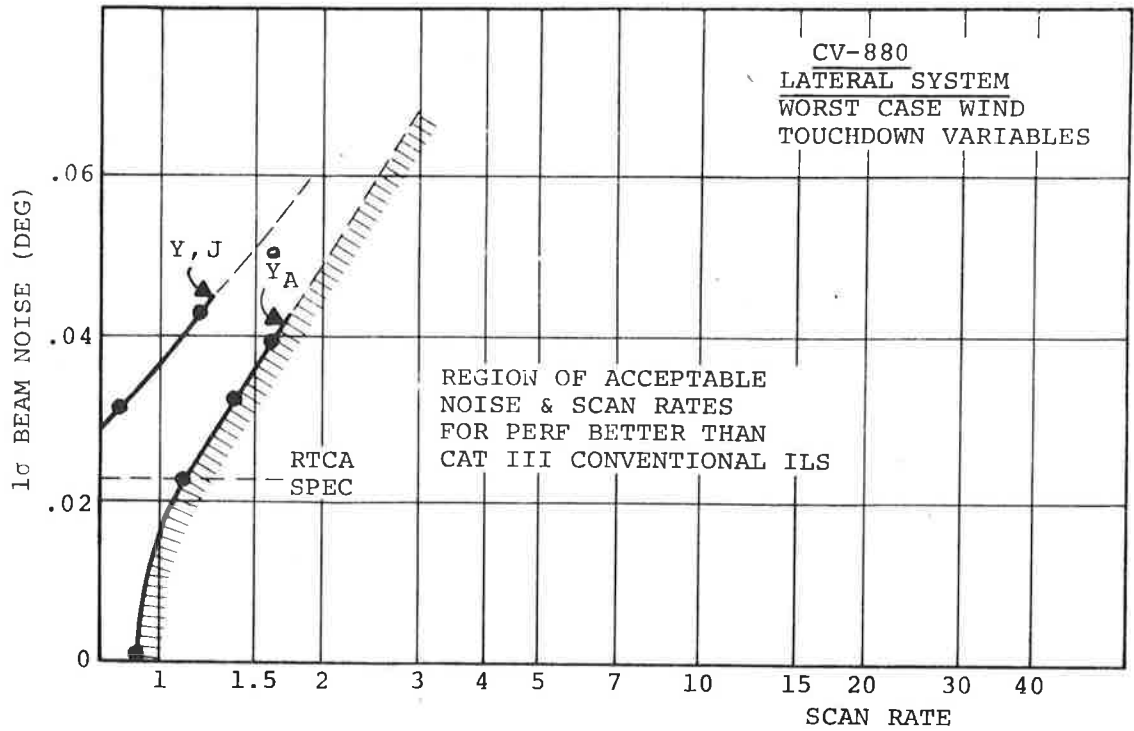


Figure 7-8(a). Scan Rate - Beam Noise Tradeoff For Performance Equivalent to Cat III Conv. ILS

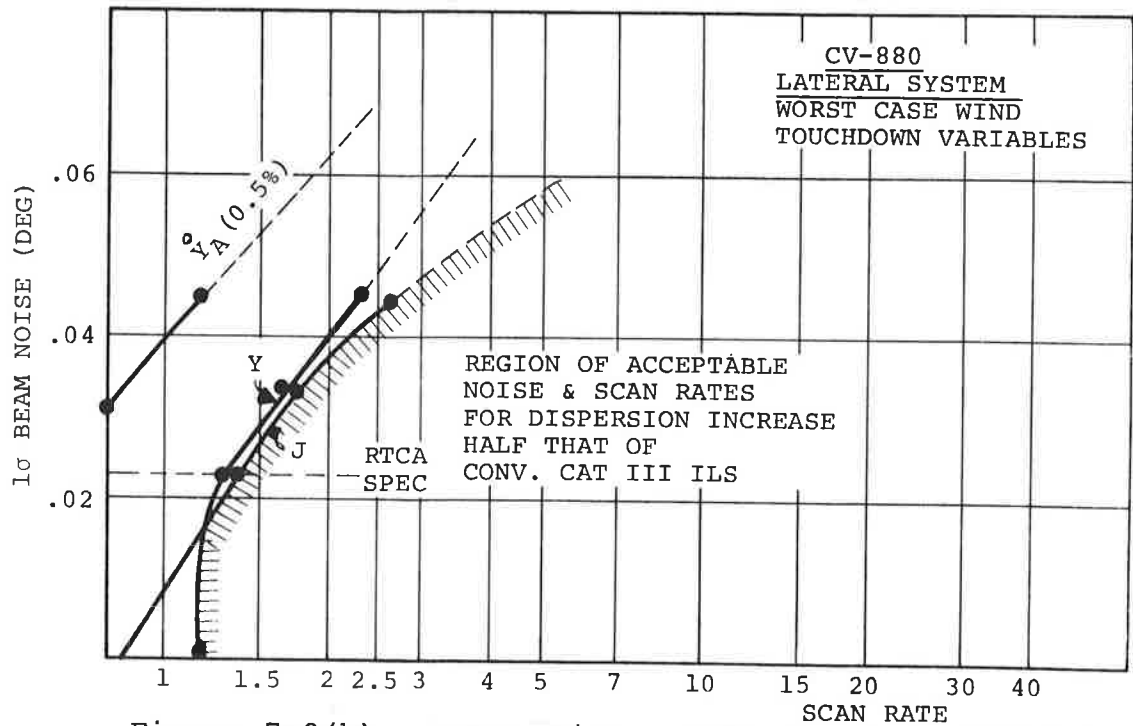


Figure 7-8(b). Beam Noise - Scan Rate Tradeoff For Dispersion Increases Half Those With Cat III Conventional ILS or 0.5%, Whichever is Greater

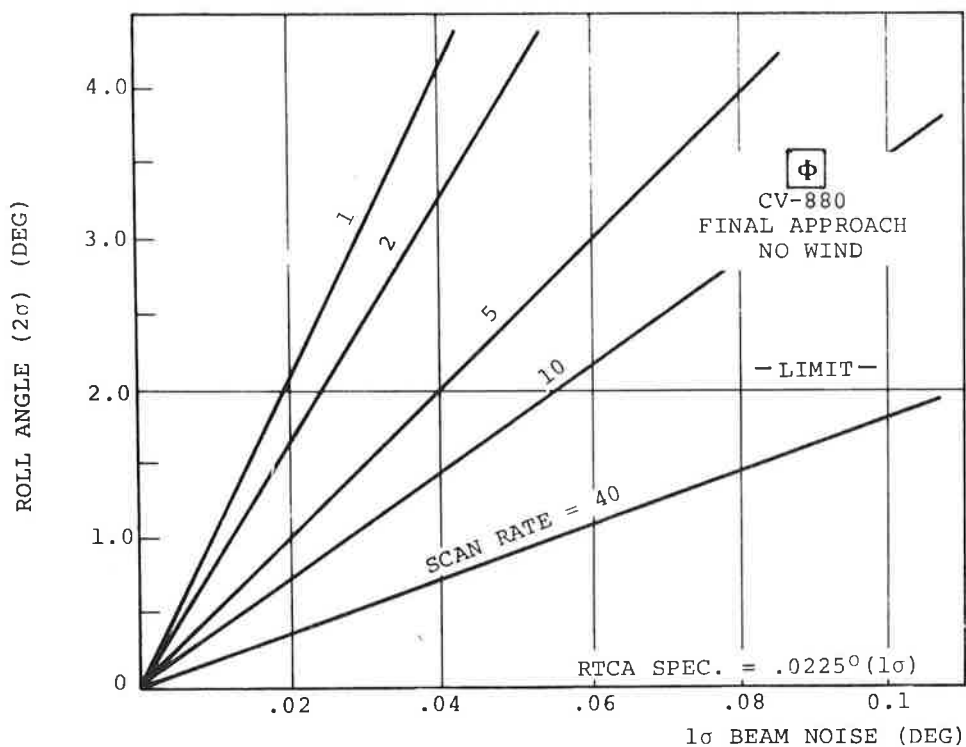


Figure 7-9.  $2\sigma$  Roll Angle ( $\phi$ ) Vs. Beam Noise  
Final Approach - No Wind

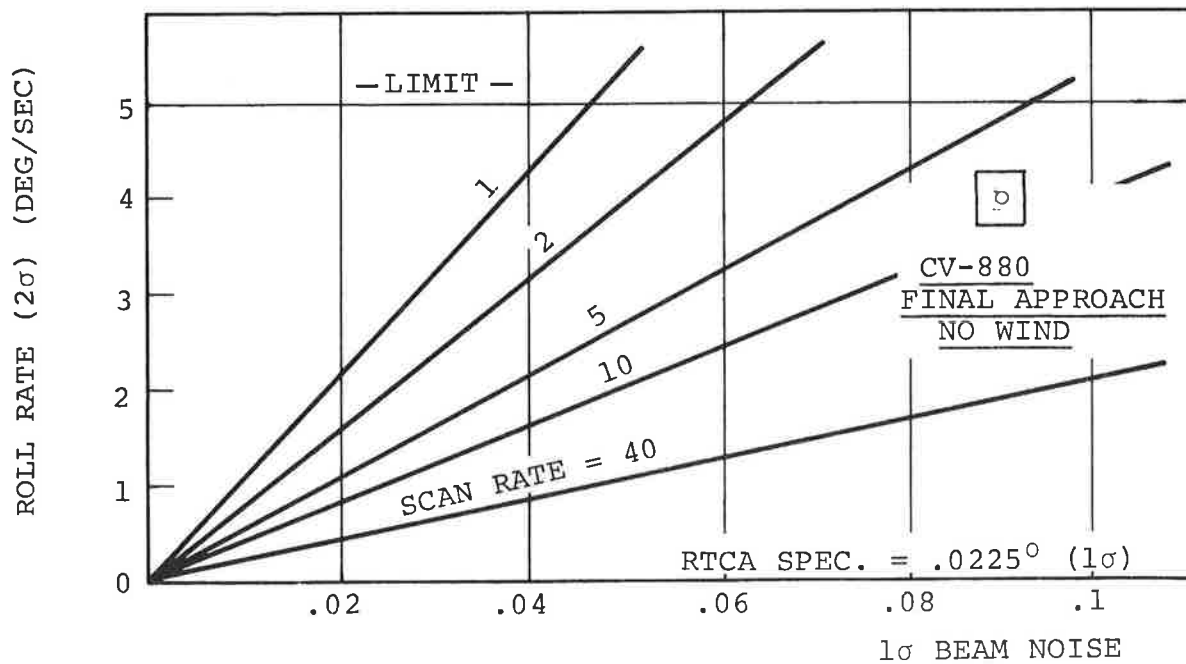


Figure 7-10.  $2\sigma$  Roll Rate ( $\rho$ ) Vs. Beam Noise  
Final Approach - No Wind



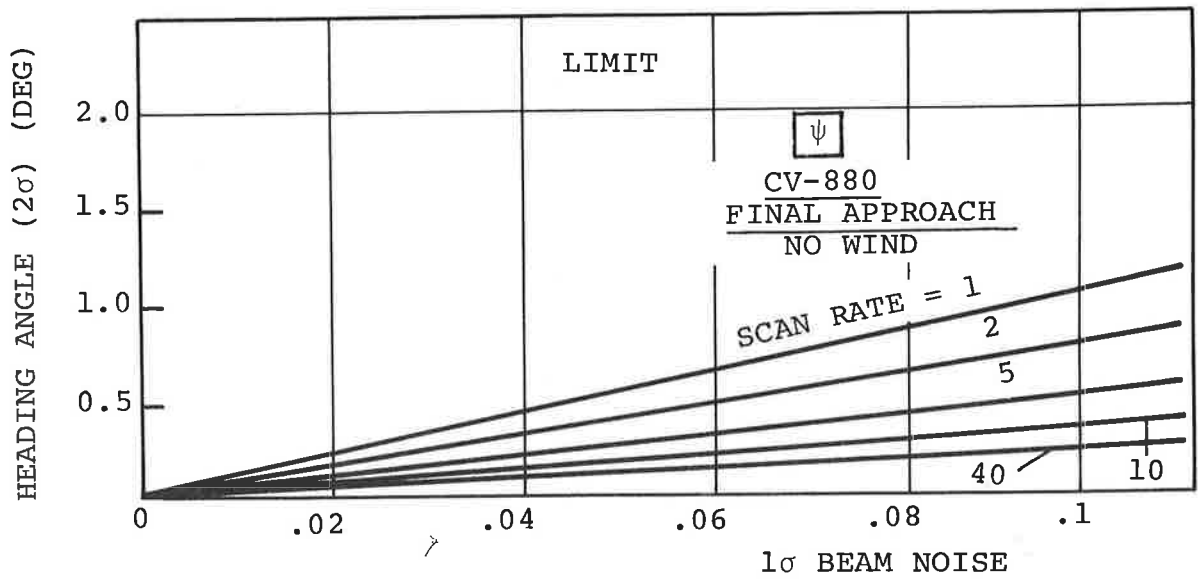


Figure 7-11. 2σ Heading Angle ( $\psi$ ) Vs. Beam Noise  
Final Approach - No Wind

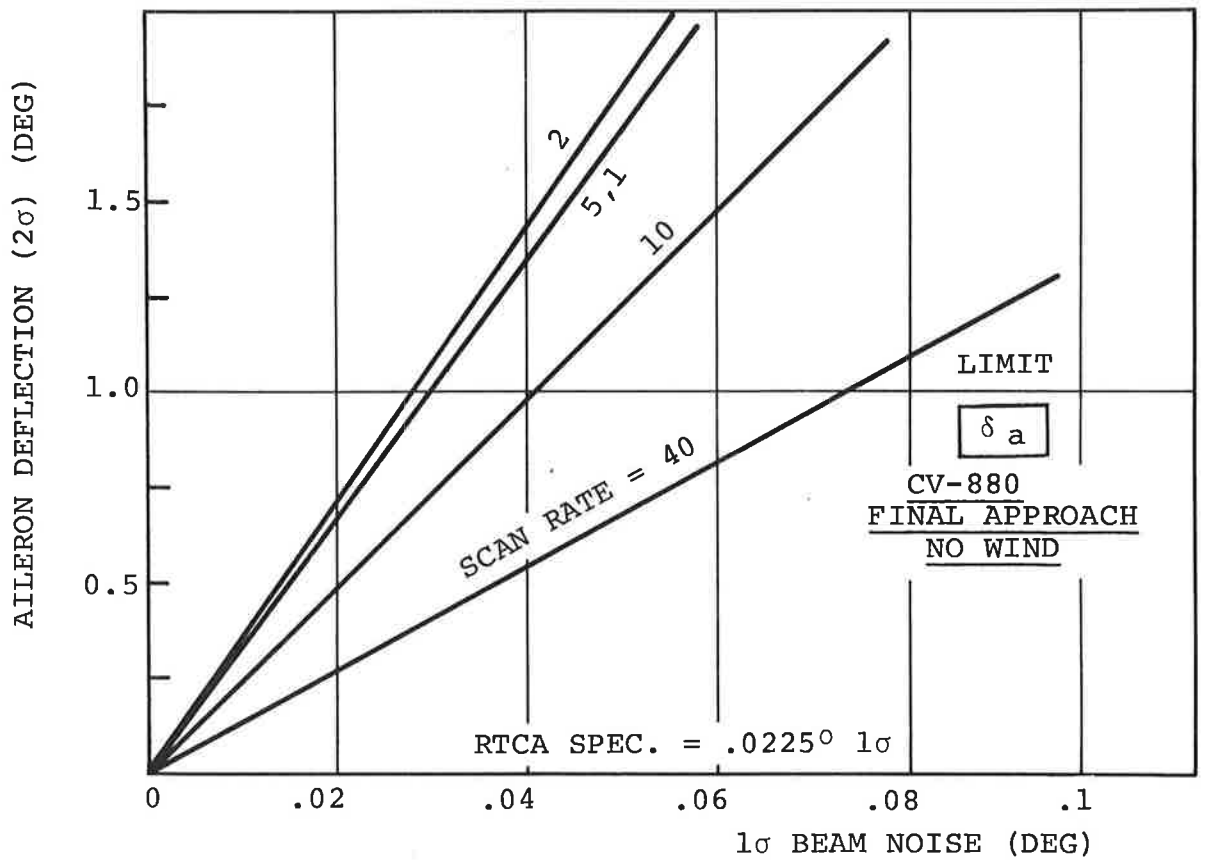


Figure 7-12. 2σ Aileron Activity ( $\delta_a$ ) Vs. Beam Noise  
Final Approach - No Wind

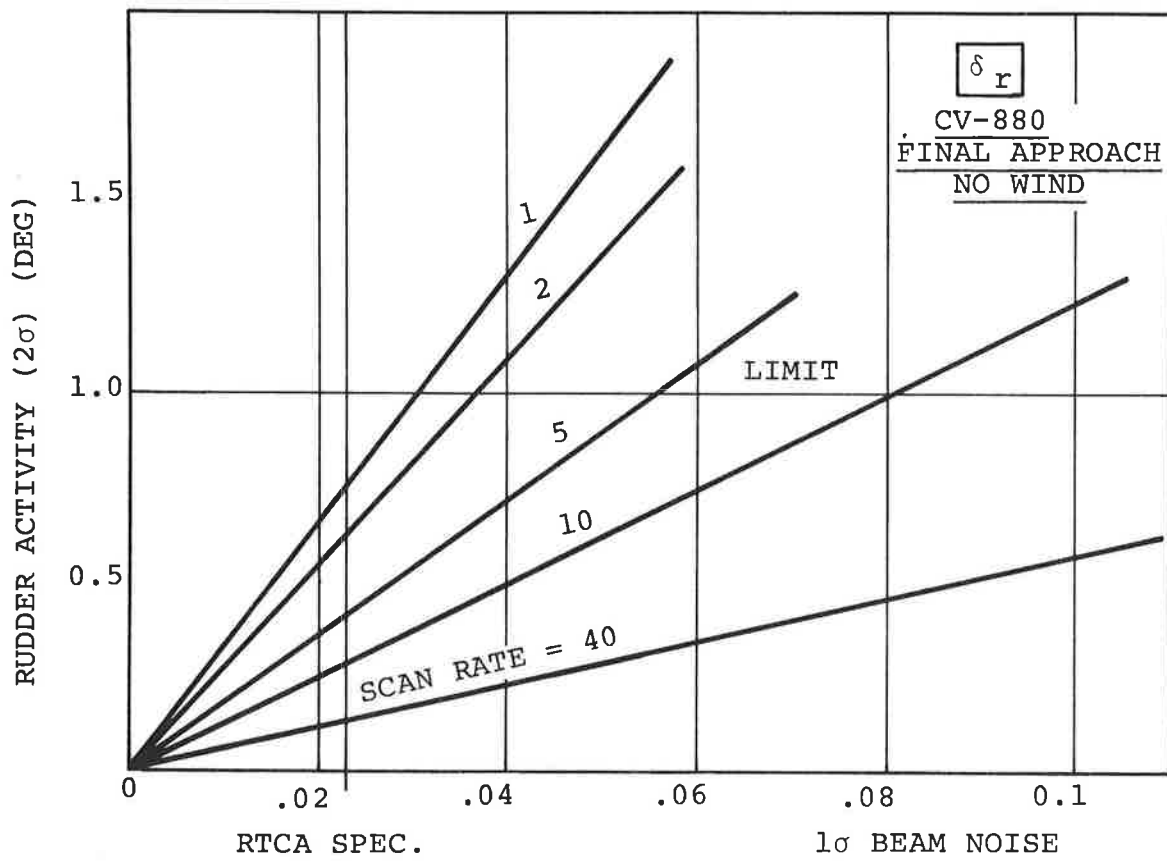


Figure 7-13.  $2\sigma$  Rudder Activity ( $\delta_a$ ) Vs. Beam Noise Final Approach - No Wind

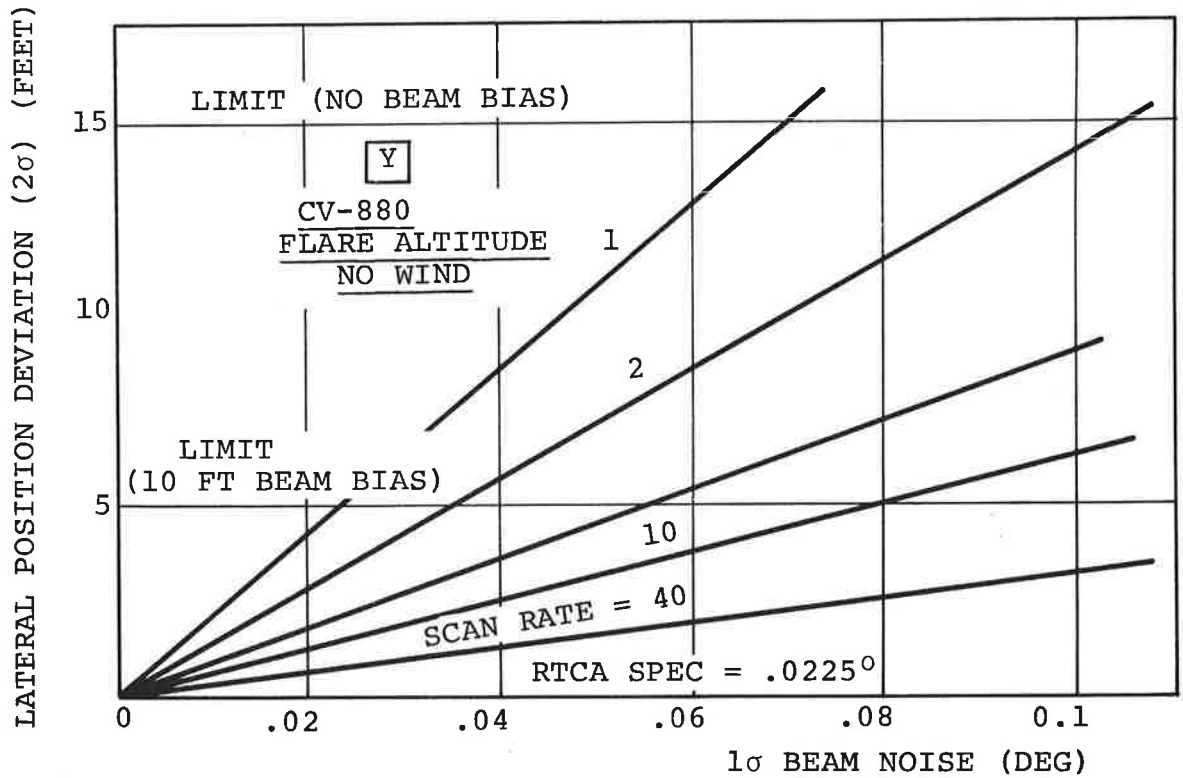


Figure 7-14. 2σ Lateral Position Deviation Vs. Beam Noise At Flare Altitude - No Wind

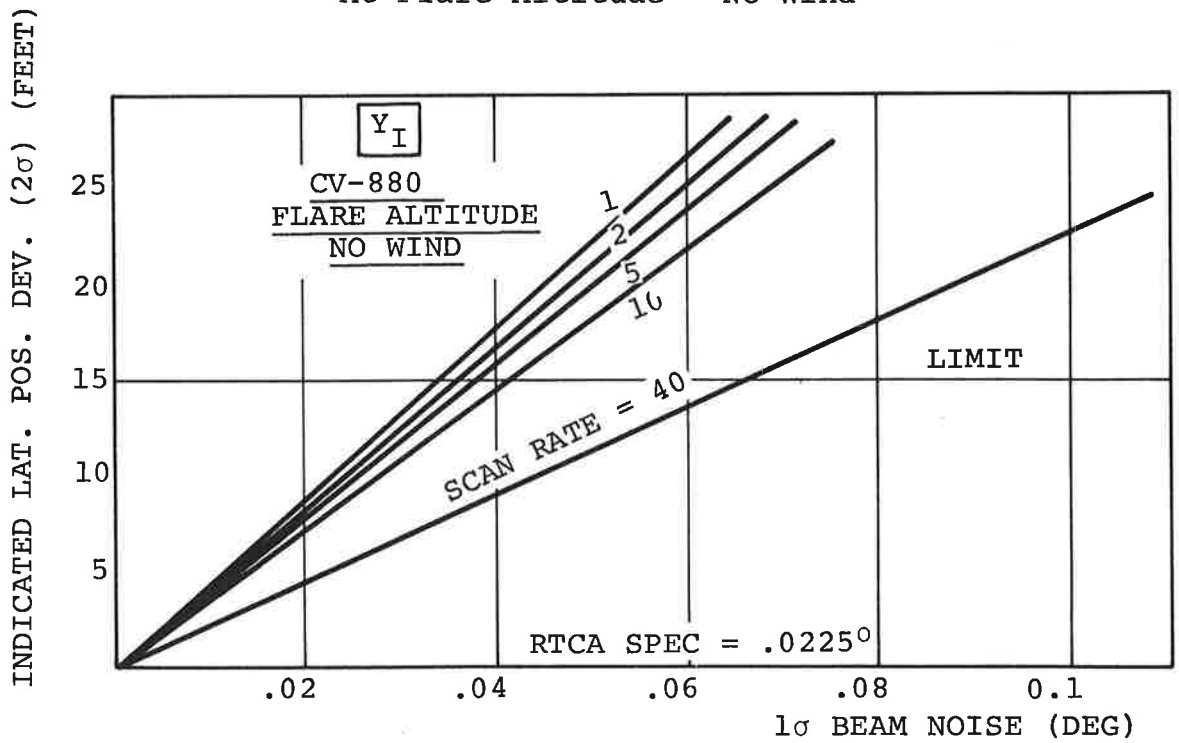


Figure 7-15. 2σ Indicated Lateral Pos. Dev. (Y<sub>I</sub>) Vs. Beam Noise - Flare Altitude - No Wind

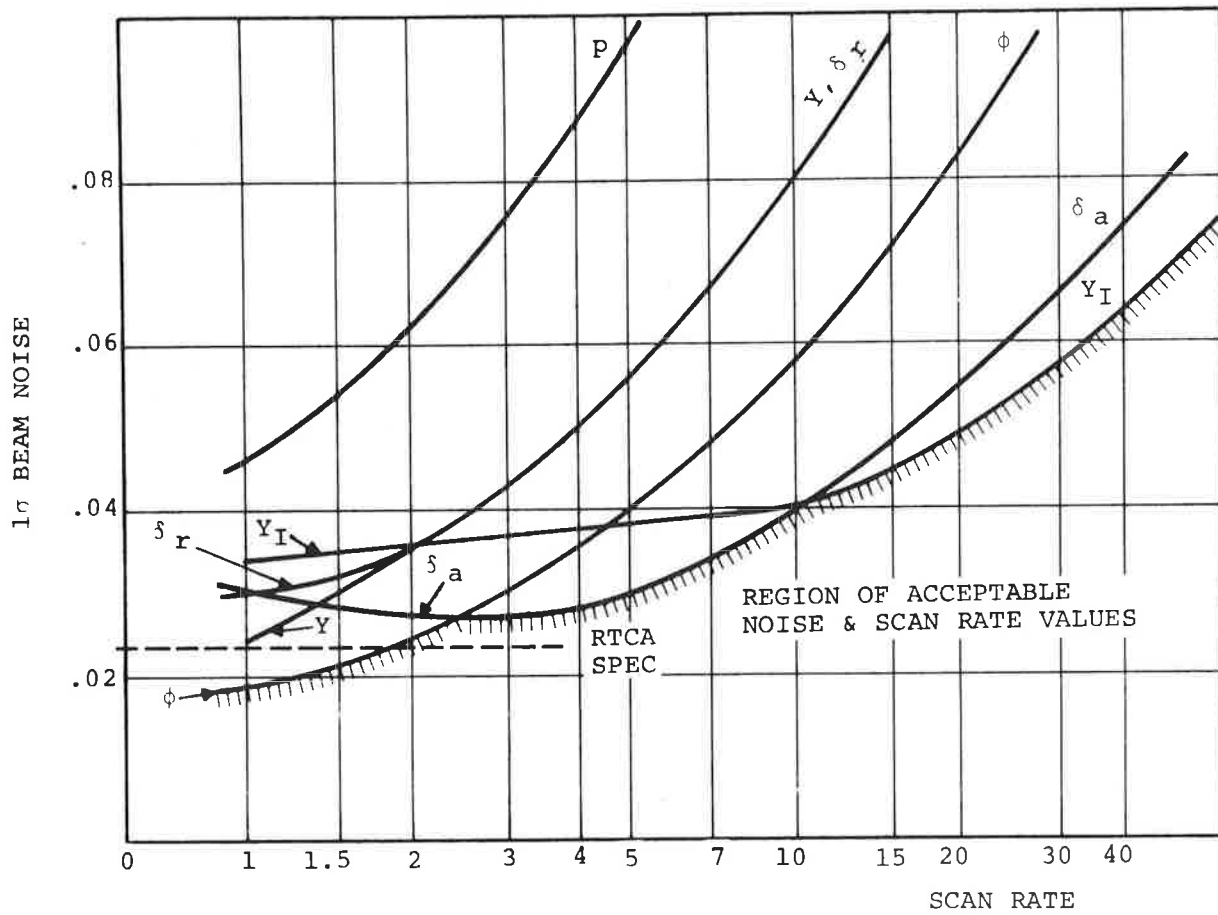


Figure 7-16(a). Beam Noise - Scan Rate Tradeoff  
 Pilot Acceptability Factors  
 CV-880 Lateral System  
 (Coupler Filter Time Constant = .025 Sec.)

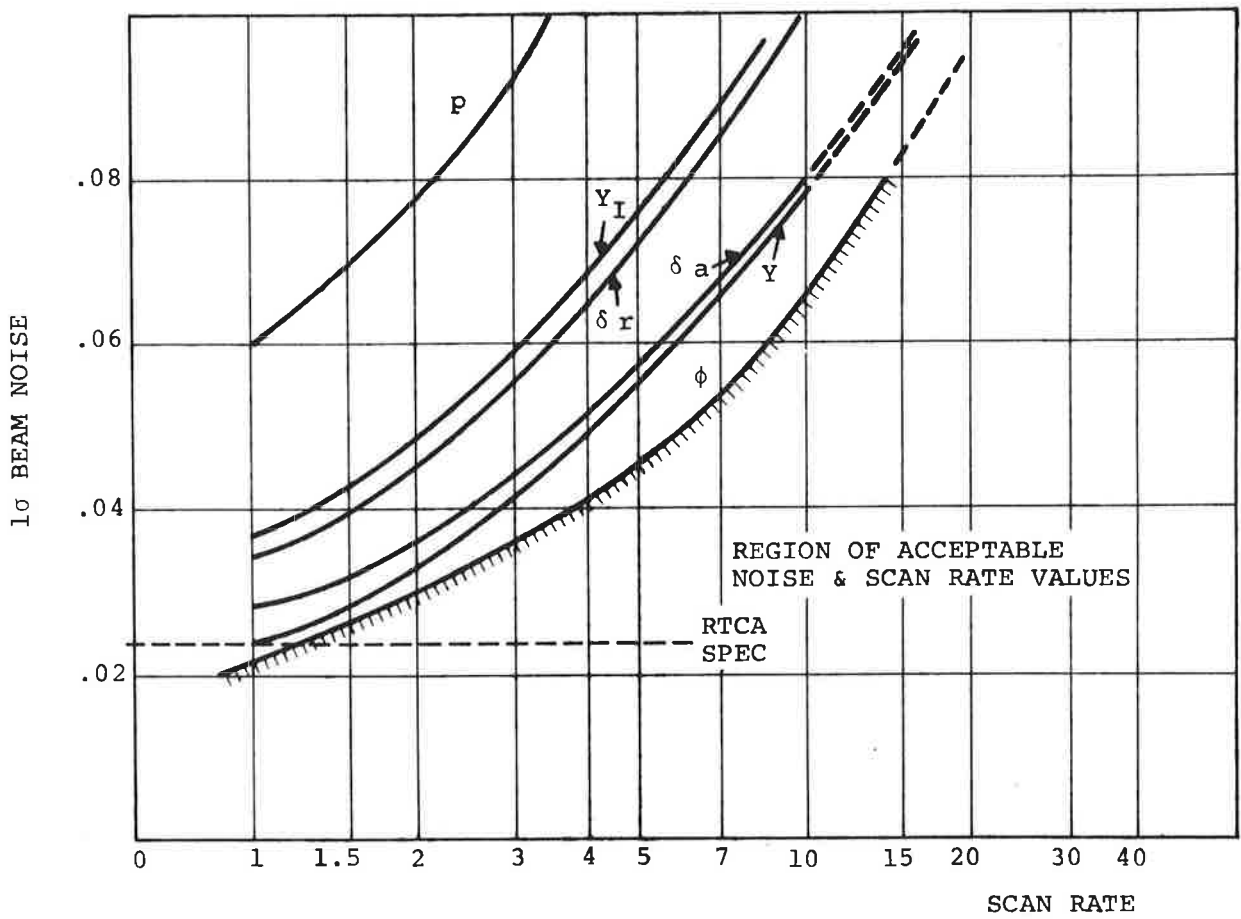


Figure 7-16(b). Beam Noise - Scan Rate Tradeoff  
 Pilot Acceptability Factors  
 CV-880 Lateral System  
 (Coupler Filter Time Constant = 0.5 Sec.)

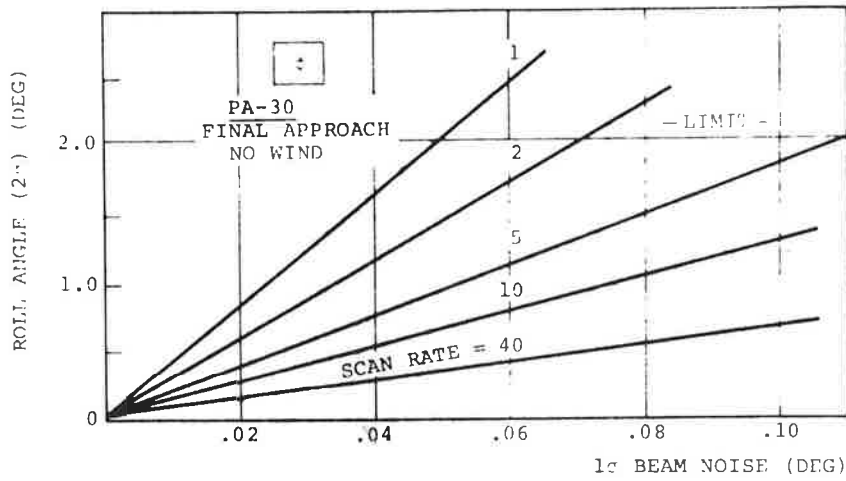


Figure 7-17.  $2\sigma$  Roll Angular Activity Vs. Beam Noise  
Final Approach - No Wind

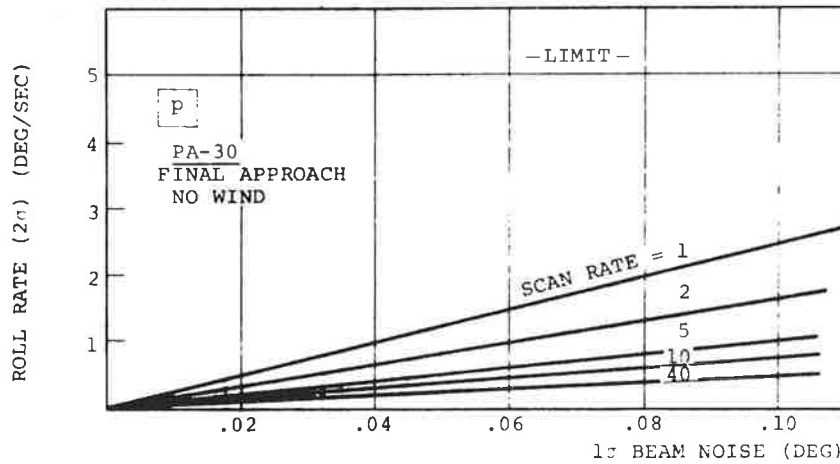


Figure 7-18.  $2\sigma$  Roll Rate Activity Vs. Beam Noise  
Final Approach - No Wind

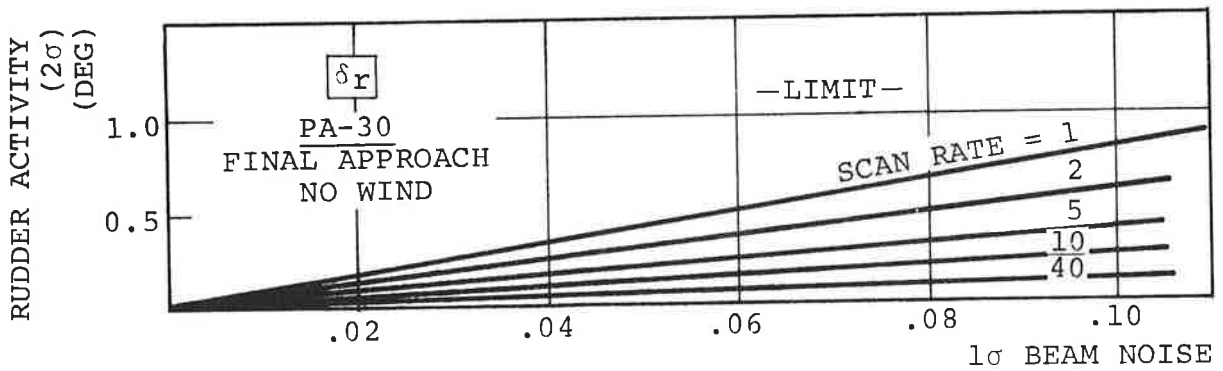


Figure 7-19.  $2\sigma$  Rudder Activity Vs. Beam Noise  
Final Approach - No Wind

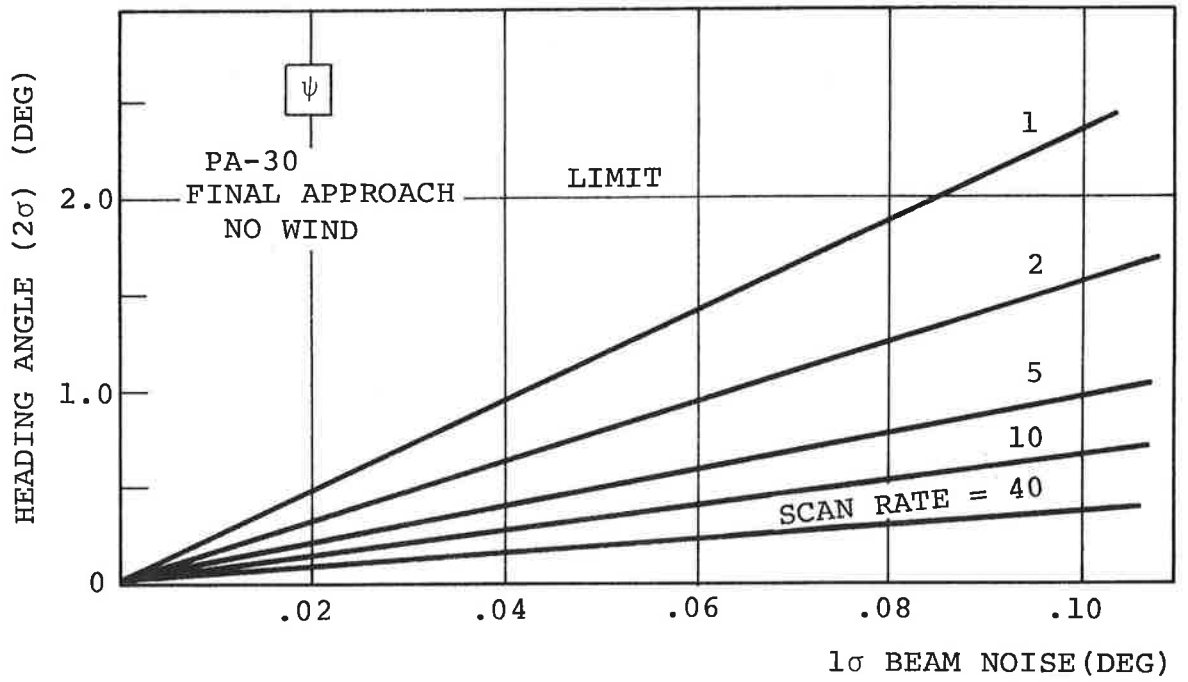


Figure 7-20.  $2\sigma$  Heading Angular Activity Vs. Beam Noise

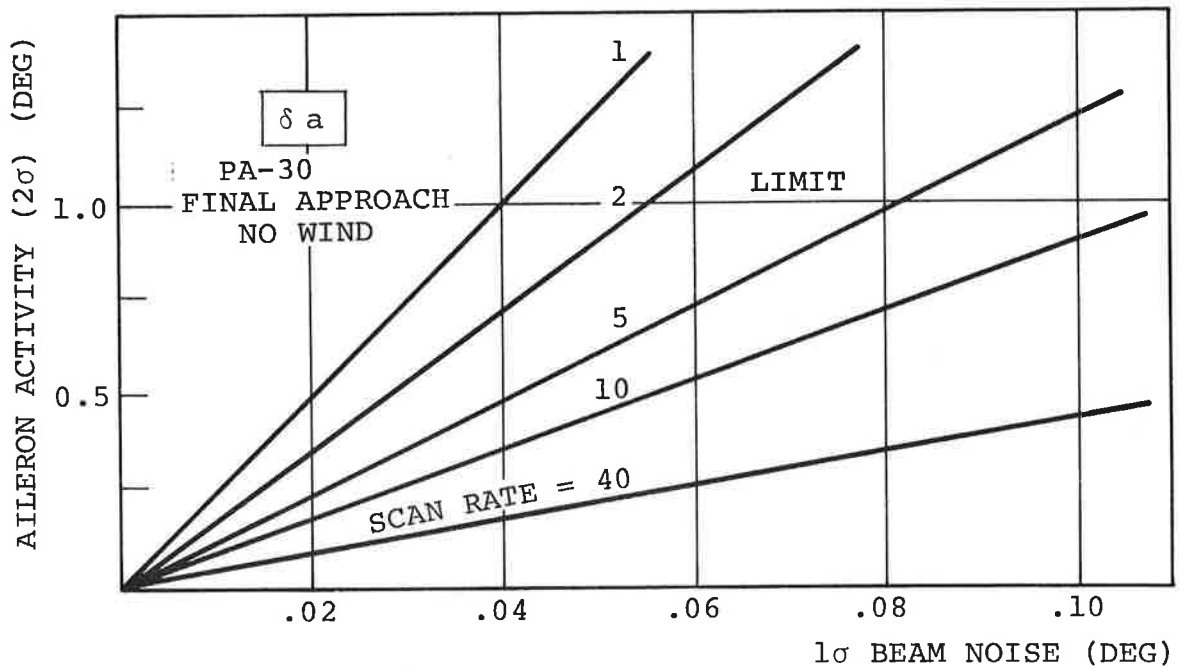


Figure 7-21.  $2\sigma$  Aileron Activity Vs. Beam Noise

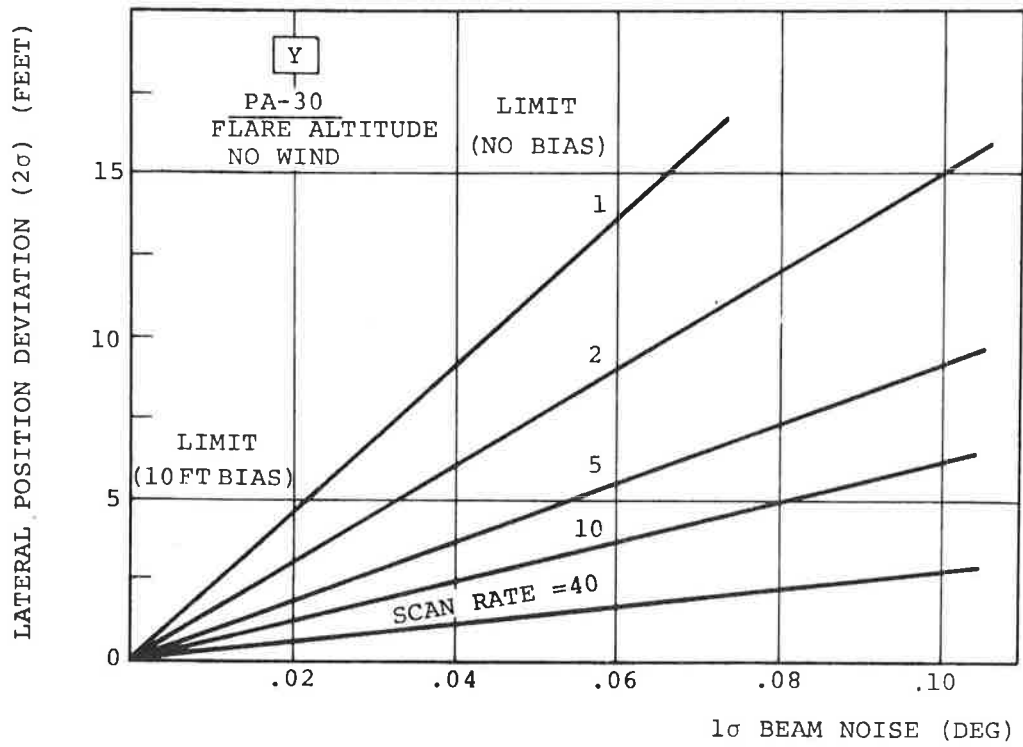


Figure 7-22.  $2\sigma$  Lateral Position Deviation Vs. Beam Noise

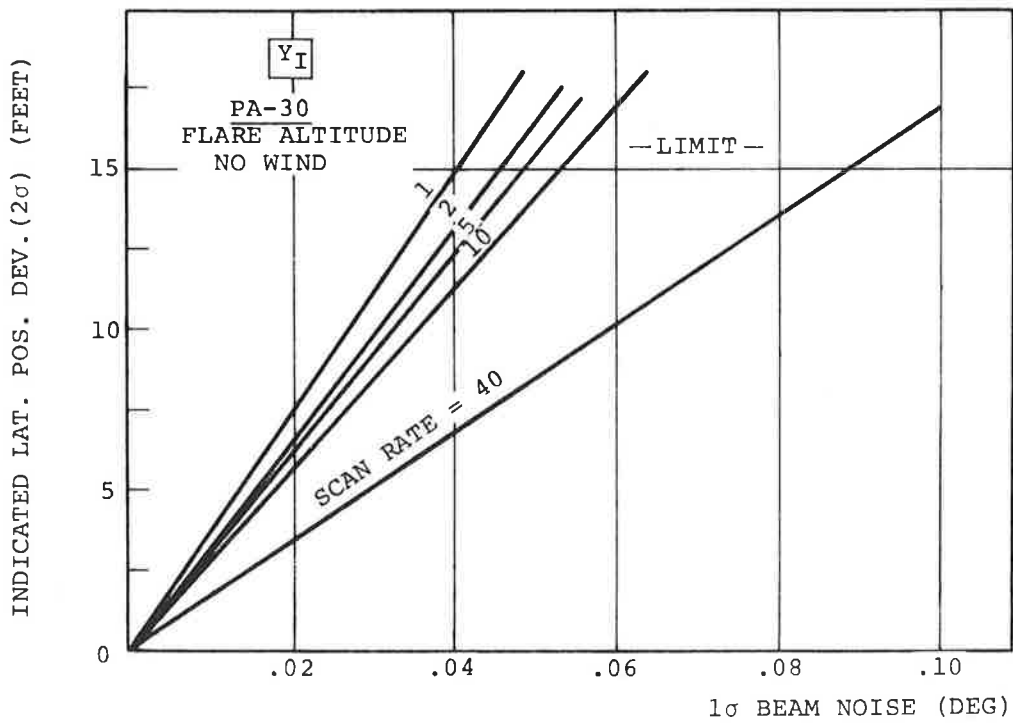


Figure 7-23.  $2\sigma$  Indicated Lat. Pos. Dev. Vs. Beam Noise



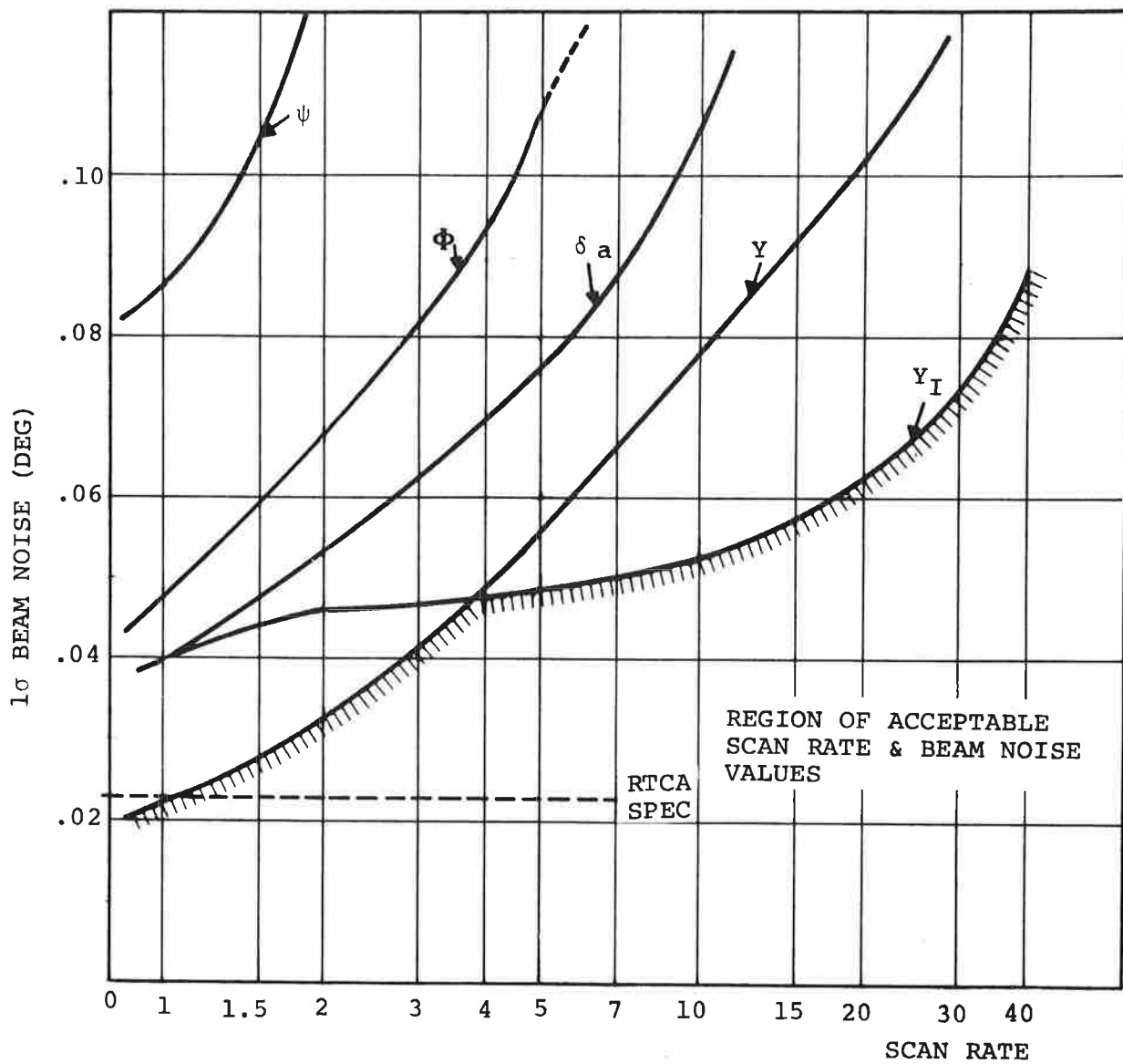


Figure 7-24(a). Beam Noise - Scan Rate Tradeoff  
 Pilot Acceptability Factors  
 PA-30 Lateral System  
 (Coupler Filter Time Constant = .025 Sec.)

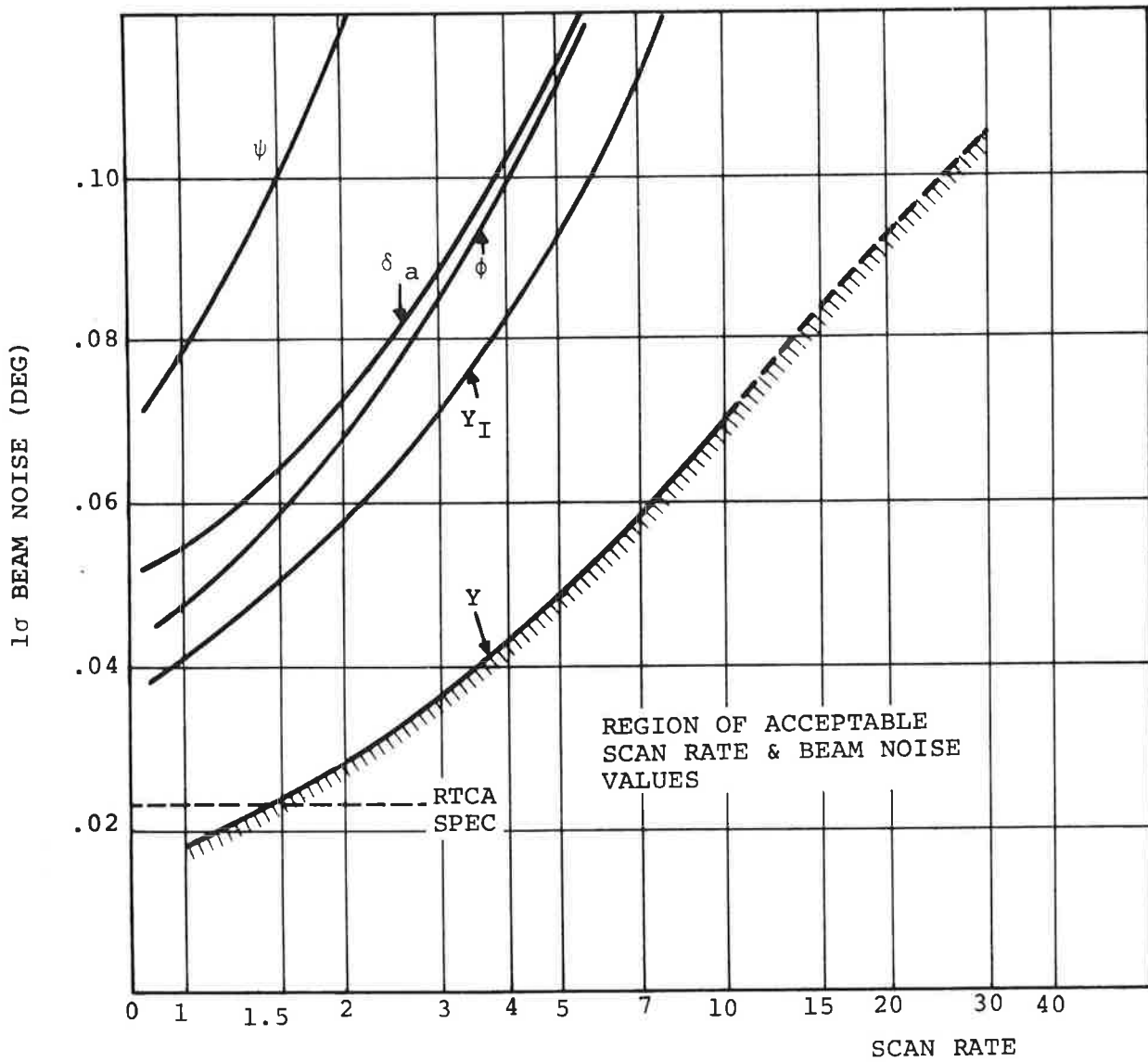


Figure 7-24(b). Beam Noise - Scan Rate Tradeoff  
 Pilot Acceptability Factors  
 PA-30 Lateral System  
 (Coupler Time Constant: 0.5 Sec.)

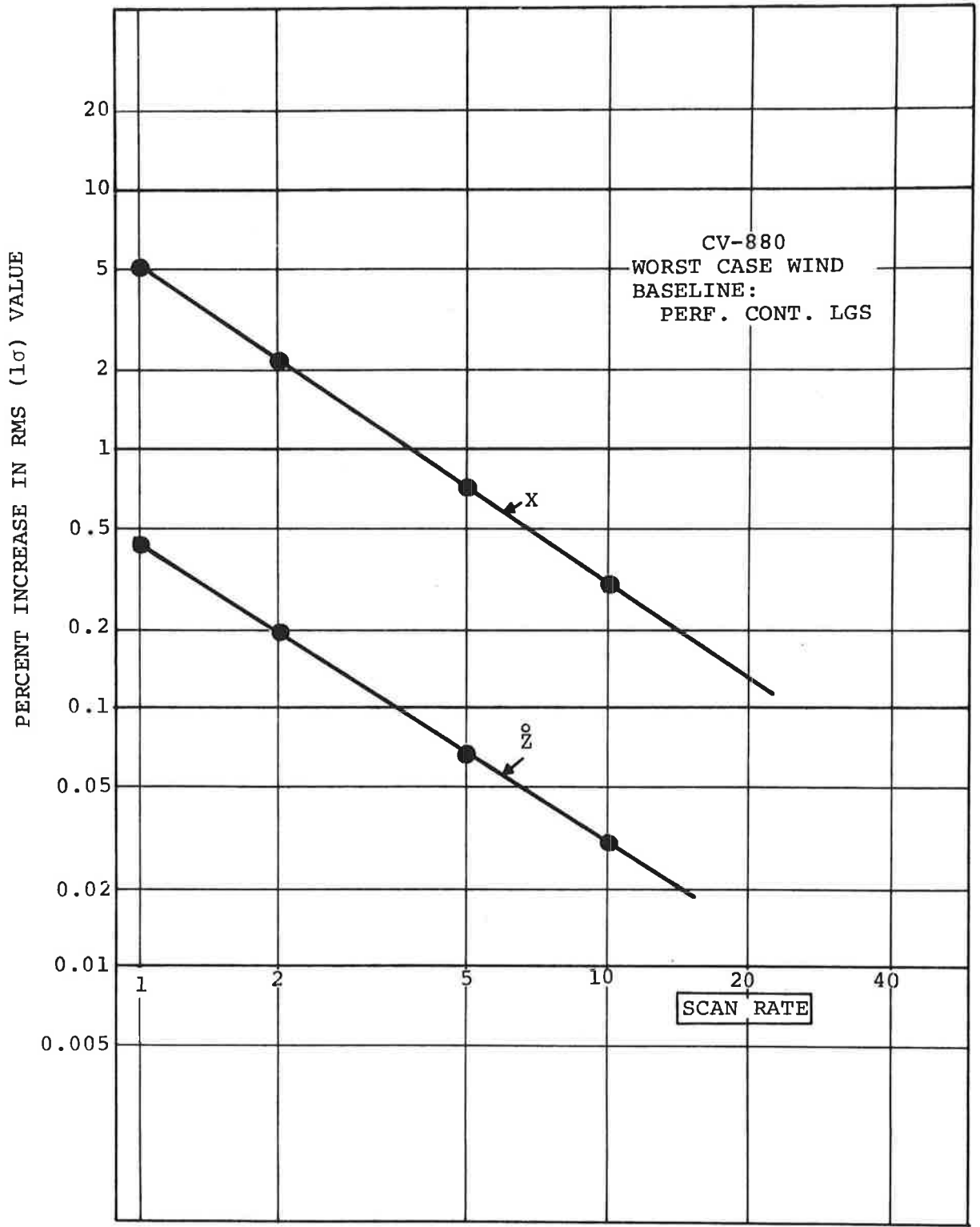


Figure 7-25. Relative Effects of Scan Rate on Longitudinal Touchdown Variables - Worst Case Wind - No Beam Noise

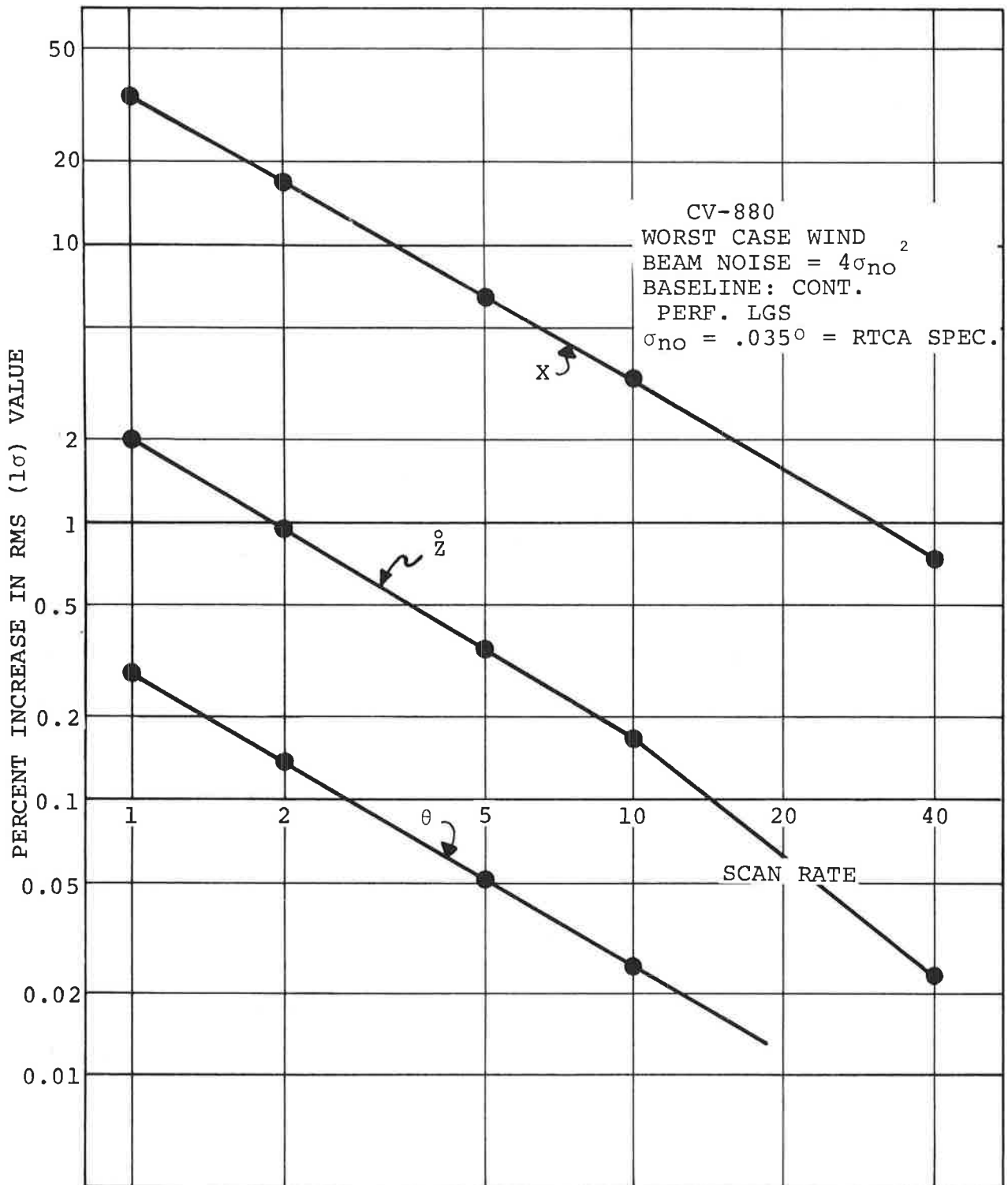


Figure 7-26. Relative Effects of Scan Rate on Longitudinal Touchdown Variables - Worst Case Wind & Beam Noise

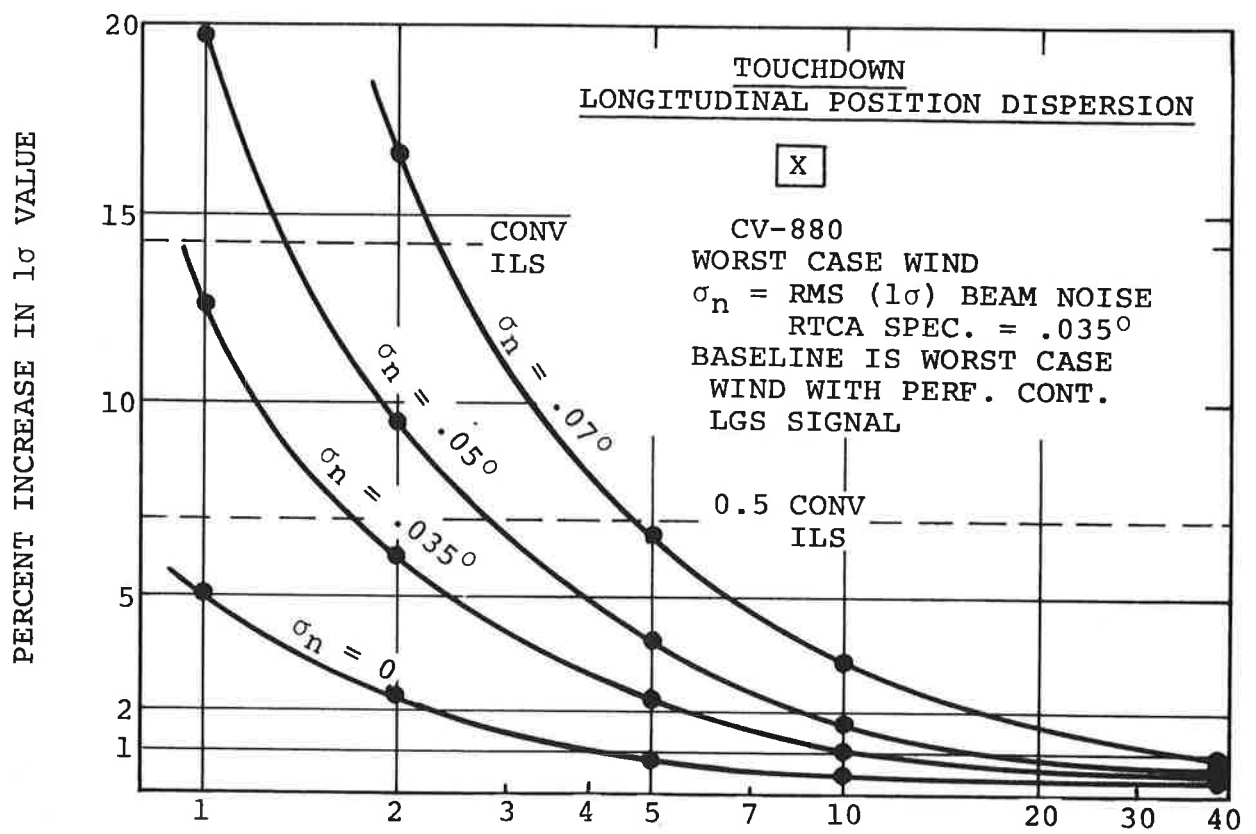


Figure 7-27(a). Longitudinal Position Dispersion Vs. Scan Rate

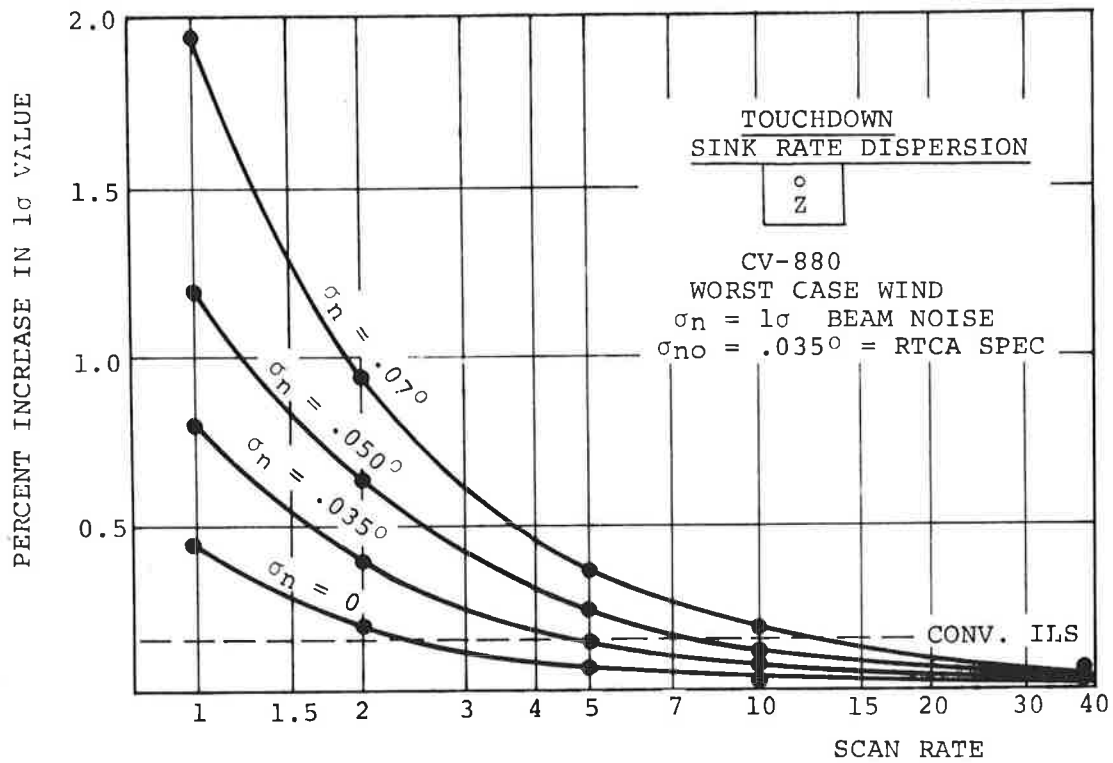


Figure 7-27(b). Sink Rate Dispersion Vs. Scan Rate

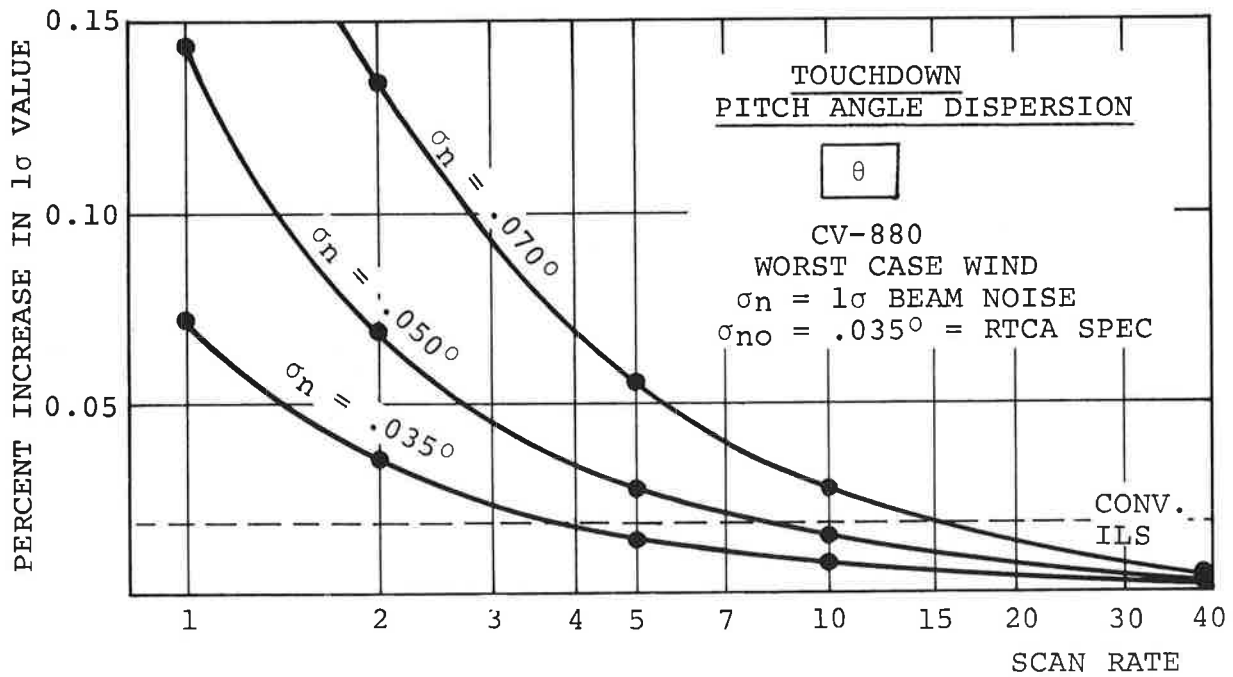


Figure 7-27(c). Pitch Angle Dispersion Vs. Scan Rate

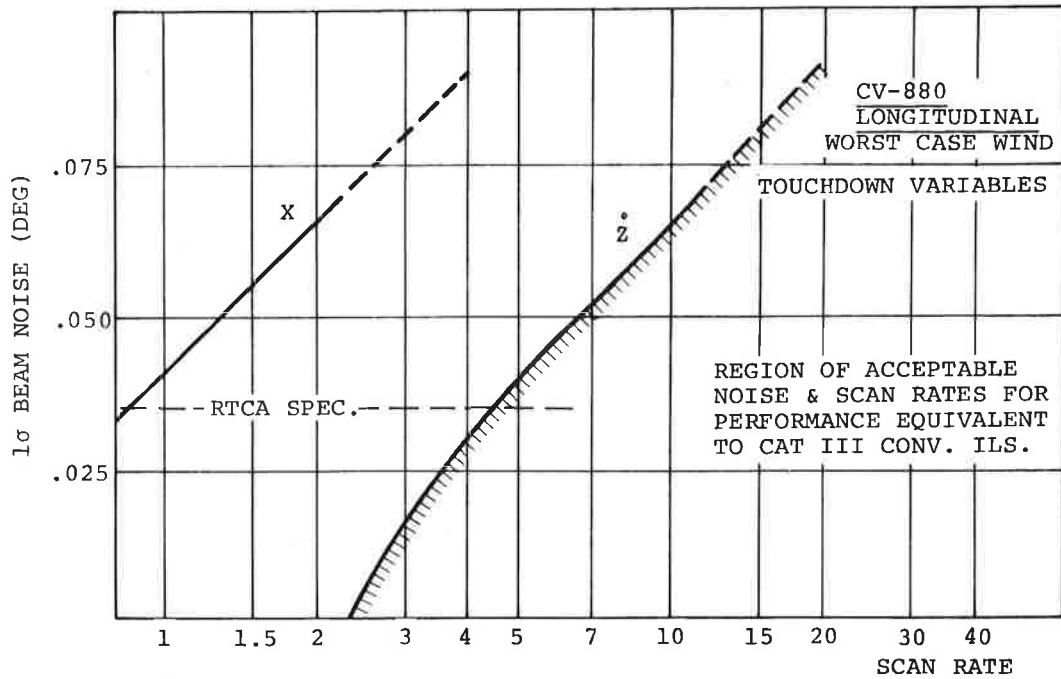


Figure 7-28(a). Scan Rate - Beam Noise Tradeoff For Performance Equivalent To Cat III Conv. ILS

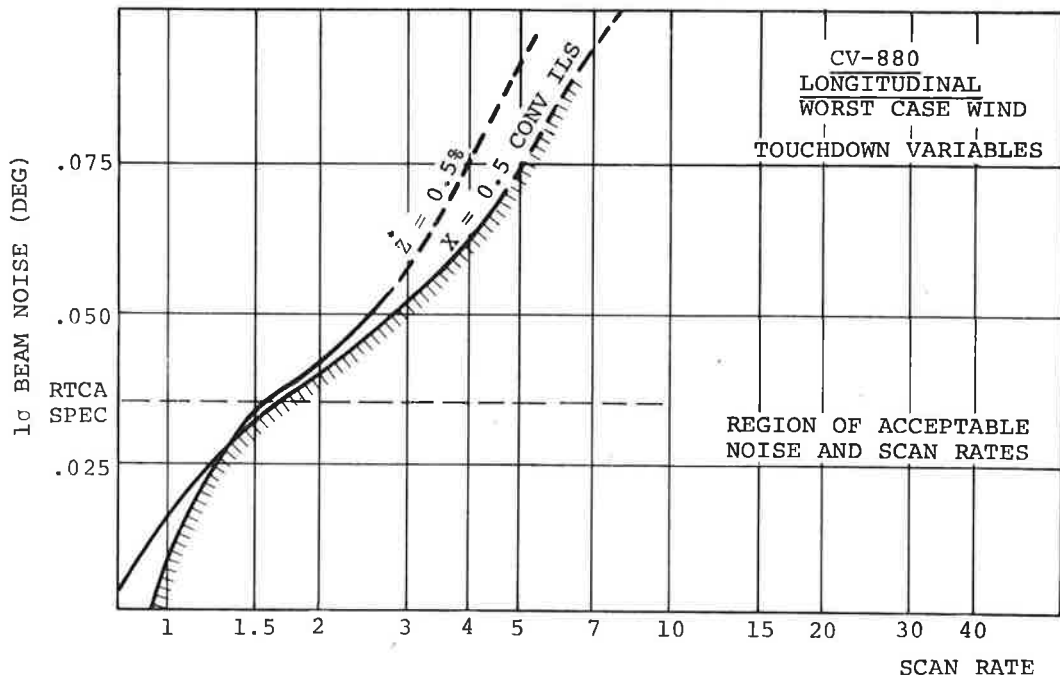


Figure 7-28(b). Scan Rate - Beam Noise Tradeoff For Long Pos. Dispersion Increase Half That With Conv. ILS and Sink Rate Disp. Increase 0.5%

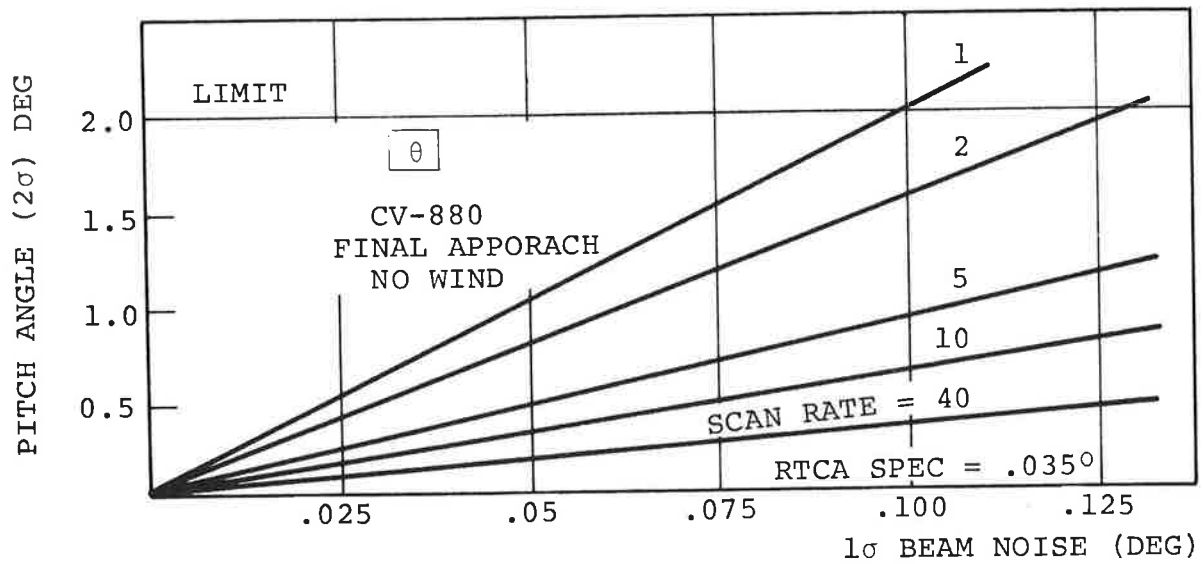


Figure 7-29.  $2\sigma$  Pitch Angular Activity Vs. Beam Noise  
Final Approach - No Wind

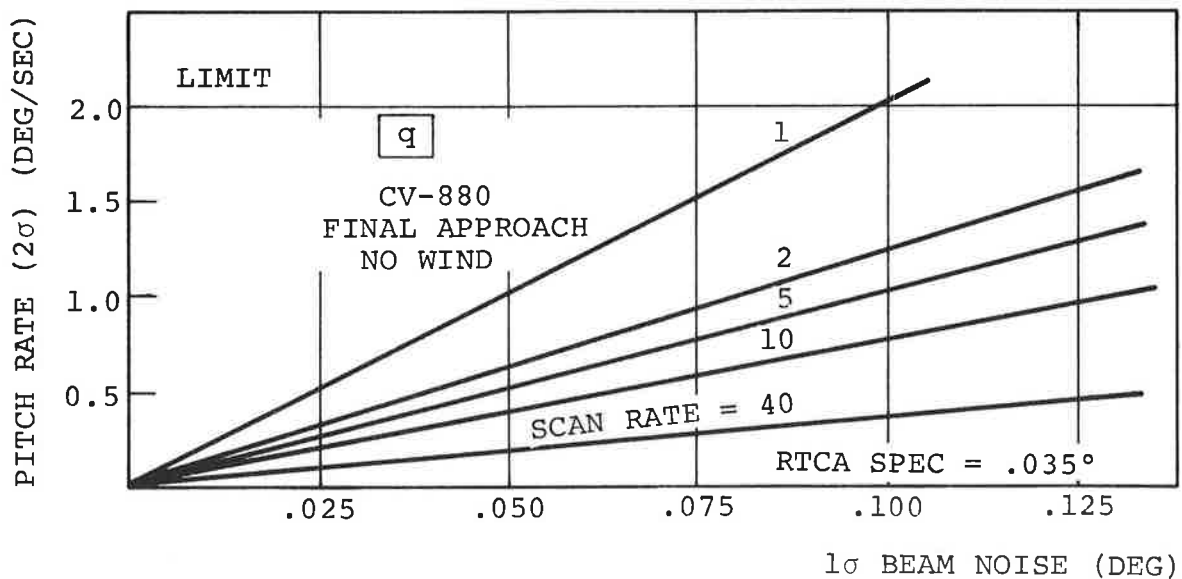


Figure 7-30.  $2\sigma$  Pitch Rate Activity Vs. Beam Noise  
Final Approach - No Wind



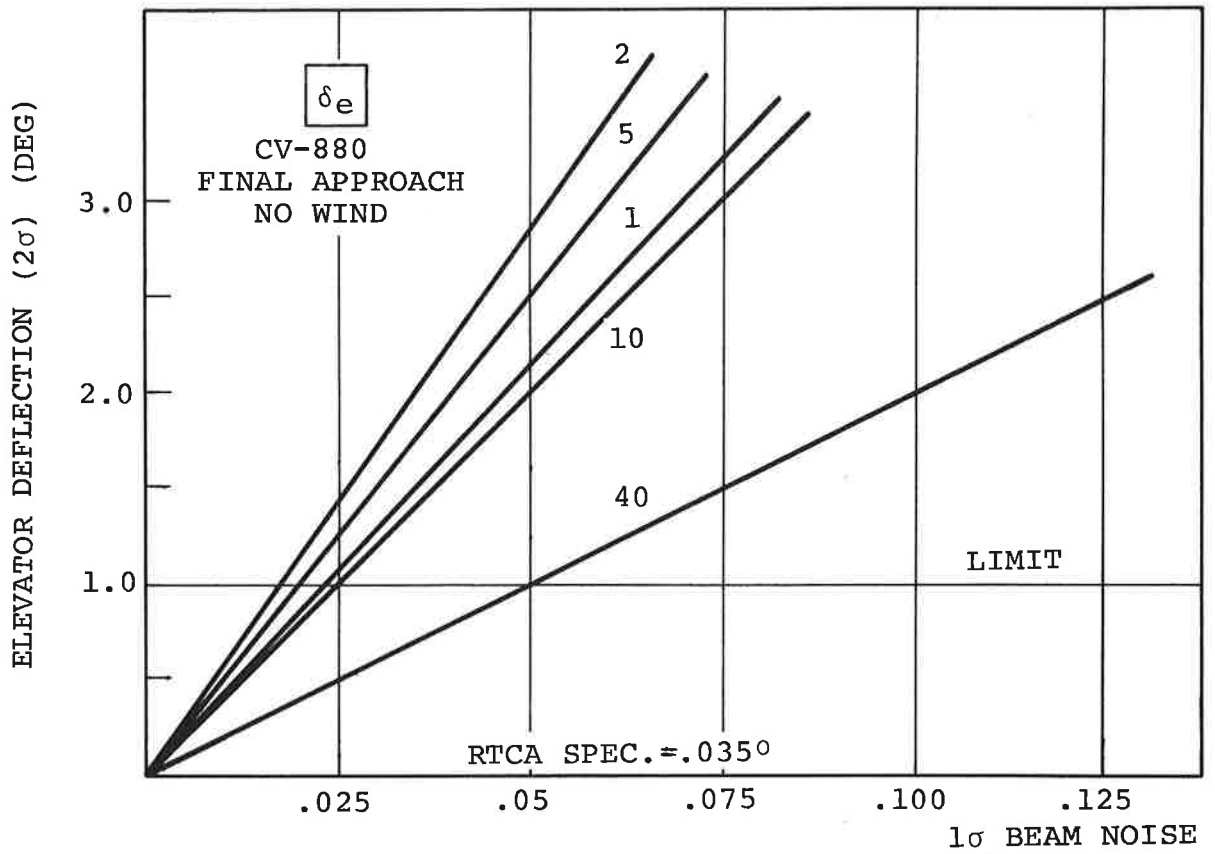


Figure 7-31.  $2\sigma$  Elevator Activity ( $\delta_a$ ) Vs. Beam Noise  
Final Approach - No Wind

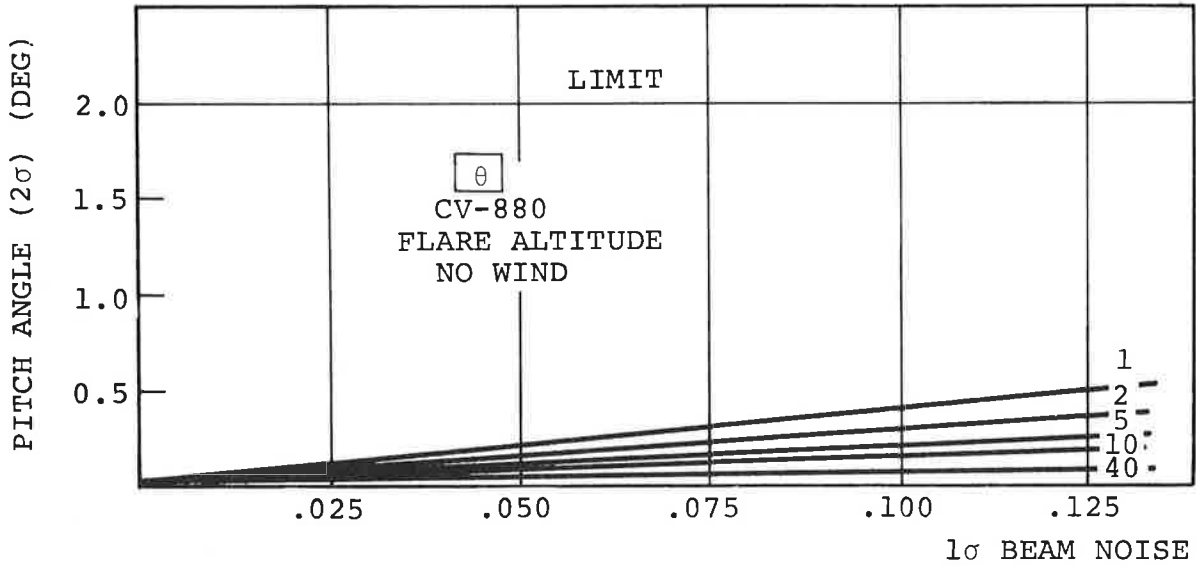


Figure 7-32. 2σ Pitch Angle Dev. Vs. Beam Noise  
Flare Altitude - No Wind

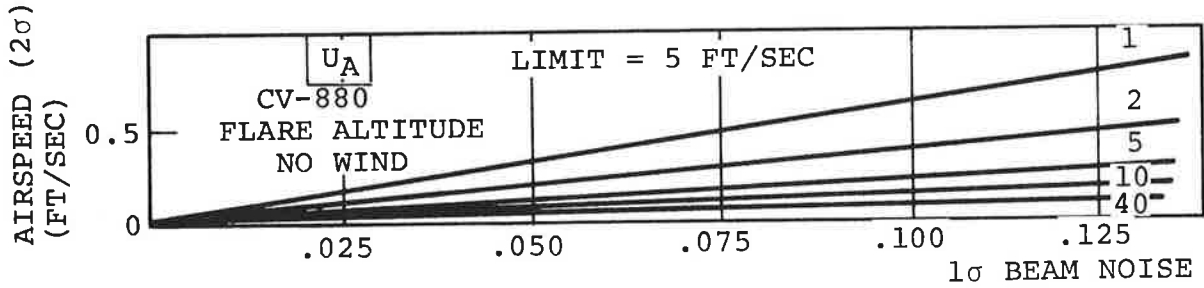


Figure 7-33. 2σ Airspeed Deviation Vs. Beam Noise  
Flare Altitude - No Wind

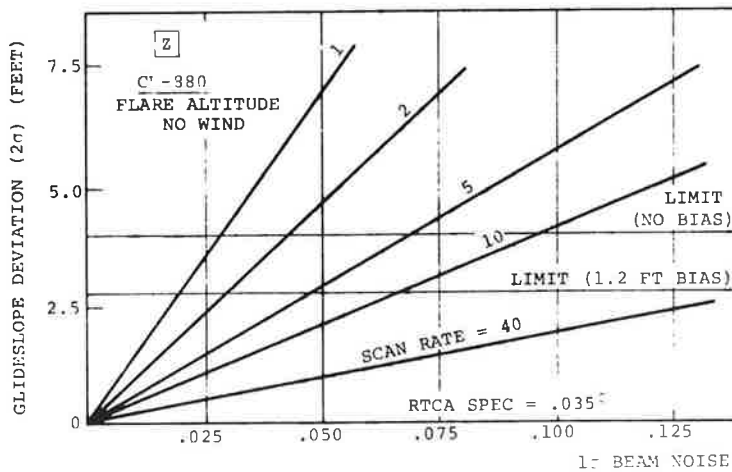


Figure 7-34. 2σ Glideslope Deviation (Z) Vs. Beam Noise  
Flare Altitude - No Wind

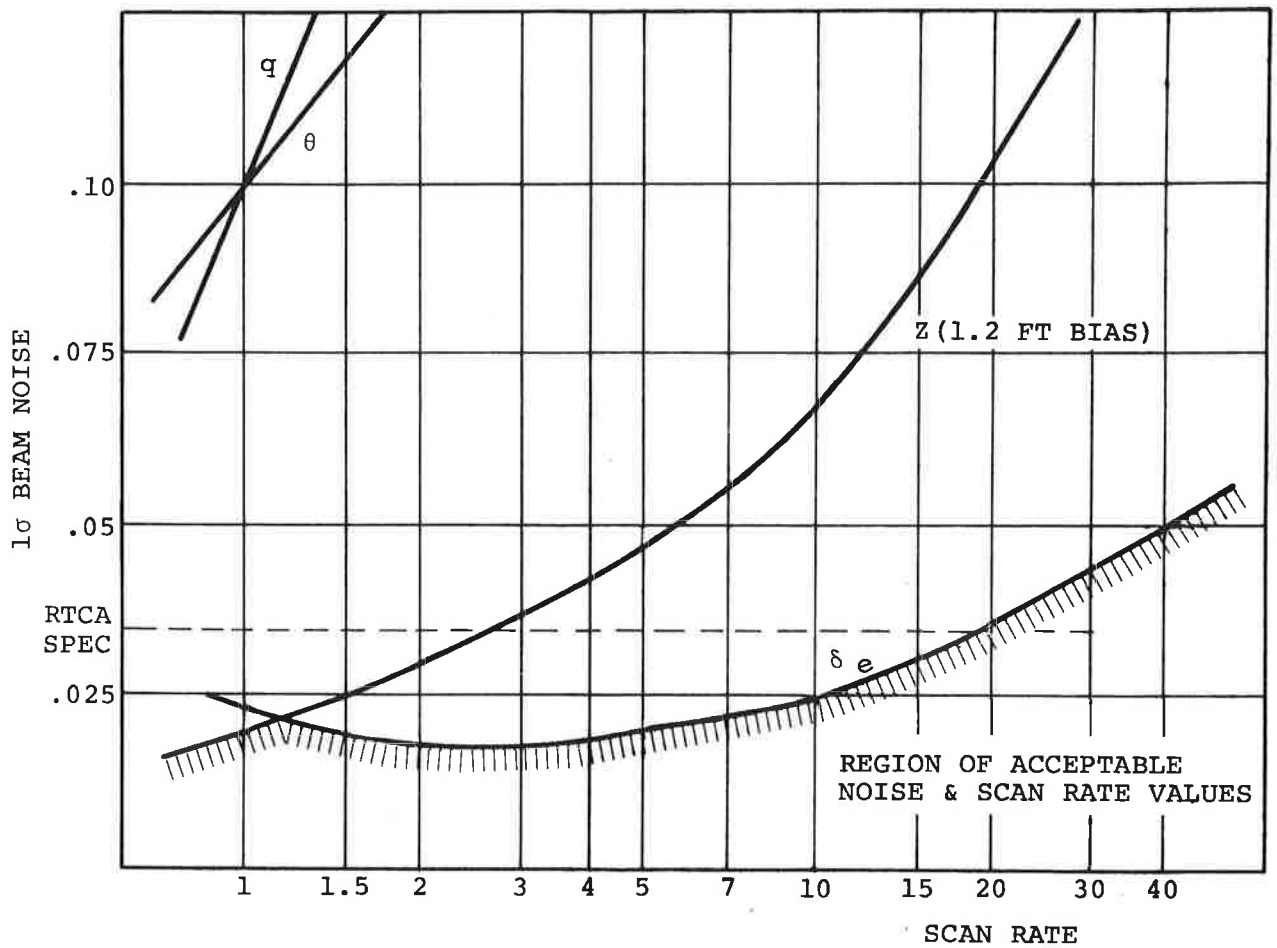


Figure 7-35(a). Beam Noise - Scan Rate Tradeoff  
 Pilot Acceptability Factors  
 CV-880 Longitudinal System  
 (Coupler Filter Time Constant: 0.025 Sec.)

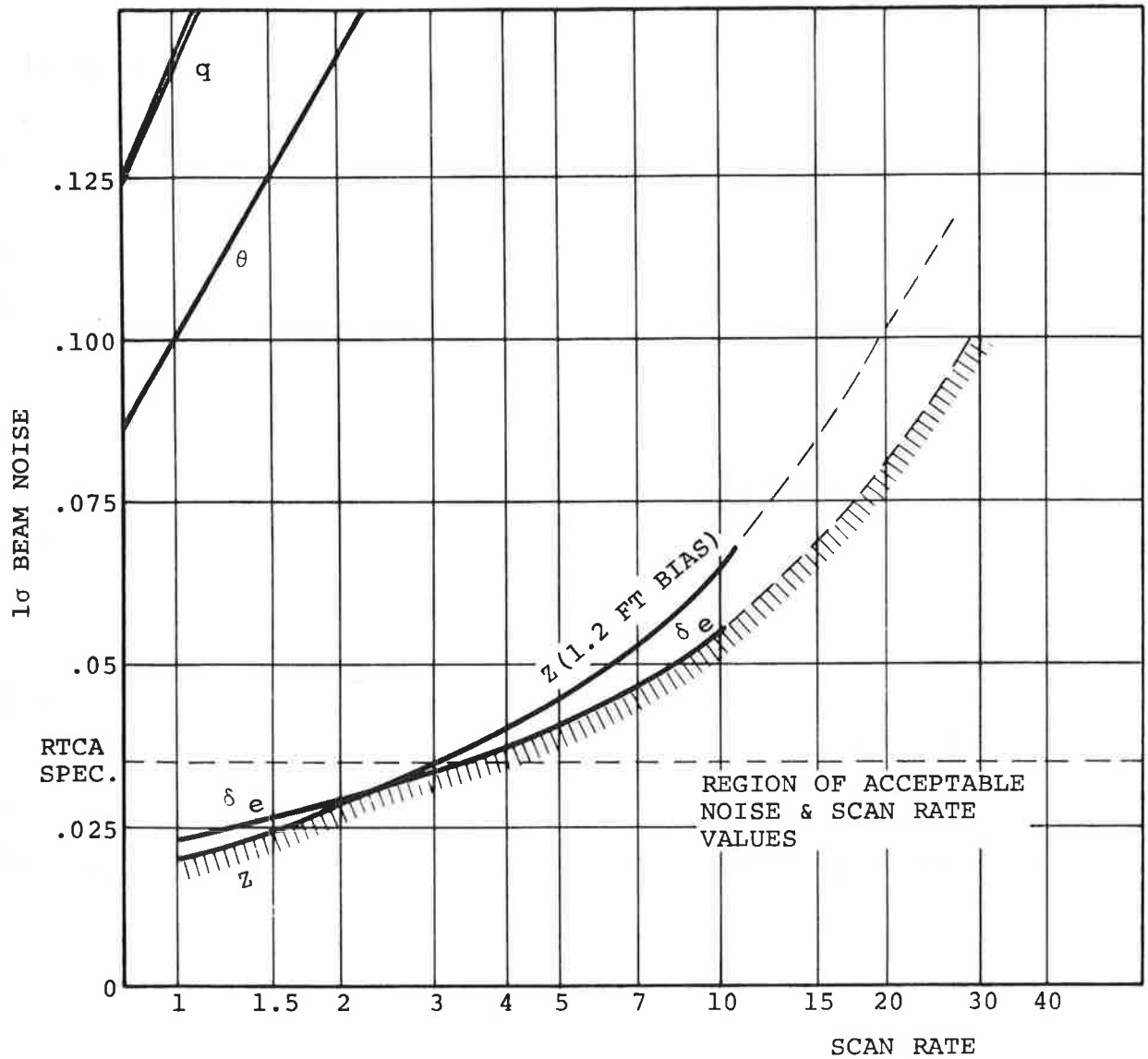


Figure 7-35(b). Beam Noise - Scan Rate Tradeoff  
 Pilot Acceptability Factors  
 CV-880 Longitudinal System  
 (Coupler Filter Time Constant: 0.5 Sec.)

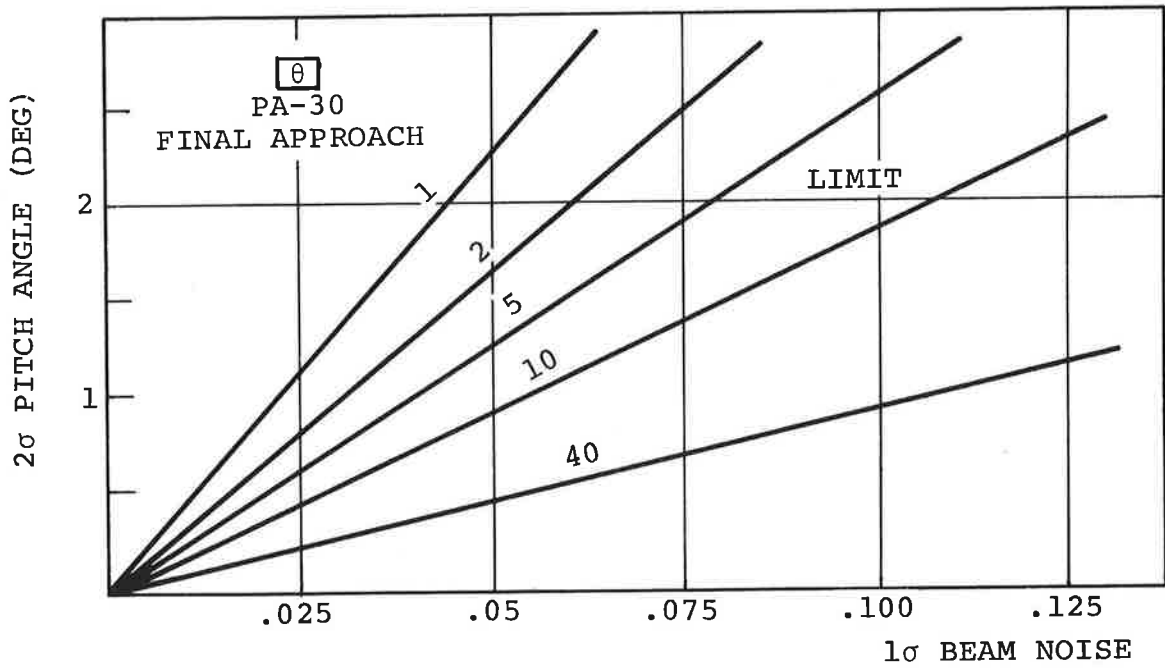


Figure 7-36.  $2\sigma$  Pitch Angular Activity Vs. Beam Noise

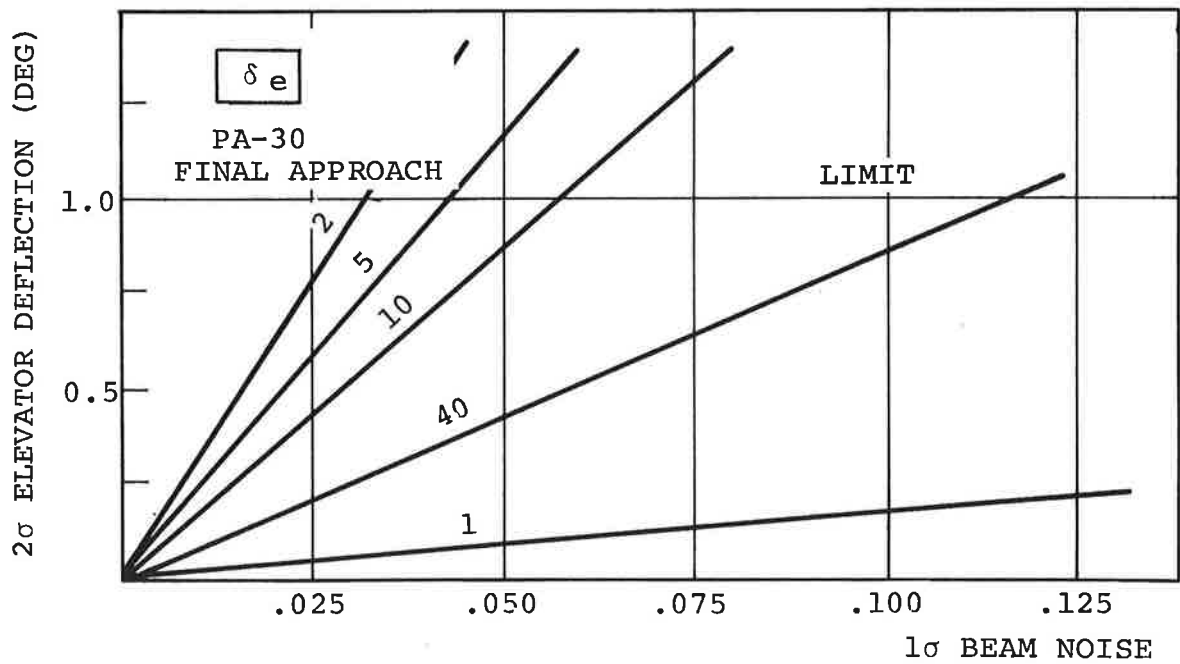


Figure 7-37.  $2\sigma$  Elevator Activity Vs. Beam Noise

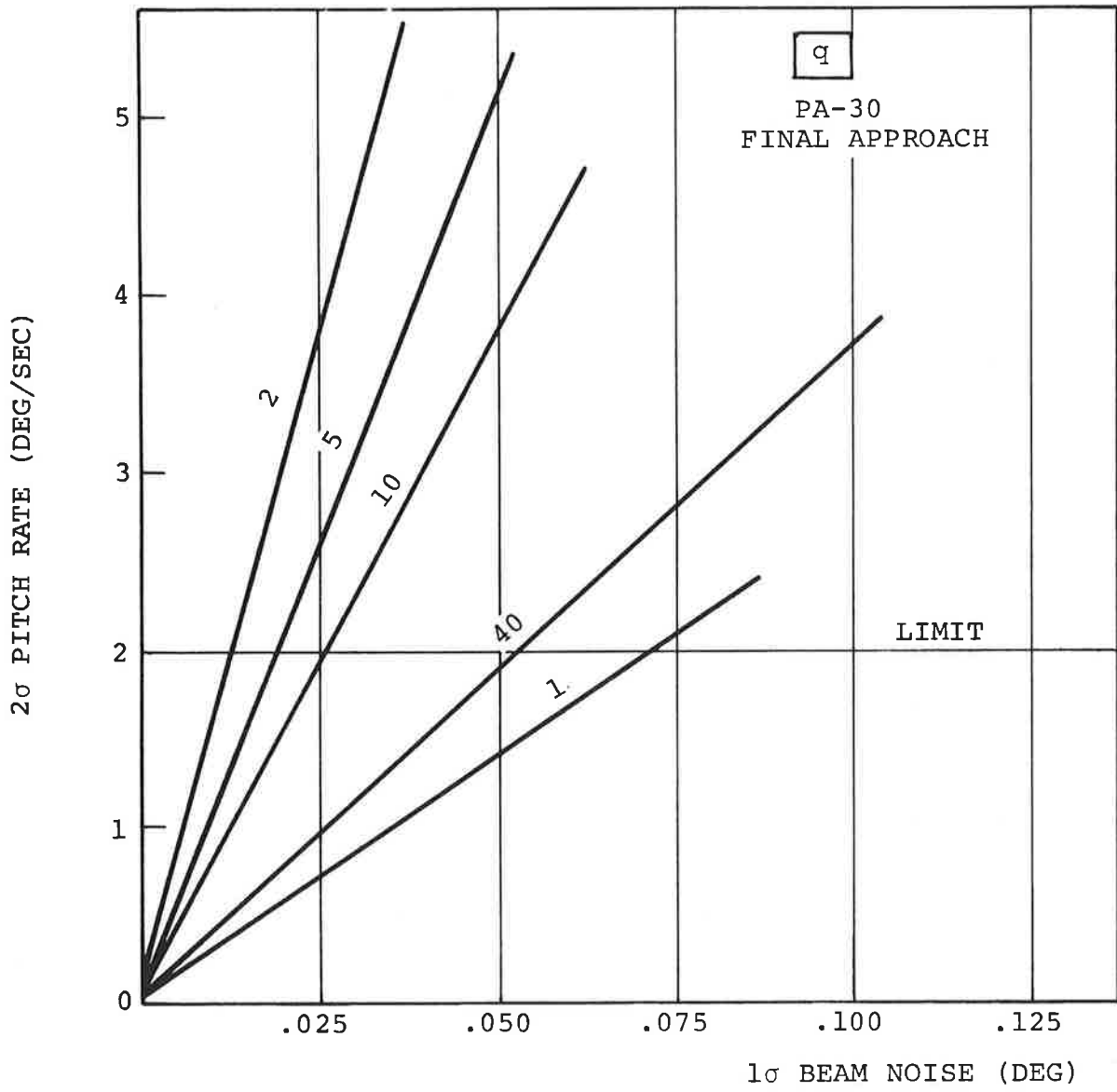


Figure 7-38.  $2\sigma$  Pitch Rate Activity Vs. Beam Noise

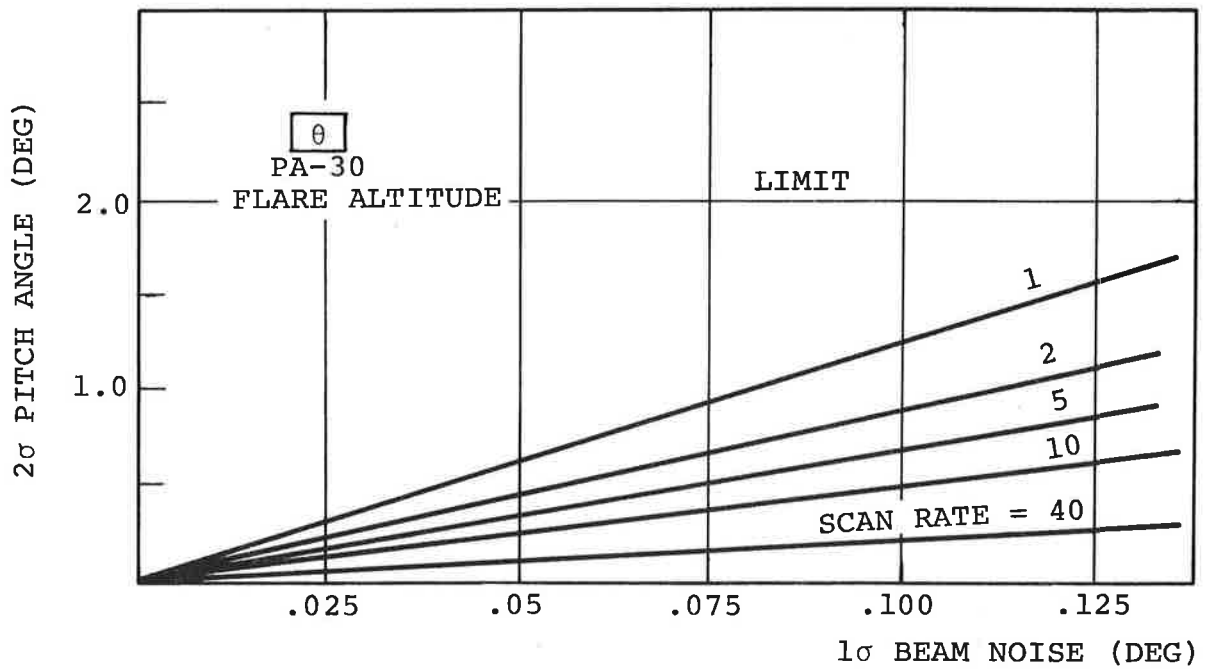


Figure 7-39.  $2\sigma$  Pitch Angle Deviation Vs. Beam Noise

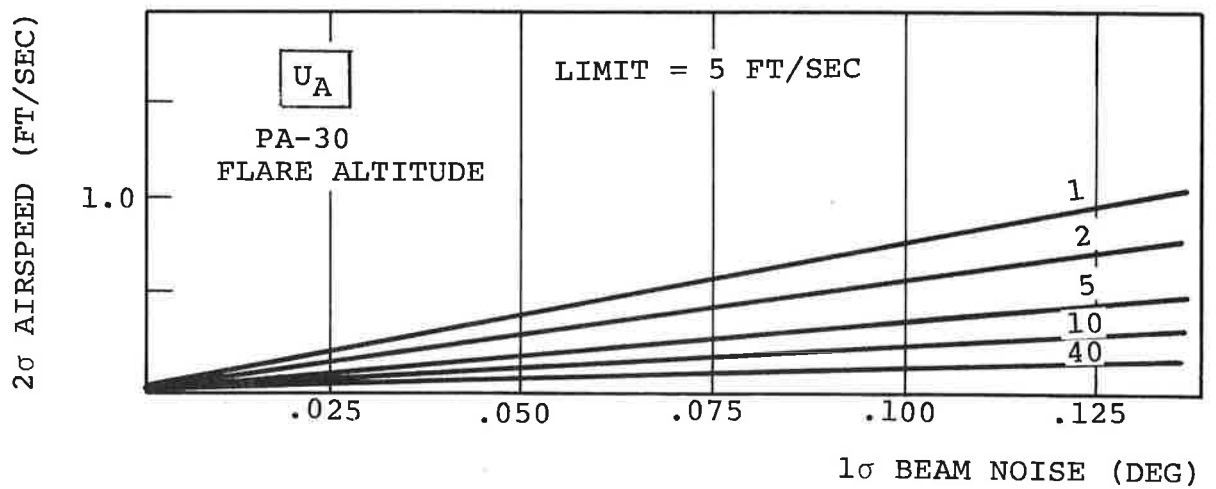


Figure 7-40.  $2\sigma$  Airspeed Deviation Vs. Beam Noise

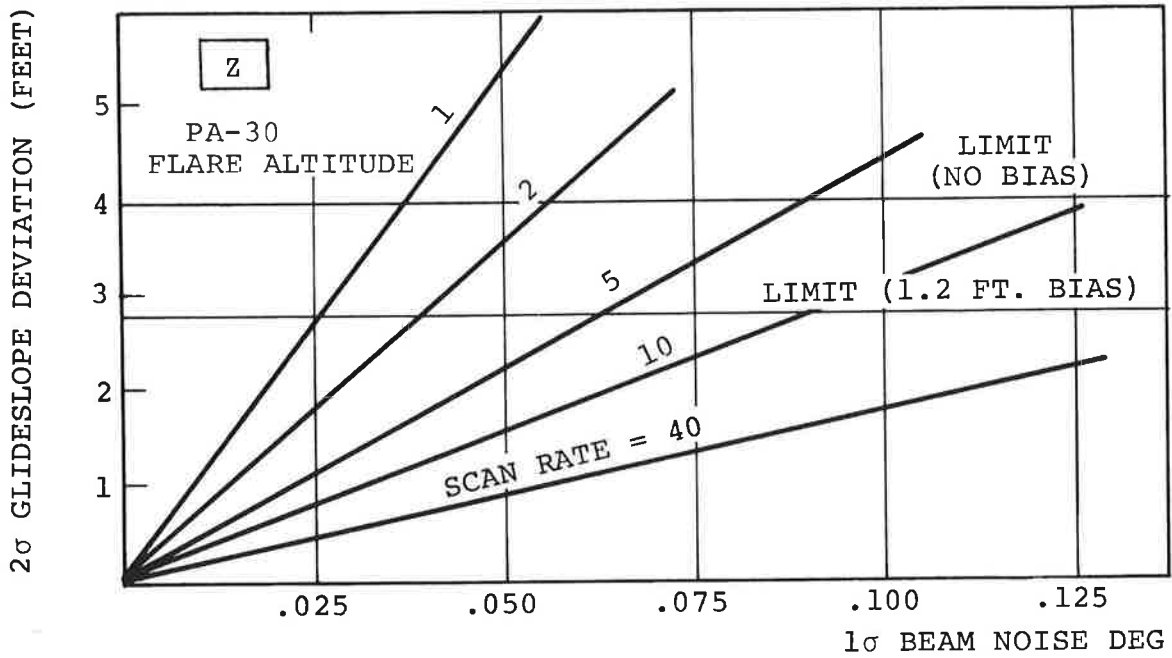


Figure 7-41.  $2\sigma$  Glideslope Deviation Vs. Beam Noise

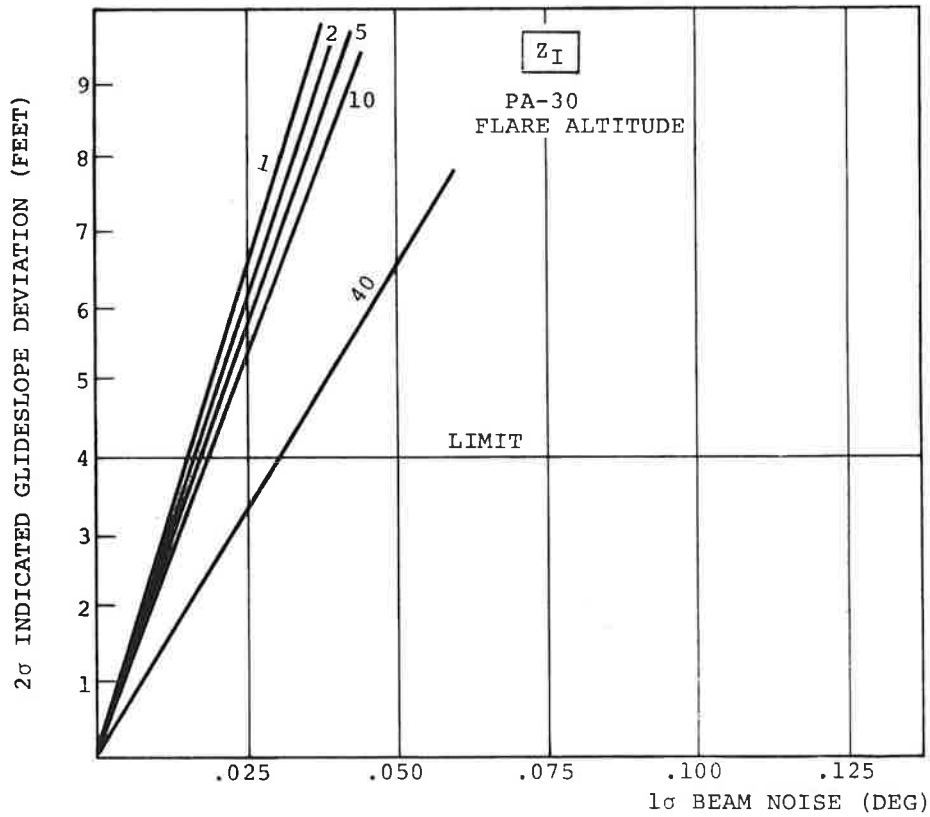


Figure 7-42.  $2\sigma$  Indicated Glideslope Deviation Vs. Beam Noise



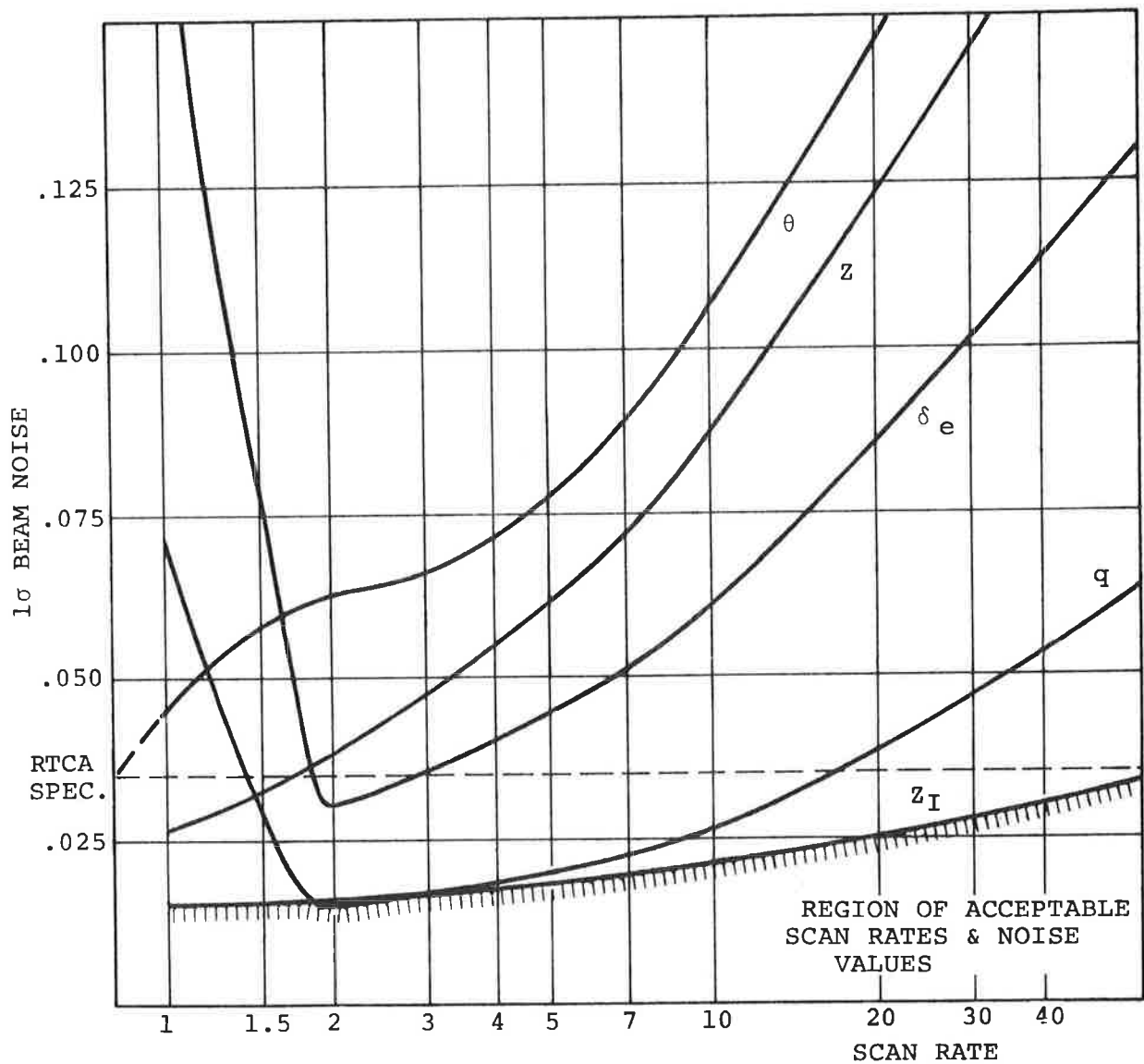


Figure 7-43(a). Beam Noise - Scan Rate Tradeoff  
Pilot Acceptability Factors  
PA-30 Longitudinal System  
(Coupler Time Constant: 0.025 Sec.)

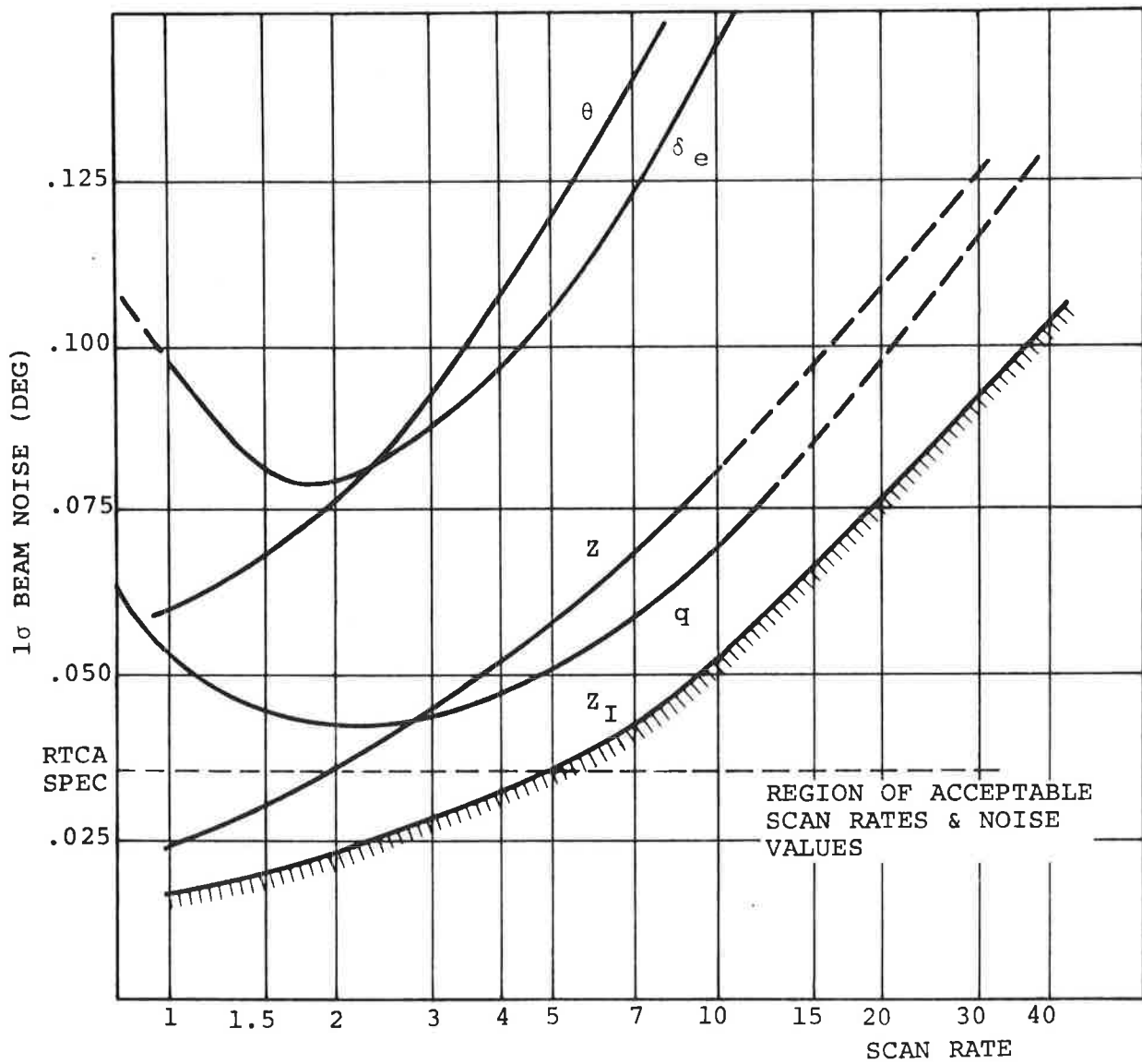


Figure 7-43(b). Beam Noise - Scan Rate Tradeoff  
 Pilot Acceptability Factors  
 PA-30 Longitudinal System  
 (Coupler Filter Time Constant: 0.5 Sec.)

## 8. CONCLUSIONS

### 8.1 GENERAL CONCLUSIONS

Figures 8-1 and 8-2 show in composite form the various important constraint curves for beam noise and scan rate for the azimuth and Elevation #1 signals, respectively.

From these figures and the data of Section 7, the following general conclusions can be drawn:

- (1) Safety factors tend to set the absolute minimum scan rate requirement and are relatively insensitive to beam noise. The critical position variables at touchdown are at least an order of magnitude more sensitive to scan rate than are velocity or altitude variables.
- (2) Pilot acceptability factors are slightly more sensitive to beam noise than scan rate and tend to limit maximum beam noise for scan rates above the absolute minimum. No particular generalization can be made concerning which acceptability factors are more critical than others.
- (3) Processing-filtering techniques are extremely significant in determining constraints imposed by pilot acceptability factors.

### 8.2 CONCLUSIONS FOR THE AZIMUTH SIGNAL

Figure 8-1 shows that scan rates as low as two per second will provide satisfactory performance with the recommended value of beam noise. At the RTCA recommended scan rate of five per second, about twice the beam noise is tolerable.

It is therefore concluded that the range of acceptable beam noise and scan rates for both the PA-30 and CV-880 is sufficient to allow significant latitude in choosing azimuth signal parameters and performance of these aircraft should not seriously constrain the choice of these parameters.

### 8.3 CONCLUSIONS FOR THE ELEVATION #1 SIGNAL

It is apparent from Figure 8-2 that pilot acceptability factors significantly limit the range of acceptable scan rates and beam noise for the Elevation #1. At the recommended beam noise value, five scans per second (the RTCA recommended scan rate) is barely adequate to meet most of the constraints.

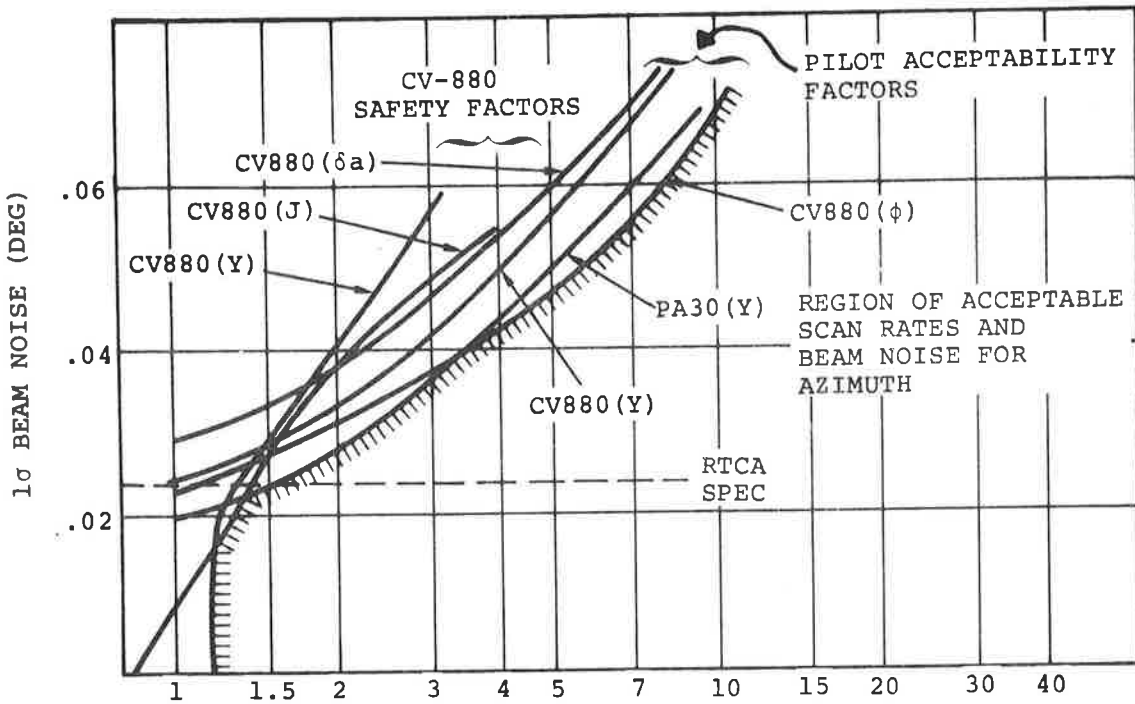


Figure 8-1. Scan Rate Beam Noise Tradeoff For Azimuth Signal

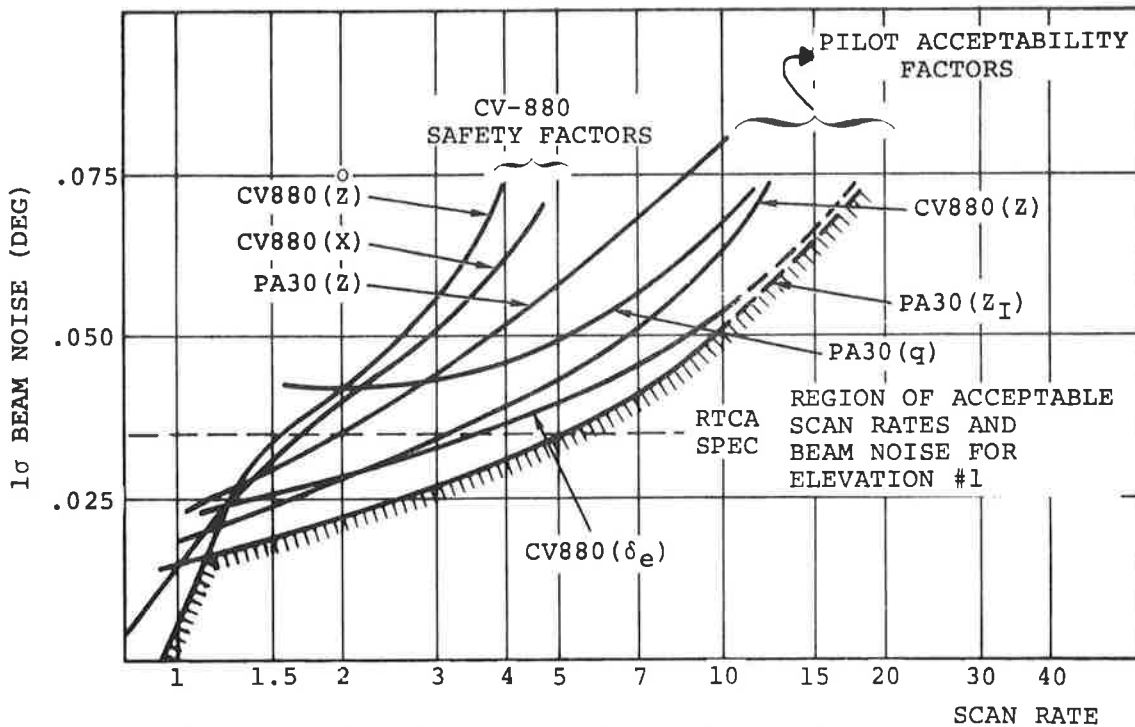


Figure 8-2. Scan Rate-Beam Noise Tradeoff For Elevation #1 Signal

It is therefore concluded that pilot acceptability factors for these aircraft may impose an eventual limitation on allowable beam noise and scan rates for elevation #1.

## 9. SUMMARY OF LIMITATIONS

### 9.1 GENERAL

Many of the limitations of this study are by now apparent; in the following sections the more important of these are summarized, including comments on further work required and possible effects on results.

### 9.2 COVARIANCE PROPAGATION METHOD

The covariance propagation method as now mechanized does not provide rigorously valid statistical results near touchdown. Two basic areas require significant work to eliminate this problem: (1) A linearization of the ground effect phenomenon so that results will more closely reflect very low altitude performance, and (2) A reformulation of the equations to include time dispersion and the effects of time dispersion implicitly. This may require some form of hybrid solution, i.e. a simultaneous integrated program including the full simulation and the linearized equations.

### 9.3 WIND MODELS

There is some evidence that turbulence does not produce the same magnitude of effects in real life as are indicated by simulation results. It is felt this may be due to the method of introducing turbulence noise into the simulation which is generally done ignoring high frequency effects and lags introduced by the airframe. Work is proceeding to include second order high frequency airframe effects to investigate their overall contribution to performance in turbulence.

### 9.4 LGS MODEL

As mentioned in Section 4, many possible significant error sources have not been considered in formulating the LGS scanning beam model. Perhaps the most important of these is the every-other-scan cyclic error which would result from a dual antenna configuration.

The filtering problem has been found to be extremely significant in defining beam noise and scan rate requirements. It should be possible to develop some general approach to simple filtering of the scanned signal, based on signal, beam noise, and sampling noise characteristics which will provide some better measure of protection against

the effects of noise than the first order filters used for this study. Work in this area is proceeding.

## 9.5 AIRCRAFT MODELS AND TOUCHDOWN CRITERIA

The portion of the approach and landing trajectory not considered to date is the rollout phase from the instant of touchdown. Touchdown criteria for safety may depend heavily on the dynamic and aerodynamic properties of the aircraft and autopilot during rollout, which are not as yet defined in terms of the simulation. In addition, the requirement for rollout guidance may affect azimuth and DME parameters.

Work is underway to model undercarriage and airframe dynamics in a form suitable for simulation.

## 9.6 PILOT ACCEPTABILITY CRITERIA

The results of Section 7 and Section 8 for pilot acceptability are based on definite but rather loosely defined criteria for acceptable performance in a zero wind environment. A change in some of the stated limits may produce a significant change in acceptable beam noise and scan rates. It is doubtful, however, that an absolute set of such criteria can ever be defined and every effort has been made in this study to remain on the conservative side.

## 9.7 STATISTICAL PROCEDURE-PROBABILITY OF SAFE LANDING

Assuming that the covariance propagation equation can be made to generate statistically valid results at touchdown, the problem remains of converting variance and covariance data into data on the probability of a safe landing. One would like this data to be in the form of an average or mean probability of safe landing over all wind conditions.

This is an extremely complex problem analytically and must take into account the following:

- (1) For highly correlated variables a joint probability function must be defined (e.g. all lateral system critical variables).
- (2) Probability must be computed over the entire range of allowable winds.
- (3) A probability density function for gust intensity must be defined in order to average the conditional probability of item (2) over all landings.

It should be possible as a method of simplification to eliminate certain variables as non-critical based on the relative relationship of all limits to variance.

The problem of averaging over all wind conditions is unlikely to be solved analytically for a general case and can probably be done only by numerical integration for specific cases.

## 9.8 DECISION WINDOW AND MISSED APPROACH

Another dimension to the problem of safe landing not considered here is the definition of decision height and decision variables which would lead to a missed approach under adverse conditions, thereby significantly affecting the probability of a safe landing.

It would be highly desirable to define decision variables and limits based on safe landing limits and the correlation between them. This is a largely impossible task to accomplish with any rigorous validity. The following comments apply however:

- (1) The only variables which are likely to be significantly correlated from decision height to touchdown are those of position. A knowledge of position deviation at decision height can therefore serve as a direct indication of successful landing probability.
- (2) Higher frequency variables (attitude, attitude rates, airspeed) at decision height are related to safe landing primarily indirectly, in that they serve as a measure of turbulence intensity and as such can be used to decide when turbulence levels have exceeded recommended or expected values.

## 9.9 SIGNAL REQUIREMENTS FOR TERMINAL AREA GUIDANCE

In addition to the problem of LGS signal requirements for safe and acceptable landings, signal requirements for coordination with other terminal area navigation aids, with terminal area air traffic control, and with desirable approach trajectories and flight interleaving must be considered.

Certain obvious tasks with respect to the above include:

- (1) Signal requirements for curved approach and development of feed forward guidance techniques.
- (2) Definition of minimum final trajectory acquisition points for various types of aircraft as a func-



- tion of LGS parameters.
- (3) Definition of dispersion in time to reach certain points in the trajectory, critical to close interleaving of flights, as a function of LGS parameters.

#### **9.10 THE USE OF DME AND ELEVATION #2 INFORMATION**

This report has not addressed the problem of DME and Elevation #2 signal requirements and uses due to the fact that this information is not used during approach by conventionally equipped aircraft.

DME will of course be required for curved approach guidance and can be used for precise gain scheduling during approach, for flare in combination with Elevation #2 information and for rollout guidance in combination with the azimuth function.

#### **9.11 LGS SIGNAL REQUIREMENTS FOR ADVANCED AUTOPILOTS**

Autopilot design will tend to take maximum advantage of whatever capabilities exist in the LGS. However, these are probably very definite tradeoffs which can be made between autopilot complexity and LGS integrity.

Work is currently underway to condition a previously designed advanced autopilot for the CV-880 to use scanning beam information. Such an autopilot must use derived beam rate data and may therefore impose more severe requirements on both scan rate and beam noise.



## Appendix A

### Notes on Digital Simulation and Covariance Propagation Methods and Mechanization

by Paul A. Madden and Mukund Desai

#### A. 1.0 Introduction

A brief description of the MIT/DL digital simulation used to simulate automatic flight of the CV 880 and PA-30 in the approach and landing flight phases is contained in the following sections. A simplified block diagram of the digital simulation appears as Fig. (A-1).

#### A. 1.1 Digital Simulation of an Automatic Landing System

The CV 880 and PA-30 aircraft and control systems were validated by digital computer simulation. Aerodynamic and LGS signal noise are simultaneously digitally simulated and input to the vehicle and control system equations.

The system of differential equations describing the vehicle, autopilot and automatic landing system were written in the form

$$\dot{\mathbf{x}} = \mathbf{f}(\mathbf{x}, \mathbf{m}, \mathbf{n}) \quad (\text{A-1})$$

where

$\mathbf{x}$  is a vector describing the system  
and is not necessarily a state vector

$\dot{\mathbf{x}}$  is a vector of derivatives

$\mathbf{m}$  is a set of control inputs

$\mathbf{n}$  is a set of system and atmospheric noise inputs

The vectors  $\mathbf{x}$  and  $\dot{\mathbf{x}}$  are subject to magnitude limits of the form

$$|\mathbf{x}| < L_x \quad (\text{A-2})$$

$$|\dot{\mathbf{x}}| < L_{\dot{x}} \quad (\text{A-3})$$

and a boundary condition

$$\mathbf{x}(0) = \mathbf{a} \quad (\text{A-4})$$

A solution of (A-2) may be obtained by direct integration from the boundary value (A-4).

To generate the aerodynamic and system noise, a digital equivalent of random gaussian noise must be supplied to either differential or difference equations representing the noise spectra filters. In the current CV880 simulation difference equations are employed since this is an efficient means of computation. The resultant solution is numerically stable independent of the sampling interval, however, the output of the system will be realistic only if the sampling is done frequently enough to result in a stair-step waveform which is a good approximation to the original continuous input waveform.

The difference equations are written in the form

$$\mathbf{n}(t + \Delta t) = \phi(t + \Delta t, t) \mathbf{n}(t) + \mathbf{D}(t + \Delta t, t) \omega(t) \quad (\text{A-5})$$

where

$\mathbf{n}$  is a vector of system and atmospheric noise sources

$\omega$  is a vector of gaussian white noise inputs

$\phi$  is the time-varying transition matrix associated with the spectral filters

$\mathbf{D}$  is defined  $\int_t^{t + \Delta t} \phi \mathbf{G} dt$

A simplified block diagram of the simulation is shown in Fig. (A-1).

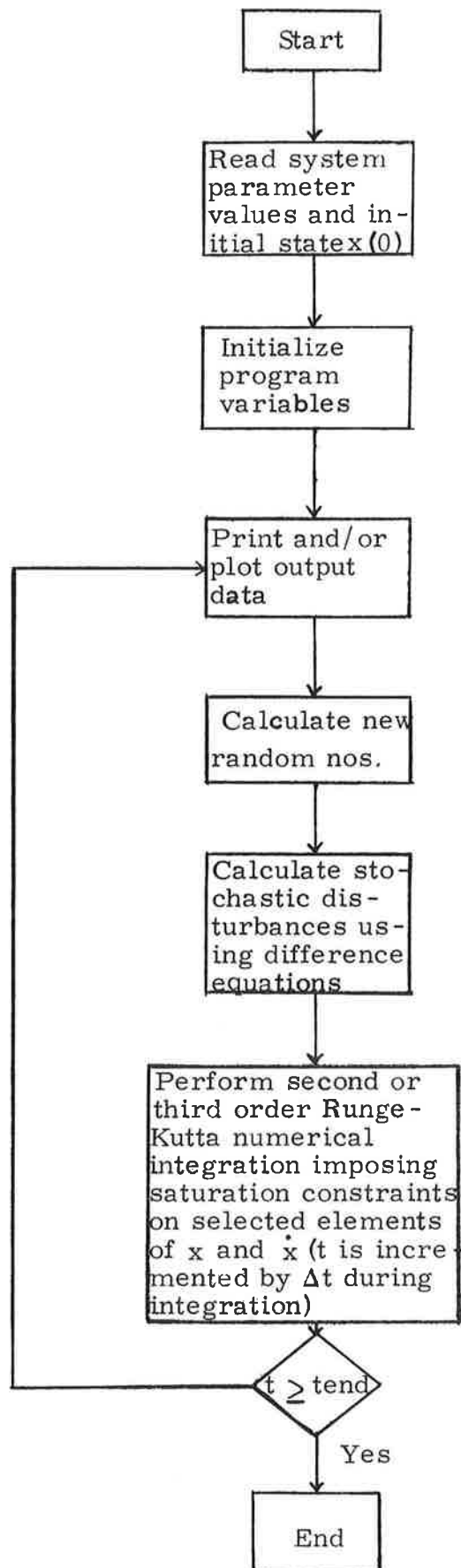


Figure A-1. Simplified block diagram of the digital simulation.

### A.2.0 Factors affecting simulation accuracy

#### A.2.1 Integration step size

Integration step size is an important consideration in the construction of a digital simulation. Several factors play an important role in step size selection.

1. Solution accuracy
2. Integration law
3. Order of the largest coupled system of differential equations in (A-1).

Step size is normally reduced until a further reduction does not yield a significant improvement in accuracy. An integration law with improved convergence characteristics usually permits an increase in step size. An upper bound on step size is often determined by the order of the largest independent set of coupled differential equations.

#### A.3.0 Program and Computer

The simulation program is written in FORTRAN IV for ease of software development and debugging. The computations were performed using an XDS 9300 computer.

#### A. 4 Discrete Representation of a Flight Vehicle and its Control System

The following sections describe the development of a linear discrete model of flight path analysis for use in error or covariance propagation programs. A discrete model is required as a result of the sampled data character of the LGS information.

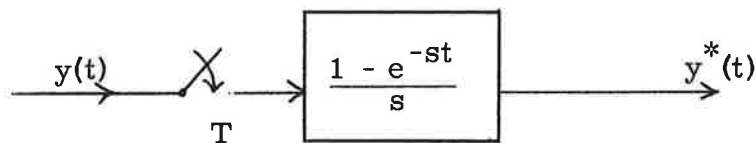
For the analysis of the statistics of the deviations of an aircraft from its nominal path in presence of noise, a state space approach (time domain) is to be favored over the frequency domain approach in view of the time discretization of the vehicle-control system can result in significant savings in computation time compared to numerical integration of the system differential equations.

##### A. 4. 1 Discrete Model for Flight Path Analysis

The deviations of an aircraft flight trajectory from its nominal approach path in a terminal area with microwave instrument landing guidance system (LGS) coverage subject to stochastic environmental disturbances and LGS measurement noise can be adequately represented by the following set of linear equations.

$$\frac{dx}{dt} = F_1 x + F_2^* x^* + G_1 u_1 + G_2^* u_2^* \quad (A-6)$$

where  $x$  is an  $n \times 1$  state vector;  $u_1$  and  $u_2$  are white gaussian noise which include the effects of stochastic input components such as wind gusts and LGS measurement noise. The starred quantities represent the output of a sampler followed by a zero order hold filter as shown in the following figure.



The statistics of the noise sources are

$$E[u_1(t)] = 0$$

$$E[u_1(t)u_1^T(\tau)] = Q_1(t)\delta(t-\tau) \quad (\delta \text{ is a delta function})$$

$$E[u_2(t_i)] = 0$$

$$E[u_2(t_i)u_2^T(t_j)] = Q_2(t_i)\delta_{ij}$$

$$\delta_{ij} = 1 \text{ for } i = j$$

$$= 0 \text{ for } i \neq j$$

The system dynamics of (A-6) contains state and noise in continuous as well as discrete form, and consequently the format of the system dynamics as represented by (A-6) is unsuitable for analysis using linear system theory. This makes it necessary to develop a discrete state representation corresponding to the continuous state representation of equation (A-6). The next section outlines the development of a discrete model.

#### A.4.2 Development of Discrete Model

At  $t_{i+1} = t_i + T$ , we have

$$x_{i+1} = \phi_1(t_{i+1}, t_i)x_i + \int_{t_i}^{t_{i+1}} \phi_1(t_{i+1}, t) \{F_2x(t_i) + G_1u_1(t) + G_2u_2(t_i)\} dt$$

$$\text{or } x_{i+1} = \phi(t_{i+1}, t_i)x_i + w(t_{i+1}, t_i) \quad (\text{A-7})$$

where  $T = \text{sampling interval}$

$$\phi(t_{i+1}, t_i) = \phi_1(t_{i+1}, t_i) + \phi_2(t_{i+1}, t_i)F_2 \quad (\text{A-8})$$

$\phi(t, t_i)$  and  $\phi(t, t_i)$  and  $\phi_2(t, t_i)$  can be easily seen to obey

$$\frac{d\phi_1}{dt} = F_1\phi_1 ; \quad \phi_1(t_i, t_i) = I \quad (\text{A-9})$$

$$\frac{d\phi_2}{dt} = F_1\phi_2 + I ; \quad \phi_2(t_i, t_i) = 0 \quad (\text{A-10})$$



$$w(t_i + 1, t_i) = w_1(t_i + 1, t_i) + w_2(t_i + 1, t_i) \quad (\text{A-11})$$

$$w_1(t_i + 1, t_i) = \int_{t_i}^{t_i + 1} \Phi_1(t_i + 1, t) G_1 u_1(t) dt \quad (\text{A-12})$$

$$\begin{aligned} w_2(t_i + 1, t_i) &= \int_{t_i}^{t_i + 1} \Phi_1(t_i + 1, t) G_2 u_2(t) dt \\ &= \Phi_2(t_i + 1, t_i) G_2 u_2(t_i) \end{aligned} \quad (\text{A-13})$$

Equation (A-7) represents a linear discrete state system; and is an exact representation of (A-6), since no approximations have been made in the development of the discrete model.

#### A.4.3 Evaluation of $\Phi$ and Statistics of $w(t_i + 1, t_i)$

Noise  $w(t_i + 1, t_i)$  may be viewed as a random sequence. It is easily seen that gaussian and white nature of the noise is preserved in  $w(t_i + 1, t_i)$ . Also, it is apparent that  $E[w(t_i + 1, t_i)] = 0$ . Let  $W = E[w(t_i + 1, t_i)w^T(t_i + 1, t_i)]$  denote the covariance of  $w$ .  $W$  can be evaluated by evaluating its two components  $W_1$  and  $W_2$  separately, with

$$W_j = E[w_j(t_i + 1, t_i)w_j^T(t_i + 1, t_i)] \quad , \quad j = 1, 2$$

From (C.3.6),  $w_1(t, t_i)$  is seen to obey

$$\frac{dw_1}{dt} = F_1 w_1 + G_1 u_1(t) \quad ; \quad w_1(t_i, t_i) = 0$$

Consequently, covariance  $W_1(t, t_i)$  obeys

$$\frac{dW_1}{dt} = F_1 W_1 + W_1^T + G_1 Q_1 G_1^T \quad , \quad W_1(t_i, t_i) = 0 \quad (\text{A-14})$$

Covariance  $W_2(t_i + 1, t_i)$  can be evaluated from the relation

$$W_2(t_i + 1, t_i) = \Phi_3(t_i + 1, t_i)G_2Q_2(t_i)G_2^T\Phi_3^T(t_i + 1, t_i) \quad (A-15)$$

The transition matrix  $\Phi$  may be evaluated from (A-8) once  $\Phi_1$  and  $\Phi_2$  are evaluated from (A-9) and (A-10) or alternatively  $\Phi$  may be evaluated by directly integrating the following equation

$$\frac{d\Phi}{dt}(t, t_i) = F_1(t)\Phi(t, t_i) + F_2(t_i) \quad ; \quad \Phi(t_i, t_i) = I \quad (A-16)$$

Transition matrix  $\Phi$ , noise and its statistics has to be calculated at each sampling instant if (A-6) has time varying components. However, great simplification obtains if  $F_1$  has time invariant elements and the only time varying components are those associated with starred (sampled) quantities.\* In this case  $\Phi_1$  and  $\Phi_3$  need only be evaluated for one sampling interval, and  $\Phi$  and the noise statistics can be evaluated from (A-8) and (A-9) at each sampling time.

#### A.4.4 Evaluation of Flight Path Statistics

Let  $\bar{x} = E[x]$  and  $X(t) = E[(x(t) - \bar{x}(t))(x(t) - \bar{x}(t))^T]$  represent the mean and covariance of  $x(t)$ .  $\bar{x}(t)$  and  $X(t)$  obey the following equations.

$$\bar{x}(t_i + 1) = \Phi(t_i + 1, t_i)\bar{x}(t_i) \quad (A-17)$$

$$X(t_i + 1) = \Phi(t_i + 1, t_i)X(t_i)\Phi^T(t_i + 1, t_i) + W(t_i + 1, t_i) \quad (A-18)$$

The above equations can be solved to give the history of the nominal path as well as of the statistics of deviations from this nominal path during the approach and landing.

\*Such a case would usually obtain when aircraft is flying with autopilot in a particular control mode.

## Appendix B

### Simulation of Atmospheric Noise

By Paul A. Madden

#### B.1 Statistical Considerations

Simulation of atmospheric noise implies the generation of time-varying functions whose statistics duplicate the spectrums of continuous atmospheric turbulence.

Exponentially correlated noise may be modeled by passing gaussian white noise through a suitable shaping filter whose dynamics adjoin the existing system providing a new system subject only to white noise input.

Let the continuous white noise autocorrelation function be given by

$$\phi(\tau) = Q \delta(\tau) \quad (\text{B-1})$$

then its PSD function is

$$\Phi(\omega) = \frac{1}{2\pi} Q \quad (\text{B-2})$$

If gaussian white noise is passed through a filter F, its output has the PSD given by

$$\Phi_n(\omega) = \left| F \right|_{s=i\omega}^2 \Phi(\omega) \quad (\text{B-3})$$

For  $F = \frac{a}{s+a}$ , the output is

$$\Phi_n(\omega) = \frac{Q}{2\pi} \frac{1}{1 + \left(\frac{\omega}{a}\right)^2} \quad (\text{B-4})$$

Equivalence of (B-4) and the assumed empirical turbulence spectrum provides the values of correlation time and Q necessary to reproduce the spectrum. For the Dryden  $\Phi_u(\omega)$  given by Table 3-1 (Chapter 3), this equivalence provides

$$\frac{1}{a} = \frac{L_u}{U_0}$$

$$Q = 4\sigma_u^2 \left(\frac{1}{a}\right) \quad (\text{B-5})$$

The filter equation may then be written

$$\dot{n} = a(w-n)$$

where  $n$  is the correlated noise output and  $w$  the gaussian white noise input.

Evaluation of the constants involved in a second-order filter necessary to reproduce the spectrum, for example, given for  $\Phi_{v,w}(\omega)$  follows in a directly analogous manner.

It is not possible to provide a continuous signal representing gaussian white noise in a digital simulation. The digital equivalent is a discrete series of uncorrelated random amplitude steps. For this step sequence, the autocorrelation function is

$$\phi(\tau) = \begin{cases} \sigma^2(1 - |\tau|/\Delta T) & |\tau| \leq \Delta T \\ 0 & |\tau| > \Delta T \end{cases} \quad (\text{B-6})$$

where  $\sigma^2$  is the mean-square value of the random step amplitudes and  $\Delta T$  is the discrete time step. The associated PSD function, defined as

$$\Phi(\omega) = \frac{1}{2\pi} \int_{-\infty}^{\infty} \phi(\tau) e^{-j\omega\tau} d\tau \quad (\text{B-7})$$

is given by

$$\Phi(\omega) = \frac{\sigma^2}{2\pi} \left[ \frac{\sin(\omega \Delta t)}{\omega} + j (\sin(\omega \Delta T) - \omega \Delta T \cos(\omega \Delta t)) \right] \quad (\text{B-8})$$

Considering only the long wavelengths ( $\omega \ll \frac{2\pi}{\Delta t}$ ), a small angle approximation may be used to give

$$\Phi(\omega) = \frac{\sigma^2 \Delta t}{2\pi} \quad \omega \ll \frac{2\pi}{\Delta t} \quad (\text{B-9})$$

Equivalencing the above discrete-step approximation for the PSD of the white noise input with the previously given (B-2) continuous function provides

$$\sigma^2 = Q / \Delta T \quad (\text{B-10})$$

For the example that led to the result for  $Q$  expressed by (B-5), the root-mean-square value of the random-step amplitude would be

$$\sigma = \left[ \frac{2w^2 \frac{1}{g} \frac{1}{a}}{\Delta T} \right]^{1/2} \quad (\text{B-11})$$

A block diagram, Fig. B.-1, shows the operations which lead from a machine-generated random number sequence to a time history of gust velocity.

## B.2 Effective Aerodynamic Noise Perturbations

The sequence of operations discussed in the last section and shown schematically in Fig. B-1 leads to a time history of the three uncorrelated gust-velocity components.

A vertical gust produces an angle-of-attack disturbance and, because of its varying intensity along the length of the aircraft, an effective pitch disturbance. Similarly, a lateral gust-velocity component produces a sideslip and effective yaw disturbance.

The pitch and yaw disturbances may be approximately represented by effective pitch and yaw rate perturbations, respectively, if the higher-frequency gust components are not admitted in evaluation of these effective rates. This is equivalent to the requirement that the gust component vary nearly linearly along the effective aerodynamic length of the aircraft. This requirement may be met with a lowpass unity-gain filter introduced in series. The break frequency of the filter is selected such that the shortest wavelength admitted is no less than about eight times the effective aerodynamic length of the aircraft. If  $\omega_b$  is the break frequency, then

$$\omega_b = 2\pi U_0 / \lambda_{\min} \quad (\text{B-12})$$

with  $\lambda_{\min}$  equal to eight times the aircraft length.

In general, it has been observed that neglect of the short wavelengths has negligible effect upon rigid-aircraft response; the energy content of these spectral components is relatively small. Their inclusion, however, is of importance in the forcing of aircraft elastic modes.

It is recalled that the empirical PSD functions are functions of the longitudinal-axis coordinate only; spanwise variations in gust intensity are thereby neglected. It is not easily possible to simulate this variation with rigor. It may be approximately accounted for, however, by considering a span-averaged gust intensity. The factor  $K$  is defined

$$K = \left[ 1 - 0.3 \frac{b}{2L} \left( 1 + \frac{b}{2L} \right) \right] \quad b < L \quad (\text{B-13})$$

where  $b$  is the wing span and  $L$  is the aircraft length. The factor  $K$  operates upon the mean-square gust intensity providing a span-averaged value. This is the gust intensity used when evaluating the vertical and longitudinal gust-velocity components. For the CV880M

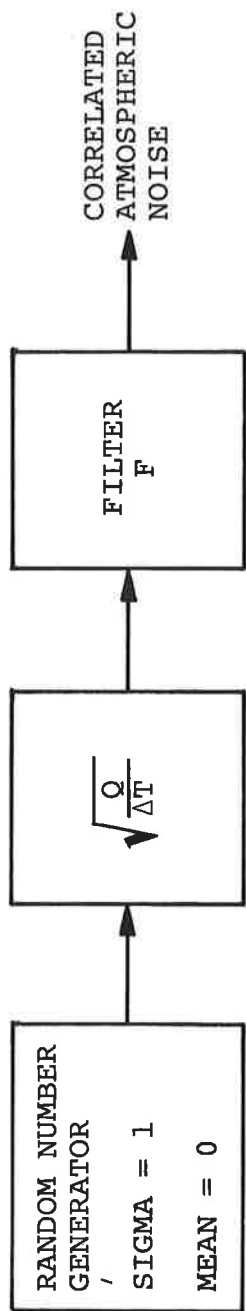


Fig. B-1 Discrete step sequence to generate time correlated atmospheric noise component.

aircraft,  $K = 0.968$ .

The aerodynamic noise perturbations may now be expressed as functions of the gust-velocity components  $u_1$ ,  $u_2$ , and  $u_3$ .

$$\begin{aligned}u_n &= u_1 \\ \alpha_n &= u_3 / U_0 \\ \dot{\alpha}_n &= \dot{u}_3 / U_0 \\ \beta_n &= u_2 / U_0 \\ q_n &= -(\dot{u}_3)_f / U_0 \\ r_n &= (\dot{u}_2)_f / U_0\end{aligned}\tag{B-14}$$

where the subscript  $f$  refers to the lowpass filtered component.

In addition to the above turbulence-induced components of aerodynamic noise, there exist also wind-shear-induced components. It is assumed that there is no mean vertical-velocity component to the air mass. The variations in mean air-mass velocity from the reference flight condition values due to wind shear must be added vectorially to the components  $u_n$  and  $\beta_n$  of (B-14). The wind-shear-induced components are evaluated as the difference between the current mean wind speed ( $w_{\text{mean}}$ ), developed in the next subsection, and the initial flight condition value.

Figures B-2 and B-3 illustrate the vector relationships between noise, inertial, response, mean wind speed, mean airspeed and ground speed for two cases,  $u_n$  and  $\beta_n$ .

The components  $u_1$ ,  $u_2$ , and  $u_3$  are space fixed, and to be completely rigorous, should be resolved through actual instantaneous yaw, pitch and, roll angles in computing  $u_n$ ,  $\beta_n$ ,  $\alpha_n$ , etc. It is assumed, however, that these angles are small and effects of ignoring the gust cross coupling negligible. In actual simulation therefore,  $u_1$ ,  $u_2$ , and  $u_3$  are generated with respect to aircraft axes.



$U_o$  = nominal airspeed  
 $U_{wo}$  = nominal headwind  
 $\dot{X}_{ao}$  = nominal groundspeed  
 $u_n$  = instantaneous gust velocity  
 $\delta U = u + u_n$  = change in true airspeed  
 $\delta \dot{X}_A = u =$  change in true groundspeed  
 Auto throttle control operates to set  
 $\delta U = 0$  i.e.  $u = -u_n$

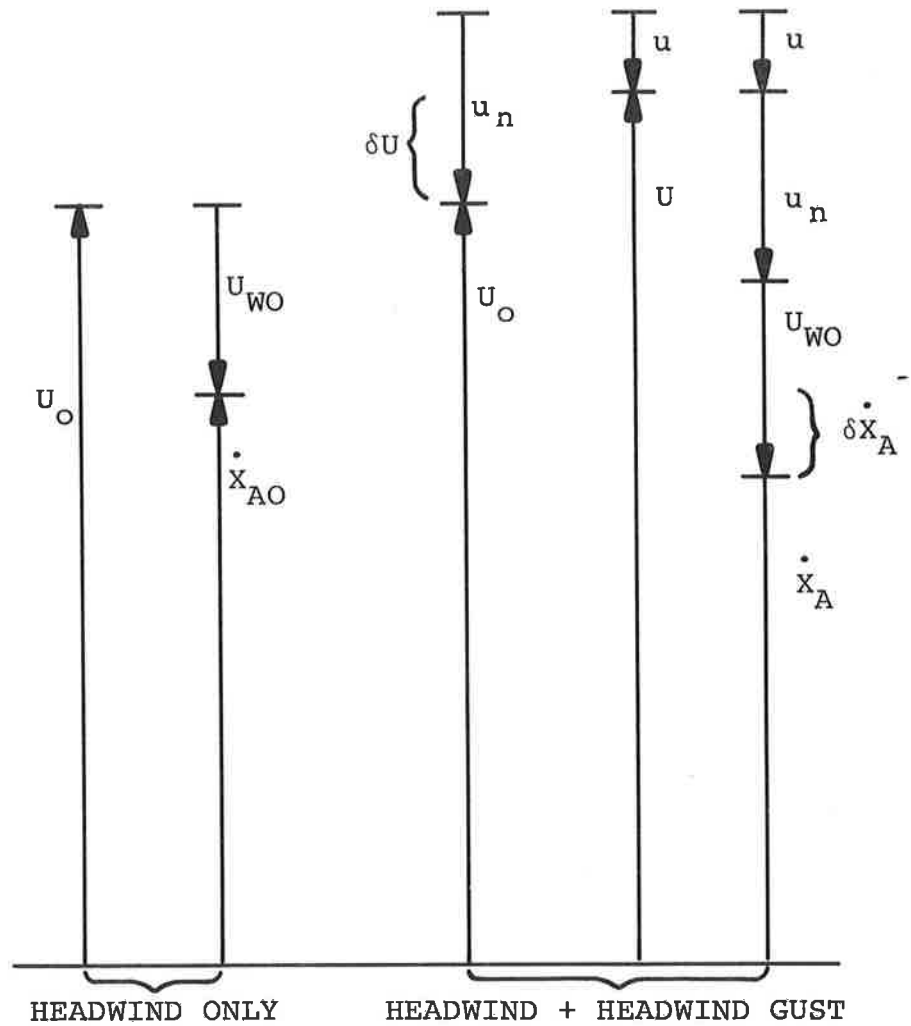


Figure B-2. Effects of Longitudinal Gust Noise on Air-Speed and Ground-Speed

$U_o$  = nominal forward airspeed  
 $V_o = U_o \beta_o$  = nominal lateral airspeed  
 $\beta_o$  = nominal sideslip angle  
 $\beta_n = v_n / (U_o \delta U)$   
 = instantaneous gust induced sideslip  
 $v_n = u_2$  = instantaneous lateral gust  
 $\delta V = (U_o + \delta U_o) \beta$  = change in lateral ground speed.

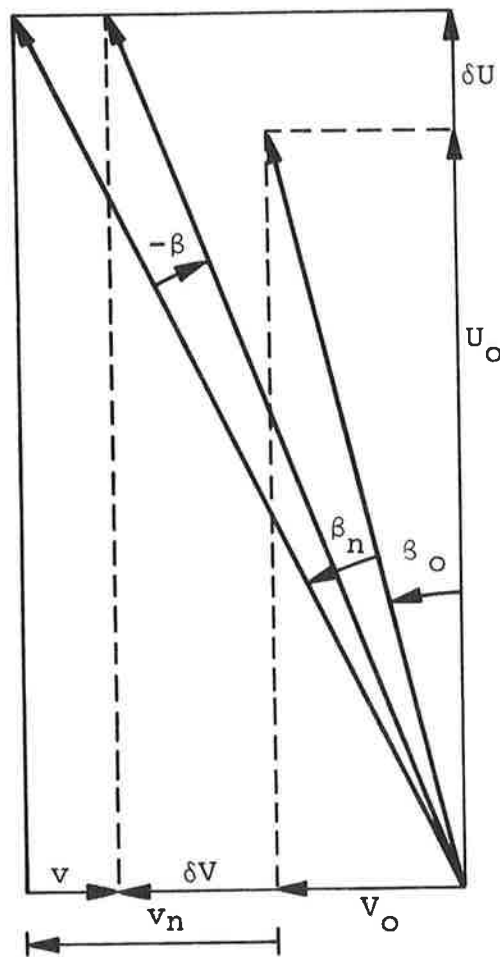


Figure B-3. Effects of Lateral Gust Noise on Sideslip Angle, Lateral Airspeed and Lateral Groundspeed

## Appendix C

### Granularity in Processed SBMILS Data

By Duncan MacKinnon

#### C.1 Introduction

The azimuth and elevation angle scanning beams of the Scanning Beam Microwave Instrument Landing System (MLS) indicate their angular position by information encoded on the transmitted signal. The encoded angular data changes as the beam sweeps through its specified angle as shown in Fig. C-1. The MLS airborne receiver measures the encoded data as the azimuth or elevation beam illuminates the aircraft. The receiver utilizes the observed measurements to estimate the actual angular relationship of the aircraft with respect to the azimuth or elevation antenna site.

Granularity (discrete changes) in the processed angular signal outputs may arise as a result of discrete quantization of the angle encoded on the modulation signal.

If quantization exists the signal measured by the receiver may be approximated by a sequence of values which are of the form

$$\langle \alpha \rangle = \langle \alpha_1, \alpha_2, \alpha_3 \dots \alpha_{N_b} \rangle \quad (\text{C-1})$$

The number  $N_b$  of elements in the sequence is equal to the number of modulation quantizations during the period  $T_b$  when the MLS receiving antenna is illuminated by the scanning beam. The sequence is monotone

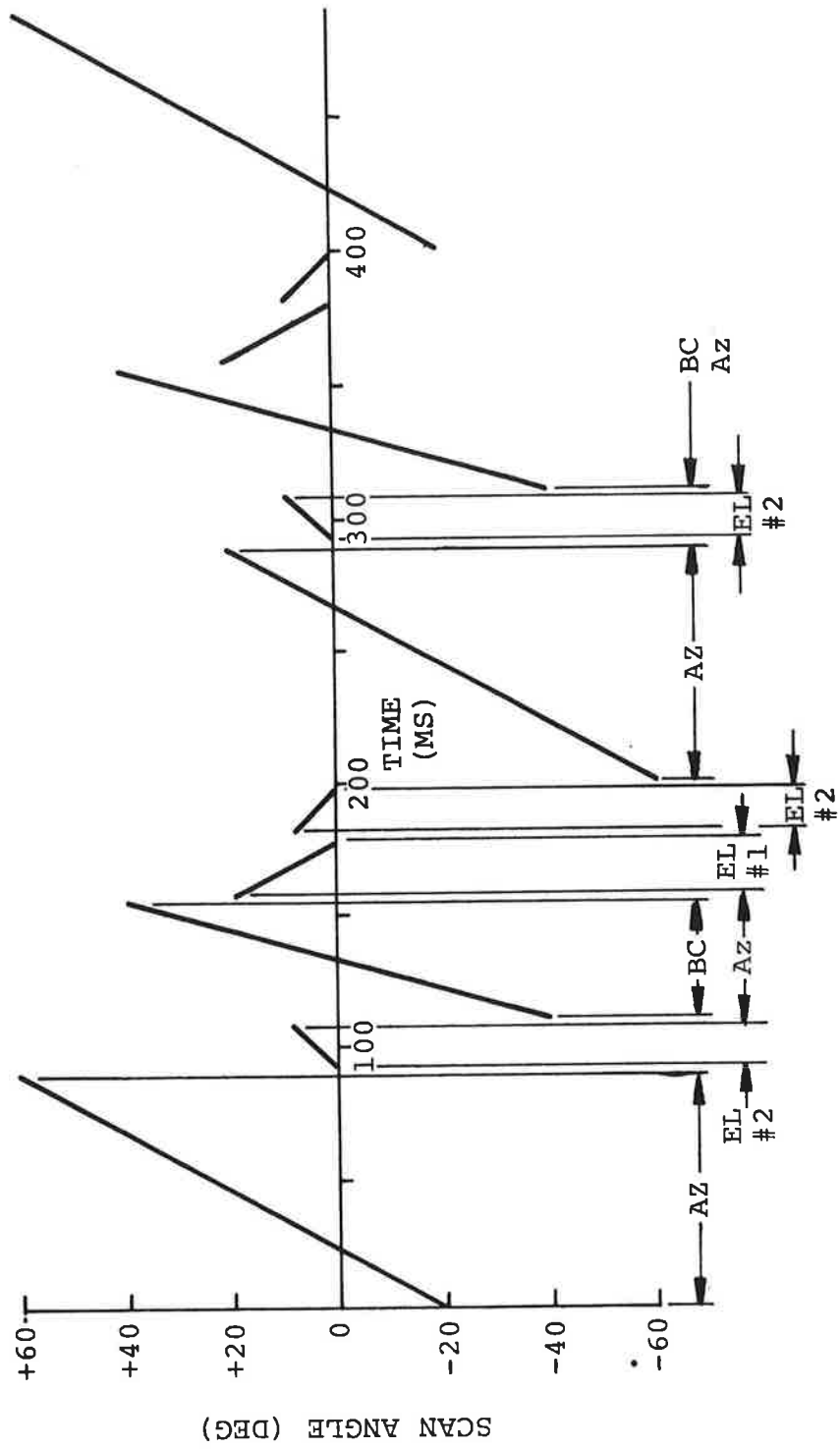


Figure C-1. Typical Scan Cycle for Mechanically Scanned Antennas

increasing or decreasing, depending on whether or not the angular modulation amplitude is increasing or decreasing with respect to time.

### C.2 The Number of Samples in the Observed Sequence

The number of elements generated as a beam sweeps past the aircraft, depends primarily upon the beamwidth  $\theta_b$  and the quantization level  $q$  of the encoded angular data

$$N_b \approx \frac{\theta_b}{q} \text{ samples} \quad (\text{C-2})$$

since the sequence elements are generated in a linear fashion as a function of angle. The quantization level  $q_r$  at the output of the MIL receiver depends upon the manner in which the sequence of measurement (C-1) is processed.

### C.3 Digital Signal Processing

In order to estimate the value of the angle of interest the sequence of measurements (C-1) must be appropriately weighted. The weighting process can be analog\* or digital in character. Digital filtering is a likely candidate as a result of small size, high accuracy and high reliability advantages. A digital output signal format is also extremely useful for interfacing with a general purpose navigation computer.

A simple digital filter to provide an estimate  $\alpha_e$  of the measured angle  $\alpha_m$  has the form

$$\alpha_e = \sum_{i=1}^{N_b} R_i \alpha_i \quad (\text{C-3})$$

where  $\beta_1 \dots \beta_{N_b}$  is a set of weighting coefficients. The characteristics of

---

\* The problem is identical for the analog system if state variable techniques are exploited.

the filter are determined by the values associated with the  $\theta$ 's.

#### C. 4 Granularity with Uniform Weighting

Suppose that the sample  $\alpha_i$  is weighted uniformly by the processor.

A suitable selection for  $\theta$  is

$$\theta_i = \frac{1}{N_b} \quad i = 1, N_b \quad (C-4)$$

in which case

$$\alpha_e = N_b^{-1} \sum_{i=1}^{N_b} \alpha_i \quad (C-5)$$

the arithmetic mean of the samples. Granularity results when the angle measured at the aircraft passes a quantization level in the modulated signal. This results in a change  $d_u$  in the receiver output equal to

$$d_u = \frac{q}{N_b} = \frac{q^2}{\theta_b} \quad (C-6)$$

The worst case occurs when  $N_b$  is equal to 1.

#### C. 5 Granularity with a Triangular Weighting

If a suitable nonuniform weighting sequence  $\theta$  is adopted, the effects of granularity may be significantly reduced. Suppose that  $\theta$  has the form shown in Fig. C-2 where

$$N_b = \text{odd number} \quad (C-7)$$

and

$$\sum_{i=1}^{N_b} \theta_i = 1.0 \quad (C-8)$$

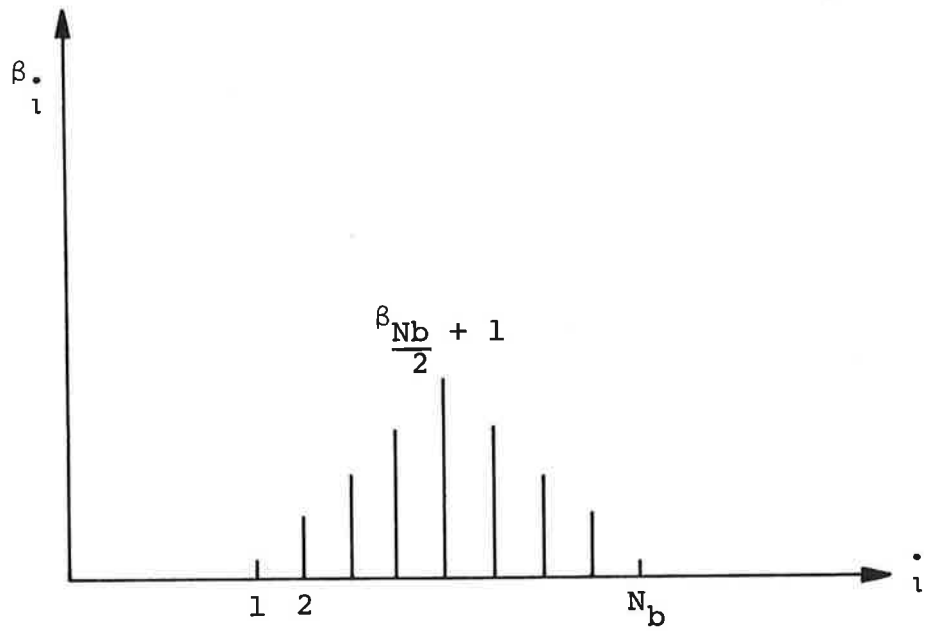


Figure C-2. Nonuniform Weighting Function

This weighting function places more confidence on measurements made near the beam center at a higher signal to noise ratio. The function is symmetrical with respect to the center value at  $(N_b/2) + 1$ . The quantization error in this case is equal to

$$d_u = qR_1 \quad (C-9)$$

Note that  $\beta_1$  can be much less than  $N_b^{-1}$  if  $N_b > 2$ .

#### C.6 Conclusions

The granularity resulting from encoded beam angle quantization depends upon the quantization level, the scanning beam width, and the weighting applied to the observed angular measurements.

Current MLS design philosophy<sup>1</sup> calls for beam widths between 0.5 and 1.0 degrees and angle encoding accuracy of 0.02 degrees. With a uniform weighting, the granularity is between  $4 \times 10^{-4}$  and  $8 \times 10^{-4}$  degrees, a negligible amount.

#### References

1. Signal Format Development Team Report to RTCA Special Committee 117, Radio Technical Commission for Aeronautics, Washington, D.C., September 1970.



## Appendix D

### Physical and Aerodynamic Characteristics of the CV880 and PA-30 Aircraft in the Approach and Landing Flight Configuration

by Paul A. Madden

#### D.1.0 Convair 880

#### D.1.1 Introduction

Physical and aerodynamic characteristics of the CV880 aircraft used as a basis for the SBMILS simulation studies are delineated in the following sections. Firstly, the aircraft approach speed is established for flight in the (defined) maximum wind condition; the nominal (no wind) flight condition (FC) is FC4 (See Reference (1).). Aerodynamic characteristics of the aircraft in the maximum wind condition follow from the derived approach speed and those characteristics given for FC4.

#### Derived Approach Speed

The approach speed is constructed following the empirical expression<sup>2</sup>

$$V_{\text{app}} = V_{\text{ref}} + \frac{1}{2} \text{ surface winds} + \text{reported gusts} \quad (\text{D-1})$$

where  $V_{\text{ref}}$  is the nominal (no wind) approach speed for FC4.

#### Physical and Aerodynamic Characteristics of the CV880

The following aerodynamic characteristics derive from the approach speed calculated using Eqn. (D-1) and aerodynamic characteristics given for FC4. The physical characteristics are identical with those of FC4.

#### D. 1. 2. 0 Physical Characteristics

##### D. 1. 2. 1 Aircraft

Gross weight	= 126,000 lbs.
Flaps	= 50 degrees (full down)
Undercarriage	= down
C. G. position	= .195% MAC
Speed brakes	= 8 degrees
$I_x$	= $1.51 \times 10^6$ slug-feet <sup>2</sup>
$I_y$	= $2.45 \times 10^6$ slug-feet <sup>2</sup>
$I_z$	= 4.07 slug-feet <sup>2</sup>

##### D. 1. 2. 2 Wing

Span	= 118.3 feet
$\bar{c}$	= 18.94 feet
Area	= 2000 feet <sup>2</sup>

##### D. 1. 2. 3 Elevator

Area	= 88.28 feet <sup>2</sup>
$\bar{c}$	= 2.44 feet
I	= 33.6 slug-feet <sup>2</sup>

##### D. 1. 2. 4 Rudder

Area	= 82.44 feet <sup>2</sup>
$\bar{c}$	= 4.69 feet
I	= 54.56 slug-feet <sup>2</sup>

##### D. 1. 2. 5 Aileron

Area	= 2 x 27.37 feet <sup>2</sup>
$\bar{c}$	= 2.96 feet
I	= 2 x 19.11 slug-feet <sup>2</sup>

### D. 1. 3. 0 Aerodynamic Characteristics

#### D. 1. 3. 1 Trim Flight Condition

$V_{app}$	= 269 fps
Mach. No.	= .241
Dynamic Pressure	= 86.0 psf
Trim $C_L$	= .733
Trim $C_D$	= .13
Trim $\alpha$	= 1.5 degrees
Zero-lift $\alpha$	= -7.5 degrees

#### D. 1. 3. 2 Longitudinal Stability Derivatives

	<u>Out of ground effect</u>	<u>In ground effect</u>
$C_{L,\alpha}$	4.66	5.56
$C_{D,\alpha}$	.317	.378
$C_{L,q}$	7.92	8.02
$C_{L,\delta_e}$	.22	
$C_{L,\delta_{te}}$	.055	
$C_{m,\alpha}$	-.996	-.985
$C_{m,\dot{\alpha}}$	-4.17	
$C_{m,q}$	-12.22	-12.22
$C_{m,\delta_e}$	-.657	
$C_{m,\dot{\delta}_e}$	-.0218	
$C_{m,\delta_{te}}$	-.164	

### D. 1. 3. 3 Elevator Hinge Moment Coefficients

$$C_{h, e, \alpha} \quad -.043$$

$$C_{h, e, \delta_e} \quad -.326$$

$$C_{h, e, \dot{\delta}_e} \quad -.023$$

$$C_{h, e, \delta_{te}} \quad -.287$$

### D. 1. 3. 4 Lateral Stability Derivatives

$$C_{l, \beta} \quad -.2390$$

$$C_{l, r} \quad .3094$$

$$C_{l, p} \quad -.3950$$

$$C_{l, \delta_r} \quad .0207$$

$$C_{l, \delta_a} \quad -.0487$$

$$C_{l, \delta_{ta}} \quad -.00722$$

$$C_{l, \delta_{tr}} \quad .00208$$

$$C_{l, \delta_s} \quad .0805$$

$$C_{n, \beta} \quad .1445$$

$$C_{n, r} \quad -.2178$$

$$C_{n, p} \quad -.0868$$

$$C_{n, \delta_r} \quad -.0995$$

$$C_{n, \delta_{tr}} \quad -.02025$$

$$C_{n, \delta_a} \quad .01862$$

$$C_{n, \delta_s} \quad .0258$$

## GLOSSARY OF TERMS

ABSORPTION The irreversible conversion of the energy of an electromagnetic wave into another form of energy as a result of its interaction with matter.

ACTIVE SECTOR That portion of a cylindrical array which is excited by the feed network. The active sector is measured in degrees.

APERTURE DISTRIBUTION The relative amplitudes of the radiating elements in the active portion of an array.

ARRAY ANTENNA An antenna comprising a number of radiating elements, generally similar, which are arranged and excited to obtain a desired radiation pattern.

ASPECT RATIO The ratio of maximum beamwidth to minimum beamwidth of a fan beam. These beamwidths are measured with respect to perpendicular cuts.

ATTENUATION Reduction of the strength of a propagating signal by virtue of an intervening medium.

BEAM BROADENING FACTOR A parameter which depicts the increase in beamwidth for a given aperture caused by a non uniform aperture distribution. It is measured in degrees.

BEAMWIDTH The angle between the half-power points on the main beam of an antenna pattern. Other than half-power points may be used, but must be indicated, e.g. "10 dB beamwidth".

BORESIGHT The direction of the center of the main beam of an antenna. The definition of beam center depends on the processing used in the system.

COLLIMATION The achievement of a plane wave by appropriate phase corrections of the excitation of the elements of an arbitrary array geometry. For a cylindrical array, the correction is a circular-to-planar correction.

CONICAL BEAM A fan beam whose beam center locus sweeps out a conical surface with its vertex at the antenna.

CONING The effect on the shape of a fan beam caused by certain antenna geometries, notably linear arrays. A linear array along the y-axis will not generate fan beams which coincide with planes passing through the z-axis.

## GLOSSARY OF TERMS (Cont)

CONTINUOUS SCAN The behavior achieved by an antenna beam which rotates smoothly in angle. Its opposite is step scan, which moves in discrete jumps.

COPHASAL DISTRIBUTION That phase distribution by which array elements are excited which achieves collimation of the resultant beam into a plane wave.

CYLINDRICAL ARRAY An antenna whose elements are located on a cylindrical surface, closed or open.

DECORRELATION The distortion of a plane wave caused by random disturbances in an intervening medium. The effect on antenna performance is similar to the effect of random phase errors in the feed system.

DEFOCUSING PHASE ERROR The phase difference between the actual far-field phase of an individual element and that which would be obtained by a perfectly collimated beam, of a cylindrical array. A cylindrical array is generally perfectly focused at two angles only.

DIFFERENCE BEAM A notched, or bilobed, pattern of an antenna. Here the boresight is defined as the direction of the central null. Typical is a monopulse pattern.

DROOP The decrease in the true elevation angle of a planar elevation fan beam at wide azimuth angles.

ELEMENT PATTERN The pattern of a single element of an array. If the other elements are not present, it is called the "isolated element pattern". If the other elements are present, and are terminated in a matched load, it is called the "active element pattern".

EMISSION Electromagnetic radiation from matter, random in nature.

FAN BEAM An antenna beam which is narrow in one dimension, wide in another. A pencil beam, on the other hand, is narrow in both dimensions. Fan beams have different shapes - see Conical Beams and Planar Beams.

## GLOSSARY OF TERMS (Cont)

FAR FIELD PATTERN The antenna pattern obtained at a distance far enough away from the antenna that further distances do not change the pattern. The usual criterion is that the distance from antenna to field point exceed  $2 D^2/\lambda$ , where D is the maximum linear dimension of the antenna, and  $\lambda$  is the wavelength. Patterns obtained within this sphere are called near-field patterns.

FLAREOUT The time immediately prior to touchdown during which the aircraft pitches up, and flies above the glide slope.

FOCUS ANGLE For a cylindrical array, the angle in the non-scan plane at which perfect collimation of the beam occurs. In general there are two focus angles for a cylindrical array.

GLIDE PATH INTERCEPT POINT (GPIP) The point on the runway which the straight-line glideslope path would intercept if guidance were maintained down to the runway surface.

GRATING LOBE An unwanted beam which occurs as a result of spacings between elements that are too wide in an array.

INSERTION LOSS The attenuation of a signal due to losses and reflections in components of a system.

LAMINATES Plastic materials made by bonding together two or more sheets of reinforcing fibers. Microwave stripline circuit laminates typically are made from materials such as teflon-fiberglass, polyethylene, polyphenylene oxide, etc. Important electrical properties such as dielectric constant and loss factor are carefully controlled parameters in strip-line laminates.

LENS FOCAL ARC The locus of points in a flat circular lens at which incoming plane waves are focused. Conversely, a probe along the focal arc will result in a plane wave if fed with a signal from an internal generator.

LINEAR ARRAY An antenna array whose elements lie on a straight line. More specifically, the element phase centers lie on a straight line.

MAIN BEAM In a properly designed antenna system, the angular region in which most of the transmitted energy is concentrated. The Main beam region is usually considered as that between the first minimums.

## GLOSSARY OF TERMS (Cont)

MICROSTRIP An electronic component board consisting of a dielectric layer surrounded on one side by a solid conducting layer, and on the other by a patterned conducting layer. The patterns form the electrical circuit.

MULTIPATH The result or a propagating signal of unwanted reflections from the ground and other reflecting objects. It results from the fact that an antenna cannot direct all the transmitted energy in one direction or set of directions only.

MUTUAL COUPLING The interaction of currents or elements of an array. This phenomenon makes it impossible to independently excite currents of arbitrary amplitude and phase. The coupling changes as the antenna is scanned.

NEAR FIELD PATTERN The antenna pattern obtained at distances not far enough away from the antenna that the pattern is independent of distance. See Far Field Pattern.

PATTERN A graphical representation of the radiation properties of the antenna as a function of space coordinates.

Note 1. In the usual case the radiation pattern is determined in the far field region and is represented as a function of directional coordinates.

Note 2. Radiation properties include radiation intensity, field strength, phase or polarization.

PHASE CENTER The point from which a phase front appears to emanate when an antenna or antenna element is excited. In general there is no unique phase center for an antenna except for the angular region of the main beam.

PHOTOENGRAVING Same as photolithography. Terms are used interchangeably.

PHOTOLITHOGRAPHY A process by which electronic circuits can be produced by use of photography and photosensitive resists. A circuit design is laid out by means of a coordinatograph on a master artwork. The master artwork is reduced 4 to 10 times producing a negative print by means of photography. The image on the print is transferred to the circuit board through a photosensitive chemical covering the circuit material by means of ultra violet light source.



## GLOSSARY OF TERMS (Cont)

PHOTORESIST Photosensitive organic chemical solutions used to define geometries in stripline and microstrip fabrication. The materials when exposed to light change their solubility properties in appropriate developer solutions. The soluble portion when removed allows the underlying metal to be removed by an etchant while the insoluble portion protects the metal from the etchant.

POLARIZATION The direction of the electric field of a wave. To say that an antenna has vertical polarization means that the resulting electric field has no component which is both perpendicular to the direction of propagation and horizontal.

PLANAR ARRAY An antenna array whose elements (actually, phase centers) lie on the surface of a plane.

PLANAR BEAMS Fan beams whose fan generates a plane passing through the antenna. (See Conical Beams)

RADIATOR Synonymous with antenna element.

REFRACTION The bending from a straight line of the direction of propagation signal caused by inhomogeneities in the dielectric constant of the intervening medium.

ROLLOUT The time immediately after touchdown of a landing aircraft during which the aircraft is on the runway surface and decelerating.

SCAN RATE The rate, measured in scans per second, at which a scanning beam illuminates an aircraft. The data rate is equal to the scan rate only when the information from every scan is within the required accuracy.

SCATTERING The process by which electromagnetic energy is diverted away from the incident direction of propagation. The effect on the signal arriving at a desired destination is to attenuate it.

SIDELOBES Beams radiating from an antenna which are outside the main beam. These are usually desired to be as low as possible, but are never eliminated.

SKEW ERROR The error in angle measurement arising from distortion of the shape of a fan beam. A horizontal linear array scanned away from broadside generates fan beams whose shape is conical rather than planar, so that the beam center changes

## GLOSSARY OF TERMS (Cont)

with elevation. The resulting error is a skew error.

SKY TEMPERATURE The equivalent black-body radiation temperature caused by emission from atmospheric constituents. (See Emission). It is a function of frequency and look angle.

SQUINT ERROR An error in angle measurement caused by asymmetries in the beam of an antenna. The peak of radiation and the bore-sight angle do not coincide (see Boresight), resulting in an error in angle measurement.

STEP SCAN The behavior achieved by an antenna beam which rotates in discrete jumps. Its opposite is continuous scan which involves smooth rotation.

STRIPLINE An electronic component board consisting of two dielectric layers surrounded by two solid conducting surfaces, and having a central conducting layer between them which the circuit is formed.

SUBSTRATE Initial metal clad stripline laminate on which the microwave circuit is fabricated using chemical processes; some typical substrates used in microwave stripline and micro-strip circuits are teflon fiberglass, polyethylene, and alumina.

SUM BEAM The normal beam shape of an antenna pattern, having a single main beam.

SWITCHING NOISE In this context, the noise generated as the components of a digitally controlled array are switched from one beam portion setting to the next under "hot-switching" conditions, where the RF energy is flowing during the switching operation.

TOUCHDOWN The time at which the wheels of an aircraft first make contact with the runway surface during landing.